THE UNIVERSITY OF CHICAGO

MULTINUCLEAR PALLADIUM CATALYSTS FOR ETHYLENE POLYMERIZATION

A DISSERTATION SUBMITTED TO
THE FACULTY OF THE DIVISION OF THE PHYSICAL SCIENCES
IN CANDIDACY FOR THE DEGREE OF
DOCTOR OF PHILOSOPHY

DEPARTMENT OF CHEMISTRY

BY
QIAN LIU

CHICAGO, ILLINOIS
DECEMBER 2016

TABLE OF CONTENTS

CHAPTER FOUR

LIST OF TABLES

CHAPTER TWO

CHAPTER THREE

CHAPTER FOUR

LIST OF FIGURES

CHAPTER ONE

CHAPTER TWO

CHAPTER THREE

CHAPTER FOUR

LIST OF SCHEMES

CHAPTER ONE

CHAPTER TWO

CHAPTER THREE

CHAPTER FOUR

LIST OF CHARTS

CHAPTER FOUR

ACKNOWLEDGEMENTS

First, I thank my advisor, Professor Richard Jordan, for his invaluable guidance and instruction throughout my graduate studies. It has been a privilege to learn from his example of both scientific rigor and professionalism. I also thank the other members of my thesis committee, Professor Michael Hopkins and Professor John Anderson, for their helpful advice and discussions.

I have been fortunate to work with many talented and helpful people in the Jordan group. I am especially grateful to Dr. Nathan D. Contrella for his mentorship when I first joined the group. Other past and current group members have provided insightful discussions, friendship, and a great environment, and I thank Dr. Benjamin Petro, Dr. Ryan Zarkesh, Dr. Jia Wei, Dr. Ge (David) Feng, Dr. Ka Cheong (Tim) Lau, Feng Zhai, Frank Olechnowicz, Rebecca Black, Alison Johnson, Erik Reinhart, Shinji Wada, Dr. Mingfang Zheng, Dr. Biyun Su, Dr. Hiroshi Terao, Jessica Sampson.

I am grateful to my undergraduate research advisors, Professor Zhangjie Shi at Peking University and Professor Xiaoyu Li at the University of Hong Kong, for their support during college and beyond, and for providing an ideal opportunity to become involved in research.

The research described in this thesis has relied on many departmental facilities, and I thank Dr. Antoni Jurkiewicz and Dr. Chang-Jin Qin for their assistance with NMR spectroscopy and mass spectrometry, respectively, and Dr. Ian Steele and Dr. Alexander Filatov for their assistance with X-ray crystallography. I am grateful to Melinda Moore, Dr. Vera Dragisich, and Laura Baker for their assistance of administrative work.

I also thank Advanced Photon Source Facility at Argonne National Lab for the X-ray analysis support. ChemMatCARS Sector 15 is principally supported by the Divisions of Chemistry (CHE) and Materials Research (DMR), National Science Foundation, under grant number NSF/CHE-1346572. Use of the Advanced Photon Source, an Office of Science User Facility operated for the

U.S. Department of Energy (DOE) Office of Science by Argonne National Laboratory, was supported by the U.S. DOE under Contract No. DE-AC02-06CH11357.

Many good friends within and outside of the Chemistry Department have provided great memories throughout graduate school. I thank my family and especially my parents for a lifetime of support and encouragement, and finally, I thank my boyfriend, Zheng, for his support through the stress and uncertainty of graduate school.

ABSTRACT

This thesis describes the synthesis of multinuclear palladium complexes that adopt self-assembled cage structures and their performances as catalysts for ethylene polymerization and ethylene/vinyl fluoride copolymerization.

Chapter One introduces tetranuclear palladium(II) alkyl catalysts that contain phosphine-bis(arenesulfonate) (Li-OPO$^-$) ligands and adopt 3-dimensional structures in which four PdMe(py) units are arranged around the periphery of a central cubic $Li_4S_4O_{12}$ cage. The intact catalyst produces high-MW linear PE and copolymerizes ethylene with vinyl fluoride to afford linear copolymer with high VF incorporation (up to 3.6 mol %). The origins of these unique polymerization properties are unknown because partial dissociation of Pd_4 catalyst into Pd_1 species occurs under polymerization conditions, which complicates mechanistic studies. Other multinuclear olefin polymerization catalysts are also discussed.

Chapter Two describes a series of methoxy-substituted phosphine-arenesulfonate (PO) and phosphine-bis(arenesulfonate) (Li-OPO$^-$) ligands, and their corresponding Pd complexes. {[κ^2-*P,O*-PPh(2-SO_3-4,5-$(OMe)_2$-Ph)(2-SO_3Li-4,5-$(OMe)_2$-Ph)]PdMe(py')}$_4$•2LiCl (**5b**) self-assembles around a $Li_4S_4O_{12}$•Li_2Cl_2 cage with *SSSS* configurations at the phosphorous centers. Solution NMR data for **5b** are consistent with the solid-state structure. **5b** partially and reversibly dissociates into monomeric Pd_1 species above room temperature, but is more robust than {[κ^2-*P,O*-PPh(2-SO_3-5-Me-Ph)(2-SO_3Li-5-Me-Ph)]PdMe(py')}$_4$ (py' = 4-(5-nonyl)pyridine) and other assemblies based on $Li_4S_4O_{12}$ cores. **5b** produces UHMWPE with a narrow MWD characteristic of single-site catalysis in hexanes at 80 ˚C. The ethylene polymerization behavior of monomeric (PO)PdMe(py) complexes [κ^2-*P,O*-P(2-OMe-Ph)$_2$(2-SO_3-5-OMe-Ph)]PdMe(py) (**3a**) and [κ^2-*P,O*-P(2-OMe-Ph)$_2$(2-SO_3-4,5-$(OMe)_2$-Ph)]PdMe(py) (**3b**) is similar to that of the bench-mark

catalyst [κ^2-*P,O*-P(2-OMe-Ph)$_2$(2-SO$_3$-5-Me-Ph)]PdMe(py), which indicates that the methoxy substituents on the arenesulfonate ring do not strongly influence the reactivity.

Chapter Three describes a phosphine-sulfonate-phosphonate ligand [(4-^{t}Bu-Ph)(2-P(O)(OH)$_2$-5-Me-Ph)(2-SO$_3^-$-5-Me-Ph)P$^+$H] ([OP-P-SO], **1-H$_3$**). **1-H$_3$** reacts with Zn(OAc)$_2$ to form tetrameric **{Zn[1-H]}$_4$**, which adopts a puckered 16-membered Zn$_4$P$_4$O$_8$ ring structure. The reaction of CH$_3$OH-free **{Zn[1-H]}$_4$** with (COD)PdMe$_2$ and pyridine ligands (L) generates tetrameric palladium complexes **4-L**. X-ray diffraction analysis of **4-(4-^{t}Bu-py)** and solution NMR data for other **4-L** complexes (L = py, 2,6-lutidine, quinolone, 4-^{t}Bu-py) show that **4-**L are isostructural with {[κ^2-*P,O*-PPh(2-SO$_3$-5-Me-Ph)(2-SO$_3$Li-5-Me-Ph)]PdMe(py')}$_4$, with a central Zn$_4$P$_4$O$_{12}$ zinc phosphonate core and four (phosphine-phosphonate)PdMeL units at the periphery. **4-L** is converted to a trimeric species {[P(4-^{t}Bu-Ph)(2-PO$_3$Zn(py)-5-Me-Ph)(2-SO$_3$-5-Me-Ph)]PdMe}$_3$ (**3-L)** in the presence of CH$_3$OH, excess pyridine ligands or Et$_2$O. **3-py** adopts a unique cage structure, which contains a 12-membered Zn$_3$P$_3$O$_6$ ring stacked with a 6-membered Pd$_3$O$_3$ ring. The solution NMR data of **3-py** are consistent with the solid-state structure. Both **4-(4-^{t}Bu-py)** and **3-py** produce linear PE with high MW and copolymerize ethylene with vinyl fluoride with up to 1.1 mol % incorporation.

Chapter Four describes the synthesis of aryl borophosphonate cage compounds [ArPO$_3$BAr']$_n$ with n = 4 or 6, by condensation reactions of ArP(O)(OH)$_2$ and Ar'B(OH)$_2$. (3,5-^{t}Bu$_2$-Ph)P(O)(OH)$_2$ (**1**) reacts with arylboronic acids that contain electron-withdrawing substituents to form borophosphonate tetramers [Ar^{1}PO$_3$BAr^2]$_4$ (Ar^1 = 3,5-^{t}Bu$_2$-Ph; Ar^2 = *o*-Br-Ph, *o*-CF$_3$-Ph, *p*-CF$_3$-Ph, *p*-CHO-Ph; **3a-d**) and hexamers [Ar^{1}PO$_3$BAr^2]$_6$ (Ar^2 = *p*-CF$_3$-Ph, *p*-CHO-Ph; **4c-d**) in 80 - 93 % NMR yield. For Ar^2 = *p*-CF$_3$-Ph and *p*-CHO-Ph, both products were observed, with the tetramer favored under dilute reaction conditions and the hexamer favored under concentrated reaction conditions. The phosphine phosphonic acid (2-PPh_2-Ph)P(O)$(OH)_2$ (**6**) reacts with arylboronic acids that contain electron-withdrawing substituents to form tetramers $[Ar^1PO_3BAr^2]_4$ (Ar^1 = 2-PPh_2-Ph; Ar^2 = *p*-CF_3-Ph, *p*-CHO-Ph; **7c-d**) in 70 - 75 % NMR yield. The reactions of **1** or **6** with (*p*-tolyl)B$(OH)_2$ (**2f**), and the reaction of **6** with (*o*-CF_3-Ph)B$(OH)_2$ (**2b**), yield only trace amounts of borophosphonate cage compounds, and instead afford the corresponding $[ArBO]_3$ boroxines and condensation products with unknown structures. These borophosphonate compounds are stable in toluene at 110 ˚C, and therefore they are potential scaffolds for the formation of multinuclear Pd catalysts.

PREFACE

Each chapter has an independent numbering system for compounds. A given compound may have a different number in different chapters. For each chapter, the relevant experimental information, references, and notes are provided at the end of the chapter.

CHAPTER ONE

Introduction to Multinuclear Phosphine-Sulfonate Palladium Alkyl Complexes

1.1 Phosphine-Sulfonate Palladium Alkyl Complexes for Olefin Polymerization

In 2002, Pugh and Drent reported that *in situ*-generated palladium alkyl catalysts based on phosphine-arenesulfonate ligands, (PO)PdR, copolymerize ethylene with alkyl acrylates to afford a linear copolymer with acrylate groups incorporated in the polyethylene backbone.[1] This polymerization behavior is quite different from that of Brookhart's cationic (α-diimine)PdR^+ catalysts, which afford highly branched ethylene/alkyl acrylate copolymers, with almost exclusively chain-end incorporation of the polar monomer.[2] The insertion copolymerization of ethylene and polar vinyl monomers is a potentially more efficient and direct method to synthesize functionalized polyethylenes, compared to alternative strategies such as post-functionalization of polyethylene, acyclic diene metathesis (ADMET) polymerization followed by hydrogenation, ring-opening metathesis polymerization (ROMP) followed by hydrogenation, and radical copolymerization. Due to its unique polymerization behavior, the (PO)PdR catalyst system has been widely studied. The scope of polar monomers that can be copolymerized with ethylene by this system has been greatly expanded (Scheme 1.1), and includes alkyl and aryl vinyl ethers,[3] vinyl fluoride,[4] vinyl chloride (terminal incorporation only),[5] acrylonitrile,[6] vinyl acetate,[7] alkyl acrylates,[1,8] acrylic acid,[9] vinyl ketones,[10] acrylamides,[11] N-vinyl-2-pyrrolidinone,[11a] styrene,[10] norbornene,[12] vinyl sulfone,[13] vinyl phosphonic acid,[14] diethyl vinyl phosphonate,[14] 3,3,3-trifluoropropene[15] and CO.[16]

Scheme 1.1

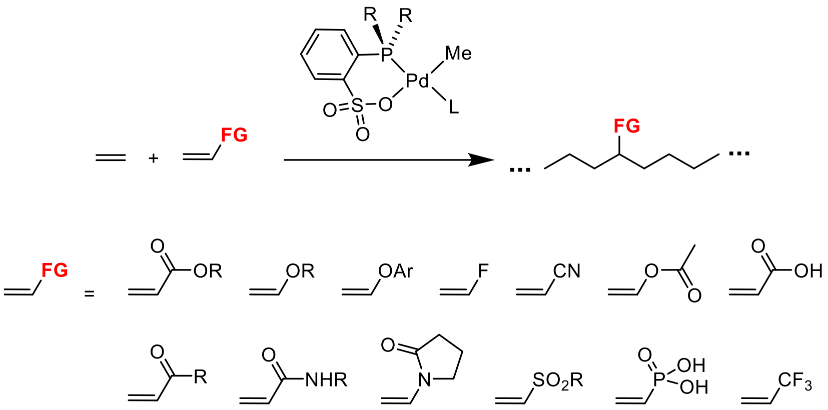

The unique polymerization properties of (PO)PdR catalysts are believed to arise from the combination of several factors, most notably the soft character of the palladium (II) metal center, the electronic asymmetry of the κ^2-*P*,*O* chelated phosphine-arenesulfonate (PO) ligand, and the overall neutral charge of the catalyst. Because Pd(II) is a soft metal center, the metal-ligand bonds are quite covalent and *trans* influence effects are pronounced. A schematic mechanism for ethylene enchainment in (PO)PdR catalyzed polymerization is shown on the right side of Scheme 1.2. Ethylene exerts a weaker *trans* influence than hydride, and therefore the *trans* arrangement of the strong phosphine ligand and the ethylene ligand in the ethylene adduct is more stable than the *trans* arrangement of phosphine and hydride in the β-H elimination product. The ethylene adduct also contains a very strong alkyl ligand *trans* to the very weak sulfonate ligand, an arrangement which is more stable than the *trans* arrangement of olefin and sulfonate ligands in the β-H elimination product. Therefore, β-H elimination, which leads to chain transfer or branching, is disfavored relative to chain growth. Similar factors disfavor β-X elimination in polar monomer copolymerization (left side of Scheme 2.1). The favorable *trans* arrangements of the phosphine and dative-X ligands, and of the sulfonate and alkyl ligands in the (PO)PdCH$_2$CHX insertion product, would be replaced by less favorable *trans* arrangements of the phosphine and X ligands, and of sulfonate and olefin ligands, after β-X elimination, while the favorable *trans* arrangement of the sulfonate and alkyl ligands is maintained in the ethylene adduct. Therefore, the β-X elimination is disfavored relative to chain growth. The neutral charge of the catalyst and the soft character of the Pd(II) center favor coordination of the polar monomer ($XCH{=}CH_2$) in the polymerization-active π-bond mode (η^2-($XCH{=}CH_2$)-Pd) over the polymerization-dormant σ-bond mode (η^1-($CH_2{=}CHX$)-Pd).

Scheme 1.2. Red letters refer to *trans*-influence (vs-very strong, s-strong, m-medium, w-weak, vw-very weak).

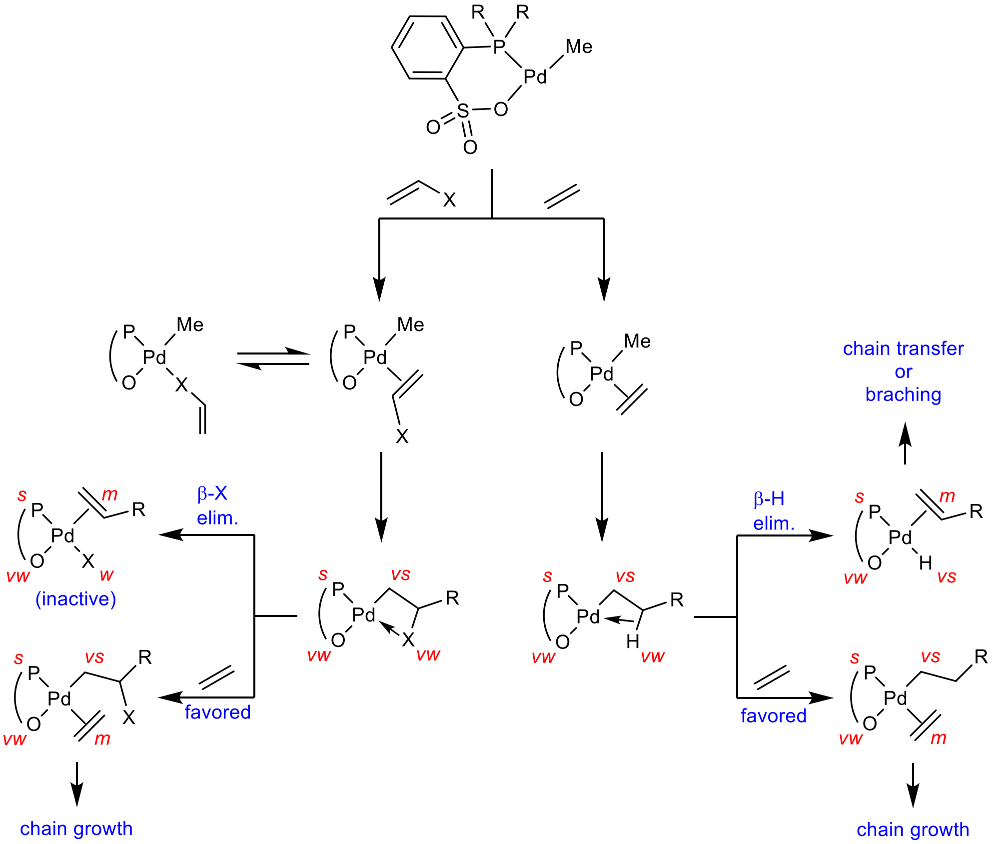

However, (PO)PdR catalysts typically exhibit low ethylene polymerization activity (< 100 $kg \cdot mol^{-1} \cdot h^{-1} \cdot atm^{-1}$) and produce polyethylene (PE) with low molecular weight (MW). Polar monomers further decease the activity and MW, and the level of incorporation of polar monomer are generally low (< 5 mol %). Therefore, there is strong interest in developing strategies to improve the performance of (PO)PdR catalysts.

1.2 Multinuclear Olefin Polymerization Catalysts

Multinuclear olefin polymerization catalysts have been reported to exhibit different polymerization behavior (activity, branching, selectivity, etc.) compared to corresponding monomeric catalysts, although the underlying reasons for the observed differences are obscure in most cases. Noh et al. reported a series of polymethylene-bridged binuclear Ti catalysts, which exhibit increased ethylene polymerization activity compared to analogous monomeric catalysts. The polymerization properties are influenced by the length of the linker.[17] One interesting example **A** (Figure 1.1) contains two linkers and shows increased activity, higher MW and higher tacticity in syndiotactic styrene homopolymerization.[17d] The high syndiotacticity was ascribed to the presence of the second bridge, which rigidifies the structure and promotes stereoselective enchainment. Marks and co-workers reported several binuclear "constrained geometry" catalysts (Figure 1.1, **B**).[18] Increased MW and α-olefin incorporation were observed for ethylene polymerization by the Zr-based binuclear catalysts, while the activity was comparable or lower than the corresponding mononuclear catalyst.[19] Increased α-olefin incorporation was observed for the Ti-based binuclear catalysts, while the activity and MW were comparable or decreased compared to mononuclear catalysts.[20] For styrene homopolymerization or ethylene/styrene copolymerization, binuclear Ti catalysts display good activity and styrene incorporation,[21] while analogous monomeric catalysts are nearly inactive.[22] These unique polymerization properties were attributed to cooperative effects between the two metal centers, which can depress the chain transfer and increase the comonomer enchainment. In other work, Salata and Marks reported a dizirconium catalyst that is based on rigid planar phenoxyiminato linker (Figure 1.1, **C**), which exhibits increased activity and MW in ethylene homopolymerization, and higher α-olefin incorporation and activity in ethylene/1-hexene and ethylene/1-octane copolymerization compared to related monomeric catalysts.[23] The close proximity of the metal centers (ca. 5.9 Å) and the conformational rigidity were invoked as reasons for these difference in polymerization properties.

Multinuclear group 10 metal olefin polymerization catalysts have also been investigated. Lee and coworkers reported dinickel catalysts based on a rigid *o*-phenylene bridge (Figure 1.1, **D**).[24] Agapie reported a similar dinickel system with a *p*-$C_6(CH_3)_4$ bridge (Figure 1.1, **E**).[25] These catalysts exhibit higher polymerization activities and increased comonomer incorporation in ethylene/2-(methoxycarbonyl)-norbornene and ethylene/2-(acetoxymethyl)-norbornene copolymerizations, which were attributed to unspecified "cooperative effects" between the metal centers. A binuclear palladium catalyst that contains a bis-chelating pyridine-imine ligand (Figure 1.1, **F**) was reported by Casalino et al. and shows a notable level of isotacticity of styrene/CO copolymerization, in contrast to a mononuclear analogue which gave atactic copolymer.[26] Dipalladium[27] and dinickel[28] catalysts linked by a macrocyclic ligand were reported by Takeuchi, Osakada, and coworkers (Figure 1.1, **G** and **H**) and displayed higher polymerization activities and MW compared to mononuclear analogues. The dipalladium catalysts incorporate higher levels of polar comonomers, such as methyl acrylate, tert-butyl acrylate, tert-butyl-butenoate.

An octanuclear Fe(II) catalyst based on a dendrimer backbone was reported to have much higher ethylene polymerization activity and produce much higher MW PE than mononuclear analogues (Figure 1.1, **I**).[29] This difference was attributed to steric crowding within the dendrimeric structure, which was proposed to weaken the electrostatic ion-pairing of the cationic (pyridine-diimine)FeR$^+$ active species with the MMAO activator derived counteranions. Similar enhanced polymerization properties were also observed for the trinuclear Fe catalyst **J**, which is linked through a macrocycle (Figure 1.1).[30] In this case, it was proposed that chain transfer was suppressed by the structure of the catalyst.

The binuclear rare earth metal samarium catalyst **K** (Figure 1.1) produces high-MW PE with high activity, while the analogous monomeric samarium alkyl complex is inactive for ethylene homopolymerization.[31] **K** also produces diblock copolymers of ethylene with methyl methacrylate/ε-caprolactone.

Figure 1.1. Multinuclear Olefin Polymerization Catalysts

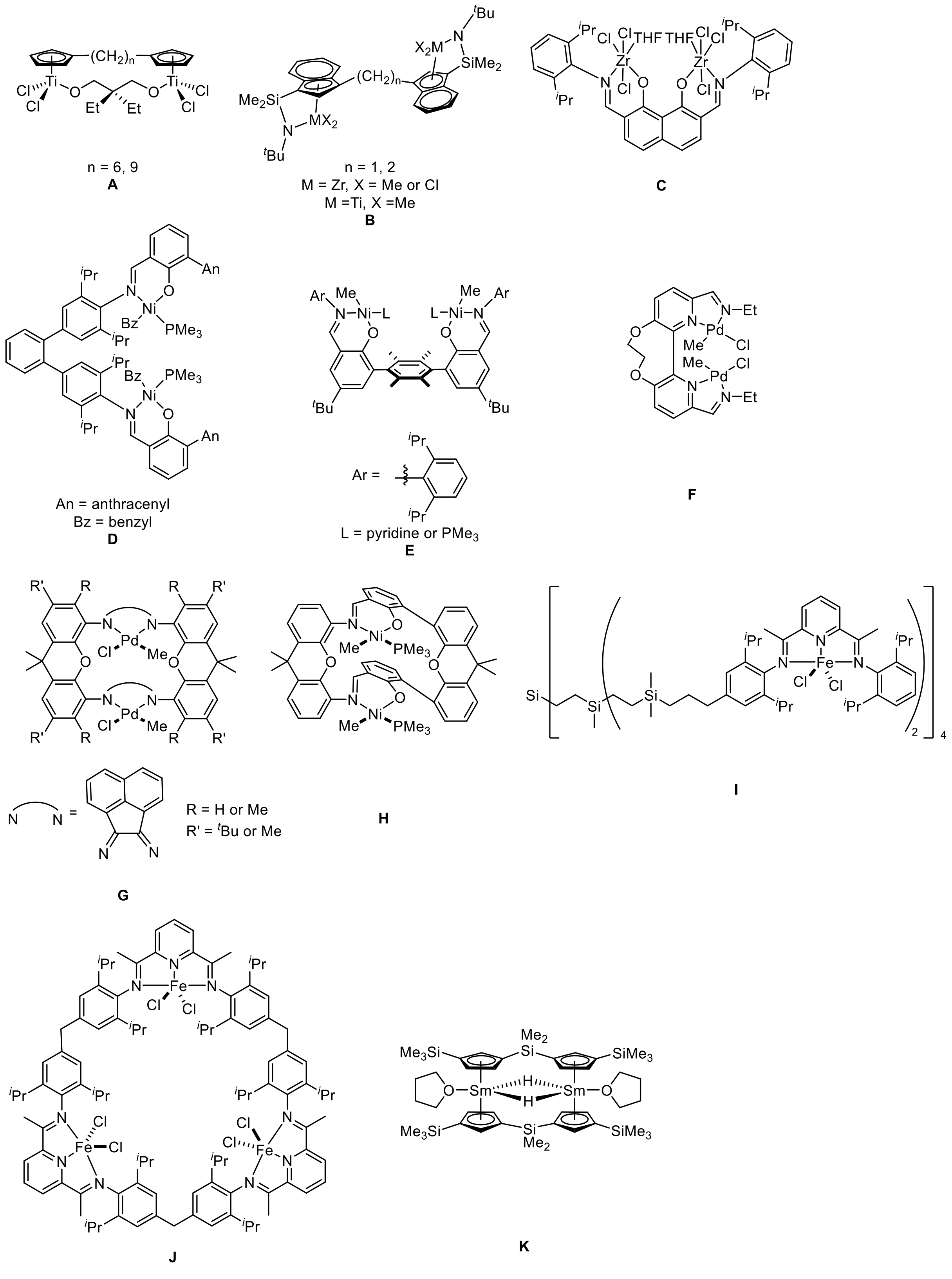

n = 6, 9
A

n = 1, 2
M = Zr, X = Me or Cl
M = Ti, X = Me
B

C

An = anthracenyl
Bz = benzyl
D

Ar =
L = pyridine or PMe$_3$
E

F

R = H or Me
R' = ^{t}Bu or Me
G

H

I

J

K

1.3 Tetranuclear Phosphine-bis(arenesulfonate) Palladium Catalysts

Palladium alkyl complexes based on the phosphine-*bis*(arensulfonate) ligand PPh(2-SO_3Li-5-Me-Ph)(2-SO_3^--5-Me-Ph) (Li[OPO]$^-$) self-assemble into tetrameric "Pd_4 cage" structures, in which four PdMeL units are arranged around the periphery of a central $Li_4S_4O_{12}$ cage.[32] The structure of [(Li-OPO)PdMe(py')]$_4$ (**L**, py' = 4-(5-nonyl)-pyridine) is shown in Figure 1.2. The four Pd centers are equivalent, but are spatially separated into two pairs, with a Pd-Pd distance of 6.04 Å in each pair.

Figure 1.2 Molecular structure of compound **L**. Hydrogen atoms are omitted.

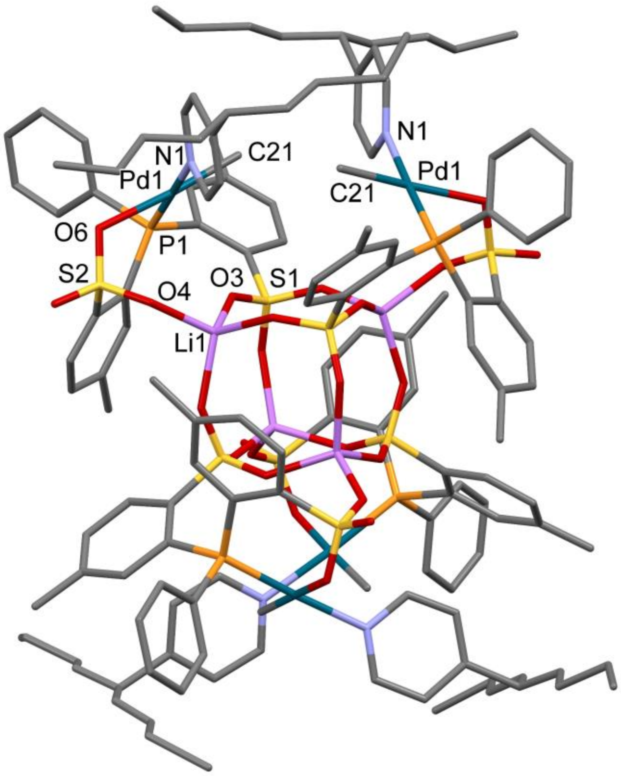

L partially dissociates into monomeric (Li-OPO)PdMe(py') "Pd_1" species in CD_2Cl_2 above -10 ˚C (Scheme 1.3). The olefin polymerization properties of **L** are strongly influenced by the extent of cage dissociation. In toluene at 80 ˚C with $[Pd_4]_0$ = 0.05 mM, **A** is completely dissociated and produces low-MW linear PE with a narrow molecular weight distribution (MWD) (Figure 1.3, black trace), similar to what is observed for conventional monomeric (PO)PdMeL catalysts. In hexanes at 80 ˚C or CH_2Cl_2 at room temperature, **A** is only partially dissociated, and produces linear PE with a broad MWD, which contains a high-MW fraction and a low-MW fraction (Figure 1.3, red trace). These results indicate that the intact tetranuclear cage Pd_4 catalyst produces the high-MW fraction, while the cage-dissociated Pd_1 species produce the low-MW fraction. **L** also copolymerizes ethylene with vinyl fluoride (VF) to form linear copolymers with a significantly higher level of VF incorporation (up to 3.6 mol %) compared to monomeric (PO)PdMeL catalysts (< 0.5 mol %).

Scheme 1.3. py’ = 4-(5-nonyl)-pyridine.

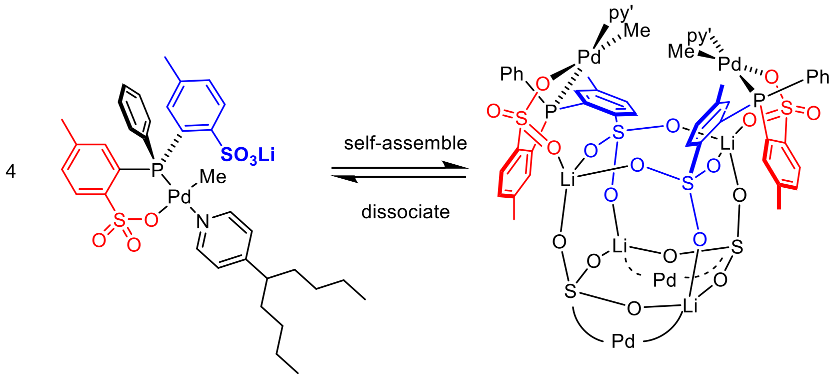

L

Figure 1.3. GPC trace of PE generated by **L** in toluene at 80 ˚C (black trace) and in hexanes at 80 ˚C (red trace). The Pd_4 catalyst is fully dissociated to Pd_1 species in toluene, but only partially dissociated in hexanes.

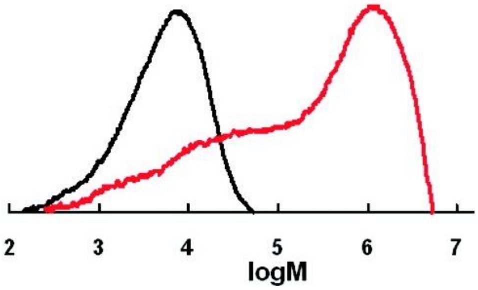

The mechanistic origins of the unusual polymerization properties of **L** are unkown. One possibility is that the high MW polymer production results from steric blockage of an axial site at each Pd center by the central $Li_4S_4O_{12}$ cage, which inhibits associative chain transfer. Another hypothesis is that, due to the proximity of the Pd centers, the growing polymer chains in the putative $[(Li\text{-}OPO)Pd(R)(CH_2{=}CH_2)]_4$ active species may interact with chains on adjacent Pd centers in a way that inhibits β-H elimination. The rigidity of the cage structure may also have an important role in high-MW polymer production. However, little is known about how the catalyst behaves under polymerization conditions. For example, the number of growing polymer chain per tetramer is unknown. Each Pd center may have a growing chain, or due to the proximity of Pd centers within each of the two pairs of PdRL units, there might be only one growing chain per pair. Additionally, the cage may undergo isomerization under polymerization conditions. Finally, the cage structure itself may influence the coordination and insertion of ethylene and polar comonomers. However, due to the partial dissociation of **L** into Pd_1 species during polymerization, it is very challenging to resolve these mechanistic issues.

1.4 Thesis Objective

The objective of this thesis is to synthesize tetranuclear Pd_4 catalysts that are structural analogues of **L** but are less susceptible to cage dissociation, and to study their olefin polymerization behavior.

Chapter 2 describes the synthesis of a tetranuclear {[κ^2-*P,O*-PPh(2-SO_3-4,5-$(OMe)_2$-Ph)(2-SO_3Li-4,5-$(OMe)_2$-Ph)]PdMe(py')}$_4$·2LiCl catalyst (**M**, Figure 1.4), which assembles around a $Li_4S_4O_{12}\cdot Li_2Cl_2$ cage core and is more thermally stable than **L**. This tetrameric Pd_4 catalyst produces high-MW PE with a narrow MWD in hexanes at 80 ˚C, characteristic of single-site catalysis. **M** also copolymerizes ethylene with vinyl fluoride into linear copolymers with a broad MWD and high VF incorporation (ca. 2.5 mol%). The analogous mononuclear complexes [κ^2-*P,O*-P(2-OMe-Ph)$_2$(2-SO_3-5-OMe-Ph)]PdMe(py) and [κ^2-*P,O*-P(2-OMe-Ph)$_2$(2-SO_3-4,5-$(OMe)_2$-Ph)]PdMe(py) were synthesized to study the electronic effects of methoxy group (**N** and **O**, Figure 1.4). The olefin polymerization behavior of these mononuclear catalysts is very similar to that of the bench-mark catalyst [κ^2-*P,O*-P(2-OMe-Ph)$_2$(2-SO_3-5-Me-Ph)]PdMe(py), which indicates that arenesulfonate methoxy substituents in **N** and **O** exert little influence.

Chapter 3 describes the synthesis of a tetrameric zinc phosphine-sulfonate-phosphonate ligand {Zn[P(4-^{t}Bu-Ph)(2-PO_3H-5-Me-Ph)(2-SO_3-5-Me-Ph)]}$_4$ (**P**, Figure 1.4). The reaction of **P** with (COD)$PdMe_2$ and a pyridine ligand (L) yields the tetrameric Pd catalyst {[κ^2-*P,SO*-P(4-^{t}Bu-Ph)(2-PO_3Zn-5-Me-Ph)(2-SO_3-5-Me-Ph)]PdMeL}$_4$ (**Q**, L = pyridine or 4-^{t}Bu-pyridine, Figure 1.4). **Q** assembles around a cubic $Zn_4P_4O_{12}$ core and is isostructural with **L**. **Q-(4-^{t}Bu-py)** is thermally robust and does not undergo significant cage dissociation at 80 ˚C in $CDCl_2CDCl_2$. However, in the presence of CH_3OH, **Q-py** is converted to a unique trimeric Pd catalyst {[P(4-^{t}Bu-Ph)(2-PO_3Zn(py)-5-Me-Ph)(2-SO_3-5-Me-Ph)]PdMe}$_3$ (**R**, Figure 1.4). **Q-(4-^{t}Bu-py)** also react with excess 4-^{t}Bu-pyridine to generate **R-(4-^{t}Bu-py)** (minor) and some unknown species (major). The reaction of **Q-(4-^{t}Bu-py)** with $B(C_6F_5)_3$ generates a poorly soluble base-free species, which reacts with 4-^{t}Bu-pyridine to regenerate **Q-(4-^{t}Bu-py)**, albeit with extensive cage isomerization. In the presence of 1 equiv of $B(C_6F_5)_3$ per 4-^{t}Bu-pyridine, **Q** produces high-MW PE with a broad MWD, characteristic of multi-site catalysis. In contrast, in the presence of 1 equiv of $B(C_6F_5)_3$ per pyridine, Pd_3 catalyst **R** produces high-MW PE with a narrow MWD, indicative of single-site catalysis. **Q** and **R** are active for ethylene/vinyl-fluoride copolymerization with up to 1.1 mol % VF incorporation.

Chapter 4 describes the synthesis of tetrameric (**S**) and hexameric (**T**) aryl borophosphonate cage compounds $[ArPO_3BAr']_n$ with a variety of Ar and Ar' groups by condensation of $ArPO_3H_2$ and $Ar'B(OH)_2$ (Figure 1.4). **S** is isostructural with the $Li_4S_4O_{12}$ core in **L**. Electronic and steric effects strongly influence the product distributions and yields of these reactions. The reactivity of simple aryl borophosphonate cages with ^{n}BuLi was explored, and showed that the aryl borophosphonate cage is compatible with ^{n}BuLi. These borophosphonate compounds are stable in toluene at 110 ˚C, and represent potential scaffolds for the generation of multinuclear Pd catalysts.

Figure 1.4. Chart of complexes.

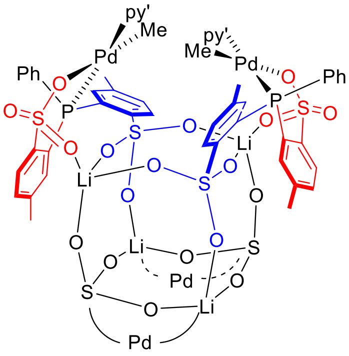

L

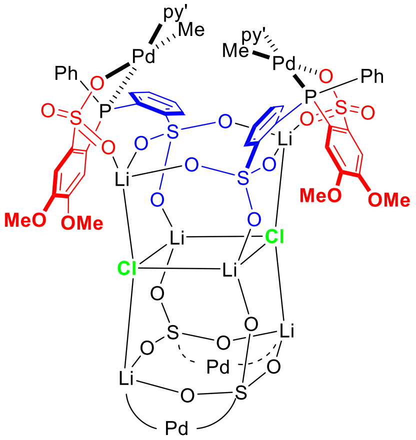

M

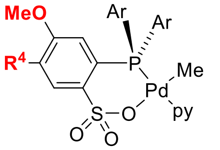

Ar = 2-OMe-Ph

N R^4 = H

O R^4 = OMe

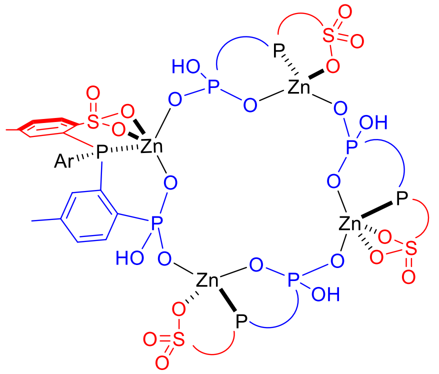

P

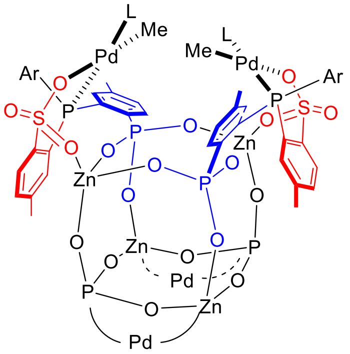

L = py, 4-^{t}Bu-py

Q

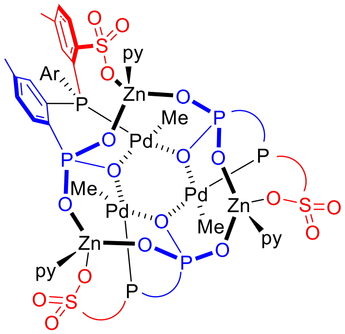

R

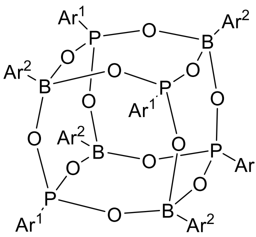

Ar^1 = 3,5-^{t}Bu$_2$-Ph, Ar^2 = *o*-Br-Ph, *o*-CF_3-Ph, *p*-CF_3-Ph, *p*-CHO-Ph

Ar^1 = 2-PPh_2-Ph, Ar^2 = *p*-CF_3-Ph, *p*-CHO-Ph

S

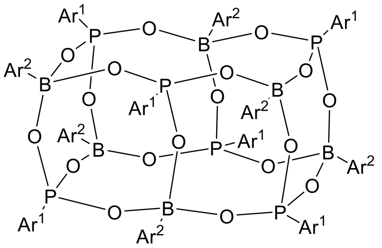

Ar^1 = 3,5-^{t}Bu$_2$-Ph

Ar^2 = *p*-CF_3-Ph, *p*-CHO-Ph

T

1.5 References and Notes

1. Drent, E.; van Dijk, R.; van Ginkel, R.; van Oort, B.; Pugh, R. I. *Chem. Commun.* **2002**, 744.

2. (a) Johnson, L. K.; Mecking, S.; Brookhart, M. *J. Am. Chem. Soc.* **1996**, *118*, 267. (b) Mecking, S.; Johnson, L. K.; Wang, L.; Brookhart, M. *J. Am. Chem. Soc.* **1998**, *120*, 888.

3. Luo, S.; Vela, J.; Lief, G. R.; Jordan, R. F. *J. Am. Chem. Soc.* **2007**, *129,* 8946.

4. (a) Weng, W.; Shen, Z.; Jordan, R. F. *J. Am. Chem. Soc.* **2007**, *129*, 15450. (b) Shen, Z.; Jordan, R. F. *Macromolecules* **2010**, *43*, 8706.

5. Leicht, H.; Göttker-Schnetmann, I.; Mecking, S. *Angew. Chem. Int. Ed.* **2013**, *52*, 3963.

6. (a) Kochi, T.; Noda, S.; Yoshimura, K.; Nozaki, K. *J. Am. Chem. Soc.* **2007**, *129*, 8948. (b) Nozaki, K.; Kusumoto, S.; Noda, S.; Kochi, T.; Chung, L. W.; Morokuma, K. *J. Am. Chem. Soc.* **2010**, *132*, 16030.

7. Ito, S.; Munakata, K.; Nakamura, A.; Nozaki, K. *J. Am. Chem. Soc.* **2009**, *131*, 14606.

8. (a) Skupov, K. M.; Marella, P. R.; Simard, M.; Yap, G. P. A.; Allen, N.; Conner, D.; Goodall, B. L.; Claverie, J. P. *Macromol. Rapid Commun.* **2007**, *28*, 2033. (b) Skupov, K. M.; Hobbs, J.; Marella, P.; Conner, D.; Golisz, S.; Goodall, B. L.; Claverie, J. P. *Macromolecules* **2009**, *42*, 6953. (c) Daigle, J.-C.; Piche, L.; Arnold, A.; Claverie, J. P. *ACS Macro Letters* **2012**, *1*, 343. (d) Piche, L.; Daigle, J.-C.; Rehse, G.; Claverie, J. P. *Chem. Eur. J.* **2012**, *18*, 3277. (e) Rünzi, T.; Guironnet, D.; Göttker-Schnetmann, I.; Mecking, S. *J. Am. Chem. Soc.* **2010**, *132*, 16623. (f) Guironnet, D.; Caporaso, L.; Neuwald, B.; Göttker-Schnetmann, I.; Cavallo, L.; Mecking, S. *J. Am. Chem. Soc.* **2010**, *132*, 4418. (g) Guironnet, D.; Roesle, P.; Rünzi, T.; Göttker-Schnetmann, I.; Mecking, S. *J. Am. Chem. Soc.* **2009**, *131*, 422.

9. (a) Daigle, J.-C.; Piche, L.; Claverie, J. P. *Macromolecules* **2011**, *44*, 1760. (b) Rünzi, T.; Fröhlich, D.; Mecking, S. *J. Am. Chem. Soc.* **2010**, *132*, 17690. (c) Kryuchkov, V. A.; Daigle, J.-C.; Skupov, K. M.; Claverie, J. P.; Winnik, F. M. *J. Am. Chem. Soc.* **2010**, *132*, 15573.

10. Borkar, S.; Newsham, D. K.; Sen, A. *Organometallics* **2008**, *27*, 3331.

11. (a) Skupov, K. M.; Piche, L.; Claverie, J. P. *Macromolecules* **2008**, *41*, 2309. (b) Friedberger, T.; Wucher, P.; Mecking, S. *J. Am. Chem. Soc.* **2012**, *134*, 1010.

12. (a) Ravasio, A.; Boggioni, L.; Tritto, I. *Macromolecules* **2011**, *44*, 4180. (b) Liu, S.; Borkar, S.; Newsham, D.; Yennawar, H.; Sen, A. *Organometallics* **2007**, *26*, 210. (c) Skupov, K. M.; Marella, P. R.; Hobbs, J. L.; McIntosh, L. H.; Goodall, B. L.; Claverie, J. P. *Macromolecules* **2006**, *39*, 4279.

13. Bouilhac, C.; Rünzi, T.; Mecking, S. *Macromolecules* **2010**, *43*, 3589.

14. Rünzi, T.; Baier, M. C.; Negele, C.; Krumova, M.; Mecking, S. *Macromol. Rapid Commun.* **2015**, *36*, 165.

15. Lanzinger, D.; Giuman, M. M.; Anselment, T. M. J.; Rieger, B. *ACS Macro Letters* **2014**, *3*, 931.

16. (a) Drent, E.; van Dijk, R.; van Ginkel, R.; van Oort, B.; Pugh, R. I. *Chem. Commun.* **2002**, 964. (b) Newsham, D. K.; Borkar, S.; Sen, A.; Conner, D. M.; Goodall, B. L. *Organometallics* **2007**, *26*, 3636. (c) Hearley, A. K.; Nowack, R. J.; Rieger, B. *Organometallics* **2005**, *24*, 2755. (d)Luo, R.; Newsham, D. K.; Sen, A. *Organometallics* **2009**, *28*, 6994.

17. (a) Noh, S. K.; Kim, J.; Jung, J.; Ra, C. S.; Lee, D. H.; Lee, H. B.; Lee, S. W.; Huh, W. S. *J. Organomet. Chem.* **1999**, *580*, 90. (b) Lee, H. W.; Park, Y. H. *Catal. Today* **2002**, *74*, 309. (c) Lee, H. W.; Ahn, A. H.; Park, Y. H. *J. Mol. Catal. A: Chem.* **2003**, *194*, 19. (d) Noh, S. K.; Kim, S.; Yang, Y.; Lyoo, W. S.; Lee, D. H. *Eur. Polym. J.* **2004**, *40*, 227.

18. Li, H.; Marks, T. J. *Proc. Natl. Acad. Sci. U.S.A.* **2006**, *103*, 15295.

19. (a) Li, H.; Li, L.; Marks, T. J. *Angew Chem., Int. Ed.* **2004**, *43*, 4937. (b) Motta, A.; Fragalà, I. L.; Marks, T. J. *J. Am. Chem. Soc.* **2009**, *131*, 3974. (c) Li, H.; Stern, C. L.; Marks, T. J. *Macromolecules* **2005**, *38,* 9015. (d) Li, L.; Metz, M. V.; Li, H.; Chen, M. C.; Marks, T. J.; Liable-Sands, L.; Rheingold, A. L. *J. Am. Chem. Soc.* **2002**, *124*, 12725.

20. (a) Li, H.; Li, L.; Marks, T. J.; Liable-Sands, L.; Rheingold, A. L. *J. Am. Chem. Soc.* **2003**, *125*, 10788. (b) Li, H.; Li, L.; Schwartz, D. J.; Metz, M. V.; Marks, T. J.; Liable-Sands, L.; Rheingold, A. L. *J. Am. Chem. Soc.* **2005**, *127*, 14756.

21. Guo, N.; Li, L.; Marks, T. J. *J. Am. Chem. Soc.* **2004**, *126*, 6542.

22. Sernetz, F. G.; Mülhaupt, R.; Waymouth, R. M. *Macromol. Chem. Phys.* **1996**, *197*, 1071.

23. Salata, M. R.; Marks, T. J. *Macromolecules* **2009**, *42*, 1920.

24. S, S.; Joe, D. J.; Na, S. J.; Park, Y.-W.; Choi, C. H.; Lee, B. Y. *Macromolecules* **2005**, *38*, 10027.

25. (a) Radlauer, M. R.; Day, M. W.; Agapie, T. *J. Am. Chem. Soc.* **2012**, *134*, 1478. (b) Radlauer, M. R.; Buckley, A. K.; Henling, L. M.; Agapie, T. *J. Am. Chem. Soc.* **2013**, *135*, 3784. (c) Radlauer, M. R.; Day, M. W.; Agapie, T. *Organometallics* **2012**, *31*, 2231.

26. Casalino, M.; De Felice, V.; Fraldi, N.; Panunzi, A.; Ruffo, F. *Inorg. Chem.* **2009**, *48,* 5913.

27. Takano, S.; Takeuchi, D.; Osakada, K.; Akamatsu, N.; Shishido, A. *Angew. Chem. Int. Ed.* **2014**, *53*, 9246.

28. Takeuchi, D.; Chiba, Y.; Takano, S.; Osakada, K. *Angew. Chem. Int. Ed.* **2013**, *52,* 12536.

29. Zheng, Z.-J.; Chen, J.; Li, Y.-S. *Journal of Organometallic Chemistry* **2004**, *689,* 3040.

30. Liu, J.; Li, Y.; Liu, J.; Li, Z. *Macromolecules* **2005**, *38*, 2559.

31. Desurmont, G.; Li, Y.; Yasuda, H.; Maruo, T.; Kanehisa, N.; Kai, Y. *Organometallics* **2000**, *19*, 1811.

32. Shen, Z.; Jordan, R. F. *J. Am. Chem. Soc.* **2010**, *132*, 52.

CHAPTER TWO

Structure and Olefin Polymerization Behavior of a Self-assembled LiCl-Templated Tetranuclear Palladium Catalyst

2.1 Introduction

Palladium alkyl complexes that contain phosphine-arenesulfonate (PO) ligands have been widely studied because they can polymerize ethylene to linear polyethylene (PE) and copolymerize ethylene with a wide range of polar CH_2=CHX vinyl monomers.[1] Analogous palladium alkyl complexes based on the phosphine-*bis*(arensulfonate) ligand PPh(2-SO_3Li-5-Me-Ph)(2-SO_3^--5-Me-Ph) (Li[OPO]$^-$) self-assemble into tetrameric "Pd_4 cage" species, which are held together by a core $Li_4S_4O_{12}$ cage (Figure 2.1, **A**).[2] Each Li center in **A** is coordinated to three oxygens from the non-Pd-bonded sulfonate group and one oxygen from the Pd-bonded sulfonate group. The four Pd centers are equivalent, but are spatially separated into two pairs, which occupy the "top" and "bottom" faces of the cage. In each pair, the Pd-Pd distance is 6.04 Å and the Pd-Me groups are positioned close to the neighboring py' ring. The four "side" faces of the cage are fully blocked by the arene rings of the Pd-bonded arene sulfonate groups. Therefore, the periphery of the cage is sterically saturated. As shown in Figure 2.2, H17, which is *para* to the phosphine on the Pd-bonded $ArSO_3^-$ arene ring from the "bottom" Pd center, is very close to the non-Pd-bonded $ArSO_3^-$ arene ring from "top" Pd center, and the distance between H17-H9 is ca. 2.522 Å. The cage has S_4 symmetry with *SSRR* configurations at the phosphorous centers.

Figure 2.1. (a) Molecular structure of {[κ^2-*P*,*O*-PPh(2-SO_3-5-Me-Ph)(2-SO_3Li-5-Me-Ph)]PdMe(py')}$_4$ (**A**, py' = 4-(5-nonyl)pyridine). Hydrogen atoms and the 5-nonyl groups are omitted from the 3-dimensional stick view. (b) Structure of {[κ^2-*P*,*O*-PPh(2-SO_3-5-R^5-Ph)(2-SO_3Li-5-R^5-Ph)]PdMe(L)}$_4$ compounds **B-D**.

(a)

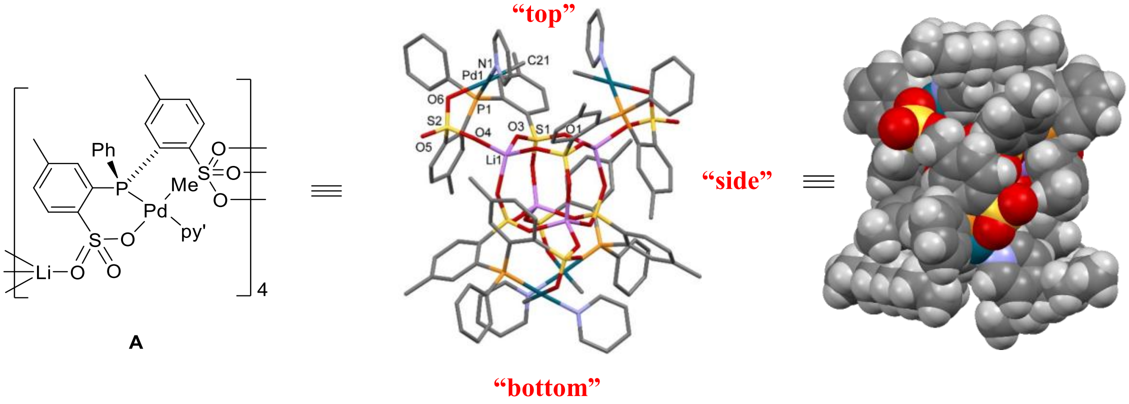

A

(b)

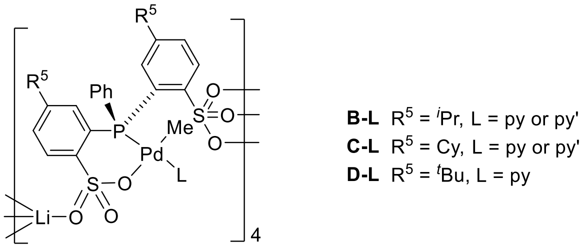

B-L R^5 = ^{i}Pr, L = py or py'
C-L R^5 = Cy, L = py or py'
D-L R^5 = ^{t}Bu, L = py

B-D

Figure 2.2. Space-filling side view of **A**. The S-S face diagonal distance is 4.676 Å.

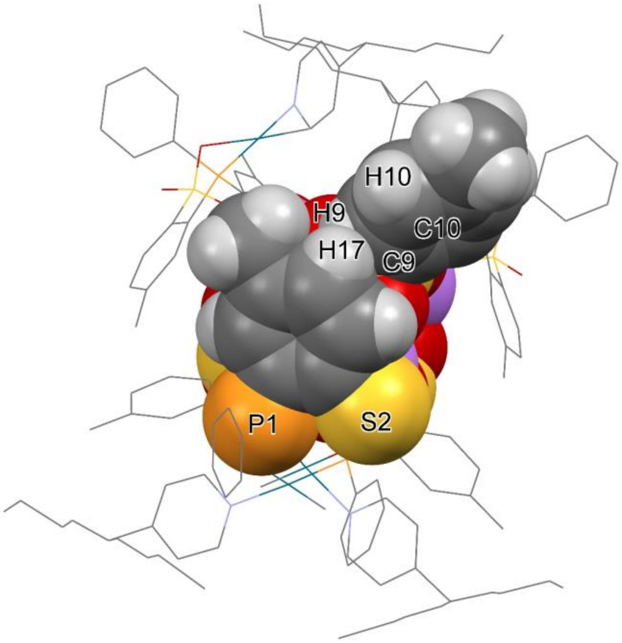

A partially dissociates into monomeric (Li-OPO)PdMe(py') "Pd_1" species in solution. The equilibrium constant for cage dissociation is $K_{eq} = [Pd_1]^4/[Pd_4] = 9.6 \times 10^2$ M^3 at 80 ˚C in $CDCl_2CDCl_2$. Under conditions where **A** is partially dissociated (in hexanes suspension at 80 ˚C or in CH_2Cl_2 solution at 25 ˚C), **A** produces linear polyethylene (PE) with a broad molecular weight distribution (MWD) that contains a high-MW fraction and a low-MW fraction. Under conditions where **A** is expected to be completely dissociated (in toluene at 80 ˚C with $[Pd_4]_0 = 0.05$ mM), **A** produces low-MW PE with a narrow MWD that is similar to what is observed for monomeric (PO)PdMeL complexes. These results suggest that the intact Pd_4 species produces the high-MW fraction, while the dissociated Pd_1 species produces the low-MW fraction. The production of high-MW PE was proposed to result from cooperative effects between the proximal Pd centers and/or steric blockage of an axial site at each Pd center by the $Li_4S_4O_{12}$ cage. **A** also copolymerizes ethylene with vinyl fluoride (VF) into linear copolymer, with a significantly higher level of VF incorporation (up to 3.6 mol %) compared to monomeric (PO)PdMeL catalysts (< 0.5 mol %).[3]

Analogous $[(\text{Li-OPO})\text{PdMe(py)}]_n$ complexes (Figure 2.1, **B-D**) with different substituents *para* to the sulfonate group (R^5) have been synthesized to study how modification of the OPO^{2-} ligand influences the cage structure and stability. The R^5 substituents have little effect on the structure of the Pd_4 assembly or free energy for dissociation into monomeric speciese. **B-py'** and **D-py** are isostructural with **A**. The solid-state structure of **B-py** is very similar, except for a minor difference in Pd-$ArSO_3$-Li connectivity at some of the Pd sites.[4]

The ΔH values for the dissociation of those Pd_4 species (**A** (8.7(3) kcal/mol)[2] < **B-py** (12.2(4) kcal/mol) ~ **C-py** (12.2(3) kcal/mol) < **D-py** (16.9(9) kcal/mol)) increase in the same order as the electron-donating ability of the R^5 substituents (Me < ^{i}Pr ~ Cy < ^{t}Bu). The experimental pK_a values of the corresponding benzoic acids are summarized in Table 2.1 and increase in the order Me < ^{i}Pr < ^{t}Bu.[5] Calculated pK_a values of the corresponding benzene sulfonic acids are very similar.[6] The trend in ΔH values for cage dissociation was ascribed to the trend in the basicity of the $ArSO_3^-$ group, based on the idea that more basic $ArSO_3^-$ units should bind Li^+ more strongly, resulting in a more robust cage. However, the trend in ΔH (Me < ^{i}Pr ~ Cy < ^{t}Bu) is counteracted by a corresponding increase of ΔS (Me < ^{i}Pr ~ Cy < ^{t}Bu), and therefore ΔG_{dissoc} is very similar for **A-D** (**A**: L = py'; **B-D**: L = py) at 80 ˚C. The trend in ΔS is hard to interpret due to the uncertainty in the nature of $ArSO_3Li$ solvation in the Pd_1 form. One hypothesis is that, due to the rigidity of the tetramer cage, the freedom of R^5 motion in the Pd_4 cage form is reduced from that in the monomeric Pd_1 form, and this effect is more pronounced for bulkier of R^5 groups.

Table 2.1. pK_a values of the corresponding benzoic acids and benzene sulfonic acids.

	$pK_{a,\,expt}$[5,7]	$pK_{a,\,calc}$[6]
	X = $-CO_2H$	X = $-SO_3H$
4-Me-C_6H_4-X	4.34	0.7
4-^{i}Pr-C_6H_4-X	4.35	0.7
4-^{t}Bu-C_6H_4-X	4.40	0.7
4-OMe-C_6H_4-X	4.46	0.9
3,4-$(OMe)_2$-C_6H_3-X	4.36	0.8
2,3,4-$(OMe)_3$-C_6H_2-X		0.7

In the present work, new Li[OPO]$^-$ ligands (**Li[2a-c]**$^-$, Scheme 2.1) containing electron-donating methoxy groups on the $ArSO_3^-$ units have been synthesized to further probe electronic and steric effects on cage assembly and thermal stability. The methoxy group is electron-donating to the *ortho* and *para* positions through the resonance effect and electron-withdrawing through the inductive effect. PPh(2-SO_3Li-5-OMe-Ph)(2-SO_3^--5-OMe-Ph) (**Li[2a]**$^-$) contains a methoxy group *para* to the sulfonate group, which should increase the basicity of the $ArSO_3^-$ group and stabilize a $Li_4S_4O_{12}$ cage. PPh(2-SO_3Li-4,5-$(OMe)_2$-Ph)(2-SO_3^--4,5-$(OMe)_2$-Ph) (**Li[2b]**$^-$) and PPh(2-SO_3Li-3,4,5-$(OMe)_3$-Ph)(2-SO_3^--3,4,5-$(OMe)_3$-Ph) (**Li[2c]**$^-$) contain additional methoxy groups on the $ArSO_3^-$ rings, which will slightly decrease the basicity of the SO_3^- group, but may have interesting steric effects on the Pd_4 assembly. Analogous monomeric PO^- ligands have also been synthesized and studied as controls.

Scheme 2.1.

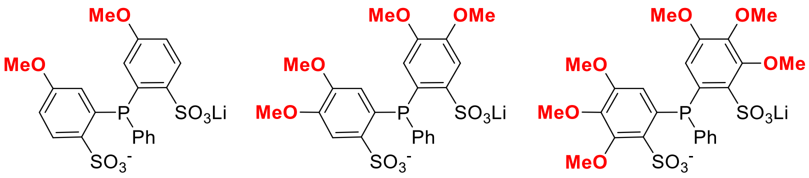

Li[2a]$^-$ **Li[2b]**$^-$ **Li[2c]**$^-$

2.2 Results and Discussion

Synthesis of Na[1a-d], Li[1c], and Li_2[2a-c]. The synthetic routes for the new ligands studied here are shown in Scheme 2.2. The appropriate methoxy-substituted aryl lithium reagents were generated by *ortho*-lithiation or lithium-halogen exchange of the corresponding arene or arylbromide **6a-c-*ⁱ*Bu** with ^{n}BuLi, and reacted with PAr_2Cl (Ar = 2-OMe-Ph or Ph) to afford PO^- pro-ligands **1a-d-^{i}Bu**. The OPO^{2-} pro-ligands **2a-c-^{i}Bu** were synthesized analogously by reaction with $PPhCl_2$.[8] **1a-d-^{i}Bu** and **2a-c-^{i}Bu** were purified by chromatography and isolated in 30 - 84 % yield. The ^{i}Bu groups were removed by reaction of **1a-d-^{i}Bu** and **2a-c-^{i}Bu** with NaI or LiI to generate **Na[1a,b,d]**, **Li[1c]** and **Li_2[2a-c]**. **Na[1a-b,d]** and **Li_2[2a-b]** precipitated from the CH_3CN reaction mixture and were isolated by filtration in 57 - 86 % yield. **Na[1c]** and **Li_2[2c]** are soluble in CH_3CN, and therefore are difficult to separate from the excess NaI and LiI in solution. LiI is soluble in THF, but **Li[1c]** and **Li_2[2c]** are not. Therefore, **Li[1c]** and **Li_2[2c]** were generated by reaction of **1c-^{i}Bu** and **2c-^{i}Bu** with LiI in CH_3CN or THF, respectively. The reaction mixture of **Li[1c]** was taken to dryness under vacuum and the resulting solid was purified by THF wash to give **Li[1c]** in 52 % yield. **Li_2[2c]** was isolated by direct filtration from the reaction mixture in 66 % yield.

Scheme 2.2

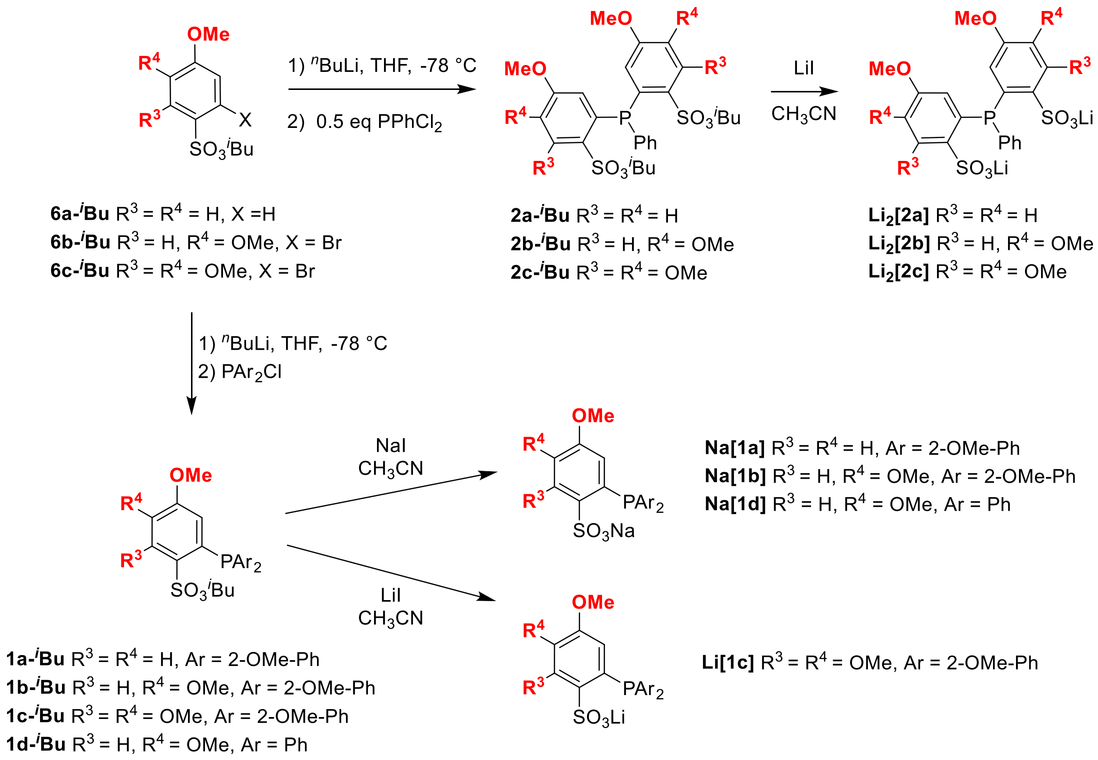

Synthesis of Methoxy-Substituted (PO)PdMe(py) Complexes. Metalation of **Na[1a-b,d]** with (COD)PdMeCl and pyridine in CH_2Cl_2 generated a clear yellow solution of **3a-b,d** (Scheme 2.3). **3a-b,d** were isolated by layering pentane onto the CH_2Cl_2 solution to give X-ray quality crystals in 59-86 % yield. The reaction of **Li[1c]** with (COD)PdMeCl and pyridine in CH_2Cl_2 gave a cloudy solution, and the formation of Pd black was observed upon attempted product isolation and recrystallization. Therefore, **3c** was not further pursued.

Scheme 2.3

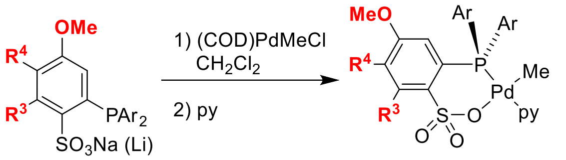

Ar = 2-OMe-Ph
Na[1a] $R^3 = R^4 = H$
Na[1b] $R^3 = H$, $R^4 = OMe$
Li[1c] $R^3 = R^4 = OMe$

Ar = Ph
Na[1d] $R^3 = H$, $R^4 = OMe$

Ar = 2-OMe-Ph
3a $R^3 = R^4 = H$
3b $R^3 = H$, $R^4 = OMe$
3c $R^3 = R^4 = OMe$

Ar = Ph
3d $R^3 = H$, $R^4 = OMe$

Another route for metalation was explored that involved the direct NMR-scale reaction of **1c-*ⁱ*Bu** with (COD)PdMeCl and pyridine (Scheme 2.4). This reaction results in clean generation of **3c**. It is likely that this reaction proceeds by initial formation of [κ^2-*P*,*O*-(**1c-*ⁱ*Bu**)]PdMeCl, displacement of chloride by pyridine, and nucleophilic attack of the free Cl$^-$ on the activated ^{i}Bu group to form **3c** and ^{i}BuCl, which is easily removed under vacuum. **3b** was synthesized by this route on a preparatory scale.

Scheme 2.4

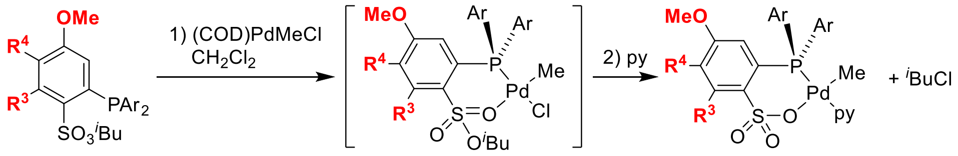

Ar= 2-OMe-Ph
1b-^{i}Bu $R^3 = H$, $R^4 = OMe$
1c-^{i}Bu $R^3 = R^4 = OMe$

Ar= 2-OMe-Ph
3b $R^3 = H$, $R^4 = OMe$
3c $R^3 = R^4 = OMe$

The solid-state structures of **3a-b,d** were determined by X-ray crystallography and are shown in Figures 2.3-2.5. In each case, κ^2-*P*,*O* coordination of the PO ligand and a *cis* relationship of the phosphine and methyl group are observed. The puckered, six-membered (PO)Pd chelate rings adopt boat conformations. In **3d**, the pyridine ring is slightly bent away from the Pd square plane, such that P-Pd-N angle is 167.9° (Figure 2.5 (b)). The Pd-C distances of **3a** (2.022(2) Å), **3b** (2.0237(18) Å) and **3d** (2.025(3) Å) are very similar, but ca. 0.08 Å shorter than those in [κ^2-*P*,*O*-P(2-OMe-Ph)$_2$(2-SO$_3$-Ph)]PdMe(2,6-lutidine) complex (2.107(2) Å).[9] The solution NMR data for **3a-b** and **3d** are consistent with the solid state structures. Both **3a** and **3b** exhibit $^3J_{P\text{-}CH3}$ values ≤ 3 Hz and $^2J_{P\text{-}CH3}$ values ≤ 4 Hz, indicating a *cis* relationship of the phosphine and methyl groups. The Pd-CH$_3$ resonance of **3d** is observed as a singlet without ^{31}P coupling in the ^{1}H and ^{13}C{^{1}H} NMR spectra, again consistent with a *cis*-P,C structure. The ^{1}H and ^{13}C{^{1}H} NMR spectra were fully assigned by COSY, HMQC and HMBC NMR experiments.

Figure 2.3 Molecular structure of **3a**. Hydrogen atoms are omitted. Selected bond lengths (Å) and angles (deg): Pd1-P1 2.2368(5), Pd1-O1 2.1618(13), Pd1-N1 2.1535(15), Pd1-C1 2.022(2), O1-S1 1.4834(14), O1-Pd1-P1 94.09(4), N1-Pd1-P1 174.86(4), N1-Pd1-O1 87.07(5), C1-Pd1-P1 87.37(6), C1-Pd1-O1 176.32(7), C1-Pd1-N1 91.77(7).

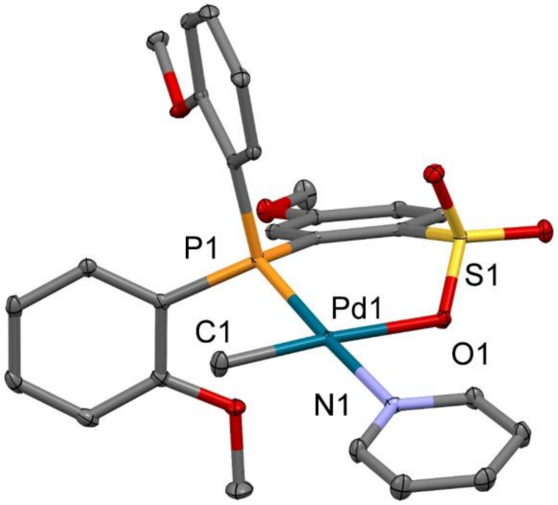

Figure 2.4 Molecular structure of **3b**. Hydrogen atoms are omitted. Selected bond lengths (Å) and angles (deg): Pd1-P1 2.2234(4), Pd1-O1 2.1768(11), Pd1-N1 2.1189(13), Pd1-C1 2.0237(18), S1-O1 1.4840(11), O1-Pd1-P1 94.88(3), N1-Pd1-P1 175.96(4), N1-Pd1-O1 88.92(5), C1-Pd1-P1 86.83(5), C1-Pd1-O1 177.78(7), C1-Pd1-N1 89.41(6).

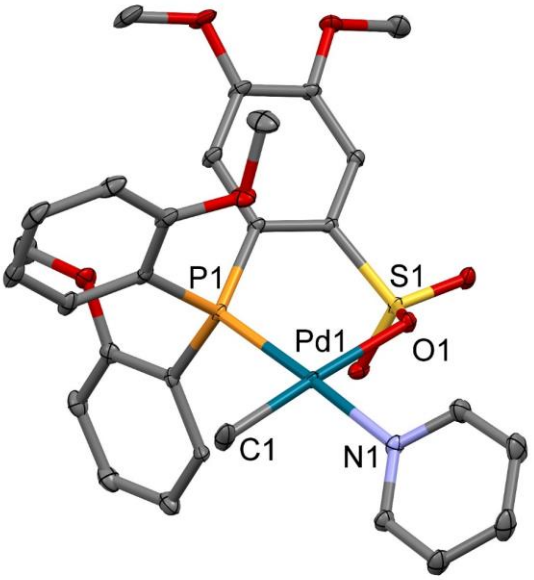

Figure 2.5 (a) Molecular structure of **3d**. Hydrogen atoms are omitted. (b) Side view of **3d**, from Me-P-O bond. Selected bond lengths (Å) and angles (deg): Pd1-P1 2.2170(7), Pd1-O1 2.1737(16), Pd1-N1 2.140(2), Pd1-C1 2.025(3), S1-O1 1.4851(17), O1-Pd1-P1 94.37(5), N1-Pd1-P1 167.87(6), N1-Pd1-O1 86.81(7), C1-Pd1-P1 88.77(8), C1-Pd1-O1 175.46(9), C1-Pd1-N1 90.80(10).

(a)

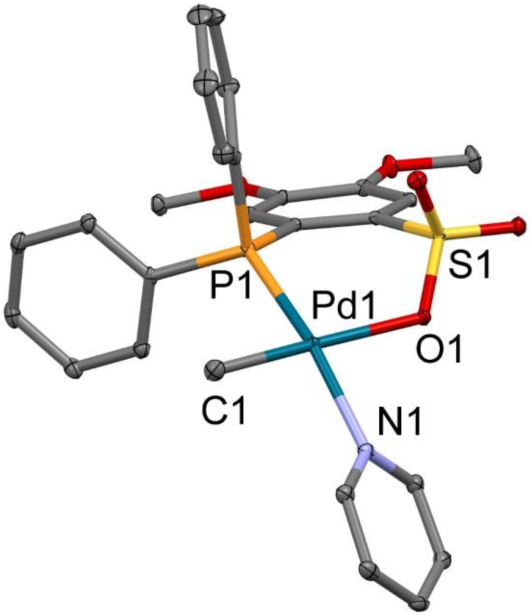

(b)

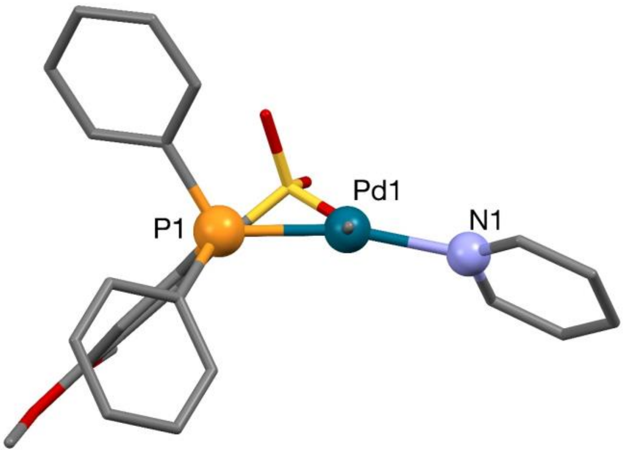

Synthesis of Methoxy-Substituted Phosphine-bis(arenesulfonate) Palladium Complexes. $[(\text{Li-OPO})\text{PdMeL}]_4$ complexes **A-D** were generally synthesized by the reaction of the appropriate $\text{Li}_2[\text{OPO}]$ with (COD)PdMeCl and L in CH_2Cl_2 at room temperature.[2,4] However, this procedure gave poor results for **Li$_2$[2a,c]** (Scheme 2.5). The NMR-scale reaction of **Li$_2$[2a]** with (COD)PdMeCl and pyridine in CD_2Cl_2 yielded a cloudy yellow solution of **4a-py**, for which no phosphorus resonance was observed in the $^{31}P\{^1H\}$ NMR spectrum. Replacement of the CD_2Cl_2 with CD_3OD, in which cage complexes form solvated monomeric species, produced clean NMR spectra of monomeric solvated **4a-py**, the purity of which was determined to be ca. 95 % by $^{31}P\{^1H\}$ NMR. These observations show that tetrameric **4a-py** (if formed) is not soluble in CD_2Cl_2. To circumvent this problem, 4-(5-nonyl)-pyridine was used instead of pyridine to increase the solubility of the resulting palladium complex in CH_2Cl_2. However, in this case the formation of Pd black was observed after overnight reaction.

The reaction of **Li$_2$[2c]** and (COD)PdMeCl with 4-(5-nonyl)-pyridine in CD_2Cl_2 gave a clear yellow solution of **4c-py'**. However, the NMR spectra of the product mixture in CD_2Cl_2 are very complicated and no high-field Pd-Me ^1H NMR resonances indicative of a self-assembled cage product were observed. Replacement of the CD_2Cl_2 solvent with CD_3OD produced fairly clean spectra consistent with monomeric solvated **4c-py'** and the $^{31}P\{^1H\}$ spectrum indicates that monomeric **4c-py'** is ca. 82 % pure. These results suggest that the failure of **4c-py'** to self-assemble to a Pd_4 species might be due to the steric bulkiness of the three methoxy groups.

Scheme 2.5

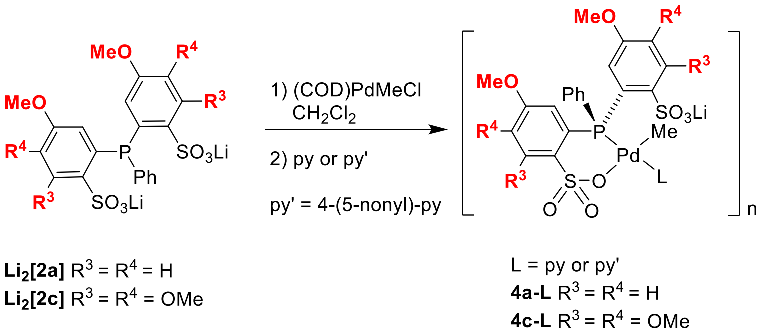

In contrast, the reaction of **Li$_2$[2b]** with (COD)PdMeCl and 4-(5-nonyl)-pyridine in CH_2Cl_2 generated a clear or slighty cloudy pale-yellow solution, from which **5b** was isolated in crystalline form in 67 % yield by layering pentane onto the CH_2Cl_2 solution and cooling to -40 °C (Scheme 2.6). Crystals of **5b** obtained in this manner lose crystallinity rapidly and do not diffract X-rays well. Crystallographic analysis of large molecules of this type is challenging due to the co-crystallization of solvent molecules, which fill the void spaces between the large molecules. The evaporation of these solvents during crystal handling leads to loss of long-range order and poor diffraction. To overcome the solvent evaporation issue, the high boiling point solvent $CHCl_2CHCl_2$ (bp = 146.5 °C) was used instead of CH_2Cl_2. X-ray quality crystals were obtained by slow diffusion of pentane into a $CHCl_2CHCl_2$ solution at room temperature. The structure of **5b** is discussed below.

Scheme 2.6

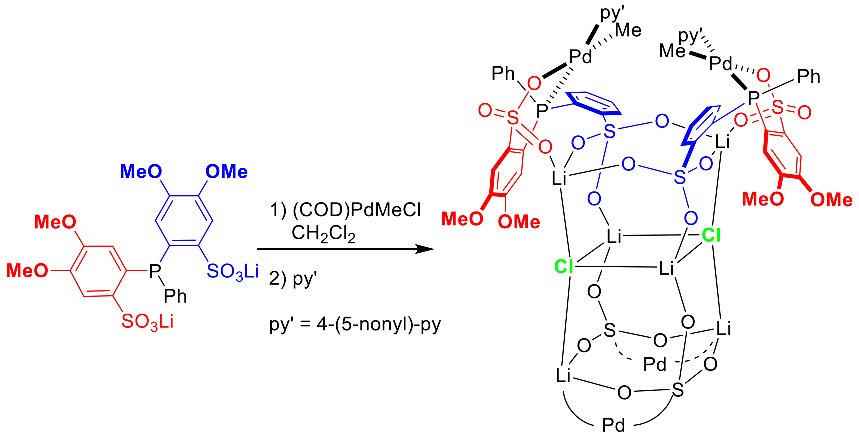

Li$_2$[2b] **5b**

Solid-State Structure of 5b. The solid-state structure of **5b** is shown in Figure 2.6. **5b** assembles into a tetrameric Pd$_4$ complex, which is structurally similar to **A** but differs in two key aspects. First, **5b** is built around a Li$_4$S$_4$O$_{12}$•Li$_2$Cl$_2$ cage, which contains a layer of Li$_2$Cl$_2$ inserted between the "top" and "bottom" Li$_2$S$_2$O$_6$ layers of the cage. Two types of tetrahedral Li$^+$ ions are present. Four Li$^+$ ions form the corners of the cage and coordinate two oxygens from two non-Pd-bonded ArSO$_3^-$ groups, one oxygen from a Pd-bonded ArSO$_3^-$ group and one Cl$^-$ ion. Two Li$^+$ ions form the inner Li$_2$Cl$_2$ layer and coordinate two oxygens from two non-Pd-bonded ArSO$_3^-$ groups and two Cl$^-$ ions. **A** lacks the Li$_2$Cl$_2$ layer.

Second, the structure of **5b** is chiral with *C*$_2$-symmetry. **5b** crystalizes as a racemic conglomerate, i.e. as a mixture of individual crystals that are enantiomerically pure but together comprise a racemate.[10] The configurations of the four P centers are *SSSS* (ent *RRRR*). In contrast, **A** has *S*$_4$ symmetry with *SSRR* configurations at the phosphorous centers. The four Pd centers in **5b** are equivalent, but are spatially separated into two pairs. In each pair, the Pd-Pd distance is 6.58 - 6.62 Å and the Pd-Me points toward the py' ring of the neighboring Pd center.

Figure 2.6 Molecular structure of **5b·6($C_2H_2Cl_4$)**. Hydrogen atoms, the 5-nonyl groups of the py' ligands and solvent molecules are omitted. (a) View of the central cage with one (κ^2-*P*,*O*-**Li[2b])**PdMe(py') unit highlighted. (b) View of the full structure. (c) Space-filling side view of **5b**. (d) Space-filling top view of **5b**. Selected bond lengths (Å) and angles (deg): Pd1-P1 2.223(3), Pd1-O1 2.185(6), Pd1-N1 2.113(7), Pd1-C1 2.025(11), S1-O1 1.481(7), O1-Pd1-P1 85.10(18), N1-Pd1-P1 177.2(2), N1-Pd1-O1 93.8(3), C1-Pd1-P1 92.7(3), C1-Pd1-O1 177.5(4), C1-Pd1-N1 88.4(4). Average bond lengths (Å) and angles (deg) related with Li1 and Li3: Li-O 1.94, Li-Cl 2.44, O-Li-O 109.6, O-Li-Cl 109.5. Average bond lengths (Å) and angles (deg) related with Li2: Li-O 1.859, Li-Cl 2.404, O-Li-O 102.3, Cl-Li-Cl 96.2, O-Li-Cl 114.8.

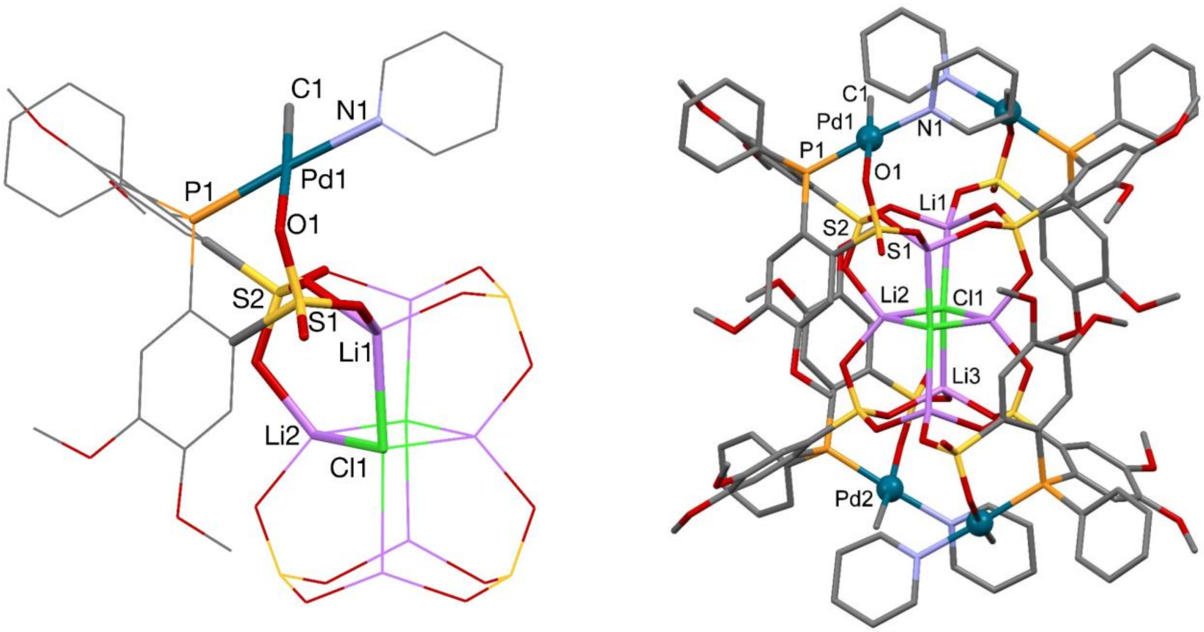
(a)
(b)

Figure 2.6, continued.

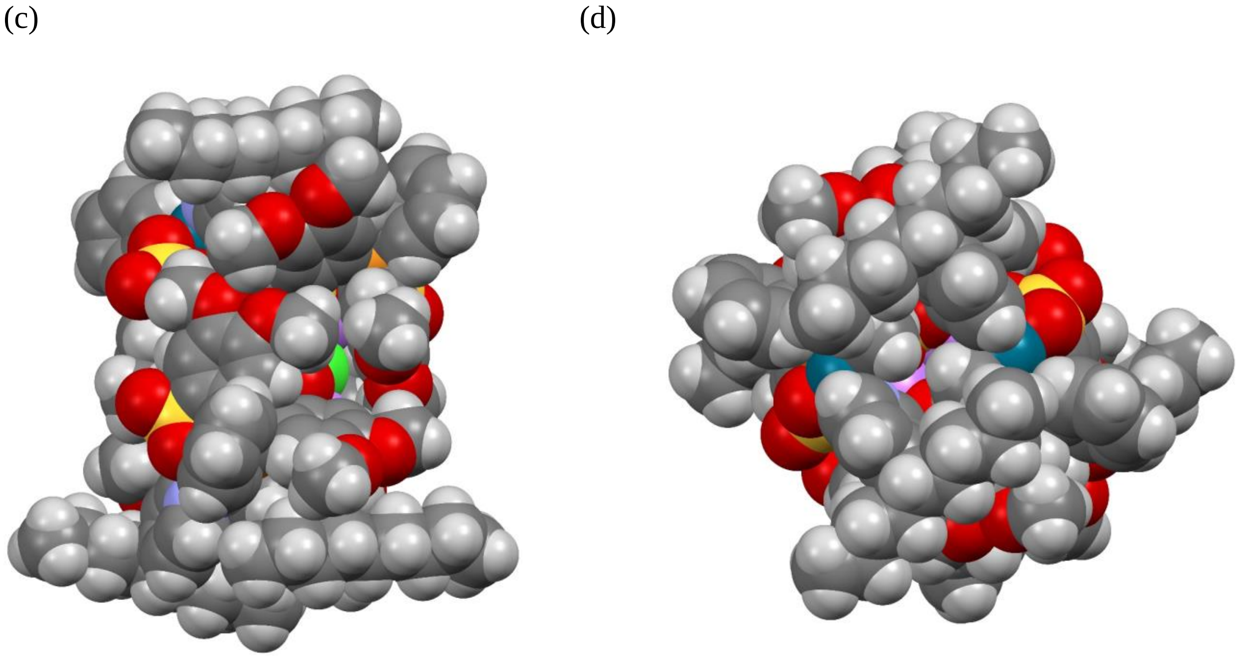

The two structural differences between **5b** and **A** provide hints to why **5b** forms with the observed composition and structure. As shown in Figure 2.7, the Pd-bonded $ArSO_3^-$ arene ring fully blocks the side face of the cage of **A**. In particular, H17 is very close to the non-Pd-bonded $ArSO_3^-$ arene ring (H17-H9 distance ca. 2.522 Å), and it is clear that replacement of H17 by a methoxy group would not be possible without significant structural distortion, i.e. the $Li_4S_4O_{12}$ cage is too small to accommodate a methoxy group at the H17 position. Inclusion of the inner Li_2Cl_2 layer in the core of **5b** elongates the cage and satisfies the steric requirement of the methoxy group at the position of H17. This point is illustrated by Figure 2.7, which shows how the Pd-bonded $ArSO_3^-$ arene ring is nicely packed with the non-Pd-bonded $ArSO_3^-$ arene ring.

Figure 2.7. Space-filling side view of **5b** with one Pd-bonded $ArSO_3^-$ unit and one non-Pd-bonded $ArSO_3^-$ unit highlighted.

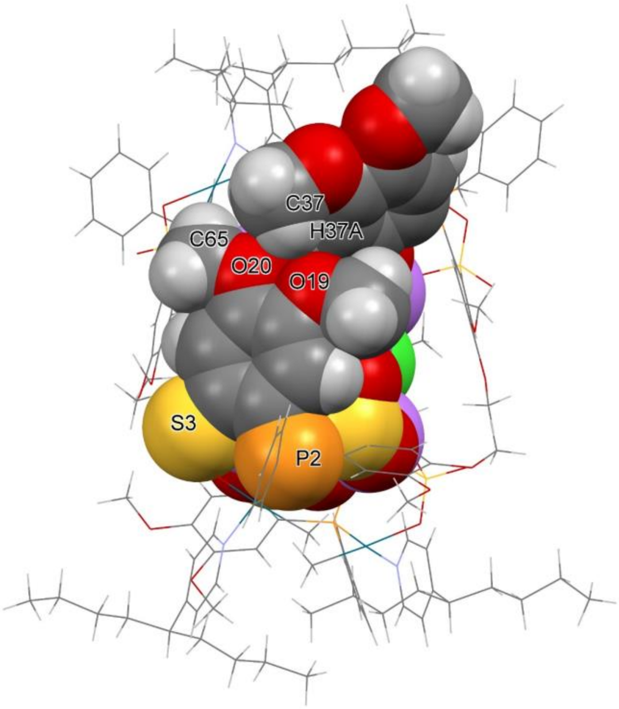

However, inclusion of the inner Li_2Cl_2 layer in **5b** has important stereochemical consequences. As shown in Figure 2.8, assembly of **5b** around the $Li_4S_4O_{12}$•Li_2Cl_2 cage with *SSRR* configurations at the phosphorous centers (as observed for **A**) will cause either a misalignment of the Li^+, Cl^- and $ArSO_3^-$ units that prevents the formation of the cage (Figure 2.8a,b) or impossibly close contacts between the two Pd-bonded $ArSO_3^-$ arene rings (Figure 2.8b,c). Therefore, inversion of the configurations of the bottom two phosphorous centers from *RR* to *SS* is required.

Figure 2.8. (a) Structure of **A** with *SSRR* configurations at the phosphorus centers. The black lines show the Li-O interactions that must be cleaved to insert the inner Li_2Cl_2 layer of **5b**. (b) Structure generated by cleavage of the Li-O interactions indicated by the black lines in (a), insertion of a Li_2Cl_2 layer and addition of methoxy groups at the H17 positions. Note that the Li^+ and Cl^- ions in the Li_2Cl_2 layer are not properly aligned with the Li^+ and $ArSO_3^-$ units on the bottom half of the molecule to close the cage. Li: purple dot; Cl: green dot. (c) Structure generated from (b) by a 90° rotation of the bottom $Li_2S_2O_6$ layer to properly align the Li^+ and Cl^- ions of the inner layer with the Li^+ and $ArSO_3^-$ units of the bottom layer to complete cage formation. Note that impossibly bad steric contacts between the Pd-bonded $ArSO_3^-$ arene units are present. (d) Structure generated from (b) by inversion of the P configurations from *RR* to *SS* in the bottom half, resolving the $Li^+/Cl^-/O$ misalignment and steric contact issues and giving the structure of **5b**.

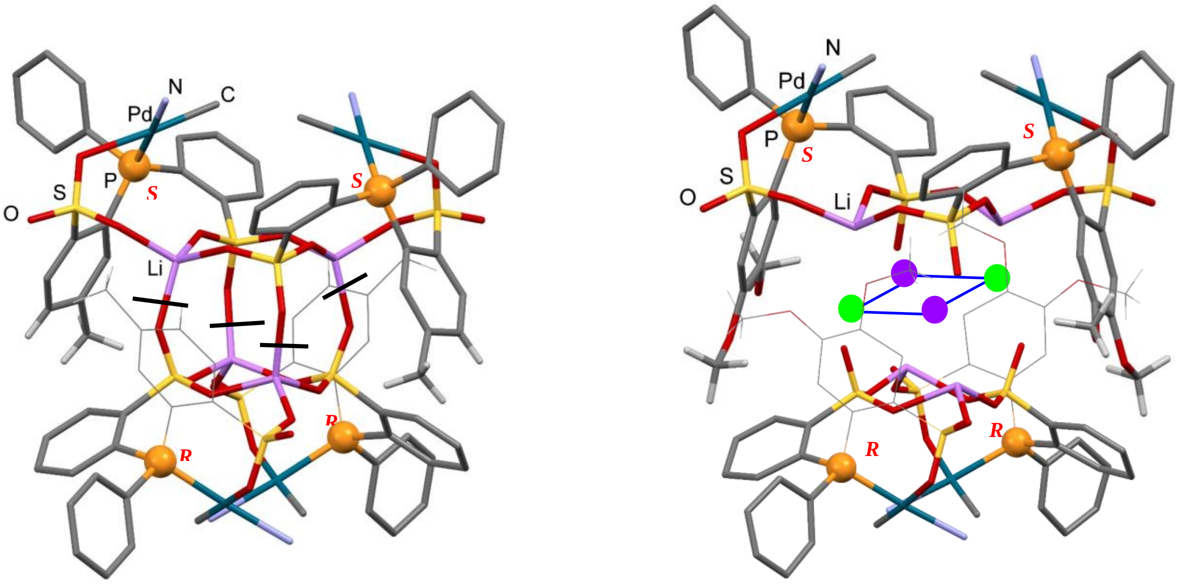
(a) (b)

Figure 2.8, continued.

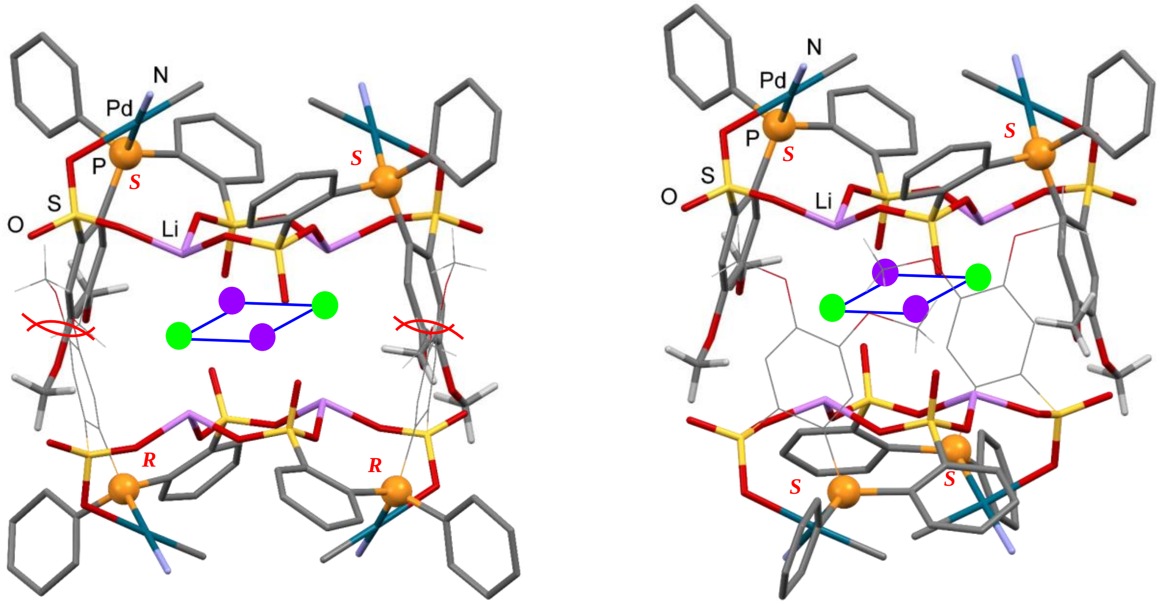
(c) (d)

Solution Structure of 5b. The $^{31}P\{^1H\}$ NMR spectrum of **5b** in CD_2Cl_2 at room temperature contains only one resonance (δ 34.0) indicative of a highly symmetric structure. The $^7Li\{^1H\}$ NMR spectrum contains two resonances at δ -0.3 and -0.5, in a 2:1 intensity ratio (Figure 2.9), consistent with the presence of two types of Li^+, as observed in the solid state structure. The Pd-Me ^1H NMR resonance appears at δ -0.17 (Figure 2.10), which is consistent with the anisotropic shielding by the adjacent 4-(5-nonyl)-pyridine ring expected according for the solid-state structure. The ^1H NMR spectrum contains two sets of $ArSO_3^-$ resonances including four $-OCH_3$ resonances, which is also expected from the solid-state structure. The hydrodynamic volume of **5b** determined by PGSE-NMR in CD_2Cl_2 at room temperature is ca. 8.0 × 10^3 Å, which is comparable to that of **A** (6.2 × 10^3 Å).[2] Collectively, these data make a compelling case that the solution structure of **5b** is closely similar to the solid-state structure. Interestingly, the $^{13}C\{^1H\}$ NMR spectrum contains two sets of resonances for the butyl chains within the 5-nonyl group, at both room temperature (Figure 2.11) or at 80 ˚C, which indicates the tetramer structure is very rigid and causes the restricted rotation of the 5-nonyl group. The space-fill view of **5b** in Figure 2.6d shows the inequivalence of the Bu groups in the 5-nonyl units.

Figure 2.9. $^{7}Li\{^{1}H\}$ NMR spectrum of **5b** in CD_2Cl_2

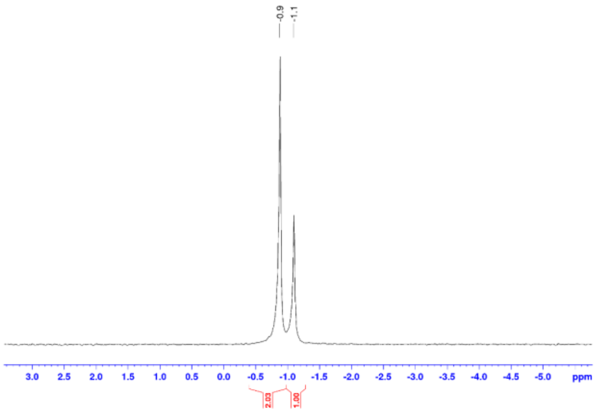

Figure 2.10. -O*Me* (left) and Pd-*Me* (right) regions of ^{1}H NMR spectrum of **5b** in CD_2Cl_2

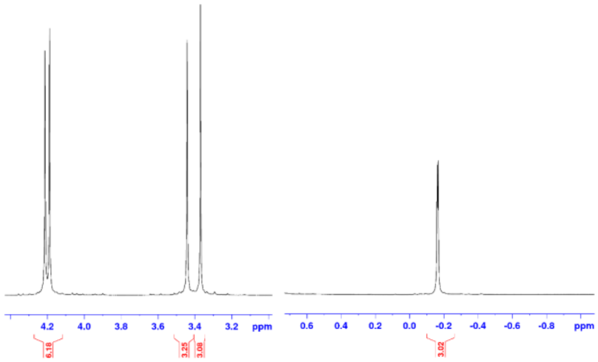

Figure 2.11. Nonyl region of $^{13}C\{^{1}H\}$ NMR spectrum of **5b** in CD_2Cl_2 at room temperature

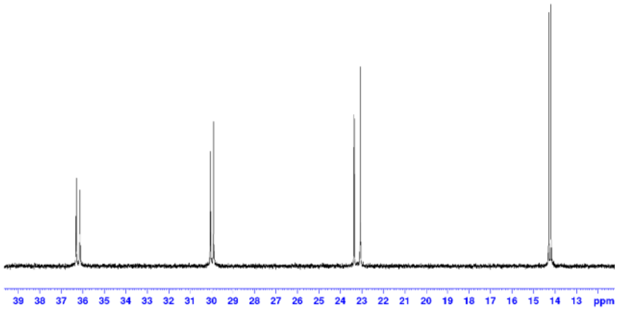

In contrast, in CD_3OD solution, the Pd-Me ^1H NMR resonance of **5b** shifts downfield to δ 0.58, the $^7Li\{^1H\}$ NMR spectrum comprises a singlet at δ 0.2, and the $^{13}C\{^1H\}$ NMR spectrum contains only one set of 5-nonyl group resonances. PGSE-NMR analysis of **5b** in CD_3OD shows that the hydrodynamic volumes is close to those of related monomeric (PO)PdMe(L) species.[2,4] Reaction of **5b** with ca. 1.1 equiv of Cryptand211, converts **5b** into a new Pd species, which has a Pd-Me ^1H NMR resonance at δ 0.62 in $CDCl_2CDCl_2$ (δ 0.44 in CD_2Cl_2), and exhibits a singlet at δ -0.5 in the $^7Li\{^1H\}$ NMR spectrum. These Pd-Me ^1H chemical shifts are within the normal range for monomeric (PO)PdMeL species, in which shielding by the pyridine ring is absent. These results show that CD_3OD and Cryptand211 convert **5b** to a monomeric Pd_1 species, as previously established for **A**.

Thermal Stability of 5b. The thermal stability of **5b** was probed by ^1H NMR spectroscopy in $CDCl_2CDCl_2$ solution over the temperature range 50-80 ˚C. Upon heating a $CDCl_2CDCl_2$ solution of **5b** (initial concentration of $[Pd_4]_0 = 4.74$ mM), a minor species with a Pd-Me resonance at ca. δ 0.6 grew in, which is assigned to the monomeric Pd_1 species (Scheme 2.7). At 80 ˚C, only 6.5% of **5b** is dissociated into the monomeric form ($[Pd_4] = 4.43$ mM; ($[Pd_1] = 1.24$ mM). Because the speciation of the LiCl that is presumably released upon dissociation of **5b** is unknown, it is not possible to specify an equilibrium constant expression and determine a $K_{eq,dissoc}$ value for comparison to values for **A-D**. However, an informative qualitative assessment of the relative stability of **5b** and **A-D** toward cage dissociation is provided by comparison of the % $[Pd_4]$ dissociation at a given initial concentration of Pd_4 ($[Pd_4]_0$). These data are provided in Table 2.2. The results indicate that **5b** is substantially more robust compared than **A-D** and is more resistant to dissociation into monomeric Pd_1 species under olefin polymerization conditions.

Scheme 2.7

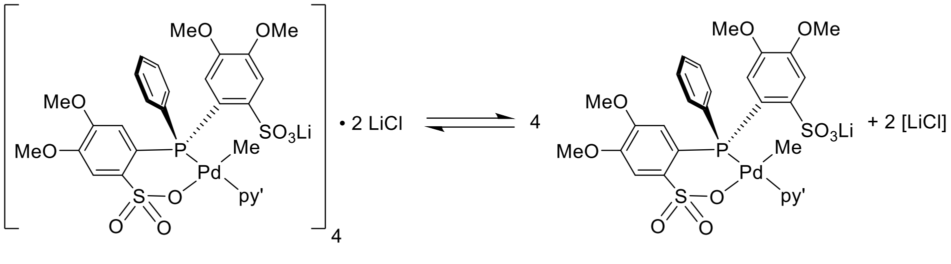

5b

Table 2.2 Values for [Pd$_4$], [Pd$_1$] and % Pd$_4$ dissociated for **A-D** and **5b**, with [Pd$_4$]$_0$ = 4.74 mM at 80 °C

Compound	K_{eq}	[Pd$_4$] (mM)	[Pd$_1$] (mM)	% Pd$_4$ dissoc
A[a]	969 mM^3	2.92	7.29	38.4
B-py[b]	1125 mM^3	2.86	7.53	39.7
C-py[b]	567 mM^3	3.12	6.48	34.2
D-py[b]	1665 mM^3	2.70	8.18	43.0
5b		4.43	1.24	6.5

[a]K_{eq} value from ref 2. [b]K_{eq} values from ref 4.

Ethylene Homopolymerization. The ethylene polymerization behavior of **3a,b** is very similar to that of the bench mark catalyst (κ^2-1-*P*(2-OMe-Ph)$_2$-2-*S**O*$_3$-5-Me-Ph)PdMe(py) (**std**, (PO^{OMe})PdMe(py), Table 2.3, entry 5, 6, 11, 12, 22). Therefore, the electronic effect of the methoxy groups is minor. **3b** has a slightly higher activity than **3a** in toluene at 80 °C. The activity and polymer MWs for **3a,b** observed for polymerizations in hexane suspension are lower than in toluene solution. Highly linear PE is formed in all cases.

Table 2.3. Ethylene Homopolymerization of **3a,b** and **5b**

Entry	Cat.	P_{C2H4} (psi)	T (°C)	Time (h)	Pd (μmol)	Yield (g)	Acitivity (kg•mol^{-1}•h^{-1})	M$_w$[e] (10^3)	PDI[e]	T$_m$[f] (°C)
1[a]	**3a**	410	80	2	10	8.92	446	29.6	2.0	136.3
2[a]	**3a**	410	80	2	10	9.89	494	29.9	1.8	134.8
3[b]	**3a**	410	80	2	10	3.16	158	29.2	2.4	132.4
4[b]	**3a**	410	80	2	10	3.14	157	29.7	2.1	132.0
5[c]	**3a**	410	80	2	0.88	1.53	869	29.7	1.7	135.1
6[c]	**3a**	410	80	2	0.88	1.73	983	27.5	1.8	134.5
7[a]	**3b**	410	80	2	10	10.3	515	26.1	1.8	134.5
8[a]	**3b**	410	80	2	10	10.1	505	25.6	1.7	135.4
9[b]	**3b**	410	80	2	10	1.22	60.9	19.0	2.2	131.8
10[b]	**3b**	410	80	2	10	1.24	62.0	18.8	2.3	131.2
11[c]	**3b**	410	80	2	0.88	2.05	1164	27.7	1.6	135.1
12[c]	**3b**	410	80	2	0.88	2.57	1462	27.0	1.8	135.1
13[a]	**5b**	410	80	2	10	1.36	68	249	9.5	138.2
14[a]	**5b**	410	80	2	10	1.25	62	412	14.3	137.3
15[a]	**5b**	410	80	1	10	0.716	72	136	6.6	135.2
16[b]	**5b**	410	80	2	10	5.65	282	1271	2.6	137.1
17[b]	**5b**	410	80	2	10	6.35	318	1473	2.3	136.5
18[d]	**5b**	80	25	24	10	0.336	1.4	922	12.5	136.2
19[d]	**5b**	80	25	24	10	0.424	1.8	1015	12.5	138.7
20[c,g]	**5b** + $B(C_6F_5)_3$	410	80	2	10	2.38	119	868	13.2	137.8
21[c,g]	**5b** + $B(C_6F_5)_3$	410	80	2	10	2.02	101	733	14.9	137.1
22[c]	**std**	410	80	2	0.88	1.95	1108	31.3	1.8	133.7
23[a,h]	**A**	410	80	2	10	6.25	312	7.87	2.6	131.7
24[b,h]	**A**	410	80	2	10	5.18	259	1000	60	138.7
25[d,h]	**A**	80	25	24	10	1.91	8.0	915	29	136.5

[a] Solvent = 50 mL toluene. [b] Solvent = 50 mL hexanes. [c] Solvent = 49 mL toluene + 1 mL chlorobenzene. [d] Solvent = 50 mL CH_2Cl_2. [e] GPC. [f] *DSC.* [g] 1 equiv of $B(C_6F_5)_3$ per py’. [h] ref 2.

In hexanes suspension at 80 °C, **5b** produces ultra-high molecular weight polyethylene (UHMWPE) with a narrow MDW (Table 2.3, entry 16, 17 and Figure 2.12). GPC analysis of these UHMWPE samples is difficult due to the poor solubility of the high molecular weight fraction of the polymer.[11] Generally, these samples were shaken at 160 °C for 1-2 days to attain complete dissolution of the polymers in trichlorobenzene.[12] Therefore, the GPC analyses are less reproducible than those for PEs with lower MWs, due to potential sample degradation during the preparation and partial loss of the high MW fraction.[13] Nevertheless, it is clear that **5b** produces very-high MW PE with a narrow MWD in hexanes at 80 °C. In contrast, in toluene at 80 °C or CH_2Cl_2 at room temperature, **5b** also produces high MW PE, but with a broad MWD (Table 2.3, entry 13-15, 18-19). In the presence of 1 equiv of $B(C_6F_5)_3$ per 4-(5-nonyl)-pyridine in toluene at 80 °C, **5b** exhibits increased activity, and produces linear PE with high-MW and a broad MWD (Table 2.3, entry 20, 21). These results show that (i) **5b** functions as a single-site catalyst and produces UHMWPE in hexanes at 80 °C, (ii) **5b** forms a multi-site catalyst system in toluene at 80 °C, presumably due to cage dissociation and (iii) the Pd_4 cage form of **5b** is more active than cage-dissociated Pd_1 form. Note that the contrasting polymerization behavior of **3a,b** and **5b** in hexanes vis-à-vis toluene implies that the unique performance of **5b** in hexanes suspension reflects the robustness of the cage structure, not a solvent effect.

Figure 2.12. Molecular weight distributions (GPC) of polyethylenes produced by **3b** and **5b**. See Table 3. Polymerization conditions: entry 7 and 14: toluene solution, 80 ˚C; entry 9 and 16: hexanes suspension, 80 ˚C.

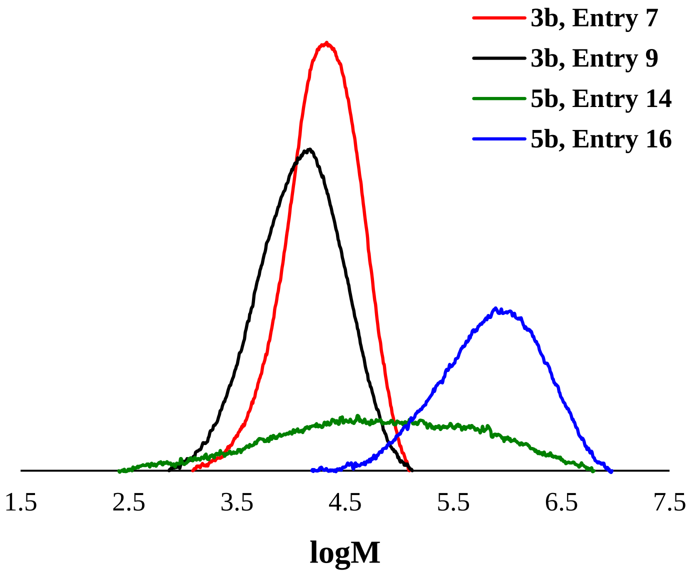

Compared to **A** (Table 2.3, entry 23-25),[2] **5b** has a similar activity in hexanes, but is much less active in toluene and CH_2Cl_2. The MWDs of polymers produced by **5b** are generally narrower than those of **A**. These polymerization results are consistent with the greater thermal stability of **5b** compared to **A**.

Ethylene/Vinyl Fluoride Copolymerization. 3a,b copolymerize ethylene and vinyl fluoride to form low-MW copolymer with ca. 0.5 % VF incorporation (Table 2.4, entry 1, 2). These results are similar to results for the bench-mark (PO)PdMe(py) complex (**std**, [κ^2-*P*,*O*-P(2-OMe-Ph)$_2$(2-SO_3-5-Me-Ph)]PdMe(py), (PO^{OMe})PdMe(py)). The microstructure of copolymers produced by **3a,b** was determined by $^{19}F\{^1H\}$ NMR and ^1H NMR spectroscopy.[3,14] VF is incorporated as in-chain -CH_2CHFCH_2- units (major) and as -CH_2CF_2H, -CH_2CFHCH_3 and -CH_2CFH_2 end groups (minor, Figure 2.13). The -CH_2CF_2H chain ends are most likely formed by β-F elimination to generate a Pd-F species,[15] followed by 1,2 VF insertion, while the -CH_2CFHCH_3 chain ends are most likely formed by β-H elimination to generate Pd-H species, followed by 2,1 VF insertion. The -CH_2CFH_2 chain ends are likely formed by ethylene insertion to the Pd-F species or 1,2 VF insertion to the Pd-H species.

Table 2.4. Ethylene /Vinyl Fluoride Copolymerization of **3a,b** and **5b**

Entry	Cat.	P_{C2H4} (psi)	P_{VF} (psi)	Pd (μmol)	Yield (mg)	Acitivity ($kg\cdot mol^{-1}\cdot h^{-1}$)	M_w[d] (10^3)	PDI[d]	VF incorp[e] (mol %)	T_m[f] (°C)
1[a]	**3a**	220	80	10	115	5.8	13.4	2.3	0.59	131.4
2[a]	**3b**	220	80	10	102	5.1	12.1	2.0	0.51	131.4
4[b]	**5b**	220	80	10	27	1.4	20.3	8.0	0.10	128.8
5[b]	**5b**	130	120	10	8.9	0.44	1.92	1.4	0.25	[g]
6[c]	**5b**	220	80	10	239	12.0	498	18.1	0.87	134.4
7[c]	**5b**	130	120	10	69	3.4	419	26.2	2.5	132.8

[a] Solvent = 40 mL toluene + 10 mL chlorobenzene; injection method. [b] Solvent = 50 mL toluene; standard method. [c] Solvent = 50 mL hexanes; standard method. [d] GPC. [e] VF incorporation in copolymer determined by ^1H NMR. [f] DSC. [g] Not determined due to the limited quantity of copolymer.

Figure 2.13. $^{19}F\{^1H\}$ NMR spectrum of ethylene/VF copolymer (*o*-dichlorobenzene-d_4, 120 °C) produced by **3b** (Table 2.4, entry 2).

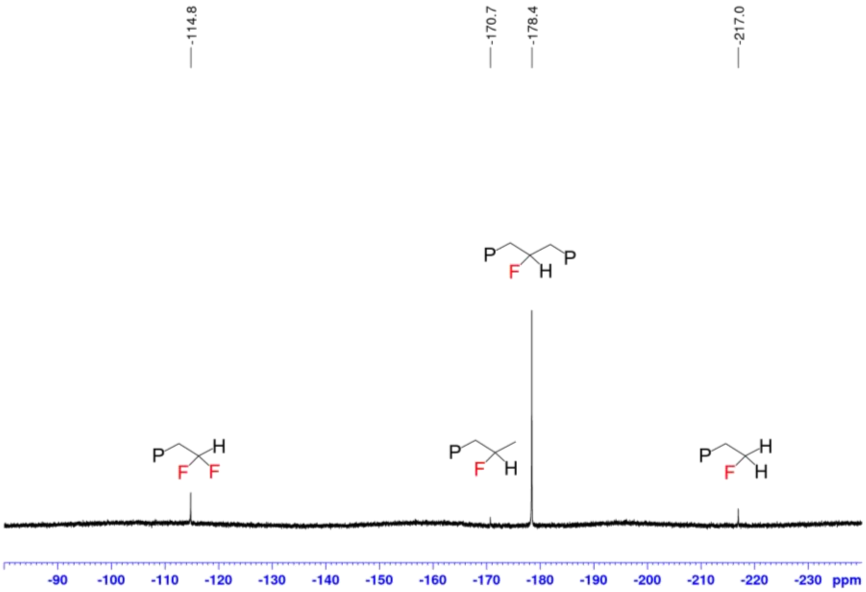

5b copolymerizes ethylene and VF in hexanes slurry at 80 ˚C to form linear copolymer with 2.5 mol % VF incorporation, which is lower than the 3.6 mol % incorporated by **A** under the same condition. The microstructure of the copolymer from **5b** is similar to that from **A** (Figure 2.14), with major in chain -CH_2CHFCH_2- incorporation, and minor VF-derived end groups *cis*-$CH_2CH{=}CHF$ and -CH_2CFHCH_3. The *cis*-$CH_2CH{=}CHF$ chain ends are most likely formed by 2,1 VF insertion to Pd-R species, followed by β-H elimination.

Figure 2.14. $^{19}F\{^1H\}$ NMR spectrum of ethylene/VF copolymer (*o*-dichlorobenzene-d_4, 120 °C) produced by **5b** (Table 2.4, entry 7).

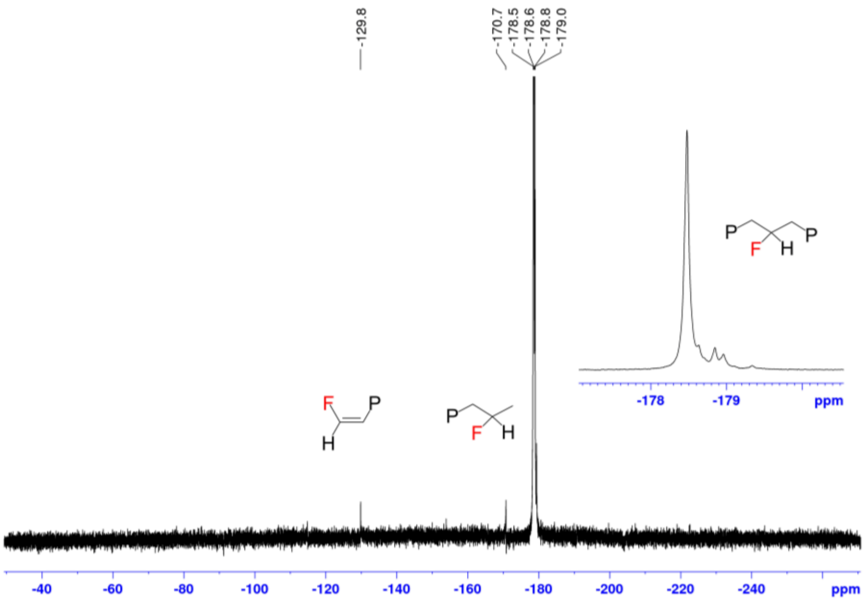

Generation of a Base-free Complex by the Reaction of 5b with B(C_6F_5)$_3$ and its Reactivity with 4-^{t}Bu-styrene. The reaction **5b** with B(C_6F_5)$_3$ in CD_2Cl_2 at room temperature generates (py')B(C_6F_5)$_3$, which was assigned based on the similarity of its ^1H and $^{19}F\{^1H\}$ NMR data with data for the analogous adduct (py)B(C_6F_5)$_3$,[16] and an insoluble product that is assumed to be the base-free derivative **7b** (Scheme 2.8). **5b** can be regenerated in ca. 90 % yield by addition of 4-(5-nonyl)-pyridine to the base-free complex based on integration of the Pd-Me region of the ^1H NMR spectrum.

Scheme 2.8

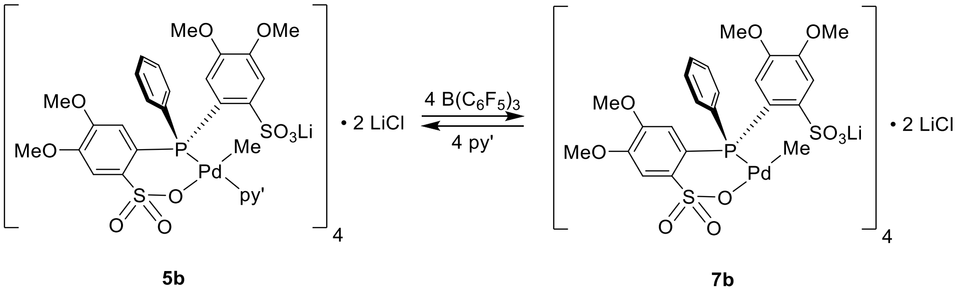

Base-free complex **7b** reacts with 4-^{t}Bu-styrene (1 equiv per Pd) in $CDCl_2CDCl_2$ at 80 °C for 2 h to form *E*-1-(4-^{t}Bu-phenyl)-propene (50 % vs. **7b**). This product likely forms by 2,1-insertion of 4-^{t}Bu-styrene into the Pd-Me bond, followed by β-H elimination (Scheme 2.9). Pd black was observed after the reaction, and **5b** was not recovered after addition of 4-(5-nonyl)-pyridine. The decomposition of **7b** and the consumption of remaining 4-^{t}Bu-styrene are most likely due to trapping of the initial form Pd-H species by 4-^{t}Bu-styrene insertion to form a (OPO)Pd(η^3-4-^{t}Bu-phenylethyl) compound and subsequent decomposition.

Scheme 2.9. Ar = Ph or 4-^{t}Bu-Ph, R = H or 4-^{t}Bu.

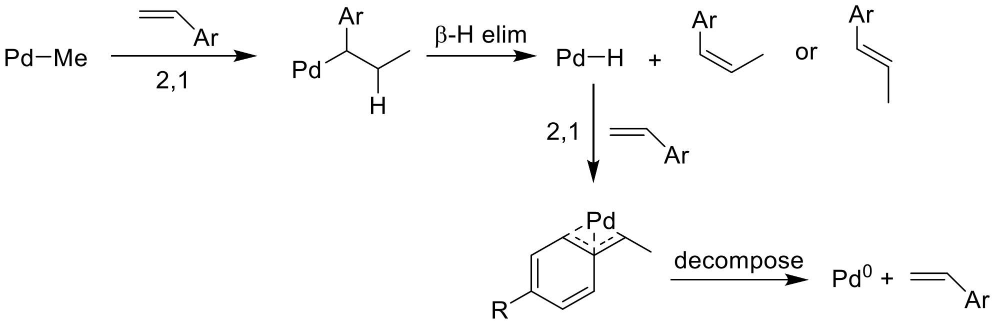

For comparison, a previous study showed that monomeric [κ^2-*P,O*-P(2-OMe-Ph)$_2$(2-SO_3-Ph)]PdMe(py) reacts rapidly with styrene in the presence of BPh_3 to form 1-phenyl-propene (Scheme 2.9).[17] (PO)Pd(η^3-phenylethyl), derived from subsequent 2,1-insertion of styrene into Pd-H bond of (PO)PdH species, was also observed and found to decompose slowly at ambient temperature to Pd black and styrene. After 2.5 h, 79 % of the starting Pd-Me converted to 1-phenyl-propene or (PO)Pd(η^3-phenylethyl) compound based on ^{1}H NMR.

The results of this experiment suggest that at least two Pd-Me groups with the Pd_4 structure are active for insertion and at least two polymer chains grow per tetrameric cage in ethylene polymerization.

2.3 Conclusions

The phosphine-arenesulfonate ligands **Na[1a-c]** and **Li[1c]**, and the phosphine-*bis*-arenesulfonate ligands **Li_2[2a-c]**, which contain 1-3 methoxy substituents on the arenesulfonate rings, have been synthesized. **Na[1a,b]** bind to Pd(II) to form (κ^2-*PO*)PdMe(pyridine) complexes **3a,b**. **3a,b** exhibit similar polymerization behavior compared to a bench mark (PO)PdMe(py) complex (**std**, [κ^2-*P,O*-P(2-OMe-Ph)$_2$(2-SO_3-5-Me-Ph)]PdMe(py)), indicating that the methoxy groups have little influence on the reactivity. **Li_2[2b]** reacts with (COD)PdMeCl and 4-(5-nonyl)-pyridine to generate Pd_4 compound **5b**, in which four PdMe(py') units are arranged around a central $Li_4S_4O_{12}$•Li_2Cl_2 cage. The structure of **5b** is similar to that of {[κ^2-*P,O*-PPh(2-SO_3-5-Me-Ph)(2-SO_3Li-5-Me-Ph)]PdMe(py')}$_4$ (**A**), except that **5b** contains a layer of Li_2Cl_2 that elongates the cage to satisfy the steric profile of the methoxy groups on the arenesulfonate rings. **5b** is more thermally stable than **A-D**, and more resistant to cage dissociation under ethylene polymerization conditions. In hexanes at 80 °C, **5b** produces linear UHMWPE with a narrow MWD. **5b** also copolymerizes vinyl fluoride with ethylene to produce linear copolymer with a broad MWD and high VF incorporation (ca. 2.5 mol %).

2.4 Experimental

General Procedures. All experiments were performed under a nitrogen atmosphere using drybox or Schlenk techniques. Nitrogen was purified by passage through Q-5 oxygen scavenger and activated molecular sieves. Methylene chloride, diethyl ether and THF were dried by passage over activated alumina. Toluene, pentane and hexane were purified by passage through BASF R3-11 oxygen scavenger and activated alumina. $CDCl_2CDCl_2$ and $CHCl_2CHCl_2$ were dried over 4 Å molecular sieves. CD_2Cl_2 was dried over P_2O_5. The following materials were obtained from commercial sources and used without further purification: 4-methoxybenzenesulfonyl chloride

(Aldrich, 99 %), 4-bromoveratrole (Aldrich, 98 %), 5-bromo-1,2,3-trimethoxybenzene (Aldrich, 97 %), chlorosulfonic acid (Aldrich, 99 %), 2-methyl-1-propanol (Aldrich, 99 %), 2-bromoanisole (Aldrich, 97 %), pyridine (Aldrich, 99.8 %), P,P-dichlorophenylphosphine (Aldrich, 97 %), chlorodiphenylphosphine (Aldrich, 96 %), dichloro(diethylamino)phosphine (Alfa aesar, 97 %), ^{n}BuLi solution (Aldrich, 2.5 M in hexanes), HCl solution (Aldrich, 2 M in diethyl ether), sodium iodide (Aldrich, > 99 %), lithium iodide (Aldrich, 99.9 %) 4,7,13,18-tetraoxa-1,10-diazabicyclo[8.5.5]eicosane (Cryptand211, Aldrich, 90 %)and 4-(5-nonyl)pyridine (TCI, 98 %). The following compounds were prepared by literature procedures: 2-bromo-4,5-di-methoxybenzenesulfonyl chloride[18] and (COD)PdMeCl.[19] Elemental analyses were performed by Robertson Microlit Laboratories. The solvent content in elemental analysis samples was quantified by ^{1}H NMR.

NMR spectra were acquired on Bruker DRX-500 or Bruker DRX-400 spectrometers at ambient temperatures unless otherwise indicated. ^{1}H and ^{13}C chemical shifts are reported relative to $SiMe_4$ and are internally referenced to residual ^{1}H and ^{13}C solvent resonances. ^{31}P chemical shifts are reported relative to externally referenced 85% H_3PO_4. ^{19}F spectra were referenced to external $BF_3•Et_2O$, and ^{19}F chemical shifts are reported relative to $CFCl_3$. ^{7}Li chemical shifts are reported relative to externally referenced LiCl in D_2O. NMR resonances were assigned based on COSY, HMQC, HMBC and ${}^{1}H\{{}^{31}P\}$ experiments, as well as trends in chemical shifts and coupling constants derived from these experiments. Coupling constants are given in Hz. Mass spectrometry was performed on Agilent 6224 TOF-MS (high resolution) or Agilent 6130 LCMS (low resolution) instruments.

Polymerization reactions were performed in a Parr 300 mL stainless steel autoclave, which was equipped with a mechanical stirrer, thermocouple and water cooling loop and controlled by a

Parr 4842 controller. Gel permeation chromatography (GPC) data were obtained on a Polymer Laboratories PL-GPC 220 instrument at 150 °C with 1,2,4-trichlorobenzene (stabilized with 125 ppm BHT) as the mobile phase. Three PLgel 10 μm Mixed-B LS columns were used. Molecular weights were calibrated using narrow polystyrene standards (ten-point calibration with M_n from 570 Da to 5670 kDa) and are corrected for linear polyethylene by universal calibration using the following Mark-Houwink parameters: polystyrene, $K = 1.75 \times 10^{-2}$ cm^3g^{-1}, $\alpha = 0.67$; polyethylene, $K = 5.90 \times 10^{-2}$ cm^3g^{-1}, $\alpha = 0.69$.[20] DSC measurements were performed on a TA Instruments DSC 2920 instrument. DSC samples (10 mg) were annealed by heating to 170 °C at 20 °C/min, cooled to 40 °C at 20 °C/min, and then analyzed while being heated to 170 °C at 20 °C/min.

6a-**

6a-^{i}Bu. A flask was charged with ^{i}BuOH (5.0 mL, 54 mmol), pyridine (8.4 mL, 0.10 mol) and $CHCl_3$ (50 mL), and cooled to 0 °C for 20 min. A solution of 4-methoxybenzenesulfonyl chloride (10 g, 50 mmol) in $CHCl_3$ (30 mL) was added, and the mixture was stirred for 18 h at room temperature. HCl solution (0.1 M in H_2O, 40 mL) was added, and the mixture was stirred for 5 min and transferred to a separatory funnel. The $CHCl_3$ layer was washed with H_2O (3 × 50 mL) and brine (10 mL), and dried over $MgSO_4$. The volatiles were removed under vacuum to yield a yellow oil. The crude product was purified by silica gel chromatography using CH_2Cl_2 as the eluent. The product was isolated as a colorless oil (11 g, 88 %). The ethyl ester of 4-methoxybenzenesulfonate, which is formed by the reaction with EtOH instead of ^{i}BuOH, was present as a minor impurity. Commercial $CHCl_3$ contains EtOH as stabilizer. ^{1}H NMR (CD_2Cl_2): δ 7.81 (d, $^3J_{HH} = 9$, 2H, H^2), 7.03 (d, $^3J_{HH} = 9$; 2H, H^3), 4.05 (q, $^3J_{HH} = 7$, 2H, $-SO_3CH_2CH_3$), 3.88 (s, 3H, $-OCH_3$), 3.75 (d, $^3J_{HH} = 6$, 2H, $-SO_3CH_2CH(CH_3)_2$), 1.91 (sept, $^3J_{HH} = 7$, 1H, $-SO_3CH_2CH(CH_3)_2$), 1.26 (t, $^3J_{HH} = 7$, 3H, $-SO_3CH_2CH_3$), 0.87 (d, $^3J_{HH} = 7$, 6H, $-SO_3CH_2CH(CH_3)_2$). $^{13}C\{^1H\}$ NMR (CD_2Cl_2): δ 164.2 (s, C^4), 130.4 (s, C^3), 127.9 (s, C^1), 114.8 (s, C^2), 76.6 (s, -$SO_3\mathit{C}H_2CH(CH_3)_2$), 67.2 (s, -$SO_3\mathit{C}H_2CH_3$), 56.1 (s, -$O\mathit{C}H_3$), 28.4 (s, -$SO_3CH_2\mathit{C}H(CH_3)_2$), 18.7 (s, -$SO_3CH_2CH(\mathit{C}H_3)_2$), 14.9 (s, -$SO_3CH_2\mathit{C}H_3$). HRMS (APCI/ESI-Mixed mode; *m*/*z*): Calcd. for $[C_{11}H_{16}O_4S + H]^+$ 245.0848, Found: 245.0859.

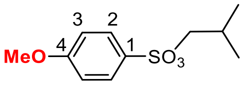

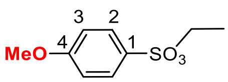

Figure 2.15. NMR spectra of **6a-^{i}Bu**

(a) ^1H (CD_2Cl_2, 500 MHz):

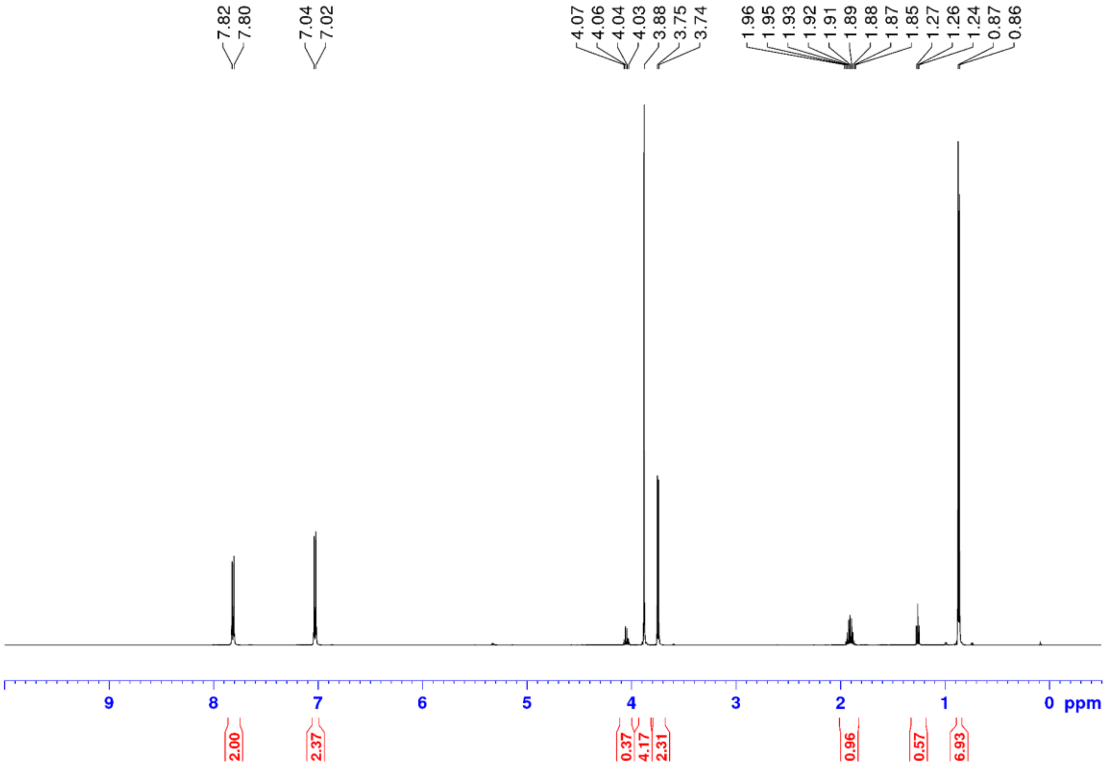

Figure 2.15, continued.

(b) $^{13}C\{^1H\}$ (CD_2Cl_2, 125 MHz):

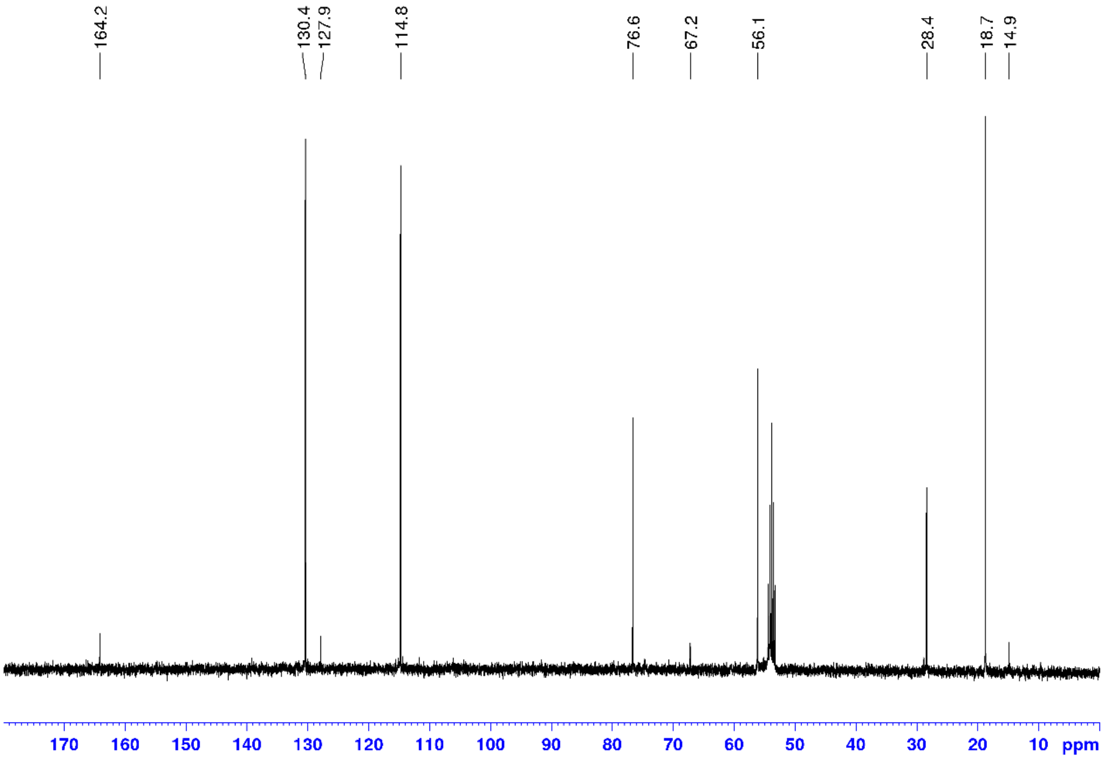

6b-^{i}Bu. **6b-^{i}Bu** was synthesized analogously to **6a-^{i}Bu** from 2-bromo-4,5-dimethoxybenzenesulfonyl chloride (9.8 g, 35 mmol), ^{i}BuOH (3.3 mL, 36 mmol), pyridine (4.8 mL, 60 mmol) and $CHCl_3$ (70 mL). The product was purified by silica gel chromatography using CH_2Cl_2 as the eluent, and isolated as a white solid (7.3 g, 60 %). ^{1}H NMR (CD_2Cl_2): δ 7.53 (s, 1H, H^6), 7.20 (s, 1H, H^3), 3.91 (s, 3H, H^8), 3.89 (s, 3H, H^7), 3.80 (d, $^3J_{HH}$ = 6, 2H, H^9), 1.98 (sept, $^3J_{HH}$ = 7, 1H, H^{10}), 0.93 (d, $^3J_{HH}$ = 7, 6H, H^{11}). $^{13}C\{^1H\}$ NMR (CD_2Cl_2): δ 153.3, 148.1, 127.0, 117.7, 114.4, 112.2, 77.1, 56.5, 56.4, 28.1, 18.5. HRMS (ESI mode; *m*/*z*): Calcd. for $[C_{12}H_{17}BrO_5S + Na]^+$ 374.9878, Found: 374.9863.

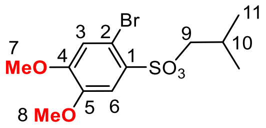

Figure 2.16. NMR spectra of **6b-^{i}Bu**

(a) ^{1}H (CD_2Cl_2, 500 MHz):

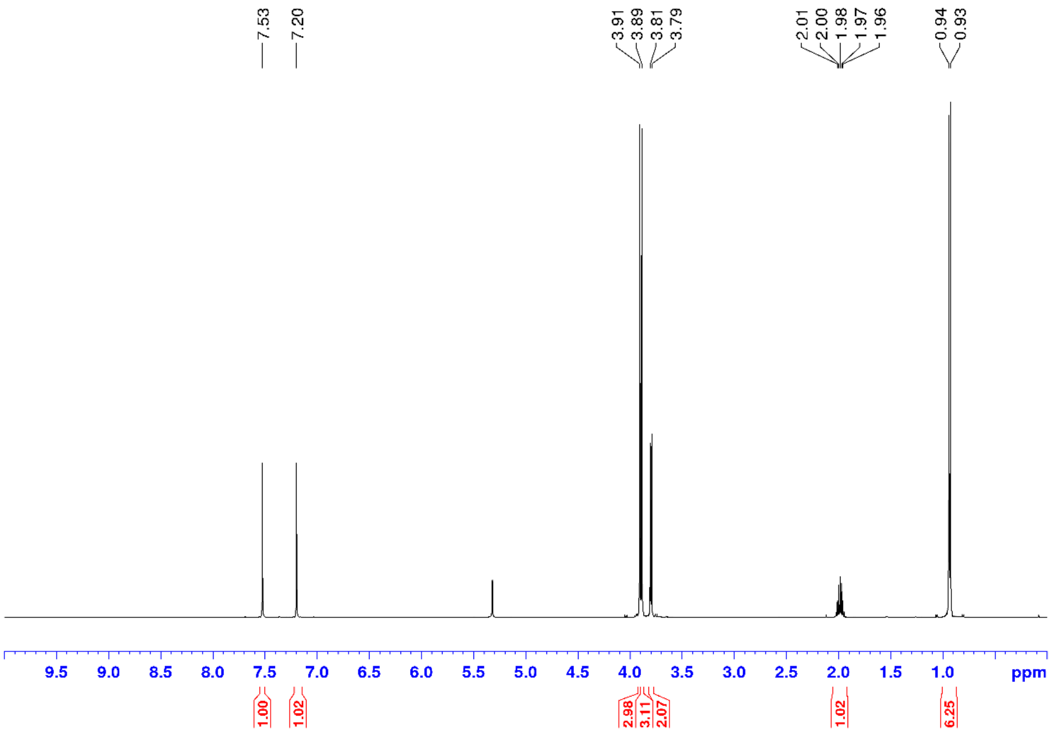

(b) $^{13}C\{^{1}H\}$ (CD_2Cl_2, 125 MHz):

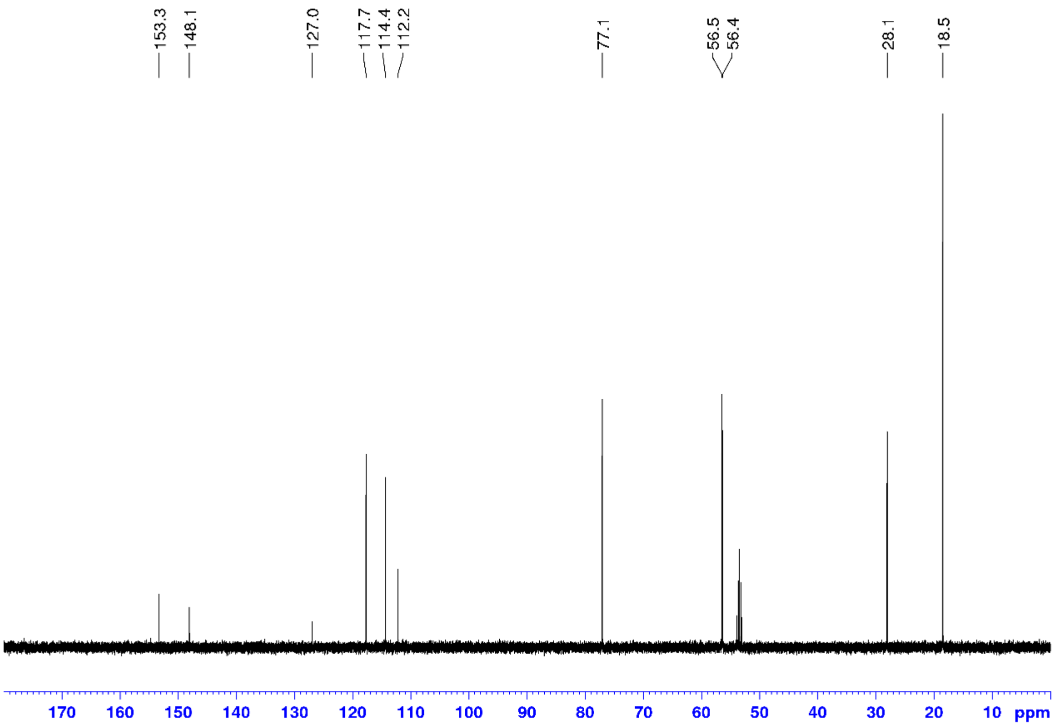

6c-^{i}Bu. A flask was charged with chlorosulfonic acid (12 mL, 0.18 mol) and cooled to 0 °C for 20 min. A solution of 5-bromo-1,2,3-trimethoxybenzene (8.0 g, 32 mmol) in CH_2Cl_2 (40 mL) was added and the mixture was stirred for 90 min. The mixture was slowly poured onto ice. After the ice had thawed, the mixture was transferred to a separatory funnel, and the aqueous layer was extracted with CH_2Cl_2 (3 × 40 mL). The organic fractions were combined and dried with $MgSO_4$, and the volatiles were removed under vacuum to a yield yellow oil. The oil was dissolved in $CHCl_3$ (60 mL), and a solution of ^{i}BuOH (4.5 mL, 49 mmol) and pyridine (8.0 mL, 99 mmol) in $CHCl_3$ (20 mL) was added. The mixture was stirred for 18 h at room temperature. HCl solution (0.1 M in H_2O, 80 mL) was added, and the mixture was stirred for 5 min and transferred to a separatory funnel. The $CHCl_3$ layer was washed with H_2O (3 × 50 mL) and brine (10 mL), and dried over $MgSO_4$. The volatiles were removed under vacuum to yield a yellow oil. The crude product was purified by silica gel chromatography using a mixture of 4/1 hexanes/ethyl acetate as the eluent. The product was isolated as a yellow oil (3.0 g, 24 %). ^{1}H NMR (CD_2Cl_2): δ 7.08 (s, 1H, H^3), 3.94 (s, 3H, H^9), 3.92 (s, 3H, H^8), 3.87 (d, $^3J_{HH}$ = 6, 2H, H^{10}), 3.84 (s, 3H, H^7), 1.98 (sept, $^3J_{HH}$ = 7, 1H, H^{11}), 0.93 (d, $^3J_{HH}$ = 6, 6H, H^{12}). $^{13}C\{^1H\}$ NMR (CD_2Cl_2): δ 157.7, 155.4, 143.3, 122.8, 116.6, 115.1, 77.2, 62.6, 61.1, 56.8, 28.5, 18.8. ESI-MS (1/1 CH_3OH/H_2O; *m/z*): Calcd. For $[2(C_{13}H_{19}O_6BrS) + Na]^+$ 789.0, Found: 789.1.

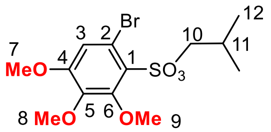

Figure 2.17. NMR spectra of **6c-^{i}Bu**

(a) ^{1}H (CD_2Cl_2, 500 MHz): δ 1.53 = H_2O

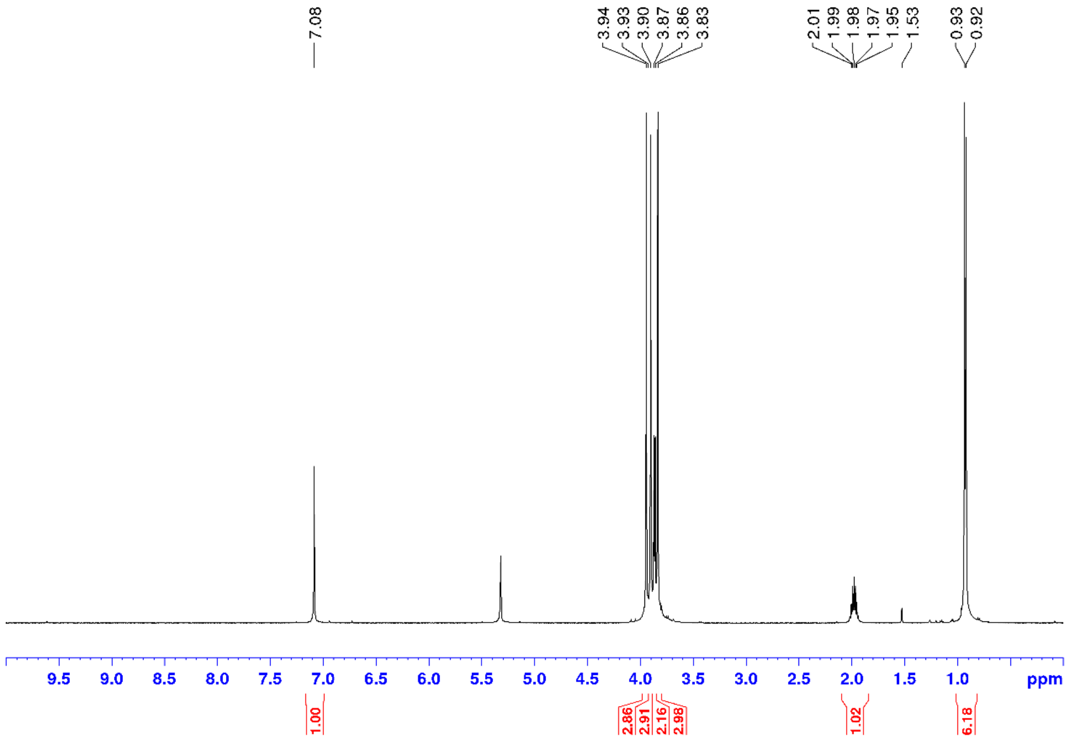

(b) $^{13}C\{^{1}H\}$ (CD_2Cl_2, 125 MHz):

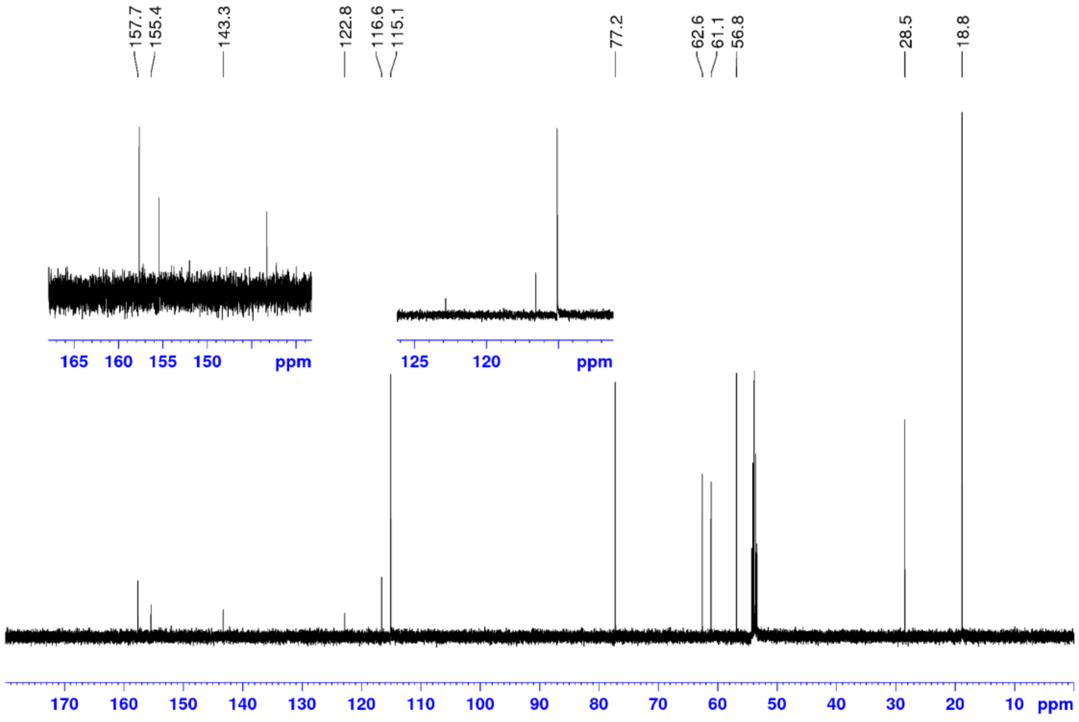

P(2-OMe-Ph)$_2$Cl. A Schlenk flask was charged with 2-bromoanisole (5.0 mL, 40 mmol) and THF (210 mL), and cooled to -78 °C. ^{n}BuLi (2.5 M solution in hexanes, 16 mL, 40 mmol) was added via syringe over 15 min. The mixture was stirred at -78 °C for 1 h and a solution of PCl_2NEt_2 (3.5 g, 20 mmol) in Et_2O (30 mL) was added. The mixture was stirred at room temperature for 18 h to yield a clear yellow solution. The volatiles were removed under vacuum. The resulting yellow solid was taken up in Et_2O (100 mL) and washed with H_2O (100 mL). The aqueous layer was extracted with Et_2O (3 × 75 mL). The combined organic fractions were washed with brine (20 mL) and dried over $MgSO_4$, and the volatiles were removed under vacuum to afford P(2-OMe-Ph)$_2$NEt$_2$ as a yellow solid (5.7 g, 87 %). A Schlenk flask was charged with P(2-OMe-Ph)$_2$NEt$_2$ (3.1 g, 10 mmol) and THF (50 mL), and cooled to -78 °C. HCl solution (2.0 M solution in diethyl ether, 10 mL, 20 mmol) was added via syringe to form a white cloudy solution. The mixture was stirred at -78 °C for 1 h and filtered, and the volatiles were removed from the filtrate under vacuum to yield a white solid (2.5 g, 89 %). The typical purity was ca. 93% by $^{31}P\{^1H\}$ NMR. The product was used without further purification. $^{31}P\{^1H\}$ NMR (CD_2Cl_2): δ 69.6. ^1H NMR (CD_2Cl_2): δ 7.43 (t, $^3J_{HH}$ = 8, 2H), 7.36-7.34 (m, 2H), 7.00 (t, $^3J_{HH}$ = 8, 2H), 6.93 (dd, $^3J_{HH}$ = 8, $^3J_{PH}$ = 5, 2H), 3.82 (s, 6H).

1a-^{i}Bu. A Schlenk flask was charged with **6a-^{i}Bu** (1.2 g, 5.0 mmol) and THF (38 mL), and cooled to -78 °C. ^{n}BuLi (2.5 M solution in hexanes, 2.0 mL, 5.0 mmol) was added via syringe over 5 min. The mixture was stirred at -78 °C for 1 h and a solution of P(2-OMe-Ph)$_2$Cl (1.4 g, 5.0 mmol) in THF (10 mL) was added. The mixture was stirred at room temperature for 18 h to yield a clear yellow solution. The volatiles were removed under vacuum. The resulting yellow oil was taken up in H_2O (50 mL) and was extracted with CH_2Cl_2 (3 × 50 mL). The combined organic fractions were washed with brine (20 mL) and dried over $MgSO_4$, and the volatiles were removed under vacuum to yield a yellow solid. The crude product was purified by silica gel chromatography, using a 4/1 hexanes/ethyl acetate mixture as the eluent. The product was isolated as a white solid (0.720 g, 30%). $^{31}P\{^{1}H\}$ NMR (CD_2Cl_2): δ -28.1. ^{1}H NMR (CD_2Cl_2): δ 8.06 (dd, $^{3}J_{HH}$ = 8, $^{4}J_{PH}$ = 4, 1H, H^{3}), 7.36 (t, $^{3}J_{HH}$ = 8; 2H, H^{10}), 6.96 (dd, $^{3}J_{HH}$ = 8, $^{4}J_{HH}$ = 3, 1H, H^{4}), 6.92 (dd, $^{3}J_{HH}$ = 8, $^{4}J_{PH}$ = 5, 2H, H^{9}), 6.85 (t, $^{3}J_{HH}$ = 8, 2H, H^{11}), 6.57 (m, 3H, H^{6} and H^{12}), 3.79 (d, $^{3}J_{HH}$ = 6, 2H, H^{15}), 3.72 (s, 6H, H^{14}), 3.64 (s, 3H, H^{13}), 1.85 (sept, $^{3}J_{HH}$ = 7, 1H, H^{16}), 0.88 (d, $^{3}J_{HH}$ = 7, 6H, H^{17}). $^{13}C\{^{1}H\}$ NMR (CD_2Cl_2): δ 163.1 (d, $^{3}J_{PC}$ = 1, C^{5}), 161.5 (d, $^{2}J_{PC}$ = 17, C^{8}), 141.6 (d, $^{1}J_{PC}$ = 33, C^{1}), 134.2 (s, C^{12}), 133.1 (d, $^{3}J_{PC}$ = 4, C^{3}), 132.7 (d, $^{2}J_{PC}$ = 26, C^{2}), 130.8 (s, C^{10}), 125.1 (d, $^{1}J_{PC}$ =16, C^{7}), 122.6 (d, $^{2}J_{PC}$ = 1, C^{6}), 121.4 (s, C^{11}), 113.3 (s, C^{4}), 110.8 (d, $^{3}J_{PC}$ = 1, C^{9}), 76.7 (d, $^{5}J_{PC}$ = 3, C^{15}), 56.0 (d, $^{4}J_{PC}$ = 1, C^{14}), 55.7 (s, C^{13}), 28.4 (s, C^{16}), 18.9 (s, C^{17}). HRMS (APCI/ESI-Mixed mode; *m*/*z*): Calcd. for $[C_{25}H_{29}O_6PS + H]^+$ 489.1501, Found: 489.1495.

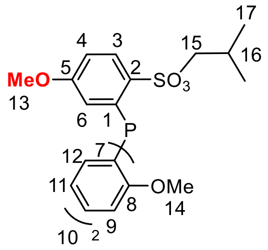

Figure 2.18. NMR spectra of **1a-^{i}Bu**

(a) $^{31}P\{^1H\}$ (CD_2Cl_2, 202 MHz):

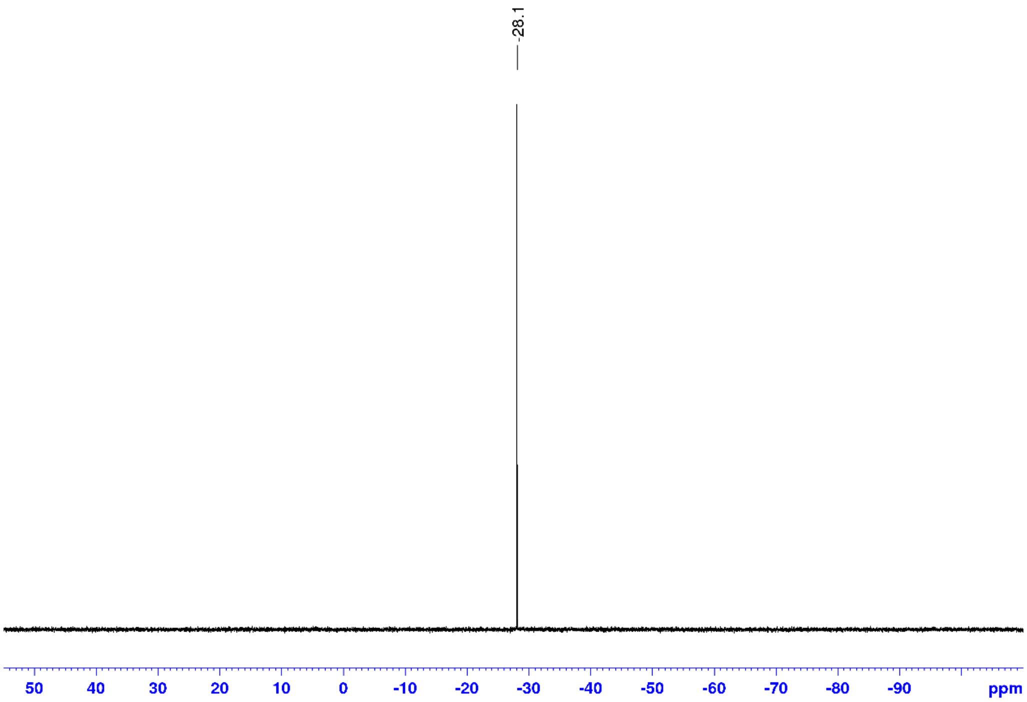

(b) ^1H (CD_2Cl_2, 500 MHz): δ 4.08, 2.00, 1.23 = EtOAc; 0.08 = grease

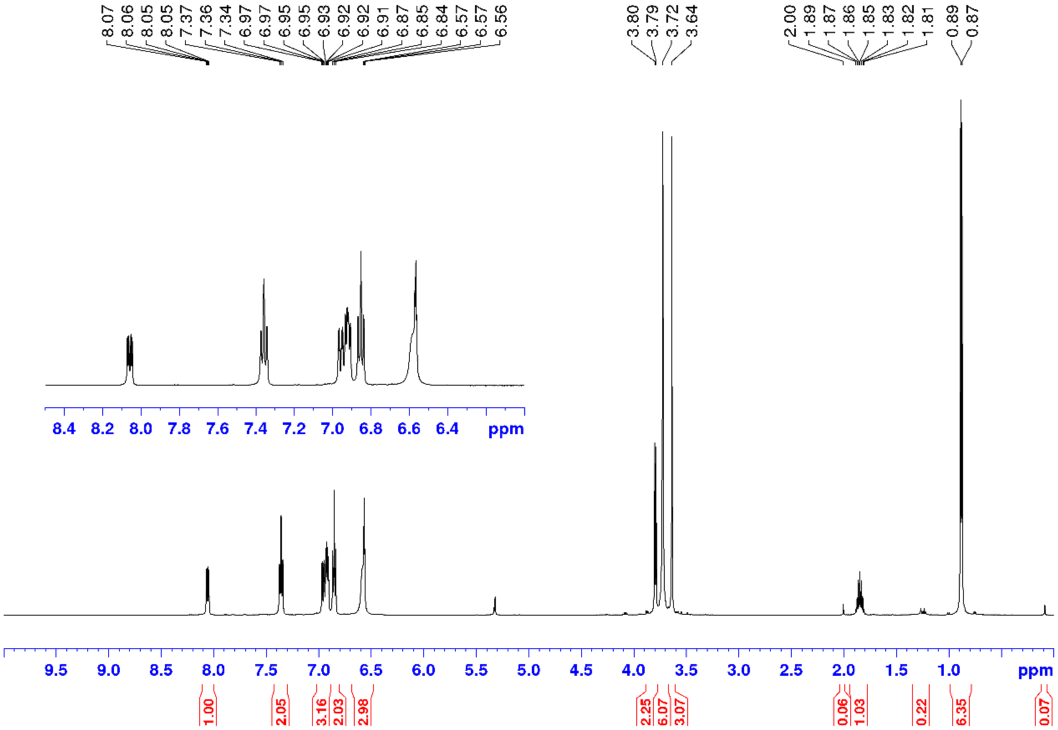

Figure 2.18, continued.

(c) $^{13}C\{^1H\}$ (CD_2Cl_2, 125 MHz):

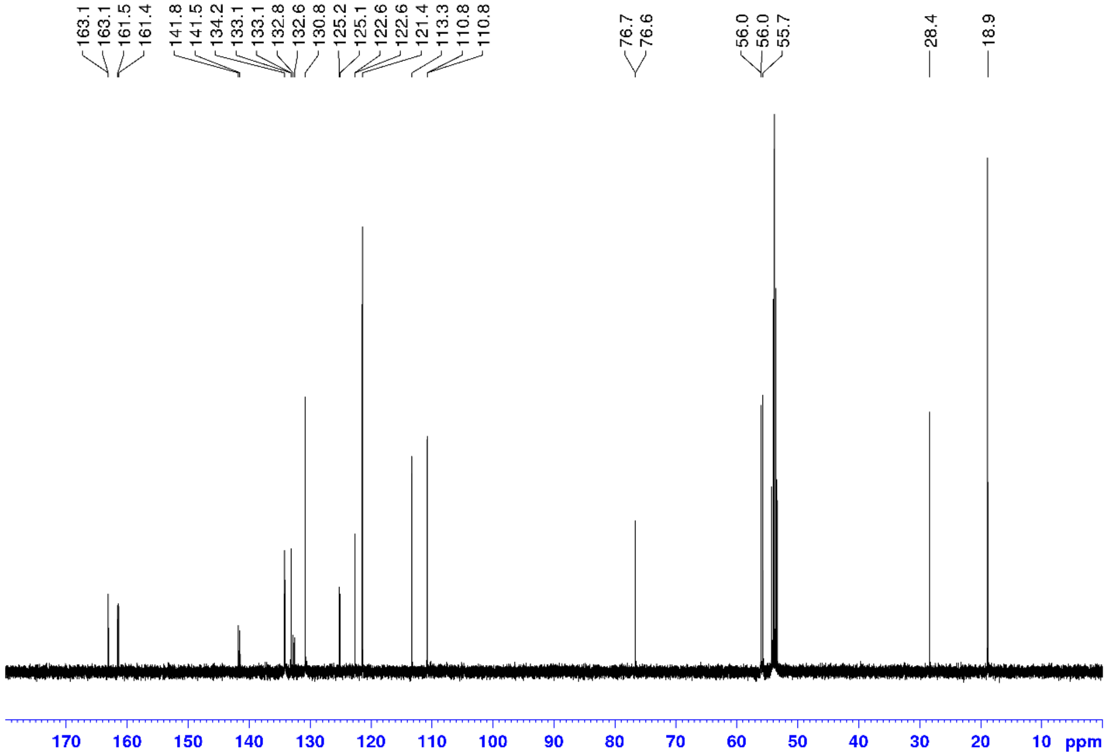

1b-^{i}Bu. 1b-^{i}Bu was synthesized analogously to **1a-^{i}Bu** from **6b-^{i}Bu** (0.71 g, 2.0 mmol) and P(2-OMe-Ph)$_2$Cl (0.56 g, 2.0 mmol). The volatiles were removed under vacuum, and the resulting yellow oil was taken up in H_2O (20 mL) and extracted with ethyl acetate (3 × 20 mL). The combined organic fractions were washed with brine (5 mL) and dried over $MgSO_4$, and the volatiles were removed under vacuum to yield a yellow solid. The crude product was purified by silica gel chromatography using a 3/1 hexanes/ethyl acetate mixture as the eluent. The product was isolated as a white solid (0.450 g, 43 %). $^{31}P\{^1H\}$ NMR (CD_2Cl_2): δ -27.6. ^1H NMR (CD_2Cl_2): δ 7.59 (d, $^4J_{PH}$ = 3, 1H, H^3), 7.35 (t, $^3J_{HH}$ = 8, 2H, H^{10}), 6.91 (dd, $^3J_{HH}$ = 8, $^4J_{PH}$ = 5, 2H, H^9), 6.85 (t, $^3J_{HH}$ = 8, 2H, H^{11}), 6.60 (br, 2H, H^{12}), 6.50 (d, $^3J_{PH}$ = 2, 1H, H^6), 3.92 (s, 3H, H^{13}), 3.84 (d, $^3J_{HH}$ = 6, 2H, H^{16}), 3.72 (s, 6H, H^{15}), 3.41 (s, 3H, H^{14}), 1.86 (sept, $^3J_{HH}$ = 7, 1H, H^{17}), 0.89 (d, $^3J_{HH}$ = 6, 6H, H^{18}). $^{13}C\{^1H\}$ NMR (CD_2Cl_2): δ 161.4 (d, $^2J_{PC}$ = 17, C^8), 152.5 (s, C^5), 149.3 (s, C^4), 134.0 (s, C^{12}), 133.2 (d, $^{2}J_{PC}$ = 28, C^{2}), 131.5 (d, $^{1}J_{PC}$ = 31, C^{1}), 130.7 (s, C^{10}), 125.7 (d, $^{1}J_{PC}$ =17, C^{7}), 121.4 (s, C^{11}), 118.4 (s, C^{6}), 113.7 (d, $^{3}J_{PC}$ = 5, C^{3}), 110.7 (s, C^{9}), 76.8 (d, $^{5}J_{PC}$ = 4, C^{16}), 56.5 (s, C^{13}), 56.0 (s, C^{15}), 55.8 (s, C^{14}), 28.4 (s, C^{17}), 18.9 (s, C^{18}). HRMS (APCI/ESI-Mixed mode; *m*/*z*): Calcd. for $[C_{26}H_{31}O_{7}PS + H]^{+}$ 519.1606, Found: 519.1616.

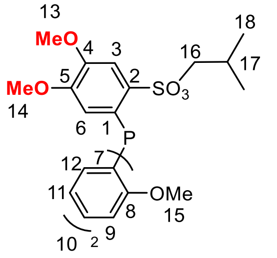

Figure 2.19. NMR spectra of **1b-^{i}Bu**

(a) ^{31}P{^{1}H} (CD$_2$Cl$_2$, 202 MHz):

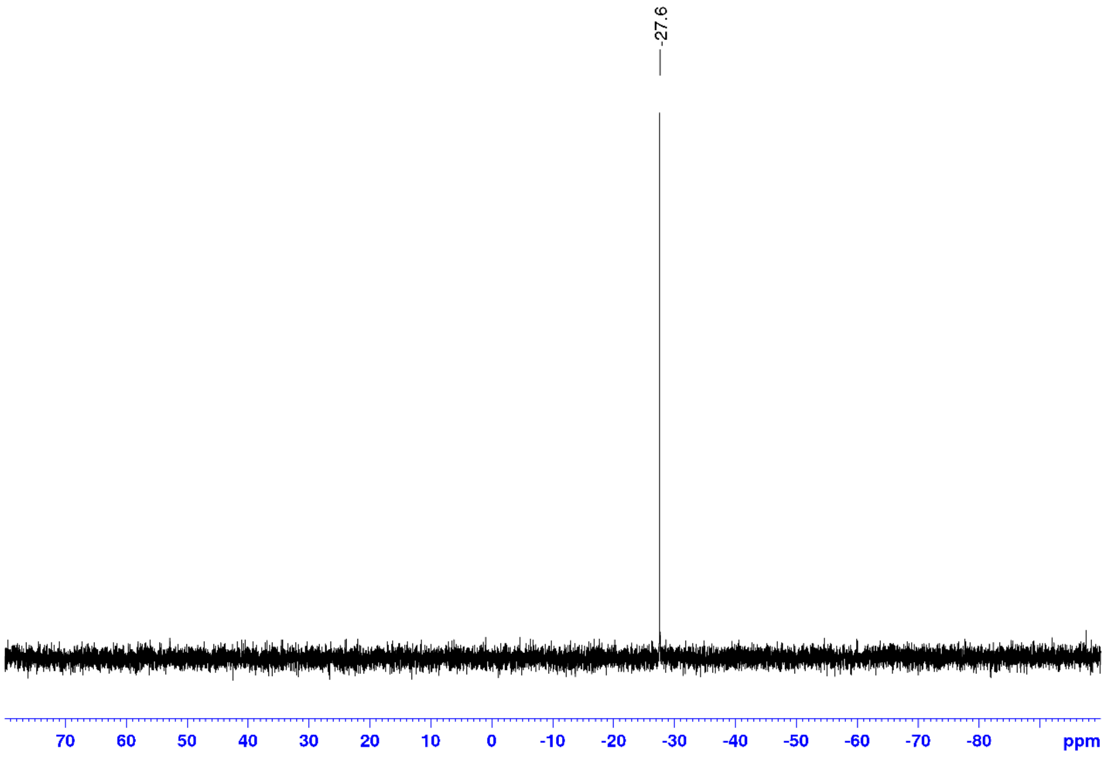

Figure 2.19, continued.

(b) ^{1}H (CD_2Cl_2, 500 MHz): δ 0.08 = grease

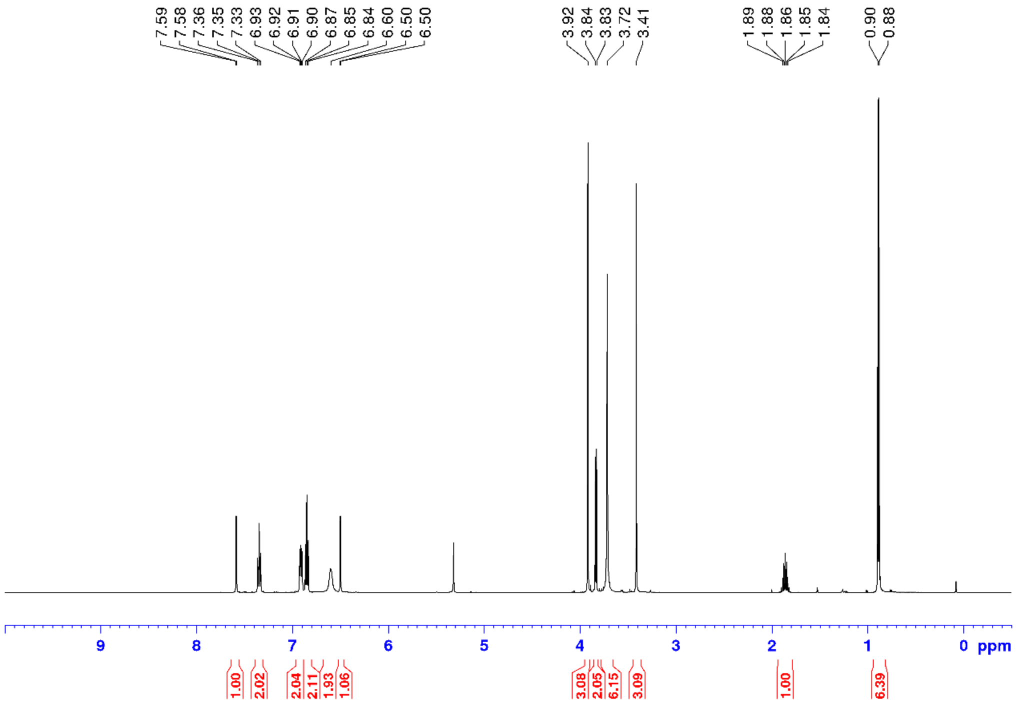

(c) $^{13}C\{^1H\}$ (CD_2Cl_2, 125 MHz):

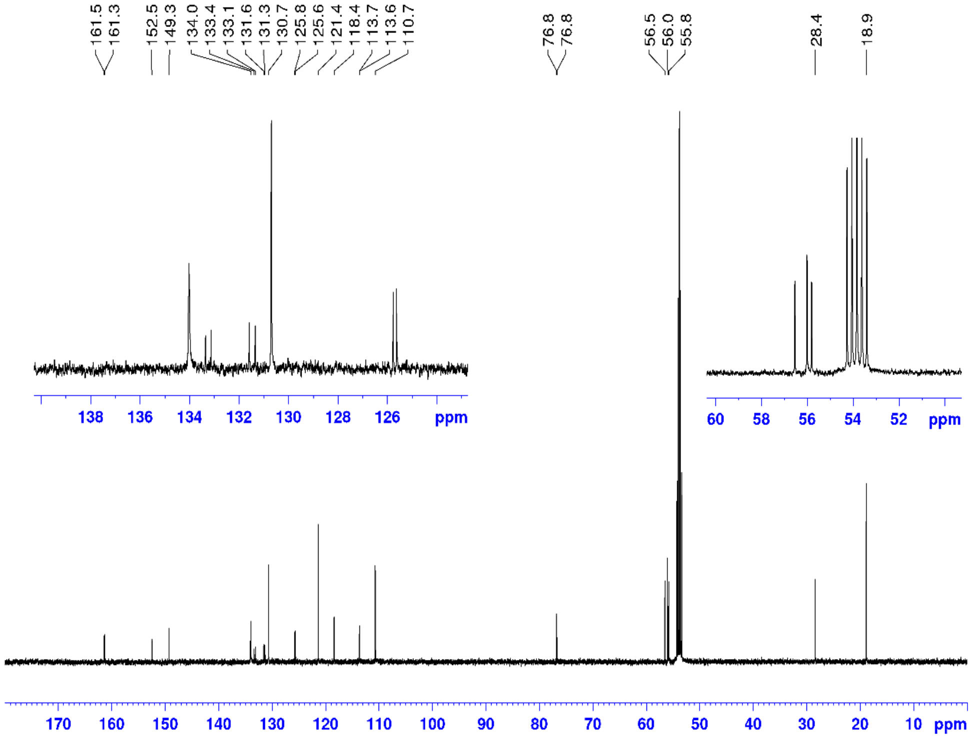

1c-^{i}Bu. 1c-^{i}Bu was synthesized analogously to **1a-^{i}Bu** from **6c-^{i}Bu** (1.2 g, 3.0 mmol) and P(2-OMe-Ph)$_2$Cl (0.85 g, 3.0 mmol). The volatiles were removed under vacuum, and the resulting yellow oil was taken up in H_2O (50 mL) and extracted with ethyl acetate (3 × 50 mL). The combined organic fractions were washed with brine (10 mL) and dried over $MgSO_4$, and the volatiles were removed under vacuum to yield a yellow solid. The crude product was purified by silica gel chromatography using a 5/1 hexanes/ethyl acetate mixture as the eluent. The product was isolated as a white solid (0.800 g, 49 %). $^{31}P\{^1H\}$ NMR (CD_2Cl_2): δ -21.9. ^1H NMR (CD_2Cl_2): δ 7.36 (t, $^3J_{HH}$ = 8, 2H, H^{10}), 6.93 (dd, $^3J_{HH}$ = 8, $^4J_{PH}$ = 5, 2H, H^9), 6.87 (t, $^3J_{HH}$ = 8, 2H, H^{11}), 6.70 (br, 2H, H^{12}), 6.32 (s, 1H, H^6), 3.99 (s, 3H, H^{13}), 3.86 (s, 3H, H^{14}), 3.75 (s, 6H, H^{16}), 3.72 (d, $^3J_{HH}$ = 6, 2H, H^{17}), 3.38 (s, 3H, H^{15}), 1.89 (sept, $^3J_{HH}$ = 7, 1H, H^{18}), 0.86 (d, $^3J_{HH}$ = 7, 6H, H^{19}). $^{13}C\{^1H\}$ NMR (CD_2Cl_2): δ 161.7 (d, $^2J_{PC}$ = 17, C^8), 156.8 (s, C^5), 154.4 (d, $^3J_{PC}$ = 4, C^3), 143.1 (s, C^4), 136.4 (d, $^1J_{PC}$ = 37, C^1), 134.5 (s, C^{12}), 130.8 (s, C^{10}), 126.6 (d, $^2J_{PC}$ = 21, C^2), 126.5 (d, $^1J_{PC}$ =19, C^7), 121.5 (s, C^{11}), 113.9 (s, C^6), 110.8 (s, C^9), 76.7 (d, $^5J_{PC}$ = 2, C^{17}), 62.1 (s, C^{13}), 60.9 (s, C^{14}), 56.1 (s, C^{16}), 55.7 (s, C^{15}), 28.5 (s, C^{18}), 18.8 (s, C^{19}). HRMS (ESI mode; *m*/*z*): Calcd. for $[C_{27}H_{33}O_8PS + H]^+$ 549.1712, Found: 549.1710.

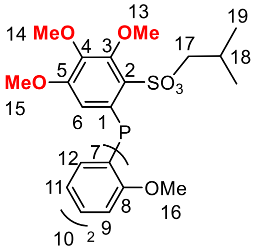

Figure 2.20. NMR spectra of **1c-^{i}Bu**

(a) $^{31}P\{^{1}H\}$ (CD_2Cl_2, 202 MHz):

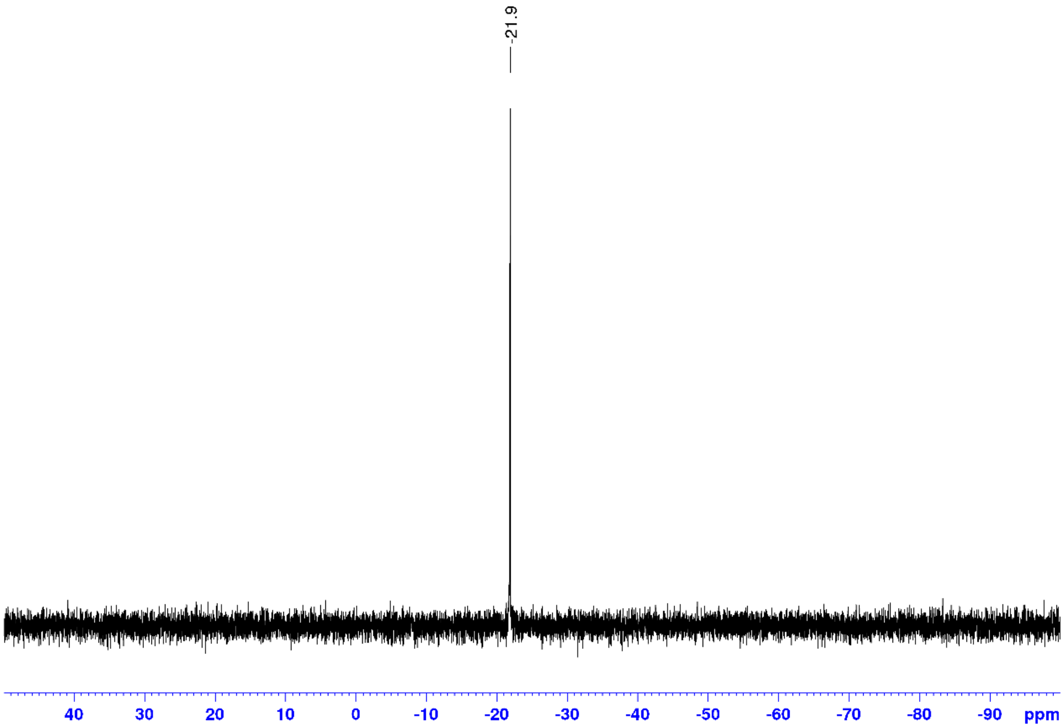

(b) ^{1}H (CD_2Cl_2, 500 MHz): δ 4.08, 2.00, 1.23 = EtOAc; 1.53 = H_2O; 0.08 = grease.

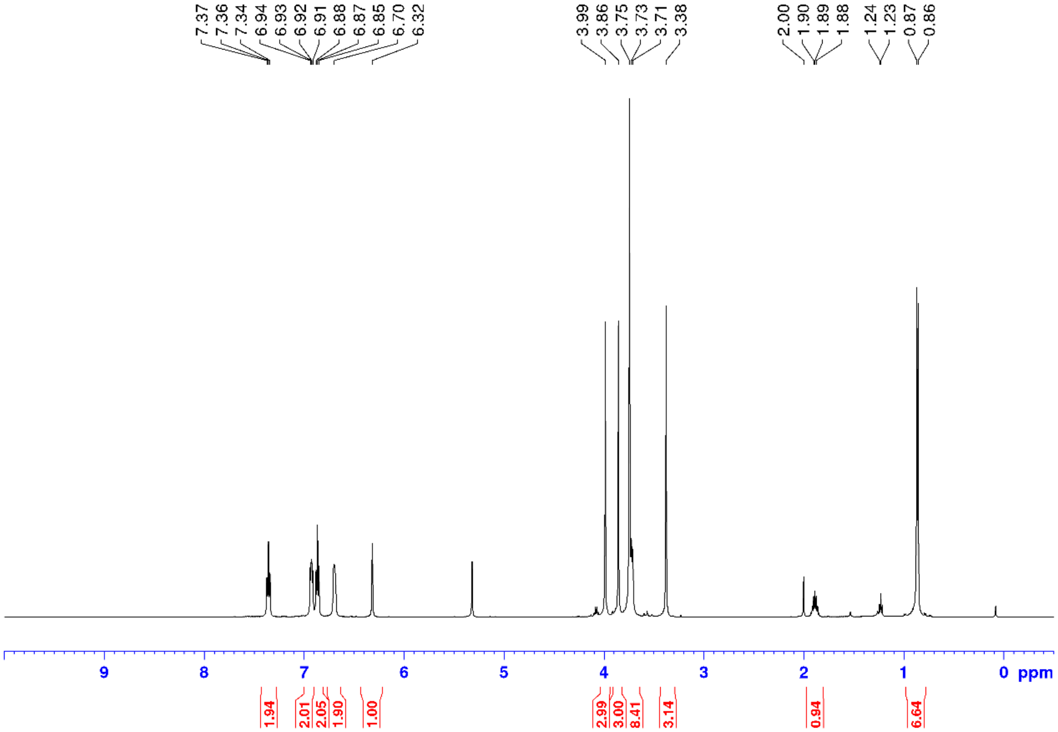

Figure 2.20, continued.

(c) $^{13}C\{^1H\}$ (CD_2Cl_2, 125 MHz):

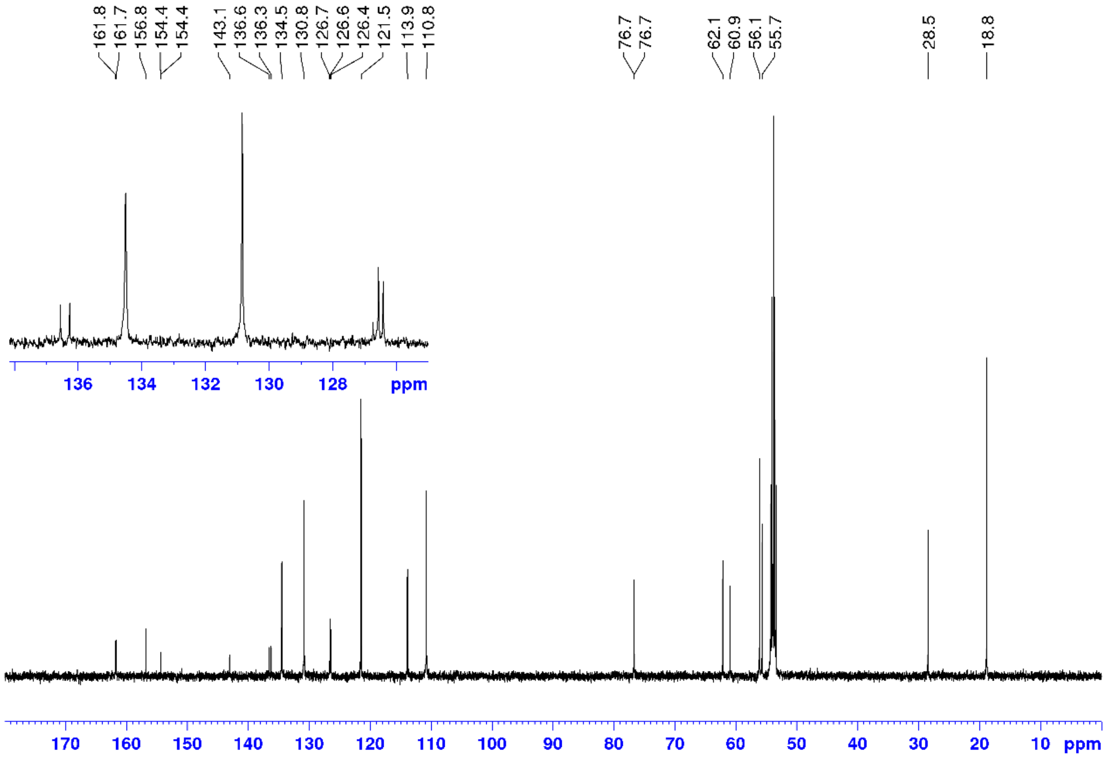

1d-^{i}Bu. 1d-^{i}Bu was synthesized analogously to **1a-^{i}Bu** from **6b-^{i}Bu** (0.53 g, 1.5 mmol) and PPh_2Cl (0.30 mL, 1.5 mmol). The volatiles were removed under vacuum, and the resulting yellow oil was taken up in H_2O (20 mL) and extracted with CH_2Cl_2 (3 × 20 mL). The combined organic fractions were washed with brine (5 mL) and dried over $MgSO_4$, and the volatiles were removed under vacuum to yield yellow solid. The crude product was purified by silica gel chromatography using a 3/1 hexanes/ethyl acetate mixture as the eluent. The product was isolated as a white solid (0.575 g, 84 %). $^{31}P\{^1H\}$ NMR (CD_2Cl_2): δ -9.4. ^1H NMR (CD_2Cl_2): δ 7.57 (d, $^4J_{PH}$ = 3, 1H, H^3), 7.36-7.33 (m, 6H, H^9 and H^{10}), 7.22 (m, 4H, H^8), 6.55 (d, $^3J_{PH}$ = 2, 1H, H^6), 3.91 (s, 3H, H^{11}), 3.74 (d, $^3J_{HH}$ = 6, 2H, H^{13}), 3.48 (s, 3H, H^{12}), 1.79 (sept, $^3J_{HH}$ = 7, 1H, H^{14}), 0.87 (d, $^3J_{HH}$ = 6, 6H, H^{15}). $^{13}C\{^1H\}$ NMR (CD_2Cl_2): δ 152.6 (s, C^5), 149.5 (s, C^4), 137.7 (d, $^1J_{PC}$ =14, C^7), 133.9 (d, $^2J_{PC}$ = 21, C^8), 133.2 (d, $^2J_{PC}$ = 25, C^2), 130.9 (d, $^1J_{PC}$ = 31, C^1), 129.2 (s, C^{10}), 128.9 (d, $^3J_{PC}$ = 7, C^9), 119.0

(s, C^6), 113.9 (d, $^3J_{PC} = 5$, C^3), 76.9 (s, $^5J_{PC} = 2$, C^{13}), 56.6 (s, C^{11}), 55.9 (s, C^{12}), 28.4 (s, C^{14}), 18.9 (s, C^{15}). HRMS (APCI/ESI-Mixed mode; *m*/*z*): Calcd. for $[C_{24}H_{27}O_5PS + H]^+$ 459.1395, Found: 459.1377.

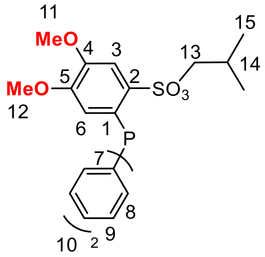

Figure 2.21. NMR spectra of **1d-^{i}Bu**

(a) $^{31}P\{^1H\}$ (CD_2Cl_2, 202 MHz):

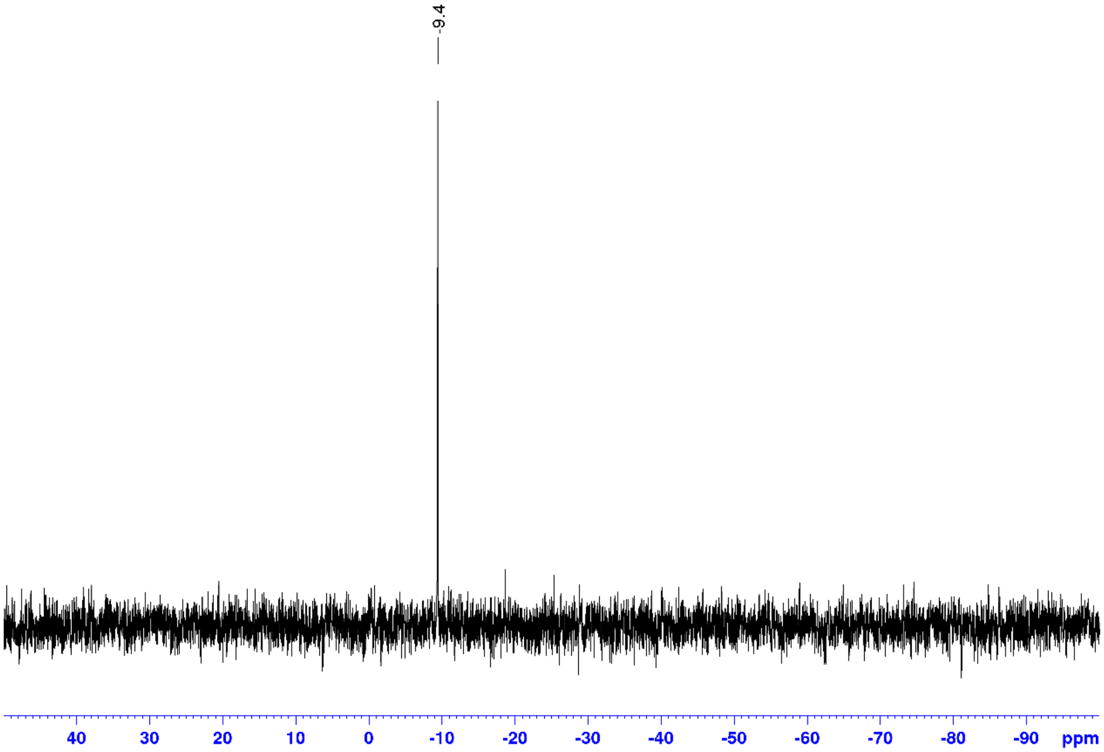

Figure 2.21, continued.

(b) ^1H (CD_2Cl_2, 500 MHz): δ 4.08, 2.00, 1.23 = EtOAc; 1.53 = H_2O; 0.08 = grease

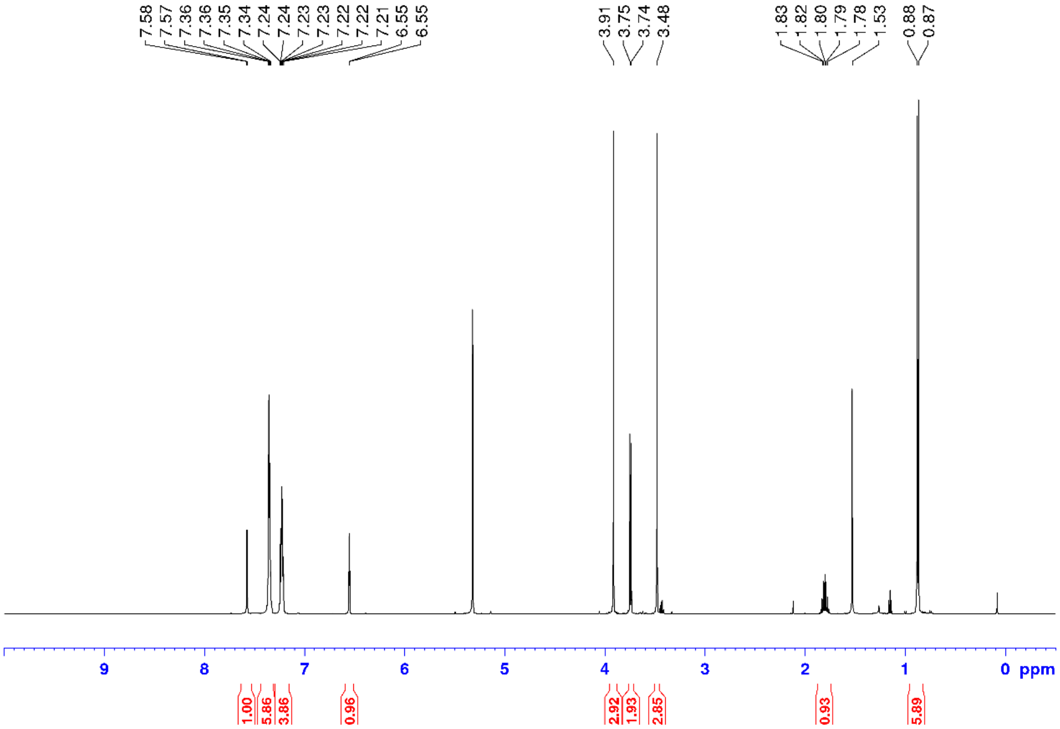

(c) $^{13}C\{^1H\}$ (CD_2Cl_2, 125 MHz):

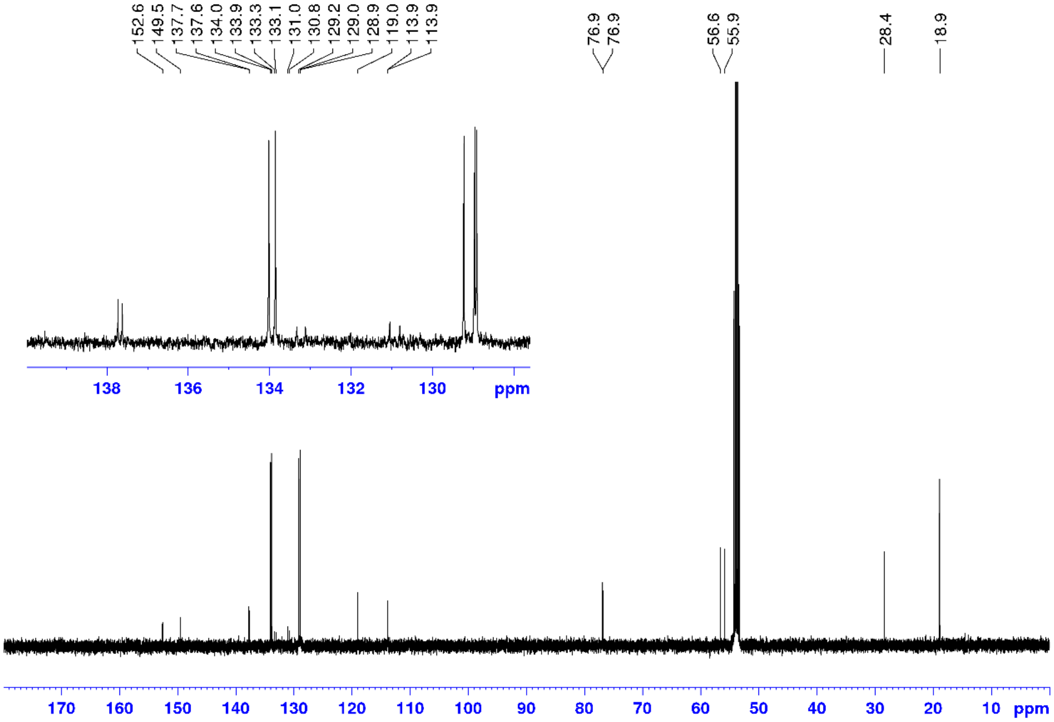

2a-^{i}Bu. 2a-^{i}Bu was synthesized analogously to **1a-^{i}Bu** from **6a-^{i}Bu** (1.4 g, 6.0 mmol) and $PPhCl_2$ (0.41 mL, 3.0 mmol). The volatiles were removed under vacuum, and the resulting yellow oil was taken up in H_2O (50 mL) and extracted with Et_2O (3 × 50 mL). The combined organic fractions were washed with brine (5 mL) and dried over $MgSO_4$, and the volatiles were removed under vacuum to yield a yellow solid. The crude product was purified by silica gel chromatograph using a 3/1 hexanes/ethyl acetate mixture as the eluent. The product was isolated as a white solid (1.4 g, 79 %). The ethyl sulfonate esters (2-SO_3Et-5-OMe-Ph)$_2$PPh and (2-SO_3Et-5-OMe-Ph)(2-$SO_3{}^i$Bu-5-OMe-Ph)PPh, which are formed from the 4-methoxybenzenesulfonate ethyl ester impurity in **6a-^{i}Bu**, were present as minor impurities. $^{31}P\{^1H\}$ NMR (CD_2Cl_2): δ -7.8. ^1H NMR (CD_2Cl_2): δ 8.05 (d, $^3J_{HH}$ = 8, $^4J_{PH}$ = 4, 2H, H^3), 7.41-7.36 (m, 3H, H^9 and H^{10}), 7.18 (t, $^3J_{PH}$ = $^3J_{HH}$ = 7, 2H, H^8), 6.97 (dd, $^3J_{HH}$ = 9, $^5J_{PH}$ = 3, 2H, H^4), 6.42 (t, $^3J_{PH}$ = 3, 2H, H^6), 3.89 and 3.77 (dd, $^2J_{HH}$ = 9, $^3J_{HH}$ = 8, 4H, $H^{12,12'}$), 3.67 (s, 6H, H^{11}), 1.95 (sept, $^3J_{HH}$ = 6, 2H, H^{13}), 0.93 and 0.92 (d, $^3J_{HH}$ = 6, 12H, H^{14} and $H^{14'}$). ESI-MS (1/1 CH_3OH/H_2O; *m/z*): Calcd. for $[C_{28}H_{35}O_8PS_2 + H]^+$ 595.2, Found: 595.1.

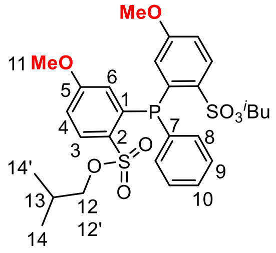

Figure 2.22. NMR spectra of **2a-^{i}Bu**

(a) $^{31}P\{^1H\}$ (CD_2Cl_2, 202 MHz): δ -8.2 = Ethyl sulfonate ester impurities

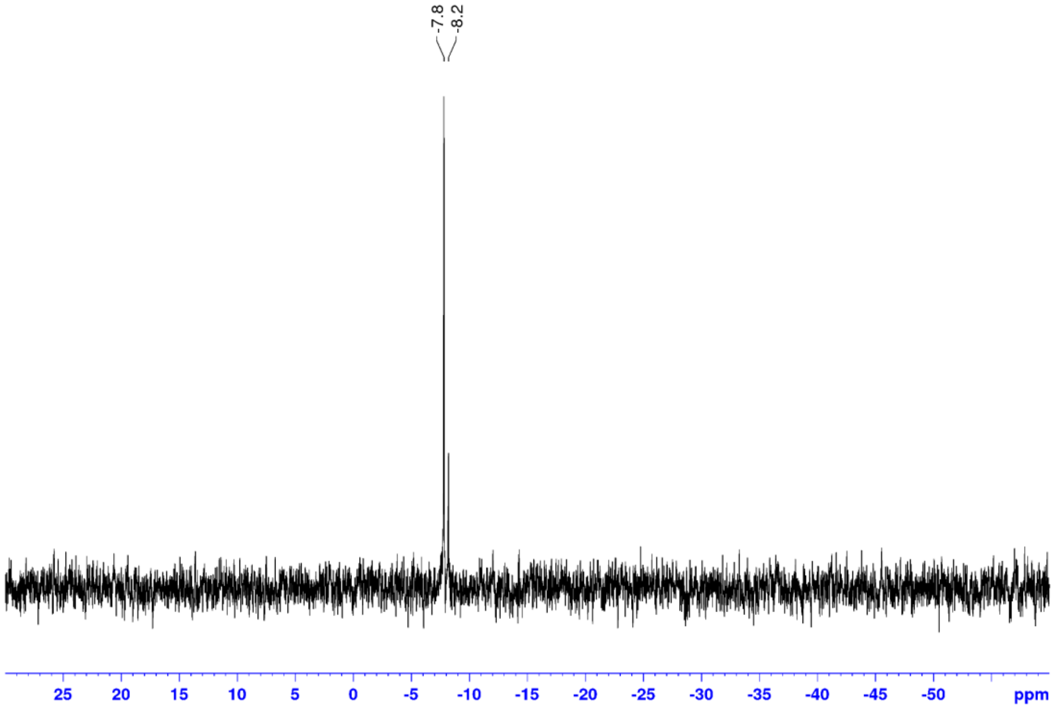

(b) ^1H (CD_2Cl_2, 500 MHz): δ 4.08, 2.00, 1.23 = EtOAc; 1.53 = H_2O; 0.08 = grease

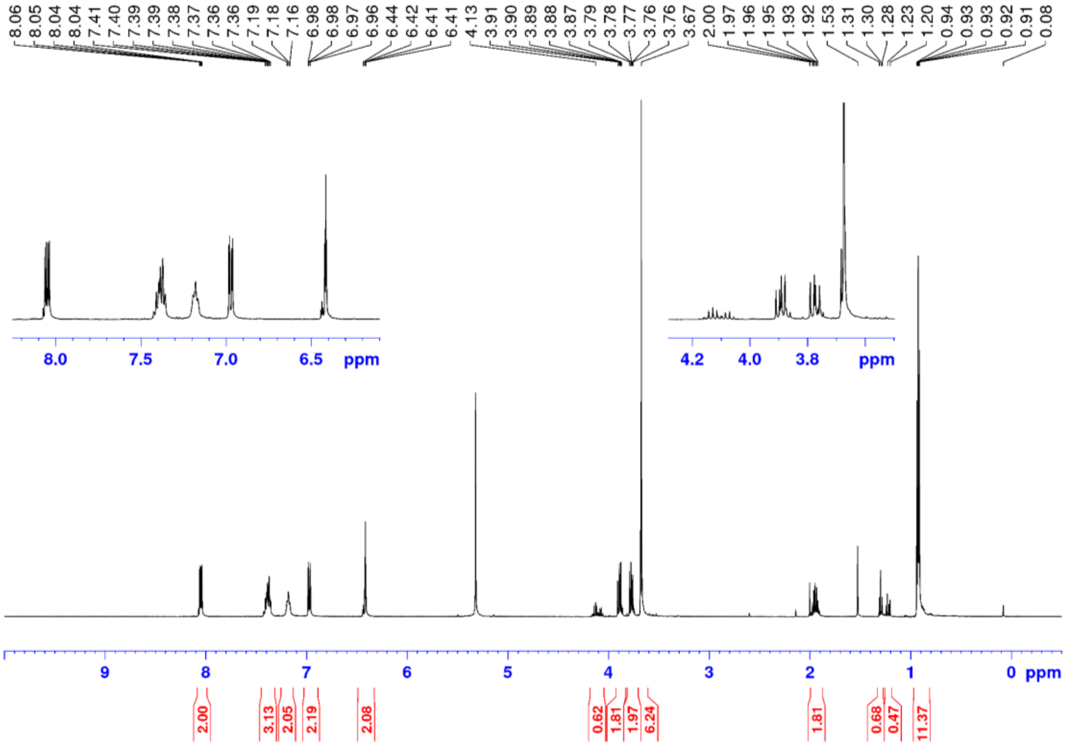

2b-^{i}Bu. 2b-^{i}Bu was synthesized analogously to **1a-^{i}Bu** from **6b-^{i}Bu** (3.5 g, 10 mmol) and $PPhCl_2$ (0.67 mL, 5.0 mmol). The volatiles were removed under vacuum, and the resulting yellow oil was taken up in H_2O (50 mL) and extracted with ethyl acetate (3 × 50 mL). The combined organic fractions were washed with brine (10 mL) and dried over $MgSO_4$, and the volatiles were removed under vacuum to yield a yellow solid. The crude product was purified by silica gel chromatography using a 3/1 hexanes/ethyl acetate mixture as the eluent. The product was isolated as a white solid (2.4 g, 73 %). $^{31}P\{^1H\}$ NMR (CD_2Cl_2): δ -8.4. ^1H NMR (CD_2Cl_2): δ 7.58 (d, $^4J_{PH}$ = 3, 2H, H^3), 7.38-7.36 (m, 3H, H^9 and H^{10}), 7.17 (t, $^3J_{PH} = {}^3J_{HH}$ = 7, 2H, H^8), 6.38 (d, $^3J_{PH}$ = 2, 2H, H^6), 3.96 (dd, $^2J_{HH}$ = 9, $^3J_{HH}$ = 7, 2H, H^{13}), 3.92 (s, 6H, H^{11}), 3.84 (dd, $^2J_{HH}$ = 9, $^3J_{HH}$ = 7, 2H, $H^{13'}$), 3.46 (s, 6H, H^{12}), 1.98 (sept, $^3J_{HH}$ = 7, 2H, H^{14}), 0.95 and 0.94 (d, $^3J_{HH}$ = 6, 12H, H^{15} and $H^{15'}$). $^{13}C\{^1H\}$ NMR (CD_2Cl_2): δ 152.6 (d, $^3J_{PC}$ = 1, C^5), 149.5 (s, C^4), 138.2 (d, $^1J_{PC}$ = 14, C^7), 134.0 (d, $^2J_{PC}$ = 22, C^8), 132.4 (d, $^2J_{PC}$ = 26, C^2), 131.5 (d, $^1J_{PC}$ = 32, C^1), 129.5 (s, C^{10}), 129.0 (d, $^3J_{PC}$ = 7, C^9), 118.5 (s, C^6), 114.1 (d, $^3J_{PC}$ =4, C^3), 77.2 (d, $^5J_{PC}$ = 3, C^{13}), 56.6 (s, C^{11}), 56.0 (s, C^{12}), 28.5 (s, C^{14}), 19.0 and 18.9 (s, C^{15} and $C^{15'}$). HRMS (APCI/ESI-Mixed mode; *m*/*z*): Calcd. for $[C_{30}H_{39}O_{10}PS_2 + H]^+$ 655.1801, Found: 655.1826.

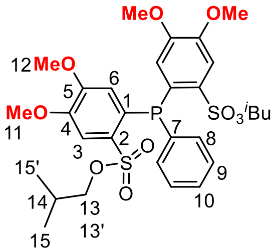

Figure 2.23. NMR spectra of **2b-^{i}Bu**

(a) $^{31}P\{^{1}H\}$ (CD_2Cl_2, 202 MHz):

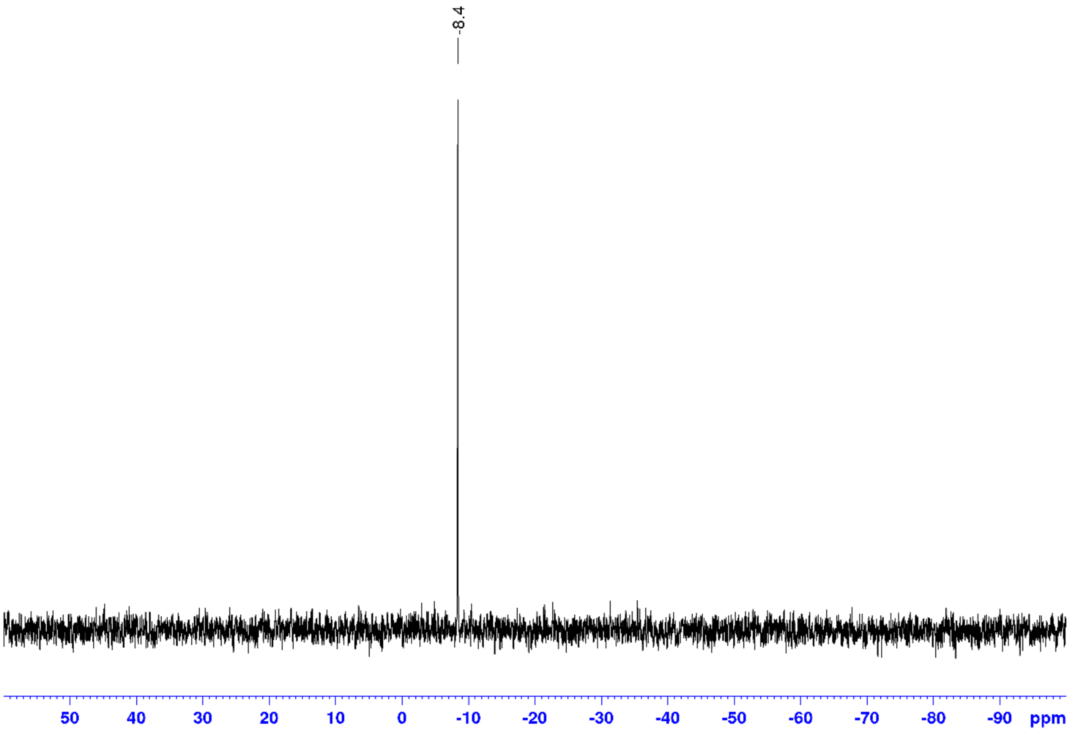

(b) ^{1}H (CD_2Cl_2, 500 MHz):

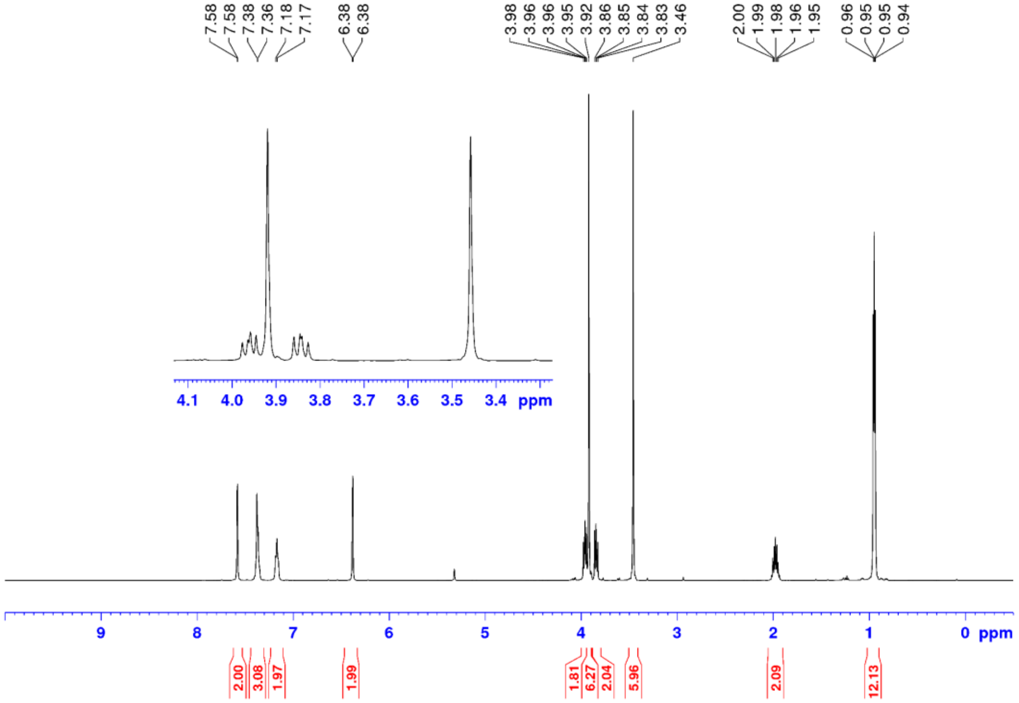

Figure 2.23, continued.

(c) ^{13}C{^{1}H} (CD_2Cl_2, 125 MHz):

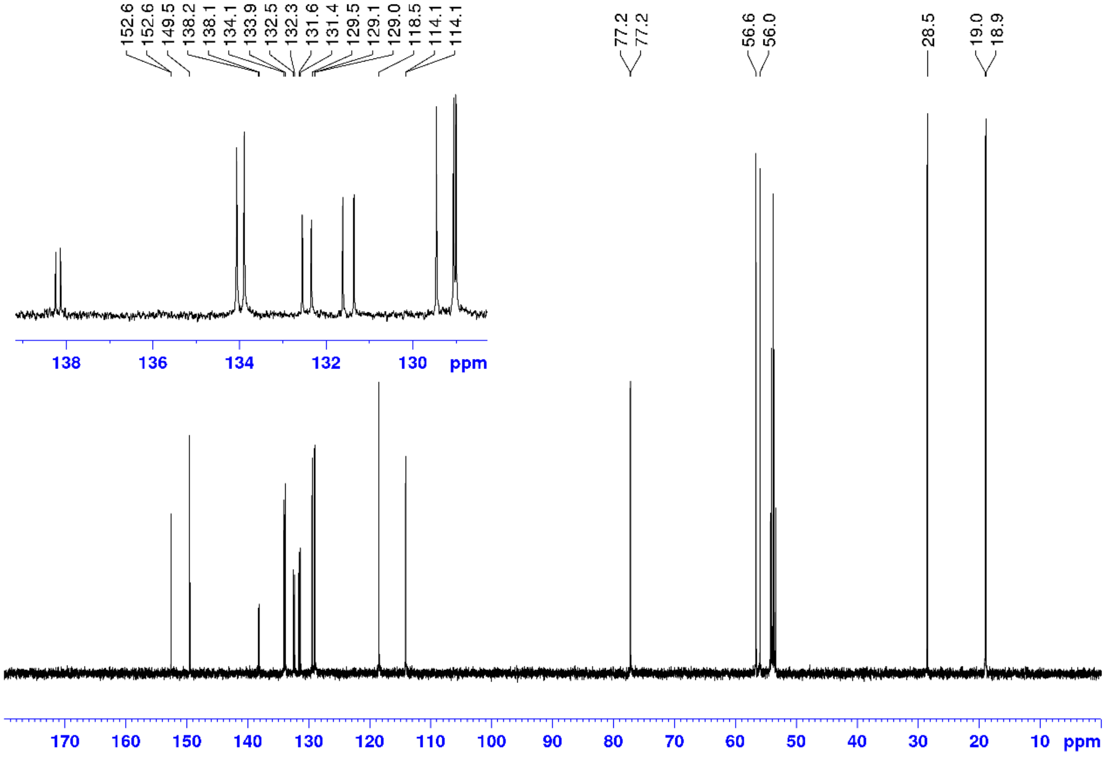

2c-^{i}Bu. 2c-^{i}Bu was synthesized analogously to **1a-^{i}Bu** from **6c-^{i}Bu** (2.3 g, 6.0 mmol) and $PPhCl_2$ (0.41 mL, 3.0 mmol). The volatiles were removed under vacuum, and the resulting yellow oil was taken up in H_2O (50 mL) and extracted with ethyl acetate (3 × 50 mL). The combined organic fractions were washed with brine (10 mL) and dried over $MgSO_4$, and the volatiles were removed under vacuum to yield a yellow solid. The crude product was purified by silica gel chromatography using a 3/1 hexanes/ethyl acetate mixture as the eluent. The product was isolated as a white solid (0.96 g, 45 %). ^{31}P{^{1}H} NMR (CD_2Cl_2): δ 6.2. ^{1}H NMR (CD_2Cl_2): δ 7.41 (br, 5H, H^8, H^9 and H^{10}), 6.23 (br, 2H, H^6), 3.97 (s, 6H, H^{11}), 3.85 (s, 8H, H^{12} and H^{14}), 3.78 (dd, $^{2}J_{HH}$ = 9, $^{3}J_{HH}$ = 7, 2H, $H^{14'}$), 3.46 (br, 6H, H^{13}), 1.91 (sept, $^{3}J_{HH}$ = 7, 2H, H^{15}), 0.88 (d, $^{3}J_{HH}$ = 6, 12H, H^{16}). ^{13}C{^{1}H} NMR (CD_2Cl_2): δ 157.1 (d, J_{PC} = 1), 154.7 (d, J_{PC} = 3), 149.2, 139.2 (d, J_{PC} = 19), 138.0, 137.7, 135.0, 129.8, 129.2, 114.1, 77.0 (d, J_{PC} = 1), 62.2, 61.0 (d, J_{PC} = 1), 55.8, 28.5, 18.8. HRMS (APCI mode; *m*/*z*): Calcd. for $[C_{32}H_{43}O_{12}PS_2 + H]^+$ 715.2011, Found: 715.2022.

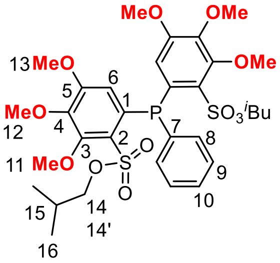

Figure 2.24. NMR spectra of **2c-^{i}Bu**

(a) $^{31}P\{^1H\}$ (CD_2Cl_2, 202 MHz):

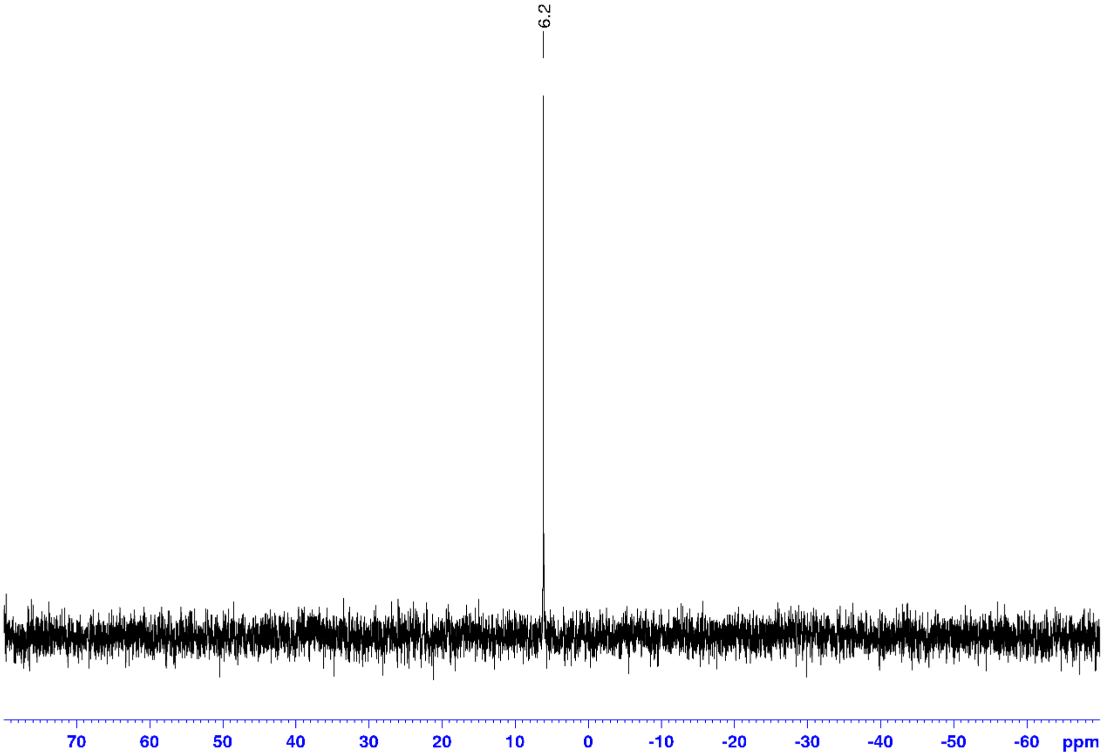

Figure 2.24, continued.

(b) ^{1}H (CD$_2$Cl$_2$, 500 MHz): δ 0.08 = grease

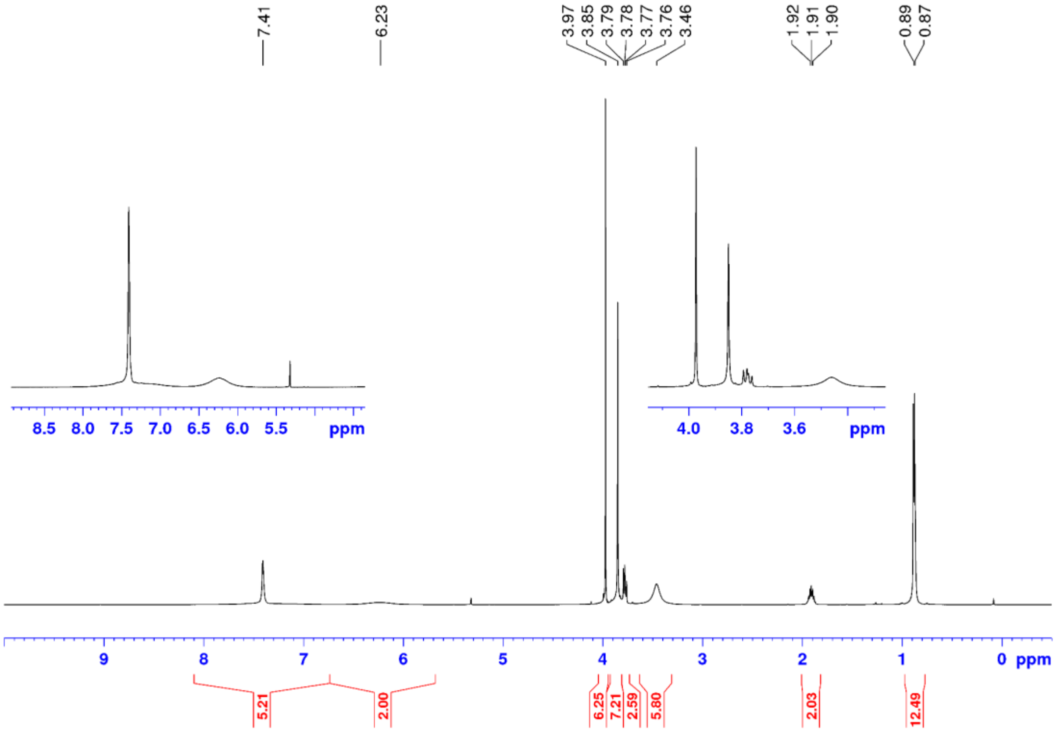

(c) ^{13}C{^{1}H} (CD$_2$Cl$_2$, 125 MHz):

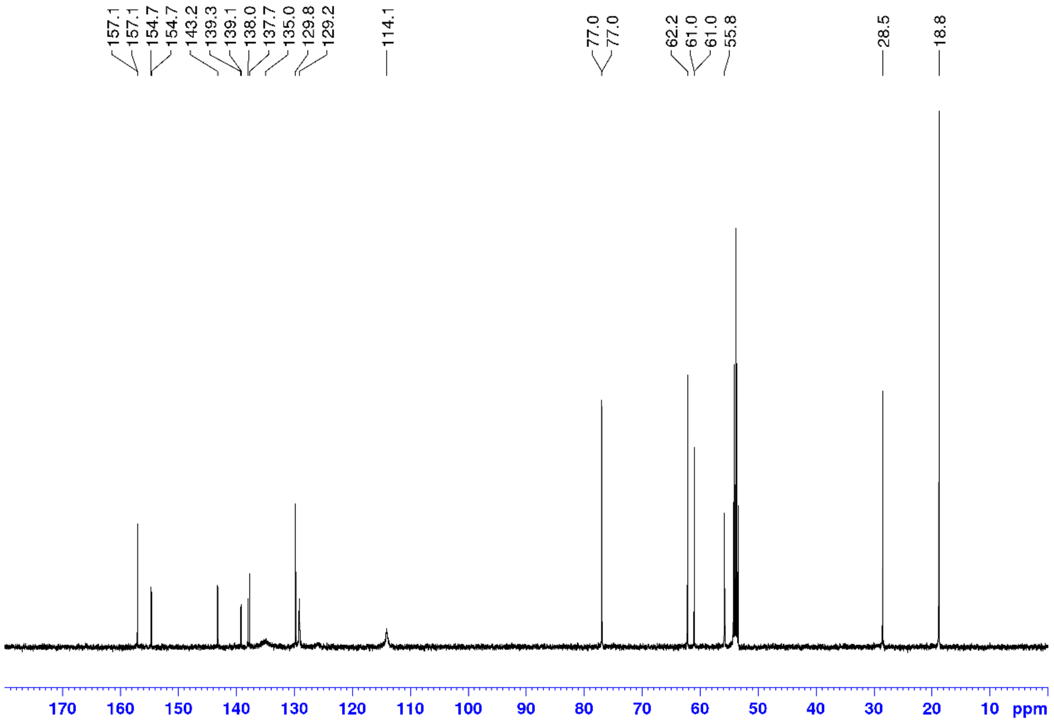

Na[1a]. A flask was charged with **1a-^{i}Bu** (0.72 g, 1.5 mmol), NaI (0.64 g, 4.0 mmol) and CH_3CN (20 mL). CH_2Cl_2 (15 mL) was added to afford a clear solution. The mixture was stirred at room temperature for 2 d to afford a white suspension, which was filtered to afford **Na[1a]** as a white powder. The product was dried under vacuum for 18 h (0.39 g, 57 %). $^{31}P\{^1H\}$ NMR (CD_3OD): δ -28.4. ^1H NMR (CD_3OD): δ 8.02 (dd, $^3J_{HH}$ = 8, $^4J_{PH}$ = 4, 1H, H^3), 7.30 (t, $^3J_{HH}$ = 8; 2H, H^{10}), 6.93 (dd, $^3J_{HH}$ = 8, $^4J_{PH}$ =5, 2H, H^9), 6.91 (dd, $^3J_{HH}$ = 9, $^4J_{HH}$ = 3, 1H, H^4), 6.80 (t, $^3J_{HH}$ = 8, 2H, H^{11}), 6.60 (br, 2H, H^{12}), 6.47 (t, $^3J_{PH}$ = $^4J_{HH}$ = 3, 1H, H^6), 3.69 (s, 6H, H^{14}), 3.56 (s, 3H, H^{13}). $^{13}C\{^1H\}$ NMR (CD_3OD): δ 162.4 (d, $^2J_{PC}$ = 16, C^8), 161.8 (s, C^5), 143.2 (d, $^1J_{PC}$ = 27, C^1), 138.2 (d, $^2J_{PC}$ = 23, C^2), 134.8 (s, C^{12}), 131.1 (s, C^{10}), 130.5 (d, $^3J_{PC}$ = 5, C^3), 127.0 (d, $^1J_{PC}$ =14, C^7), 122.3 (s, C^6), 121.9 (s, C^{11}), 113.8 (s, C^4), 111.5 (s, C^9), 56.0 (s, C^{14}), 55.5 (s, C^{13}). HRMS (ESI mode; *m*/*z*): Calcd. for $[C_{21}H_{20}NaO_6PS + Cl]^-$ 489.0304, Found: 489.0325.

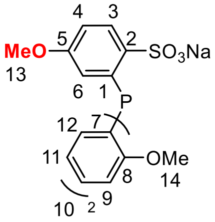

Figure 2.25. NMR spectra of **Na[1a]**

(a) $^{31}P\{^1H\}$ (CD_3OD, 202 MHz):

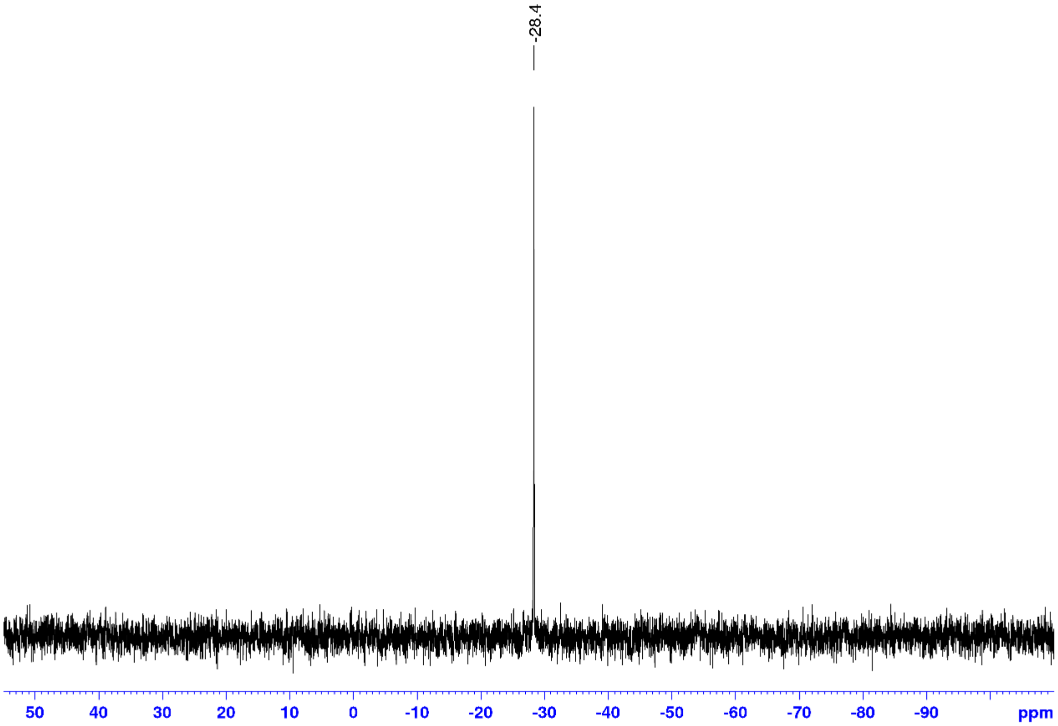

(b) ^1H (CD_3OD, 500 MHz): δ 4.88 = H_2O; 2.04 = CH_3CN

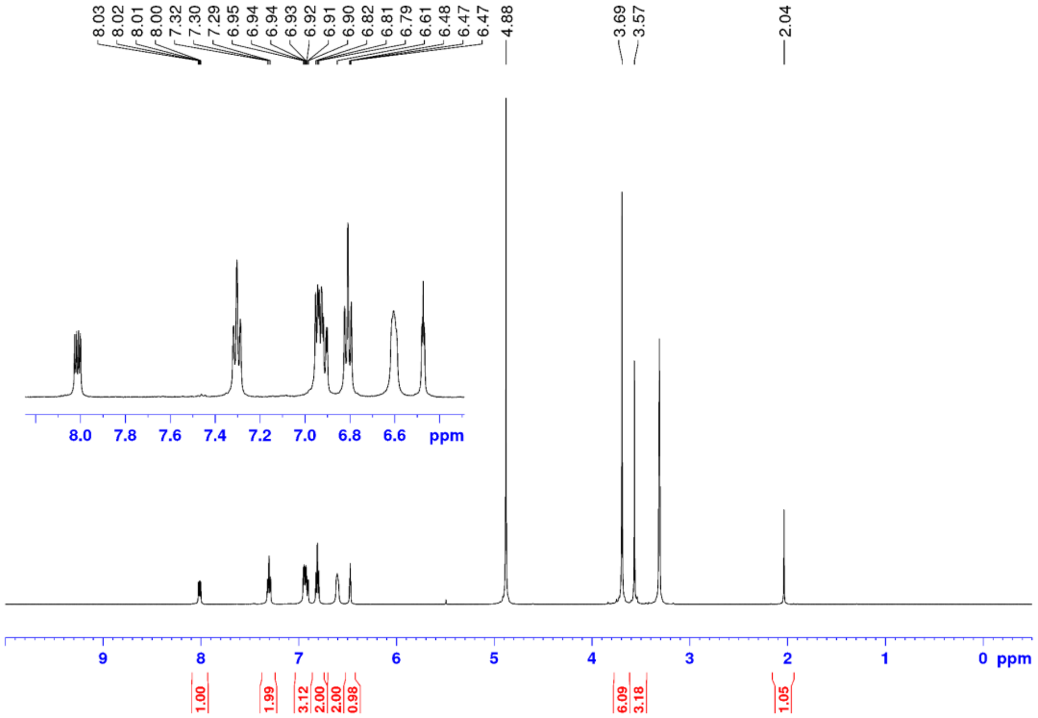

Figure 2.25, continued.

(c) $^{13}C\{^1H\}$ (CD_3OD, 125 MHz): δ 0.8 = CH_3CN

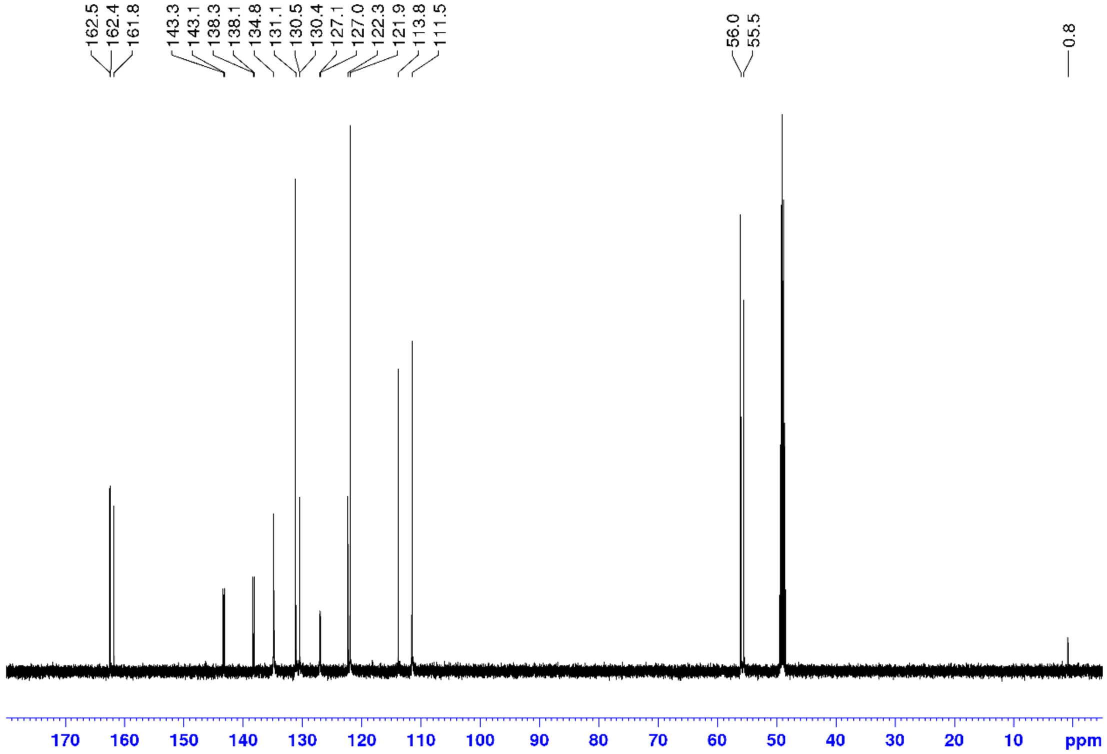

Na[1b]. Na[1b] was synthesized analogously to **Na[1a]** from **1b-*i*Bu** (0.36 g, 0.70 mmol), NaI (0.450 g, 3.0 mmol) and CH_3CN (5 mL). The mixture was stirred at room temperature for 2 d to afford a white suspension, which was filtered to afford **Na[1b]** as a white powder. The product was dried under vacuum for 18 h (0.29 g, 85 %). $^{31}P\{^1H\}$ NMR (CD_3OD): δ -27.7. ^1H NMR (CD_3OD): δ 7.68 (d, $^4J_{PH}$ = 4, 1H, H^3), 7.29 (t, $^3J_{HH}$ = 8, 2H, H^{10}), 6.93 (dd, $^3J_{HH}$ = 8, $^4J_{PH}$ = 4, 2H, H^9), 6.81 (t, $^3J_{HH}$ = 8, 2H, H^{11}), 6.64 (br, 2H, H^{12}), 6.46 (d, $^3J_{PH}$ = 2, 1H, H^6), 3.89 (s, 3H, H^{13}), 3.69 (s, 6H, H^{15}), 3.36 (s, 3H, H^{14}). $^{13}C\{^1H\}$ NMR (CD_3OD): δ 162.5 (d, $^2J_{PC}$ = 16, C^8), 150.9 (s, C^5), 149.9 (s, C^4), 144.5 (d, $^2J_{PC}$ = 29, C^2), 134.8 (s, C^{12}), 130.9 (s, C^{10}), 128.1 (d, $^1J_{PC}$ =11, C^7), 128.0 (d, $^1J_{PC}$ = 23, C^1), 121.8 (s, C^{11}), 119.2 (s, C^6), 112.6 (s, C^3), 111.4 (s, C^9), 56.4 (s, C^{13}), 56.0 (s, C^{15}), 55.9 (s, C^{14}). HRMS (ESI mode; *m/z*): Calcd. for $[C_{22}H_{22}NaO_7PS + Cl]^-$ 519.0410, Found: 519.0430.

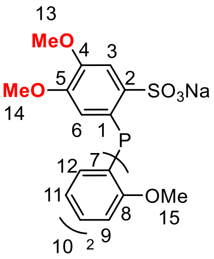

Figure 2.26. NMR spectra of **Na[1b]**

(a) $^{31}P\{^1H\}$ (CD_3OD, 202 MHz):

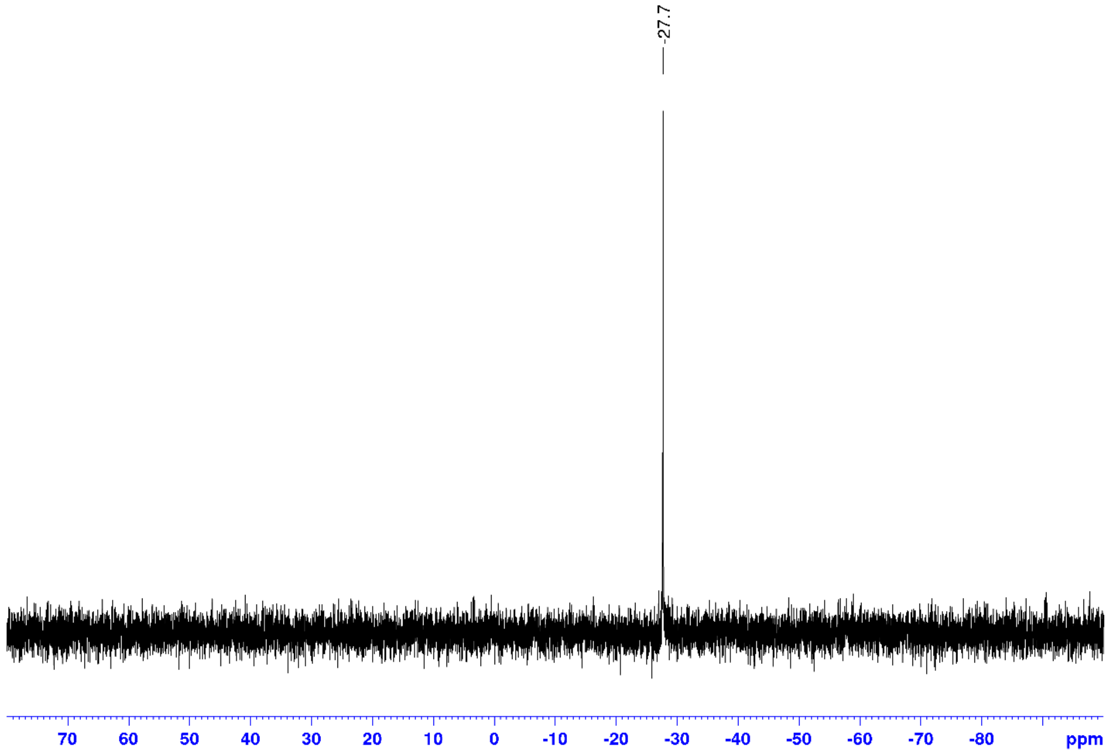

Figure 2.26, continued.

(b) ^1H (CD_3OD, 500 MHz): δ 4.88 = H_2O; 2.16 = acetone; 2.04 = CH_3CN

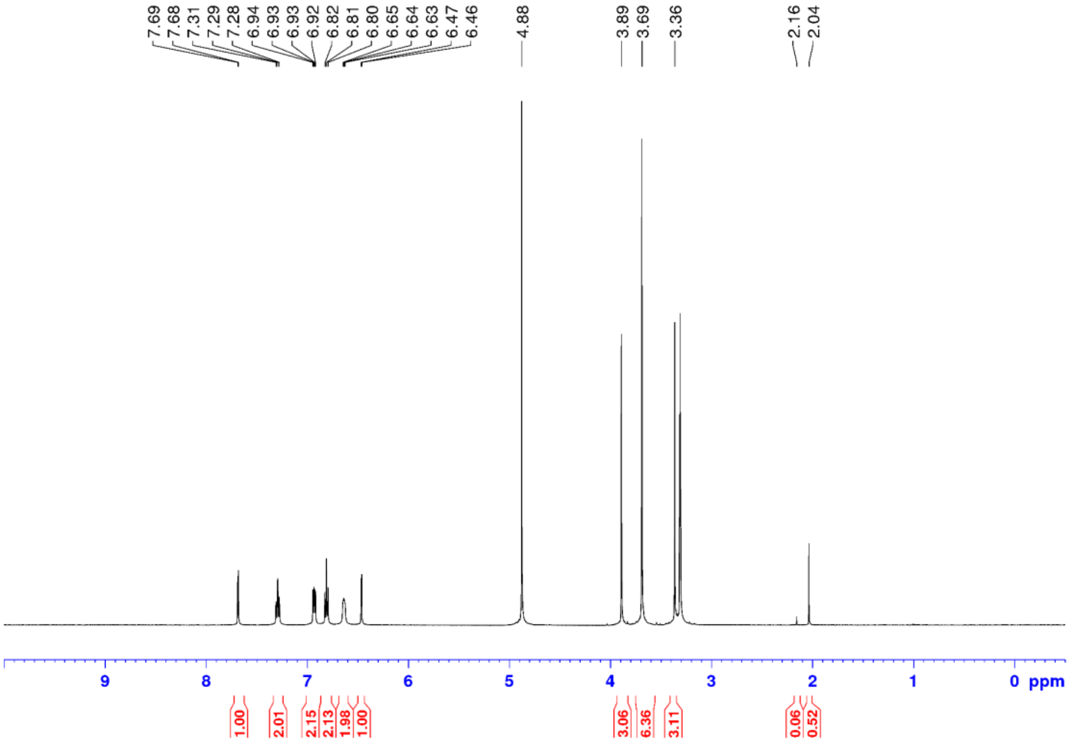

(c) $^{13}C\{^1H\}$ (CD_3OD, 125 MHz):

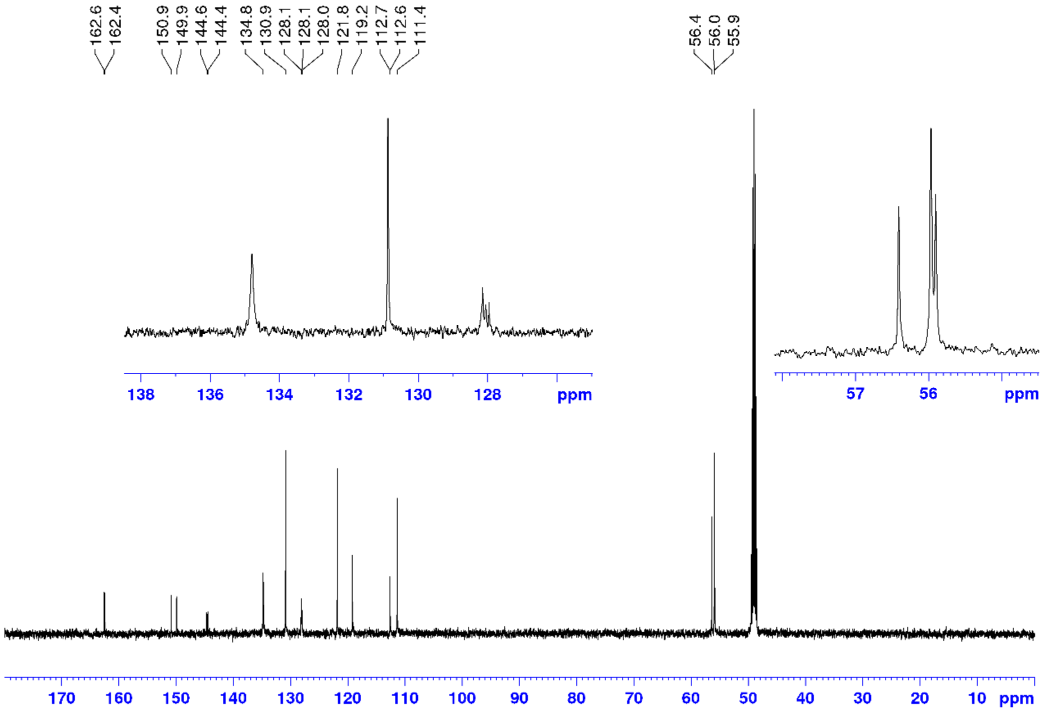

Li[1c]. A vial was charged with **1c-^{i}Bu** (0.31 g, 0.60 mmol), LiI (0.35 g, 2.6 mmol) and CH_3CN (10 mL), and covered with aluminum foil. The mixture was stirred at room temperature for 4 d. The volatiles were removed under vacuum. THF was added to afford a white suspension, which was filtered to afford **Li[1c]** as a white powder. The product was dried under vacuum for 18 h (0.14 g, 52 %). $^{31}P\{^{1}H\}$ NMR (CD_3OD): δ -22.7. ^{1}H NMR (CD_3OD): δ 7.29 (t, $^{3}J_{HH}$ = 8, 2H, H^{10}), 6.93 (dd, $^{3}J_{HH}$ = 8, $^{4}J_{PH}$ = 5, 2H, H^{9}), 6.82 (t, $^{3}J_{HH}$ = 7, 2H, H^{11}), 6.68 (br, 2H, H^{12}), 6.27 (d, $^{3}J_{PH}$ = 2, 1H, H^{6}), 3.97 (s, 3H, H^{13}), 3.84 (s, 3H, H^{14}), 3.70 (s, 6H, H^{16}), 3.32 (s, 3H, H^{15}). ESI-MS (1/1 CH_3OH/H_2O; *m/z*): Calcd. for $[C_{23}H_{24}O_8PS + 2H]^+$ 493.1, Found: 493.2; Calcd. for $[C_{23}H_{24}O_8PS]^-$ 491.1, Found: 491.3.

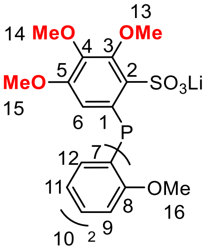

Figure 2.27. NMR spectra of **Li[1c]**

(a) $^{31}P\{^1H\}$ (CD_3OD, 202 MHz):

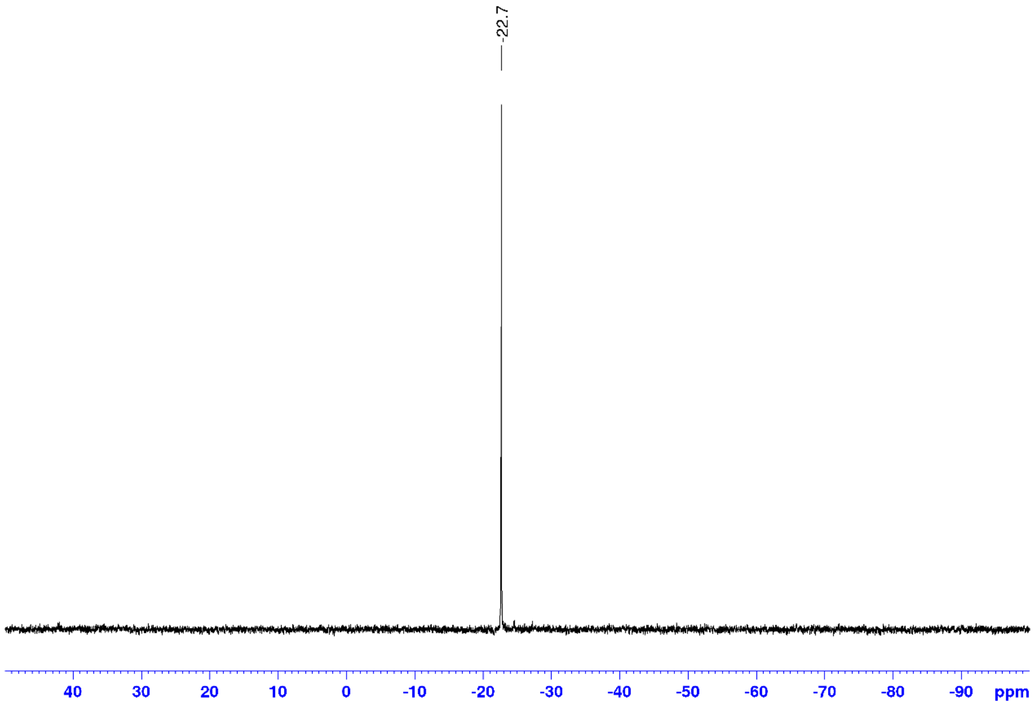

(b) ^1H (CD_3OD, 500 MHz): δ 4.88 = H_2O; 3.73 and 1.87 = THF; 2.16 = acetone

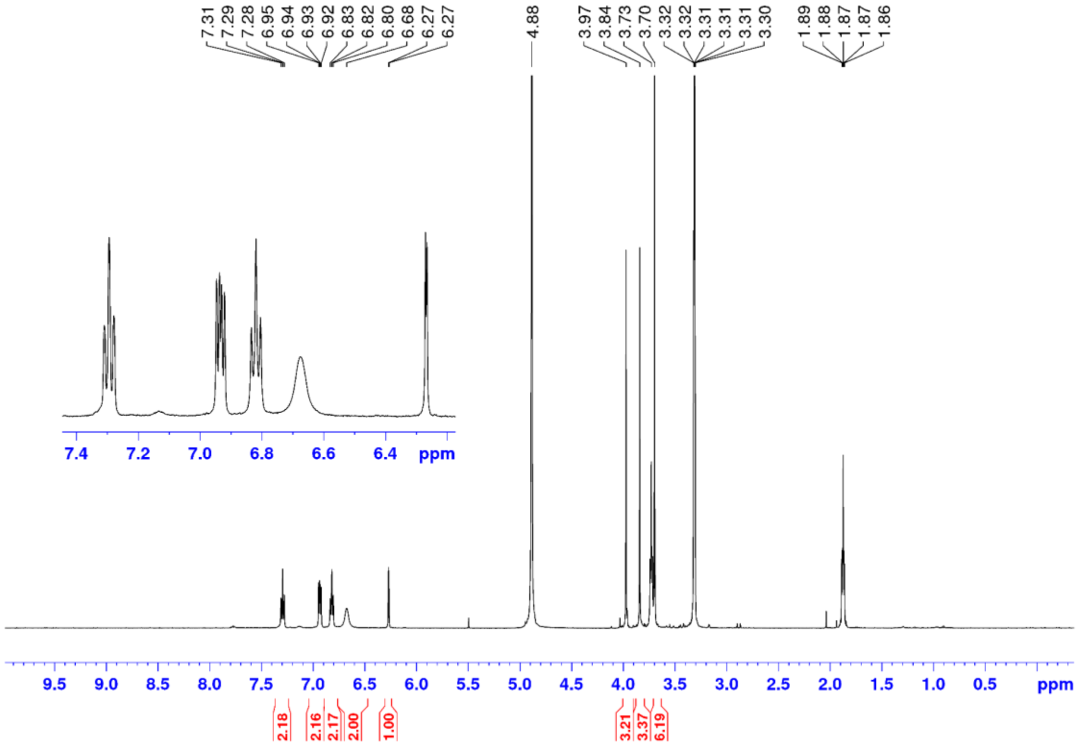

Na[1d]. Na[1d] was synthesized analogously to **Na[1a]** from **1d-^{i}Bu** (0.57 g, 1.2 mmol), NaI (0.57 g, 3.6 mmol) and CH_3CN (15 mL). The mixture was stirred at room temperature for 2 d to afford a white suspension, which was filtered to afford **Na[1d]** as a white powder. The product was dried under vacuum for 18 h (398 mg, 78 %). $^{31}P\{^{1}H\}$ NMR (CD_3OD): δ -9.9. ^{1}H NMR (CD_3OD): δ 7.69 (d, $^{4}J_{PH}$ = 4, 1H, H^3), 7.30-7.25 (m, 6H, H^9 and H^{10}), 7.24 (m, 4H, H^8), 6.53 (d, $^{3}J_{PH}$ = 3, 1H, H^6), 3.89 (s, 3H, H^{11}), 3.42 (s, 3H, H^{12}). $^{13}C\{^{1}H\}$ NMR (CD_3OD): δ 151.0 (s, C^5), 150.2 (s, C^4), 144.7 (d, $^{2}J_{PC}$ = 28, C^2), 140.4 (d, $^{1}J_{PC}$ =28, C^7), 134.6 (d, $^{2}J_{PC}$ = 20, C^8), 129.3 (s, C^{10}), 129.2 (d, $^{3}J_{PC}$ = 2, C^9), 128.1 (d, $^{1}J_{PC}$ = 25, C^1), 119.7 (s, C^6), 112.6 (d, $^{3}J_{PC}$ = 6, C^3), 56.4 (s, C^{11}), 56.0 (s, C^{12}). HRMS (ESI mode; *m*/*z*): Calcd. for $[C_{20}H_{18}O_5PSNa + Cl]^-$ 459.0199, Found: 459.0218.

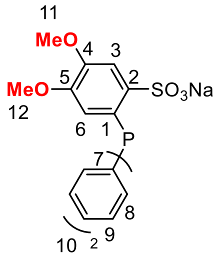

Figure 2.28. NMR spectra of **Na[1d]**

(a) $^{31}P\{^{1}H\}$ (CD_3OD, 202 MHz):

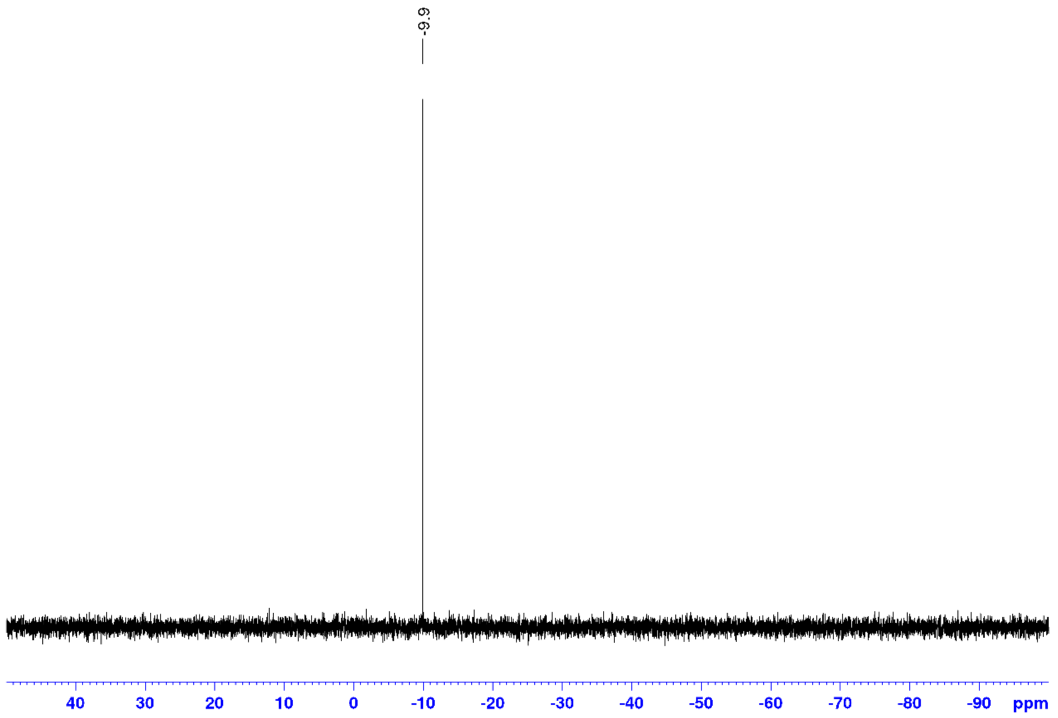

(b) ^{1}H (CD_3OD, 500 MHz): δ 4.88 = H_2O; 0.10 = grease

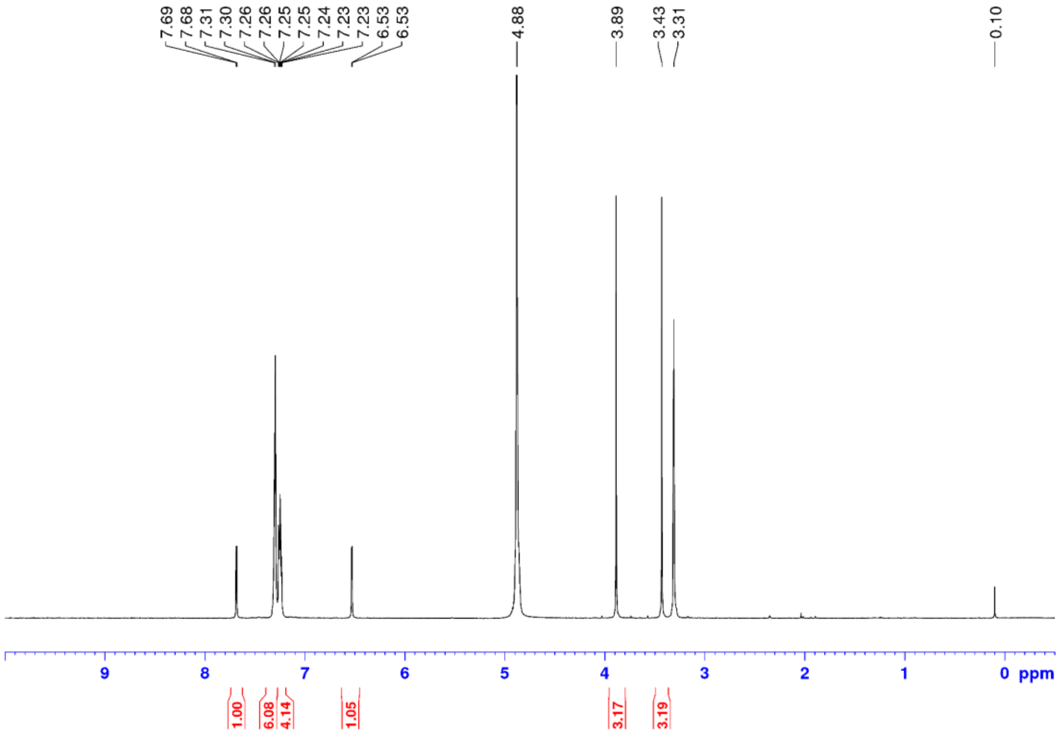

Figure 2.28, continued.

(c) $^{13}C\{^1H\}$ (CD_3OD, 125 MHz):

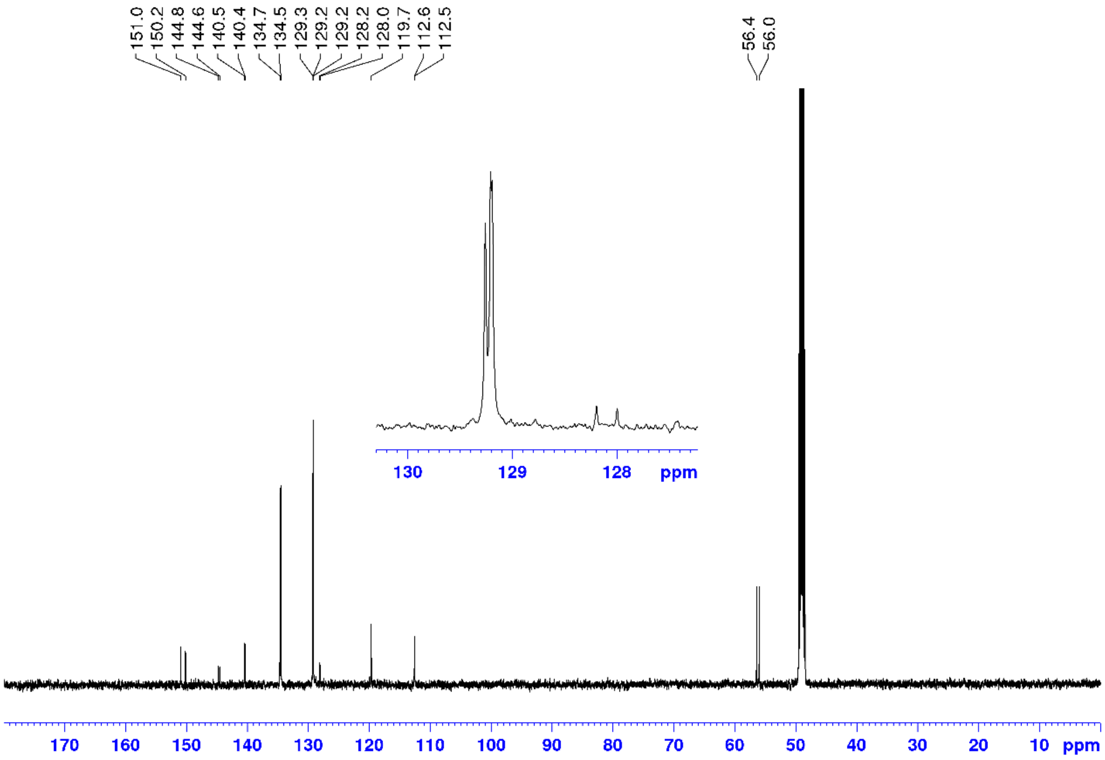

Li_2[2a]. A vial was charged with **2a-^{i}Bu** (1.4 g, 2.3 mmol), LiI (1.0 g, 7.5 mmol) and CH_3CN (10 mL), and covered with aluminum foil. The mixture was stirred at room temperature for 2 d to afford a white suspension, which was filtered to afford **Li_2[2a]** as a white powder. The product was dried under vacuum for 18 h (0.98 mg, 86 %).$^{31}P\{^1H\}$ NMR (CD_3OD): δ -11.7. ^1H NMR (CD_3OD): δ 7.98 (dd, $^3J_{HH}$ = 8, $^4J_{PH}$ = 4, 2H, H^3), 7.28 (s, 3H, H^9 and H^{10}), 7.15 (s, 2H, H^8), 6.92 (dd, $^3J_{HH}$ = 8, $^5J_{PH}$ = 2, 2H, H^4), 6.42 (s, 2H, H^6), 3.60 (s, 6H, H^{11}). $^{13}C\{^1H\}$ NMR (CD_3OD): δ 161.9 (s, $^3J_{PC}$ =4, C^5), 142.0 (d, $^2J_{PC}$ = 26, C^2), 140.2 (d, $^1J_{PC}$ = 15, C^7), 139.4 (d, $^1J_{PC}$ = 28, C^1), 134.9 (d, $^2J_{PC}$ = 20, C^8), 130.8 (d, $^3J_{PC}$ =5, C^3), 129.1 (d, $^3J_{PC}$ = 2, C^9), 129.1 (s, C^{10}), 122.7 (s, C^4), 113.7 (s, C^6), 55.6 (s, C^{11}). ESI-MS (1/1 CH_3OH/H_2O; *m/z*): Calcd. for $[C_{20}H_{17}O_8PS_2 + 3H]^+$ 483.0, Found: 483.1; Calcd. for $[C_{20}H_{17}O_8PS_2 + H]^-$ 481.0, Found: 481.1.

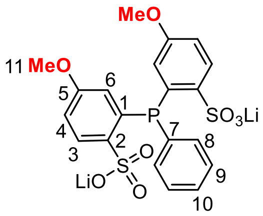

Figure 2.29. NMR spectra of **Li₂[2a]**

(a) $^{31}P\{^{1}H\}$ (CD_3OD, 202 MHz):

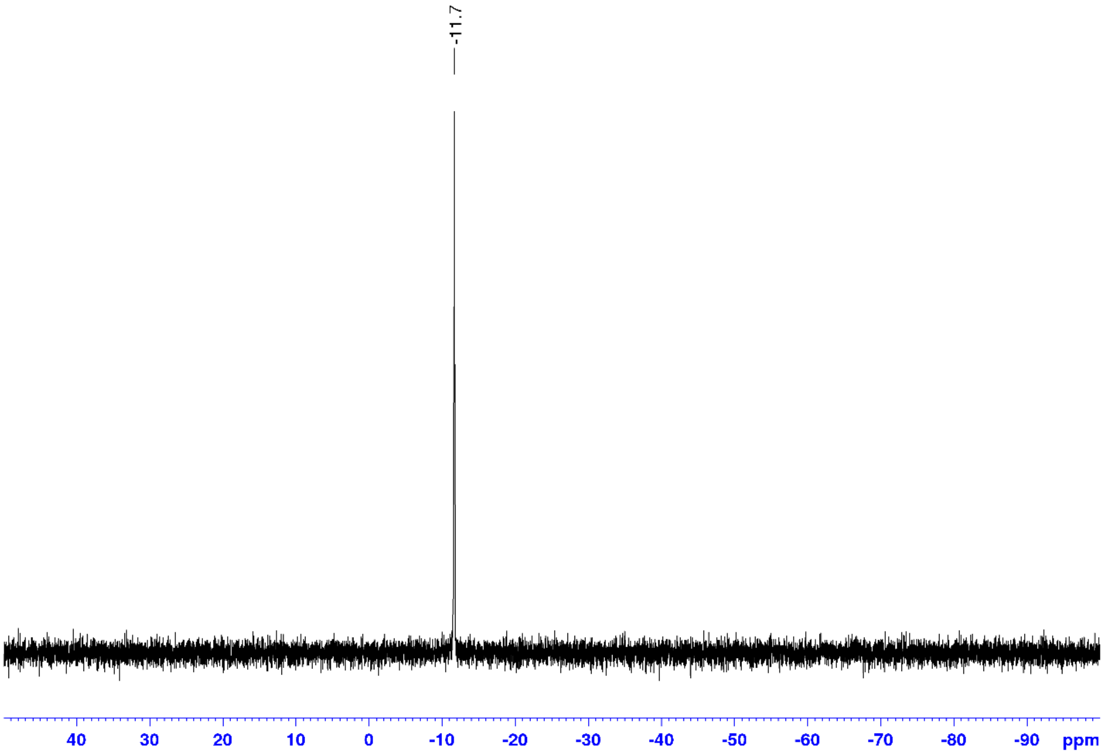

Figure 2.29, continued.

(b) ^{1}H (CD$_3$OD, 500 MHz): δ 4.88 = H_2O; 2.03 = CH_3CN

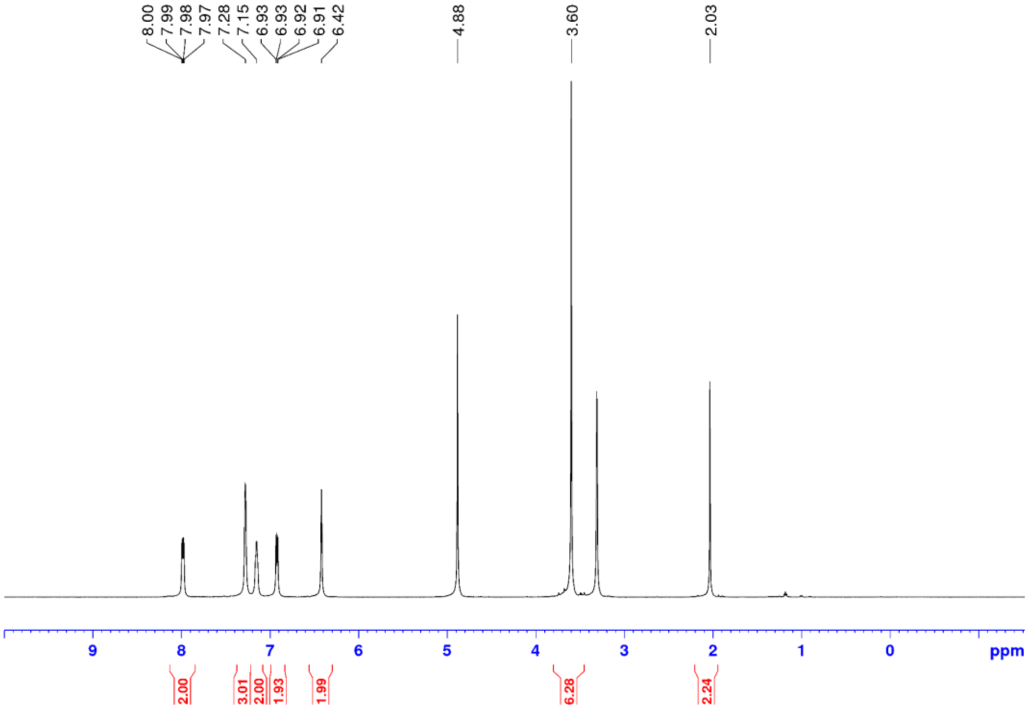

(c) ^{13}C{^{1}H} (CD$_3$OD, 125 MHz):

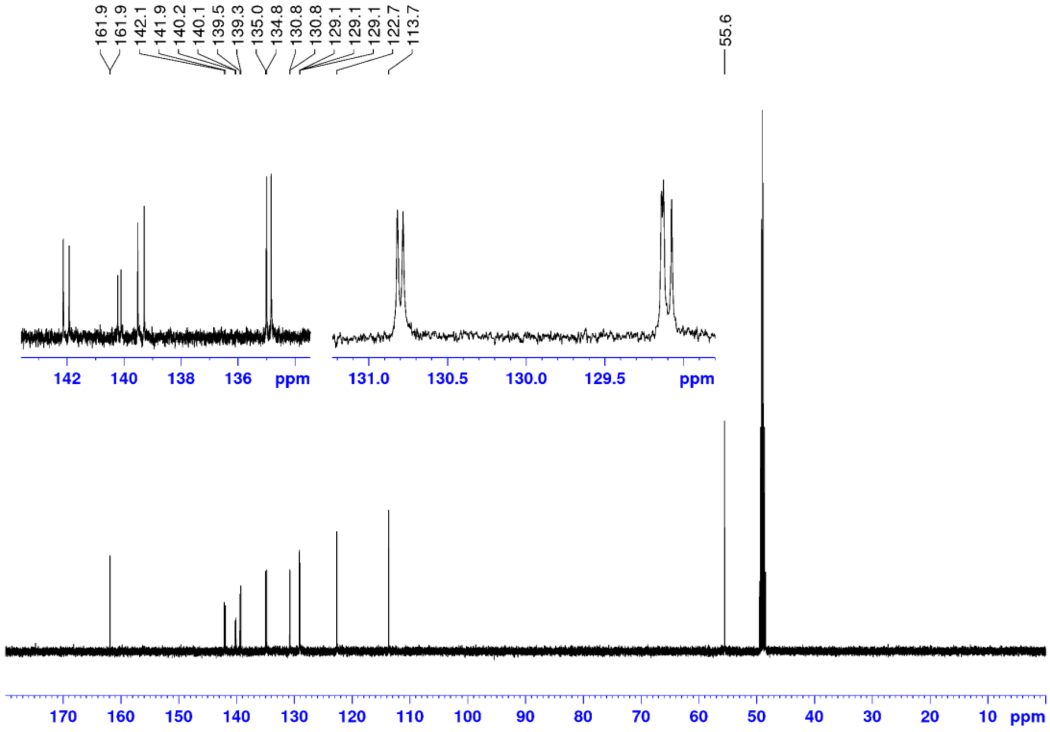

Li$_2$[2b]. **Li$_2$[2b]** was synthesized analogously to **Li$_2$[2a]** from **2b-^{i}Bu** (0.50 g, 0.80 mmol), LiI (0.60 g, 4.5 mmol) and CH_3CN (10 mL). **Li$_2$[2b]** was collected by filtration as a white powder and dried under vacuum for 18 h (0.30 g, 72 %). ^{31}P{^{1}H} NMR (CD_3OD): δ -13.2. ^{1}H NMR (CD_3OD): δ 7.65 (d, $^4J_{PH}$ = 4, 2H, H^3), 7.28-7.26 (m, 3H, H^9 and H^{10}), 7.17 (m, 2H, H^8), 6.46 (d, $^3J_{PH}$ = 2, 2H, H^6), 3.88 (s, 6H, H^{11}), 3.43 (s, 6H, H^{12}). ^{13}C{^{1}H} NMR (CD_3OD): δ 151.0 (s, C^5), 149.9 (s, C^4), 143.0 (d, $^2J_{PC}$ = 27, C^2), 141.4 (d, $^1J_{PC}$ = 15, C^7), 134.6 (d, $^2J_{PC}$ = 20, C^8), 129.3 (d, $^1J_{PC}$ = 27, C^1), 129.0 (d, $^3J_{PC}$ = 6, C^9), 128.9 (s, C^{10}), 119.5 (s, C^6), 112.9 (d, $^3J_{PC}$ =5, C^3), 56.4 (s, C^{11}), 56.0 (s, C^{12}). HRMS (ESI mode; *m/z*): Calcd. for $[C_{22}H_{21}Li_2O_{10}PS_2 + H]^+$ 555.0712, Found: 555.0690.

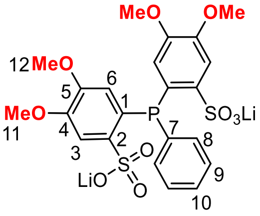

Figure 2.30. NMR spectra of **Li₂[2b]**

(a) $^{31}P\{^1H\}$ (CD_3OD, 202 MHz):

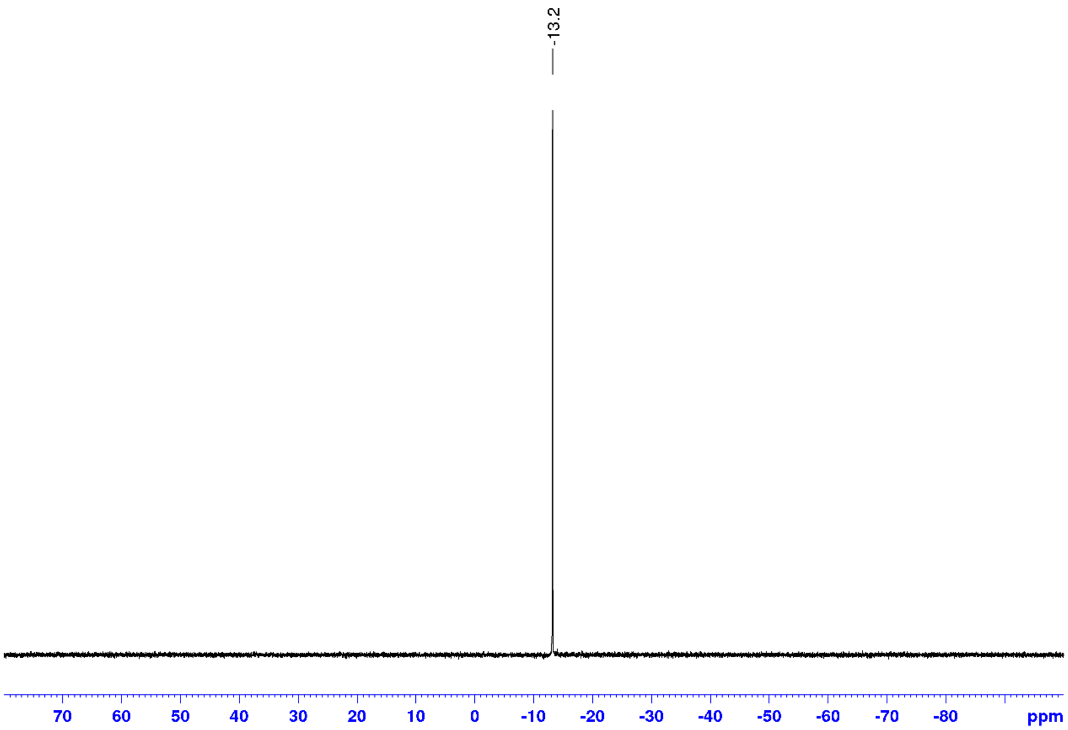

(b) ^1H (CD_3OD, 500 MHz): δ 4.88 = H_2O, 2.04 = CH_3CN

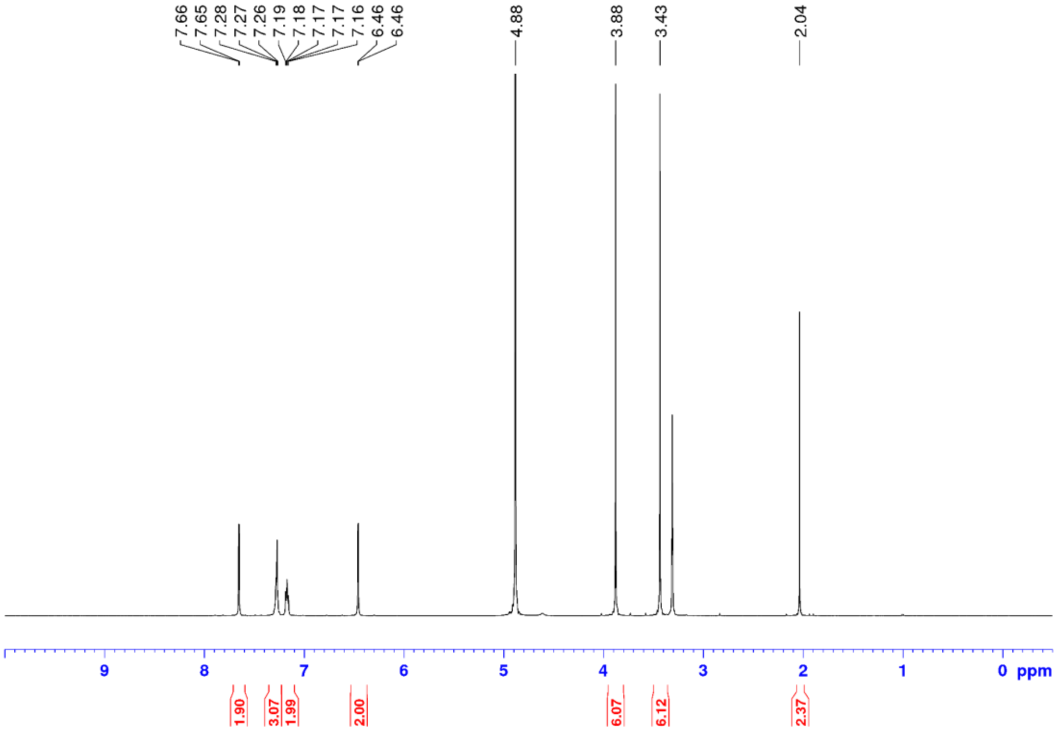

Figure 2.30, continued.

(c) $^{13}C\{^1H\}$ (CD_3OD, 125 MHz):

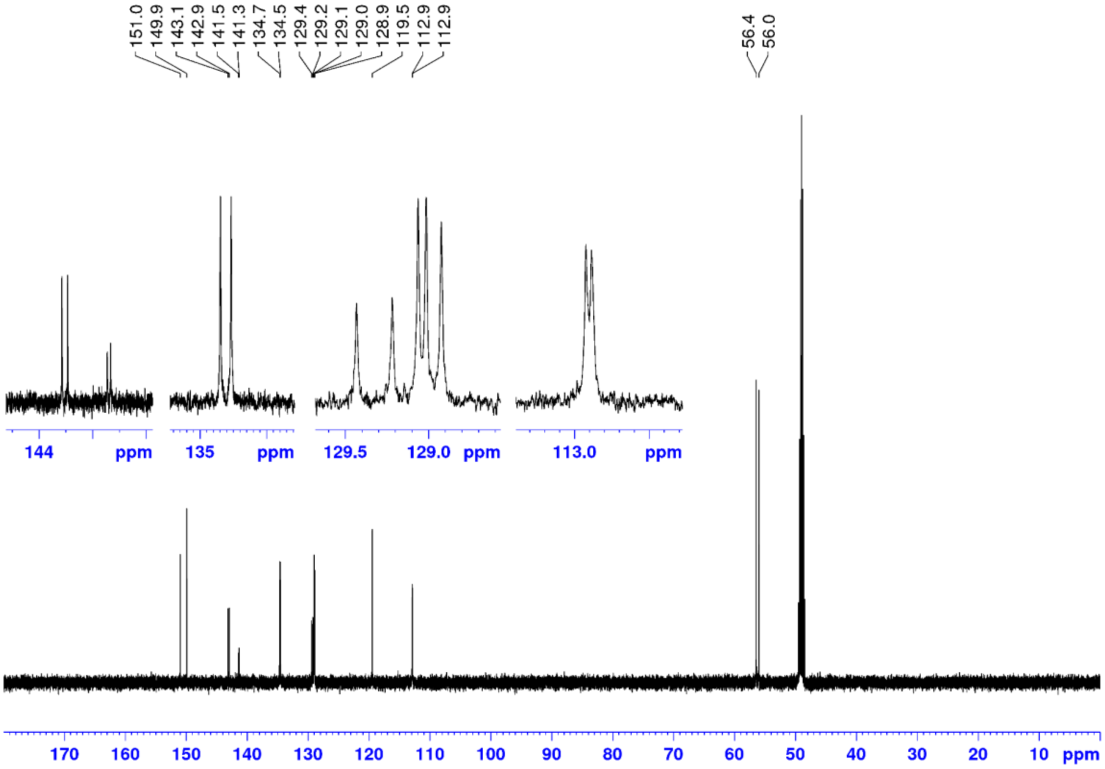

Li_2[2c]. Li_2[2c] was synthesized analogously to **Li_2[2a]** from **2c-^{i}Bu** (0.18 g, 0.30 mmol), LiI (0.10 mg, 0.70 mmol) and THF (5 mL). **Li_2[2c]** was collected by filtration as a white powder and dried under vacuum for 18 h (0.10 g, 66 %).$^{31}P\{^1H\}$ NMR (CD_3OD): δ 2.3. ^1H NMR (CD_3OD): δ 7.29 (m, 3H, H^9 and H^{10}), 7.22 (s, 2H, H^8), 6.24 (s, 2H, H^6), 3.94 (s, 6H, H^{11}), 3.83 (s, 6H, H^{12}) 3.40 (s, 6H, H^{13}). ESI-MS (1/1 CH_3OH/H_2O, *m/z*): Calcd. for $[C_{24}H_{25}O_{12}PS_2 + 3H]^+$ 603.1, Found: 603.2; Calcd. for $[C_{24}H_{25}O_{12}PS_2 + H]^-$ 601.1, Found: 601.2.

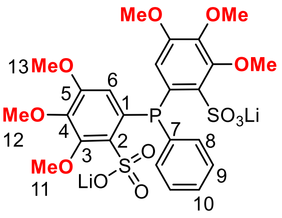

Figure 2.31. NMR spectra of **Li_2[2c]**

(a) $^{31}P\{^1H\}$ (CD_3OD, 202 MHz):

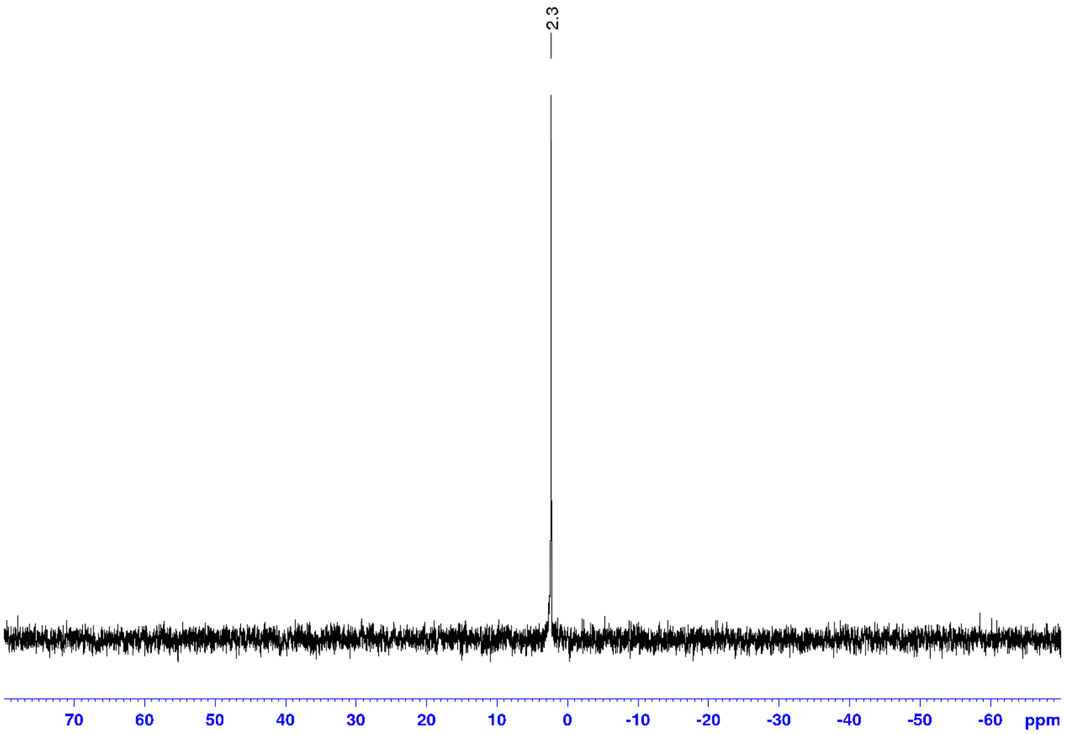

(b) ^1H (CD_3OD, 500 MHz): δ 4.88 = H_2O; 3.73 and 1.87 = THF

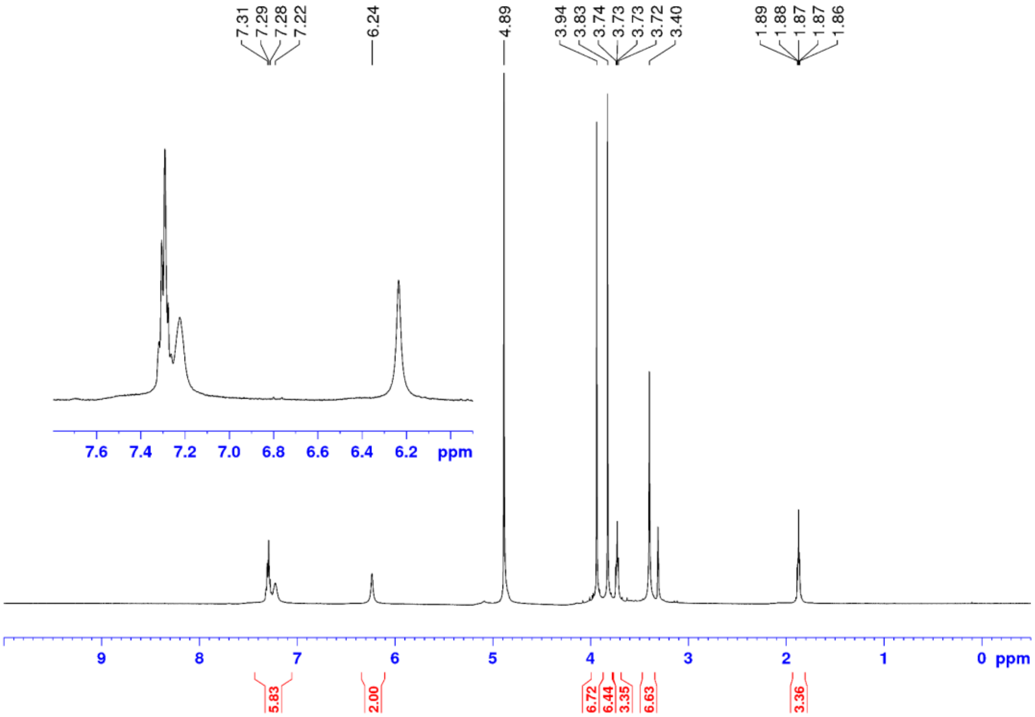

3a. A vial was charged with **Na[1a]** (0.14 g, 0.30 mmol), (COD)PdMeCl (80 mg, 0.30 mmol) and CH_2Cl_2 (6 mL), and the mixture was stirred at room temperature for 1h to afford a cloudy yellow solution. Pyridine (24 μL, 0.30 mmol) was added, and the mixture was stirred for 18 h, filtered through a Celite pipette, layered with pentane and cooled to -40 °C. After 1 d, colorless X-ray quality crystals formed. The crystals were collected by filtration and dried under vacuum for 18 h (0.11 g, 59 %). ^{31}P{^{1}H} NMR (CD_2Cl_2): δ 21.8. ^{1}H NMR (CD_2Cl_2): δ 8.76 (dd, $^{3}J_{HH}$ = 5, $^{4}J_{HH}$ = 2, 2H, H^{13}), 8.01 (dd, $^{3}J_{HH}$ = 9, $^{4}J_{PH}$ = 6, 1H, H^{3}), 7.88 (tt, $^{3}J_{HH}$ = 8, $^{4}J_{HH}$ = 1, 1H, H^{15}), 7.54 (t, $^{3}J_{HH}$ = 8, 2H, H^{10}), 7.48 (t, $^{3}J_{HH}$ = 7, 2H, H^{14}), 7.56-7.46 (br, overlap with H^{10} and H^{14}, 2H, H^{12}), 7.03 (t, $^{3}J_{HH}$ = 8, 2H, H^{11}), 6.99 (dd, $^{3}J_{HH}$ = 8, $^{4}J_{PH}$ =5, 2H, H^{9}), 6.95 (dd, $^{3}J_{HH}$ = 8, $^{4}J_{HH}$ = 2, 1H, H^{4}), 6.78 (dd, $^{3}J_{PH}$ = 12, $^{4}J_{HH}$ = 3, 1H, H^{6}), 3.71 (s, 6H, H^{17}), 3.67 (s, 3H, H^{16}), 0.26 (d, $^{3}J_{PH}$ = 3, 3H, Pd-C*H*$_3$). ^{13}C{^{1}H} NMR (CD_2Cl_2): δ 161.0 (d, $^{2}J_{PC}$ = 3, C^{8}), 159.8 (d, $^{3}J_{PC}$ = 9, C^{5}), 150.7 (s, C^{13}), 141.6 (d, $^{2}J_{PC}$ = 15, C^{2}), 138.7 (s, C^{15}), 137.8 (br, C^{12}), 133.6 (s, C^{10}), 129.8 (d, $^{3}J_{PC}$ = 9, C^{3}), 129.6 (d, $^{1}J_{PC}$ = 48, C^{1}), 125.5 (d, $^{4}J_{PC}$ =2, C^{14}), 121.3 (d, $^{2}J_{PC}$ = 3, C^{6}), 120.9 (d, $^{3}J_{PC}$ = 12, C^{11}), 116.5 (d, $^{1}J_{PC}$ =56, C^{7}),[21] 114.2 (s, C^{4}), 111.8 (d, $^{3}J_{PC}$ = 5, C^{9}), 55.8 (s, C^{17}), 55.7 (s, C^{16}), 0.3 (d, $^{2}J_{PC}$ = 4, Pd-*C*H$_3$). The broadening of the H^{12} and C^{12} resonances is due to fast exchange of the two anisyl rings. HRMS (ESI mode; *m*/*z*): Calcd. for $[C_{27}H_{28}NO_6PPdS + H]^+$ 632.0488, Found: 632.0492.

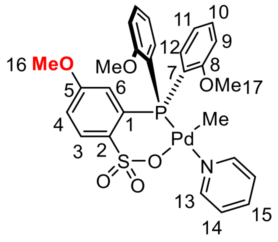

Figure 2.32. NMR spectra of **3a**

(a) $^{31}P\{^{1}H\}$ (CD_2Cl_2, 202 MHz):

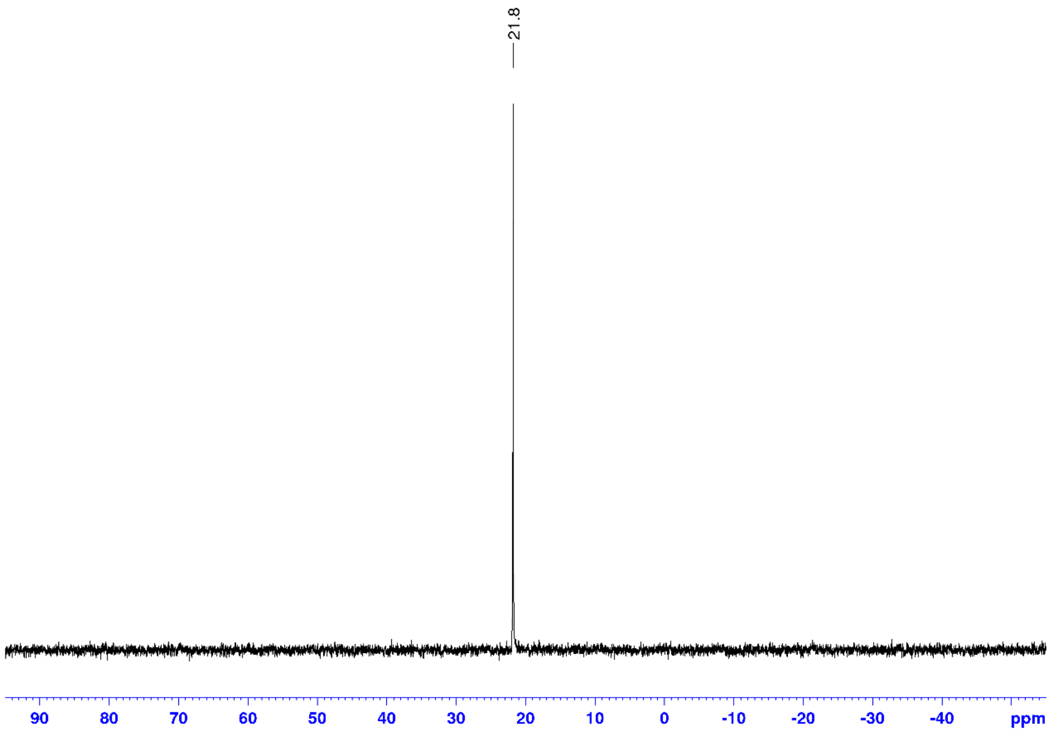

(b) ^{1}H (CD_2Cl_2, 500 MHz):

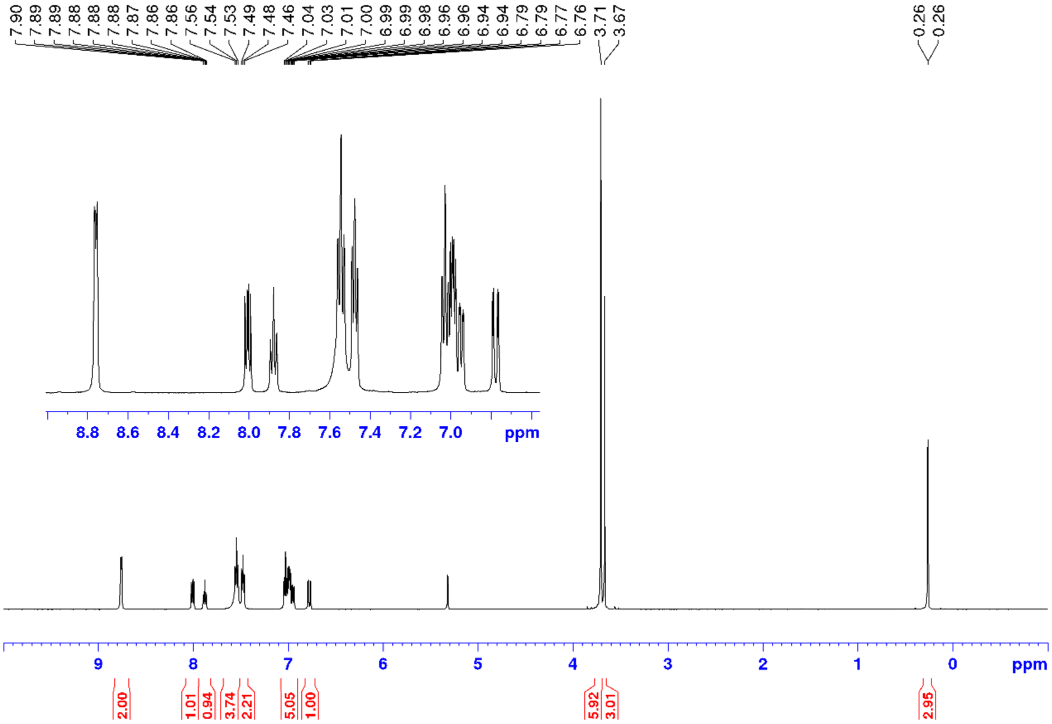

Figure 2.32, continued.

(c) $^{13}C\{^1H\}$ (CD_2Cl_2, 125 MHz):

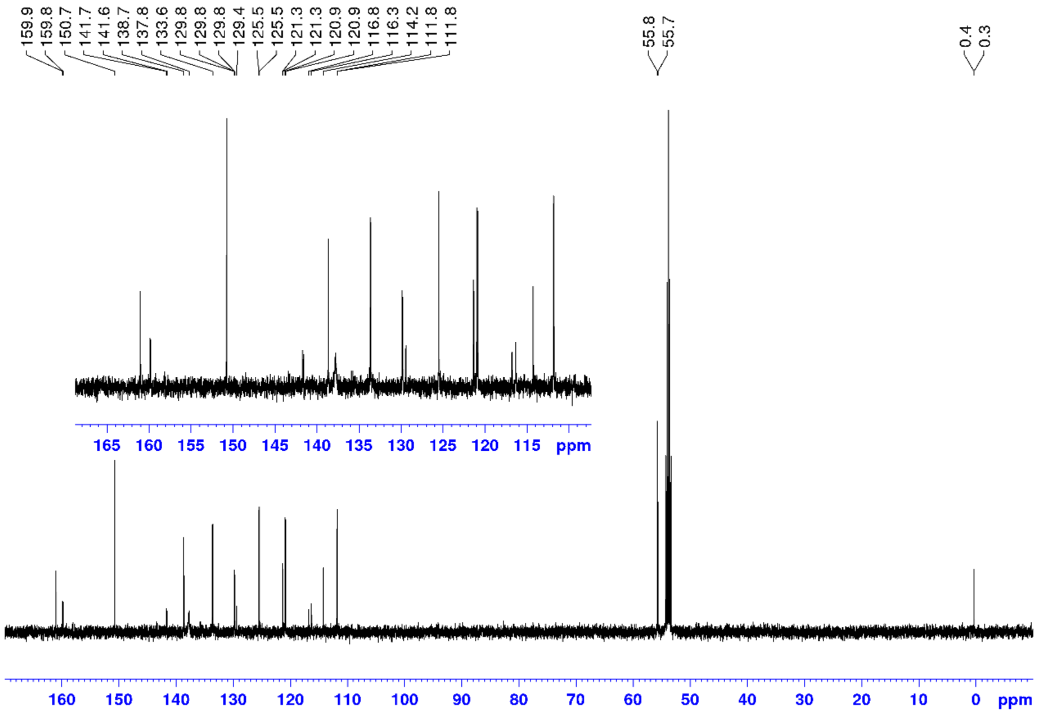

(d) COSY (CD_2Cl_2, aryl region):

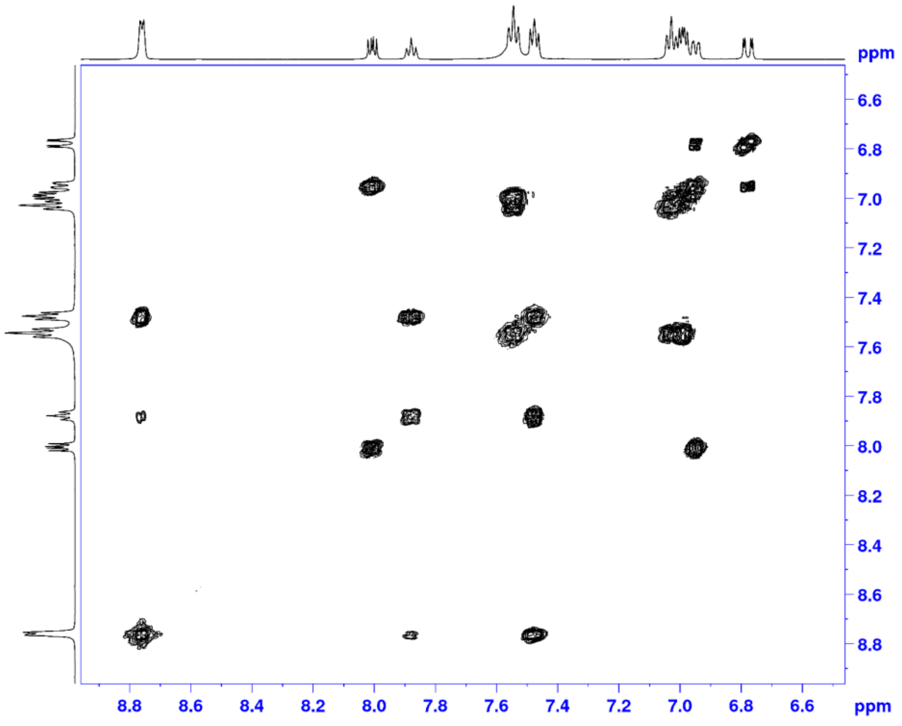

Figure 2.32, continued.

(e) HMQC (CD_2Cl_2, -OMe region):

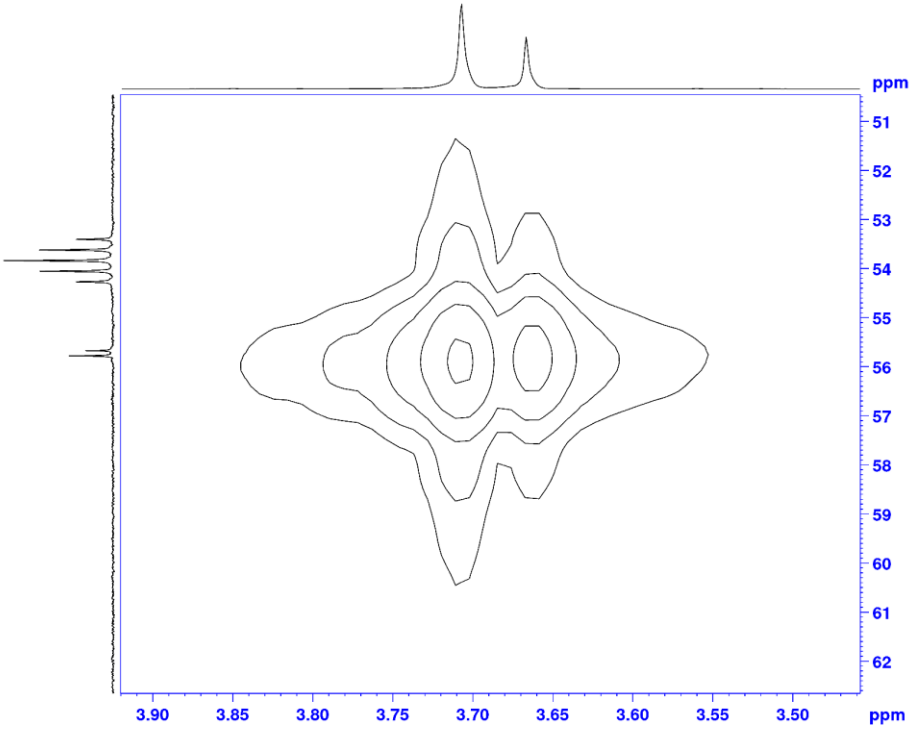

(f) HMQC (CD_2Cl_2, aryl region):

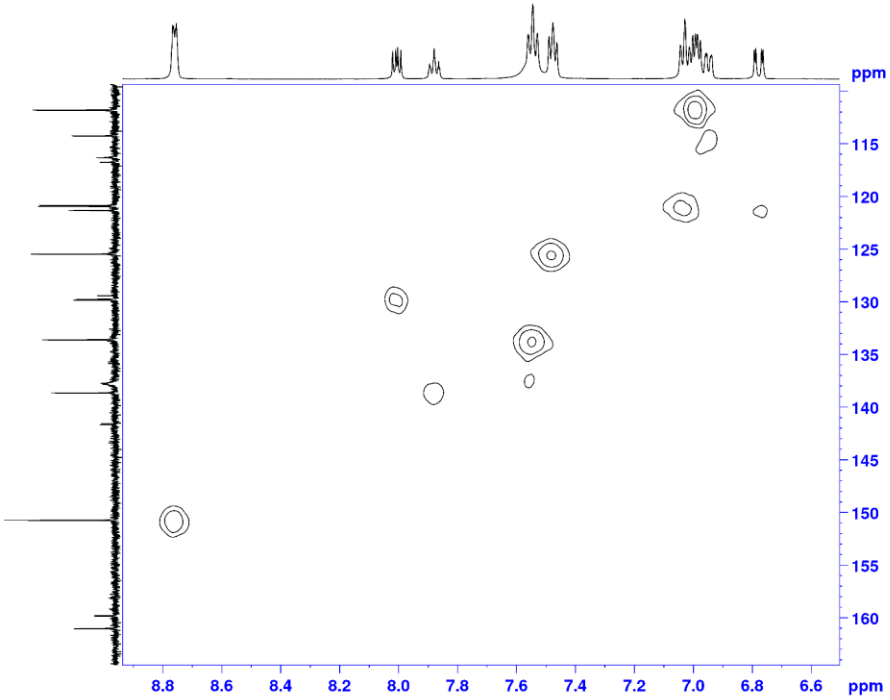

Figure 2.32, continued.

(g) HMBC (CD_2Cl_2, C-aryl region):

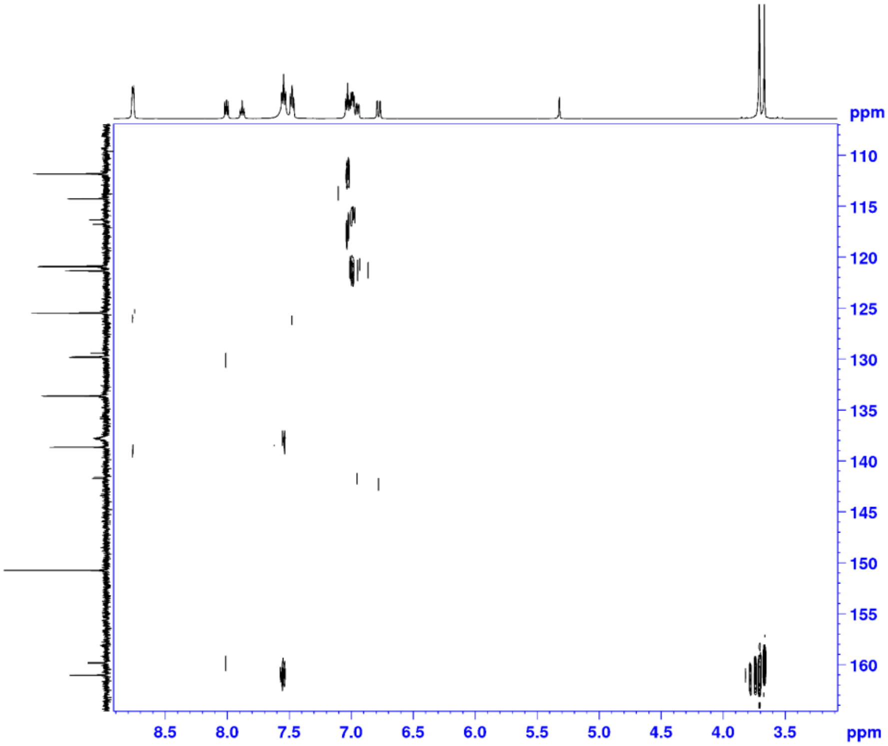

3b. Route 1. 3b was synthesized analogously to **3a** from **Na[1b]** (0.15 g, 0.30 mmol), (COD)PdMeCl (80 mg, 0.30 mmol), pyridine (25 µL, 0.30 mmol) and CH_2Cl_2 (5 mL). The CH_2Cl_2 solution was layered with pentane and cooled to -40 °C. After 1 d, colorless X-ray quality crystals formed. The crystals were collected by filtration and dried under vacuum for 18 h (0.17 g, 86 %). $^{31}P\{^1H\}$ NMR (CD_2Cl_2): δ 21.0. ^1H NMR (CD_2Cl_2): δ 8.76 (dd, $^3J_{HH}$ = 5, $^4J_{HH}$ = 2, 2H, H^{13}), 7.88 (tt, $^3J_{HH}$ = 8, $^4J_{HH}$ = 2, 1H, H^{15}), 7.61 (d, $^4J_{PH}$ = 4, 1H, H^3), 7.54 (t, $^3J_{HH}$ = 8, 2H, H^{10}), 7.48 (t, $^3J_{HH}$ = 7, 2H, H^{14}), 7.62-7.46 (br, overlap with H^3, H^{10} and H^{14}, 2H, H^{12}), 7.03 (t, $^3J_{HH}$ = 8, 2H, H^{11}), 6.99 (dd, $^3J_{HH}$ = 8, $^4J_{PH}$ =5, 2H, H^9), 6.68 (d, $^3J_{PH}$ = 11, 1H, H^6), 3.90 (s, 3H, H^{16}), 3.71 (s, 6H, H^{18}), 3.50 (s, 3H, H^{17}), 0.29 (d, $^3J_{PH}$ = 3, 3H, Pd-CH_3). $^{13}C\{^1H\}$ NMR (CD_2Cl_2): δ 161.0 (d, $^2J_{PC}$ = 3, C^8), 150.8 (s, C^{13}), 150.5 (s, C^4), 149.0 (d, $^3J_{PC}$ = 8, C^5), 143.3 (d, $^2J_{PC}$ = 16, C^2), 138.6 (s, C^{15}), 137.5 (br, C^{12}), 133.5 (s, C^{10}), 125.5 (s, C^{14}), 120.9 (d, $^3J_{PC}$ = 11, C^{11}), 118.9 (d, $^1J_{PC}$ = 53, C^1), 117.6 (d, $^2J_{PC}$ = 4, C^6), 117.0 (d, $^1J_{PC}$ =57, C^7), 111.7 (d, $^3J_{PC}$ = 5, C^3), 111.6 (d, $^3J_{PC}$ = 12, C^9), 56.4 (s, C^{16}), 56.0 (s, C^{17}), 55.8 (s, C^{18}), 0.3 (d, $^2J_{PC}$ = 4, Pd-CH_3). The broadening of the H^{12} and C^{12} resonances is due to fast exchange of the two anisyl rings. HRMS (APCI/ESI-Mixed mode; *m*/*z*): Calcd. for $[C_{28}H_{30}NO_7PPdS + H]^+$ 662.0594, Found: 662.0609.

3b. Route 2. A vial was charged with **1b-^{i}Bu** (52 mg, 0.10 mmol), (COD)PdMeCl (26 mg, 0.10 mmol) and CH_2Cl_2 (3 mL), and the mixture was stirred at room temperature for 1h to afford a clear yellow solution. Pyridine (8.1 µL, 0.10 mmol) was added, and the mixture was stirred for 18 h, filtered through Celite, and layered with pentane and cooled to -40 °C. After 1 d, colorless X-ray quality crystals formed. The crystals were collected by filtration and dried under vacuum for 18 h (34 mg, 51 %).

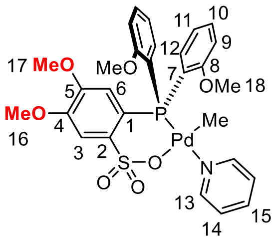

Figure 2.33. NMR spectra of **3b**

(a) $^{31}P\{^1H\}$ (CD_2Cl_2, 202 MHz):

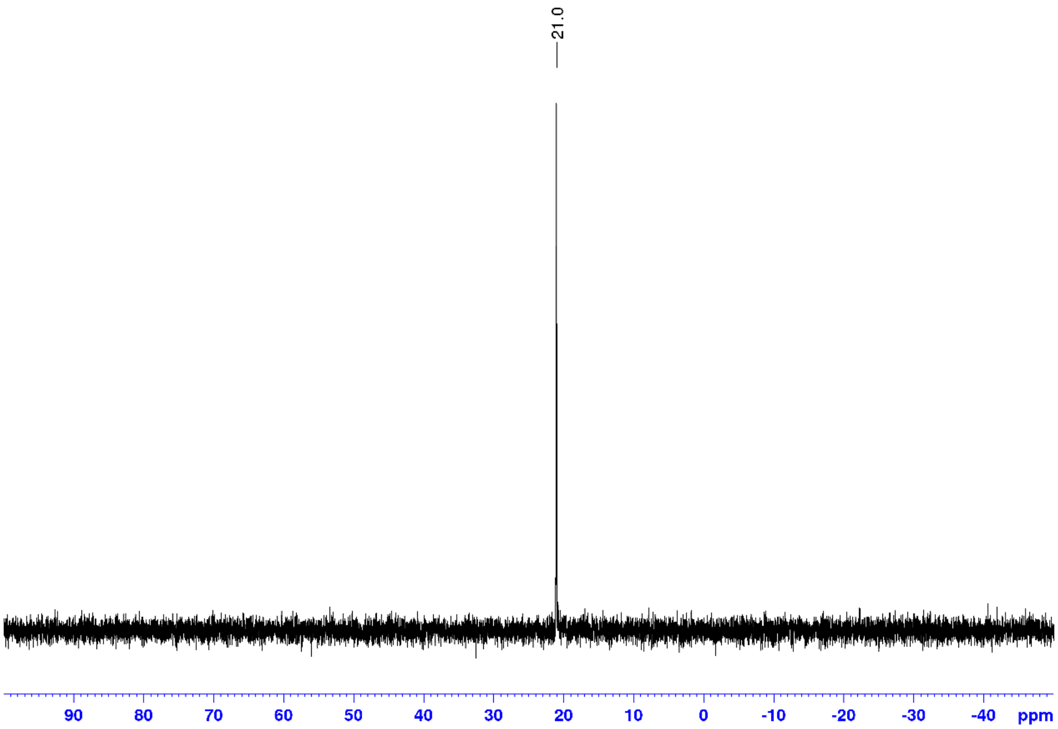

(b) ^1H (CD_2Cl_2, 500 MHz): δ 5.33 = CH_2Cl_2

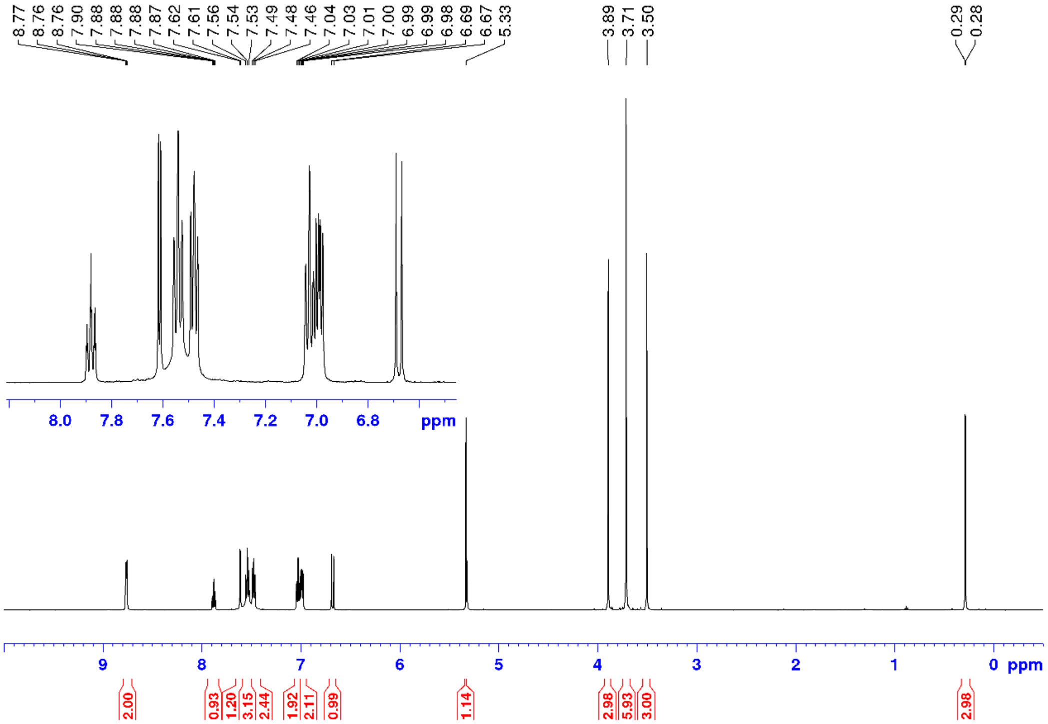

Figure 2.33, continued.

(c) $^{13}C\{^1H\}$ (CD_2Cl_2, 125 MHz):

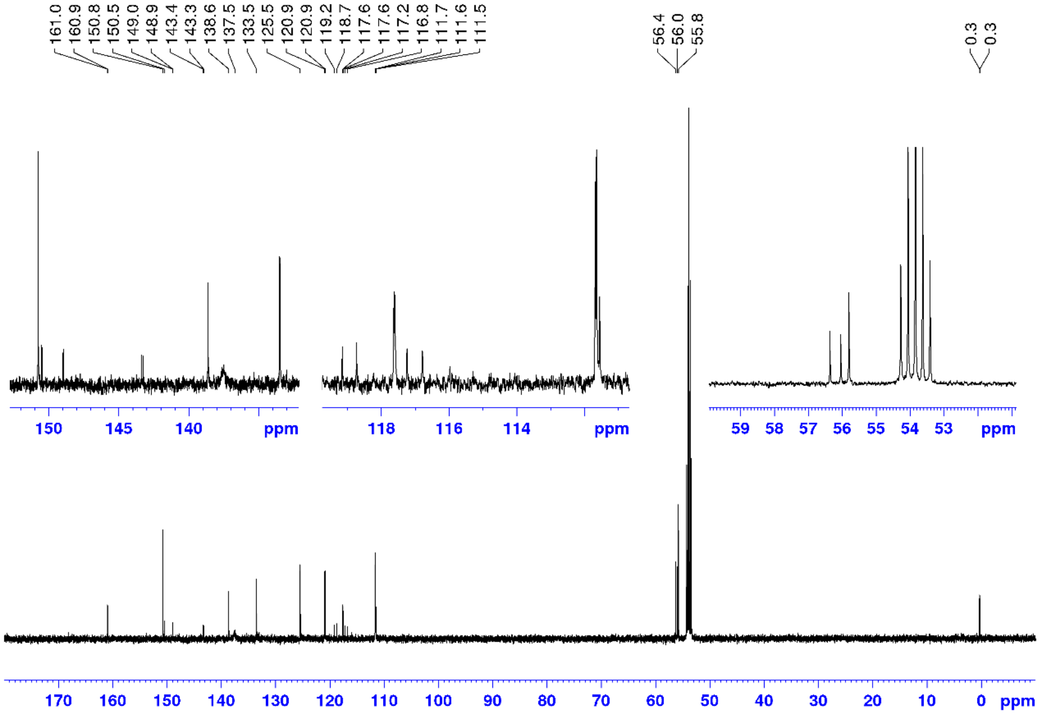

(d) COSY (CD_2Cl_2, aryl region):

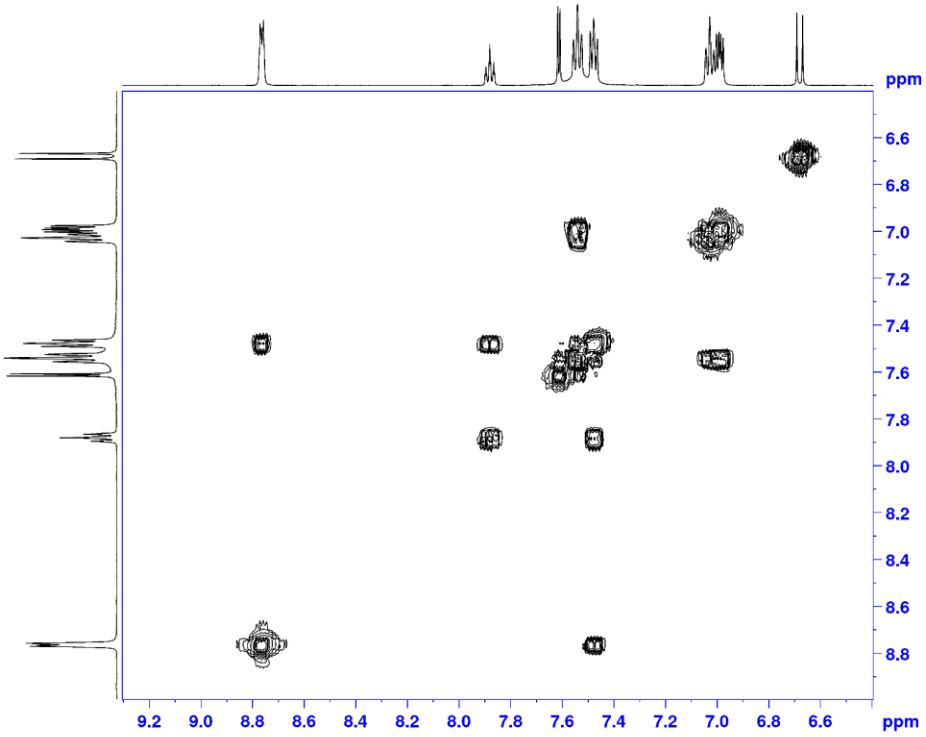

Figure 2.33, continued.

(e) HMQC (CD_2Cl_2, -OMe region):

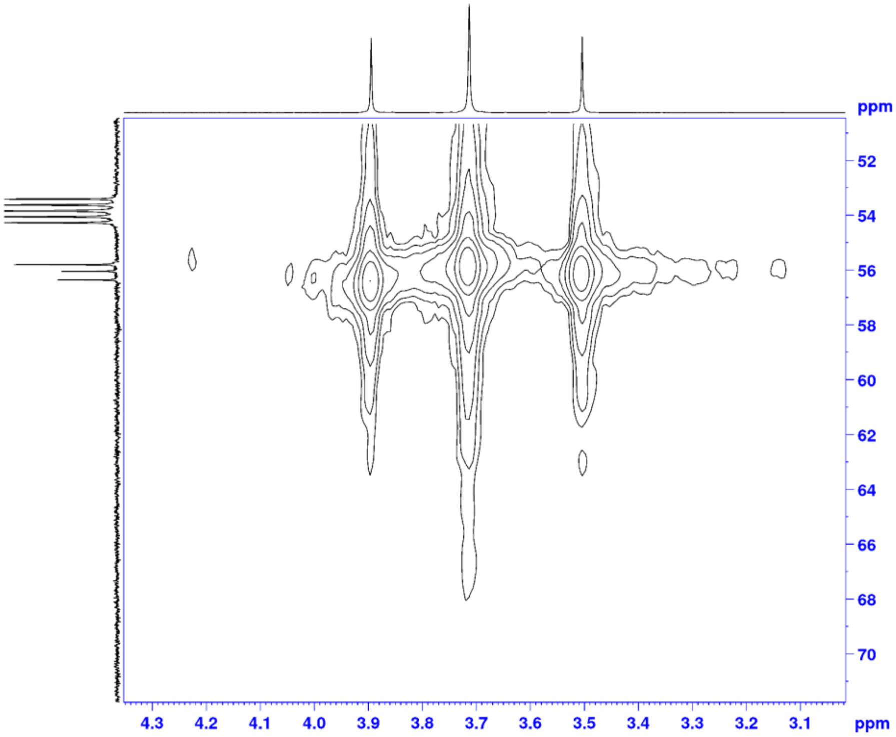

(f) HMQC (CD_2Cl_2, aryl region):

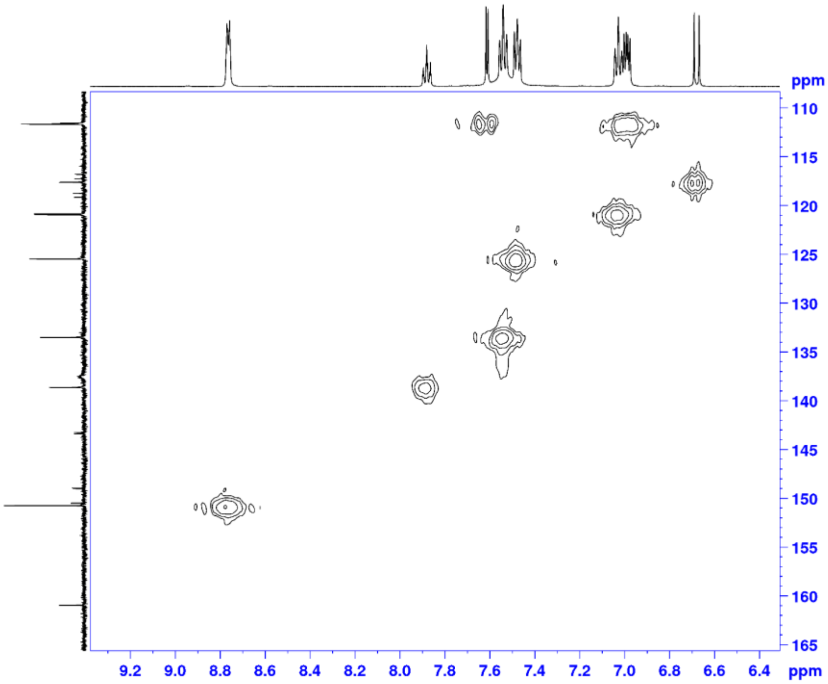

Figure 2.33, continued.

(g) HMBC (CD_2Cl_2, C-aryl region):

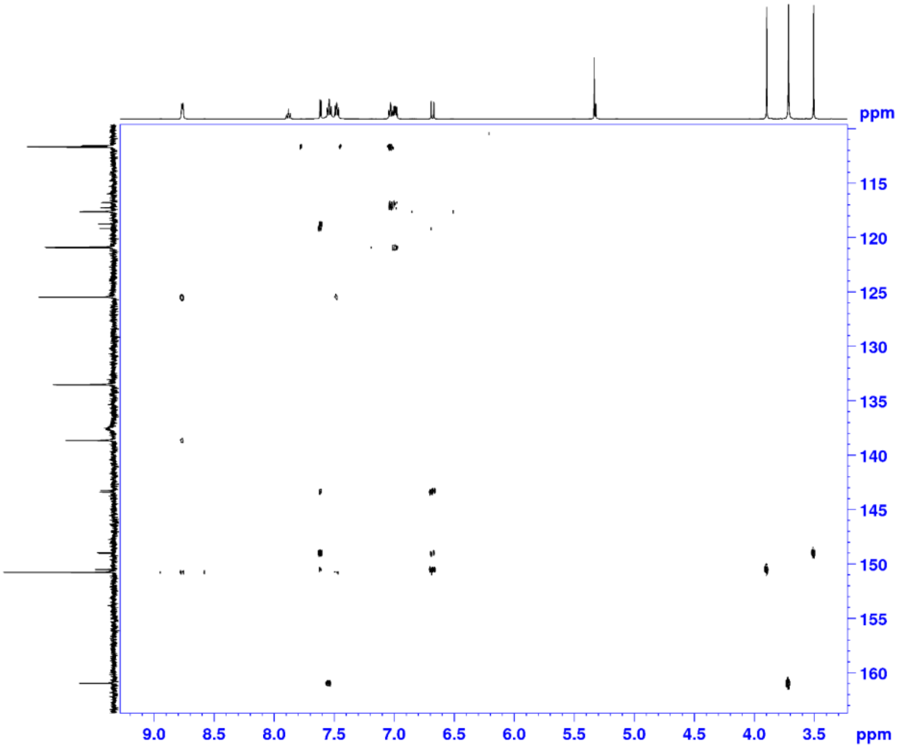

3c. Route 1. 3c was synthesized analogously to **3a** from **Li[1c]** (50 mg, 0.10 mmol), (COD)PdMeCl (26 mg, 0.10 mmol), pyridine (8.1 μL, 0.10 mmol) and CH_2Cl_2 (5 mL). The CH_2Cl_2 solution was filtered through Celite, layered with pentane and cooled to -40 °C. After 1 d, Pd black was observed and this route was not pursued further.

3c. Route 2. A J-Young valved NMR tube was charged with **1c-^{i}Bu** (11 mg, 0.020 mmol) and (COD)PdMeCl (10 mg, 0.037 mmol), and CD_2Cl_2 was added by vacuum transfer. The mixture was thawed and formed a clear yellow solution. $^{31}P\{^1H\}$ NMR (CD_2Cl_2): δ 25.0. ^1H NMR (CD_2Cl_2) Pd-*Me* region: δ 0.81 (d, $^3J_{PH}$ = 3Hz). After 18 h, pyridine (1.6 μL, 0.020 mmol) was added, and the reaction was monitored by NMR and found to be complete after 3 d. $^{31}P\{^1H\}$ NMR (CD_2Cl_2): δ 20.1. ^1H NMR (CD_2Cl_2) Pd-*Me* region: δ 0.46 (d, $^3J_{PH}$ = 2 Hz). These data indicate that **3c** was successfully generated by this route. However, due to decomposition upon attempted product purification, **3c** was not further pursued.

3d. 3d was synthesized analogously to **3a** from **Na[1d]** (0.21 g, 0.50 mmol), (COD)PdMeCl (0.13 mg, 0.50 mmol), pyridine (41 µL, 0.50 mmol) and CH_2Cl_2 (10 mL). The CH_2Cl_2 solution was layered with pentane and cooled to -40 °C. After 1 d, colorless X-ray quality crystals formed. The crystals were collected by filtration and dried under vacuum for 18 h (0.25 g, 84 %). $^{31}P\{^1H\}$ NMR (CD_2Cl_2): δ 27.8. ^1H NMR (CD_2Cl_2): δ 8.77 (d, $^3J_{HH}$ = 5, 2H, H^{11}), 7.90 (t, $^3J_{HH}$ = 8, 1H, H^{13}), 7.69 (s, 1H, H^3), 7.60 (m, 4H, H^8), 7.53-7.47 (m, 8H, H^9, H^{10} and H^{12}), 6.36 (d, $^3J_{PH}$ = 10, 1H, H^6), 3.90 (s, 3H, H^{14}), 3.47 (s, 3H, H^{15}), 0.55 (s, 3H, Pd-C*H*$_3$). $^{13}C\{^1H\}$ NMR (CD_2Cl_2): δ 151.1 (s, C^4), 150.6 (s, C^{11}), 149.8 (d, $^3J_{PC}$ = 8, C^5), 144.1 (br, C^2), 138.9 (s, C^{13}), 134.5 (d, $^2J_{PC}$ = 12, C^8), 131.4 (s, C^{10}), 130.8 (d, $^1J_{PC}$ =55, C^7), 129.0 (d, $^3J_{PC}$ = 11, C^9), 125.6 (s, C^{12}), 119.0 (d, $^1J_{PC}$ = 43, C^1), 117.8 (s, C^6), 112.3 (d, $^3J_{PC}$ = 9, C^3), 56.6 (s, C^{14}), 56.1 (s, C^{15}), 0.5 (s, Pd-*C*H_3). HRMS (APCI/ESI-Mixed mode; *m*/*z*): Calcd. for $[C_{26}H_{25}NO_5PPdS + H]^+$ 602.0382, Found: 602.0346.

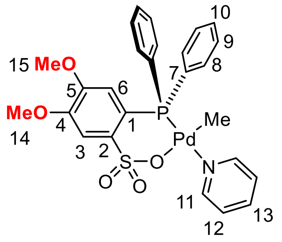

Figure 2.34. NMR spectra of **3d**

(a) $^{31}P\{^{1}H\}$ (CD_2Cl_2, 202 MHz):

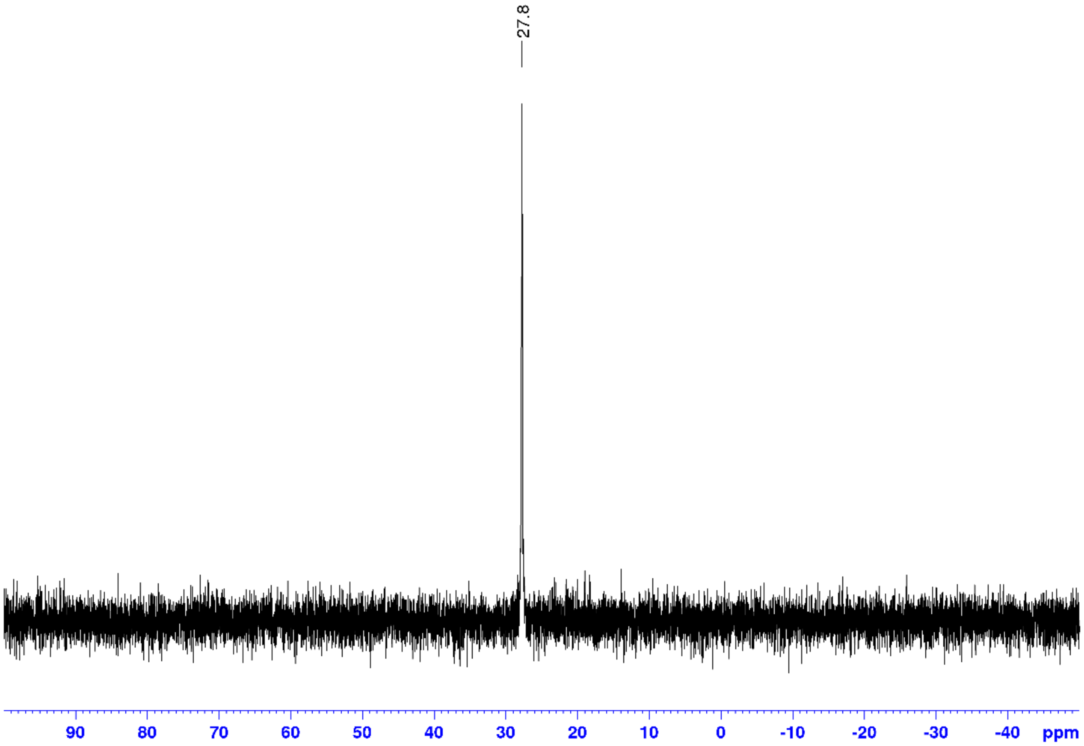

(b) ^{1}H (CD_2Cl_2, 500 MHz): δ 3.43 and 1.15 = Et_2O

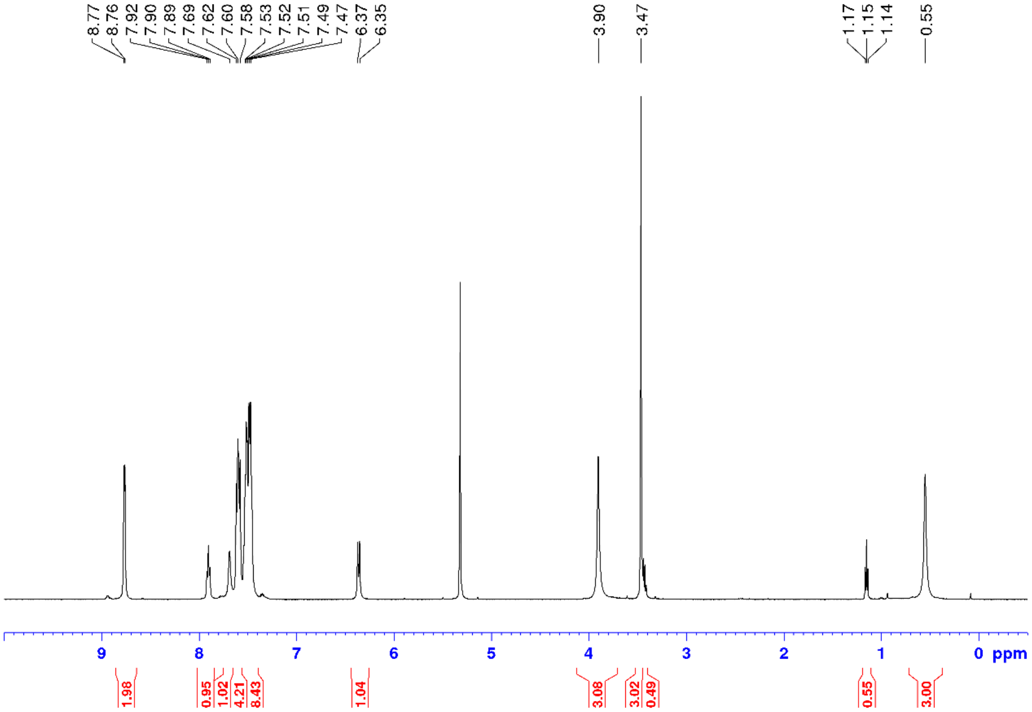

Figure 2.34, continued.

(c) ^{13}C{^{1}H} (CD_2Cl_2, 125 MHz):

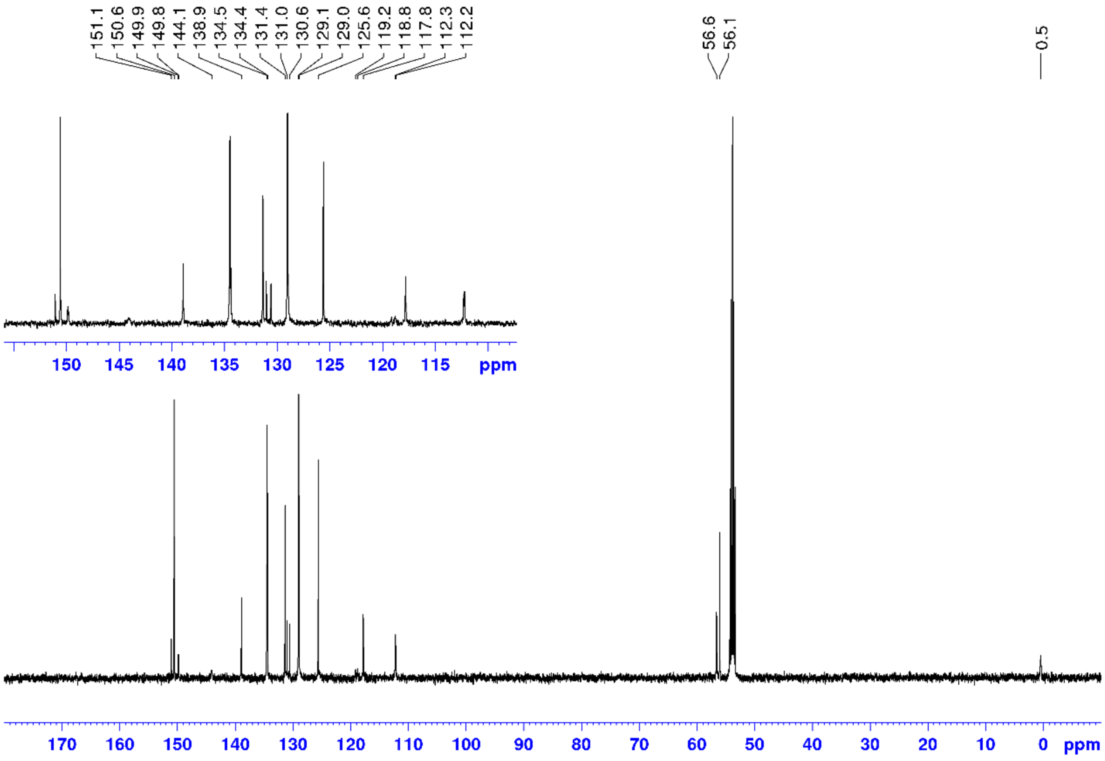

4a-py. A J-Young valved NMR tube was charged with **Li_2[2a]** (20 mg, 0.040 mmol) and (COD)PdMeCl (11 mg, 0.040 mmol), and CD_2Cl_2 was added by vacuum transfer. The mixture was thawed and formed a cloudy white solution. After 1 h, pyridine (3.2 μL, 0.040 mmol) was added, and the reaction was monitored by NMR. No ^{31}P NMR resonance was observed after 2 d. The volatiles were removed under vacuum, CD_3OD was added, and NMR spectra were obtained. ^{31}P{^{1}H} NMR (CD_3OD): δ 32.9 (major, 95 %). ^{1}H NMR (CD_3OD) Pd-*Me* region: δ 0.55 (d, $^{3}J_{PH}$ = 3 Hz). These data indicate that monomeric solvated **4a-py** was successfully generated, but tetrameric **4a-py** (if formed) is not soluble in CD_2Cl_2. Therefore, **4a-py** was not further pursued.

4a-py'. The synthesis of **4a-py'** was attempted analogously to **3a** from **Li_2[2a]** (50 mg, 0.10 mmol), (COD)PdMeCl (26 mg, 0.10 mmol), 4-(5-nonyl)-pyridine (23 μL, 0.10 mmol) and CH_2Cl_2 (2 mL). After 18 h, Pd black was observed and **4a-py'** was not further pursued.

4c-py'. A J-Young valved NMR tube was charged with **Li_2[2c]** (10 mg, 0.016 mmol) and (COD)PdMeCl (4.0 mg, 0.015 mmol), and CD_2Cl_2 was added by vacuum transfer. The mixture was thawed and formed a cloudy white solution. After 1 h, 4-(5-nonyl)-pyridine (3.8 μL, 0.016 mmol) was added, and the reaction was monitored by NMR. After 18 h, very complicated NMR spectra were observed. The volatiles were removed under vacuum, CD_3OD was added, and NMR spectra were obtained. $^{31}P\{^1H\}$ NMR (CD_3OD): δ 43.2 (major, 82 %). ^1H NMR (CD_3OD) Pd-*Me* region: δ 0.65 (d, $^3J_{PH}$ = 1 Hz). These data indicate that monomeric solvated **4c-py'** was successfully generated, but the tetrameric **4c-py'** is not formed, presumably due to the steric bulkiness of the three methoxy groups. Therefore, **4c-py'** was not further pursued.

5b. 5b was synthesized analogously to **3a** from **Li_2[2b]** (0.17 g, 0.30 mmol), (COD)PdMeCl (82 mg, 0.30 mmol), 4-(5-nonyl)-pyridine (72 μL, 0.30 mmol) and CH_2Cl_2 (10 mL). **5b** was crystallized by layering pentane onto the CH_2Cl_2 solution and cooling to -40 °C. **5b** was collected by filtration and dried under vacuum for 18 h (0.18 g, 67 %). X-ray quality crystals of **5b**•6($CHCl_2CHCl_2$) were grown by diffusing pentane into a $CHCl_2CHCl_2$ solution at room temperature. $^{31}P\{^1H\}$ NMR (CD_2Cl_2): δ 34.1. ^1H NMR (CD_2Cl_2): δ 8.68 (d, $^3J_{HH}$ = 5, 2H, H^{11}), 8.08 (d, $^4J_{PH}$ = 4, 1H, H^3), 7.73 (d, $^4J_{PH}$ = 5, 1H, $H^{3'}$), 7.56-7.52 (m, 5H, H^8, H^9 and H^{10}; the H^8 resonance is broadened into the baseline due to restricted rotation around the P-C^7 bond), 6.67 (d, $^3J_{HH}$ = 6, 1H, H^{12}), 6.52 (d, $^3J_{PH}$ = 10, 1H, H^6), 6.16 (d, $^3J_{PH}$ = 11, 1H, $H^{6'}$), 4.21 (s, 3H, $H^{19'}$), 4.19 (s, 3H, H^{19}), 3.44 (s, 3H, H^{20}), 3.37 (s, 3H, $H^{20'}$), 2.27 (sept, $^3J_{HH}$ = 5, 1H, H^{14}), 1.25-0.84 (m, 18H, H^{15}, H^{16}, H^{17} and H^{18}), -0.16 (d, $^3J_{PH}$ = 3, 3H, Pd-C*H*$_3$). $^{13}C\{^1H\}$ NMR (CD_2Cl_2): δ 157.9 (s, C^{13}), 152.6 (d, $^4J_{PC}$ = 2, C^4), 151.5 (s, C^{11}), 150.9 (d, $^4J_{PC}$ = 2, $C^{4'}$), 150.7 (d, $^3J_{PC}$ = 8, $C^{5'}$), 149.8 (d, $^3J_{PC}$ = 10, C^5), 140.6 (d, $^2J_{PC}$ = 15, C^2), 139.2 (d, $^2J_{PC}$ = 9, $C^{2'}$), 132.1 (d, $^1J_{PC}$ = 43, C^7), 131.7 (s, C^8), 129.2 (br, C^9 and C^{10}), 124.3 (s, C^{12}), 118.8 (d, $^1J_{PC}$ = 19, C^1), 118.6 (s, C^6), 118.4 (d, $^1J_{PC}$

= 27, C$^{1'}$), 115.8 (d, $^{2}J_{PC}$ = 7, C$^{6'}$), 114.2 (d, $^{3}J_{PC}$ = 8, C^{3}), 114.0 (d, $^{3}J_{PC}$ = 10, C$^{3'}$), 58.4 (s, C^{19}), 56.6 (s, C$^{20'}$), 56.5 (s, C$^{19'}$), 55.3 (s, C^{20}), 46.2 (s, C^{14}), 36.3 and 36.1 (s, C$^{15,15'}$), 30.1 and 29.9 (s, C$^{16,16'}$), 23.4 and 23.1 (s, C$^{17,17'}$), 14.3 and 14.2 (s, C$^{18,18'}$), -1.0 (s, Pd-*C*H$_3$). ^{13}C{^{1}H} NMR ($CDCl_2CDCl_2$, 353 K), 5-nonyl group region: 35.2 and 35.2 (s, C$^{15,15'}$), 29.3 and 29.2 (s, C$^{16,16'}$), 22.4 and 22.3 (s, C$^{17,17'}$), 13.6 and 13.6 (s, C$^{18,18'}$). The observation that the butyl chains of the 5-nonyl group are inequivalent indicates that the tetramer structure is maintained at high temperature. ^{7}Li{^{1}H} NMR (CD_2Cl_2): δ -0.9, -1.1. ^{31}P{^{1}H} NMR (CD_3OD): δ 33.6. ^{1}H NMR (CD_3OD): δ 8.74 (s, 2H, H^{11}), 7.80 (br, 2H, H^{8}, this resonance is broad due to the restricted rotation around the P-C^{7} bond), 7.68 (d, $^{4}J_{PH}$ = 4, 2H, H$^{3,3'}$), 7.53-7.47 (m, 3H, H^{9} and H^{10}), 7.36 (d, $^{3}J_{HH}$ = 6, 2H, H^{12}), 6.53 (d, $^{3}J_{PH}$ = 10, 2H, H$^{6,6'}$), 3.91 (s, 6H, H$^{19,19'}$), 3.51 (s, 6H, H$^{20,20'}$), 2.64 (sept, $^{3}J_{HH}$ = 5, 1H, H^{14}), 1.74-1.56 (m, 4H, H^{15}), 1.36-1.17 (m, 8H, H^{16} and H^{17}), 0.85 (t, $^{3}J_{HH}$ = 7, 6H, H^{18}), 0.55 (d, $^{3}J_{PH}$ = 2, 3H, Pd-C*H*$_3$). ^{13}C{^{1}H} NMR (CD_3OD): δ 159.9 (s), 151.5 (s), 150.6 (d, J_{PC} = 9), 142.3 (s), 136.9 (br), 133.9 (s), 133.5 (s), 131.9 (s), 129.7 (d, J_{PC} = 11), 125.6 (s), 118.3 (s), 115.9 (s), 113.9 (s), 56.5 (s, C^{19}), 56.1 (s, C^{20}), 46.9 (s, C^{14}), 36.9 (s, C^{15}), 30.8 (s, C^{16}), 23.7 (s, C^{17}), 14.3 (s, C^{18}), -2.0 (s, Pd-*C*H$_3$). ^{7}Li{^{1}H} NMR (CD_3OD): δ 0.2. HRMS (APCI/ESI-Mixed mode; *m*/*z*): Calcd. for $[C_{74}H_{94}N_2O_{20}P_2Pd_2S_4Li_2 - Li + 2H]^+$ 1743.3148, Found: 1743.3160.[22] EA: Calcd. for $[C_{37}H_{47}Cl_{0.5}Li_{1.5}NO_{10}PPdS_2]_4$, %: C, 49.63; H, 5.29; N, 1.56; Cl, 1.98; Li, 1.16; P, 3.46; S, 7.16. Found: C, 48.81; H, 5.45; N, 1.50; Cl, 1.69; Li, 1.07; P, 3.35; S, 5.77.

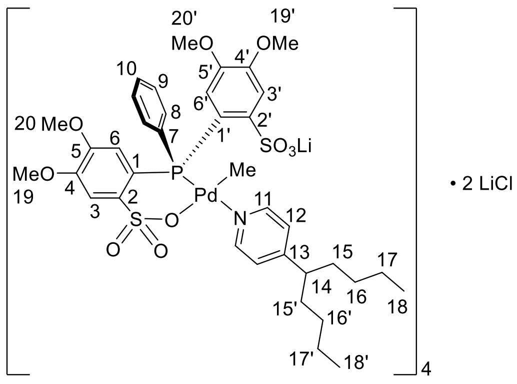

Figure 2.35. NMR spectra of **5b**

(a) $^{31}P\{^1H\}$ (CD_2Cl_2, 202 MHz):

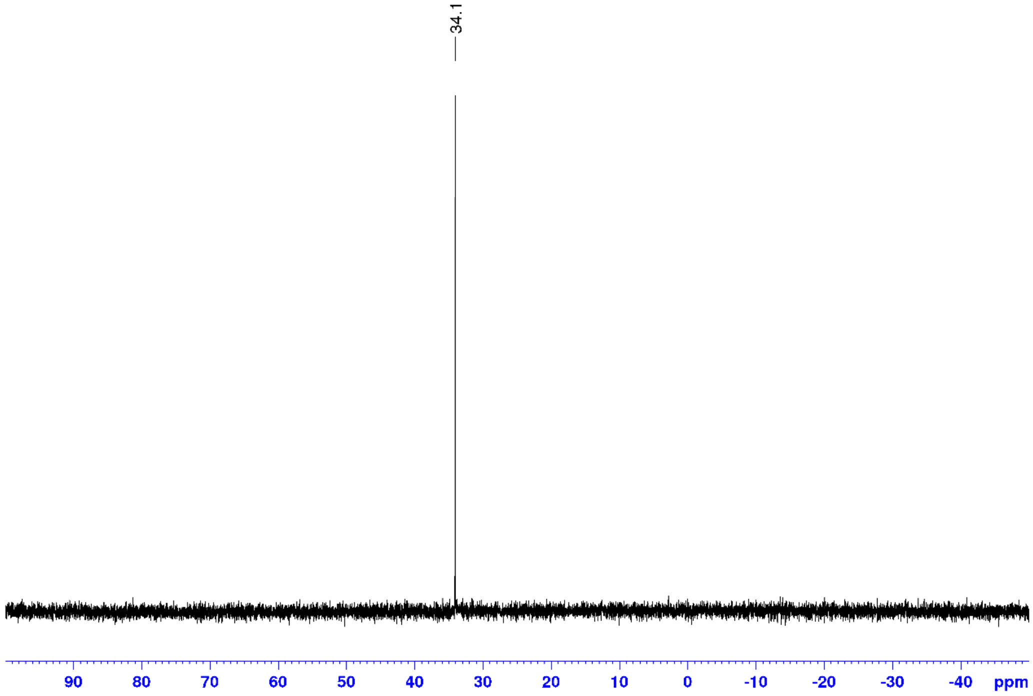

(b) ^1H (CD_2Cl_2, 500 MHz):

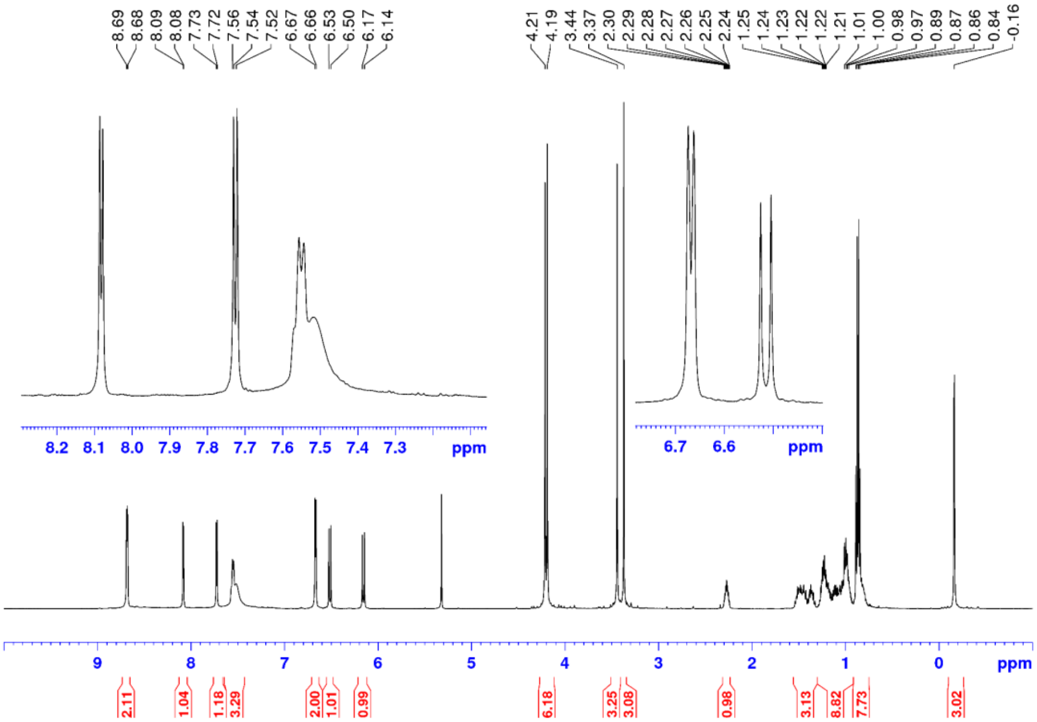

Figure 2.35, continued.

(c) $^{13}C\{^{1}H\}$ (CD_2Cl_2, 125 MHz):

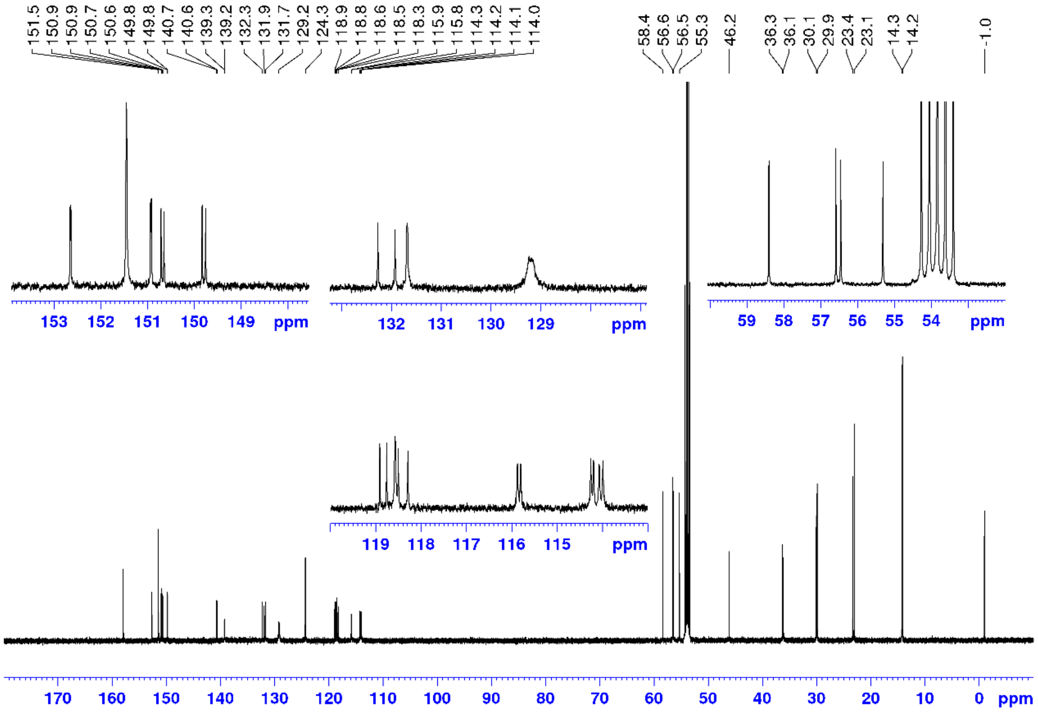

(d) $^{13}C\{^{1}H\}$ of 5-nonyl group region C^{15}-C^{18} at 353 K ($CDCl_2CDCl_2$, 125 MHz):

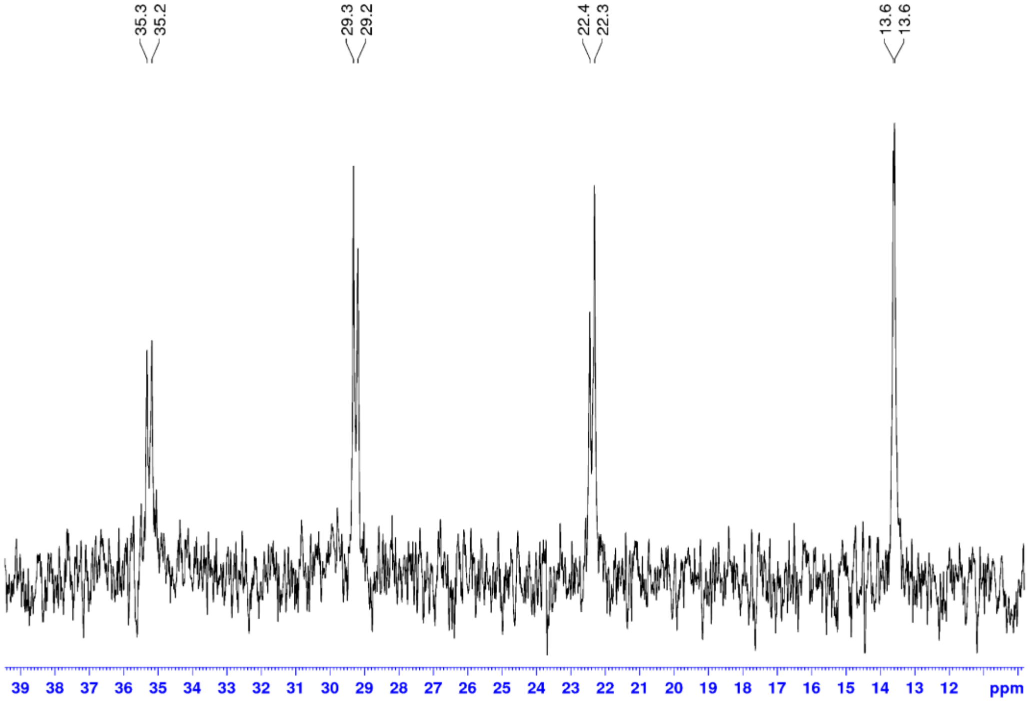

Figure 2.35, continued.

(e) ^{7}Li{^{1}H} (CD_2Cl_2, 155 MHz):

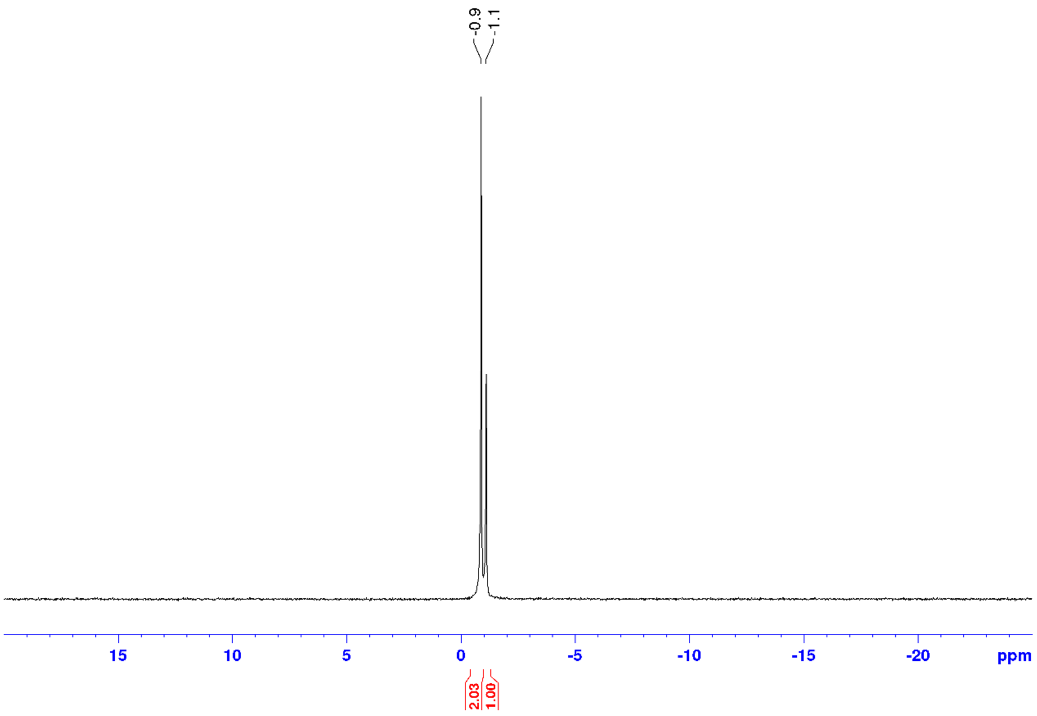

(f) NOESY (CD_2Cl_2, at 263 K):

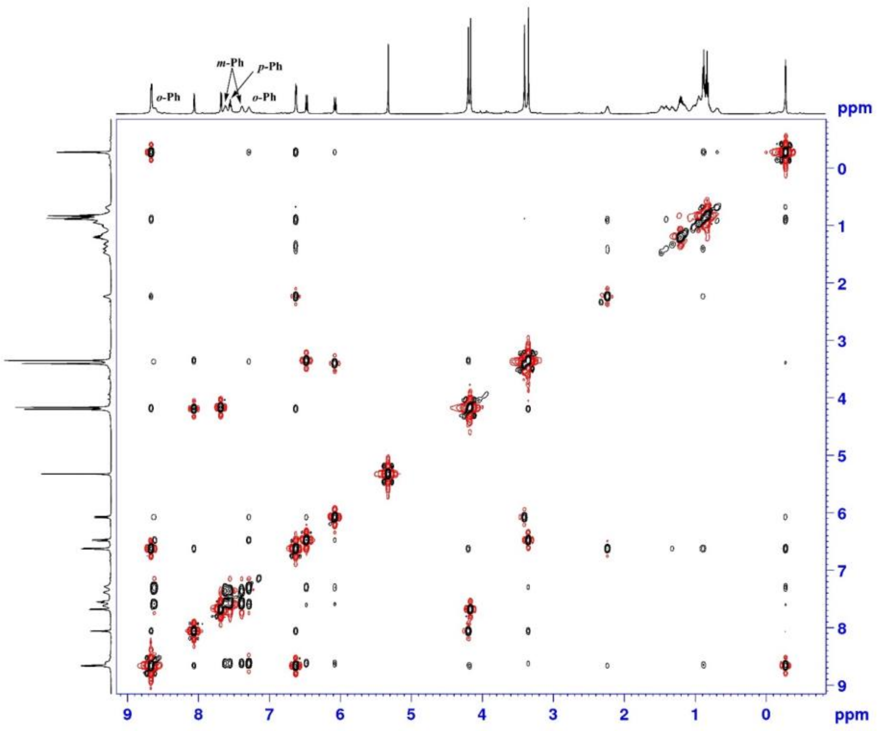

Figure 2.35, continued.

(g) HMQC (CD_2Cl_2, aliphatic region):

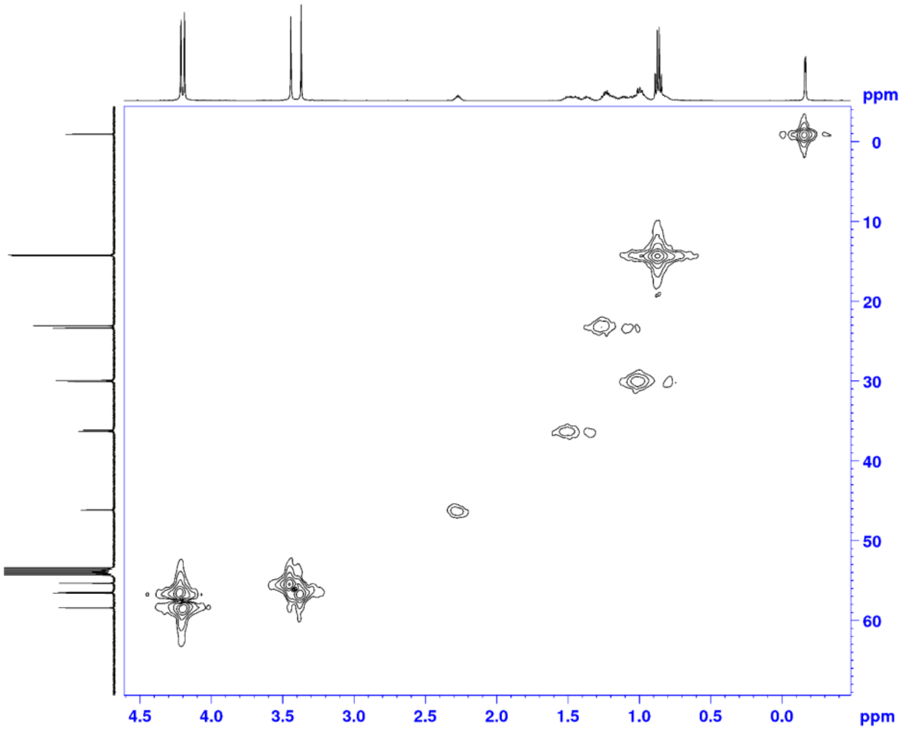

(h) HMQC (CD_2Cl_2, aryl region):

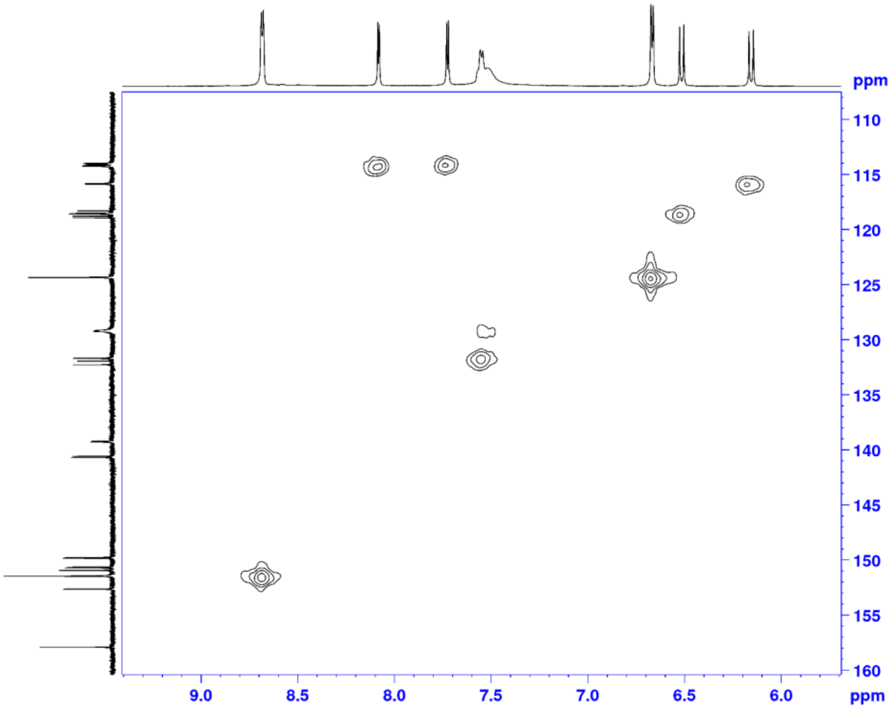

Figure 2.35, continued.

(i) HMBC (CD_2Cl_2):

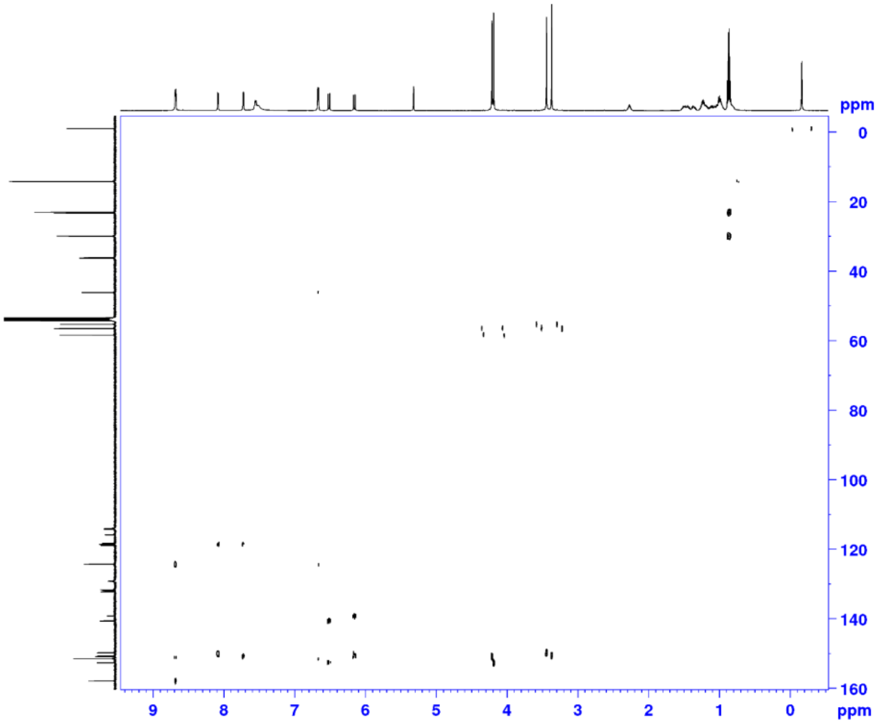

(j) HMBC (CD_2Cl_2, C-aryl region expansion):

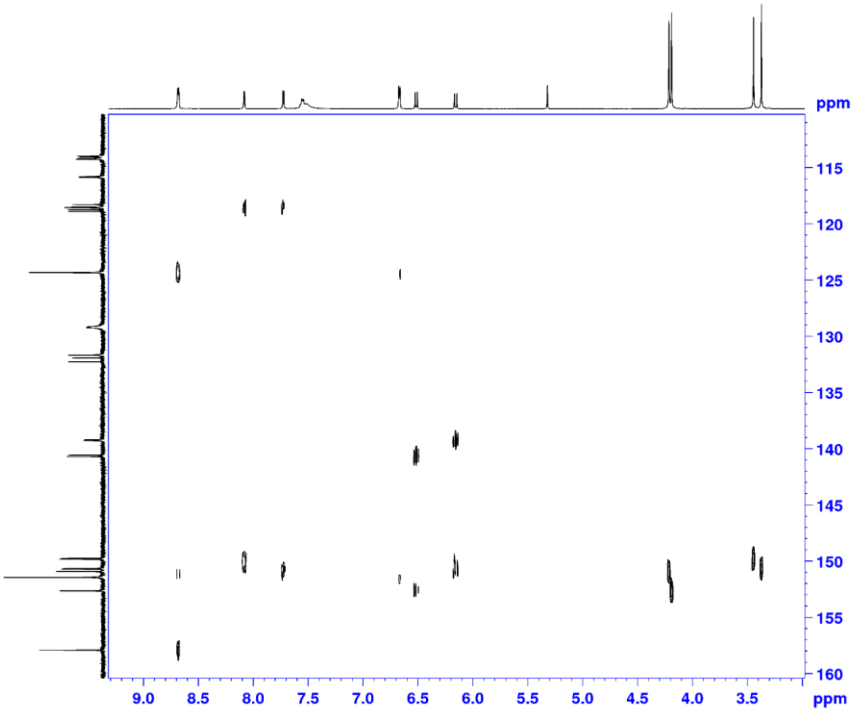

Figure 2.35, continued.

(k) $^{31}P\{^{1}H\}$ (CD_3OD, 202 MHz):

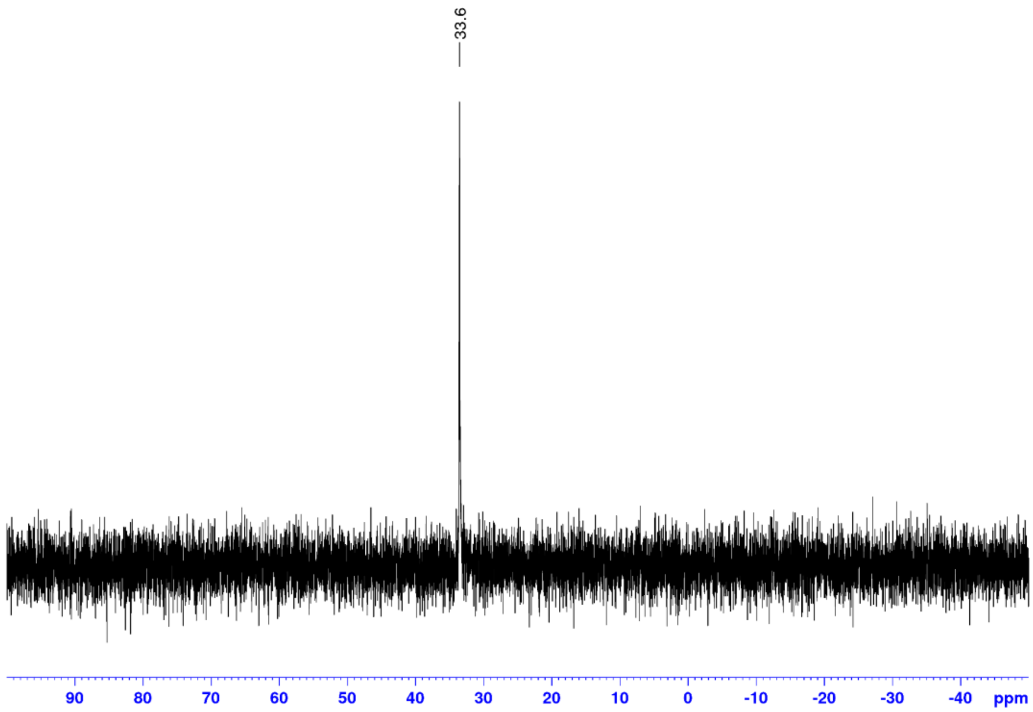

(l) ^{1}H (CD_3OD, 500 MHz): δ 5.49 = CH_2Cl_2; 4.88 = H_2O

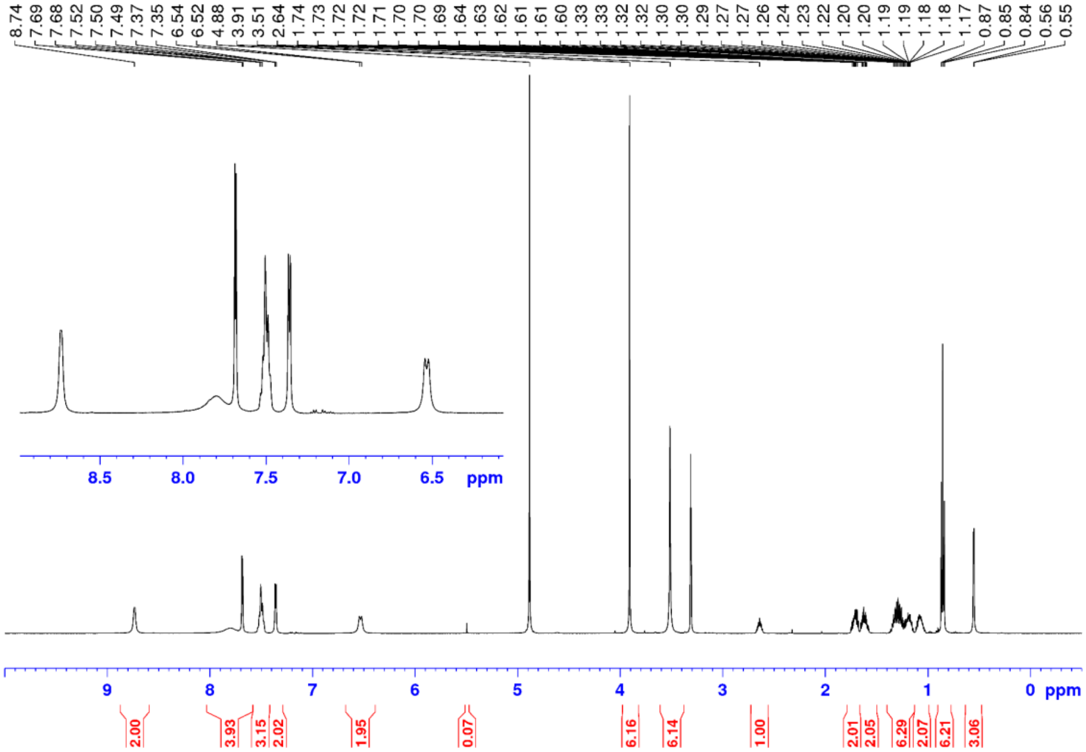

Figure 2.35, continued.

(m)$^{13}C\{^1H\}$ (CD_3OD, 125 MHz):

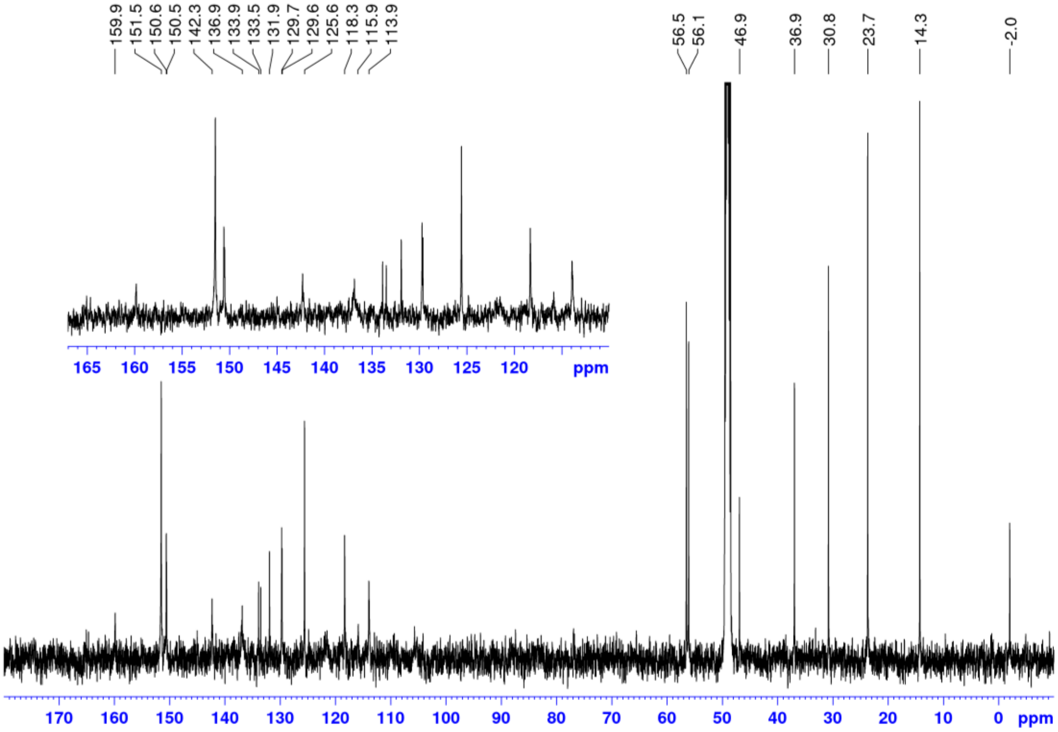

(n) $^7Li\{^1H\}$ (CD_3OD, 155 MHz):

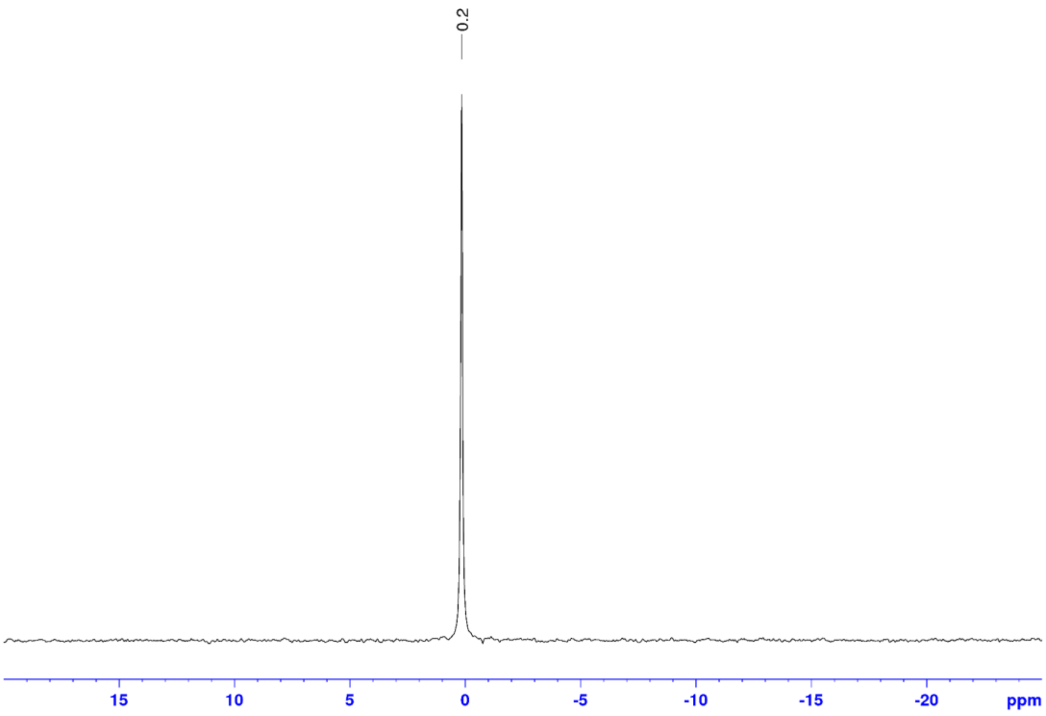

Reaction of 5b with Cryptand211. A J-Young valved NMR tube was charged with **5b** (4.1 mg, 0.0046 mmol), and CD_2Cl_2 was added by vacuum transfer. A solution of Cryptand211 in CH_2Cl_2 (200 μL, 0.026 M, 0.0052 mmol) was added and the reaction was monitored by NMR. $^{31}P\{^1H\}$ NMR (CD_2Cl_2): δ 30.9. ^1H NMR (CD_2Cl_2) Pd-*Me* region: δ 0.49 (d, $^3J_{PH} = 2$ Hz). $^7Li\{^1H\}$ NMR (CD_2Cl_2): δ -0.5. These data indicate that Cryptand211 converted **5b** to a monomeric Pd_1 species.

Reaction of 5b with $B(C_6F_5)_3$ and 4-(5-nonyl)-pyridine. A J-Young valved NMR tube was charged with **5b** (5.1 mg, 0.0057 mmol) and $B(C_6F_5)_3$ (3.3 mg, 0.0064 mmol), and CD_2Cl_2 was added by vacuum transfer. The reaction was monitored by NMR. The formations of (py')$B(C_6F_5)_3$ and an insoluble product that is assumed to be the base-free derivative **7b** were observed. After 1 h, 4-(5-nonyl)-pyridine (1.3 μL, 0.0056 mmol) was added and the reaction was monitored by NMR. **5b** was regenerated in 90 % yield based on integration of the Pd-Me region of the ^1H NMR spectrum.

Reaction of 5b + $B(C_6F_5)_3$ with 4-^{t}Bu-Styrene. A J-Young valved NMR tube was charged with **5b** (4.2 mg, 0.0047 mmol) and $B(C_6F_5)_3$ (2.5 mg, 0.0049 mmol), and CD_2Cl_2 was added by vacuum transfer. 4-^{t}Bu-Styrene (0.92 μL, 0.0050 mmol) was added and the reaction was monitored by NMR. No reaction was observed at room temperature. The volatiles were removed under vacuum and $CDCl_2CDCl_2$was added. The NMR tube was heated at 80 °C and the reaction was monitored by NMR. After 2 h, the reaction was complete. *E*-1-(4-^{t}Bu-phenyl)-propene was generated in 50 % based on ^1H NMR integration and the formation of Pd black was observed. 4-(5-nonyl)-pyridine (1.2 μL, 0.0065 mmol) was added and the reaction was monitored by NMR. No regeneration of **5b** was observed.

Ethylene Homopolymerization. In a glovebox, a 200 mL glass autoclave liner was charged with solution of the catalyst in chlorobenzene (1 mL), and toluene (49 mL) was then added. For catalyst loadings larger than 5 μmol, the catalyst and $B(C_6F_5)_3$ (if applicable) were weighed directly into the glass liner and 50 mL solvent was added. The glass liner was placed in a stainless steel autoclave, which was sealed and removed from the glovebox. The autoclave was heated to the target temperature and pressurized with ethylene while the contents were stirred. After 2 h, the autoclave was cooled to 25 °C and vented. Acetone (50 mL) was added to precipitate the polymer. The polymer was collected by filtration, rinsed with acetone, and dried under vacuum.

Ethylene/VF Copolymerization. (a) Standard Method: In the glove box, the catalyst (10 μmol) was weighed into a glass autoclave liner. Solvent (50 mL) was added. The liner was placed in the autoclave, and the autoclave was assembled and brought out of the box. The autoclave was pressurized with VF to the desired pressure and ethylene was added until the total pressure reached 250 or 300 psi, while stirring (100 rpm). The reactor was heated to the desired temperature (80 °C) and stirring was increased to 170 rpm. After 2 h, the autoclave was cooled to 25 °C and vented. Acetone (50 mL) was added to precipitate the polymer. The polymer was collected by filtration, rinsed with acetone, and dried under vacuum.

(b) Injection-Method: This method is designed to minimize catalyst decomposition prior to exposure to monomers. In the standard method, the catalyst solution was heated to the target temperature without monomer, and during this period (ca. 20-25 min) catalyst decomposition may occur. In the injection method, the solvent and monomers are heated to the target temperature first and then the catalyst solution is injected from an injection cylinder, which minimizes the chance for catalyst decomposition.

In the glove box, the catalyst (10 μmol) was weighed into a vial, and dissolved in chlorobenzene (5 mL). The catalyst solution was transferred into the injection cylinder with chlorobenzene (5 mL) and the injection cylinder was connected to the autoclave. Toluene (40 mL) was added to glass autoclave liner. The liner was placed in the autoclave, and the autoclave was assembled in the box. The injection cylinder and autoclave were brought out of the box. The autoclave was pressurized with VF to the desired pressure and ethylene was added until the total pressure reached 300 psi, while the mixture was stirred (100 rpm). The reactor was heated to the desired temperature (80 °C) and the catalyst solution was injected from the injection cylinder by 450 psi of N_2. The stirring rate was increased to 170 rpm after the temperature stabilized at 80 °C. After 2 h, the autoclave was cooled to 25 °C and vented. Acetone (50 mL) was added to precipitate the polymer. The polymer was collected by filtration, rinsed with acetone, and dried under vacuum.

Pulsed-Gradient Spin-Echo (PGSE) NMR Experiments. All PGSE measurements were performed on a Bruker 500 MHz spectrometer using the Stejskal-Tanner method. Two identical pulsed field gradients with duration $\delta = 0.004$ s separated by a delay time $\Delta = 0.01418$ s were incorporated into a spin-echo sequence, one before and the other after the 180° pulse. ^{1}H NMR spectra were recorded in CD_2Cl_2 or CD_3OD at 295.5 K without sample spinning. During each experiment, the gradient strength (G) was varied between 0 and 26 G/cm while keeping all other factors constant. The gradient was calibrated using a solution of 2% H_2O in D_2O. After obtaining the spectra, careful integration was carried out. In all studies, the integral of the Pd-Me resonance were used to evaluate signal intensity. A linear plot of $\ln(I/I_0)$ (I = integral of a peak in the presence of G; I_0 = integral of the peak without a gradient) versus G^2 was generated. According to eq 1, the slope of this line is proportional to the diffusion coefficient and thus inversely proportional to the hydrodynamic radius of the molecule according to the Stokes-Einstein equation (eq 2). Hydrodynamic volumes were estimated by eq 3.

$$\ln(I/I_0) = -\gamma_H^2 \delta^2 G^2 (\Delta - \delta/3) D \quad (1)$$

where γ_H = magnetogyric ratio of ^{1}H; δ = length of the gradient pulse; Δ = delay between the midpoints of the gradients; D = diffusion coefficient.

$$r_H = k_B T/(6\pi\eta D) \quad (2)$$

where r_H = hydrodynamic radius, k_B = Boltzmann constant; T = temperature; η = viscosity of the solvent.

$$V_H = 4\pi r_H^3/3 \quad (3)$$

where V_H = hydrodynamic volume.

Figure 2.36. Linear plot of PGSE data (eq 1) for **5b** in CD_2Cl_2 solution at 22.5 °C. Δ = 0.01418 s. The intrinsic viscosity of CD_2Cl_2 at 22.5 °C is 0.42 × 10^{-6} Pa•s. From eq 1-3, V_H = 8.0 × 10^3 Å.[23]

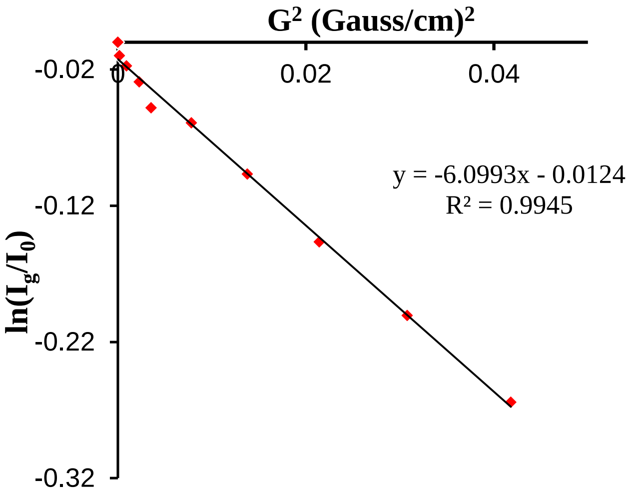

Figure 2.37. Linear plot of PGSE data (eq 1) for **5b** in CD_3OD solution at 22.5 °C. $\Delta = 0.01418$ s. The intrinsic viscosity of CD_3OD at 22.5 °C is 0.554×10^{-6} Pa•s. From eq 1-3, $V_H = 2.0 \times 10^3$ Å.

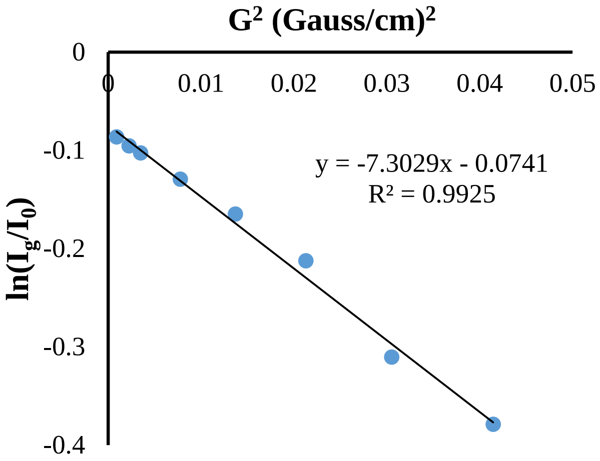

NMR studies of the equilibrium between Pd_4 and Pd_1 species for 5b. Pd_4 cage species **5b** undergoes partial reversible dissociation to monomeric Pd_1 species above room temperature. NMR studies of **5b** dissociation were conducted in $CDCl_2CDCl_2$ over the temperature range 50-80 ˚C by ^1H NMR (Figure 2.38). The resonance at ca. δ 0.6 is assigned to Pd_1 species, based on the Pd-*Me* chemical shifts observed for **5b** in CD_3OD and the product of the reaction of **5b** with Cryptand211.

Figure 2.38. (a) Variable temperature NMR spectra of **5b** in $CDCl_2CDCl_2$ from 50-80 ˚C. (b) Pd-Me region expansion.

(a)

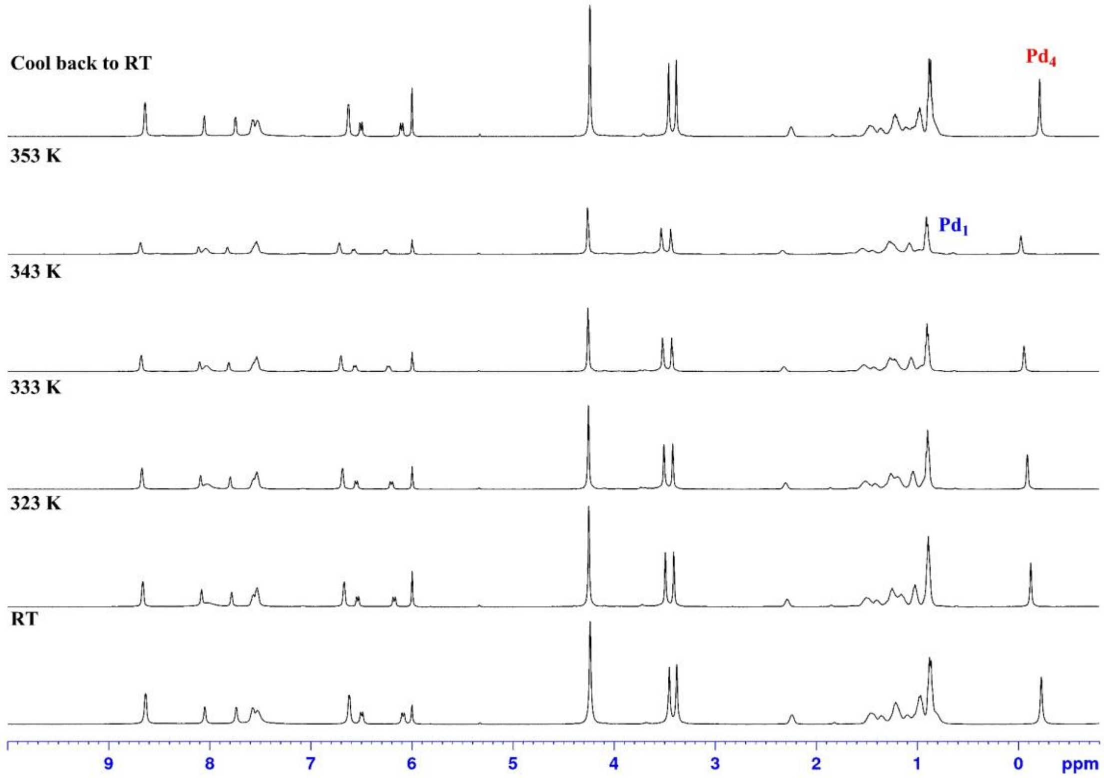

Figure 2.38, continued.

(b)

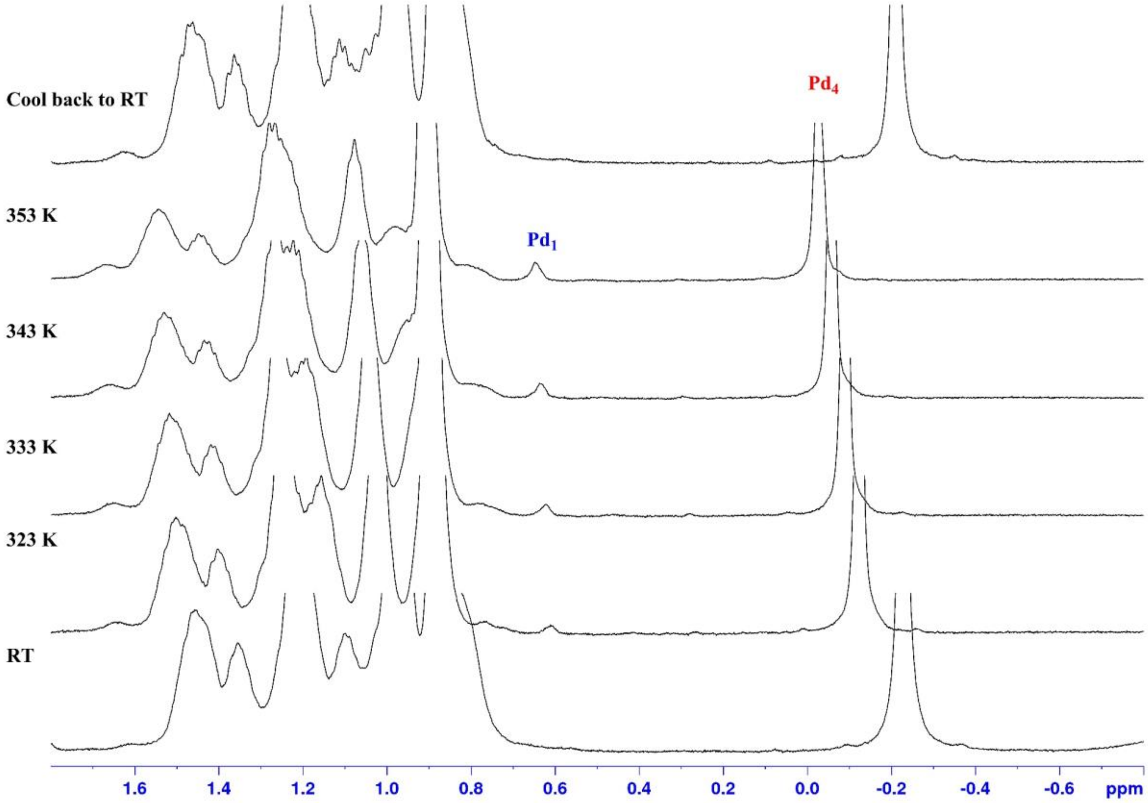

It is not possible to define the speciation and hence the concentration or activity of the Li$^+$ and Cl$^-$ ions, due to possible ion-pairing of the Li$^+$ and Cl$^-$ ions with Pd$_1$ species, or possible aggregation between Li$^+$ and Cl$^-$ ions, or possible precipitation of LiCl. Therefore, it is not possible to define the equilibration expression. However, a qualitative assessment of the stability of **5b** toward cage dissociation versus that of [(Li-OPO)PdMeL]$_4$ compounds **A-D** (**A**: L = py'; **B-D**: L = py) is provided by comparison of the [Pd$_4$]/[Pd$_1$] ratio at a constant [Pd$_4$]$_0$ at 80 °C. These data are given in Table 2.2.

It is possible to define apparent K_{eq} values for the dissociation of **5b**, if assumptions are made concerning the speciation of LiCl in the cage dissociated Pd_1 form. This section treats the equilibrium under two limiting situations.

Scenario 1: Four Li^+ ions are associated with each Pd_1 species, and the remaining 2 Li^+ and 2 Cl^- ions are free (solvated) ions, so that the equilibrium is

$$Pd_4 \rightleftharpoons 4\ Pd_1 + 2\ Li^+ + 2\ Cl^-$$

$$\boldsymbol{K_{eq,apparent} = [Pd_1]^4[Li^+]^2[Cl^-]^2/[Pd_4]}$$

Table 2.5. Analysis of equilibrium between Pd_4 and Pd_1 species for **5b** in $CDCl_2CDCl_2$, under the assumption of scenario 1.

Temp (K)	$[Pd_4]^a$ (10^{-3} M)	$[Pd_1]^a$ (10^{-3} M)	$[Li^+]^a$ (10^{-3} M)	$[Cl^-]^a$ (10^{-3} M)	$K_{eq,apparent}^{\Theta}$ (10^{-25} M^7)	$\ln(K_{eq,apparent}^{\Theta})^b$	1000/T
353	4.43	1.24	0.62	0.62	789	-50.9	2.83
343	4.54	0.811	0.4055	0.4055	25.7	-54.3	2.92
333	4.65	0.392	0.196	0.196	0.0749	-60.2	3.00
323	4.69	0.219	0.1095	0.1095	0.000705	-64.8	3.10

[a] **5b**: 9.7 mg, 2.71 μmol; $CDCl_2CDCl_2$: 0.924 g, 0.572 mL; $[Pd_4]_0$ = 4.74 mM. [b] c^{Θ} = 1M

Figure 2.39. Van't Hoff plot of **5b**, under the assumption of scenario 1. $\Delta H_{\text{apparent}}$ = 106 kcal/mol, $\Delta S_{\text{apparent}}$ = 199 cal/mol·K and $\Delta G_{\text{apparent}}$ (80 °C) = 35.7 kcal/mol.

$$\mathrm{Pd_4} \rightleftharpoons 4\ \mathrm{Pd_1} + 2\ \mathrm{Li^+} + 2\ \mathrm{Cl^-}$$

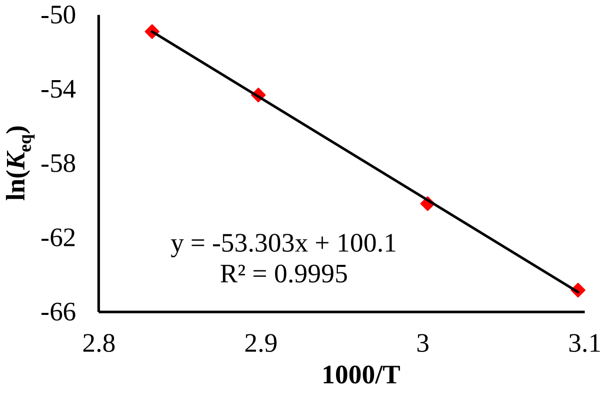

Scenario 2: All of the $\mathrm{Li^+}$ and $\mathrm{Cl^-}$ ions are associated with $\mathrm{Pd_1}$ species, so that equilibrium is

$$\mathrm{Pd_4} \rightleftharpoons 4\ \mathrm{Pd_1}$$

$$\boldsymbol{K_{eq,apparent}} = [\boldsymbol{Pd_1}]^4/[\boldsymbol{Pd_4}]$$

Table 2.6. Analysis of equilibrium between $\mathrm{Pd_4}$ and $\mathrm{Pd_1}$ species for **5b** in $\mathrm{CDCl_2CDCl_2}$, under the assumption of scenario 2.

Temp (K)	$[\mathrm{Pd_4}]^a$ (10^{-3} M)	$[\mathrm{Pd_1}]^a$ (10^{-3} M)	$K_{\text{eq,apparent}}^{\Theta}$ (10^{-12} $\mathrm{M^9}$)	$\ln(K_{\text{eq,apparent}}^{\Theta})^b$	1000/T
353	4.43	1.24	534	-21.4	2.83
343	4.54	0.811	95.3	-23.1	2.92
333	4.65	0.392	5.08	-26.0	3.00
323	4.69	0.219	0.490	-28.3	3.10

[a] **5b**: 9.7 mg, 2.71 μmol; $\mathrm{CDCl_2CDCl_2}$: 0.924 g, 0.572 mL; $[\mathrm{Pd_4}]_0$ = 4.74 mM. [b] c^{Θ} = 1M.

Figure 2.40. Van't Hoff plot of **5b**, under the assumption of scenario 2. $\Delta H_{\text{apparent}}$ = 53 kcal/mol, $\Delta S_{\text{apparent}}$ = 108 cal/mol·K and $\Delta G_{\text{apparent}}$ (80 °C) = 15 kcal/mol.

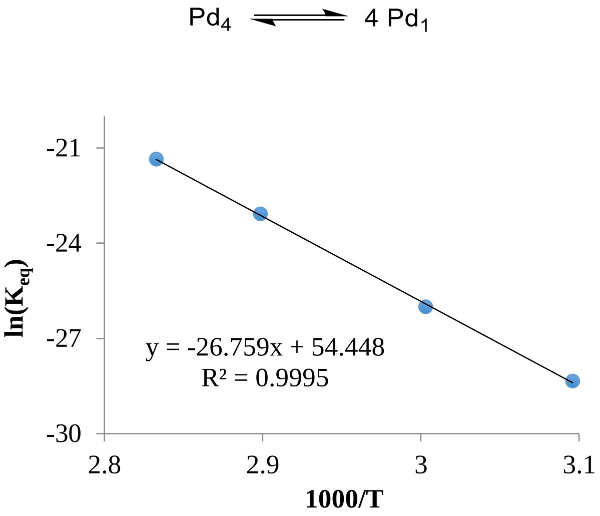

X-ray Crystallography. Data were collected on a Bruker D8 Venture diffractometer using Mo Kα radiation (0.71073 Å). Direct methods were used to locate many atoms from the E-map. Repeated difference Fourier maps enabled location of all expected non-hydrogen atoms. Following anisotropic refinement of all non-H atoms, ideal H atom positions were calculated. Final refinement was anisotropic for all non-H atoms and isotropic-riding for H atoms.

Specific details for structure refinement for 3a·2(CH_2Cl_2). Crystals were grown by layering pentane onto a CH_2Cl_2 solution and cooling to -40 °C under nitrogen. All atoms were refined with anisotropic thermal parameters. Hydrogen atoms were included in idealized positions for structure factor calculations.

Specific details for structure refinement for 3b·CH_2Cl_2. Crystals were grown by layering pentane onto a CH_2Cl_2 solution and cooling to -40 °C under nitrogen. All atoms were refined with anisotropic thermal parameters. Hydrogen atoms were included in idealized positions for structure factor calculations. One of the Ph-OMe substituents and a solvent molecule of CH_2Cl_2 were found to be disordered. Each was individually modeled over two orientations with the application of SIMU/RIGU restraints on thermal parameters for two parts.

Specific details for structure refinement for 3d. Crystals were grown by layering pentane onto a CH_2Cl_2 solution and cooling to -40 °C under nitrogen. All atoms were refined with anisotropic thermal parameters. Hydrogen atoms were included in idealized positions for structure factor calculations.

Specific details for structure refinement for 5b·6($CHCl_2CHCl_2$). Crystals were grown by diffusing pentane into $CHCl_2CHCl_2$ solution at room temperature under nitrogen. All atoms were refined with anisotropic thermal parameters except two disordered atoms of a nonyl dangling group. Several soft restrains were utilized on distances (SADI) and rigid body (RIGU) restrains. Hydrogen atoms were included in idealized positions for structure factor calculations. In addition to well resolved solvent molecules, crystal contained many disordered solvent molecules located in large solvent accessible voids. The diffuse contribution to scattering was treated by application of the program SQUEZZE[24] as implemented in Platon[25] using the “fab” file construct. SQUEEZE algorithm located a void, centered at (0, 0, 1), with a volume of 3944 $Å^3$ and the electron count of 1522. Such electron count may be consistent with 18 additional $CHCl_2CHCl_2$ solvent molecules.

Table 2.7. X-ray crystallographic parameters of **3a·2(CH_2Cl_2).**

Empirical formula	$C_{29}H_{32}Cl_4NO_6PPdS$
Formula weight	801.78
Temperature/K	100(2)
Crystal system	triclinic
Space group	*P*-1
a/Å	11.4869(5)
b/Å	12.1515(5)
c/Å	13.0397(5)
α/°	78.4180(10)
β/°	80.2470(10)
γ/°	67.7760(10)
Volume/Å^3	1641.81(12)
Z	2
ρ_{calc}g/cm^3	1.622
μ/mm^{-1}	1.045
F(000)	812.0
Crystal size/mm^3	0.36 × 0.2 × 0.18
Radiation	MoKα (λ = 0.71073)
2Θ range for data collection/°	4.734 to 57.51
Index ranges	$-14 \leq h \leq 14$, $-15 \leq k \leq 16$, $-17 \leq l \leq 17$
Reflections collected	32815
Independent reflections	7777 [R_{int} = 0.0268, R_{sigma} = 0.0240]
Data/restraints/parameters	7777/0/392
Goodness-of-fit on F^2	1.040
Final R indexes [I>=2σ (I)]	R_1 = 0.0262, wR_2 = 0.0591
Final R indexes [all data]	R_1 = 0.0321, wR_2 = 0.0616
Largest diff. peak/hole / e Å^{-3}	1.05/-0.86

Table 2.8. X-ray crystallographic parameters of **$3b{\cdot}CH_2Cl_2$.**

Empirical formula	$C_{29}H_{32}Cl_2NO_7PPdS$
Formula weight	746.88
Temperature/K	100(2)
Crystal system	monoclinic
Space group	$P2_1/n$
a/Å	11.4737(8)
b/Å	20.1607(14)
c/Å	13.5917(10)
α/°	90
β/°	91.464(2)
γ/°	90
Volume/Å^3	3143.0(4)
Z	4
ρ_{calc}g/cm^3	1.578
μ/mm^{-1}	0.924
F(000)	1520.0
Crystal size/mm^3	0.18 × 0.18 × 0.16
Radiation	MoKα (λ = 0.71073)
2Θ range for data collection/°	4.588 to 60.992
Index ranges	$-15 \leq h \leq 16$, $-27 \leq k \leq 28$, $-19 \leq l \leq 18$
Reflections collected	250766
Independent reflections	8717 [R_{int} = 0.0442]
Data/restraints/parameters	8717/449/486
Goodness-of-fit on F^2	1.058
Final R indexes [I>=2σ (I)]	$R_1 = 0.0265$, $wR_2 = 0.0574$
Final R indexes [all data]	$R_1 = 0.0366$, $wR_2 = 0.0610$
Largest diff. peak/hole / e Å^{-3}	0.98/-0.45

Table 2.9. X-ray crystallographic parameters of **3d.**

Empirical formula	$C_{26}H_{26}NO_5PPdS$
Formula weight	601.91
Temperature/K	100(2)
Crystal system	monoclinic
Space group	$P2_1/n$
a/Å	10.4843(7)
b/Å	21.4281(13)
c/Å	11.2502(7)
α/°	90
β/°	97.925(2)
γ/°	90
Volume/Å^3	2503.3(3)
Z	4
ρ_{calc}g/cm^3	1.597
μ/mm^{-1}	0.927
F(000)	1224.0
Crystal size/mm^3	0.14 × 0.12 × 0.08
Radiation	MoKα (λ = 0.71073)
2Θ range for data collection/°	4.98 to 54.318
Index ranges	$-13 \leq h \leq 13$, $-27 \leq k \leq 26$, $-14 \leq l \leq 14$
Reflections collected	35006
Independent reflections	5506 [$R_{int} = 0.0454$]
Data/restraints/parameters	5506/0/319
Goodness-of-fit on F^2	1.046
Final R indexes [I>=2σ (I)]	$R_1 = 0.0311$, $wR_2 = 0.0587$
Final R indexes [all data]	$R_1 = 0.0491$, $wR_2 = 0.0637$
Largest diff. peak/hole / e Å^{-3}	0.59/-0.48

Table 2.10. X-ray crystallographic parameters of **5b·6(CHCl$_2$CHCl$_2$).**

Empirical formula	$C_{160}H_{200}Cl_{26}Li_6N_4O_{40}P_4Pd_4S_8$
Formula weight	4588.53
Temperature/K	100(2)
Crystal system	orthorhombic
Space group	$P2_12_12$
a/Å	23.055(3)
b/Å	23.056(2)
c/Å	23.990(3)
α/°	90
β/°	90
γ/°	90
Volume/Å^3	12752(2)
Z	2
ρ_{calc}g/cm^3	1.195
μ/mm^{-1}	0.695
F(000)	4680.0
Crystal size/mm^3	0.21 × 0.14 × 0.12
Radiation	MoKα (λ = 0.71073)
2Θ range for data collection/°	4.216 to 50.16
Index ranges	$-27 \leq h \leq 26$, $-27 \leq k \leq 27$, $-28 \leq l \leq 26$
Reflections collected	164653
Independent reflections	20879 [R_{int} = 0.0565, R_{sigma} = 0.0565]
Data/restraints/parameters	20879/183/1147
Goodness-of-fit on F^2	1.045
Final R indexes [I>=2σ (I)]	R_1 = 0.0563, wR_2 = 0.1297
Final R indexes [all data]	R_1 = 0.0788, wR_2 = 0.1371
Largest diff. peak/hole / e Å^{-3}	0.59/-0.43
Flack parameter	0.068(6)

2.5 References and Notes

1. (a) Nakamura, A.; Ito, S.; Nozaki, K. *Chem. Rev.* **2009**, *109*, 5215. (b) Nakamura, A.; Anselment, T. M. J.; Claverie, J.; Goodall, B.; Jordan, R. F.; Mecking, S.; Rieger, B.; Sen, A.; van Leeuwen, P. W. N. M.; Nozaki, K. *Acc. Chem. Res.* **2013**, *46*, 1438. (c) Ito, S.; Nozaki, K. *The Chemical Record* **2010**, *10*, 315.

2. Shen, Z.; Jordan, R. F. *J. Am. Chem. Soc.* **2010**, *132*, 52.

3. Shen, Z.; Jordan, R. F. *Macromolecules* **2010**, *43,* 8706.

4. Wei, J.; Shen, Z.; Filatov, A. S.; Liu, Q.; Jordan, R. F. *Organometallics* in press.

5. (a) Braude, E. A., CHAPTER 4 - Ultraviolet and Visible Light Absorption. In *Determination of Organic Structures by Physical Methods,* Academic Press: 1955; pp 131. (b) Dippy, J. F. J. *Chem. Rev.* **1939**, *25*, 151.

6. Calculated using ACD/Labs Percepta Predictors, I-Lab 2.0, Algorithm Version: v5.0.0.184

7. Serjeant, E. P.; Dempsey, B., *Ionisation constants of organic acids in aqueous solution*. Pergamon Press: Oxford ; New York, 1979.

8. ^{i}Bu-protected **[6a-c]-^{i}Bu** were used due to the poor solubility of **Li[6a-c]** in THF.

9. Kochi, T.; Noda, S.; Yoshimura, K.; Nozaki, K. *J. Am. Chem. Soc.* **2007**, *129*, 8948.

10. Flack, H. D. *Helv. Chim. Acta* **2003**, *86*, 905.

11. (a) Zhang, H.-x.; Shin, Y.-j.; Lee, D.-h.; Yoon, K.-B. *Polym. Bull.* **2011**, *66*, 627. (b) *Engineered materials handbook*. Array ed.; ASM International: Materials Park, OH, 1995.

12. In contrast, the lower MW PE samples require only 2 h complete dissolution under the same condition.

13. GPC analysis conducted by ExxonMobil shows ca. 50~60 % recovery after analysis for high-MW PE, while for low-MW PE, ca. 100 % recovery was obtained.

14. (a) Baklouti, A.; Chaabouni, M. M. *J. Fluorine Chem.* **1981**, *19*, 181. (b) Macnaughtan, M. L.; Gary, J. B.; Gerlach, D. L.; Johnson, M. J. A.; Kampf, J. W. *Organometallics* **2009**, *28*, 2880. (c) Boz, E.; Wagener, K. B.; Ghosal, A.; Fu, R.; Alamo, R. G. *Macromolecules* **2006**, *39*, 4437. (d) Weng, W.; Shen, Z.; Jordan, R. F. *J. Am. Chem. Soc.* **2007**, *129*, 15450. (e) Wada, S.; Jordan, R. F. *J. Am. Chem. Soc.* submitted.

15. High polarity solvent chlorobenzene may promote β-F elimination to form Pd-F complexed, and result in the formation of $-CH_2CF_2H$ end group.

16. Vela, J.; Lief, G. R.; Shen, Z.; Jordan, R. F. *Organometallics* **2007**, *26*, 6624.

17. Borkar, S.; Newsham, D. K.; Sen, A. *Organometallics* **2008**, *27*, 3331.

18. Evans, P.; McCabe, T.; Morgan, B. S.; Reau, S. *Org. Lett.* **2005**, *7*, 43.

19. Rulke, R. E.; Ernsting, J. M.; Spek, A. L.; Elsevier, C. J.; van Leeuwen, P. W. N. M.; Vrieze, K. *Inorg. Chem.* **1993**, *32*, 5769.

20. Grinshpun, V.; Rudin, A. *Die Makromolekulare Chemie, Rapid Communications* **1985**, *6*, 219.

21. An increased J_{PC} of ipso C^7 was observed in the complex compared to those in free ligand.

22. The mass spectroscopy analysis is very challenging for **5b**, which is due to the cage fragmentation under the APCI/ES MS conditions. The highest intensity peak was assigned to Pd_2 $\{[(Li\text{-}OPO)PdMe(py')]_2 - Li^+ + 2\ H^+\}$ signal.

23. Volume ($V_{\text{x-ray}}$) for **5b** and **A** that are derived from X-ray analyses were calculated by dividing unit cell volume (V) by formula units per cell (Z). $V_{\text{x-ray}}$ for **5b** and **A** are 6.4×10^3 Å and 5.4×10^3 Å, respectively. These results are ca. 15-20 % smaller compared to the PGSE-NMR result.

24. (a) van der Sluis, P.; Spek, A. L. *Acta Cryst. A.* **1990**, *46*, 194. (b) Spek, A. *Acta Cryst. C.* **2015**, *71*, 9.

25. Spek, A. *Acta Cryst. D.* **2009**, *65*, 148.

CHAPTER THREE

Multinuclear Palladium Olefin Polymerization Catalysts Based On Self-Assembled Zinc Phosphonates Compounds

3.1 Introduction

Palladium alkyl complexes that contain the phosphine-bis(arensulfonate) ligand PPh(2-SO_3Li-5-Me-Ph)(2-SO_3^--5-Me-Ph) (Li[OPO]$^-$) self-assemble into tetrameric structures, in which four (Li-OPO)PdMeL units are arranged on the periphery of a cubic cage formed by the non-Pd-bonded $ArSO_3Li$ group and one oxygen from the Pd-bonded $ArSO_3^-$ group. One example [(Li-OPO)PdMe(py')]$_4$ (**A**, py' = 4-(5-nonyl)-pyridine) is shown in Figure 3.1.[1] However, **A** undergoes partial reversible dissociation into a monomeric Pd_1 species (Li-OPO)PdMe(py') in CH_2Cl_2 above -10 ˚C. Compound **A** polymerizes ethylene to linear PE and copolymerizes ethylene with vinyl fluoride (VF) to produce linear copolymers containing up to 3.6 mol % VF (Scheme 3.1).[1-2] The polymerization behavior is strongly influenced by the extent of dissociation of **A** to monomeric Pd_1 species under polymerization conditions. Under conditions where **A** is only partially dissociated (hexanes slurry at 80 °C, CH_2Cl_2 solution at 25 °C), **A** produces linear PE that has a broad bimodal MWD and contains a high MW fraction (ca. 10^6 Da) and low MW fraction (ca. 10^4 Da). Under conditions where **A** is completely dissociated (dilute toluene solution at 80 °C), **A** produces linear PE with low MW (ca. 10^4 Da) and a narrow MWD. These results suggest the intact Pd_4 species produce the high MW fraction, while the Pd_1 species produces the low MW fraction. For comparison, the mononuclear Pd_1 complex (PO^{OMe})PdMe(py) produces PE with a Schultz-

Flory MWD with a MW ca. 10^4 Da.[3] We are interested in synthesizing analogs of **A** that are more robust under polymerization conditions, in order to pursue mechanistic studies to probe why the intact cage produces high-MW polymer and to develop new applications in copolymerization.

Figure 3.1. {[κ^2-*P*,*O*-PPh(2-SO_3-5-Me-Ph)(2-SO_3Li-5-Me-Ph)]PdMe(py')}$_4$ (**A**, py' = 4-(5-nonyl)pyridine). Hydrogen atoms and 5-nonyl groups are omitted in x-ray structure.

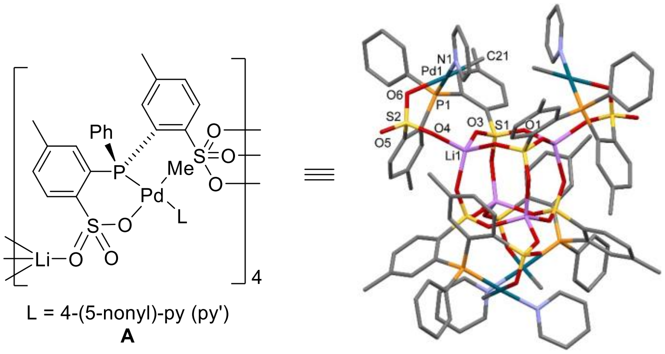

Scheme 3.1

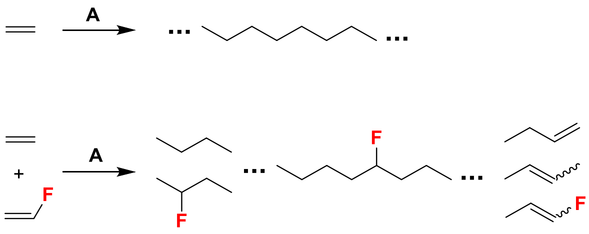

Several analogous Pd_4 cage complexes based on PPh(2-SO_3Li-5-R-Ph)(2-SO_3^--5-R-Ph) ligands (R = ^{i}Pr, Cy, ^{t}Bu) that incorporate more electronic-donating 5-R substituents on the arenesulfonate rings were synthesized. However, they also partially dissociate into monomeric Pd_1 species in solution and exhibit similar thermal stability compared to **A**.[4]

The interactions between the Li^+ cations and the sulfonate oxygens in **A** and its analogs are inherently weak. A potentially powerful strategy for enhancing the stability of the central cage in the Pd_4 assemblies is to use a stronger Lewis acid/base pair such as Zn^{2+} and PO_3^{2-} to form the central cage.

Molecular zinc phosphonate clusters with two, three, four, six, seven, or twelve zinc atoms that exhibit a diverse range of structures have been isolated and structurally characterized by X-ray diffraction (Scheme 3.2).[5] Several dimeric zinc phosphonate compounds,[6] such as $Zn_2(3,5\text{-}^t Bu_2\text{-}2\text{-}OH\text{-}Ph\text{-}CH_2\text{-}PO_3)_2(TMEDA)_2(H_2O)_2\cdot 0.5CH_3CN$ (**B**),[6d] have been characterized and shown to contain a central eight-membered $Zn_2P_2O_4$ ring. Each zinc center in **B** is five coordinate and binds a bidentate TMEDA ligand, two bridging phosphonate oxygens, and one H_2O molecule. The trinuclear Zn phosphonate compound $Zn_3Cl_2(3,5\text{-}Me_2\text{-}Pz)_4(^t BuPO_3)_2$, (**C**, 3,5-$Me_2$-PzH = 3,5-dimethylpyrazole) adopts an interesting core structure with the three zinc centers held together by two triply bridging $^t BuPO_3^{2-}$ ligands.[7] Tetranuclear zinc phosphonate compounds have been reported to possess several different structures, such as the "open-book" planar tricyclic structure exhibited by $[Zn_4(2,4,6\text{-}^i Pr_3\text{-}Ph\text{-}PO_3)_2\{2,4,6\text{-}^i Pr_3\text{-}Ph\text{-}P(O)_2(OH)\}_2(3,5\text{-}Me_2\text{-}PzH)_4(3,5\text{-}Me_2\text{-}Pz)_2]\bullet 5MeOH$[8] (**D**) and the 3-dimensional "stacked" bridging structure exhibited by $[Zn_4(FMPA)_4(phen)_4]\bullet 7MeOH$ (**E**, FMPA = ferrocenyl-CH_2-PO_3H_2, phen = 1,10-phenanthroline)[9].

Scheme 3.2

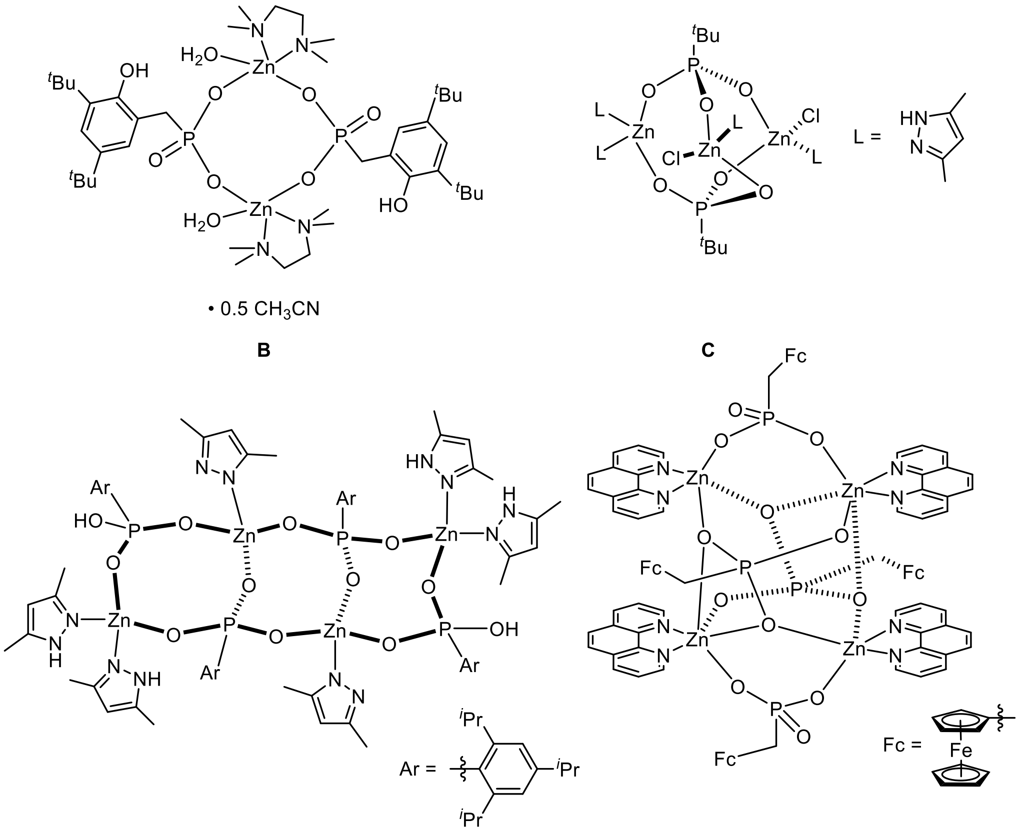

[^{t}BuPO$_3$Zn(2-apy)]$_4$ (**F**, 2-apy = 2-amino-pyridine, Scheme 3.3) was the first tetrameric D4R ("double 4-ring") cubic $Zn_4P_4O_{12}$ cage structure to be reported,[10] and is isostructural with the $Li_4S_4O_{12}$ cage of **A**. Murugavel and coworkers synthesized **F** by the reaction of ^{t}BuP(O)(OH)$_2$ and Zn(OAc)$_2$ in the presence of auxiliary ligand 2-amino-pyridine (2-apy). Crystals of **F** were obtained directly from the reaction mixture. The core of the cluster is a D4R zinc phosphonate cage and the 2-apy ligands cap the zinc corners. The 2-apy ligands are probably critical for the formation and crystallization of **F**. In studies of analogous cubic zinc phosphate compounds,[11] Murugavel found that the reaction of P(O-(2,6-^{i}Pr$_2$-Ph))O$_3$H$_2$ and Zn(OAc)$_2$ in the presence of a capping ligand L yielded L-capped cage compound {LZnO$_3$P(O-2,6-^{i}Pr$_2$-Ph)}$_4$ that could be isolated in crystalline form. In the absence of L, the reaction of (2,6-^{i}Pr$_2$-Ph)OPO$_3$H$_2$ and Zn(OAc)$_2$

yielded [Zn-{O_3P(O-2,6-$^iPr_2$-Ph)}(MeOH)]$_n$ that lost solvent rapidly to form a material whose powder X-ray diffraction pattern is similar to those of layered phosphonates such as [Zn(O_3PPh)(OH_2)]$_n$.[12] The NH_2 group of the 2-apy ligand in **F** engages in intra- and inter-molecular H-bonding, the latter of which links the [$^tBuPO_3Zn$(2-apy)]$_4$ cages into a 3-D polymer. The metrical parameters for the core cage of [$^tBuPO_3Zn$(2-apy)]$_4$ are similar to those of the $Li_4S_4O_{12}$ cage in **A**. The thermal behavior of solid [$^tBuPO_3Zn$(2-apy)]$_4$ has been studied by TGA and DSC. The first weight loss occurs in the temperature range of 170–200 ˚C and corresponds to the loss of the 2-apy ligand, which indicates that the $Zn_4P_4O_{12}$ core itself is quite robust. However, NMR spectroscopic measurements are unavailable due to the poor solubility of **F** in organic solvents.

Scheme 3.3

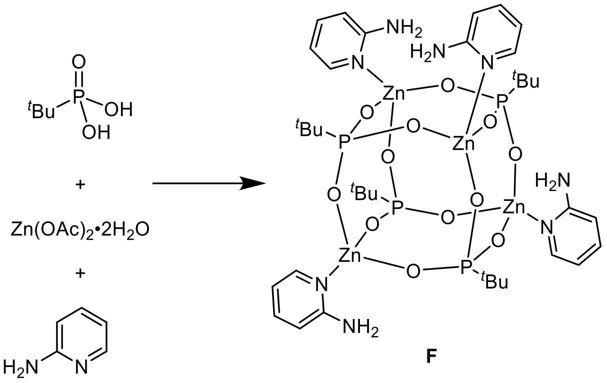

The objective of the present work was to synthesize Pd_4 catalysts that are based on zinc phosphonate cages analogous to that found in **F**. It was envisioned that the reaction of the zwitterionic phosphine-phosphonate-sulfonate proligand [PH^+(4-^{t}Bu-Ph)(2-PO_3H_2-5-Me-Ph)(2-SO_3^--5-Me-Ph)] (**1**-H_3, Scheme 3.4) with Zn(OAc)$_2$ would generate a cubic $Zn_4P_4O_{12}$ cage in which an oxygen from the $ArSO_3^-$ group would function as the Zn-capping ligand analogous to the 2-apy ligand in **F**. Subsequent metalation with an appropriate Pd compound would then deliver the targeted Pd_4 zinc phosphonate cage catalyst. The orientation of the Pd units and the Pd-Pd distances in this target were anticipated to be similar to those in **A** because of the close similarity of the structures and metrical parameters of the $Li_4S_4O_{12}$ cage in **A** and the $Zn_4P_4O_{12}$ cage in **F**. A dimeric Pd compound [{(κ^2-*P*,*SO*-(P(4-^{t}Bu-Ph)(2-PO_3Et_2-5-Me-Ph)(2-SO_3^--5-Me-Ph)))PdMe}$_2$(μ-Cl)]MgCl based on a similar phosphine-*diethylphosphonate*-sulfonate ligand was shown to self-assemble around the Mg^{2+} cation with a Pd-Pd distance of ca. 3.874 Å. After abstraction of Cl^- from [{(κ^2-*P*,*SO*-(P(4-^{t}Bu-Ph)(2-PO_3Et_2-5-Me-Ph)(2-SO_3^--5-Me-Ph)))PdMe}$_2$(μ-Cl)]MgCl using $AgB(C_6F_5)_4$, this species polymerizes ethylene to low-MW linear PE.[13]

Scheme 3.4. Ar = 4-^{t}Bu-Ph.

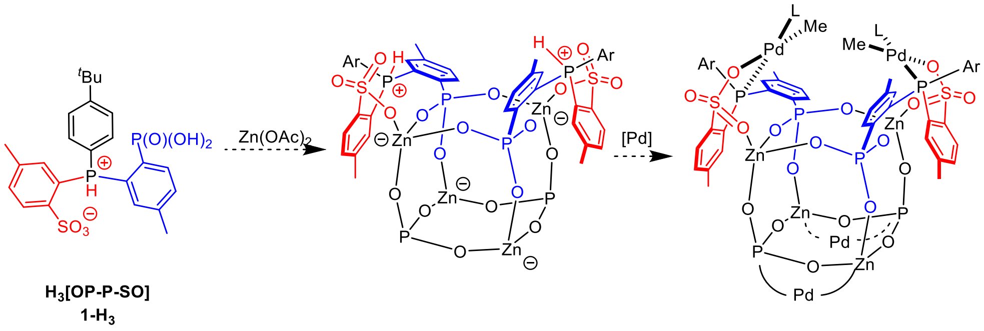

3.2 Results and Discussion

Synthesis of Phosphine-phosphonate-sulfonate (OP-P-SO) Proligand 1-H_3. Proligand **1**-H_3 was synthesized via the diethyl phosphonate intermediates Li[**1**-Et_2] and H[**1**-Et_2] as shown in Scheme 3.5. The reaction of (4-^{t}Bu-Ph)PCl_2 with 2 equiv of $HNEt_2$ gave mono-protected (4-^{t}Bu-Ph)PCl(NEt_2). Reaction of this compound with *ortho*-lithiated diethyl *para*-toluene-phosphonate and removal of the NEt_2 protecting group by reaction with HCl afforded (4-^{t}Bu-Ph)(2-P(O)(OEt)$_2$-5-Me-Ph)PCl. The reaction of this intermediate with Li[*para*-toluene-sulfonate] generated Li[**1**-

Et_2] in 79 % NMR yield based on $^{31}P\{^1H\}$ NMR. Li[**1**-Et_2] was acidified with aqueous HCl to form H[**1**-Et_2] in 98 % yield. H[**1**-Et_2] was purified by recrystallization from CH_2Cl_2/Et_2O. H[**1**-Et_2] was converted to **1**-H_3 by reaction with $SiMe_3Br$ followed by quenching with CH_3OH. **1**-H_3 is only sparingly soluble in CH_3OH. The product mixture was concentrated and sonicated for 2 h to form a white suspension, from which **1**-H_3 was isolated by filtration in 78 % yield. **1**-H_3 was characterized by $^{31}P\{^1H\}$,^1H, $^1H\{^{31}P\}$, $^{13}C\{^1H\}$ and COSY NMR experiments.

Scheme 3.5

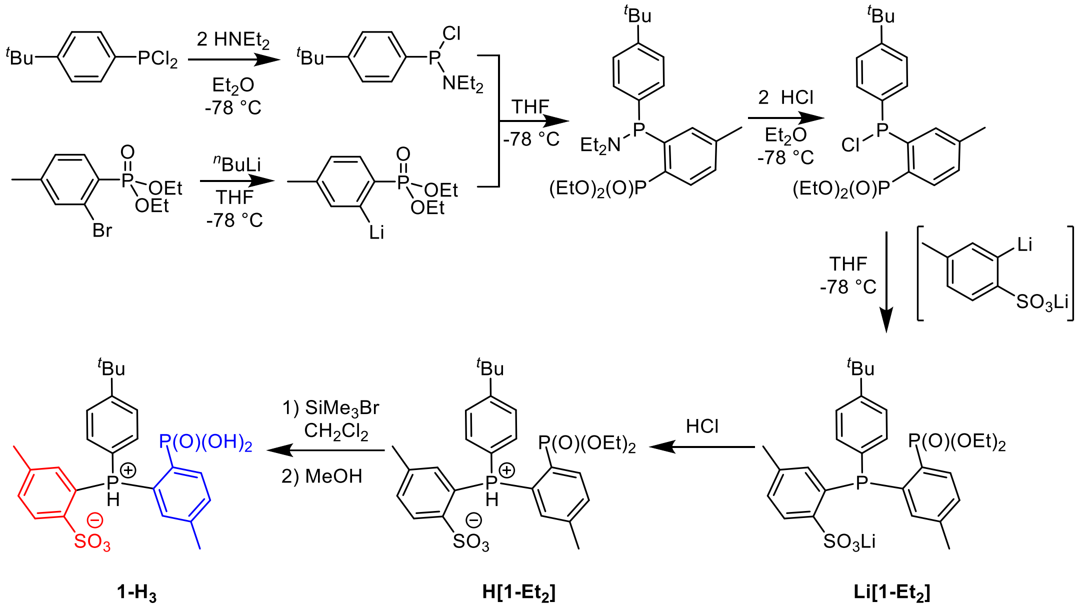

Li[**1**-Et_2] and H[**1**-Et_2] were previously synthesized by the sequential reaction of (4-^{t}Bu-Ph)PCl_2 with *ortho*-lithiated *para*-toluene-sulfonate and *ortho*-lithiated diethyl *para*-toluene-phosphonate without any protection/deprotection steps.[13] This procedure afforded Li[**1**-Et_2] in ca. 60 % NMR yield. However, the product contained major impurities including (4-^{t}Bu-Ph)(2-SO_3Li-5-Me-Ph)$_2$P and (4-^{t}Bu-Ph)(2-P(O)(OEt)$_2$-5-Me-Ph)$_2$P which were difficult to remove. The protection deprotection route in Scheme 3.5 minimized the formation these impurities and increased the crude yield of Li[**1**-Et_2] from 60 % to 79 %.

Synthesis of the Tetrameric Zinc Phosphonate Compound {Zn[1-H]}$_4$. The reaction of **1**-H$_3$ with Zn(OAc)$_2$•2H$_2$O in CH$_3$OH with a small amount of CH$_2$Cl$_2$ to dissolve **1**-H$_3$ generates a clear solution (Scheme 3.6). Concentration of the reaction mixture under vacuum induces precipitation or crystallization of the tetrameric compound {Zn[**1**-H]}$_4$ directly from the reaction mixture. Isolated {Zn[**1**-H]}$_4$ contains a variable amount of CH$_3$OH (2 to 64 equiv per {Zn[**1**-H]}$_4$ unit). Drying solid {Zn[**1**-H]}$_4$ under vacuum at room temperature for 1 d reduces the CH$_3$OH content to ca. 1.5 equiv per {Zn[**1**-H]}$_4$ unit. Complete CH$_3$OH removal requires heating at 50 °C under vacuum for 2 d. CH$_3$OH may or may not have an effect on the reactivity of {Zn[**1**-H]}$_4$ depending on the reaction, as discussed below.

Scheme 3.6. Ar = 4-^{t}Bu-Ph.

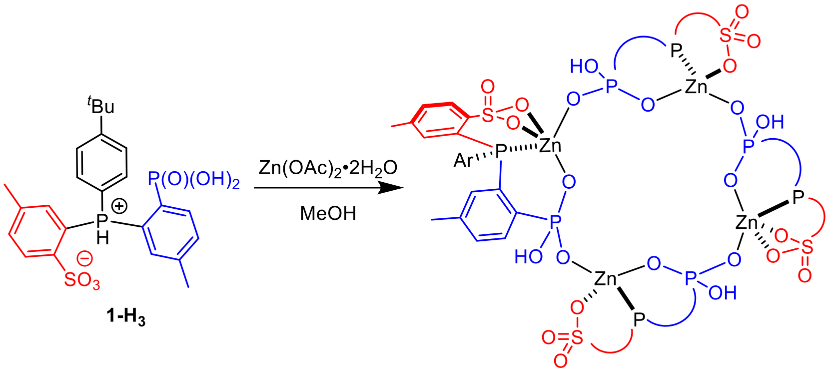

{Zn[1-H]}$_4$

Crystallization of {Zn[**1**-H]}$_4$ from a concentrated reaction mixture (ca. 0.02 M in Zn^{2+}) affords X-ray quality crystals of {Zn[**1**-H](CH$_3$OH)}$_4$•12CH$_3$OH, the solid-state structure of which is shown in Figure 3.2. {Zn[**1**-H](CH$_3$OH)}$_4$•12CH$_3$OH is held together by a puckered 16-membered Zn$_4$P$_4$O$_8$ ring. The Zn atoms are 5 or 6 coordinate, with one CH$_3$OH ligand, one phosphine ligand, two oxygens from bridging ArPO$_3^{2-}$ groups, and one or two oxygens from the ArSO$_3^-$ group. The acidic protons were located on the ArPO$_3^{2-}$ oxygens. {Zn[**1**-H](CH$_3$OH)}$_4$ has

C_i symmetry with *SSRR* configurations at the phosphorus centers. In addition to the four Zn^{2+}-coordinated CH$_3$OH molecules, twelve additional CH$_3$OH molecules are present within the voids between the {Zn[**1**-H](CH$_3$OH)}$_4$ molecules. The Zn^{2+}-coordinated CH$_3$OH molecules form intramolecular H-bonds to oxygens from the ArSO$_3^-$ or ArPO$_3$H$^-$ groups. The non- Zn^{2+}-coordinated CH$_3$OH molecules are H-bonded to oxygens from the ArSO$_3^-$ groups or protons from the ArPO$_3$H$^-$ groups. All of the CH$_3$OH molecules are involved in an extensive H-bonding network inside and outside of the {Zn[**1**-H]}$_4$ cluster.

Figure 3.2. Molecular structure of {Zn[**1**-H](CH$_3$OH)}$_4$•12CH$_3$OH. Hydrogen atoms except acidic protons and non-Zn^{2+}-coordinated CH$_3$OH molecules are omitted. Selected bond lengths (Å) and angles (deg): Zn1-O5 2.136(2), Zn2-O1 2.059(2), Zn1-O6 2.015(2), Zn2-O12 2.536(3), Zn2-O13 2.407(3), Zn1-P1 2.6115(9), Zn2-P4 2.4845(8), Zn1-O4 1.959(2), Zn1-O9 1.913(2), Zn2-O2 1.974(2), Zn2-O10 1.978(2), P2-O2 1.498(2), P2-O4 1.513(2), P3-O9 1.498(2), P3-O10 1.506(2), O9-Zn1-O4 120.01(9), O2-Zn2-O10 116.99(9), O2-P2-O4 112.96(12), O9-P3-O10 116.24(13).

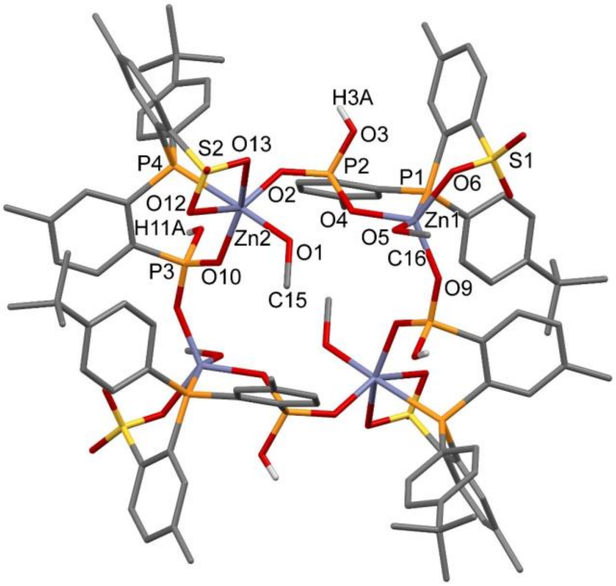

A micro-crystal (dimensions 10 x 12 x 15 μm) of $\{Zn[\mathbf{1}\text{-}H](CH_3OH)_{0.5}\}_4 \bullet \{Zn[\mathbf{1}\text{-}H](CH_3OH)_{0.75}\}_4 \bullet 6CH_3OH \bullet 2H_2O$ was obtained by crystallization of $\{Zn[\mathbf{1}\text{-}H]\}_4$ from a more concentrated reaction mixture (ca. 0.03 M in Zn^{2+}), and its structure was determined by X-ray diffraction with synchrotron radiation. The resolution of this structure is low, but the results are sufficient for the determination of atom connectivity and comparison with the structure of $\{Zn[\mathbf{1}\text{-}H](CH_3OH)\}_4 \bullet 12CH_3OH$. Two $\{Zn[\mathbf{1}\text{-}H](CH_3OH)_n\}_4$ molecules are present in the asymmetric unit. The first (cluster 1), shown in Figure 3.3, is a $\{Zn[\mathbf{1}\text{-}H](CH_3OH)_{0.5}\}_4$ cluster that has the same structure as $\{Zn[\mathbf{1}\text{-}H](CH_3OH)\}_4$ in Figure 3.2, except that the four $ArSO_3^-$ groups only donate one oxygen to each Zn^{2+} center and only two Zn^{2+}-coordinated CH_3OH molecules are present. The second is a 50/50 disordered mixture of cluster 1 and a $\{Zn[\mathbf{1}\text{-}H](CH_3OH)\}_4$ cluster that has the same structure of cluster 1, but contains four Zn^{2+}-coordinated CH_3OH molecules. Six non-Zn^{2+}-coordinated CH_3OH molecules and one non-coordinated H_2O molecule form an intensive H-bonding network that links the clusters.

Figure 3.3. Molecular structure of the $\{Zn[\mathbf{1}\text{-}H](CH_3OH)_{0.5}\}_4$ molecule (Cluster 1) in $\{Zn[\mathbf{1}\text{-}H](CH_3OH)_{0.5}\}_4 \bullet \{Zn[\mathbf{1}\text{-}H](CH_3OH)_{0.75}\}_4 \bullet 6CH_3OH \bullet 2H_2O$. Hydrogen atoms except acidic protons, H_2O molecules and non-Zn^{2+}-coordinated CH_3OH molecules are omitted.

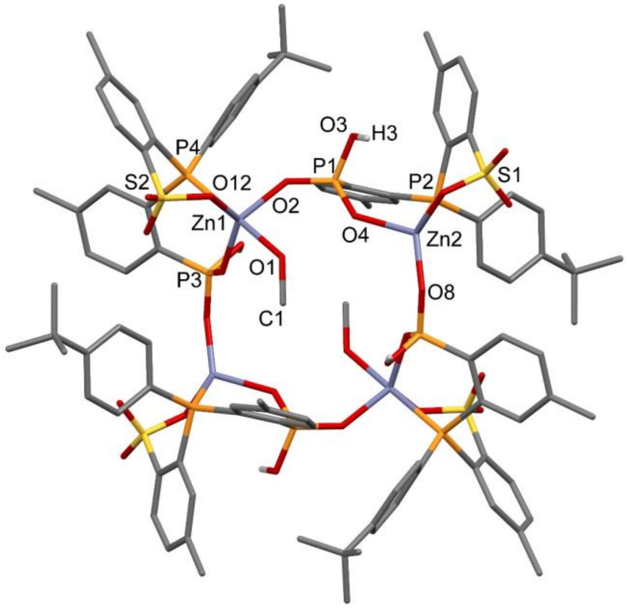

Although there are some differences in the solid-state structures of $\{Zn[\mathbf{1}\text{-}H](CH_3OH)\}_4 \bullet 12CH_3OH$ and $\{Zn[\mathbf{1}\text{-}H](CH_3OH)_{0.5}\}_4 \bullet \{Zn[\mathbf{1}\text{-}H](CH_3OH)_{0.75}\}_4 \bullet 6CH_3OH \bullet 2H_2O$, the core structure of each compound is composed of the same puckered 16-membered $Zn_4P_4O_8$ ring and has the same configurations at the phosphorus centers. The observation that this core structure can accommodate different levels of CH_3OH ligation suggests that it is quite stable. This core structure is similar to that in the diuclear zinc phosphonate compound **B** in Scheme 3.2,[6d] in that both compounds contain μ^2-κ^1,κ^1 bridging phosphonate units.

Solution Behavior of {Zn[1-H]}$_4$. Isolated $\{Zn[\mathbf{1}\text{-}H]\}_4 \bullet nCH_3OH$ (n = 0 to 64) is only soluble in DMSO. The $^{31}P\{^1H\}$ NMR spectrum of $\{Zn[\mathbf{1}\text{-}H]\}_4 \bullet nCH_3OH$ (n = 0 to 64) in dmso-d_6 contains only one phosphine resonance (δ -17.6) and one broad phosphonate resonance (δ 12.1) (Figure

3.4). The broad phosphonate resonance is consistent with the location of the acidic protons on the $ArPO_3^{2-}$ oxygen, where fast intermolecular exchange is expected. The ^1H NMR spectrum of {Zn[**1**-H]}$_4$ is broad, but contains only one set of resonances, which is consistent with {Zn[**1**-H]}$_4$ adopting a symmetric structure in solution. The CH_3OH resonance appears at δ 3.17, the chemical shift of free CH_3OH in dmso-d_6.[14] This observation and the variable amounts of Zn^{2+}-coordinated-CH_3OH observed in the crystal structures show that the CH_3OH is labile and does not influence the macrocyclic zinc phosphonate ring structure. The hydrodynamic volume of {Zn[**1**-H]}$_4$ determined by PGSE-NMR in dmso-d_6 at room temperature is ca. 5.1×10^3 Å, which is ca. four times larger than that for **1**-H_3 (ca. 1.3×10^3 Å). These results suggest that {Zn[**1**-H]}$_4$ adopts the same tetrameric structure in solution as in the solid state.

Figure 3.4. $^{31}P\{^1H\}$ NMR spectrum of {Zn[**1**-H]}$_4$ in dmso-d_6 at 25 °C. Assignments: δ 12.1 = *P*=O; -17.6 = *P*Ar_3.

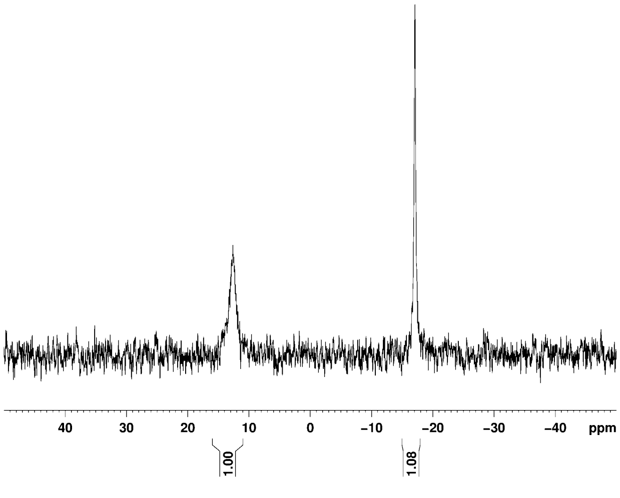

Factors that Influence the Structure of {Zn[1-H]}$_4$ and Implications for the Synthesis of Pd_4 Cage Catalysts. The reason that {Zn[**1**-H]}$_4$ adopts a 2-dimensional ring structure instead of 3-dimensional $Zn_4P_4O_{12}$ cage structure is that the phosphine units are coordinated to Zn^{2+} centers and the remaining acidic protons are located on $ArPO_3^{2-}$ oxygens. One possible explanation for this arrangement is that the non-Zn^{2+}-bonded phosphonate oxygen is more basic than the phosphine. Although the exact pK_a values for the $ArP(OZn)_2O^-$ and PAr_3 centers in {Zn[**1**-H]}$_4$ are unknown, the pK_a trend is expected to be similar to that for $PhPO_3H_2$ and PPh_3. In H_2O, phenylphosphonic acid has pK_a values of 1.83 and 7.07,[15] and triphenylphosphine has a pK_a value of 2.7.[16] Therefore, the location of the acidic proton at the $ArP(OZn)_2O^-$ oxygen, as in the observed 2D ring structure, rather than at the phosphine, as in the targeted 3D cage structure in Scheme 3.4, is reasonable based on pK_a values of these sites. Moreover, Zn^{2+} is a relatively soft Lewis acid compared to H^+. Therefore, the coordination of soft Lewis base phosphine to Zn^{2+} in the 2D structure, instead of to H^+ in the 3D structure, is also reasonable based on Lewis acid/base arguments. Another possible explanation for the observed 2D ring structure is that acidic protons at $ArP(OZn)_2OH$ units are capable of forming H-bonds, while such interactions at the phosphine are very rare. The extensive H-bonding stabilizes and favors the observed 2D ring structure.

Importantly, although {Zn[**1**-H]}$_4$ does not adopt a 3D $Zn_4P_4O_{12}$ cage structure, it has the correct composition and stereochemical configurations at the phosphorous centers for the ultimate formation of a Pd_4 cage catalyst. Therefore, its reactivity with Pd precursors was explored.

Reaction of {Zn[1-H]}$_4$ with (TMEDA)PdMe$_2$. The NMR scale reaction of {Zn[**1**-H]}$_4$•1.3CH_3OH with (TMEDA)$PdMe_2$ and pyridine in CD_2Cl_2 resulted in very complicated and broad $^{31}P\{^1H\}$ and ^1H NMR spectra, with at least four Pd-Me ^1H resonances (Scheme 3.7). Layering Et_2O onto the CH_2Cl_2 reaction mixture solution in a preparatory-scale experiment afforded a 23 % yield of colorless crystals, which were identified as {Zn^+(TMEDA)[κ^2-*P*,P*O*-P(4-^{t}Bu-Ph)(2-PO_3-5-Me-Ph)(2-SO_3^--5-Me-Ph)PdMe(py)]}$_2$ (**2**) by X-ray crystallography (Figure 3.5). Compound **2** adopts a dimeric C_i-symmetric structure in which two (*O*P-*P*-SO)PdMe(py) units are held together through an 8-membered $Zn_2P_2O_4$ ring, with *RS* configurations at the phosphorus centers. Each Zn^{2+} is four-coordinate and binds to two oxygens from bridging $ArPO_3^{2-}$ groups and two nitrogens from the bidentate ligand TMEDA. The OP-P-SO ligand chelates to each Pd(II) center through the phosphine and one phosphonate oxygen (κ^2-*P*,*PO*), leaving the $ArSO_3^-$ groups essentially free in the solid-state structure. The Pd1-O4 distance is 3.146 Å, which is equal to the sum of the van der Waals radii of palladium and oxygen (3.15 Å). Similar arrangements of pendant $ArSO_3^-$ groups in Pd catalysts have been reported previously. In the complex [Li-(Crytand211)][[κ^2-*P*,*O*-PPh(2-SO_3-5-Me-Ph)$_2$]PdMe(py')], a weak interaction of the dangling $ArSO_3^-$ group with the Pd center was observed with a Pd-O distance of ca. 3.08 Å.[1] Another case is [κ^2-*P*,*PO*-P(4-^{t}Bu-Ph)(2-PO_3Et_2-5-Me-Ph)(2-$SO_3(B(C_6F_5)_3)$-5-Me-Ph)]PdMe(2,6-lutidine), in which the $ArSO_3^-$ group is positioned above one of the axial sites of the Pd center with a Pd-O distance of ca. 3.043 Å.[13] Several binuclear zinc phosphonate compounds that adopt the same core structure as that observed in **2** have been reported.[6] The compound [Zn_2(3,5-^{t}Bu$_2$-2-OH-Ph-CH$_2$-PO_3)$_2$(TMEDA)$_2$(H_2O)$_2$]·0.5CH_3CN[6d] contains a bidentate TMEDA ligand and has a very similar structure to **2** (**B**, Scheme 3.2). The main structural difference is that in **B**, the zinc centers are 5-coordinate due to the presence of an extra H_2O ligand.

Scheme 3.7. Ar = 4-^{t}Bu-Ph.

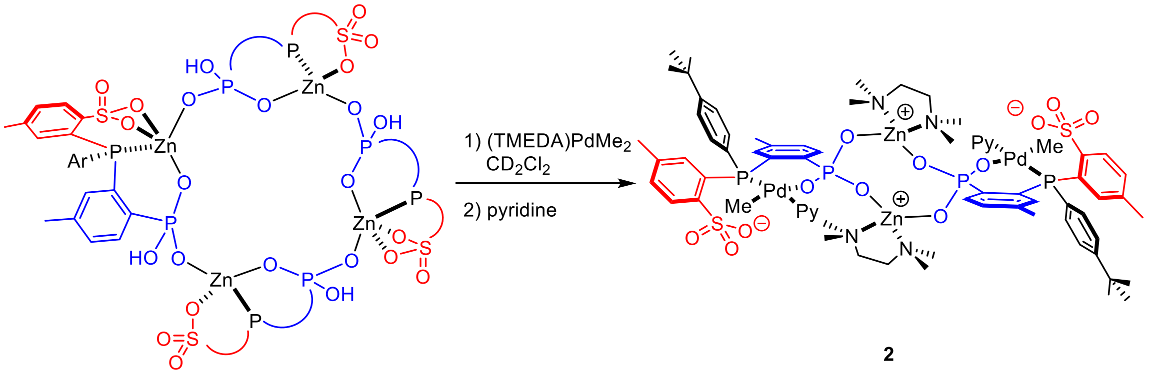

{Zn[1-H]}$_4$

2

Figure 3.5. Molecular structure of **2**•4CH_2Cl_2. Hydrogen atoms and solvent molecules are omitted. Selected bond lengths (Å) and angles (deg): Pd1-C1 2.030(5), Pd1-N1 2.104(4), Pd1-O3 2.126(3), Pd1-P1 2.2136(13), Zn1-O2 1.907(3), Zn1-O1 1.928(3), Zn1-N2 2.068(4), Zn1-N3 2.087(4), P2-O1 1.515(4), P2-O2 1.521(3), P2-O3 1.519(3), C1-Pd1-N1 89.08(19), C1-Pd1-O3 174.16(19), N1-Pd1-O3 85.20(13), C1-Pd1-P1 89.80(16), N1-Pd1-P1 177.57(11), O3-Pd1-P1 95.96(9), O2-Zn1-O1 117.22(14), N2-Zn1-N3 87.08(16), O1-P2-O2 111.57(19).

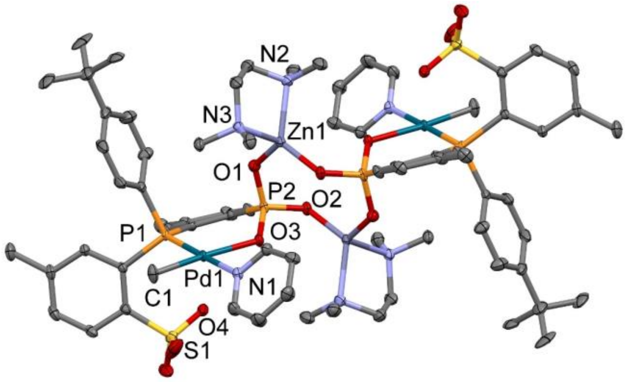

The NMR spectra of crystalline **2** in CD_2Cl_2 solution are complicated and similar to those of the reaction mixture from Scheme 3.7. While it is clear that **2** forms several species in solution, the precise speciation is unknown. A variety of structures could form by exchange between the (free) $ArSO_3^-$ groups and the Pd-bonded $ArPO_3^{2-}$ groups (OP*PSO*-Pd *vs.* *O*P*P*SO-Pd), self-assembly of stereoisomers with different relative configurations at the phosphorus centers, and assembly of structures with different nuclearity.

The key result of these studies is that the reaction of {Zn[**1**-H]}$_4$·1.3MeOH with (TMEDA)$PdMe_2$ and py failed to form a tetrameric 3D $Zn_4P_4O_{12}$ cage structure, but instead formed a 2D ring structure. A likely reason for this finding is that TMEDA occupies two coordination sites at each Zn^{2+} center, which precludes the coordination of a third $ArPO_3^{2-}$ unit that is required to generate a 3D cage structure.

Reaction of {Zn[1-H]}$_4$ with (COD)PdMe$_2$ to Form Tetrameric Pd$_4$ Compounds with Central $Zn_4P_4O_{12}$ Core. To avoid the presence of the hard, bidentate ligand TMEDA, which coordinates to Zn^{2+} and prevents cage formation, (COD)PdMe$_2$ (COD = 1,5-cyclooctadiene) was utilized as the Pd precursor. Due to the poor back-bonding ability of Zn(II), zinc-olefin complexes are rare, with only a few reports of compounds with Zn-π-interactions.[17]

The reaction of CH_3OH-free {Zn[**1**-H]}$_4$ with (COD)PdMe$_2$ and pyridine in CD_2Cl_2 resulted in quite clean $^{31}P\{^1H\}$ and ^1H NMR spectra of {[κ^2-*P,SO*-P(4-^{t}Bu-Ph)(2-PO$_3$Zn-5-Me-Ph)(2-SO$_3$-5-Me-Ph)]PdMe(py)}$_4$ (**4**-py, Scheme 3.8). The $^{31}P\{^1H\}$ NMR spectrum contains major phosphine (δ 35.5) and phosphonate (δ 8.8) resonances (76 % of total intensity, Figure 3.6a). No P-P coupling was observed, which indicates the absence of κ^2-*P*-P*O* Pd chelation in **4**-py (in which case P-P coupling would be observed), and suggests that the OP-P-SO ligand chelates to the Pd center with phosphine and sulfonate groups in a κ^2-*P*-S*O* coordination mode. In the ^1H NMR spectrum, the major (> 80 %, based on integration of the Pd-Me region) Pd-Me resonance is a doublet at δ -0.20 with a small J_{PH} = 3 Hz (Figure 3.6b). The high-field shift of Pd-Me resonance is consistent with anisotropic shielding by an adjacent py ring, and the small J_{PH} value indicates a *cis* arrangement of the phosphine and methyl ligands.[18] The major species exhibits only one set of OP-P-SO ligand resonances, suggesting that it is highly symmetric. PGSE-NMR analysis of the major Pd-Me resonance in CD_2Cl_2 at room temperature shows that the hydrodynamic volume of **4**-py is ca. 6.5 × 10^3 Å, which is very similar to that for **A** (6.2 × 10^3 Å). These results are consistent with a tetrameric $Zn_4P_4O_{12}$ cage structure for **4**-py that is analogous to that of the $Li_4S_4O_{12}$ cage in **A**. However, the ^1H NMR spectrum of **4**-py contains a set of minor Pd-Me resonances with similar intensities (total < 20 %), indicating that other species are present. One likely possibility is that cages with lower symmetry due to different connectivities or different relative configurations at the phosphorous centers may be present.

Scheme 3.8. Ar = 4-^{t}Bu-Ph.

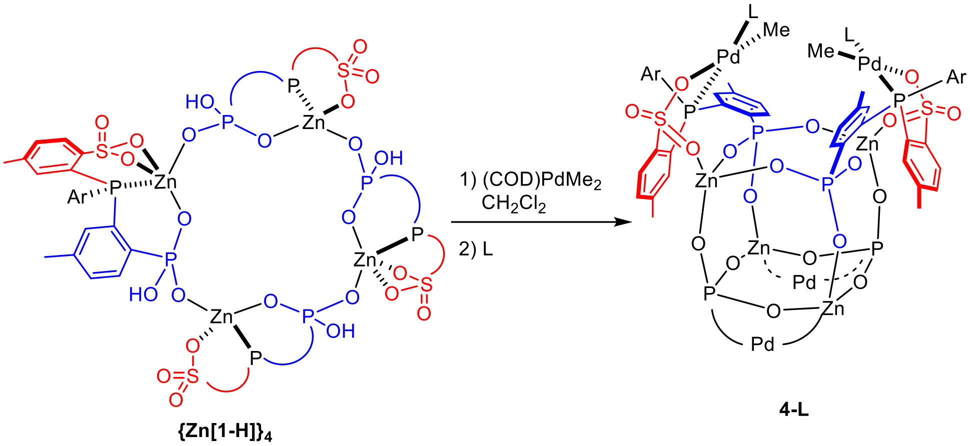

Figure 3.6. NMR spectra of the **4**-py reaction mixture (CD_2Cl_2). (a) $^{31}P\{^1H\}$ NMR spectrum. (b) ^1H spectrum (Pd-Me region): δ 0.27 = $(COD)PdMe_2$; 0.21 = CH_4; 0.09 = grease.

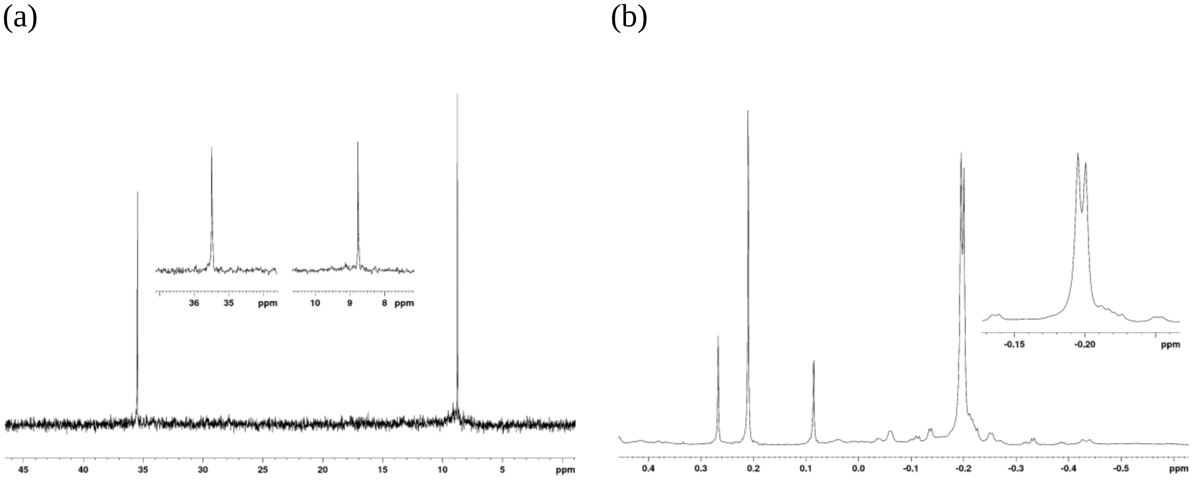
(a)

(b)

Separation of the major stereoisomer of **4**-py from the minor species was unsuccessful, because these compounds have very similar solubilities and **4**-py does not crystallize well.

Therefore, several substituted pyridine ligands were screened in Scheme 3.8 to generate a cleaner and more crystalline product, including 4-*t*Bu-pyridine, 4-Ph-pyridine, 3-Br-4-Cl-pyridine, 4-(5-nonyl)-pyridine, 2,6-lutidine, 4-Me-2,6-lutidine, 4-Br-2,6-lutidine, quinoline, and acridine. In all these cases, the $^{31}P\{^{1}H\}$ spectrum of the reaction mixture contains major resonances at δ 36.4 - 29.5 (phosphine) and 9.4 - 7.9 (phosphonate) without P-P coupling, and the ^{1}H spectrum containes a major high-field Pd-Me resonance at δ -0.06 – -0.36 with a small J_{PH} coupling (ca. 3 Hz), along with minor Pd-Me resonances possibly from stereoisomers. For **4**-(4-*t*Bu-py), the major phosphine and phosphonate ^{31}P NMR resonances appear at δ 36.4 and 9.4, respectively, and the major Pd-Me ^{1}H NMR resonance appears at δ -0.29 (J_{PH} = 3 Hz). Recrystallization conditions were also screened, including different solvents combinations of solvents (CH_2Cl_2, CH_2ClCH_2Cl, $CHCl_2CHCl_2$, toluene, 1,2-diclorobenzene, pentane, hexanes and heptane) and different temperatures (room temperature, 10 °C, -10 °C and -40 °C). Ultimately, **4**-(4-*t*Bu-py) was obtained in crystalline form.

Structure of 4-(4-*t*Bu-py). **4**-(4-*t*Bu-py) was obtained in crystalline form by crystallization from $CHCl_2CHCl_2$ solution at room temperature and analyzed by X-ray crystallography (Figure 3.7). Due to the large amount of disordered solvent filling the voids between the **4**-(4-*t*Bu-py) molecules and additional loss of long range order resulting from solvent evaporation, the diffraction intensity dropped rapidly at high angles. However, the data are of sufficient quality to be useful for the comparison of connectivity and for qualitative comparison of metrical parameters with previous results for **A**. The X-ray analysis confirms that **4**-(4-*t*Bu-py) adopts the target cubic $Zn_4P_4O_{12}$ cage structure and is structurally analogous to **A**. The key cage dimensions of **4**-(4-*t*Bu-py) and **A** are summarized in Table 3.1 and are quite similar. In **4**-(4-*t*Bu-py), the phosphorus and sulfonate oxygens chelate to Pd, which is consistent with the absence P-P coupling in $^{31}P\{^{1}H\}$

NMR spectrum. The structure has approximate S_4 symmetry. The four Pd units are nearly equivalent, which is consistent with the symmetry implied by the $^{31}P\{^1H\}$ and ^1H NMR spectra, and are arranged in two pairs with *SS* and *RR* configurations at the phosphorous centers. The Pd-Me groups lie directly under the 4-^{t}Bu-py ring of the neighboring Pd unit (Figure 3.6 (b)), which is consistent with the high-field Pd-Me ^1H NMR chemical shift.

Figure 3.7. Molecular structure of **4**-(4-^{t}Bu-py). (a) Hydrogen atoms, tolyl Me groups and ^{t}Bu groups are omitted. Only the nitrogen atom of the 4-^{t}Bu-py group is shown. (b) Top view of **4**-(4-^{t}Bu-py) highlighting the relative orientation of the Pd-Me and 4-^{t}Bu-py units. Hydrogen atoms are omitted. (c) Space-filling view of the whole structure.

(a)

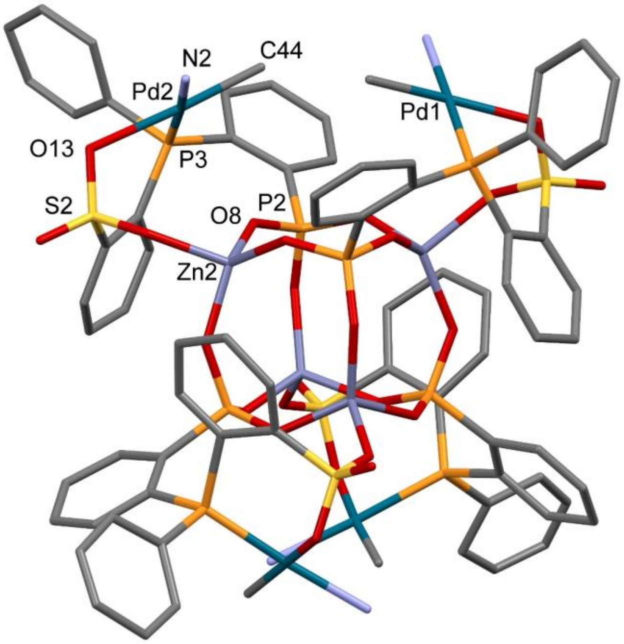

Figure 3.7, continued.

(b)

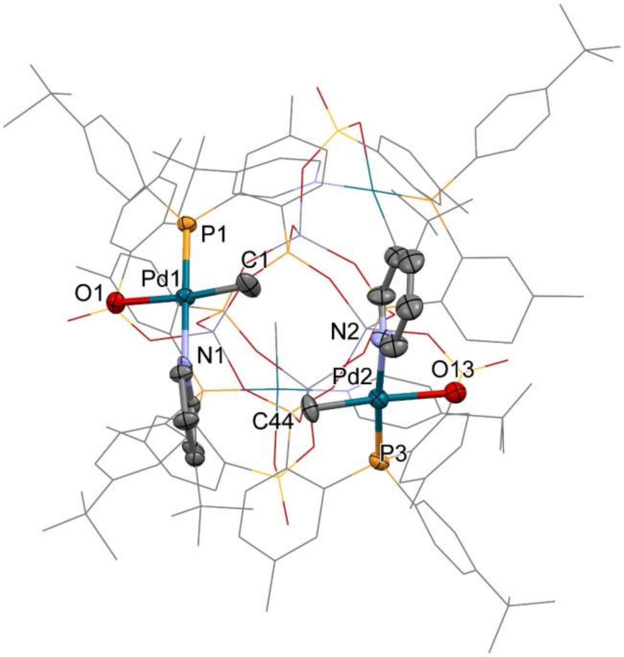

(c)

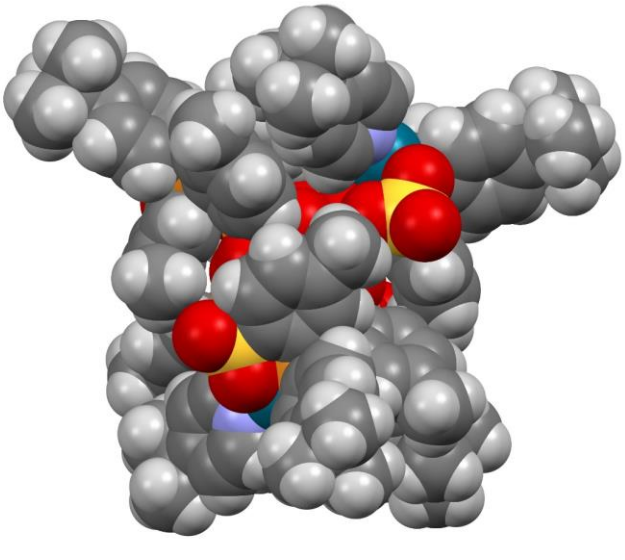

Table 3.1. Cage dimension parameters.

	4-(4-^{t}Bu-py)		**A**[b]	
Edge (Å)	Zn---P	3.19(4)	Li---S	3.21
Face Diagonal (Å)	P---P	4.72(11)	S---S	4.62
	Zn---Zn	4.28(9)	Li---Li	4.45
Body diagonal (Å)	Zn---P	5.51(3)	Li---S	5.51
Pd-Pd distance (Å)[a]	Pd---Pd	6.26(14)	Pd---Pd	6.04
Angles between Pd planes angles (°) [a]		74.86 (2.06)		73.96

[a] within each pair of proximal Pd units. [b] ref 1.

Possible Stereoisomers of 4-L. As noted above, the **4**-L compounds are formed as a mixture of highly symmetric major species (presumed to have S_4-symmetric structures analogues to that of **4**-(4-^{t}Bu-py)) and minor species that are likely to be stereoisomers that differ in the configurations of one or more phosphorous centers. Figure 3.8 shows an unsymmetrical stereoisomer with *RSRR* configurations at the phosphorous centers. No obvious steric hindrance is present in this stereoisomer, which illustrates that the formation of different stereoisomers is possible.

Figure 3.8. Possible stereoisomerism in **4**-(4-^{t}Bu-py). (a) Structure of the major stereoisomer of **4**-(4-^{t}Bu-py) determined by X-ray diffraction with *SSRR* configurations at the phosphorous centers. The top left phosphine has an *S* configuration. (b) Model of the structure of a stereoisomer of **4-**(4-^{t}Bu-py) in which the configuration of the top left phosphine has been inverted, given an overall *RSRR* configuration. The Zn-O interactions are indicated by the black dashed lines. (c) Schematic illustration of the structural change resulting from the inversion of the configuration of the top left phosphine. Pd unit: blue dot. Zn corner: pink dot. P corner: yellow dot.

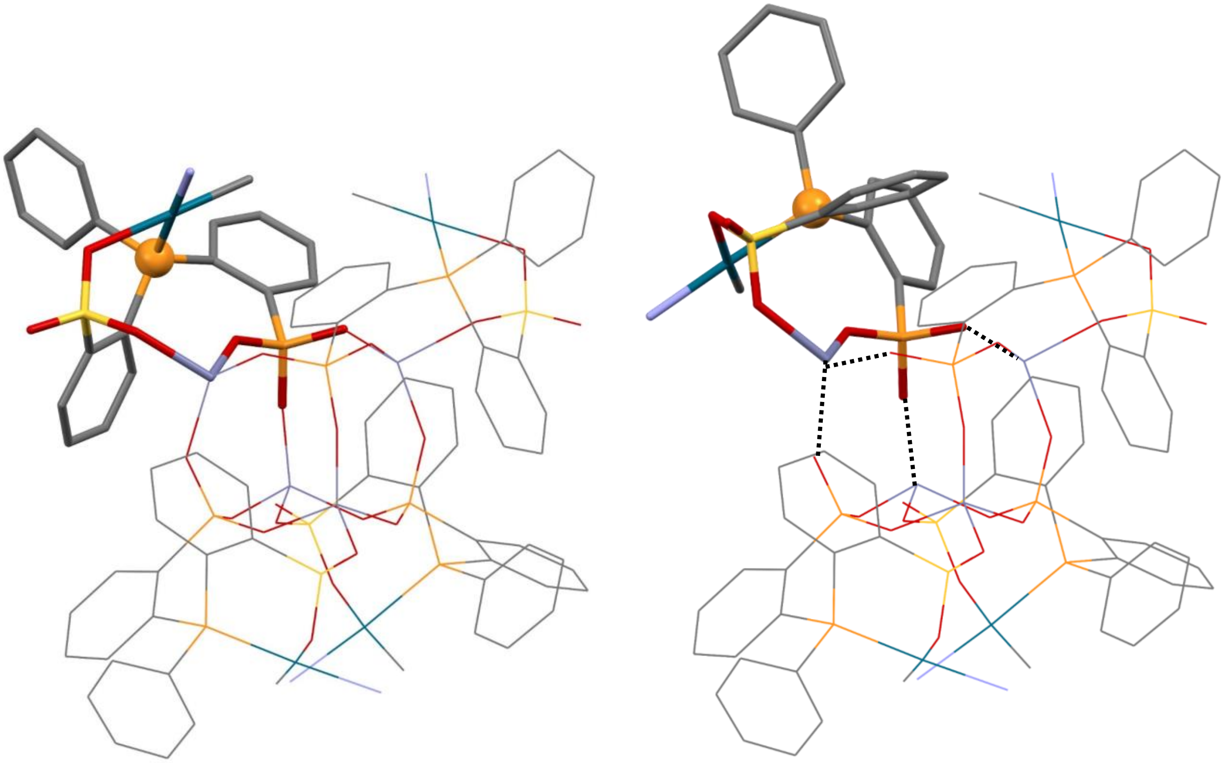

(a)

(b)

Figure 3.8, continued.

(c)

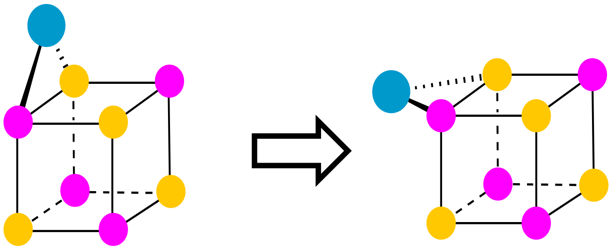

4-(4-^{t}Bu-py) was isolated on a preparatory scale by recrystallization from $CHCl_2CHCl_2$/pentane solution at -40 °C. The isolated material comprises ca. 80 % of the major S_4-symmetric stereoisomer and 20 % of the other Pd-Me species (most likely other stereoisomers) based on integration of the Pd-Me region of the ^{1}H NMR spectrum. This sample was used in further thermal stability and polymerization studies.

Reaction of 4-py with CH_3OH to Produce a Trimeric Pd_3 Cluster. Dissolution of **4**-py in CD_3OD at room temperature results in complete conversion to a trimeric species {[P(4-^{t}Bu-Ph)(2-PO_3Zn(py)-5-Me-Ph)(2-SO_3-5-Me-Ph)]PdMe}$_3$ (**3**-py, Scheme 3.9a). **3**-py is only sparingly soluble in CD_3OD and directly crystallized as **3**-py•CH_3OH from the CD_3OD solution. The structure of **3**-py was determined by X-ray diffraction. **3**-py has a C_3-symmetric structure with *RRR* (ent *SSS*) configurations at the phosphorous centers. As shown in Figure 3.9, **3**-py•CH_3OH is held together by a two-layered ring structure composed of a 12-membered $Zn_3P_3O_6$ ring and a 6-membered Pd_3O_3 ring. The $ArPO_3^{2-}$ groups form μ-κ^1,κ^1-OPO bridges between two Zn centers and μ-κ^1,κ^1-O bridges between two Pd centers. Two Zn centers are four-coordinate, with one oxygen from an $ArSO_3^-$ groups, two oxygens from bridging $ArPO_3^{2-}$ groups and one nitrogen from a pyridine ligand. One Zn^{2+}-coordinated-CH_3OH molecule per trimer cluster was observed and is disordered among the three Zn centers. The square-planer Pd center is ligated by the phosphine, two phosphonate oxygens, and the Me group. The Pd-Me group is buried in a deep pocket formed by the $ArSO_3^-$, $ArPO_3^{2-}$ and P(4-^{t}Bu-Ph) arene rings (Figure 3.10). This result is in direct contrast with the observations for lithium sulfonate related cages, that CH_3OH converts tetrameric Pd_4 cage species into full solvated monomeric Pd_1 species (Scheme 3.9b,c).[1,4,19]

Scheme 3.9. Ar = 4-^{t}Bu-Ph, L = py.

(a)

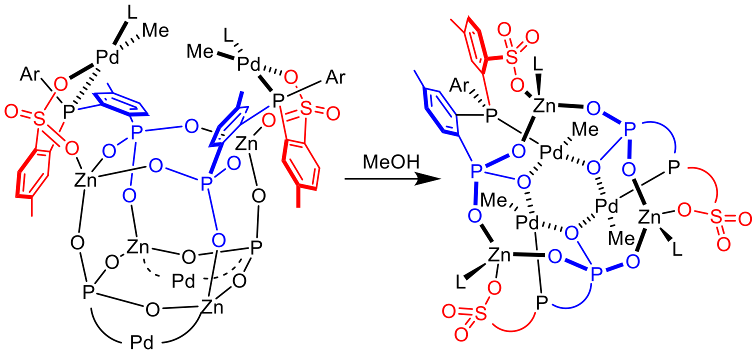

4-L **3-L**

(b)

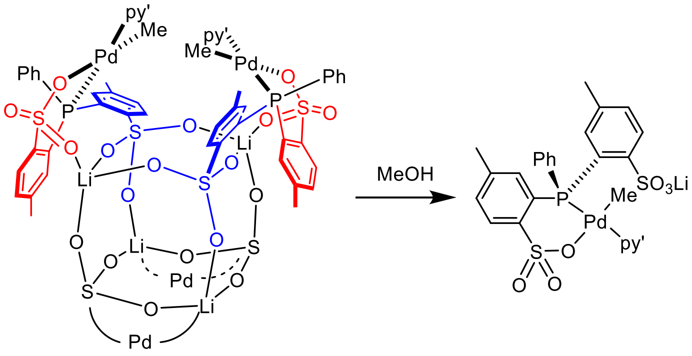

py' = 4-(5-nonyl)-py

A

Scheme 3.9, continued.

(c)

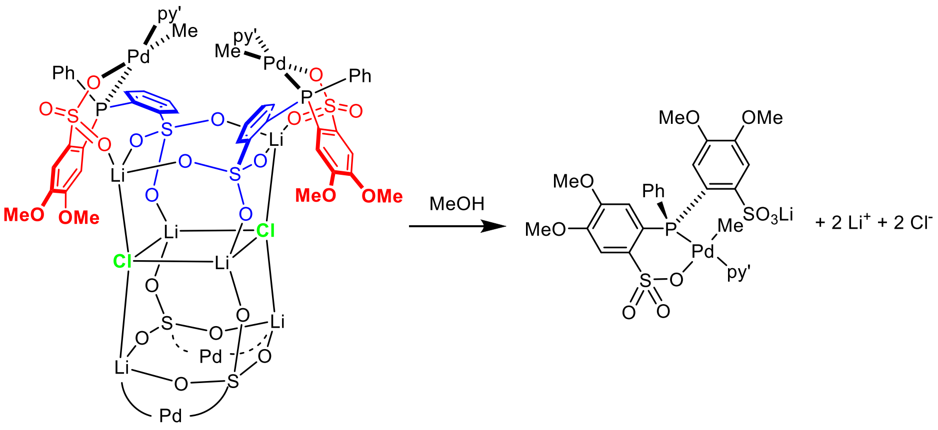

Figure 3.9. Molecular structure of **3**-py•CH_3OH. Hydrogen atoms, tolyl Me groups, ^{t}Bu groups and the CH_3OH molecule are omitted. Selected bond lengths (Å) and angles (deg): Pd1-C1 2.007(9), Pd1-O1 2.104(5), Pd1-P2 2.197(2), Zn1-O2 1.921(5), Zn1-O3 1.916(6), Zn1-O4 1.957(6), Zn1-N1 1.981(7), Zn1-Pd1 3.0265(17), S1-O4 1.467(6), P1-O1 1.541(6), P1-O2 1.510(5), P1-O3 1.516(6), C1-Pd1-O1 90.3(3) and 176.0(3), O1-Pd1-O1 87.9(3), C1-Pd1-P2 92.5(3), P2-Pd1-O1 89.45(15) and 176.48(17), Pd1-O1-Pd1 125.3(3), O3-Zn1-O2 117.1(2), O2-P1-O3 111.8(4), P1-O2-Zn1 130.7(3), P1-O3-Zn1 131.7(4).

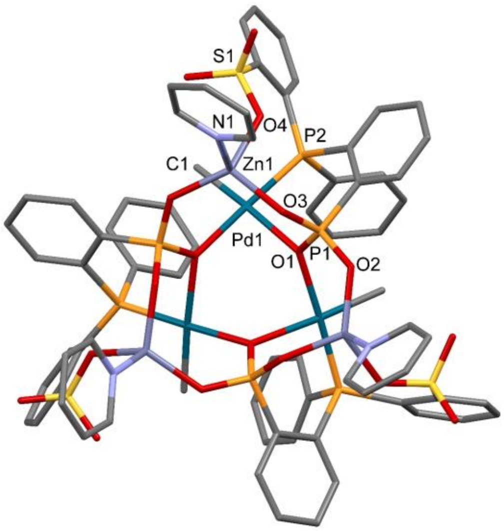

Figure 3.10. View of **3**-py highlighting the relative orientation of the Pd-Me and OP-P-SO ligand arene units.

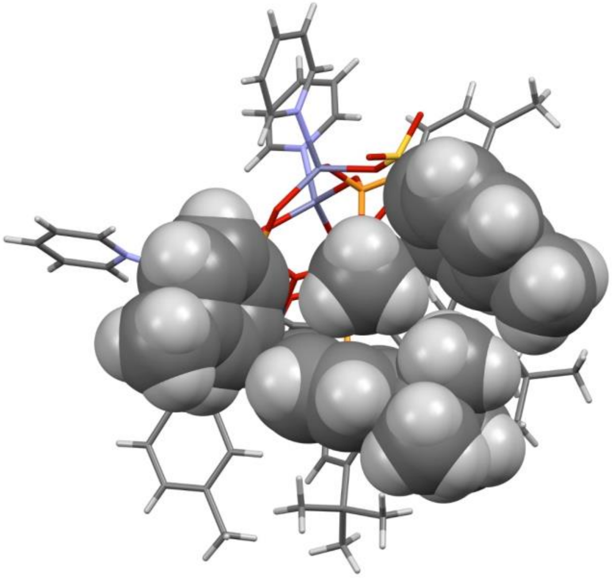

3-py was isolated on a preparatory scale by filtration, washed with CH_3OH, and dried under vacuum. The $^{31}P\{^1H\}$ and ^1H NMR spectra of isolated **3**-py in CD_2Cl_2 are broad but sharpen upon the addition of CD_3OD. Based on the ^1H NMR integration, ca. 0.85 equiv of pyridine per Pd-Me unit was present. Addition of excess pyridine in the CD_2Cl_2 NMR sample also sharpens the NMR spectrum, which further confirms the substoichiometric amount of pyridine in the isolated material. Fast exchange on the ^1H NMR chemical shift time scale of free and coordinated pyridine was also observed. These results show that the pyridine of **3**-py is quite labile, and was partially removed by the CH_3OH wash and the vacuum drying protocol. In the $^{31}P\{^1H\}$ NMR spectrum of **3**-py in CD_2Cl_2/CD_3OD or in CD_2Cl_2 in the presence of excess pyridine, the phosphine and phosphonate resonances appear at δ 42.7 and 19.4, respectively, and P-P coupling (J_{PP} = 12 Hz) is observed, which is consistent with the P-P*O* Pd chelation observed in the solid-state structure. In the ^1H NMR spectrum of **3**-py, the Pd-Me resonance appears at δ -0.81, which is upfield-shifted compared to the Pd-Me resonance of **4**-py (δ -0.20). This unusually high-field chemical shift is consistent with the strong anisotropic shielding expected from the solid-state structure. The hydrodynamic volume of **3**-py determined by PGSE-NMR in CD_2Cl_2 at 25 °C is ca. 4.5×10^3 Å, which is ca. ¾ of the value for **4**-py (6.5×10^3 Å). Therefore, the solution structure must be very similar to the solid-state structure. The conversion of **4**-py to **3**-py is also induced by Et_2O, which was discovered during attempts to recrystallize **4**-py from CH_2Cl_2/Et_2O and toluene/Et_2O solutions. The conversion of **4**-py to **3**-py in CH_3OH contrasts with the completely solvolysis of **A** to monomeric Pd_1 species in this solvent, and reflects the greater strength of the Zn^{2+}-phosphonate versus Li^+-sulfonate interactions in these system.

The NMR-scale reaction of **4**-(4-*t*Bu-py) and excess 4-*t*Bu-py in CD_2Cl_2 at room temperature resulted in completely conversion of **4**-(4-*t*Bu-py) to a mixture of a small amount of **3**-(4-*t*Bu-py) (ca. 10 %) and unknown species including a species with low-field Pd-Me ^{1}H resonances (δ 0.91 and 0.80, ca. 80 %, major) and other minor species (Figure 3.11).

Figure 3.11. NMR spectra of the reaction of **4**-(4-^{t}Bu-py) and excess 4-^{t}Bu-py (CD_2Cl_2). (a) $^{31}P\{^1H\}$ NMR spectrum. (b) ^1H spectrum: δ 0.91 and 0.80 = unknown species.

(a)

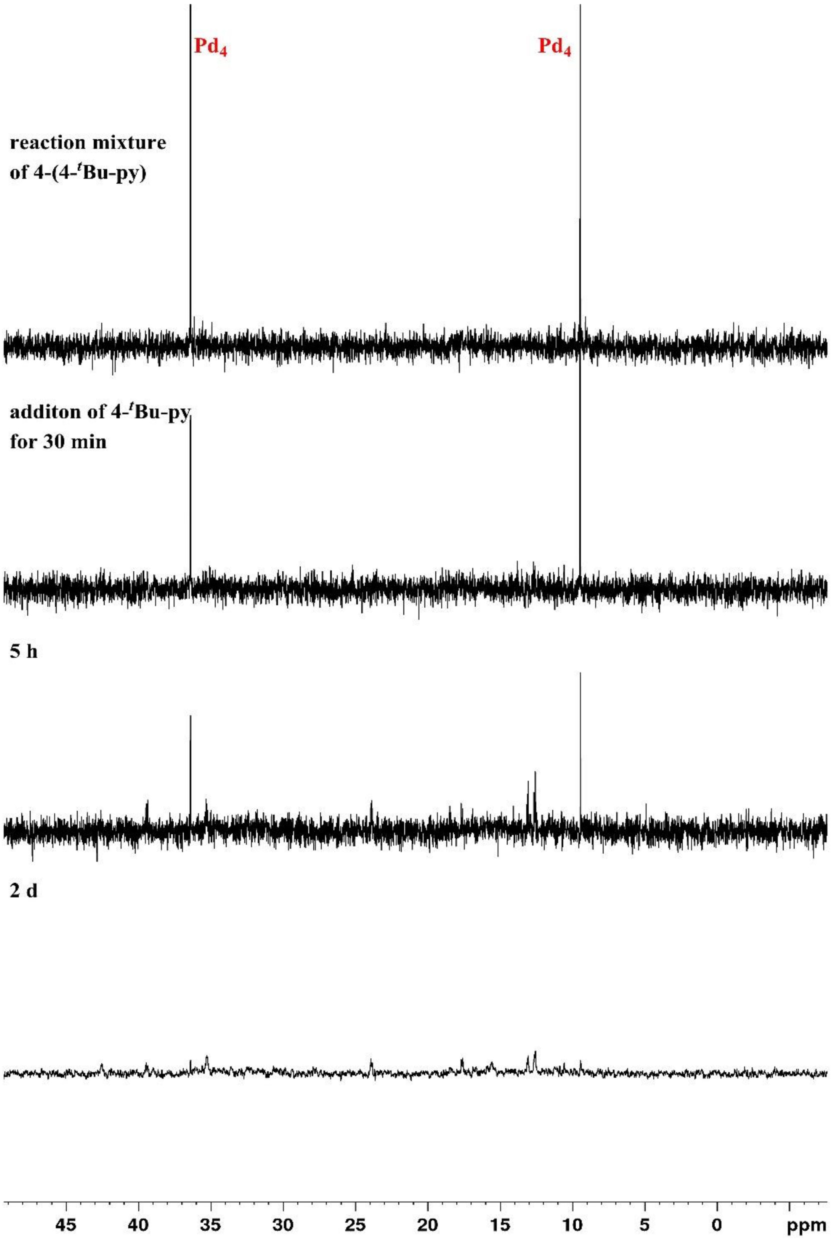

Figure 3.11, continued.

(b)

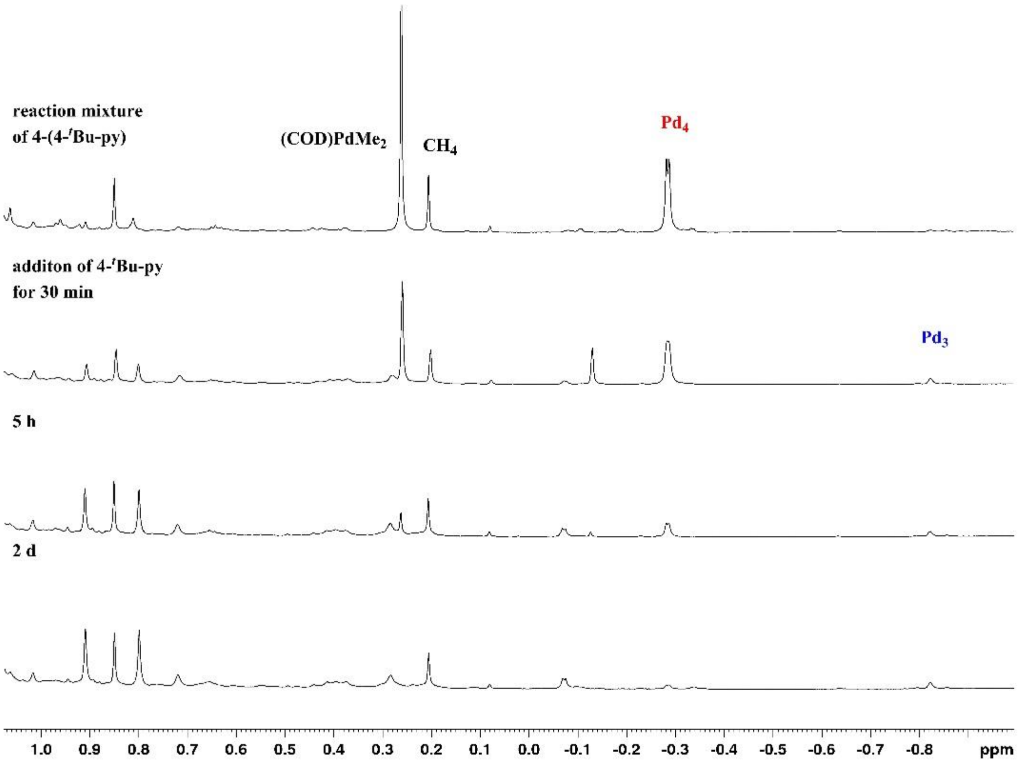

The facile conversion of **4**-py to **3**-py in CH_3OH dictates that it is critical that {Zn[**1**-H]}$_4$ is CH_3OH-free in the synthesis of **4**-py. The reaction of {Zn[**1**-H]}$_4$•1.6 CH_3OH with (COD)PdMe$_2$ and pyridine in CD_2Cl_2 resulted in a mixture of **4**-py (major) and **3**-py (minor).

The key structural differences between **4**-(4-^{t}Bu-py) and **3**-py are the location of the pyridine ligand (at Pd *vs.* Zn) and the coordination mode of the OP-P-SO ligand to Pd (*P*-S*O* *vs.* *P*-P*O*). The more favorable hard/soft matching of the hard (nitrogen-based) pyridine ligand with Zn^{2+} *vs.* Pd^{2+} may explain why **3**-L is apparently favored over **4**-L when L is a pyridine ligand.

Reaction of {Zn[1-H]}$_4$ with (COD)PdMe$_2$ and Tetrahydrothiophene. The hypothesis that the preference for pyridine ligands to bind to Zn^{2+} *vs.* Pd^{2+} drives the conversion of **4**-L to **3**-L, raises the question of whether replacement of pyridine ligand with a softer ligand may favor **4**-L over **3**-L. The NMR-scale reaction of CH_3OH-free $\{Zn[\mathbf{1}\text{-H}]\}_4$ with (COD)$PdMe_2$ and tetrahydrothiophene (THT) in CD_2Cl_2 resulted in the formation of a species assigned as **4**-THT in 49 % NMR yield based on integration of the Pd-Me region of the ^1H NMR spectrum. In the $^{31}P\{^1H\}$ NMR spectrum of **4**-THT, major phosphine and phosphonate resonances are observed at δ 31.2 and 9.2 as singlets. The absence of P-P coupling suggests that the phosphorous and sulfonate oxygen chelate to the Pd center, as in **4**-py. In the ^1H NMR spectrum, a major Pd-Me resonance is present at δ 0.26, which is consistent with the absence of anisotropic shielding from the saturated THT ring. Several minor, Pd-Me ^1H resonances with similar intensities and several minor ^{31}P resonances with similar intensities were also observed and are tentatively assigned to stereoisomers of **4**-THT that differ in the relative configurations at the phosphorous centers.

4-THT was isolated on a preparatory scale by recrystallization from toluene/hexanes solution. Dissolution of **4**-THT in CD_3OD results in conversion of **4**-THT to a new species, **3**-THT, which precipitates from CD_3OD solution as an amorphous solid. The $^{31}P\{^1H\}$ spectrum of **3**-THT in CD_2Cl_2/CD_3OD mixed solvent contains doublets for the phosphine (δ 43.1) and phosphonate (δ 19.6) centers with J_{PP} = 11 Hz, which is consistent with the phosphine and phosphonate groups being chelated to the Pd center (*P*-P*O*-Pd). The Pd-Me ^1H NMR resonance appears at high field, δ -0.79, indicative of pronounced anisotropic shielding by one or more arene rings of the OP-P-SO ligand. The THT ^1H NMR resonances appear at δ 2.80 and 1.93, and are close to positions for free THT (δ 2.78, 1.90) in CD_2Cl_2, which indicates that THT is labile. These data strongly suggest that **3**-THT is structurally analogous to **3**-py.

Unfortunately, neither **3**-THT nor **4**-THT could be isolated in pure form or crystallized, so their structures could not be confirmed. However, addition of excess THT to a solution of **3**-THT in CD_2Cl_2 converts **3**-THT back to **4**-THT. This is in direct contrast to the observation noted above that excess 4-^{t}Bu-pyridine converts **4**-(4-^{t}Bu-py) to a mixture and supports the hypothesis that soft L ligand favors tetrameric **4**-L over trimeric **3**-L. Therefore, use of other soft ligands may provide more isolable and robust **4**-L complexes.

Thermal stability of 4-L and 3-L. Heating a solution of **4**-(4-^{t}Bu-py) in $CDCl_2CDCl_2$ over the temperature range 50-80 ˚C did not produce significant changes in the $^{31}P\{^1H\}$ and ^1H NMR spectra. While one minor unknown resonance grew in at ca. δ 0.27 (< 3 %) in the ^1H NMR spectrum, the intensity of the major Pd-Me resonance remained constant at ca. 80 % (based on ^1H NMR Pd-Me region integration) during the experiment, and no Pd-black was observed. These results indicate that **4**-(4-^{t}Bu-py) is quite robust and, in contrast to **A** does not undergo cage dissociation under these conditions.

3-py is also quite robust. The NMR spectra of a sample of **3**-py containing 0.85 equiv pyridine per Pd in $CDCl_2CDCl_2$ solution at room temperature and 80 ˚C are broad. Addition of CD_3OD to the NMR sample sharpens the spectrum at room temperature, but only partially sharpens the spectrum at 80 ˚C. No indication of cluster dissociation was observed by comparing the room temperature and 80 ˚C spectra with or without CD_3OD. In $CDCl_2CDCl_2/CD_3OD$, the Pd-Me ^1H NMR resonance of **3**-py appears at δ -0.92 at room temperature and at δ -0.68 at 80 ˚C.

Base-free Complexes Derived from 4-L and 3-L. The reaction of **4**-(4-^{t}Bu-py) with $B(C_6F_5)_3$ in CD_2Cl_2 at room temperature generates $(py)B(C_6F_5)_3$ and a poorly soluble species presumed to be a base-free complex derived by loss of 4-^{t}Bu-py from **4**-(4-^{t}Bu-py). The ^1H NMR spectrum of the cloudy reaction mixture contains resonances for $(py)B(C_6F_5)_3$,[3] and broad resonances at δ 7.92 - 6.94 and 2.60 - 2.01, presumably from the base-free complex. No Pd-Me resonance was observed in the ^1H NMR spectrum and no resonances were observed in the $^{31}P\{^1H\}$

NMR spectrum (Figure 3.12). The addition of 1 equiv of 4-*t*Bu-py to the base-free complex in CD_2Cl_2 at room temperature regenerates **4**-(4-*t*Bu-py) in 39 % yield (based on integration of Pd-Me region of ^{1}H NMR spectrum) along with minor species (total 61 %), likely stereoisomers of **4**-(4-*t*Bu-py), which exhibit doublet of Pd-Me ^{1}H resonances with similar intensities ($^3J_{PH}$ = 3 Hz) ^{31}P resonances with similar intensities.

Figure 3.12. NMR spectra of the reaction of **4**-(4-*t*Bu-py) and $B(C_6F_5)_3$. (a) ^{31}P{^{1}H} NMR spectrum. (b) ^{1}H spectrum.

(a)

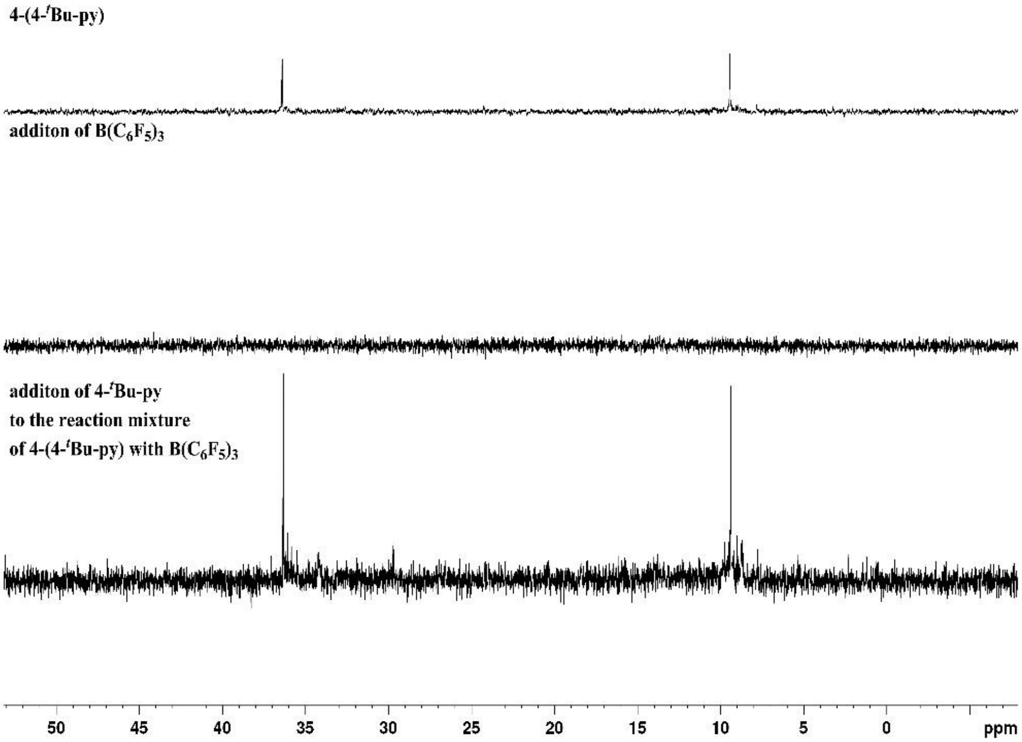

Figure 3.12, continued.

(b)

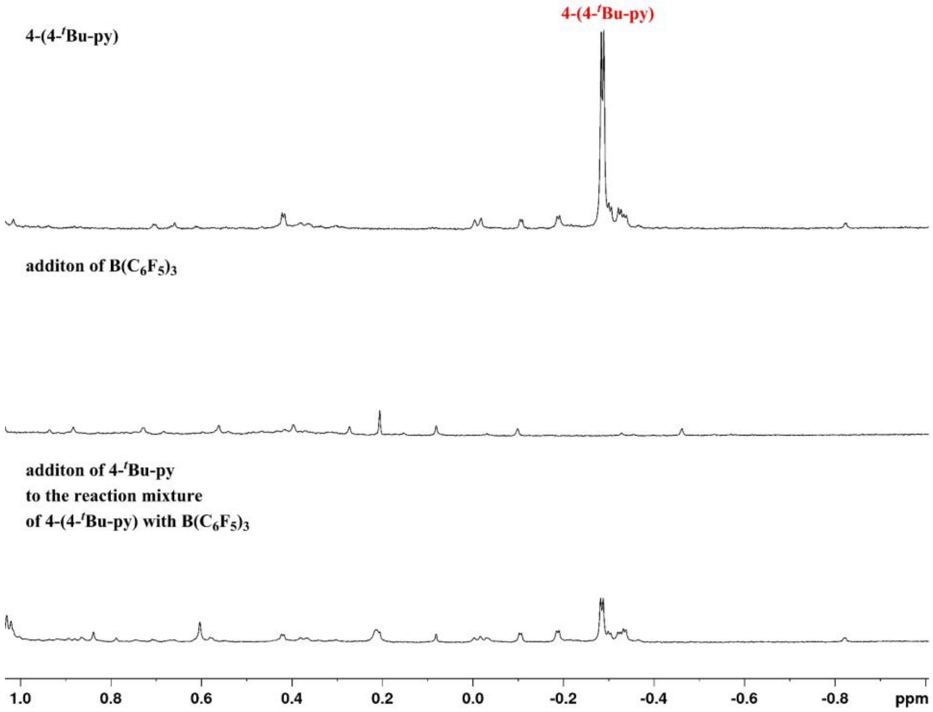

Similarly, the reaction of **3**-py with $B(C_6F_5)_3$ generates a base-free species that is poorly soluble in $CDCl_2CDCl_2$. The ^{1}H NMR spectrum of the reaction mixture (at room temperature or 80 ˚C) contains signals for the (py)$B(C_6F_5)_3$ adduct and broad resonances which are presumed to arise from the base-free complex. **3**-py was regenerated in 96 % yield by addition of pyridine to the base-free complex **3**. Thus, again, **3**-py is more robust than **4**-py.

Ethylene Homopolymerization. The ethylene polymerization behavior of **4**-(4-^{t}Bu-py) and **3**-py was briefly explored. A sample of **4**-(4-^{t}Bu-py) that contains ca. 80 % of the major stereoisomer was used for polymerization studies. $B(C_6F_5)_3$ was added to trap the 4-^{t}Bu-py ligand, in order to minimize potential cage isomerization and conversion to **3**-(4-^{t}Bu-py) induced by 4-^{t}Bu-py when it is released by displacement by ethylene. In the presence of 1 equiv of $B(C_6F_5)_3$ per

4-^{t}Bu-pyridine, **4**-(4-^{t}Bu-py) produced high-MW linear PE with a broad MWD (PDI = 15 and 91, Table 3.2, entry 1, 2) at 80 ˚C in toluene solution and in hexanes suspension, with comparable activities. Preliminary GPC results indicate that the polymer produced in hexanes has a remarkably high MW, with M_w > 6 million Da (separation limits of the GPC columns and the high end of the range of calibration standards). The broad MWDs indicate that in the presence of $B(C_6F_5)_3$, **4**-(4-^{t}Bu-py) functions as a multi-site catalyst. Thus result is not surprising given the extensive cage isomerization observed in the reaction of base-free complex derived from **4**-(4-^{t}Bu-py) with 4-^{t}Bu-py.

A sample of **3**-py that contains 2.55 equiv of pyridine per trimer was used for ethylene polymerization studies. $B(C_6F_5)_3$ was not required in this case since **3**-py is more robust than **4**-py. In toluene at 80 ˚C, **3**-py produced high MW linear PE with a moderately broad MWD (PDI = 4.1, Table 3.2, entry 3). The broadening may result from the presence of growing active species that maintain the core structure of **3**-py but contain different numbers of pyridine ligands. In contrast, in the presence of 1 equiv of $B(C_6F_5)_3$ per pyridine in toluene at 80 ˚C, **3**-py exhibits an increased activity and yields high-MW linear PE with a narrow MWD (PDI = 2.7, Table 3.2, entry 6), characteristic of single-site catalysts.

Table 3.2. Ethylene Homopolymerization of **4**-(4-^{t}Bu-py) and **3**-py[a]

Entry	Cat.	*T* (°C)	Solvent (50 mL)	Yield (g)	Acitivity (kg•mol^{-1}•h^{-1})	M$_w$[d] (10^3)	PDI[d]	T$_m$[e] (°C)
1[b]	**4**-(4-^{t}Bu-py) + B(C$_6$F$_5$)$_3$	80	toluene/chlorobenzene (49/1)	4.74	237	436	15	136.9
2[b]	**4**-(4-^{t}Bu-py) + B(C$_6$F$_5$)$_3$	80	hexanes/chlorobenzene (49/1)	5.11	256	> 6000	91	135.4
3[b]	**3**-py	80	toluene	2.18	108	466	4.1	138.1
4[b]	**3**-py	25	CH$_2$Cl$_2$	0.142	7.1	1010	21	137.2
5[c]	**3**-py	25	CH$_2$Cl$_2$	0.534	4.4	1438	14	137.0
6[b]	**3**-py + B(C$_6$F$_5$)$_3$	80	toluene/chlorobenzene (49/1)	7.64	378	691	2.7	136.6

[a] P_{C2H4} = 410 psi, 1 equiv of B(C$_6$F$_5$)$_3$ per 4-^{t}Bu-pyridine or per pyridine when applicable. [b] Time = 2 h, [Pd] = 10 μmol. [c] Time = 24 h, [Pd] = 5 μmol. [d] GPC. [e] *DSC*.

Ethylene/Vinyl Fluoride Copolymerization. **4**-(4-^{t}Bu-py) copolymerizes ethylene and VF at 80 ˚C in the presence of 1 equiv of B(C$_6$F$_5$)$_3$ per 4-^{t}Bu-pyridine to produce linear copolymer with 0.96 mol % VF incorporation. Only in-chain -CH$_2$CFHCH$_2$- units were observed (Table 3.3, entry 1). **3**-py also copolymerizes ethylene with VF in the presence of 1 equiv of B(C$_6$F$_5$)$_3$ per pyridine in toluene at 80 ˚C to produce linear copolymer with in-chain -CH$_2$CFHCH$_2$- (major) and chain-end -CH$_2$CFHCH$_3$ (minor) units (Table 3.3, entry 3,4). Increasing the VF pressure from 80 psi to 120 psi resulted in a decrease in catalyst activity and an increase in VF incorporation from 0.43 to 1.1 mol %.

Table 3.3. Ethylene /Vinyl Fluoride Copolymerization of **4**-(4-^{t}Bu-py) and **3**-py with $B(C_6F_5)_3$ [a]

Entry	Cat.	P_{C2H4} (psi)	P_{VF} (psi)	Yield (mg)	Acitivity ($kg \cdot mol^{-1} \cdot h^{-1}$)	M_w [b] (10^3)	PDI[b]	VF incorp[c] (mol %)	T_m [d] (°C)
1	**4**-(4-^{t}Bu-py) + $B(C_6F_5)_3$	130	120	39	2.0	42.2	4.1	0.96	131.4
2	**3**-py + $B(C_6F_5)_3$	220	80	94	4.9	50.3	2.4	0.43	134.7
3	**3**-py + $B(C_6F_5)_3$	130	120	20	1.0	23.0	2.3	1.1	131.6

[a] Solvent = 49 mL toluene + 1 mL chlorobenzene, [Pd] = 10 μmol, 1 equiv $B(C_6F_5)_3$ per L, temperature = 80 °C. [b] GPC. [c] VF incorporation in copolymer determined by ^1H NMR. [d] DSC.

3.3 Conclusions

The phosphine-phosphonate-sulfonate ligand (4-^{t}Bu-Ph)(2-$P(O)(OH)_2$-5-Me-Ph)(2-SO_3^--5-Me-Ph)P^+H (OP-P-SO, **1**-H_3) was investigated as a building block for the self-assembly of multinuclear Pd catalysts based on 3-dimensional zinc phosphonate scaffolds. The reaction of **1**-H_3 with $Zn(OAc)_2$•$2H_2O$ yields {Zn[**1**-H]}$_4$, which adopts a 2-dimensional 16-membered $Zn_4P_4O_8$ ring structure. This structure can accommodate variable amounts of CH_3OH molecules, which coordinate to the Zn centers and form an intermolecular H-bonding network in the solid state. These observations, along with solution NMR studies, indicate that the core structure of {Zn[**1**-H]}$_4$ is quite stable. {Zn[**1**-H]}$_4$•1.3CH_3OH reacts with (TMEDA)$PdMe_2$ and pyridine to generate {Zn^+(TMEDA)[κ^2-*P*,P*O*-P(4-^{t}Bu-Ph)(2-PO_3-5-Me-Ph)(2-SO_3^--5-Me-Ph)PdMe(py)]}$_2$ (**2**), which was characterized by X-ray diffraction. **2** adopts a 2-dimensional 8-membered $Zn_2P_2O_4$ ring structure. The bidentate coordination of TMEDA to Zn in **2** consumes two coordination sites, which may be the key factor that prevents the formation of a 3-dimensional cage. The reaction of CH_3OH-free {Zn[**1**-H]}$_4$ with (COD)$PdMe_2$ and 4-^{t}Bu-py generates **4**-(4-^{t}Bu-py). X-ray diffraction analysis shows that **4**-(4-^{t}Bu-py) adopts the target 3-dimensional $Zn_4P_4O_{12}$ cage structure and is isostructural with {[κ^2-*P*,*O*-PPh(2-SO_3-5-Me-Ph)(2-SO_3Li-5-Me-

Ph)]PdMe(py')}$_4$ (**A**). The $^{31}P\{^1H\}$ and ^1H NMR spectra of **4**-(4-^{t}Bu-py) are consistent with the solid-state structure. In the ^1H NMR spectrum of **4**-(4-^{t}Bu-py), several minor Pd-Me ^1H NMR resonances with similar intensities were also present and assigned to stereoisomers. Similar results were observed for the reactions with other pyridine ligands. CH_3OH or Et_2O convert **4**-py to a trimeric cluster **3**-py. **3**-py adopts a unique two-layered ring structure composed of a 12-membered $Zn_3P_3O_6$ ring and a 6-membered Pd_3O_3 ring. Excess 4-^{t}Bu-pyridine ligands convert **4**-(4-^{t}Bu-py) to a mixture of unknown species and a small amount of **3**-(4-^{t}Bu-py). In the presence of 1 equiv of $B(C_6F_5)_3$ per 4-^{t}Bu-pyridine at 80 ˚C in toluene or in a hexanes suspension, **4**-(4-^{t}Bu-py) produces high-MW linear PE with a broad MWD, characteristic of multi-site catalysis. **4**-(4-^{t}Bu-py) copolymerizes ethylene and VF to linear copolymer with ca. 0.96 mol % VF incorporation. In the presence of 1 equiv of $B(C_6F_5)_3$ per pyridine, **3**-py produces high-MW linear PE with a narrow MWD at 80 ˚C in toluene, characteristic of single-site catalysis. **3**-py also copolymerizes ethylene and VF to linear copolymer with ca. 1.1 mol % VF incorporation. Modifications to the phosphine-phosphonate-sulfonate ligand could lead to the formation of a more sterically-favored analogue of **4**-L, that maintains a high symmetry. This may result in the clean isolation a **4**-L analogue and reduce the formation of low symmetry stereoisomers.

3.4 Experimental

General Procedures. All experiments were performed under a nitrogen atmosphere using drybox or Schlenk techniques. Nitrogen was purified by passage through Q-5 oxygen scavenger and activated molecular sieves. Methylene chloride, diethyl ether and THF were dried by passage over activated alumina. Toluene, pentane and hexane were purified by passage through BASF R3-11 oxygen scavenger and activated alumina. $C_2D_2Cl_4$, $C_2H_4Cl_2$ and $C_2H_2Cl_4$ were dried over 4 Å molecular sieves. CD_2Cl_2 was dried over P_2O_5. The following materials were obtained from commercial sources and used without further purification: bromotrimethylsilane (Aldrich, 97 %), zinc acetate dihydrate (Aldrich, 99.999 %), diethylamine (Aldrich, 99.5 %), ^{n}BuLi solution (Aldrich, 2.5 M in hexanes), HCl solution (Aldrich, 2 M in diethyl ether), pyridine (Aldrich, 99.8 %), 2,6-lutidine (Aldrich, 99 %), 4-bromo-2,6-dimethylpyridine (Aldrich, 97 %), 2,4,6-trimethylpyridine (Aldrich, 99 %), quinoline (Aldrich, 98 %), acridine (Aldrich, 97 %), 3-bromo-4-chloropyridine (Matrix, 98 %), 4-phenylpyridine (TCI, 98 %) and 4-(5-nonyl)pyridine (TCI, 98 %). The following compounds were prepared by literature procedures (4-^{t}Bu-Ph)PCl_2,[20] diethyl (2-bromo-4-tolyl)phosphonate,[20a,21] (TMEDA)$PdMe_2$,[22] (COD)$PdMe_2$[23]. *para*-toluenesulfonic acid (Aldrich, 98 %, monohydrate) was dried by azeotropic distillation in benzene. 4-^{t}Bu-pyridine (Aldrich, 96 %) was purified by vacuum distillation. Elemental analyses were performed by Robertson Microlit Laboratories. The solvent content in elemental analysis samples was quantified by ^{1}H NMR. NMR spectra were acquired on Bruker DRX-500 or Bruker DRX-400 spectrometers at ambient temperatures unless otherwise indicated. ^{1}H and ^{13}C chemical shifts are reported relative to $SiMe_4$ and are internally referenced to residual ^{1}H and ^{13}C solvent resonances. ^{31}P chemical shifts are reported relative to externally referenced 85% H_3PO_4. ^{19}F spectra were referenced to external $BF_3{\bullet}Et_2O$, and ^{19}F chemical shifts are reported relative to $CFCl_3$. Coupling constants are reported in Hz. NMR resonances were assigned based on COSY, NOESY, HMQC, HMBC and ^{1}H{^{31}P} experiments, as well as trends in chemical shifts and coupling constants derived from these experiments. Mass spectrometry was performed on Agilent 6224 TOF-MS (high resolution) or Agilent 6130 LCMS (low resolution) instruments.

Polymerization reactions were performed in a Parr 300 mL stainless steel autoclave, which was equipped with a mechanical stirrer, thermocouple and water cooling loop and controlled by a Parr 4842 controller. Gel permeation chromatography (GPC) data were obtained on a Polymer

Laboratories PL-GPC 220 instrument at 150 °C with 1,2,4-trichlorobenzene (stabilized with 125 ppm BHT) as the mobile phase. Three PLgel 10 μm Mixed-B LS columns were used. Molecular weights were calibrated using narrow polystyrene standards (ten-point calibration with M_n from 570 Da to 5670 kDa) and are corrected for linear polyethylene by universal calibration using the following Mark-Houwink parameters: polystyrene, $K = 1.75 \times 10^{-2}$ cm^3g^{-1}, $\alpha = 0.67$; polyethylene, $K = 5.90 \times 10^{-2}$ cm^3g^{-1}, $\alpha = 0.69$.[24] DSC measurements were performed on a TA Instruments DSC 2920 instrument. Samples (10 mg) were annealed by heating to 170 °C at 20 °C/min, cooled to 40 °C at 20 °C/min, and then analyzed while being heated to 170 °C at 20 °C/min.

(4-*t*Bu-Ph)P(NEt$_2$)Cl.[20] A Schlenk flask was charged with (4-*t*Bu-Ph)PCl$_2$ (4.2 g, 18 mmol) and Et$_2$O (75 mL), and cooled to -78 °C. HNEt$_2$ (3.7 mL, 36 mmol) was added via syringe to form a white cloudy solution. The mixture was stirred at -78 °C for 1 h and filtered, and the volatiles were removed from the filtrate under vacuum to yield a white solid (4.4 g, 91 %). The product was pure by NMR and used without further purification. $^{31}P\{^1H\}$ NMR (CD$_2$Cl$_2$): δ 144.8 (s). ^{1}H NMR (CD$_2$Cl$_2$): δ 7.65-7.62 (m, 2H), 7.50-7.47 (m, 2H), 3.17-3.09 (m, 4H), 1.34 (s, 9H), 1.09 (t, $^3J_{HH}$ = 7, 6H).

(4-*t*Bu-Ph)(2-P(O)(OEt)$_2$-5-Me-Ph)(2-SO$_3$Li-5-Me-Ph)P (Li[1-Et$_2$]). Revision of the procedure reported in literature.[13] A Schlenk flask was charged with diethyl (2-bromo-4-tolyl)phosphonate (4.6 g, 15 mmol) and THF (115 mL), and cooled to -78 °C. *n*BuLi (2.5 M in hexanes, 6.0 mL, 15 mmol) was added via syringe over 10 min. The mixture was stirred at -78 °C for 1 h and a solution of (4-*t*Bu-Ph)P(NEt$_2$)Cl (4.1 g, 15 mmol) in Et$_2$O (30 mL) was added. The mixture was stirred at room temperature for 18 h to yield a clear yellow solution. The violates were removed under vacuum and the crude (4-*t*Bu-Ph)(2-P(O)(OEt)$_2$-5-Me-Ph)P(NEt$_2$) was dissolved in Et$_2$O (60 mL). The Et$_2$O solution was cooled to -78 °C and stirred for 1h. HCl solution (2.0 M in diethyl ether, 15 mL, 30 mmol) was added via syringe to form a cloudy white solution. The reaction mixture was stirred for 2 h, and filtered through a frit. The white solid was rinsed with 40 mL Et_2O. The filtrate and wash were combined and taken to dryness under vacuum to afford a yellow solid, (4-^{t}Bu-Ph)(2-P(O)(OEt)$_2$-5-Me-Ph)PCl, which was dried under vacuum for 18 h. The yellow solid was dissolved in Et_2O (30 mL) in a Schlenk flask. Another Schlenk flask was charged with *para*-toluenesulfonic acid (2.6 g, 15 mmol) and THF (115 mL), and cooled to -78 °C. ^{n}BuLi (2.5 M in hexanes, 12 mL, 30 mmol) was added via syringe over 10 min to yield a yellow solution and the mixture was stirred at -78 °C for 1 h. The mixture was then cannula transferred into the (4-^{t}Bu-Ph)(2-P(O)(OEt)$_2$-5-Me-Ph)PCl Et_2O solution. The mixture was stirred at room temperature for 18 h to yield a clear yellow solution. The volatiles were removed under vacuum. The resulting yellow solid was taken up in H_2O (280 mL) and washed with hexanxes/benzene (3/1, 280 mL). The aqueous layer was separated and extracted with CH_2Cl_2 (4 x 300 mL). The combined CH_2Cl_2 layers were dried with $MgSO_4$, and the solvent was removed under vacuum to yield Li[**1**-Et$_2$] as a white solid (5.5 g, 64 %). The NMR data for **Li[1-Et$_2$]** agree with literature data.[13]

(4-^{t}Bu-Ph)(2-P(O)(OEt)$_2$-5-Me-Ph)(2-SO$_3^-$-5-Me-Ph)PH$^+$ (H[1-Et$_2$]). A flask was charged with Li[**1**-Et$_2$] (5.5 g, 9.7 mmol) and water (200 mL). The solution was transfered to a separatory funnel and aqueous HCl (1 M) was added until the *p*H was ca. 2. The resulting white suspension was extracted with CH_2Cl_2 (3 x 100 mL). The organic layers were combined, and dried with $MgSO_4$, and the solvent was removed under vacuum, affording H[**1**-Et$_2$] as a white solid (5.3 g, 98 %). H[**1**-Et$_2$] was recrystallized by layering Et_2O onto CH_2Cl_2 solution and solution was cooling to -40 ˚C (3.7 g, 70%). The NMR data for **H[1-Et$_2$]** agree with literature data.[13]

(4-^{t}Bu-Ph)(2-P(O)(OH)$_2$-5-Me-Ph)(2-SO$_3^-$-5-Me-Ph)P$^+$H (1-H$_3$). A Schlenk flask was charged with H[**1**-Et$_2$] (0.74 g, 1.3 mmol) and CH_2Cl_2 (30 mL), and bromotrimethylsilane (1.0 mL, 7.6 mmol) was added. The mixture was stirred at room temperature for 2 d and the volatiles were removed under vacuum. N_2-purged CH_3OH was added to yield a colorless clear solution and the mixture was stirred at room temperature for 2 h. The solution was concentrated to yield a white suspension, which was sonicated for 2 h. The product was isolated by filtration as a white solid (0.52 g, 78 %). ^{31}P{^{1}H} NMR (DMSO-d_6): δ 11.9 (d, J_{PP} = 6 Hz, *P*=O), -19.5 (d, J_{PP} = 6 Hz, *P*-H^{+}). ^{1}H NMR (DMSO-d_6): δ 11.11 (br, 3H, -O*H* and -P*H*$^{+}$), 7.78-7.73 (m, 2H, H^{9} and H^{3}), 7.34 (d, $^{3}J_{HH}$ = 6, 2H, H^{15}), 7.25 (d, $^{3}J_{HH}$ = 8, 1H, H^{10}), 7.19 (d, $^{3}J_{HH}$ = 8, 1H, H^{4}), 7.03 (s, 1H, H^{6}), 6.93 (s, 1H, H^{12}), 6.90 (dd, $^{3}J_{PH}$ = $^{3}J_{HH}$ = 8, 2H, H^{14}), 2.21 (s, 3H, H^{17}), 2.19 (s, 3H, H^{18}), 1.27 (s, 9H, H^{20}). ^{13}C{^{1}H} NMR (DMSO-d_6): δ 150.0 (s, C^{16}), 148.1 (d, J_{PC} = 28), 140.2 (s), 139.9 (d, J_{PC} = 20), 138.4 (s), 136.2 (dd, J_{PC} = 176, 38, C^{8}), 135.3 (s, C^{12}), 135.1 (d, J_{PC} = 26, C^{6}), 134.6 (d, J_{PC} = 25), 134.3 (d, J_{PC} = 14), 132.6 (d, J_{PC} = 18, C^{14}), 132.3 (d, J_{PC} = 11, C^{9}), 129.1 (s, C^{4}), 129.0 (s, C^{10}),127.3 (d, J_{PC} = 5, C^{3}), 125.0 (d, J_{PC} = 5, C^{15}), 34.3 (s, C^{19}), 31.1 (s, C^{20}), 21.1 (s, C^{18}), 20.9 (s, C^{17}). HRMS (*m*/*z*): Calcd. for $[C_{24}H_{28}O_6P_2S - H]^-$ 505.1004, Found: 505.1030.

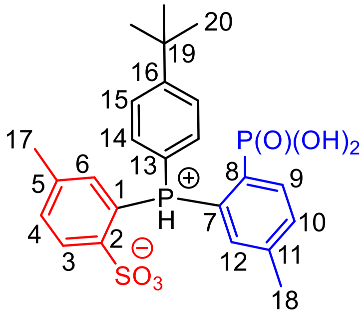

Figure 3.13. NMR spectra of **1-H$_3$**

(a) $^{31}P\{^1H\}$ (DMSO-d_6, 202 MHz):

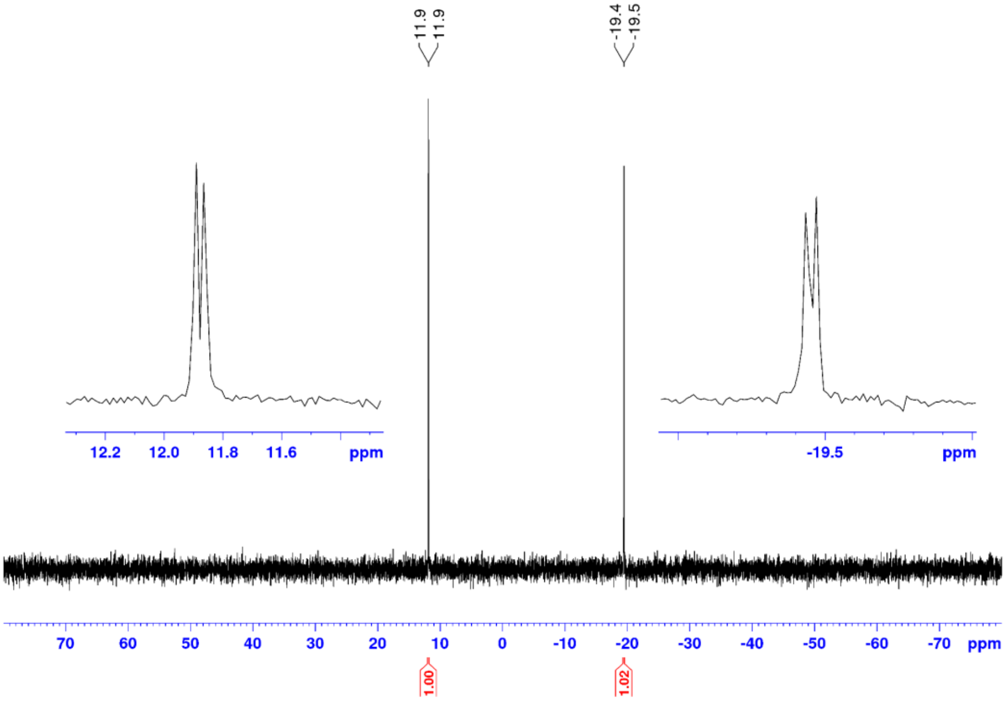

(b) ^1H (DMSO-d_6, 500 MHz): δ 3.16 = CH_3OH

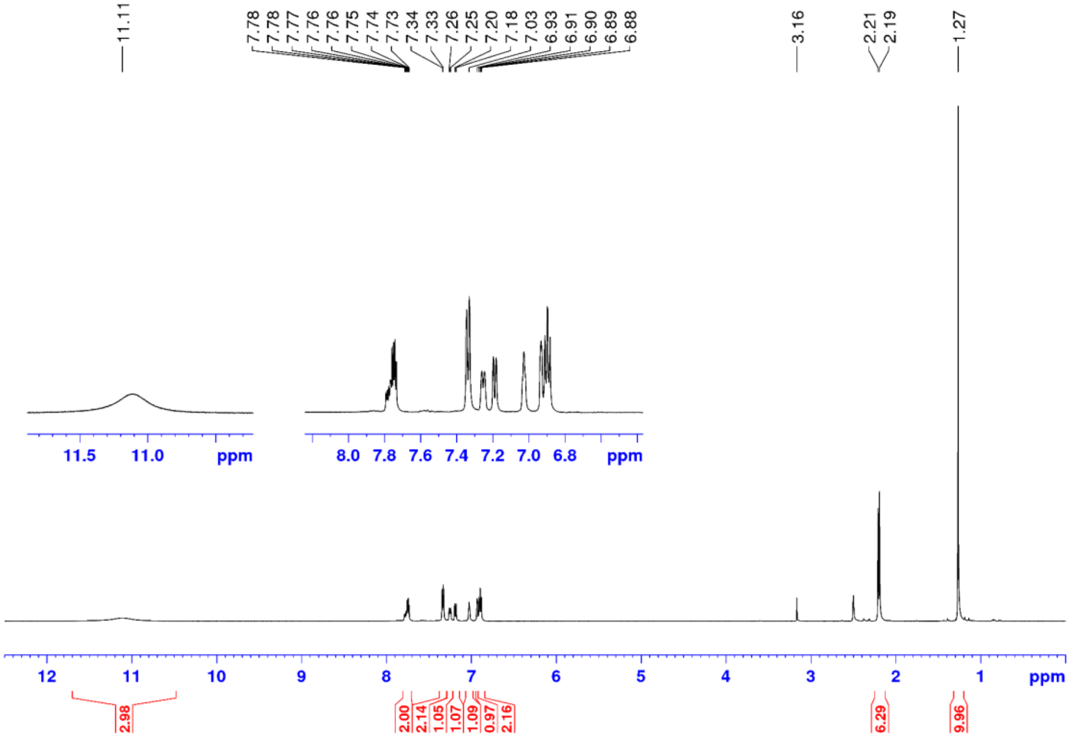

Figure 3.13, continued.

(c) $^{1}H\{^{31}P\}$ (DMSO-d_6, 500 MHz): δ 3.16 = CH_3OH

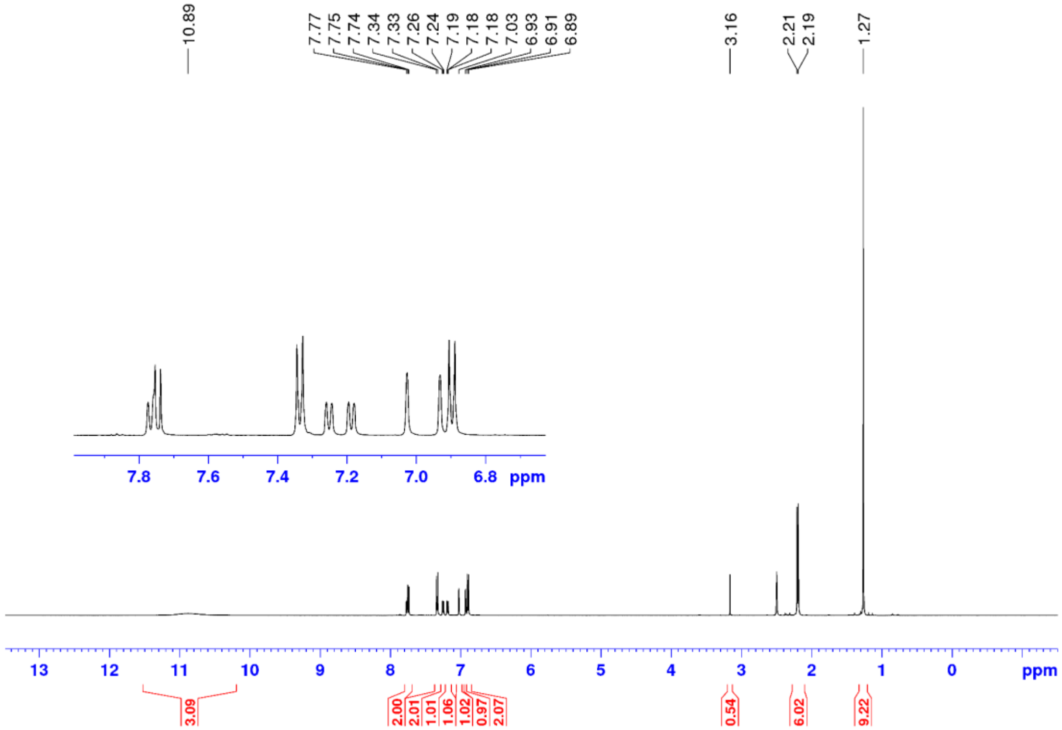

(d) $^{13}C\{^{1}H\}$ (DMSO-d_6, 125 MHz):

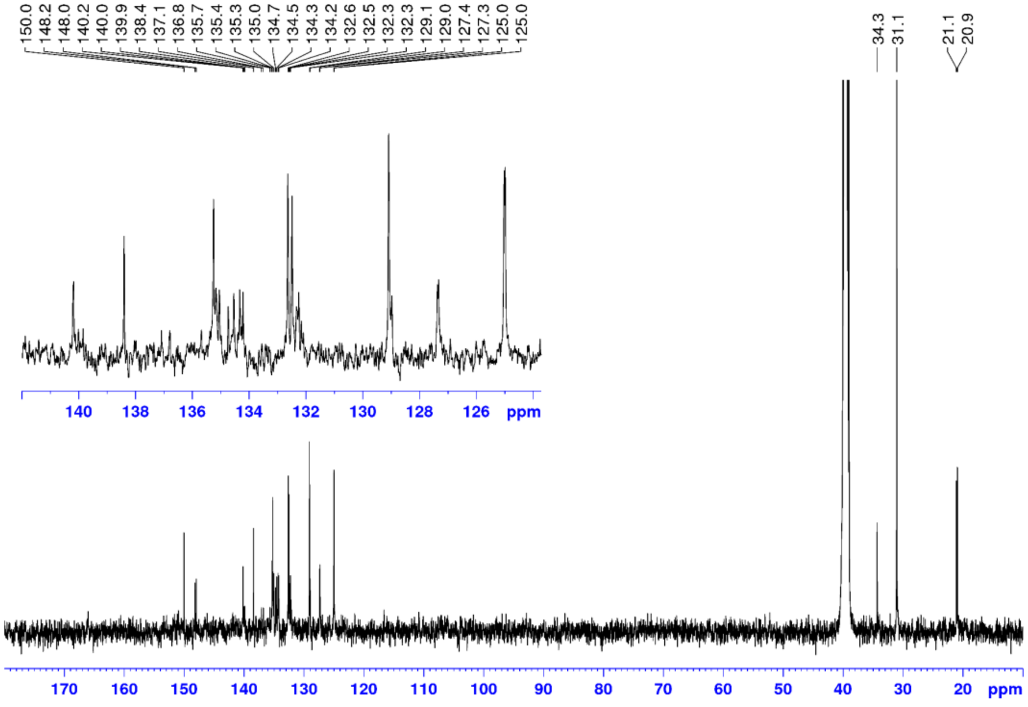

Figure 3.13, continued.

(e) COSY (DMSO-d_6, aryl region):

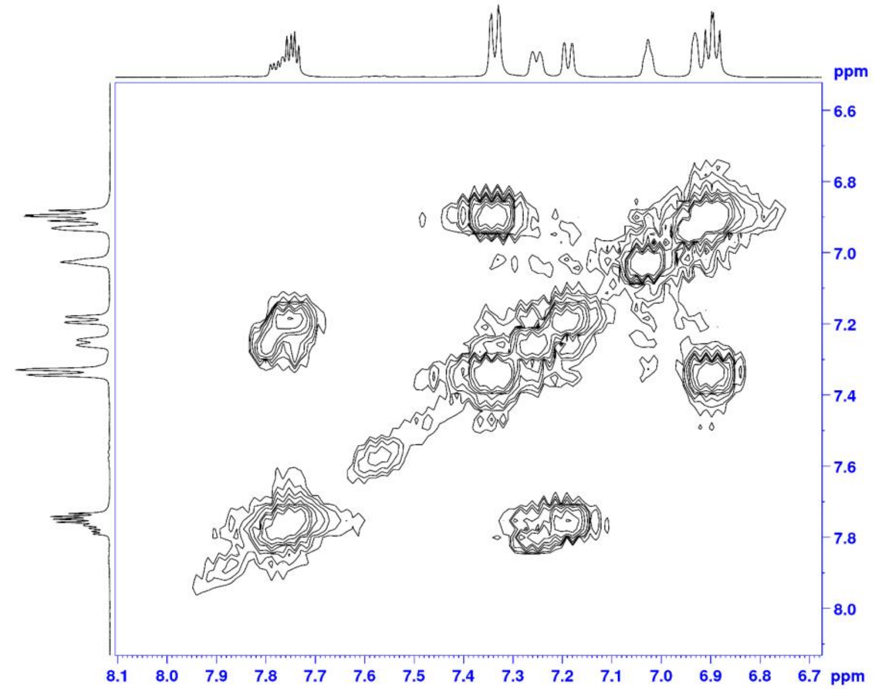

(f) COSY (DMSO-d_6, aryl region):

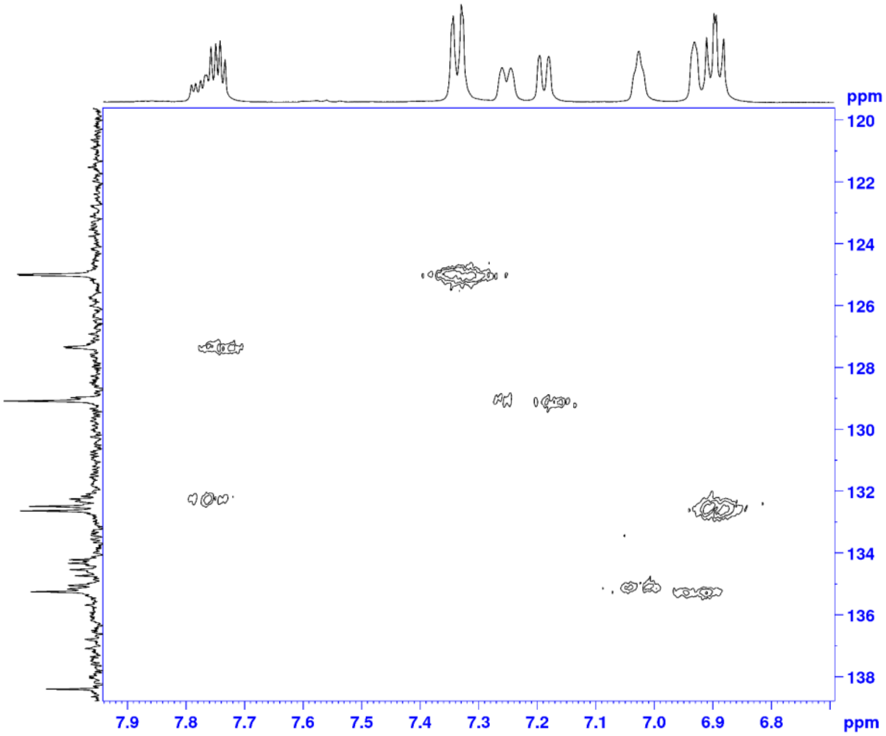

{Zn[1-H]}$_4$. A Schlenk flask was charged with **1**-H_3 (0.71 g, 1.4 mmol), zinc acetate dihydrate (0.31 g, 1.4 mmol) and N_2-purged CH_3OH (70 mL) to yield a white suspension. CH_2Cl_2 (15 mL) was added by syringe until the solution became clear. The mixture was stirred at room temperature for 2 h, concentrated under vacuum to ca. 50 mL, and left at room temperature for 18 h without stirring to precipitate or crystallize {Zn[**1**-H]}$_4$ out of solution. The product was isolated by filtration and washed with CH_3OH to afford a white solid. The product was heated to 50 ˚C for 2 d under vacuum to yield CH_3OH-free {Zn[**1**-H]}$_4$ (0.67 mg, 84 %). X-ray quality crystals were grown from CH_3OH solution at room temperature. $^{31}P\{^1H\}$ NMR (DMSO-*d*$_6$): δ 12.2 (s, *P*=O), -17.7 (s, Zn-*P*). ^1H NMR (DMSO-*d*$_6$): δ 10.58 (br, 1H, -O*H*), 7.82 (br, 2H, H^3 and H^9), 7.31-7.27 (br, 4H, H^4, H^{10} and H^{15}), 6.96 (br, 2H, H^6 and H^{12}), 6.80 (br, 2H, H^{14}), 2.19 (s, 6H, H^{17} and H^{18}), 1.25 (s, 9H, H^{20}). $^{13}C\{^1H\}$ NMR (DMSO-*d*$_6$): δ 151.4 (br), 146.6 (br), 146.4 (br), 139.7 (br), 139.1 (br), 135.6 (s), 134.8 (d, J_{PC} = 12), 133.1 (d, J_{PC} = 15), 130.2 (br), 129.8 (br), 127.3 (s), 124.9 (d, J_{PC} = 7), 34.4 (s, C^{19}), 31.0 (s, C^{20}), 21.1 (s, C^{18}), 20.9 (s, C^{17}). Four carbon resonances were not observed due to the broadness of the spectrum and possible overlapping among resonances. HRMS (*m*/*z*): Calcd. for $[C_{96}H_{104}Zn_3O_{24}P_8S_4 - Zn + 3H]^+$ 2217.1668, Found: 2217.1676. When the product was dried under vacuum at room temperature for 1 d, (instead of at 50 ˚C for 2 d), the isolated material contained ca. 1.3 equiv CH_3OH per {Zn[**1**-H]}$_4$. ^1H NMR (DMSO-*d*$_6$): δ 10.82 (br, 1H, -O*H*), 7.83 and 7.82 (d, $^3J_{HH}$ = 8 Hz, 2H, H^3 and H^9), 7.31-7.26 (br, 4H, H^4, H^{10} and H^{15}), 6.93 (br, 2H, H^6 and H^{12}), 6.79 (br, 2H, H^{14}), 2.18 (s, 6H, H^{17} and H^{18}), 1.25 (s, 9H, H^{20}).

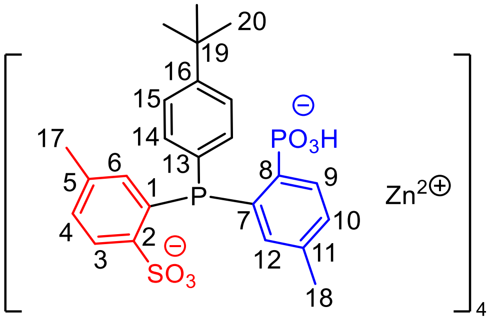

Figure 3.14. NMR spectra of **{Zn[1-H]}$_4$**

(a) $^{31}P\{^1H\}$ (DMSO-d_6, 202 MHz):

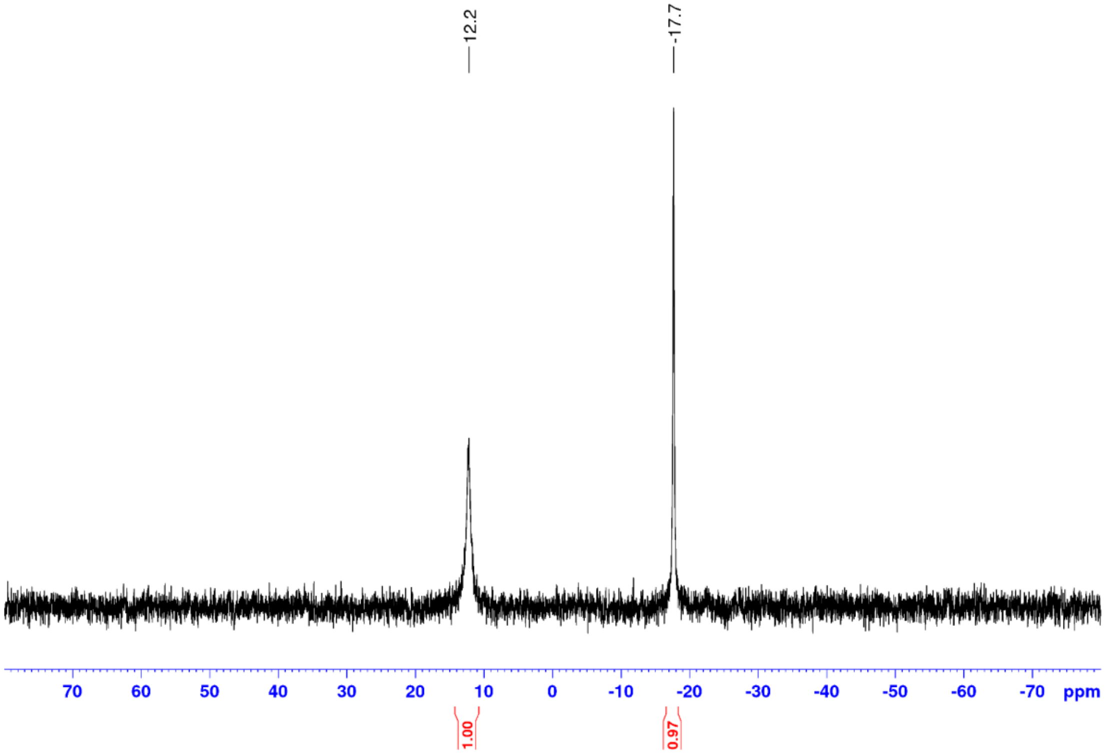

Figure 3.14, continued.

(b) ^1H (DMSO-d_6, 500 MHz):

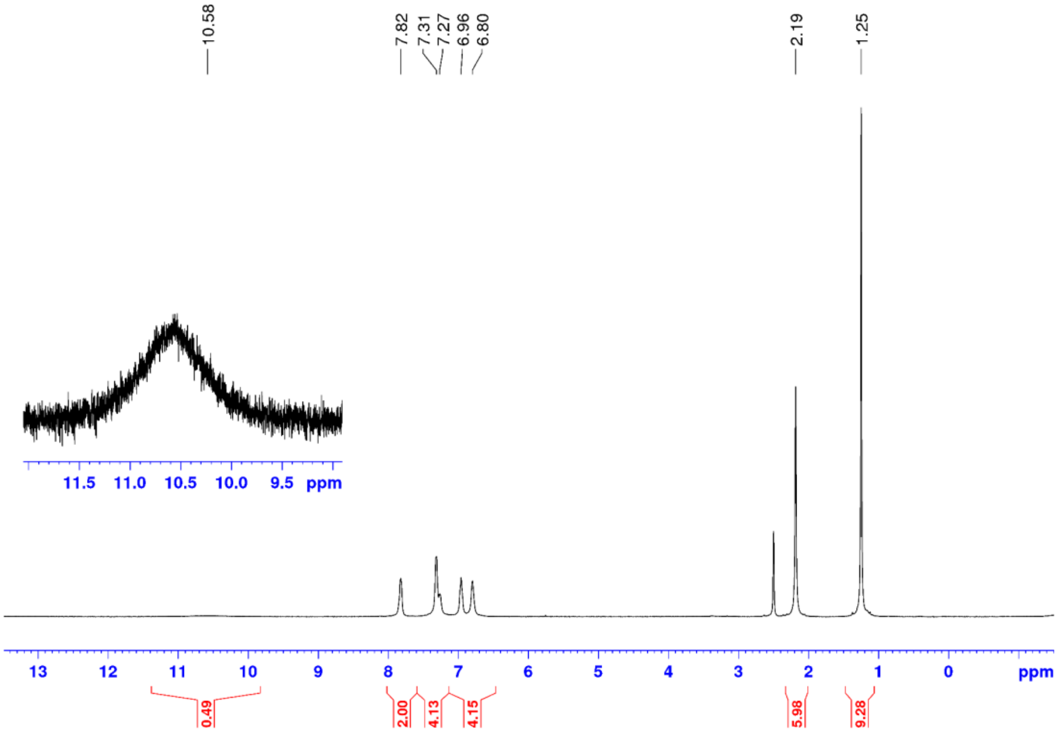

(c) $^{13}C\{^1H\}$ (DMSO-d_6, 125 MHz):

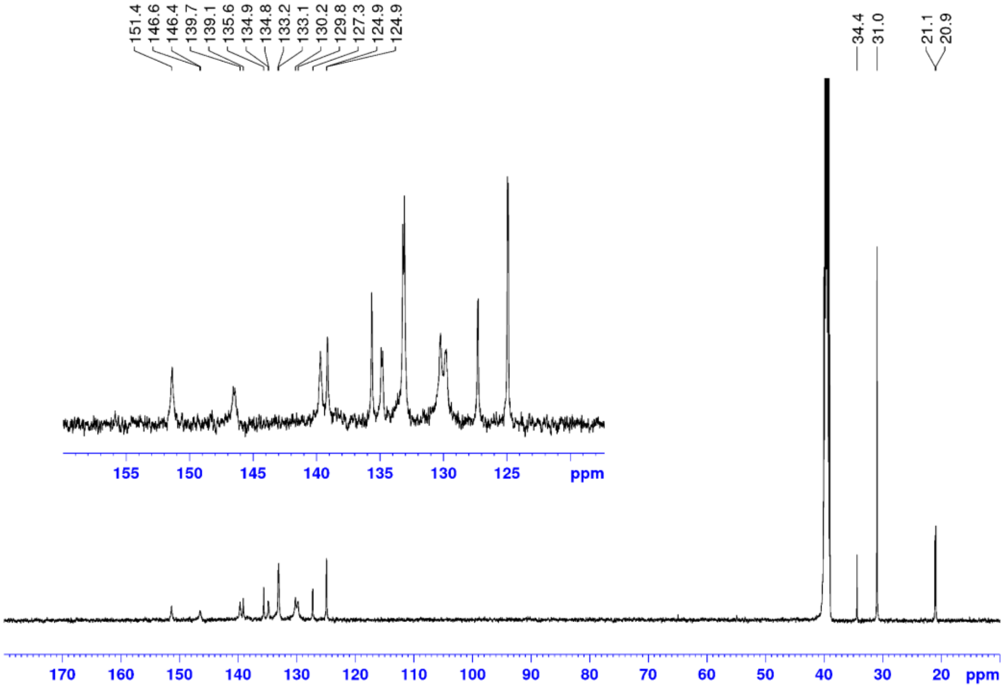

Figure 3.14, continued.

(d) ^{1}H for **{Zn[1-H]}$_4$**•1.3CH$_3$OH (DMSO-d_6, 500 MHz): δ 3.17 = CH$_3$OH

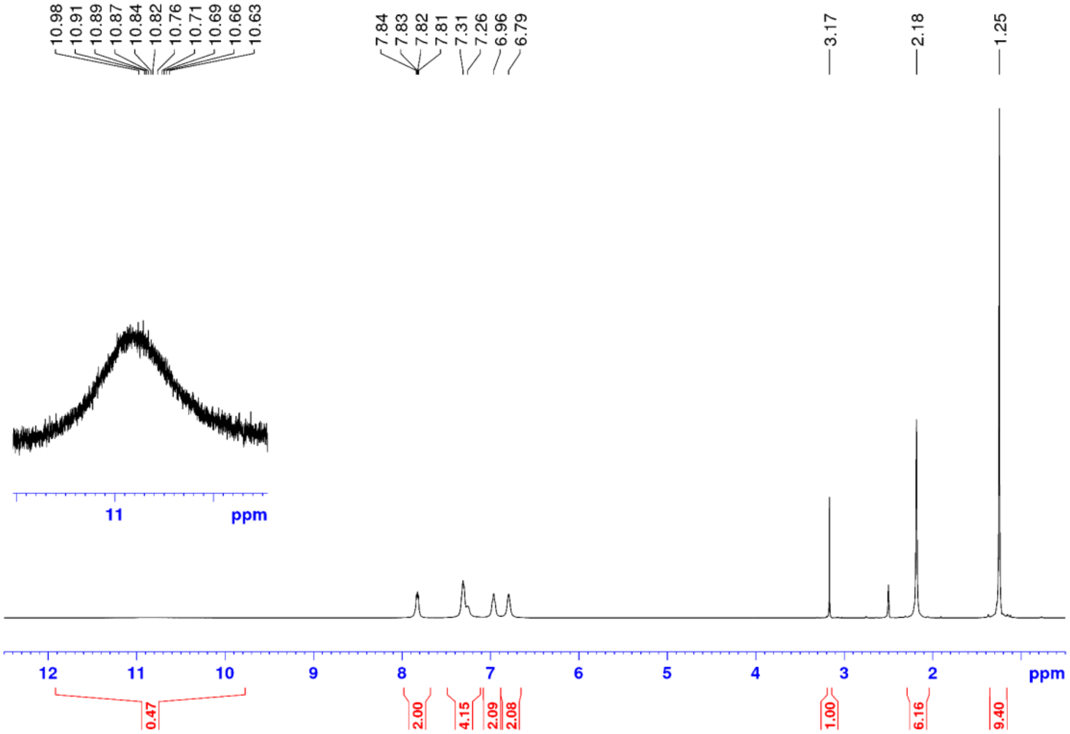

{Zn(TMEDA)[κ^2-*P*,P*O*-P(4-^{t}Bu-Ph)(2-P*O*$_3$$^{2-}$-5-Me-Ph)(2-SO$_3$$^-$-5-Me-Ph)PdMe(py)]}$_2$ (2). A vial was charged with {Zn[**1**-H]}$_4$•1.3CH$_3$OH (49 mg, 0.020 mmol), (TMEDA)PdMe$_2$ (21 mg, 0.020 mmol) and CH$_2$Cl$_2$ (1 mL). The yellow solution was stirred at room temperature for 1 h. Pyridine (6.8 μL, 0.020 mmol) was added, and the solution was stirred for an additional 18 h. The mixture was filtered through Celite, and Et$_2$O was diffused into the filtrate at room temperature to afford colorless X-ray quality crystals (10 mg, 23 %).

General procedure for screening of ligands (L) for NMR-scale generation of 4-L compound. A J-Young valved NMR tube was charged with 1.0 equiv of {Zn[**1**-H]}$_4$ and 1.0 equiv of (COD)PdMe$_2$, and CD$_2$Cl$_2$ was added by vacuum transfer. The mixture was thawed and formed a clear yellow solution. Gas evolution (CH$_4$) was observed. The NMR tube was agitated at room temperature for 1 h to afford a clear yellow solution. The ligand L (1.0 equiv) was added, and the tube was agitated for an additional 18 h and analyzed by NMR. The following ligands were screened: 4-^{t}Bu-pyridine, 4-Ph-pyridine, 3-Br-4-Cl-pyridine, 4-(5-nonyl)-pyridine, 4-Me-2,6-lutidine, 4-Br-2,6-lutidine, quinoline, and acridine. In all cases, the major ^{31}P resonances for the reaction mixture appeared at δ 36.4 – 29.5 (phosphine) and 9.4 – 7.9 (phosphonate), and no P-P coupling was observed. The major ^{1}H Pd-Me resonance appeared in the range δ -0.06 – -0.36 as a doublet with a small J_{PH} value (ca. 3 Hz). These major ^{31}P and ^{1}H resonances were assigned to **4-L**. Minor Pd-Me ^{1}H resonances ascribed to minor stereoisomers were also observed. The highest major/minor stereoisomer ratio was observed for quinoline and 4-^{t}Bu-pyridine.

Figure 3.15. NMR spectra of **4-py**

(a) ^{31}P{^{1}H} (CD_2Cl_2, 202 MHz):

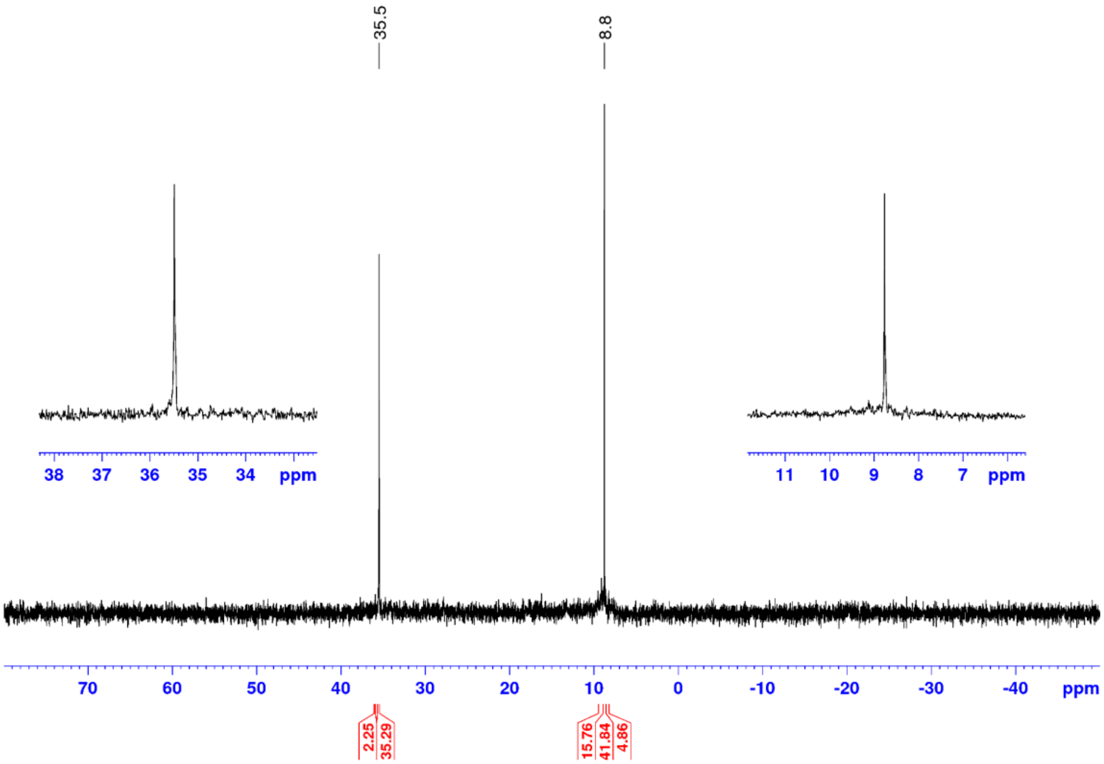

Figure 3.15, continued.

(b) ^{1}H (CD_2Cl_2, 202 MHz): δ 5.56, 2.35 = COD; 5.41, 0.27 = (COD)$PdMe_2$; 0.21 = CH_4; 0.09 = grease.

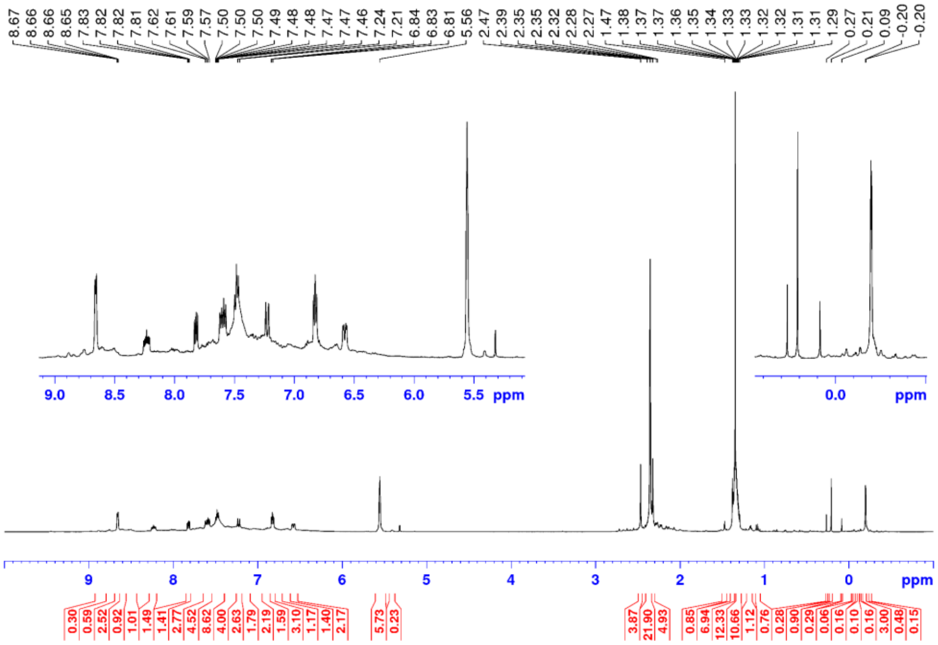

Figure 3.16. NMR spectra of **4-(quinoline)**

(a) $^{31}P\{^1H\}$ (CD_2Cl_2, 202 MHz):

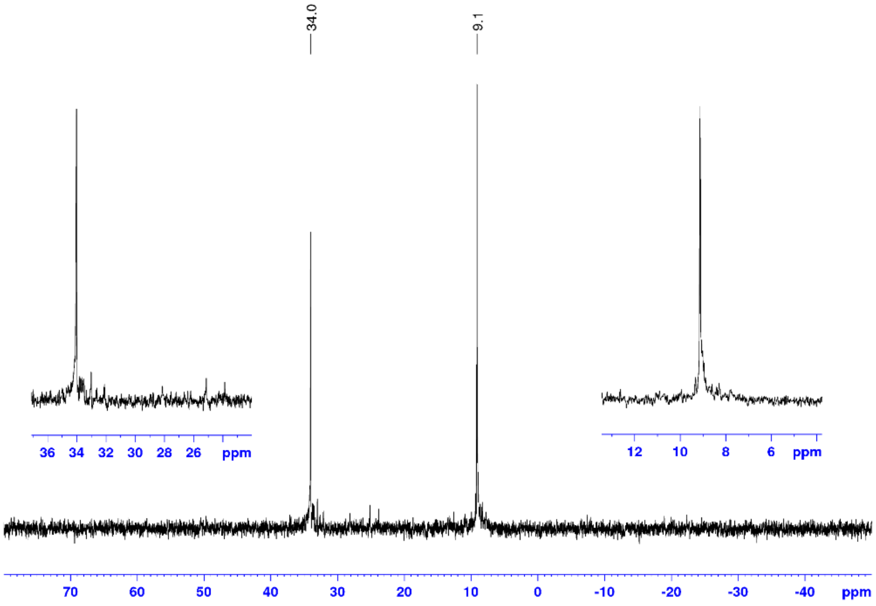

Figure 3.16, continued.

(b) ^{1}H (CD_2Cl_2, 202 MHz): δ 5.56, 2.35 = COD; 0.21 = CH_4.

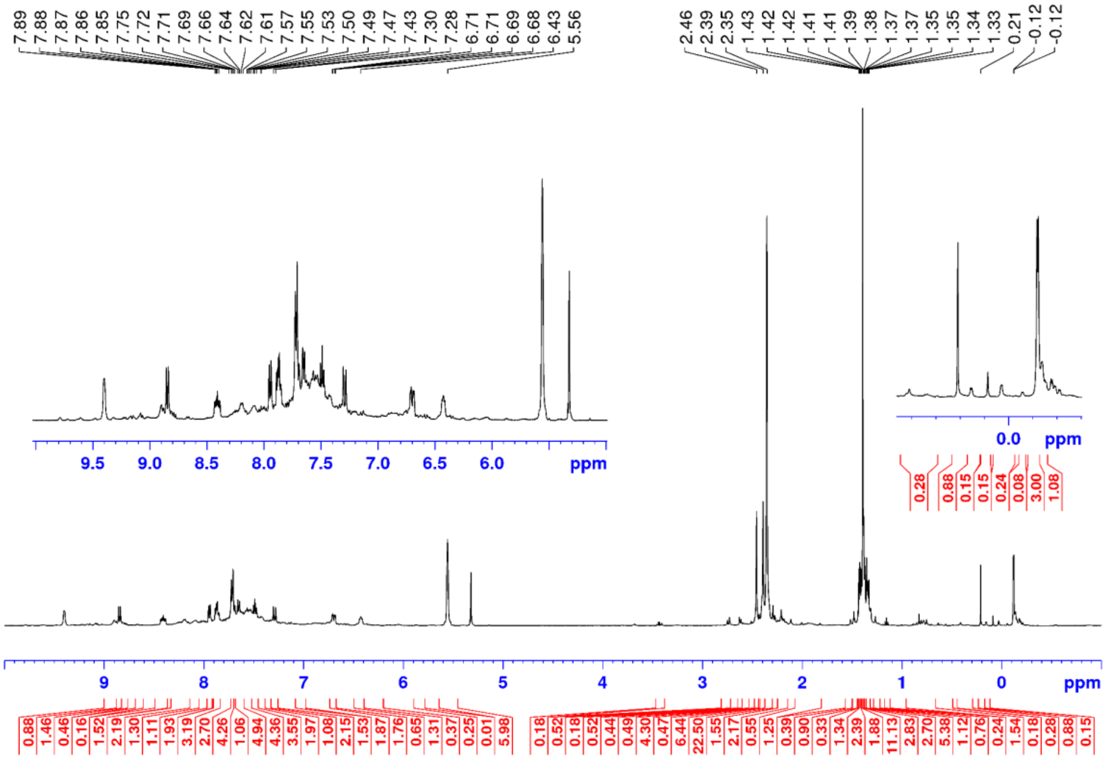

General procedure for prep scale synthesis of 4-L. A vial was charged with 1.0 equiv of {Zn[**1**-H]}$_4$, 1.0 equiv of (COD)$PdMe_2$ and CH_2Cl_2. The yellow solution was stirred at room temperature for 1 h. The ligand L (1.0 equiv) was added, and the mixture was stirred for an additional 18 h. The mixture was filtered through Celite and the volatiles were removed under vacuum to afford a yellow solid, which was further recrystallized. The following ligands L were studied: pyridine, 2,6-lutidine, quinoline and 4-^{t}Bu-pyridine. Recrystallization conditions included different combinations of CH_2Cl_2, $C_2H_4Cl_2$, $C_2H_2Cl_4$, toluene, 1,2-diclorobenzene, pentane, hexanes and heptane solvents, and different temperatures including room temperature, 10 °C, -10 °C and -40 °C. For most cases, precipitates or tiny crystals that did not diffract X-rays well were obtained. The sample of **4**-(2,6-lutidine) for NMR analysis was obtained from toluene/pentane solution at -40 °C as a yellow precipitates.

Figure 3.17. NMR spectra of **4-(2,6-lutidine)**

(a) $^{31}P\{^{1}H\}$ (CD_2Cl_2, 202 MHz):

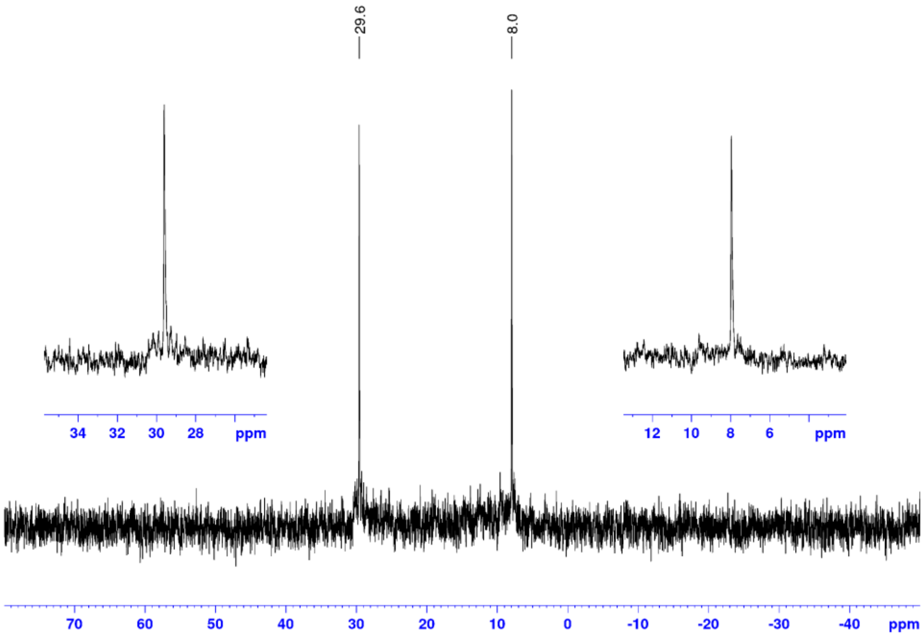

(b) ^{1}H (CD_2Cl_2, 202 MHz):

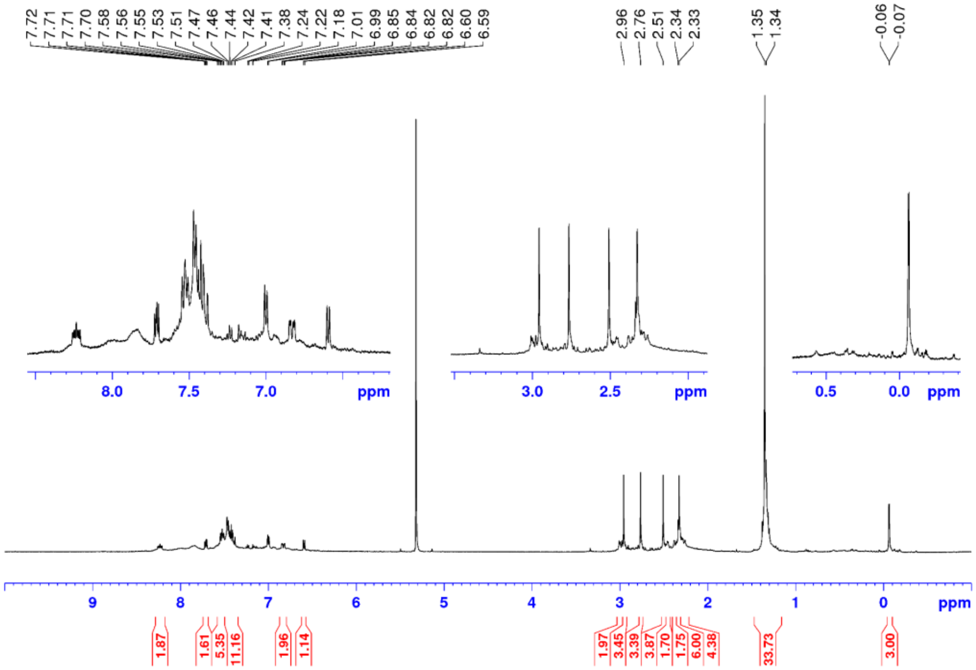

4-(4-^{t}Bu-py). A vial was charged with {Zn[**1**-H]}$_4$ (0.18 g, 0.31 mmol), (COD)PdMe$_2$ (77 mg, 0.31 mmol) and CH$_2$Cl$_2$ (5 mL). The mixture was stirred at room temperature for 1 h to afford a yellow clear solution. 4-^{t}Bu-py (46 µL, 0.31 mmol) was added, and the mixture was stirred for an additional 18 h. The mixture was filtered through Celite and the volatiles were removed under vacuum to afford a yellow solid. The solid was recrystallized by layering pentane onto a C$_2$H$_2$Cl$_4$/toluene solution and cooling to -40 °C. **4**-(4-^{t}Bu-py) was collected by filtration and dried under vacuum for 18 h (122 mg, 77 %). X-ray quality crystals were grown by slow evaporation of the C$_2$H$_2$Cl$_4$ solution at room temperature. ^{31}P{^{1}H} NMR (CD$_2$Cl$_2$): δ 36.4 (s, Pd-*P*), 9.4 (s, *P*=O). ^{1}H NMR (CD$_2$Cl$_2$): δ 8.54 (d, $^3J_{HH}$ = 5, 2H, H^{17}), 8.29 (m, 1H, H^9), 7.80 (dd, $^3J_{HH}$ = 8, $^4J_{PH}$ = 5, 1H, H^3), 7.63 (d, $^3J_{HH}$ = 8, 1H, H^{10}), 7.60 (d, $^3J_{HH}$ = 8, 1H, H^4), 7.46-7.44 (br, 4H, H^{14} and H^{15}; H^{14} resonance is broadened due to the restricted rotation around the P-C^{13} bond), 7.23 (d, $^3J_{PH}$ = 12, 1H, H^6), 6.81 (d, $^3J_{HH}$ = 6, 2H, H^{18}), 6.61 (dd, $^3J_{PH}$ = 12, $^4J_{PH}$ = 4, 1H, H^{12}), 2.48 (s, 3H, H^{20}), 2.31 (s, 3H, H^{21}), 1.38 (s, 9H, H^{25}), 1.15 (s, 9H, H^{23}), -0.29 (d, $^3J_{PH}$ = 3, 3H, Pd-C*H*$_3$). ^{13}C{^{1}H} NMR (CD$_2$Cl$_2$): δ 161.8 (s), 154.4 (s), 151.3 (s), 142.5 (d, J_{PC} = 7), 141.5 (d, J_{PC} = 12), 140.6 (d, J_{PC} = 13), 139.9 (d, J_{PC} = 10), 138.8 (m), 136.9 (m), 134.9 (s), 134.6 (m), 131.3 (d, J_{PC} = 32), 131.0 (s), 130.4 (d, J_{PC} = 10), 130.1 (s), 129.6 (s), 129.2 (s), 126.0 (br), 122.0 (s), 35.1 (s), 35.0 (s), 31.3 (s), 30.3 (s), 21.8 (s), 21.5 (s), 0.2 (s, Pd-*C*H$_3$).

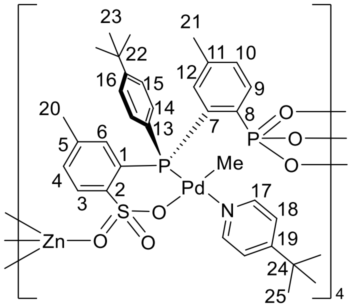

Figure 3.18. NMR spectra of **4-(4-^{t}Bu-py)**

(a) $^{31}P\{^1H\}$ (CD_2Cl_2, 202 MHz):

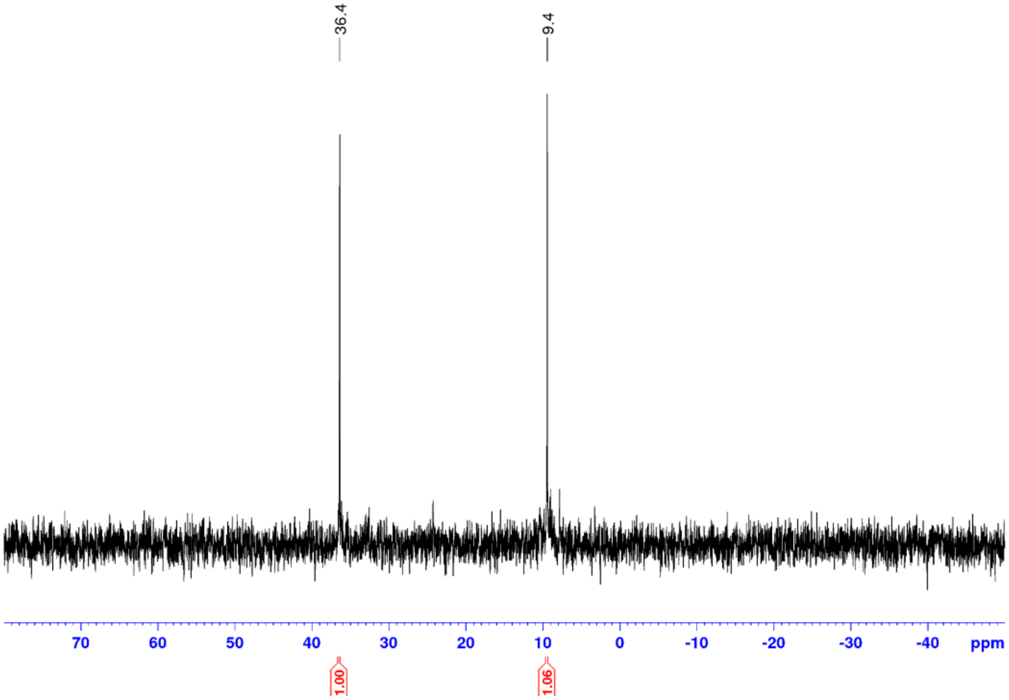

(b) ^1H (CD_2Cl_2, 500 MHz): δ 6.03 = $C_2H_2Cl_4$

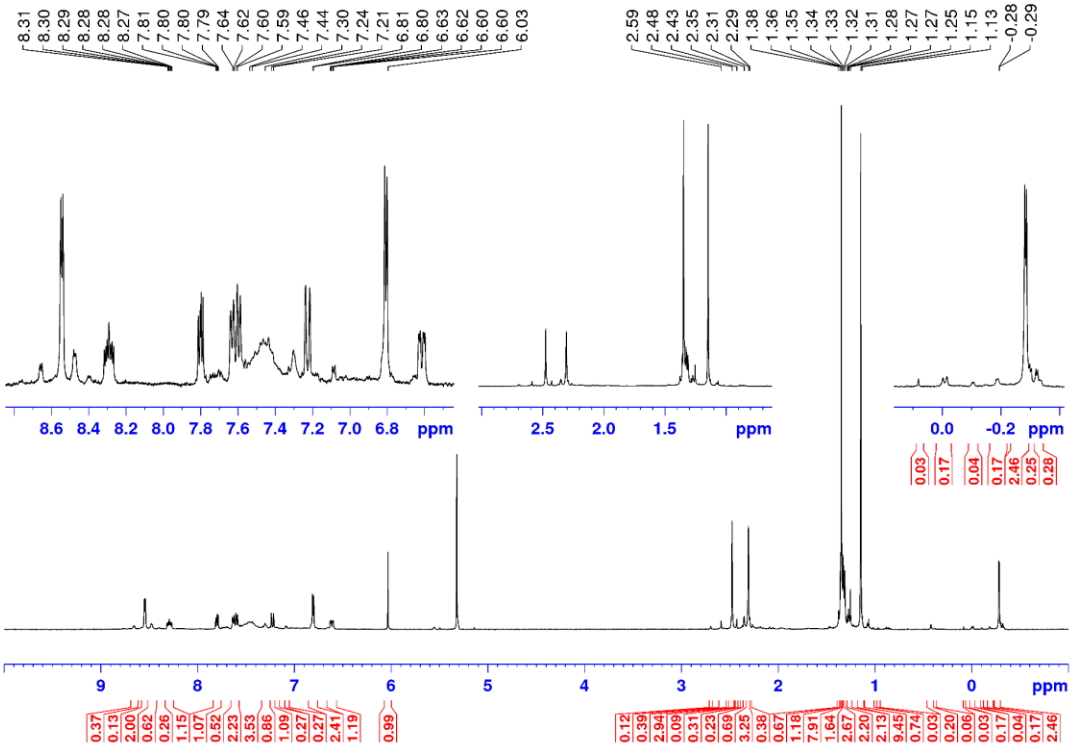

Figure 3.18, continued.

(c) $^{13}C\{^1H\}$ (CD_2Cl_2, 125 MHz): δ 74.7 = $C_2H_2Cl_4$

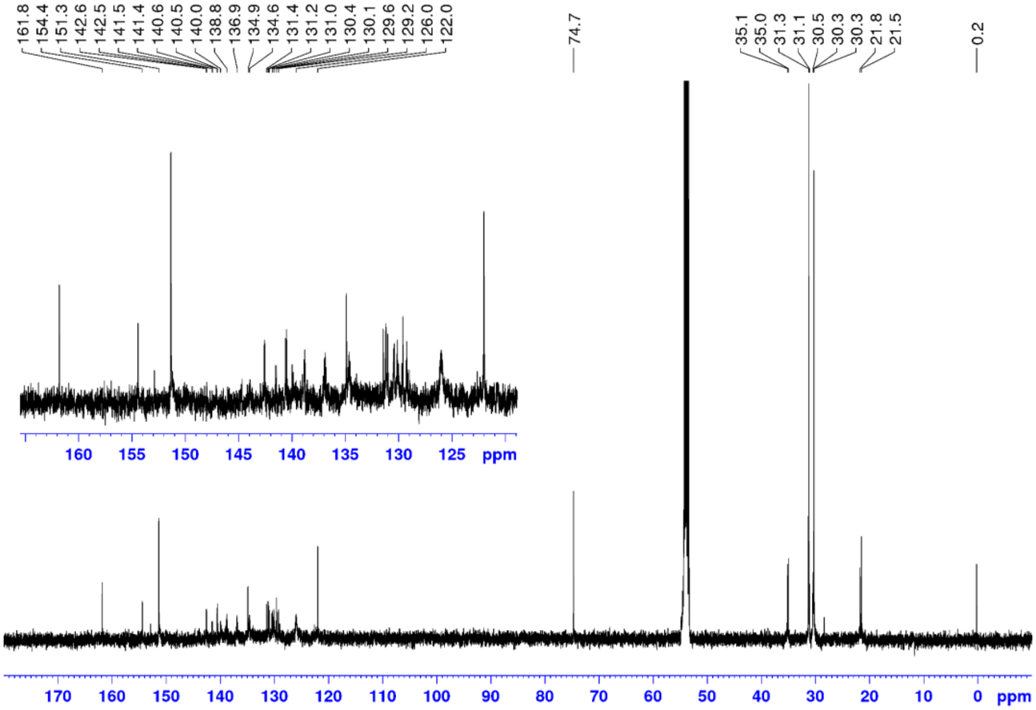

(d) COSY (CD_2Cl_2, aryl region):

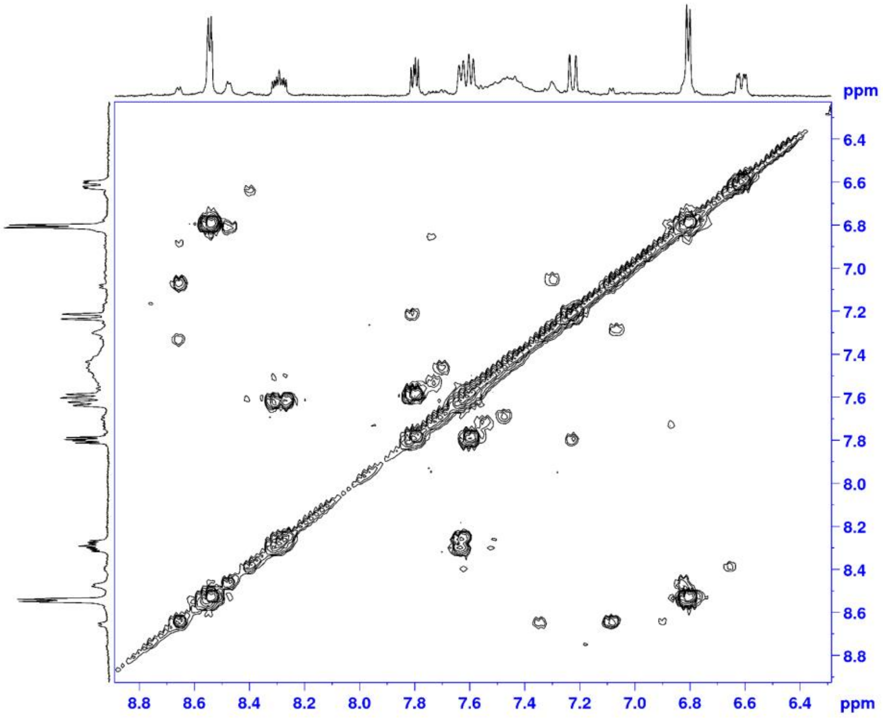

3-py. A vial was charged with CH_3OH-free $\{Zn[\mathbf{1}\text{-}H]\}_4$ (0.11 mg, 0.20 mmol), (COD)$PdMe_2$ (49 mg, 0.20 mmol) and CH_2Cl_2 (5 mL), and the mixture was stirred at room temperature for 1 h to afford a clear yellow solution. Pyridine (16 μL, 0.20 mmol) was added, and the mixturewas stirred for an additional 18 h. The mixture was filtered through Celite and the volatiles were removed under vacuum to afford a yellow solid. The solid was dissolved in N_2-purged CH_3OH (5 mL). The solution was left at room temperature for 18 h and X-ray quality crystals formed. The crystals were collected by filtration and dried under vacuum for 18 h (82 mg, 54 %, the pyridine content was 0.85 equiv as determined by ^{1}H NMR in CD_2Cl_2/CD_3OD). $^{31}P\{^{1}H\}$ NMR (CD_2Cl_2/CD_3OD): δ 42.7 (d, J_{PP} = 12 Hz, Pd-*P*), 19.4 (d, J_{PP} = 12 Hz, *P*=O). ^{1}H NMR (CD_2Cl_2/CD_3OD): δ 8.87 (dd, $^{3}J_{PH}$ = 15, $^{3}J_{HH}$ = 8, 1H, H^{3}), 8.55 (d, $^{3}J_{HH}$ = 4, 2H, H^{17}), 8.22 (d, $^{3}J_{HH}$ = 8, 1H, H^{4}), 7.91-7.80 (m, 3H, H^{9}, H^{19} and $H^{14'}$), 7.43 (t, $^{3}J_{HH}$ = 6, 2H, H^{18}), 7.29-7.22 (m, 3H, H^{15} and H^{10}), 6.99 (t, $^{3}J_{PH} = {}^{3}J_{HH}$ = 8, 1H, H^{14}), 6.89 (dd, $^{3}J_{PH}$ = 11, $^{4}J_{PH}$ = 4, 1H, H^{12}), 6.44 (d, $^{3}J_{PH}$ = 13, 1H, H^{6}), 2.20 (s, 3H, H^{20}), 2.09 (s, 3H, H^{21}), 1.28 (s, 9H, H^{23}), -0.84 (d, $^{3}J_{PH}$ = 2, 3H, Pd-CH_3). $^{13}C\{^{1}H\}$ NMR (CD_2Cl_2/CD_3OD): δ 155.7 (s, C^{16}), 149.5 (s, C^{17}), 143.9 (d, $^{4}J_{PC}$ = 9), 140.9 (d, $^{4}J_{PC}$ = 2, $C^{4'}$), 140.8 (d, J_{PC} = 9), 140.6 (d, J_{PC} = 29, C^{3}), 140.1 (dd, J_{PC} = 8, 3), 139.1 (d, J_{PC} = 8, C^{19}), 138.1 (dd, J_{PC} = 187, 18), 135.3 (d, J_{PC} = 14, C^{12}), 135.1 (d, J_{PC} = 7, C^{6}), 134.1 (s, C^{14}), 133.1 (dd, J_{PC} = 11, 7), 132.1 (s, C^{15}), 132.0 (d, J_{PC} = 11), 131.5 (dd, J_{PC} = 13, 2, C^{10}), 130.7 (d, J_{PC} = 7, $C^{14'}$), 127.5 (dd, J_{PC} = 199, 49), 127.2 (d, J_{PC} = 7), 125.4 (s, C^{4}), 125.3 (d, J_{PC} = 3, C^{18}), 35.4 (s, C^{22}), 31.1 (s, C^{23}), 21.3 (s, C^{20} and C^{21}), 1.5 (s, Pd-CH_3).

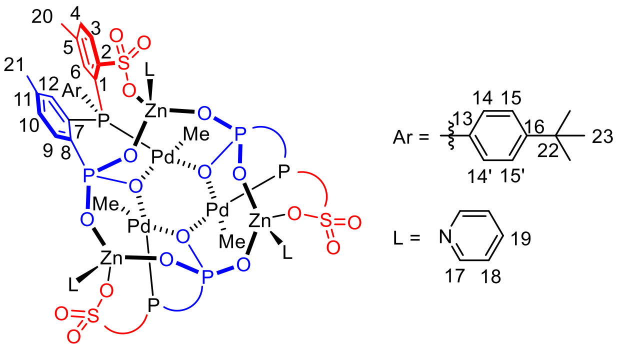

Figure 3.19. NMR spectra of **3-py**

(a) $^{31}P\{^{1}H\}$ (CD_2Cl_2/CD_3OD, 202 MHz):

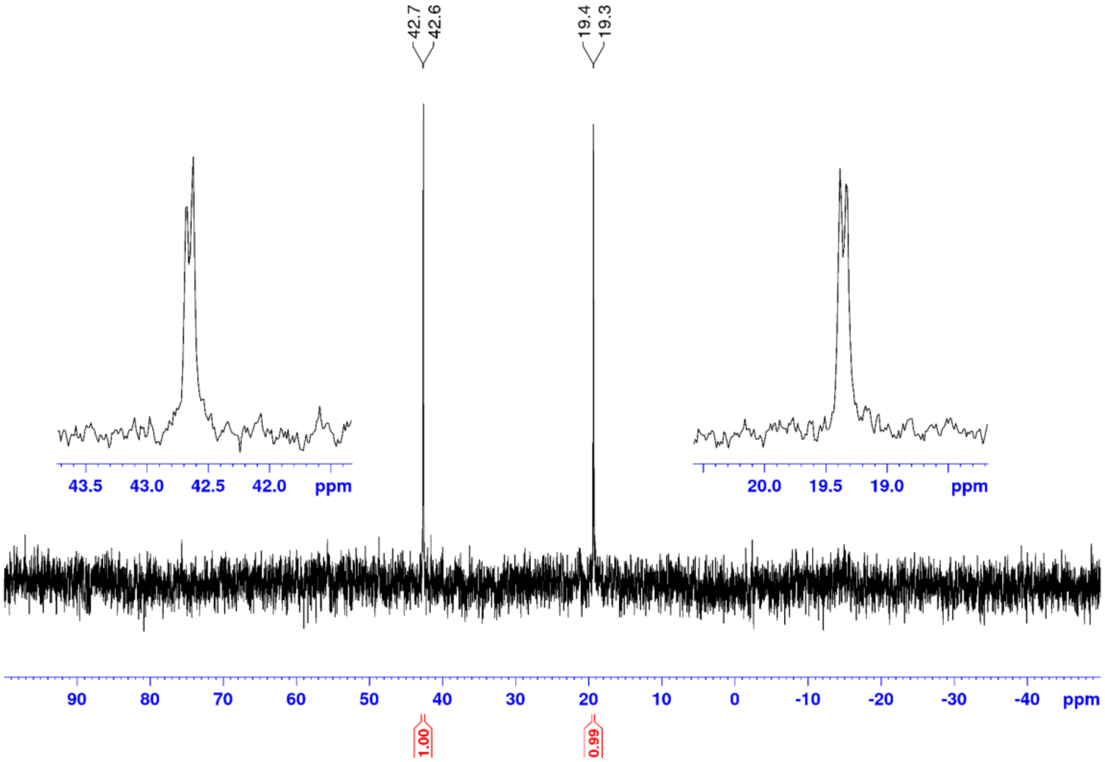

Figure 3.19, continued.

(b) ^{1}H (CD_2Cl_2/CD_3OD, 500 MHz): δ 4.29 = H_2O, 3.32 = CH_3OH, 0.05 = grease

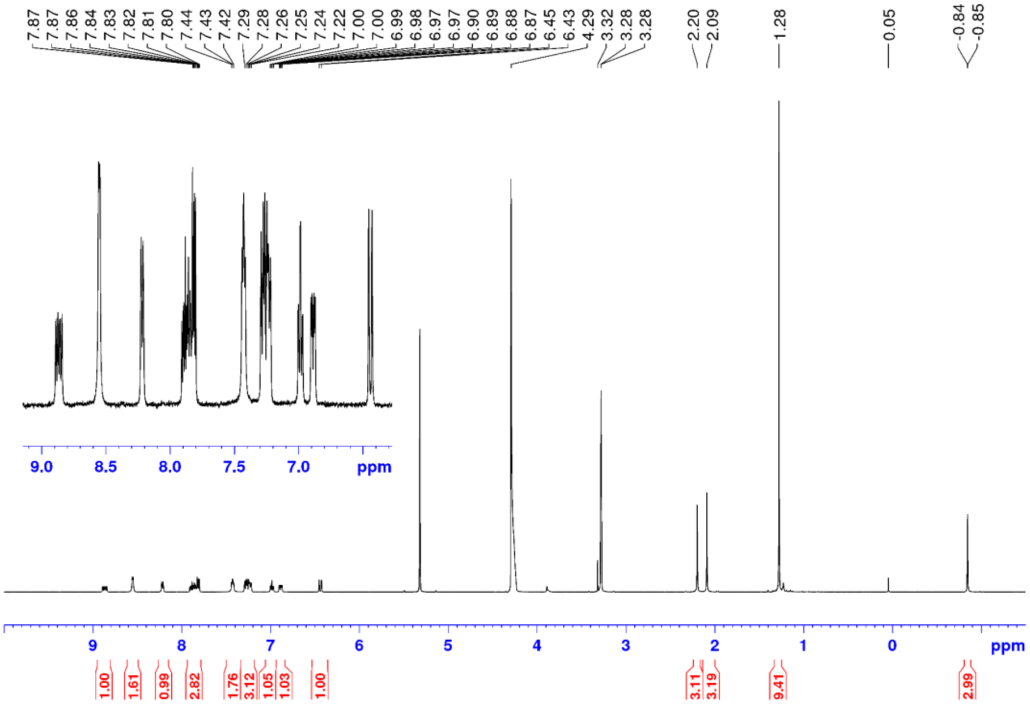

(c) $^{13}C\{^1H\}$ (CD_2Cl_2/CD_3OD, 125 MHz):

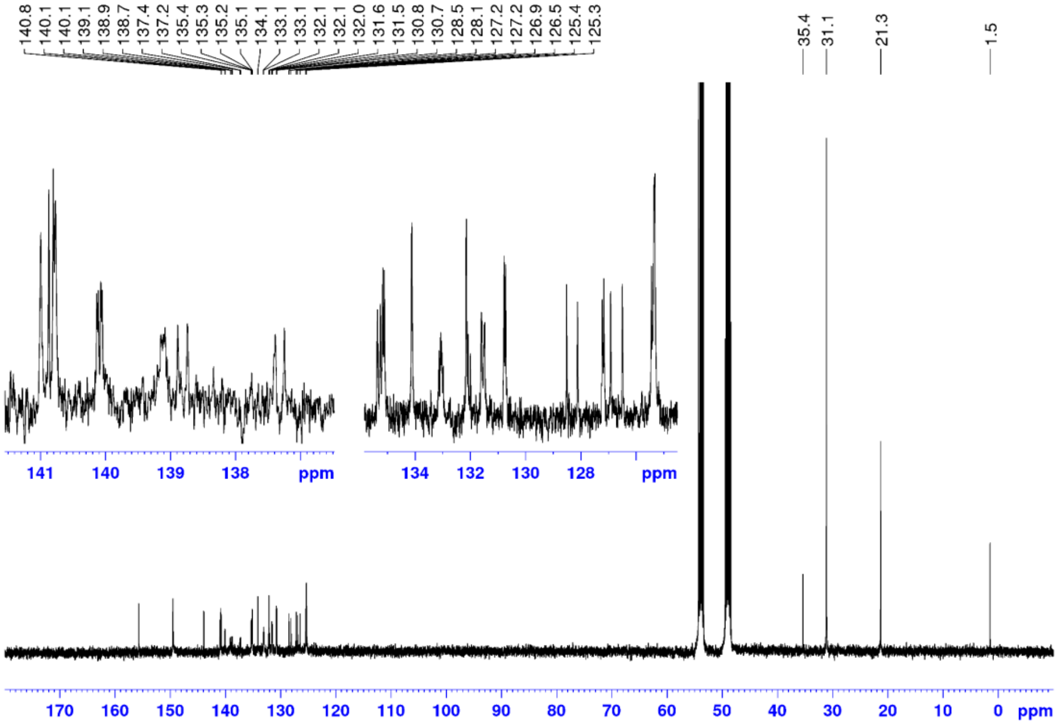

Figure 3.19, continued.

(d) ^{1}H (CD_2Cl_2/CD_3OD, 500 MHz): δ 4.28 = H_2O, 3.32 = CH_3OH, 0.05 = grease

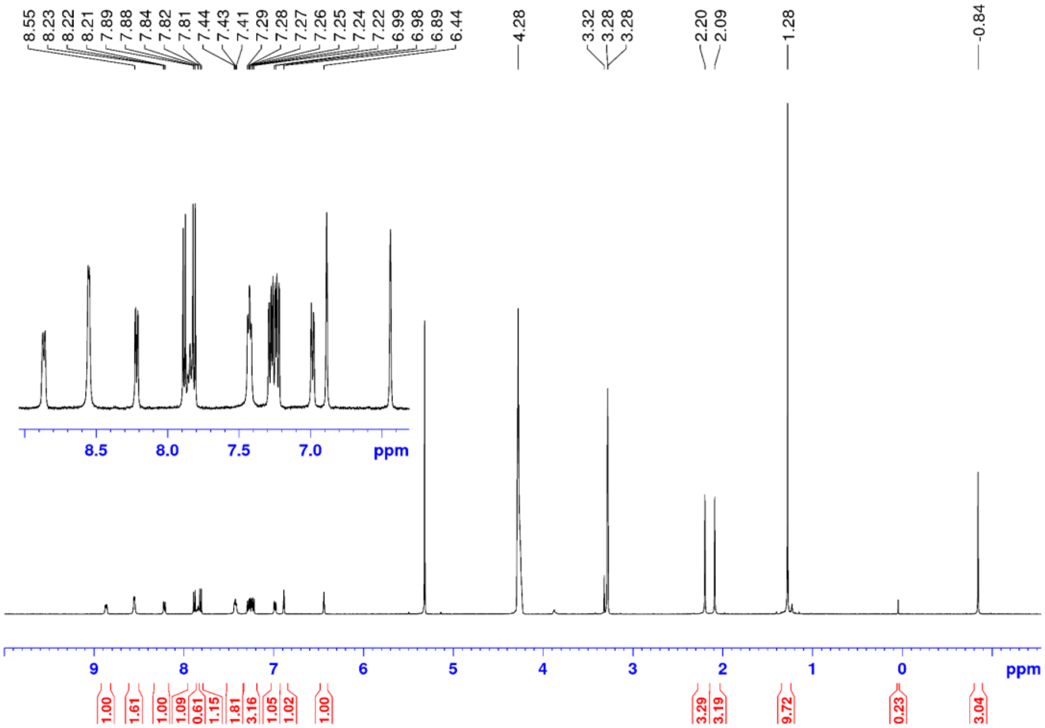

(e) COSY (CD_2Cl_2/CD_3OD, aryl region):

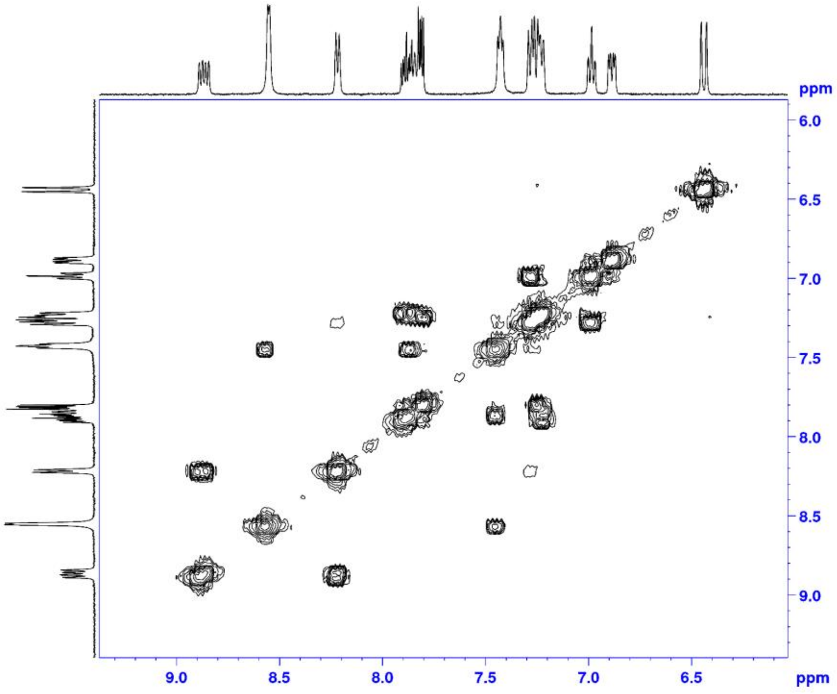

Figure 3.19, continued.

(f) COSY (CD_2Cl_2/CD_3OD, aliphatic region):

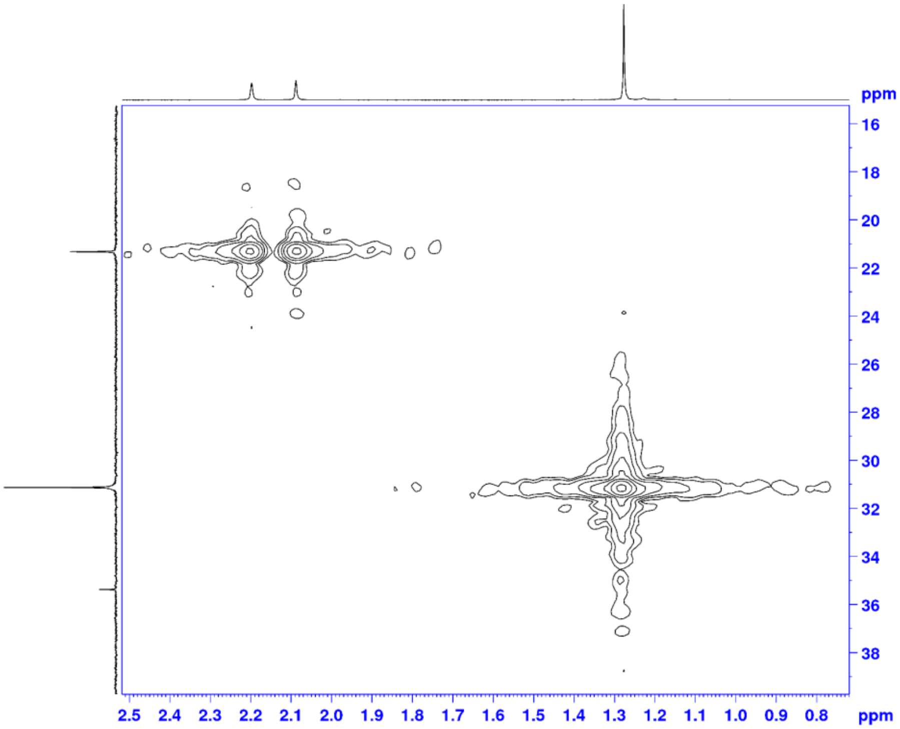

(g) COSY (CD_2Cl_2/CD_3OD, aryl region):

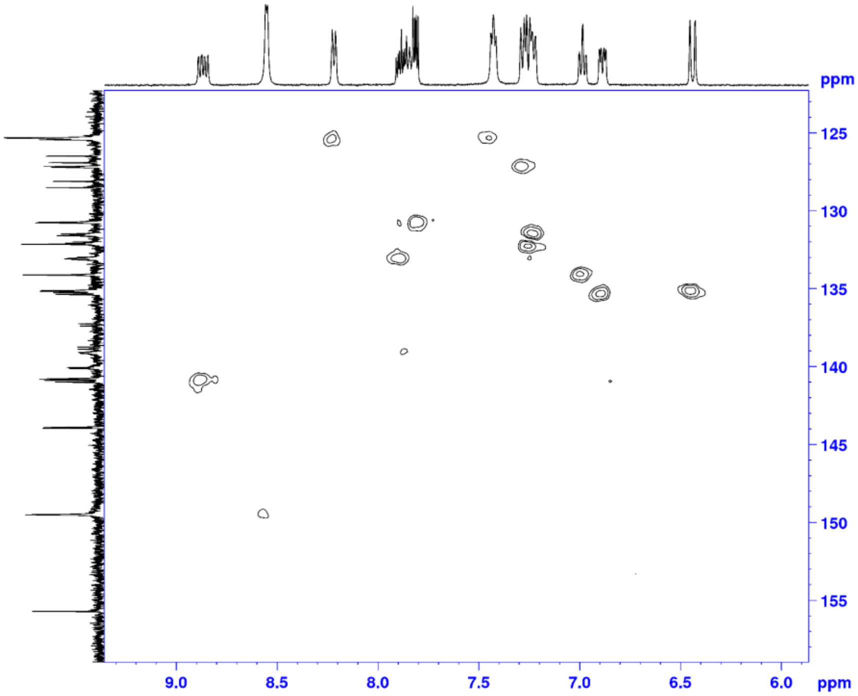

Figure 3.19, continued.

(h) ^{1}H (CD_2Cl_2/ex pyridine, 500 MHz): δ 1.67 = H_2O, 0.08 = grease

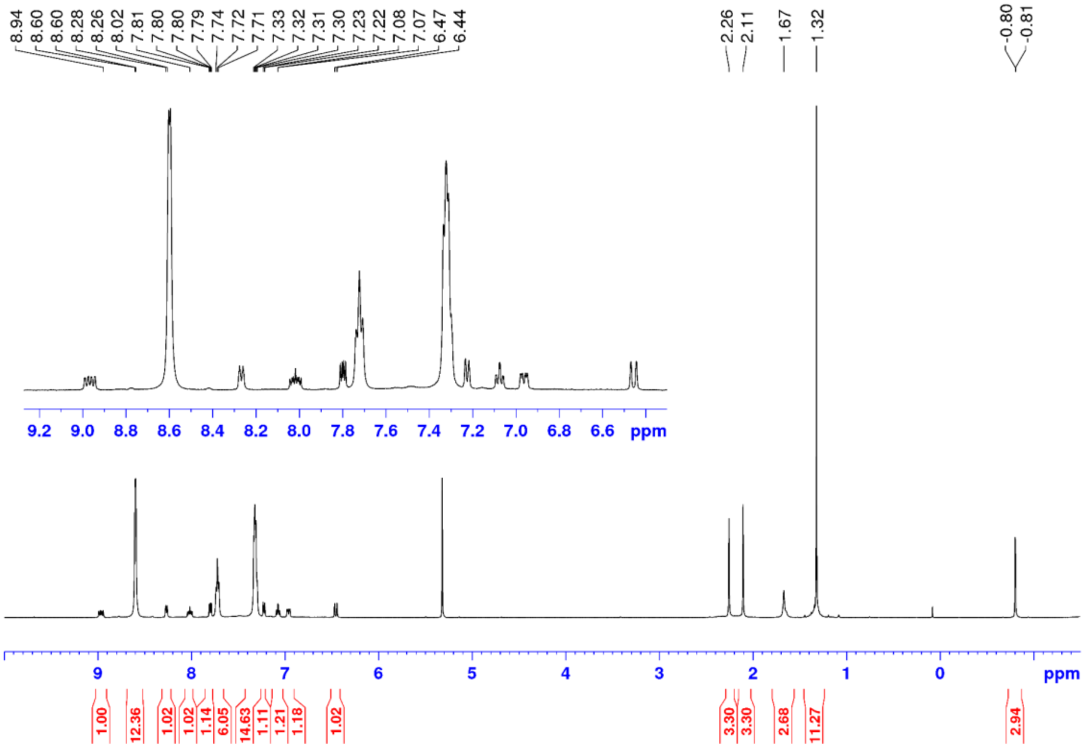

Base-free complex generaction of 4-(4-^{t}Bu-pyridine) or 3-py with $B(C_6F_5)_3$. A J-Young valved NMR tube was charged with 1.0 equiv of **4**-(4-^{t}Bu-pyridine) or **3**-py and 1.0 equiv of $B(C_6F_5)_3$ per L, and CD_2Cl_2 was added by vacuum transfer. The reaction was monitored by NMR. After 1 h, L (1.0 equiv) was added and the reaction was monitored by NMR.

Interconversion of 4-THT and 3-THT. A vial was charged with {Zn[**1**-H]}$_4$ (59 mg, 0.10 mmol), (COD)$PdMe_2$ (25 mg, 0.10 mmol) and CH_2Cl_2 (2.5 mL). The mixture was stirred at room temperature for 1 h to afford a clear yellow solution. Tetrahydrothiophene (9.1 µL, 0.10 mmol) was added, and the mixture was stirred for an additional 18 h. The mixture was filtered through Celite and the volatiles were removed under vacuum to afford a yellow solid. The solid was recrystallized by layering hexanes onto a toluene solution and cooling to -40 °C. **4**-THT was collected by filtration and dried under vacuum for 18 h (34 mg, 44 %). A J-Young valved NMR tube was charged with **4**-THT and CD_2Cl_2. $^{31}P\{^1H\}$ NMR (CD_2Cl_2): δ 31.2 (s), 9.2 (s). ^1H NMR (CD_2Cl_2): δ 0.26 ($^3J_{PH}$ = 3 Hz, Pd-C*H*$_3$). The volatiles were removed under vacuum and the resulting solid was dissolved in CD_3OD to yield a cloudy solution. CD_2Cl_2 was added and NMR spectra were obtained and indicated that **3**-THT had formed. $^{31}P\{^1H\}$ NMR (CD_2Cl_2): δ 43.1 (d, J_{PP} = 11 Hz, Pd-*P*), 19.6 (d, J_{PP} = 11 Hz, *P*=O). ^1H NMR (CD_2Cl_2): δ -0.79. The volatiles were removed under vacuum and the resulting solid was dissolved in CD_2Cl_2 to yield a clear yellow solution. Tetrahydrothiophene (ex) was added and the regeneration of **4**-THT was observed by NMR.

Ethylene homopolymerization. In a glovebox, catalyst and $B(C_6F_5)_3$ (if applicable; 1 equiv per pyridine) were weighed directly into a 200 mL glass autoclave liner and 50 mL solvent was added. The glass liner was placed in a stainless steel autoclave, which was sealed and removed from the glovebox. The autoclave was heated to the target temperature and pressurized with ethylene while the contents were stirred. After 2 h, the autoclave was cooled to 25 °C and vented. Acetone (50 mL) was added to precipitate the polymer. The polymer was collected by filtration, rinsed with acetone, and dried under vacuum.

Ethylene/VF Copolymerization. In the glove box, the catalyst (10 μmol) catalyst and $B(C_6F_5)_3$ (1.0 equiv per pyridine) were weighed into a glass autoclave liner. Solvent (50 mL) was added. The liner was placed in the autoclave, and the autoclave was assembled and brought out of the box. The autoclave was pressurized with VF to the desired pressure and ethylene was added until the total pressure reached 250 or 300 psi, while the contents were stirred (100 rpm). The reactor was heated to the desired temperature (80 °C) and stirring was increased to 170 rpm. After

2 h, the autoclave was cooled to 25 °C and vented. Acetone (50 mL) was added to precipitate the polymer. The polymer was collected by filtration, rinsed with acetone, and dried under vacuum.

Pulsed-Gradient Spin-Echo (PGSE) NMR Experiments. All PGSE measurements were performed on a Bruker 500 MHz spectrometer using the Stejskal-Tanner method. Two identical pulsed field gradients with duration $\delta = 0.004$ s separated by a delay time $\Delta = 0.01418$ s or 0.05418 s were incorporated into a spin-echo sequence, one before and the other after the 180° pulse. ^1H NMR spectra were recorded in DMSO-d_6 or CD_2Cl_2 at 295.5 K without sample spinning. During each experiment, the gradient strength (G) was varied between 0 and 26 G/cm while keeping all other factors constant. The gradient was calibrated using a 2% solution of H_2O in D_2O. After obtaining the spectra, careful integration was carried out. In all studies, the integral of the Pd-Me resonance were used to evaluate signal intensity. A linear plot of $\ln(I/I_0)$ (I = integral of a peak in the presence of G; I_0 = integral of the peak without a gradient) versus G^2 was generated. According to eq 1, the slope of this line is proportional to the diffusion coefficient and thus inversely proportional to the hydrodynamic radius of the molecule according to the Stokes-Einstein equation (eq 2). Hydrodynamic volumes were estimated by eq 3.

$$\ln(I/I_0) = -\gamma_H^2\delta^2G^2(\Delta - \delta/3)D \qquad (1)$$

where γ_H = magnetogyric ratio of ^1H; δ = length of the gradient pulse; Δ = delay between the midpoints of the gradients; D = diffusion coefficient.

$$r_H = k_BT/(6\pi\eta D) \qquad (2)$$

where r_H = hydrodynamic radius, k_B = Boltzmann constant; T = temperature; η = viscosity of the solvent.

$$V_H = 4\pi r_H^3/3 \qquad (3)$$

where V_H = hydrodynamic volume.

Figure 3.20. Linear plot of PGSE data for **1**-H_3 and {Zn[**1**-H]}$_4$ in DMSO-d_6 at 22.5 °C. Δ = 0.01418 s. The intrinsic viscosity of DMSO-d_6 at 22.5 °C is 1.99×10^{-6} Pa•s. From eq 1-3, V_H (**1**-H_3) = 1.3×10^3 Å, V_H ({Zn[**1**-H]}$_4$) = 5.1×10^3 Å.

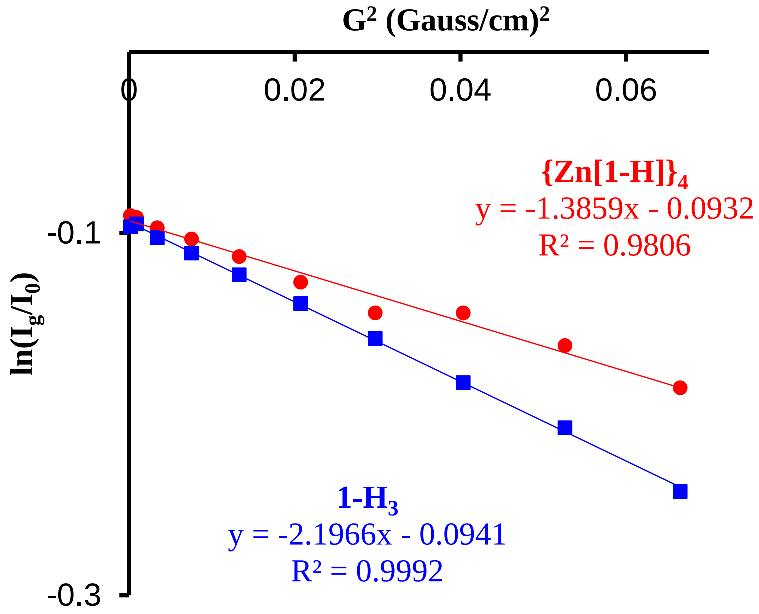

Figure 3.21. Linear plot of PGSE data for **3**-py and **4**-py in CD_2Cl_2 at 22.5 °C. $\Delta = 0.05418$ s. The intrinsic viscosity of CD_2Cl_2 at 22.5 °C is 0.42×10^{-6} Pa•s. From eq 1-3, V_H (**3**-py) = 4.5×10^3 Å, V_H (**4**-py) = 6.5×10^3 Å.

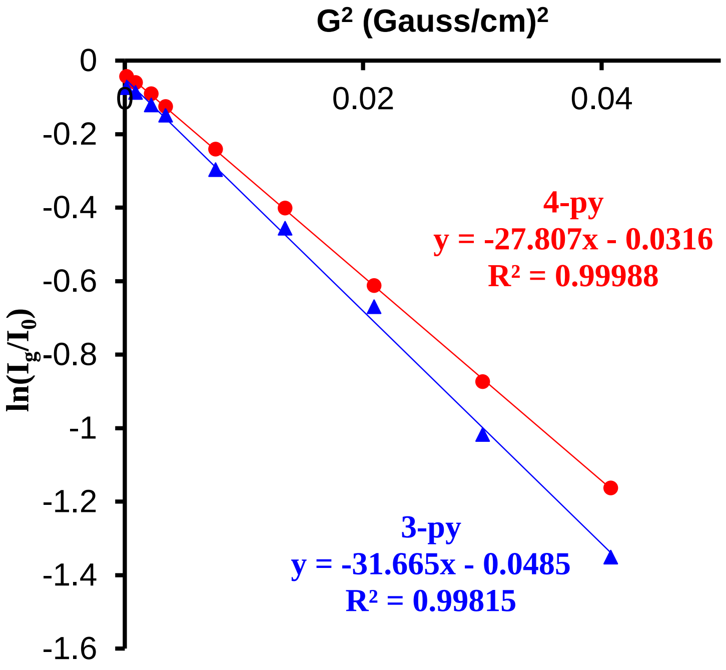

X-ray Crystallography. Data were collected on a Bruker D8 Venture diffractometer using Mo Kα radiation (0.71073 Å). Direct methods were used to locate many atoms from the E-map. Repeated difference Fourier maps enabled location of all expected non-hydrogen atoms. Following anisotropic refinement of all non-H atoms, ideal H atom positions were calculated. Final refinement was anisotropic for all non-H atoms and isotropic-riding for H atoms. ORTEP diagrams are drawn with 50 % probability ellipsoids.

Specific details for structure refinement for {Zn[1-H]}$_4$•16CH$_3$OH: All atoms were refined anisotropically. All H atoms were located on the difference Fourier map and allowed to be refined at 0.84 Å within a default 0.02 Å standard deviation with their thermal parameters constrained to be 1.5 times of the U_{eq} value of the O atoms. While the differentiation between S and P was not easily possible by the size of the respective thermal ellipsoids, the S-O and P-O bond lengths are significantly different. This fact was used to assign the site to be S or P.

Specific details for structure refinement for {Zn[1-H](CH$_3$OH)$_{0.5}$}$_4$•{Zn[1-H](CH$_3$OH)$_{0.75}$}$_4$•6CH$_3$OH•2H$_2$O. All atoms except those of two half-occupied solvent methanol molecules were refined with anisotropic thermal parameters using rigid body (RIGU) restraints. Hydrogen atoms were included in idealized positions for structure factor calculations. The H-atom positions were identified by the formation of H-bonding network.

Specific details for structure refinement for 2·4CH$_2$Cl$_2$. All elements including disordered carbon atoms of the ^{t}Bu group were refined anisotropically. The disorder was modeled with two orientations using appropriate geometric restraints (SADI, SAME, RIGU). EADP constraints were utilized on the thermal parameters of the C-atoms in the second orientation. Hydrogen atoms were included in idealized positions for structure factor calculations. All structures are drawn with thermal ellipsoids at 40% probability.

The initial refinement revealed two significant residual electron density peaks. The distance between them was similar to the Pd-P distance in the molecule and these peaks were assigned to these elements. The disorder was refined with 9:1 Pd1-P1 to Pd1X-P1X ratio. The whole body disorder could not be modeled due to the low admixture of the second orientation. Additionally, treatment of the data as a 2-component non-merohedral twin was explored. This refinement showed less than 10% of the second component and no improvements of refined parameters, so the final refinement was carried out without twin refinement.

The crystal contains 4 CH_2Cl_2 molecules per unit cell, which are involved in the formation of hydrogen bonds with dangling $–SO_3^-$ groups that are not coordinated to metal atoms.

Table 3.4. Hydrogen bonds (Å and °).

D-H...A	d(D-H)	d(H...A)	d(D...A)	<(DHA)
C(37)-H(37B)...O(6)#2	0.99	2.29	3.264(11)	168.9
C(38)-H(38A)...O(5)#3	0.99	2.14	3.118(9)	167.1

Symmetry transformations used to generate equivalent atoms:
#1 -x+1,-y+2,-z+1 #2 -x+1,-y+1,-z+1 #3 -x,-y+1,-z+1

Specific details for structure refinement for 3-py·0.5(CH_3OH)·(solvent)$_x$. The crystal was refined as an inversion twin; BASF refined to 0.39. The crystal contained many disordered solvent molecules located in large solvent-accessible voids. The diffuse contribution to scattering was treated by application of the program SQUEZZE[25] as implemented in Platon[26] using the "fab" file construct. This construct allows the solvent density distribution to be added to calculation of structure factors rather than modifying the observed intensities through the subtraction of a solvent contribution. SQUEEZE algorithm located a void, centered at (-0.127, 0.421, 0.011), with a volume of 5392 $Å^3$ and the electron count of 1333.

Specific details for structure refinement for 4-(4-^{t}Bu-py). All atoms were refined anisotropically using advanced rigid body restraints (RIGU). Several soft geometric restraints (SADI) were also used. Hydrogen atoms were included in idealized positions for structure factor calculations. In addition to well-resolved solvent molecules, the crystal contained many disordered solvent molecules located in large solvent-accessible voids. The diffuse contribution to scattering was treated by application of the program SQUEZZE[25] as implemented in Platon[26] using the "fab" file construct. The SQUEEZE algorithm located a void, centered at (0, 0, 0) and (0, 0.5, 1) with a volume of 3920 Å^3 and an electron count of 1426.

Table 3.5. X-ray crystallographic parameters of **$\{Zn[1\text{-}H]\}_4\bullet 16CH_3OH$.**

Empirical formula	$C_{56}H_{84}O_{20}P_4S_2Zn_2$
Formula weight	1395.97
Temperature/K	100(2)
Crystal system	triclinic
Space group	P-1
a/Å	13.1866(14)
b/Å	15.7525(16)
c/Å	18.2841(19)
α/°	104.606(3)
β/°	102.901(3)
γ/°	106.430(3)
Volume/Å^3	3342.9(6)
Z	2
ρ_{calc}g/cm^3	1.387
μ/mm^{-1}	0.944
F(000)	1464.0
Crystal size/mm^3	0.26 × 0.13 × 0.12
Radiation	MoKα (λ = 0.71073)
2Θ range for data collection/°	4.254 to 53.246
Index ranges	$-16 \leq h \leq 16$, $-19 \leq k \leq 19$, $-22 \leq l \leq 23$
Reflections collected	100503
Independent reflections	13975 [R_{int} = 0.0686, R_{sigma} = 0.0533]
Data/restraints/parameters	13975/10/805
Goodness-of-fit on F^2	1.032
Final R indexes [I>=2σ (I)]	R_1 = 0.0453, wR_2 = 0.0984
Final R indexes [all data]	R_1 = 0.0731, wR_2 = 0.1090
Largest diff. peak/hole / e Å^{-3}	0.95/-0.50

Table 3.6. X-ray crystallographic parameters of **$\{Zn[1\text{-}H](CH_3OH)_{0.5}\}_4 \bullet \{Zn[1\text{-}H](CH_3OH)_{0.75}\}_4 \bullet 6CH_3OH \bullet 2H_2O$.**

Empirical formula	$C_{101.5}H_{128}O_{30.5}P_8S_4Zn_4$
Formula weight	2473.51
Temperature/K	100(2)
Crystal system	triclinic
Space group	P-1
a/Å	17.735(3)
b/Å	18.333(4)
c/Å	20.480(4)
α/°	88.775(3)
β/°	77.444(3)
γ/°	64.264(2)
Volume/$Å^3$	5834.7(19)
Z	2
ρ_{calc}g/cm^3	1.408
μ/mm^{-1}	0.249
F(000)	2570.0
Crystal size/mm^3	0.015 × 0.012 × 0.01
Radiation	synchrotron ($\lambda = 0.41328$)
2Θ range for data collection/°	2.104 to 23.868
Index ranges	$-17 \le h \le 17$, $-16 \le k \le 16$, $-20 \le l \le 20$
Reflections collected	55787
Independent reflections	9250 [$R_{int} = 0.1875$, $R_{sigma} = 0.1329$]
Data/restraints/parameters	9250/1239/1367
Goodness-of-fit on F^2	1.047
Final R indexes [I>=2σ (I)]	$R_1 = 0.0730$, $wR_2 = 0.1564$
Final R indexes [all data]	$R_1 = 0.1547$, $wR_2 = 0.1974$
Largest diff. peak/hole / e $Å^{-3}$	1.20/-0.48

Table 3.7. X-ray crystallographic parameters of **$2\cdot4CH_2Cl_2$.**

Empirical formula	$C_{76}H_{106}Cl_8N_6O_{12}P_4S_2Zn_2Pd_2$
Formula weight	2110.85
Temperature	100(2) K
Wavelength	0.71073 Å
Crystal system	Triclinic
a/Å	11.4193(6)
b/Å	12.8741(6)
c/Å	17.5168(8)
α/°	79.296(2)
β/°	82.969(2)
γ/°	64.394(2)
Volume	2279.30(19) $Å^3$
Z	1
Density (calculated)	1.538 Mg/m^3
Absorption coefficient	1.317 mm^{-1}
F(000)	1080
Crystal size	0.290 x 0.220 x 0.210 mm^3
Theta range for data collection	2.162 to 27.147°.
Index ranges	-14<=h<=14, -16<=k<=16, -22<=l<=22
Reflections collected	65230
Independent reflections	10105 [R(int) = 0.0424]
Completeness to theta = 25.242°	99.9 %
Refinement method	Full-matrix least-squares on F^2
Data / restraints / parameters	10105 / 29 / 545
Goodness-of-fit on F^2	1.031
Final R indices [I>2sigma(I)]	R1 = 0.0564, wR2 = 0.1239
R indices (all data)	R1 = 0.0702, wR2 = 0.1320
Extinction coefficient	n/a
Largest diff. peak and hole	1.612 and -1.291 $e.Å^{-3}$

Table 3.8. X-ray crystallographic parameters of **3-py·0.5(CH_3OH)·(solvent)$_x$.**

Empirical formula	$C_{90.50}H_{101}N_3O_{18.50}P_6Pd_3S_3Zn_3$
Formula weight	2324.05
Temperature	100(2) K
Wavelength	0.71073 Å
Crystal system	Hexagonal
Space group	$P6_3$
a/Å	22.4386(16)
b/Å	22.4386(16)
c/Å	31.755(2)
α/°	90
β/°	90
γ/°	120
Volume	13846(2) $Å^3$
Z	4
Density (calculated)	1.115 Mg/m^3
Absorption coefficient	1.054 mm^{-1}
F(000)	4716
Crystal size	0.160 x 0.140 x 0.040 mm^3
Theta range for data collection	2.191 to 25.060°.
Index ranges	-26<=h<=26, -26<=k<=26, -37<=l<=37
Reflections collected	109281
Independent reflections	16372 [R(int) = 0.0583]
Completeness to theta = 25.060°	99.8 %
Refinement method	Full-matrix least-squares on F^2
Data / restraints / parameters	16372 / 108 / 780
Goodness-of-fit on F^2	1.038
Final R indices [I>2sigma(I)]	R1 = 0.0435, wR2 = 0.0994
R indices (all data)	R1 = 0.0604, wR2 = 0.1070
Absolute structure parameter	0.39(2)
Extinction coefficient	n/a
Largest diff. peak and hole	1.011 and -0.574 $e.Å^{-3}$

Table 3.9. X-ray crystallographic parameters of **4-(4-*t*Bu-py).**

Empirical formula	$C_{136}H_{164}N_4O_{24}P_8Pd_4S_4Zn_4$
Formula weight	3301.78
Temperature/K	100(2)
Crystal system	monoclinic
Space group	$P2_1/n$
a/Å	21.978(3)
b/Å	41.049(6)
c/Å	22.418(3)
α/°	90
β/°	90.459(3)
γ/°	90
Volume/Å^3	20225(5)
Z	4
ρ_{calc}g/cm^3	1.084
μ/mm^{-1}	0.965
F(000)	6752.0
Crystal size/mm^3	0.014 × 0.012 × 0.008
Radiation	MoKα (λ = 0.71073)
2Θ range for data collection/°	4.14 to 45.918
Index ranges	$-18 \leq h \leq 23$, $-44 \leq k \leq 41$, $-23 \leq l \leq 23$
Reflections collected	97451
Independent reflections	22029 [R_{int} = 0.0857, R_{sigma} = 0.1201]
Data/restraints/parameters	22029/2047/1664
Goodness-of-fit on F^2	1.033
Final R indexes [I>=2σ (I)]	R_1 = 0.0915, wR_2 = 0.2265
Final R indexes [all data]	R_1 = 0.1579, wR_2 = 0.2639
Largest diff. peak/hole / e Å^{-3}	1.00/-0.63

3.5 References and Notes

1. Shen, Z.; Jordan, R. F. *J. Am. Chem. Soc.* **2010**, *132*, 52.

2. Shen, Z.; Jordan, R. F. *Macromolecules* **2010**, *43*, 8706.

3. Vela, J.; Lief, G. R.; Shen, Z.; Jordan, R. F. *Organometallics* **2007**, *26*, 6624.

4. Wei, J.; Shen, Z.; Filatov, A. S.; Liu, Q.; Jordan, R. F. *Organometallics* in press.

5. Goura, J.; Chandrasekhar, V. *Chem. Rev.* **2015**, *115*, 6854.

6. (a) Chandrasekhar, V.; Sahoo, D.; Metre, R. K. *CrystEngComm* **2013**, *15*, 7419. (b) Guo, L. R.; Bao, S. S.; Zheng, L. M. *Solid State Sci.* **2009**, *11*, 310. (c) Fan, Y. T.; Xue, D. X.; Li, G.; Hou, H. W.; Du, C. X.; Lu, H. J. *J. Mol. Struct.* **2004**, *707*, 153. (d) Howlader, R.; Walawalkar, M. G.; Murugavel, R. *Inorg. Chim. Acta* **2013**, *405*, 147.

7. Chandrasekhar, V.; Kingsley, S.; Rhatigan, B.; Lam, M. K.; Rheingold, A. L. *Inorg. Chem.* **2002**, *41*, 1030.

8. Chandrasekhar, V.; Sasikumar, P.; Boomishankar, R.; Anantharaman, G. *Inorg. Chem.* **2006**, *45*, 3344.

9. Wu, J.; Song, Y.; Zhang, E.; Hou, H.; Fan, Y.; Zhu, Y. *Chem. Eur. J.* **2006**, *12*, 5823.

10. Murugavel, R.; Shanmugan, S. *Chem. Commun.* **2007**, 1257.

11. Murugavel, R.; Kuppuswamy, S.; Boomishankar, R.; Steiner, A. *Angew. Chem. Int. Ed.* **2006**, *45*, 5536.

12. (a) Alberti, G. *Acc. Chem. Res.* **1978**, *11*, 163. (b) Cao, G.; Hong, H. G.; Mallouk, T. E. *Acc. Chem. Res.* **1992**, *25*, 420. (c) Clearfield, A. *J. Mol. Catal.* **1984**, *27*, 251. (d) Murugavel, R.; Davis, P.; Walawalkar, M. G. *Zeitschrift für anorganische und allgemeine Chemie* **2005**, *631*, 2806. (e) Segawa, K.; Kihara, N.; Yamamoto, H. *J. Mol. Catal.* **1992**, *74*, 213.

13. Contrella, N. D.; Jordan, R. F. *Organometallics* **2014**, *33*, 7199.

14. Fulmer, G. R.; Miller, A. J. M.; Sherden, N. H.; Gottlieb, H. E.; Nudelman, A.; Stoltz, B. M.; Bercaw, J. E.; Goldberg, K. I. *Organometallics* **2010**, *29*, 2176.

15. Jaffé, H. H.; Freedman, L. D.; Doak, G. O. *J. Am. Chem. Soc.* **1953**, *75*, 2209.

16. Abdur-Rashid, K.; Fong, T. P.; Greaves, B.; Gusev, D. G.; Hinman, J. G.; Landau, S. E.; Lough, A. J.; Morris, R. H. *J. Am. Chem. Soc.* **2000**, *122*, 9155.

17. (a) Bukhaltsev, E.; Goldberg, I.; Cohen, R.; Vigalok, A. *Organometallics* **2007**, *26*, 4015. (b) Wooten, A.; Carroll, P. J.; Maestri, A. G.; Walsh, P. J. *J. Am. Chem. Soc.* **2006**, *128*, 4624. (c) Lichtenberg, C.; Engel, J.; Spaniol, T. P.; Englert, U.; Raabe, G.; Okuda, J. *J. Am. Chem. Soc.* **2012**, *134*, 9805.

18. Kochi, T.; Noda, S.; Yoshimura, K.; Nozaki, K. *J. Am. Chem. Soc.* **2007**, *129*, 8948.

19. For disccusion related to Scheme 3.9c, see chapter 2.

20. (a) Contrella, N. D.; Sampson, J. R.; Jordan, R. F. *Organometallics* **2014**, *33*, 3546. (b) Kyba, E. P. *J. Am. Chem. Soc.* **1976**, *98*, 4805.

21. Bonnaventure, I.; Charette, A. B. *J. Org. Chem.* **2008**, *73*, 6330.

22. De Graaf, W.; Boersma, J.; Smeets, W. J. J.; Spek, A. L.; Van Koten, G. *Organometallics* **1989**, *8*, 2907.

23. (a) Calvin, G.; Coates, G. E. *Journal of the Chemical Society (Resumed)* **1960**, 2008. (b) Foley, S. R.; Stockland, R. A.; Shen, H.; Jordan, R. F. *J. Am. Chem. Soc.* **2003**, *125*, 4350. (c) Lau, K.-C.; Petro, B. J.; Bontemps, S.; Jordan, R. F. *Organometallics* **2013**, *32*, 6895.

24. Grinshpun, V.; Rudin, A. *Die Makromolekulare Chemie, Rapid Communications* **1985**, *6*, 219.

25. (a) Spek, A. *Acta Cryst. C.* **2015**, *71*, 9. (b) van der Sluis, P.; Spek, A. L. *Acta Cryst. A.* **1990**, *46*, 194.

26. Spek, A. *Acta Cryst. D.* **2009**, *65*, 148.

CHAPTER FOUR

Synthesis of Borophosphonate Cage Compounds: Influence of Substituent and Concentration Effects on Product Distribution in Condensation Reactions of Aryl Phosphonic Acids and Boronic Acids

4.1 Introduction

Borophosphonates of general formula $[RPO_3BR']_4$ adopt 3-dimensional cubic cage structures (Chart 4.1, **A**), in which the edges are formed by B-O-P bonds.[1] These compounds, which are isoelectronic and isostructural with polyhedral oligomeric silsesquioxanes $(RSi)_8O_{12}$ (**B**, POSS),[2,3] have attracted interest due to their potential applications as building blocks for more complex structures and materials and as scaffolds for multicenter catalysts. Several borophosphate compounds of general formula $[EtOPO_3BR']_6$ (**C**) have also been reported and adopt hexameric cage structures that are similar to the cubanoid structure observed for borophosphonates and POSSs.[4]

Chart 4.1

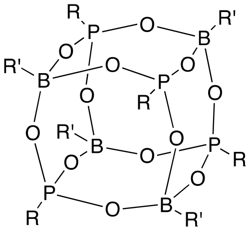
A

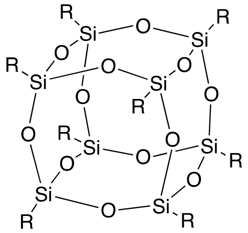
B

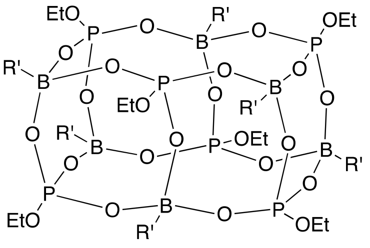
C

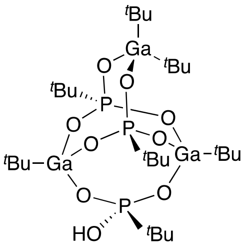
D

Borophosphonate cages have been synthesized by several methods (Scheme 1). Roesky and co-workers reported that alkyl (R = ^{t}Bu, Me, Et) and phenyl phosphonic acids react with trialkylboranes (R' = Et, ^{s}Bu) by alkane elimination to generate borophosphonates in 66 - 95 % yield (Scheme 4.1, route **a**).[1] Roesky, Mason and their coworkers used this method to generate analogous structures with other Group 13 metals (Al, Ga, In).[1a,5,6] The reaction of ^{t}BuP(O)(OH)$_2$ with GaMe$_3$ under mild conditions (room temperature in THF), yields the tetrameric gallophosphonate cage [^{t}BuPO$_3$GaMe]$_4$. In contrast, the reaction of ^{t}BuP(O)(OH)$_2$ with the bulkier gallium alkyl Ga^{t}Bu$_3$ yields different condensation products depending on the reaction conditions, and provides insight to the stepwise nature of the growing process. The single-ring dimer [^{t}Bu(OH)PO$_2$Ga^{t}Bu$_2$]$_2$ is formed at -50 °C in THF, the trimer (^{t}BuGa)$_2$(^{t}Bu$_2$Ga)(O$_3$P^{t}Bu)$_2${O$_2$P(OH)^{t}Bu} (Chart 4.1, **D**) is observed after 15 h in refluxing toluene, and the tetrameric cage [^{t}BuPO$_3$Ga^{t}Bu]$_4$ is ultimately formed after 2 h in refluxing diglyme.[6b,7,8] A mixture of tetrameric and hexameric aluminophosphonate cages, [^{t}BuPO$_3$AlMe]$_4$

and [^{t}BuPO$_3$AlMe]$_6$, is formed when the small trialkylaluminum AlMe$_3$ is used.[9] In a similar system, in addition to tetrameric and hexameric cages, [MePO$_3$Al^{t}Bu]$_4$ and [MePO$_3$Al^{t}Bu]$_6$, an interesting decamer [MePO$_3$Al^{t}Bu]$_{10}$ consisting of two tetramers, each with an open edge and linked through a cyclic dimer, was also observed.[5b,5c] Kuchen reported that ^{t}BuP(O)(OSiMe$_3$)$_2$ reacts with PhBCl$_2$ by Me$_3$SiCl elimination to form the corresponding tetrameric borophosphonate cage (Scheme 4.1, route **b**), though the yield was only 14 %.[10,11]

Scheme 4.1

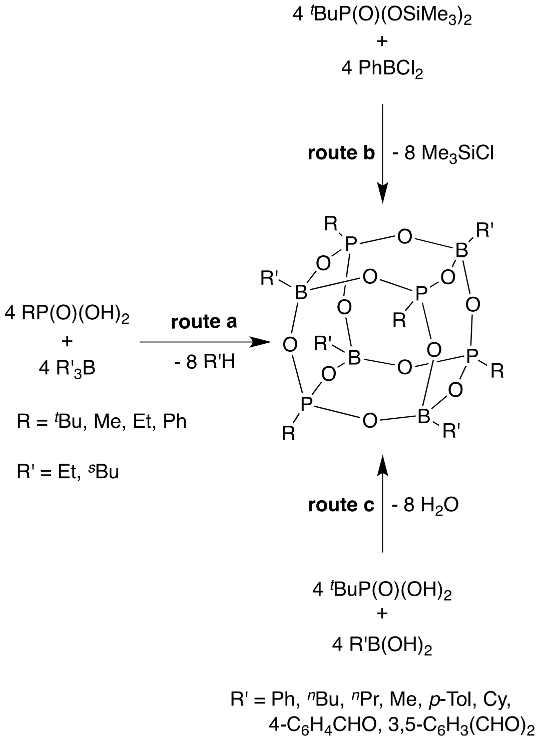

Recently, Severin and co-workers reported that condensation reactions of ^{t}BuP(O)(OH)$_2$ and R'B(OH)$_2$ in refluxing toluene, using a Dean-Stark trap to remove the H$_2$O byproduct, generate tetrameric borophosphonate cages in high yield (Scheme 4.1, route **c**).[12] A wide range of R'B(OH)$_2$ reactants are converted to cage products, including alkyl (R' = ^{n}Bu, ^{n}Pr, Me, Cy) and sterically undemanding aryl (R’ = Ph, *p*-tol, *p*-CHO-Ph, 3,5-$(CHO)_2$-Ph) boronic acids. However, similar reactions of the sterically smaller alkylphosphonic acids $^{n}BuP(O)(OH)_2$ and $^{n}HexP(O)(OH)_2$ with boronic acids produced mixtures of condensation products which could not be separated and were not characterized. Reactions of $PhP(O)(OH)_2$ with boronic acids gave insoluble products which were also not characterized. Severin concluded that phosphonic acids that are both sterically demanding and solubilizing are required for a controlled condensation reaction.

Scheme 4.2 illustrates several possible condensation pathways of phosphonic acids with boronic acids. In addition to tetrameric cages $[RPO_3BR']_4$, 1:1 borophosphonate products with different structures and degrees of oligomerizations are possible. In particular, hexameric cages analogous to **C** (Chart 4.1) may be expected when sterically small $RP(O)(OH)_2$ and $R'B(OH)_2$ reactants are used. Boronic acids are well known to reversibly and rapidly self-condense to boroxines $(R'BO)_3$, with condensation being particularly favored for electron-donating R’ groups.[13] Arylboroxines are destabilized by *ortho* substituents, which distort the planar structure[14] and reduce the overlap between the π-orbitals of phenyl ring and the empty boron p orbital. Finally, phosphonic acids are also known to self-condense to linear or cyclic phosphonic acid anhydrides ($HO[PRO_2]_nOH$ or $[RP(O)O]_n$).[15]

Scheme 4.2

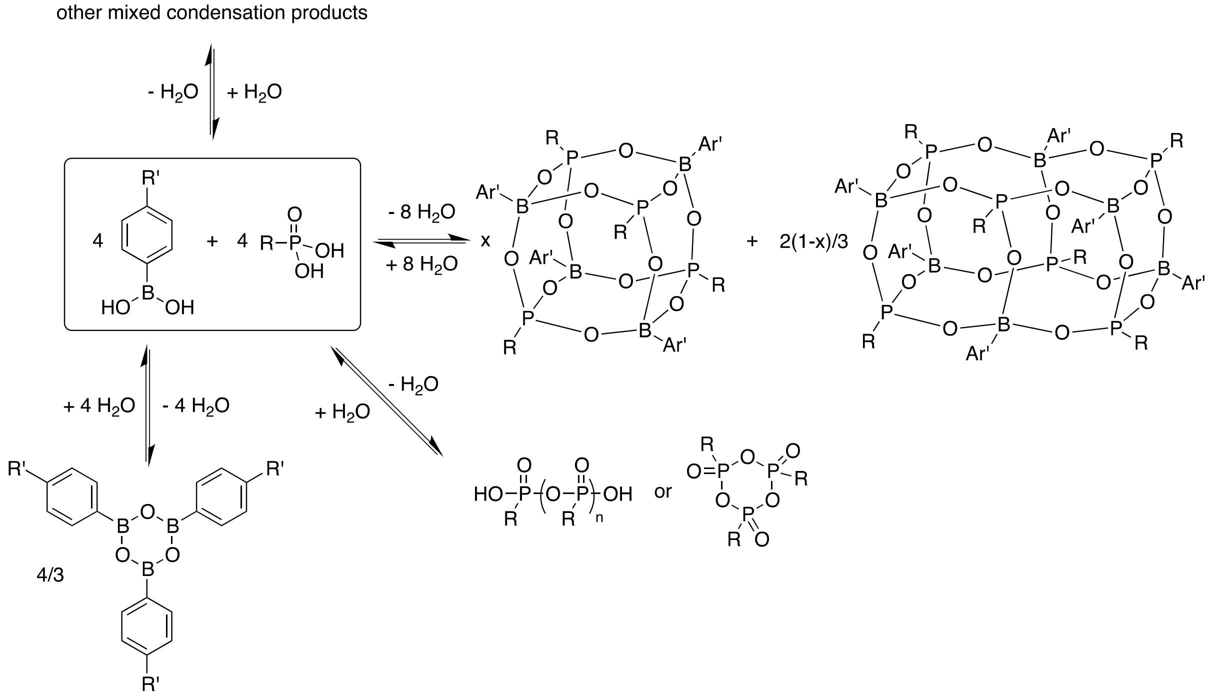

This chapter describes the synthesis of [ArPO$_3$BAr']$_4$ and [ArPO$_3$BAr']$_6$ borophosphonate cages that contain aryl substituents at both P and B *via* Severin-type condensation reactions. The product distribution is influenced by the steric properties and solubility of the phosphonic acid, the steric and electronic properties of the boronic acid, and the concentrations of the reactants.

4.2 Results and Discussion

Reaction of (3,5-^{t}Bu$_2$-Ph)P(O)(OH)$_2$ (1) with arylboronic acids that contain electron-withdrawing substituents. Based on the guidelines outlined by Severin noted above, (3,5-^{t}Bu$_2$-Ph)P(O)(OH)$_2$ (**1**), which incorporates solubilizing ^{t}Bu groups and is not sterically hindered at the phosphorous center, is an attractive candidate of controlled condensation reactions with boronic acids. Compound **1** reacts in toluene with (*o*-Br-Ph)B(OH)$_2$ (**2a**) and (*o*-CF$_3$-Ph)B(OH)$_2$ (**2b**), which contain electron-withdrawing substituents in the *ortho* position, to generate the tetrameric cages [(3,5-^{t}Bu$_2$-Ph)PO$_3$B(*o*-Br-Ph)]$_4$ (**3a**) and [(3,5-^{t}Bu$_2$-Ph)PO$_3$B(*o*-CF$_3$-Ph)]$_4$ (**3b**) in 84 % and 93 % yield, respectively, as determined by ^{31}P{^{1}H} NMR. Compounds **3a** and **3b** were isolated in 48 - 50 % yield by recrystallization from hexane. High-resolution mass spectral data, multinuclear NMR data, and an X-ray crystallographic analysis of **3a** (*vide infra*) established that **3a** and **3b** have tetrameric cage structures as shown in Scheme 4.3.

Scheme 4.3

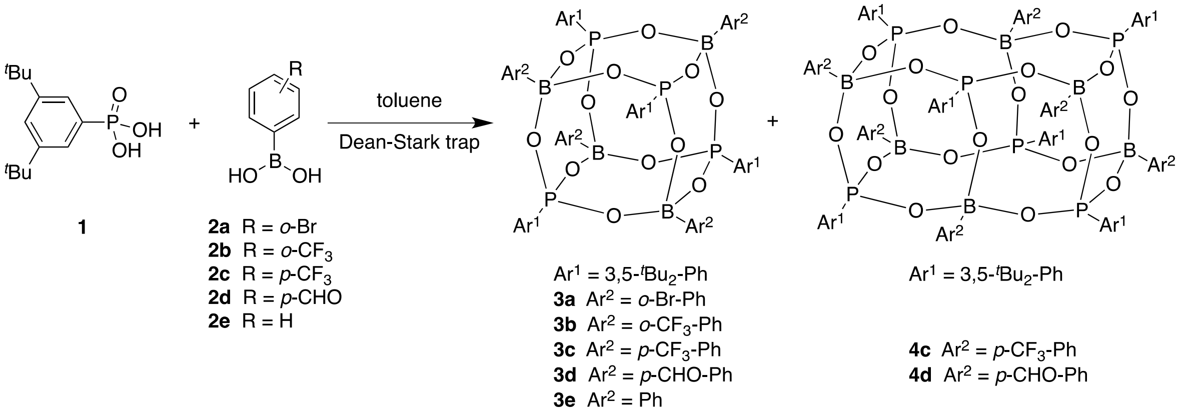

The reactions of **1** with (*p*-CF$_3$-Ph)B(OH)$_2$ (**2c**) and (*p*-CHO-Ph)B(OH)$_2$ (**2d**), which contain electron-withdrawing substituents in the *para* position, are less selective. These sterically-open boronic acids react to form mixtures of tetrameric and hexameric borophosphonate cages, and interestingly, the concentration of the reactants strongly influences the product distribution. The reaction of **1** with **2c** at low initial concentration ([**1**]$_0$ = [**2c**]$_0$ = 2.5 mM) generates [(3,5-^{t}Bu$_2$-Ph)PO$_3$B(*p*-CF$_3$-Ph)]$_4$ (**3c**) as the major product, along with a small amount of [(3,5-^{t}Bu$_2$-Ph)PO$_3$B(*p*-CF$_3$-Ph)]$_6$ (**4c**) as shown by ^{31}P{^{1}H} NMR analysis of the product mixture (Figure 4.1, **a**). The yields of **3c** and **4c** were determined to be 81 % and 7 % respectively, by ^{1}H NMR. **4c** is less soluble than **3c** and was removed by precipitation with hexane followed by filtration. **3c** was isolated in analytically pure form by removing the solvent from the filtrate and washing with hexane. However, the isolated yield of **3c** was low (12 %), due in part to competitive conversion to **4c** during workup. In contrast, the reaction of **1** with **2c** at high initial concentration ([**1**]$_0$ = [**2c**]$_0$ = 25 mM), produces **4c** as the major product (72 %, vs. 16 % **3c**) (Figure 4.1, **b**). **4c** was isolated by recrystallization from toluene in 49 % yield.

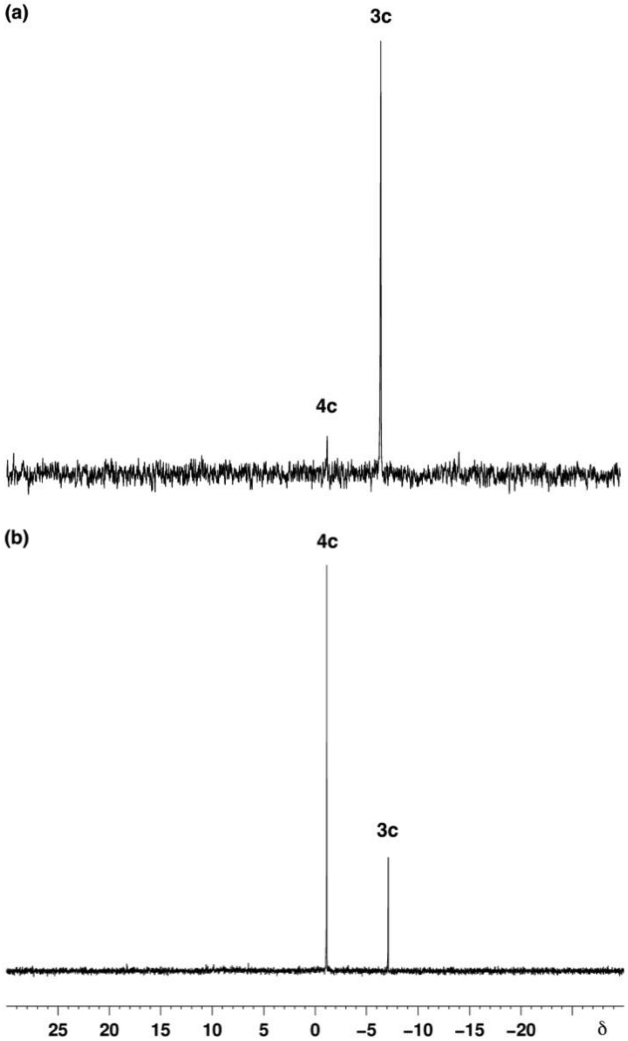

Figure 4.1. $^{31}P\{^1H\}$ NMR spectra of product mixtures from the reaction of (3,5-^{t}Bu$_2$-Ph)P(O)(OH)$_2$ (**1**) and (p-CF_3-Ph)B(OH)$_2$ (**2c**) in toluene. (a) Low initial concentration of reactants: ([**1**]$_0$ = [**2c**]$_0$ = 2.5 mM), NMR solvent = C_6D_6. Peak assignments [(3,5-^{t}Bu$_2$-Ph)PO$_3$B(p-

CF_3-Ph)]$_4$ (**3c**) δ -6; [(3,5-^{t}Bu$_2$-Ph)PO_3B(*p*-CF_3-Ph)]$_6$ (**4c**) δ -1. (b) High initial concentration of reactants: ([**1**]$_0$ = [**2c**]$_0$ = 25 mM), NMR solvent = toluene. Peak assignments: **3c** δ -7; **4c** δ -1.

Similar results were obtained for the reaction of **1** with **2d**. At low initial concentration ([**1**]$_0$ = [**2d**]$_0$ = 2.5 mM), the tetramer [(3,5-^{t}Bu$_2$-Ph)PO_3B(*p*-CHO-Ph)]$_4$ (**3d**) was the major product (81 %, ^{1}H NMR) and only a small amount (5 %) of the hexamer [(3,5-^{t}Bu$_2$-Ph)PO_3B(*p*-CHO-Ph)]$_6$ (**4d**) was formed. Compound **3d** was isolated by precipitation from the reaction mixture in 44 % yield. At high initial concentration ([**1**]$_0$ = [**2d**]$_0$ = 25 mM), a mixture of **3d** (44 %) and **4d** (36 %) is formed. The conversion of **3d** to **4d** is slower than the conversion of **3c** to **4c** noted above, but **4d** was enriched to 52 % when the product mixture from the high concentration reaction was cooled and left at room temperature for 18 h and was isolated by recrystallization from toluene in 36 % yield. Similarly, NMR studies show that **1** reacts with PhB$(OH)_2$ (**2e**) at low initial concentration ([**1**]$_0$ = [**2e**]$_0$ = 2.5 mM) to yield [(3,5-^{t}Bu$_2$-Ph)PO_3BPh]$_4$ (**3e**) as the major product (73 %, ^{1}H NMR).

Interconversion of tetrameric and hexameric cages. To probe hexamer/tetramer interconversion further, the isomerization of pure **4c** was studied by ^{1}H NMR. Heating a solution of **4c** in toluene-*d*$_8$ at 105 °C results in slow (3 weeks) formation of an equilibrium mixture of **3c** and **4c** (K_{eq} = [**3c**]^3/[**4c**]^2 = 2.4(1) x 10^{-3} M, Scheme 4.4). This equilibrium shifts toward **4c** at room temperature (K_{eq} = [**3c**]^3/[**4c**]^2 = 1.2(1) x 10^{-3} M), which is consistent with the expectation (based on stoichiometry) that **3c** should be entropically favored. The conversion of pure **4c** to the equilibrium **4c**/**3c** mixture is much slower than the conversion of **3c** and **4c** observed in the **1**/**2c** reaction mixture, suggesting that the latter process is catalyzed by other species in the mixture (e.g. RP(O)$(OH)_2$, H_2O, other condensation products).

The product mixture from the dilute reaction ($[\mathbf{1}]_0 = [\mathbf{2c}]_0 = 2.5$ mM) is enriched in **3c** relative to the expected equilibrium concentration ([**3c**]/[**4c**]: obs. 17, calcd. 2.6; see the supporting information for details). Conversely, the product mixture from the concentrated reaction ($[\mathbf{1}]_0 = [\mathbf{2c}]_0 = 25$ mM) is enriched in **4c** ([**3c**]/[**4c**]: obs. 0.33, calcd. 1.0). These deviations from the equilibrium ratios suggest that kinetic factors influence the product distribution. The high reactant concentrations favor intermolecular condensations relative to intramolecular reactions and produce larger (hexameric) aggregates.

Scheme 4.4

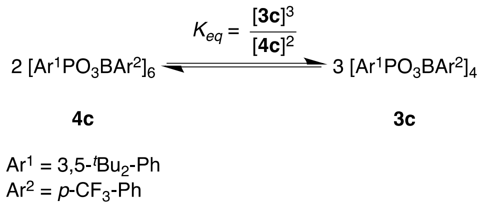

Reaction of 1 with (*p*-tolyl)B(OH)₂. The reaction of **1** with (*p*-tolyl)B(OH)$_2$ (**2f**), which contains an electron-donating methyl substituent, results in complete consumption of the starting materials but generates a mixture of products (Scheme 4.5). The $^{31}P\{^1H\}$ NMR spectrum of the reaction mixture contains a sharp signal at δ -8.0, in the range expected for $[(3,5\text{-}^t\text{Bu}_2\text{-Ph})\text{PO}_3\text{B}(p\text{-tolyl})]_4$ (**3f**), and a broad resonance at δ 20 to -10 (Figure 4.2, **a**). The presence of **3f** was confirmed by MALDI-MS, but ions derived from other mixed condensation products were also observed by MALDI-MS and APCI-MS analysis of the reaction mixture. For comparison, the self-condensation of **1** under the same reaction conditions in the absence of boronic acid generates products that exhibit broad $^{31}P\{^1H\}$ resonances at δ ca. 15, 9 and 0 (Figure 4.2, **b**). These results suggest that the reaction of **1** and **2f** generates, in addition to **3f**, other mixed borophosphonate condensation products as well as condensation products derived from **1**. The ^{1}H NMR spectrum of the product mixture contains prominent resonances for *p*-tolylboroxine (**5f**), corresponding to a 20 % yield.

Scheme 4.5

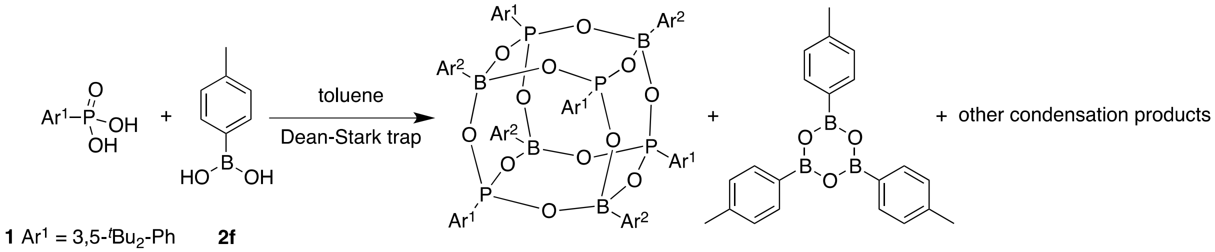

1 Ar^1 = 3,5-^{t}Bu$_2$-Ph **2f**
6 Ar^1 = 2-PPh$_2$-Ph

Ar^2 = *p*-CH$_3$-Ph
3f Ar^1 = 3,5-^{t}Bu$_2$-Ph (trace)
7f Ar^1 = 3,5-^{t}Bu$_2$-Ph (trace)

5f (20-25 %)

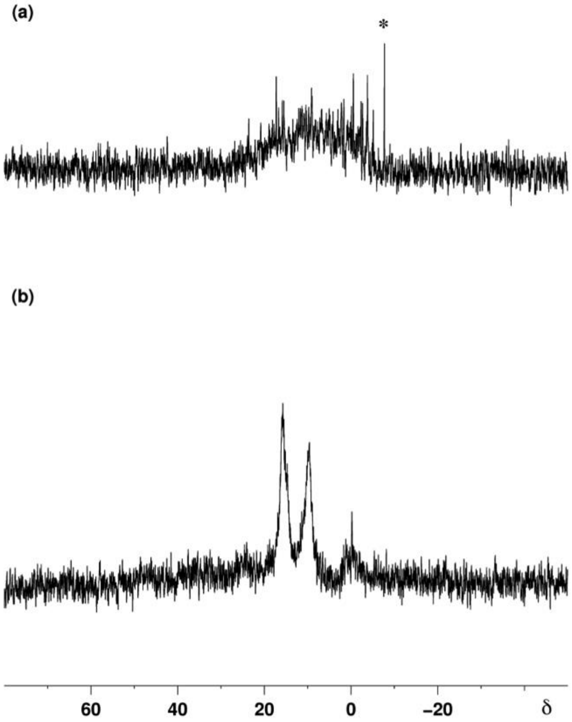

Figure 4.2. $^{31}P\{^1H\}$ NMR spectra (in C_6D_6) of product mixtures from (a) the reaction of (3,5-^{t}Bu$_2$-Ph)P(O)(OH)$_2$ (**1**) and (*p*-tolyl)B(OH)$_2$ (**2f**) and (b) the self-condensation of (3,5-^{t}Bu$_2$-Ph)P(O)(OH)$_2$ (**1**). * = [(3,5-^{t}Bu$_2$-Ph)PO$_3$B(*p*-tolyl)]$_4$ (**3f**, δ -8).

Reaction of (2-PPh$_2$-Ph)P(O)(OH)$_2$ (6) with arylboronic acids. The reactions of (2-PPh$_2$-Ph)P(O)(OH)$_2$ (**6**)[16] with boronic acids were explored because the corresponding cages are potentially interesting as ligands. Compound **6** reacts cleanly with (*p*-CF$_3$-Ph)B(OH)$_2$ (**2c**) and (*p*-CHO-Ph)B(OH)$_2$ (**2d**) to afford the tetrameric products ([(2-PPh$_2$-Ph)PO$_3$B(*p*-CF$_3$-Ph)]$_4$ (**7c**) and [(2-PPh$_2$-Ph)PO$_3$B(*p*-CHO-Ph)]$_4$ (**7d**), even at high concentration (Scheme 4.6). **7c** and **7d** are formed in 75 % and 70 % NMR yield respectively, and were isolated by recrystallization from toluene in 34 - 40 % yield. The $^{31}P\{^1H\}$ NMR spectra of **7c** and **7d** each contain phosphonate resonances in the range δ -9 to -10, and a phosphine resonance at δ -14. The diphenylphosphino substituent is thus able to solubilize the reaction intermediates and is sufficiently sterically-demanding to favor the selective formation of tetramers.

Scheme 4.6

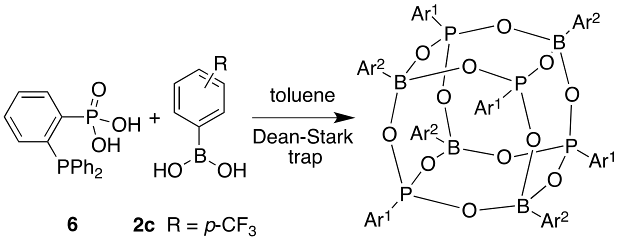

6 **2c** R = p-CF_3 **2d** R = p-CHO

Ar^1 = 2-PPh_2-Ph
7c Ar^2 = p-CF_3-Ph
7d Ar^2 = p-CHO-Ph

The reaction of **6** with (p-tolyl)$B(OH)_2$ (**2f**) is similar to that of **1**. The reactants are fully consumed, but only a trace amount of $[(2\text{-}PPh_2\text{-}Ph)PO_3B(p\text{-tolyl})]_4$ (**7f**) is formed, as determined by $^{31}P\{^1H\}$ NMR and confirmed by MALDI-MS. The major products are *p*-tolylboroxine (25 %) and condensation products of unknown structures.

Role of Boroxine Formation. As noted above, **1** and **6** react with $PhB(OH)_2$ and aryl boronic acids that contain electron-withdrawing substituents (Br, CHO, CF_3) to afford high yields of tetrameric or hexameric cages, but when *p*-tolylboronic acid is used, only low yields of cage products are formed and *p*-tolylboroxine is the major boron-containing product. In principle, phosphonic acids can also condense with boroxines to form borophosphonate cages. Indeed, the reaction of **1** with *o*-CF_3-phenylboroxine generates tetrameric cage **3b** in high yield (85 % by ^{19}F NMR). In contrast, the reaction of **1** with *p*-tolylboroxine yields cage **3f** in only 10 % NMR yield, with 20 % of the *p*-tolylboroxine remaining after the reaction.

These results suggest that the relative stabilities of borophosphonate cages and boroxines influence the product distribution. Electron-withdrawing substituents on the boron aryl group stabilize the "borate-like" 4-coordinate boron centers in the borophosphonate cages and destabilize the 3-coordinate boron centers in the boroxines.[13] In contrast, electron-donating groups have the opposite effect, and so cage formation is disfavored in these cases. This effect is less important when alkylphosphonic acids rather than arylphosphonic acids are used. Severin reported high yields of cage when $^{t}BuP(O)(OH)_2$ was reacted with (*p*-CHO-Ph)$B(OH)_2$ (70 %) or (*p*-tolyl)$B(OH)_2$ (67 %). The ^{t}Bu group is more electron-donating than aryl groups, so it better-stabilizes the "phosphonium-like" 4-coordinate RPO_3 centers in the cage structure.

Steric Limitations on Cage Formation. The reaction of **6** with (*o*-CF_3-Ph)$B(OH)_2$ (**2b**) is unselective, generating a mixture of products. The reactants are fully consumed, but multiple species are observed by $^{31}P\{^1H\}$ NMR (multiple resonances in the range δ 51 to -15). A weak $[M+H]^+$signal for $[(2\text{-}PPh_2\text{-}Ph)PO_3B(o\text{-}CF_3\text{-}Ph)]_4$ (**7b**) is observed in the APCI mass spectrum of the reaction mixture, and (*o*-CF_3-Ph)-boroxine is formed in 40 % yield, as determined by ^{1}H NMR. It is likely that the presence of *ortho* substituents on both the phosphonic acid and boronic acid disfavors cage formation in this case.

Solid State Structures. The solid-state structure of **3a** (Figure 4.3) is similar to those of $[^{t}BuPO_3BAr']_4$ (Ar' = *p*-tol, *p*-CHO-Ph, and 3,5-$(CHO)_2$-Ph).[12] The $P_2B_2O_4$ rings that comprise the faces of the cubic core adopt a flattened chair-chair conformation,[17] and the B-O and P-O distances and the P-O-B, P-O-P, and B-O-B angles are similar to those observed in previous studies.[12]

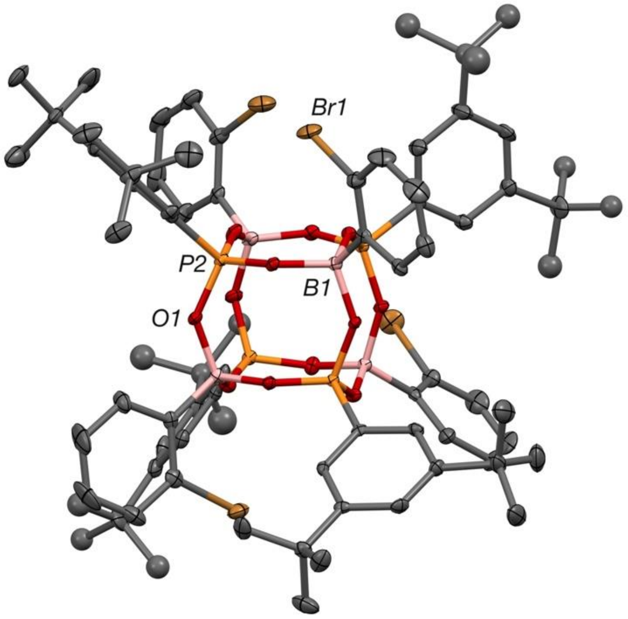

Figure 4.3. Molecular structure of **3a**. Hydrogen atoms are omitted. Four of the ^{t}Bu groups are disordered over several positions; in these cases, the positions of the methyl carbons were refined isotropically and one position of the methyl carbons is shown as a sphere. Average bond lengths (Å) and angles (^{o}) (number of data, range): P-O: 1.522(7) (12, 1.511(2) - 1.533(2)); B-O: 1.483(7) (12, 1.472(3) - 1.496(3)); P-C_{ipso}: 1.766(2) (4, 1.766(3) - 1.767(2)); B-C_{ipso}: 1.600(3) (4, 1.595(4) - 1.603(3)); P-O-B: 141.2(4.5) (12, 135.7(1) - 149.1(2)); O-P-O: 111.39(1.05) (12, 113.39(9) - 119.62(9)); O-B-O: 108.7(0.8) (12, 107.6(2) - 110.8(2)).

3d also adopts a cubic cage structure. In this case, two types of cages with the same atom connectivity but different spatial orientation of the oxygen bridges are co-crystallized, one of which is shown in Figure 4.4. These conformational isomers result from the flexibility of the oxygen bridges. While the cages are relatively rigid and the boron and phosphorous atoms occupy essentially the same positions in the two conformers, the oxygen atoms may lie in or out of the plane passing through the B-P-B atoms (Figure 4.5, see the experimental section for further details).

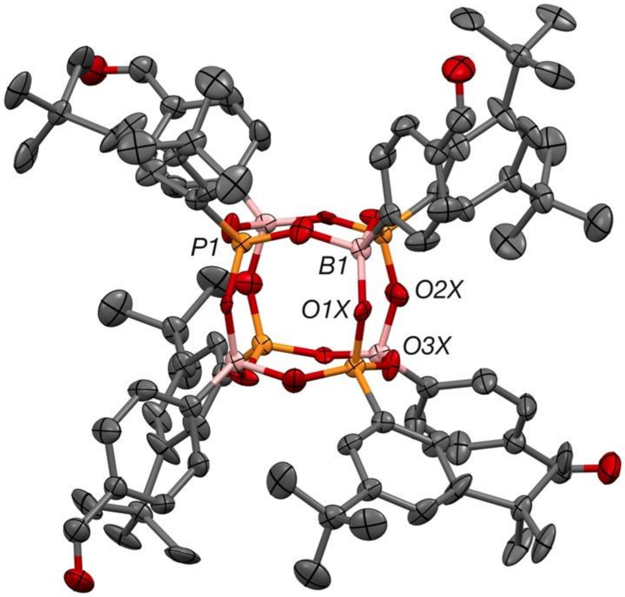

Figure 4.4 Molecular structure of **3d**. Hydrogen atoms are omitted. The oxygen atoms are disordered over two positions, only one of which is shown. One ^{t}Bu group is disordered over two positions, only one of which is shown. Average bond lengths (Å) and angles (°) (number of data, range): P-O: 1.51(5) (3, 1.48(1) - 1.57(9)); B-O: 1.47(8) (3, 1.46(1) - 1.482(9)); P-C_{ipso}: 1.767(3); B-C_{ipso}: 1.602(4); P-O-B: 142.8(6.9) (3, 135.9(6) - 149.7(7)); O-P-O: 110.9(3.1) (3, 107.4(5) - 112.8(5)); O-B-O: 108.3(19.9) (3, 87.4(5) - 127.1(6)).

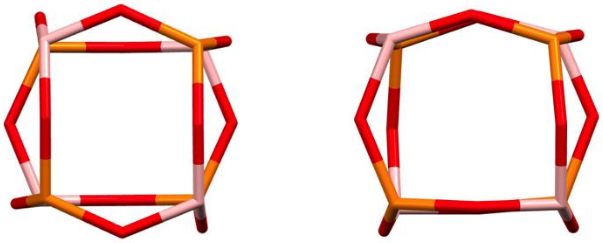

Figure 4.5. Core structures of the two co-crystallized conformational isomers of **3d**.

The solid-state structure of **4d** is shown in Figure 4.6. The hexameric cage features two 12-membered rings and six 8-membered rings. The 12-membered $P_3B_3O_6$ rings adopt a [6’6’] conformation,[18] in which four O atoms pucker into the cage (e.g. O6), while two pucker out (e.g. O7). The inward pucker generates close contact between the B-aryl and P-aryl groups that flank the inward-puckered oxygen, forcing these flanking groups to adopt near mutually parallel conformations, as illustrated in Figure 4.7. This arrangement, in turn, generates close steric interactions between the B-aryl and P-aryl groups that flank the outward-puckered oxygens. Such steric interactions would be particularly severe if either the B-aryl or P-aryl groups contain *ortho* substituents, which provides an explanation for the observation that only tetrameric structures are formed in these cases.

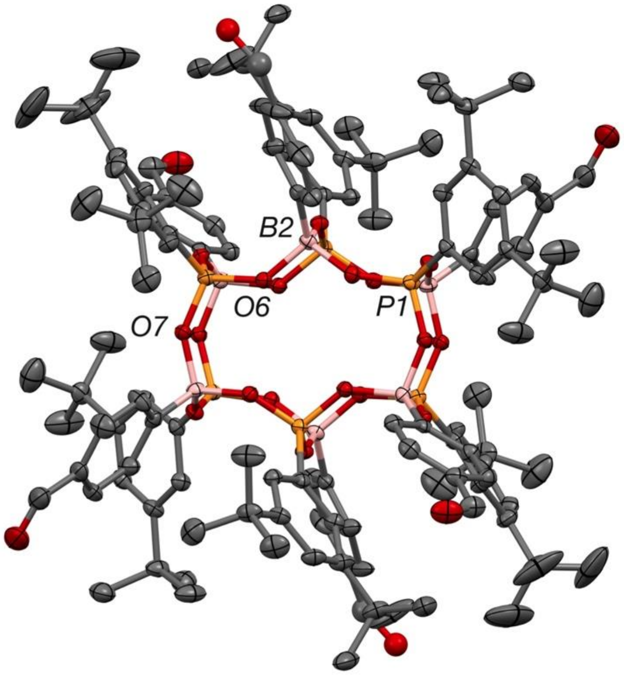

Figure 4.6. Molecular structure of **4d·C_6H_6·2C_7H_8**. Hydrogen and solvent atoms are omitted. The formyl group is disordered over two positions, only one of which is shown. Average bond lengths (Å) and angles (°) (number of data, range): P-O: 1.524(7) (9, 1.514(3) - 1.536(3)); B-O: 1.489(6) (9, 1.479(5) - 1.495(6)); P-C*ipso*: 1.769(5) (3, 1.767(5) - 1.771(4)); B-C*ipso*: 1.591(7) (3, 1.588(7) - 1.593(6)); P-O-B: 137.5(5.1) (9, 127.8(3) - 144.2(3)); O-P-O: 110.6(2.8) (9, 104.9(2) - 114.2(2)); O-B-O: 107.7(2.4) (9, 102.5(3) - 110.1(3)).

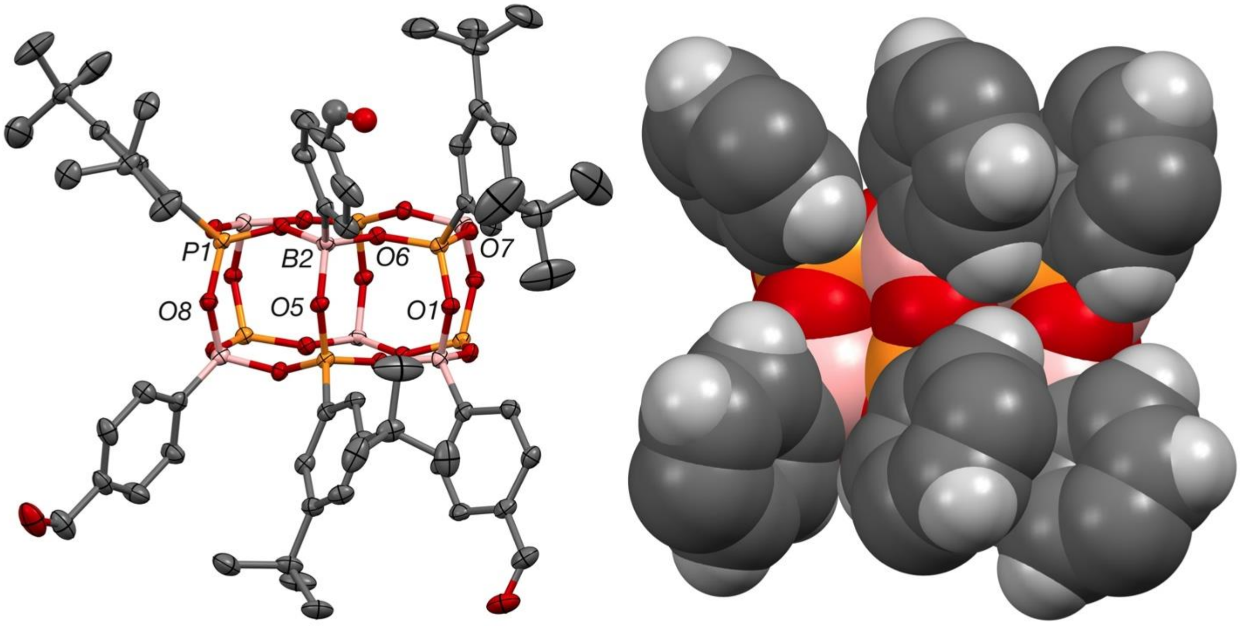

(a) **(b)**

Figure 4.7. Alternate view of **4d** that illustrates key steric interactions. (a) Side view of **4d** in which hydrogen atoms and the aryl groups at the back are omitted. O6 is inward-puckered and O1, O5, O7 and O8 are outward-puckered. (b) Space-filling view in the same perspective as in (a); the aryl-hydrogen atoms are shown, but the formyl and ^{t}Bu substituents are omitted.

Functionalization of borophosphonate compounds. Borophosphonate cage compounds are stable in toluene at 110 ˚C, and therefore they are potential scaffolds for multinuclear palladium catalysts. The lithiation reactions of borophosphonate compounds were explored, as such reactions are widely used in ligand synthesis and would provide a means of constructing multinuclear palladium catalysts from simple borophosphonate cage compounds. The key objective of these experiments was to determine if the borophosphonate cage is stable to alkyl lithium reagents. The attempted functionalization of **3a** by reaction with ^{n}BuLi followed by addition of Ph_2PCl was unsuccessful (Scheme 4.7). A substantial amount of unreacted **3a** was observed after the reaction (ca. 64 % based on $^{31}P\{^1H\}$ NMR), and prolonging the lithiation reaction time from 1 h to 18 h did not improve the conversion of **3a**. The use of other lithium reagents such as MeLi and *ᵗ*BuLi did not increase the conversion of **3a**. However, a key finding of this experiment is that the borophosphonate cage is stable to the strongly nucleophilic and basic alkyl lithium reagent. The apparent failure of lithiation of **3a** is likely due to inaccessibility of the Br group, which is on the *ortho* position of the B-aryl ring and sterically hindered by the cage core and P-aryl groups

Scheme 4.7

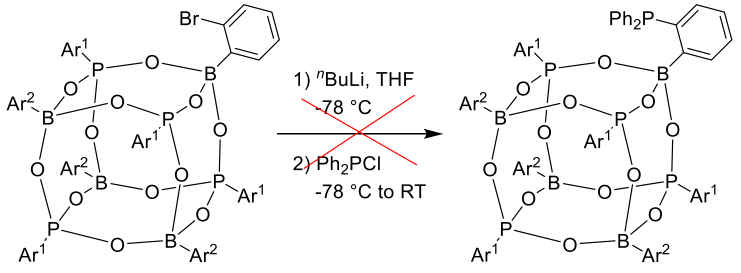

Ar^1 = 3,5-^{t}Bu$_2$-Ph
3a Ar^2 = *o*-Br-Ph

Ar^1 = 3,5-^{t}Bu$_2$-Ph
9a Ar^2 = *o*-PPh$_2$-Ph

To test this hypothesis, [^{t}BuPO$_3$B(4-Br-Ph)]$_4$ (**8**), in which the Br group is at the *para* position of the B-aryl ring, was synthesized by the condensation of ^{t}BuP(O)(OH)$_2$ and (4-Br-Ph)B(OH)$_2$ and isolated by recrystallization from toluene/hexane solution in 74 % yield (Scheme 4.8). The reaction of **8** with ^{n}BuLi followed by addition of Ph_2PCl successfully generated the fully Ph_2P-functionalized cage **9b** in 68 % yield, with 86 % overall Ph_2P installation based on $^{31}P\{^1H\}$ NMR (Scheme 4.8). Although **9b** was not isolated in pure form due to the similar solubility of the fully and partially Ph_2P-functionalized cages, this reaction shows that constructing multinuclear palladium catalysts on the borophosphonate cage compounds via this approach should be possible.

Scheme 4.8

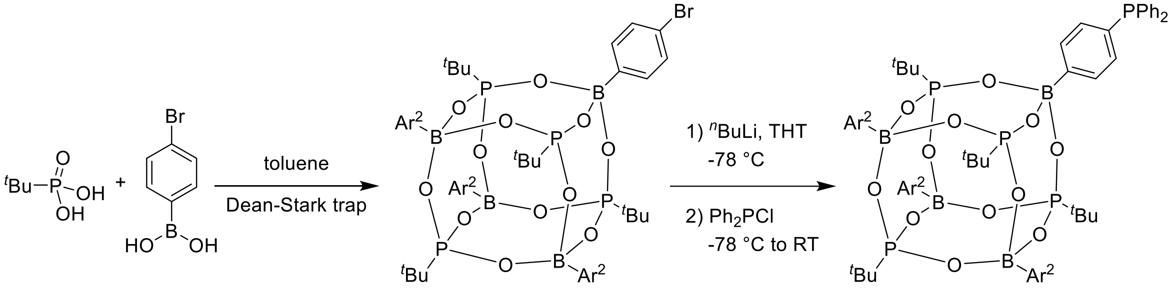

8 Ar^2 = *p*-Br-Ph

9b Ar^2 = *p*-PPh_2-Ph

4.3 Conclusions

Tetrameric $[ArPO_3BAr']_4$ and hexameric $[ArPO_3BAr']_6$ borophosphonate cages that contain aryl groups at B and P were synthesized by the condensation reactions of aryl phosphonic acids and aryl boronic acids using Severin's method. Aryl boronic acids that contain electron-withdrawing substituents afford cages with the highest yields, while aryl boronic acids with electron-donating groups form mixtures of condensation products and boroxines. Steric effects strongly influence the product distribution and yield. When both starting acids are *ortho*-substituted, the reaction produces only trace amounts of tetrameric cages. When either the aryl phosphonic acid or the aryl boronic acid has an *ortho* substituent, the reaction selectively produces the tetrameric cage. When neither reactant is *ortho*-substituted, the reaction produces a mixture of tetramer and hexamer. In this case, the tetramer is favored at low reactant concentrations, and the hexamer is favored at high reactant concentrations, reflecting the relative rates of intramolecular and intermolecular condensation reactions as the cages are formed. The hexameric and tetrameric cages can interconvert in solution. The sensitivity of hexamer formation to the steric profile of the B and P aryl groups is attributed to the inward puckering of some of the oxygen atoms in the molecular structure, which places these aryl groups in close proximity.

4.4 Experimental

General Procedures. All experiments were performed under a nitrogen atmosphere using drybox or Schlenk techniques. Nitrogen was purified by passage through Q-5 oxygen scavenger and activated molecular sieves. Toluene and hexane were purified by passage through BASF R3-11 oxygen scavenger and activated alumina. Compound **6** was prepared by the literature route.[16] Arylboroxines were prepared by azeotropic distillation of the corresponding arylboronic acids with toluene for 6 h.[19] The following materials were obtained from commercial sources and used without further purification: 1-bromo-3,5-di-tert-butylbenzene (Aldrich, 97 %), ^{n}BuLi solution (Aldrich, 2.5 M in hexanes), MeLi solution (Aldrich, 1.6 M in diethyl ether), ^{t}BuLi solution (Aldrich, 1.7 M in pentane), diethyl chlorophosphate (Aldrich, 97 %), chlorodiphenylphosphine (Aldrich, 96 %), tert-butylphosphonic acid (Aldrich, 98 %), 4-bromophenylboronic acid (Aldrich, 95 %), and bromotrimethylsilane (Aldrich, 97 %). Phenylboronic acid (Aldrich, 95 %), 4-tolylboronic acid (Matrix, 97 %), 2-bromophenylboronic acid (Matrix, 98 %), 2-(trifluoromethyl)phenylboronic acid (Matrix, 98 %), 4-(trifluoromethyl)phenylboronic acid (Matrix, 97 %), and 4-formylphenylboronic acid (Acros, 97%) were recrystallized from H_2O prior to use. Elemental analyses were performed by Robertson Microlit Laboratories. The solvent content in elemental analysis samples was quantified by ^{1}H NMR. NMR spectra were acquired on Bruker DRX-500 or Bruker DRX-400 spectrometers at ambient temperatures unless otherwise indicated. ^{1}H and ^{13}C chemical shifts are reported relative to $SiMe_4$ and are internally referenced to residual ^{1}H and ^{13}C solvent resonances. ^{31}P chemical shifts are reported relative to externally referenced 85% H_3PO_4. ^{19}F spectra were referenced to external $BF_3{\bullet}Et_2O$, and ^{19}F chemical shifts are reported relative to $CFCl_3$. ^{11}B chemical shifts are reported relative to externally referenced

BF_3•Et_2O. Coupling constants are reported in Hz. NMR signals are assigned based on COSY, HMQC, and $^1H\{^{31}P\}$ experiments, as well as trends in chemical shifts and coupling constants derived from these experiments. C_6D_6, THF-*d₈*, and toluene-*d₈* were dried over Na/benzophenone. CD_2Cl_2 was dried over P_2O_5. Mass spectrometry was performed on an Agilent 6224 TOF-MS instrument (high resolution) or an Agilent 6130 LCMS (low resolution).

(3,5-^{t}Bu$_2$-Ph)P(O)(OH)$_2$ (1). A Schlenk flask was charged with 1-bromo-3,5-di-*tert*-butylbenzene (5.384 g, 20.00 mmol) and Et_2O (120 ml), and cooled to 0 °C. ^{n}BuLi solution (2.5 M, 8.0 ml, 20 mmol) was added via syringe over 5 to 10 min. The mixture was stirred at 0 °C for 30 min and then warmed to room temperature for another 1 h. The clear colorless solution was cooled to -78 °C and a solution of diethyl chlorophosphate (2.9 ml, 20 mmol) in diethyl ether (30 ml) was added. The mixture was stirred at room temperature for 18 h to yield a cloudy colorless solution. The reaction mixture was then transferred to a separatory funnel that contained H_2O (50 ml). The aqueous layer was extracted with Et_2O (3 × 50 ml). The combined organic fractions were washed with brine (20 ml) and dried over $MgSO_4$, and the volatiles were removed under vaccum to yield a colorless oil. The crude product was purified by silica gel chromatography, using a 2:1 hexanes: ethyl acetate mixture as the eluent. The product was isolated as clear oil and directly dissolved in CH_2Cl_2 (150 ml). Bromotrimethylsilane (8.5 ml, 64 mmol, excess) was added at room temperature and the reaction mixture was stirred at room temperature for 2 days. The volatiles were removed under vaccum and the crude product was dissolved in MeOH (100 ml) and stirred for 2 h. The MeOH was removed under vaccum to yield a viscous oil. Hexane was added to the oil to afford **1** as a white solid. **1** was dried in vacuum oven (3.721 g, 69%). $^{31}P\{^1H\}$ NMR (CD_2Cl_2): δ 24.2. ^1H NMR (CD_2Cl_2): δ 11.44 (s, 2H, O*H*), 7.74 (d, $^3J_{PH}$ = 15, 2H, H^2), 7.68 (s, 1H, H^4), 1.34 (s, 18H, H^6). $^{13}C\{^1H\}$ NMR (CD_2Cl_2): δ 151.5 (d, $^3J_{PC}$ = 15, C^3), 127.7 (d, $^4J_{PC}$ = 2, C^4), 126.9 (d, $^1J_{PC}$ = 192, C^1), 125.4 (d, $^2J_{PC}$ = 11, C^2), 35.3 (s, C^5), 31.4 (s, C^6). HRMS (*m/z*): Calcd. for $[C_{14}H_{23}PO_3 + H]^+$ 271.1463, Found: 271.1456.

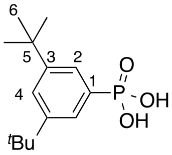

1

Figure 4.8. NMR spectra of (3,5-^{t}Bu$_2$-Ph)P(O)(OH)$_2$ (**1**)

(a) $^{31}P\{^1H\}$ NMR (CD_2Cl_2, 202 MHz):

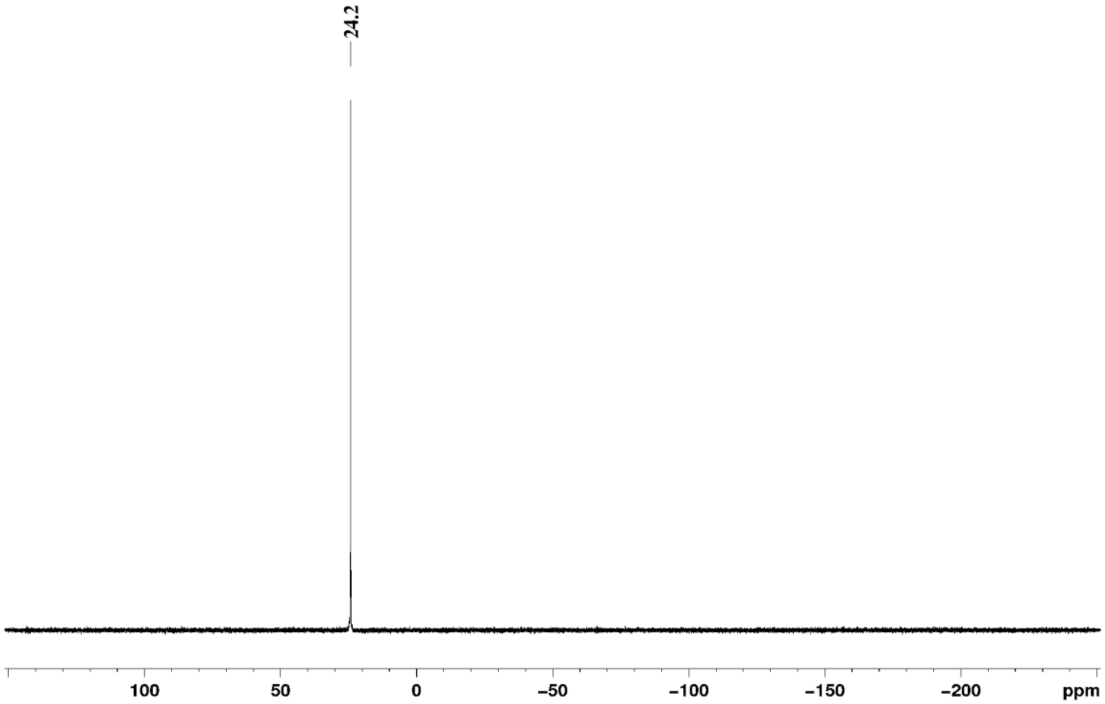

Figure 4.8, continued.

(b) ^{1}H NMR (CD_2Cl_2, 500 MHz):

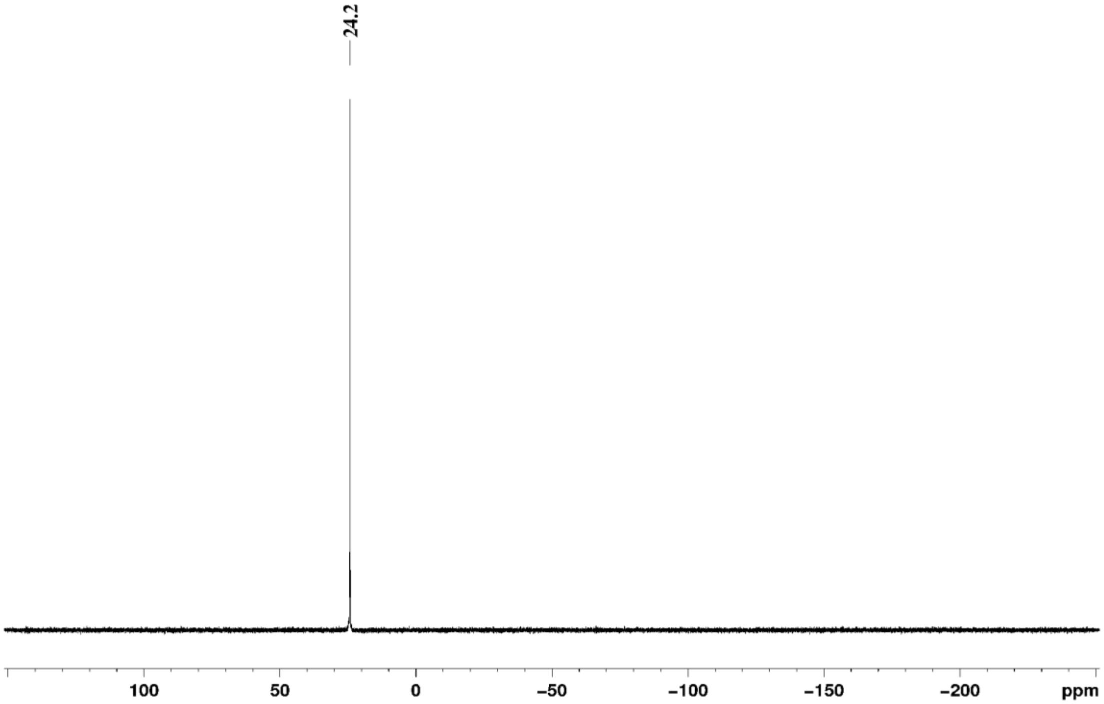

(c) $^{13}C\{^1H\}$ NMR (CD_2Cl_2, 125 MHz):

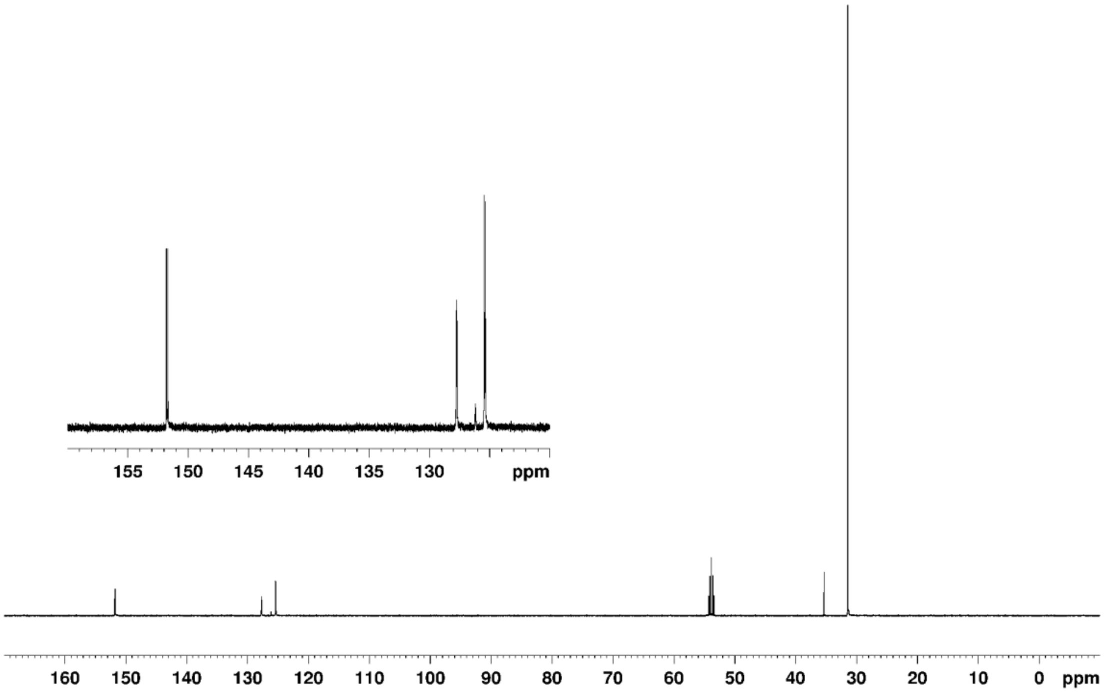

[(3,5-^{t}Bu$_2$-Ph)PO$_3$B(*o*-Br-Ph)]$_4$ (3a). A Schlenk flask equipped with Dean-Stark trap was charged with **1** (324 mg, 1.20 mmol), 2-bromophenylboronic acid (241 mg, 1.20 mmol), and toluene (48 ml). The mixture was refluxed for 3 h. The volatiles were removed under vacuum to afford a white solid. This material was recrystallized from hot hexane to afford **3a** as a white crystalline solid, which was dried under vacuum (250 mg, 48 %). X-ray quality crystals were grown by slow evaporation of a hexane solution of **3a**. ^{31}P{^{1}H} NMR (C_6D_6): δ -9.6. ^{1}H NMR (C_6D_6): δ 8.31 (dd, $^3J_{PH}$ = 17, $^4J_{HH}$ = 2; 2H, H^2), 7.96 (dd, $^3J_{HH}$ = 8, $^4J_{HH}$ = 2, 1H, H^8), 7.64 (d, $^4J_{HH}$ = 1, 1H, H^4), 7.53 (dd, $^3J_{HH}$ = 8, $^4J_{HH}$ = 0.5; 1H, H^{11}), 6.96 (dt, $^3J_{HH}$ = 7, $^4J_{HH}$ = 0.5; 1H, H^9), 6.81 (dt, $^3J_{HH}$ = 8, $^4J_{HH}$ = 2; 1H, H^{10}), 1.16 (s, 18H, H^6). ^{13}C{^{1}H} NMR (C_6D_6): δ 151.4 (d, $^3J_{PC}$ = 18, C^3), 143.0 (broad, C^7), 134.6 (s, C$^{B\text{-}Ar}$), 133.6 (s, C$^{B\text{-}Ar}$), 129.5 (s, C$^{B\text{-}Ar}$), 127.3 (d, $^4J_{PC}$ = 4, C^4), 127.1 (d, $^2J_{PC}$ = 13, C^2), 126.4 (s, C$^{B\text{-}Ar}$), 126.1 (d, $^1J_{PC}$ = 236, C^1), 35.2 (d, $^4J_{PC}$ = 2, C^5), 31.3 (s, C^6), one resonance (C$^{B\text{-}Ar}$) is obscured by the solvent peak (127.8-128.9). ^{11}B{^{1}H} NMR (toluene-*d$_8$*): δ 3.7. HRMS (*m*/*z*): Calcd. for $[C_{80}H_{100}B_4P_4O_{12}Br_4 + H]^+$ 1741.3308, Found: 1741.3348. EA: Calcd. for $C_{80}H_{100}B_4P_4O_{12}Br_4$, %: C, 55.21; H, 5.79. Found: C, 55.09; H, 5.79.

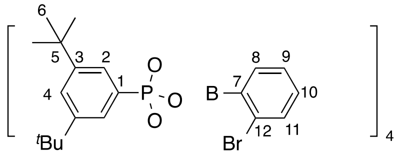

3a

Figure 4.9. NMR spectra of [(3,5-^{t}Bu$_2$-Ph)PO$_3$B(*o*-Br-Ph)]$_4$ (**3a**)

(a) ^{31}P{^{1}H} NMR (C_6D_6, 202 MHz):

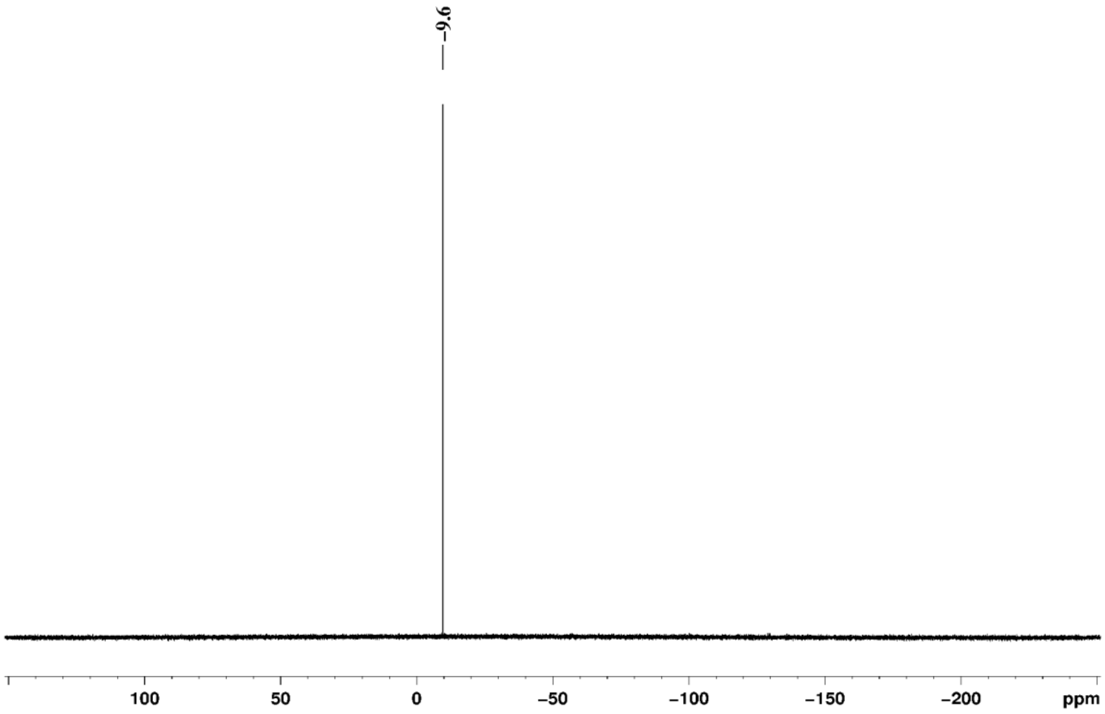

(b) ^{1}H NMR (C_6D_6, 500 MHz):

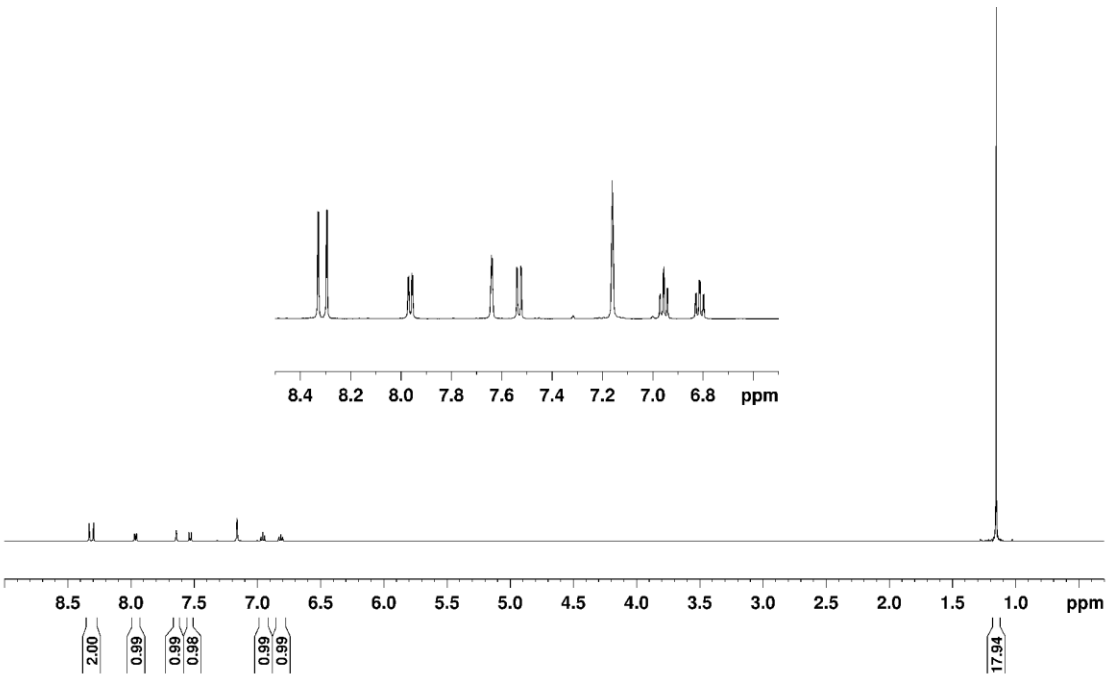

Figure 4.9, continued.

(c) $^{13}C\{^{1}H\}$ NMR (C_6D_6, 125 MHz):

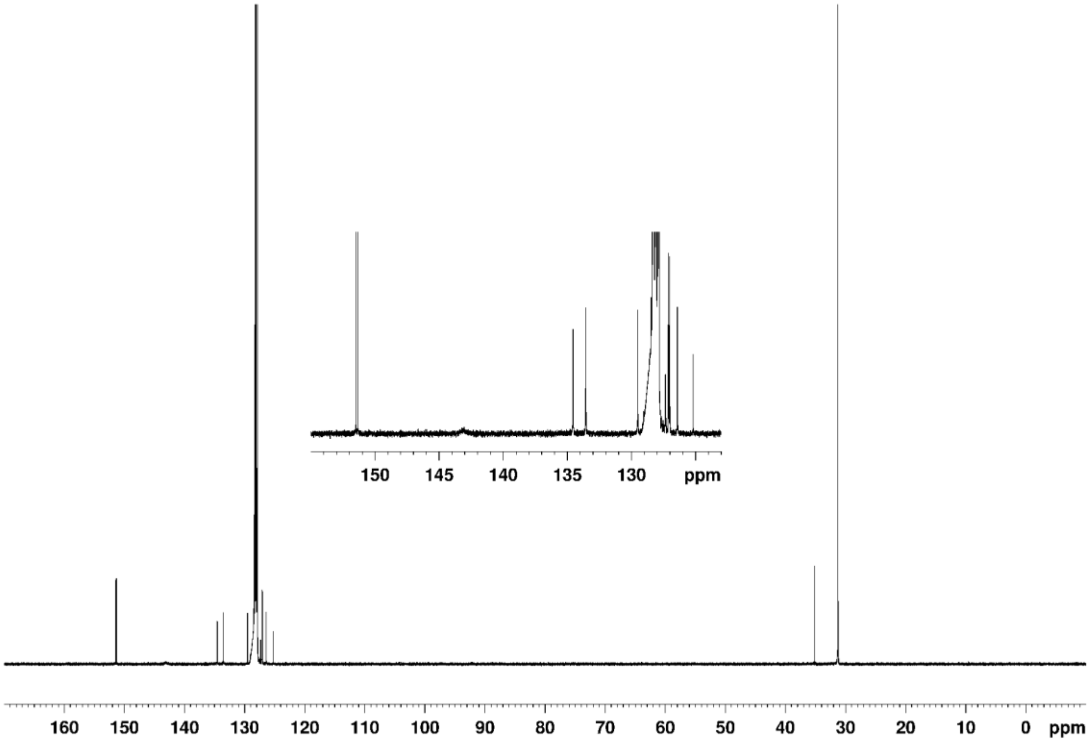

(d) $^{11}B\{^{1}H\}$ NMR (toluene-d_8, 128 MHz):

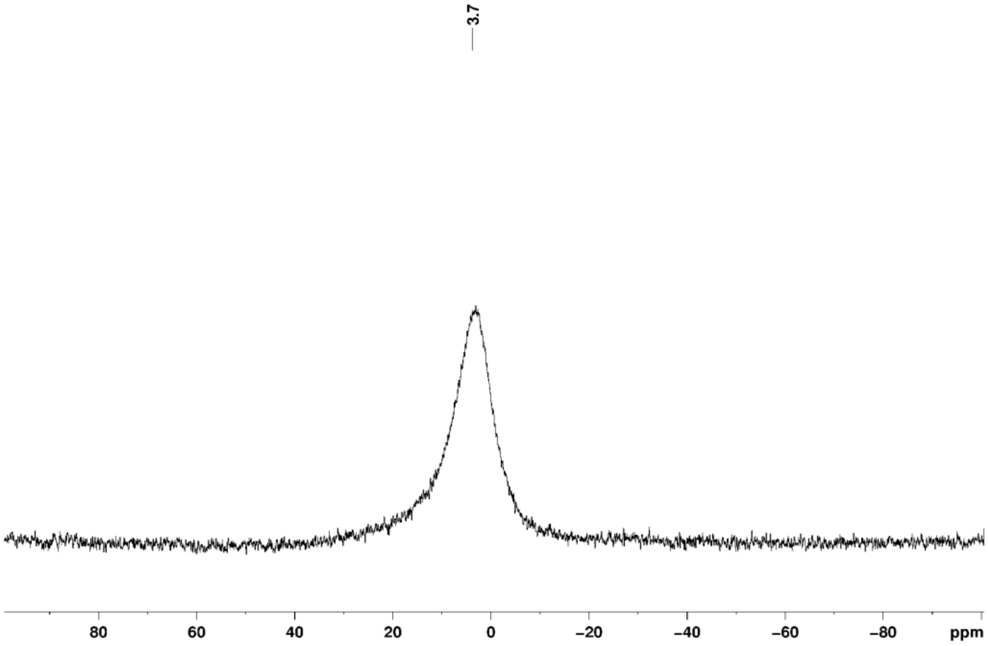

[(3,5-^{t}Bu$_2$-Ph)PO$_3$B(*o*-CF$_3$-Ph)]$_4$ (3b). **3b** was synthesized analogously to **3a** from **1** (811 mg, 3.00 mmol) and 2-(trifluoromethyl)phenylboronic acid (569 mg, 2.99 mmol) in toluene (120 ml). The volatiles were removed under vacuum to afford a white solid. This material was recrystallized from hot hexane to afford **3b** as a white crystalline solid, which was dried under vacuum (640 mg, 50 %). ^{31}P{^{1}H} NMR (C_6D_6): δ -9.5. ^{1}H NMR (C_6D_6): δ 8.23 (d, $^3J_{HH}$ = 7, 1H, H^8), 8.04 (dd, $^3J_{PH}$ = 12, $^4J_{HH}$ = 2; 2H, H^2), 7.65 (d, $^4J_{HH}$ = 1, 1H, H^4), 7.62 (d, J = $^3J_{HH}$, 1H, H^{11}), 7.11 (t, $^3J_{HH}$ = 8, 1H, H^9), 7.00 (t, $^3J_{HH}$ = 8, 1H, H^{10}), 1.09 (s, 18H, H^6). ^{13}C{^{1}H} NMR (C_6D_6): δ 151.3 (d, $^3J_{PC}$ = 17, C^3), 141.5 (broad, C^7), 134.6 (s, C^8), 133.3 (q, $^2J_{FC}$ = 31, C^{12}), 130.9 (s, C^9), 127.3 (d, $^4J_{PC}$ = 4, C^4), 126.6 (d, $^2J_{PC}$ = 13, C^2), 126.4 (q, $^3J_{FC}$ = 6, C^{11}), 126.1 (q, $^1J_{FC}$ = 273, C^{13}), 125.8 (d, $^1J_{PC}$ = 236, C^1), 35.0 (d, $^4J_{PC}$ = 2, C^5), 31.1 (s, C^6), C^{10} is obscured by the solvent peak (127.8-128.9). ^{19}F{^{1}H} NMR (C_6D_6): δ -56.9. ^{11}B{^{1}H} NMR (toluene-*d$_8$*): δ 3.6. HRMS (*m*/*z*): Calcd. for $[C_{84}H_{100}B_4P_4O_{12}F_{12} + H]^+$ 1697.6424, Found: 1697.6484. EA: Calcd. for $C_{84}H_{100}B_4P_4O_{12}F_{12}$•0.2 THF, %: C, 59.46; H, 5.94. Found: C, 59.24; H, 6.03.

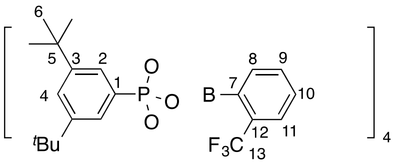

3b

Figure 4.10. NMR spectra of $[(3,5\text{-}^t\text{Bu}_2\text{-Ph})\text{PO}_3\text{B}(o\text{-CF}_3\text{-Ph})]_4$ (**3b**)

(a) ^{31}P{^{1}H} NMR (C_6D_6, 202 MHz)

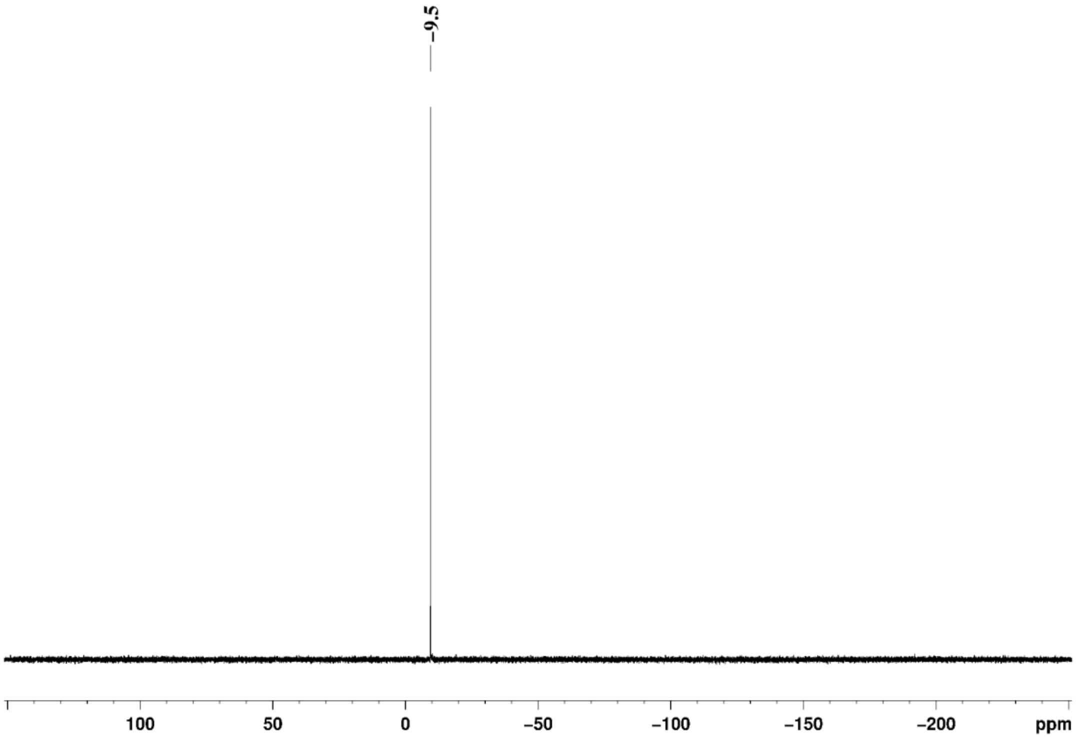

(b) ^{1}H NMR (C_6D_6, 500 MHz)

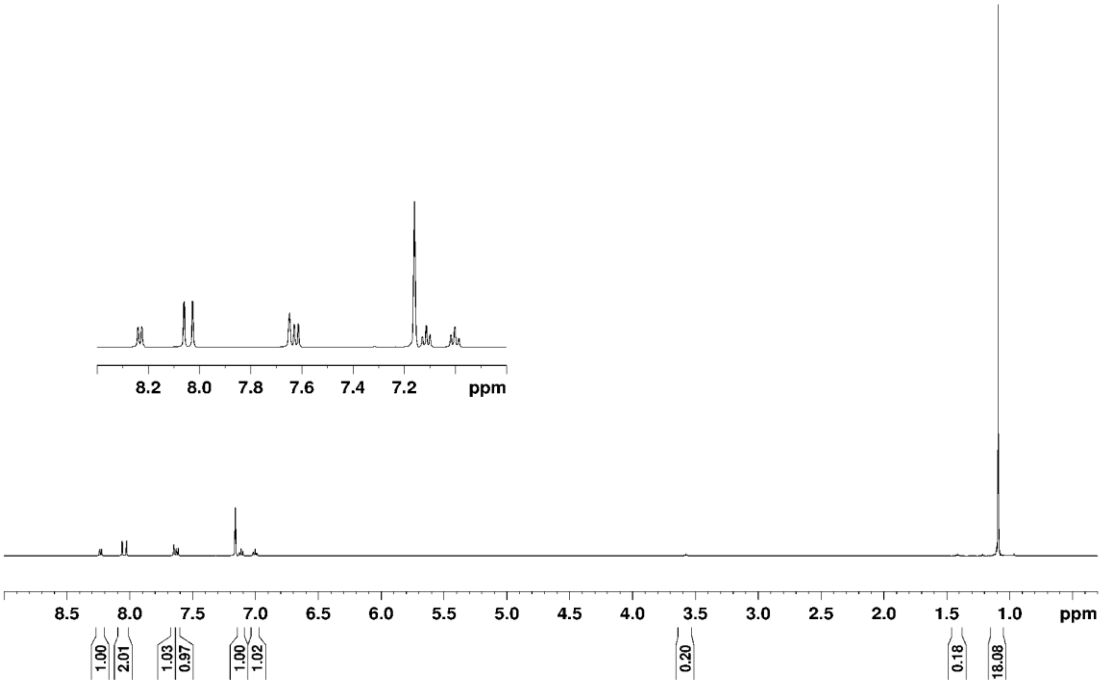

Figure 4.10, continued.

(c) $^{13}C\{^{1}H\}$ NMR (C_6D_6, 125 MHz)

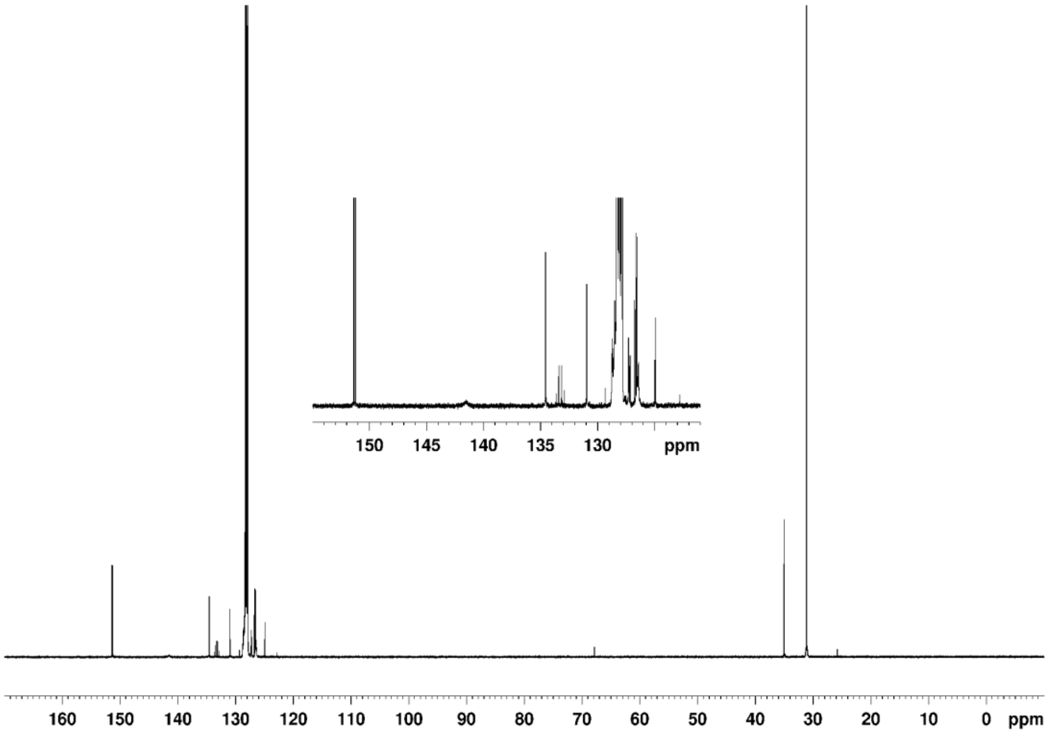

(d) $^{19}F\{^{1}H\}$ NMR (C_6D_6, 470 MHz)

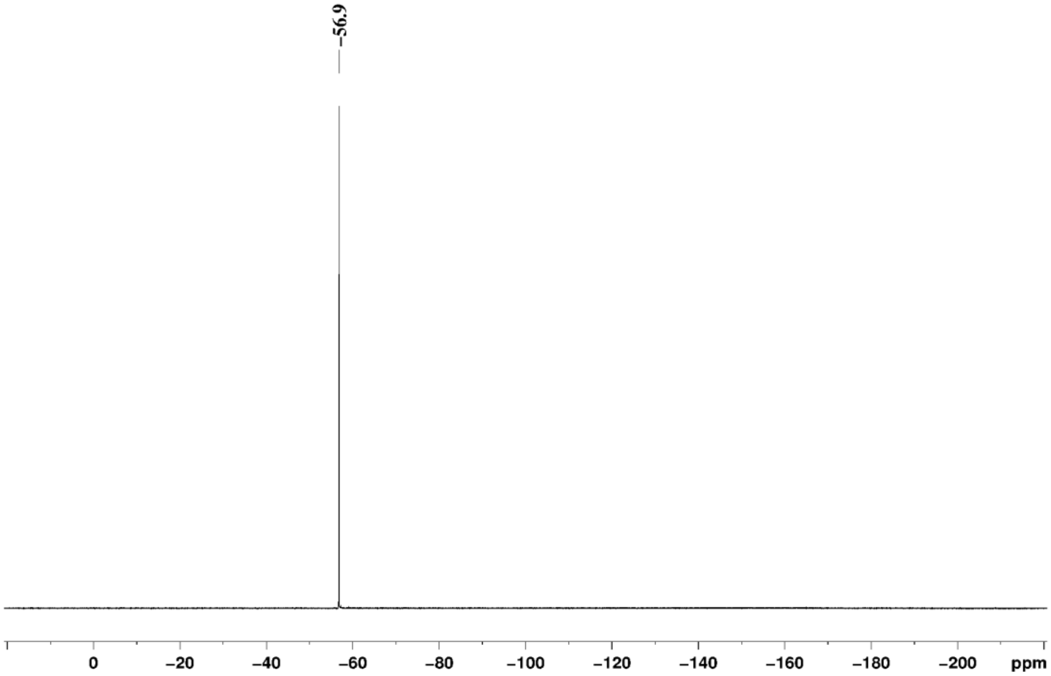

Figure 4.10, continued.

(e) $^{11}B\{^1H\}$ NMR (toluene-d_8, 128 MHz)

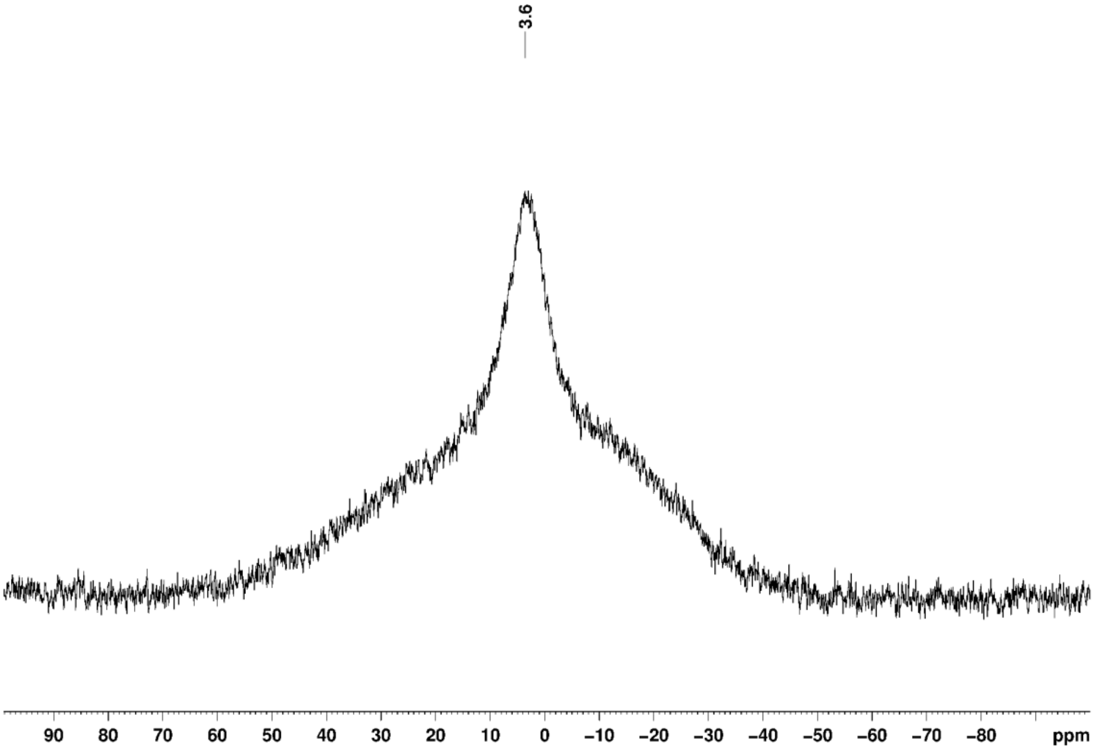

[(3,5-^{t}Bu$_2$-Ph)PO$_3$B(*p*-CF$_3$-Ph)]$_4$ (3c). 3c was synthesized analogously to **3a** from **1** (81 mg, 0.30 mmol) and 4-(trifluoromethyl)phenylboronic acid (57 mg, 0.30 mmol) in toluene (120 ml). The volatiles were removed with a rotovap to afford a yellow solid. The crude product was redissolved in toluene (1 ml), hexane (10 ml) was added, and a white precipitate formed. The mixture was filtered. The filtrate was taken to dryness under vacuum to afford **3c** as a yellow solid. The solid was washed with hexane and dried under vacuum (15 mg, 12 %). $^{31}P\{^1H\}$ NMR (THF-d_8): δ -6.9. ^1H NMR (THF-d_8): δ 7.79 (d, $^3J_{HH}$ = 8, 2H, H^8), 7.75 (s, 1H, H^4), 7.72 (dd, $^3J_{PH}$ = 16, $^4J_{HH}$ = 2; 2H, H^2), 7.52 (d, $^3J_{HH}$ = 8, 2H, H^9), 1.22 (s, 18H, H^6). $^{13}C\{^1H\}$ NMR (THF-d_8): δ 152.5 (d, $^3J_{PC}$ = 17, C^3), 132.0 (s, C^8), 130.2 (q, $^2J_{FC}$ = 32, C^{10}), 128.8 (d, $^4J_{PC}$ = 4, C^4), 125.9 (d, $^2J_{PC}$ = 13, C^2), 125.8 (d, $^1J_{PC}$ = 234, C^1), 125.5 (q, $^1J_{FC}$ = 271, C^{11}), 124.7 (q, $^3J_{FC}$ = 4, C^9), 35.6 (d, $^4J_{PC}$ =

2, C^5), 31.2 (s, C^6), C^7 resonance is not observed. $^{19}F\{^1H\}$ NMR (THF-d_8): δ -62.9. $^{11}B\{^1H\}$ NMR (toluene-d_8): δ 3.4. HRMS (*m*/*z*): Calcd. for $[C_{84}H_{100}B_4P_4O_{12}F_{12} + H]^+$ 1697.6424, Found: 1697.6522.

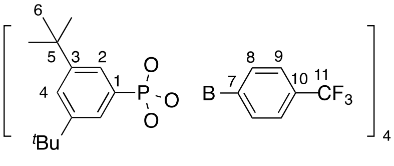

3c

Figure 4.11. NMR spectra of $[(3,5\text{-}^t\text{Bu}_2\text{-Ph})PO_3B(p\text{-}CF_3\text{-Ph})]_4$ (**3c**)

(a) $^{31}P\{^1H\}$ NMR (THF-d_8, 202 MHz)

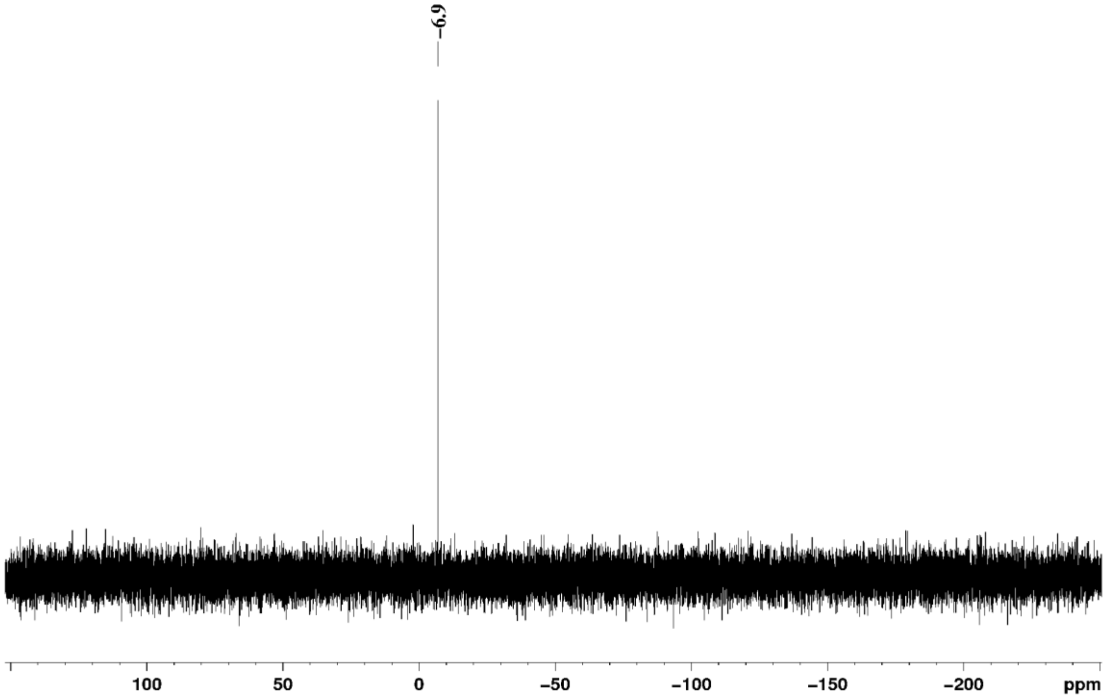

Figure 4.11, continued.

(b) ^{1}H NMR (THF-d_8, 500 MHz)

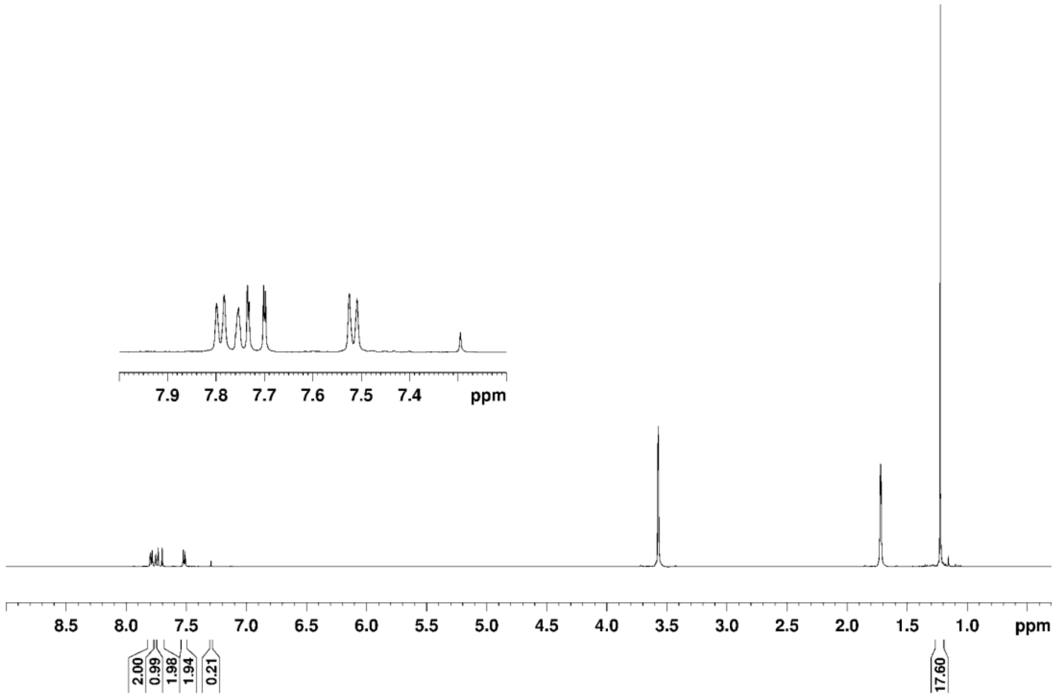

(c) ^{13}C{^{1}H} NMR (THF-d_8, 125 MHz)

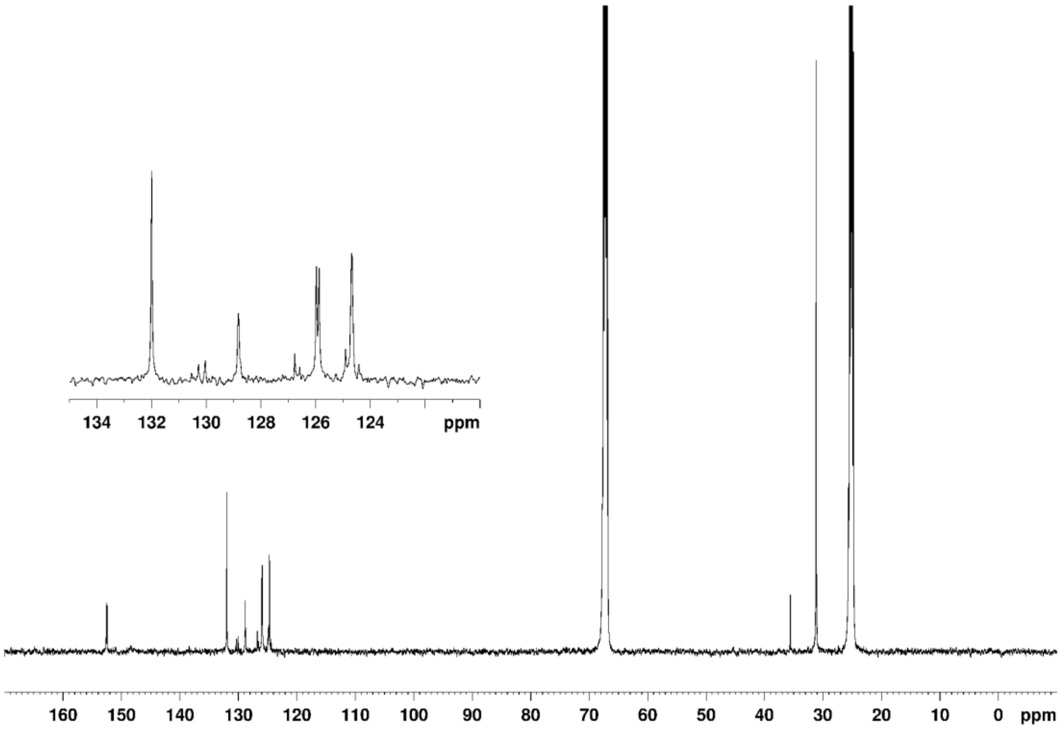

Figure 4.11, continued.

(d) $^{19}F\{^{1}H\}$ NMR (THF-d_8, 470 MHz)

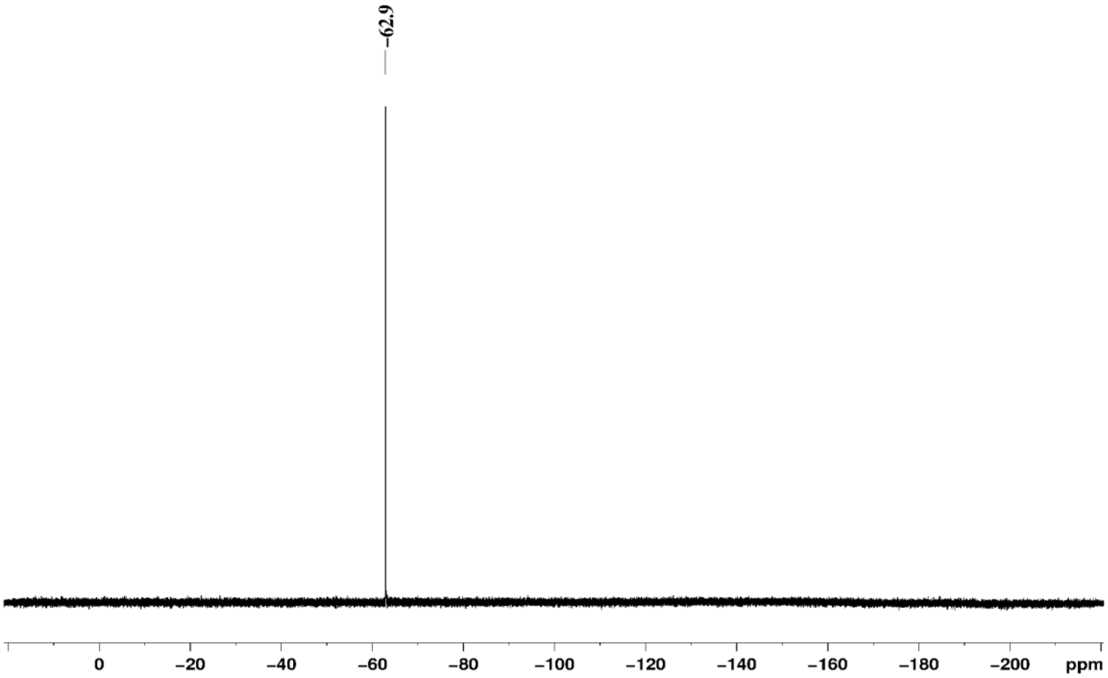

(e) $^{11}B\{^{1}H\}$ NMR (toluene-d_8, 128 MHz)

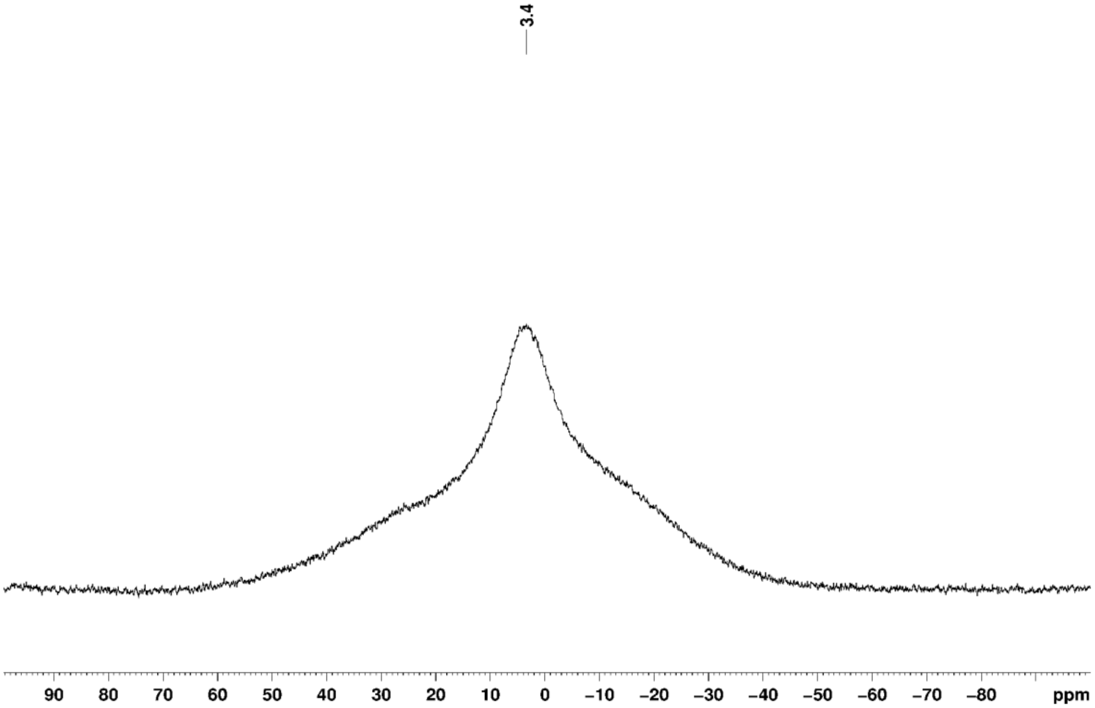

[(3,5-^{t}Bu$_2$-Ph)PO$_3$B(p-CF$_3$-Ph)]$_6$ (4c). 4c was synthesized analogously to **3a** from **1** (81 mg, 0.30 mmol) and 4-(trifluoromethyl)phenylboronic acid (57mg, 0.30 mmol) in toluene (12 ml). The volatiles were removed under vacuum to afford a yellow solid. This material was recrystallized from hot toluene to afford **4c** as a white powder, which was dried under vacuum (63 mg, 49 %). ^{31}P{^{1}H} NMR (THF-d_8): δ 0.3. ^{1}H NMR (THF-d_8): δ 7.48 (d, $^3J_{HH}$ = 8, 2H, H^8), 7.45(s, 1H, H^4), 7.42 (dd, $^3J_{PH}$ = 16, $^4J_{HH}$ = 2; 2H, H^2), 7.12 (d, $^3J_{HH}$ = 8, 2H, H^9), 1.15 (s, 18H, H^6). ^{13}C{^{1}H} NMR (THF-d_8): δ 151.5 (d, $^3J_{PC}$ = 16, C^3), 132.0 (s, C^8), 129.4 (q, $^2J_{FC}$ = 32, C^{10}), 128.0 (d, $^4J_{PC}$ = 3, C^4), 125.7 (d, $^1J_{PC}$ = 214, C^1), 125.6 (d, $^2J_{PC}$ = 12, C^2), 125.2 (d, $^1J_{FC}$ = 271, C^{11}), 124.3 (d, $^3J_{FC}$ = 4, C^9), 35.2 (d, $^4J_{PC}$ = 1, C^5), 31.1 (s, C^6), C^7 resonance is not observed. ^{19}F{^{1}H} NMR (THF-d_8): δ -62.8. ^{11}B{^{1}H} NMR (toluene-d_8): δ 3.7. HRMS (m/z): Calcd. for [$C_{126}H_{150}B_6P_6O_{18}F_{18}$ + H]$^+$ 2545.9597, Found: 2545.9663.

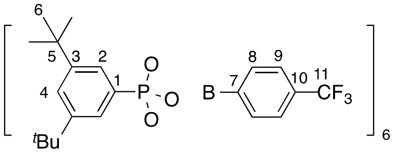

4c

Figure 4.12. NMR spectra of [(3,5-^{t}Bu$_2$-Ph)PO$_3$B(p-CF$_3$-Ph)]$_6$ (**4c**)

(a) ^{31}P{^{1}H} NMR (THF-d_8, 202 MHz)

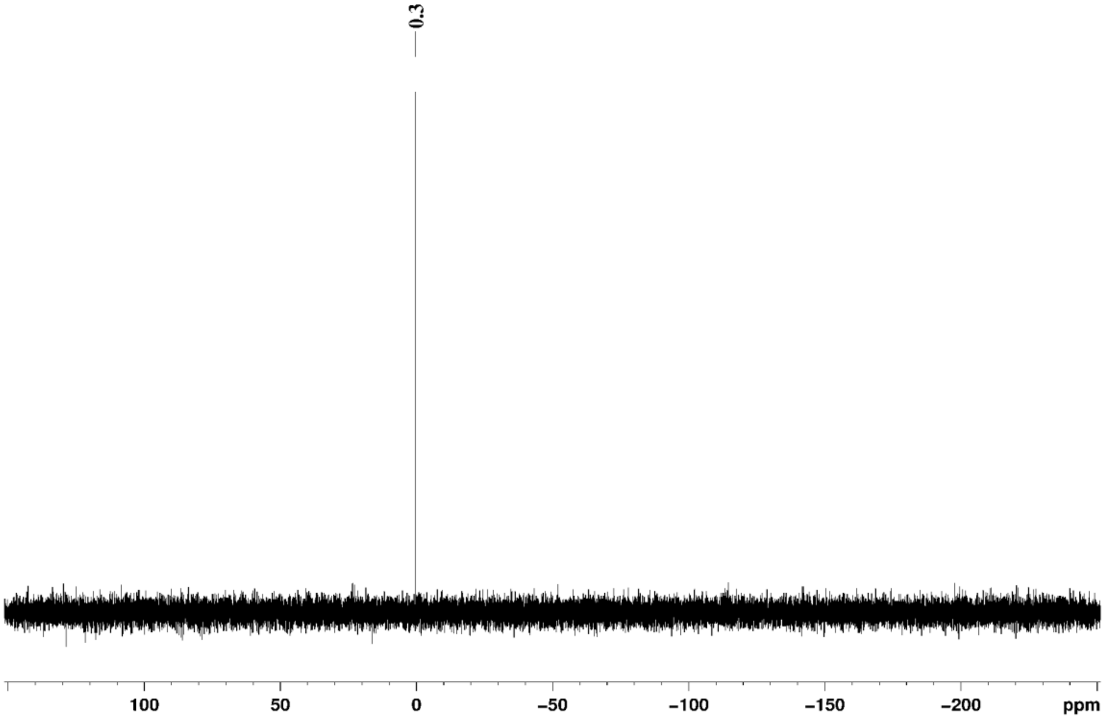

(b) ^{1}H NMR (THF-d_8, 500 MHz)

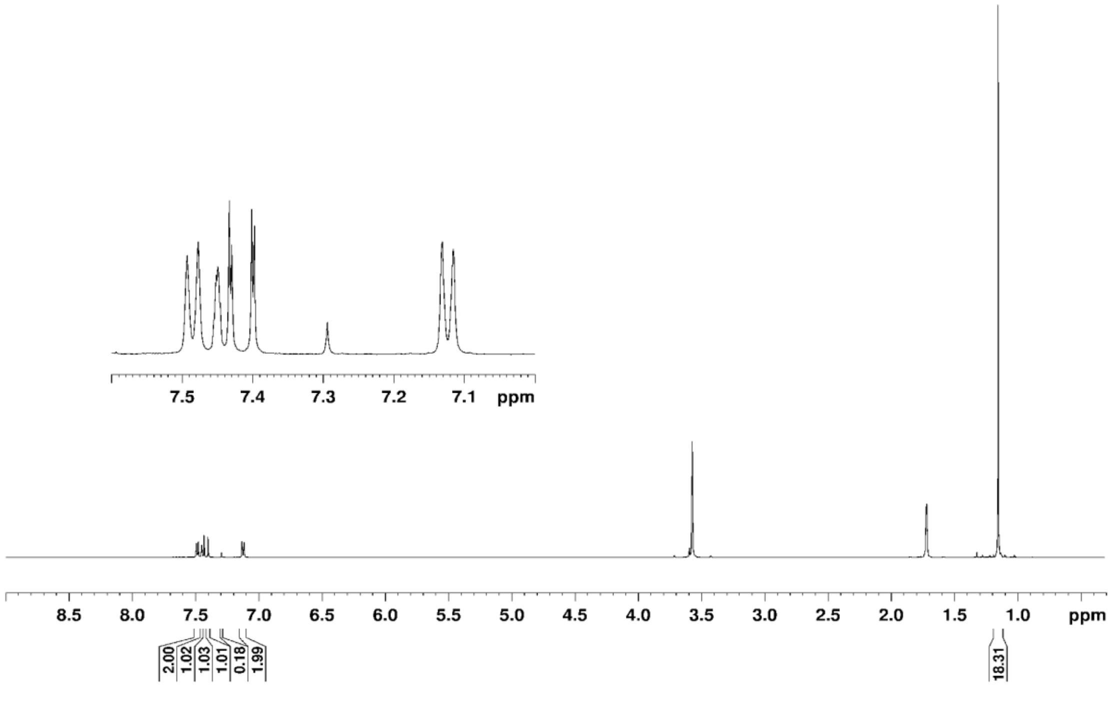

Figure 4.12, continued.

(c) $^{13}C\{^{1}H\}$ NMR (THF-d_8, 100 MHz)

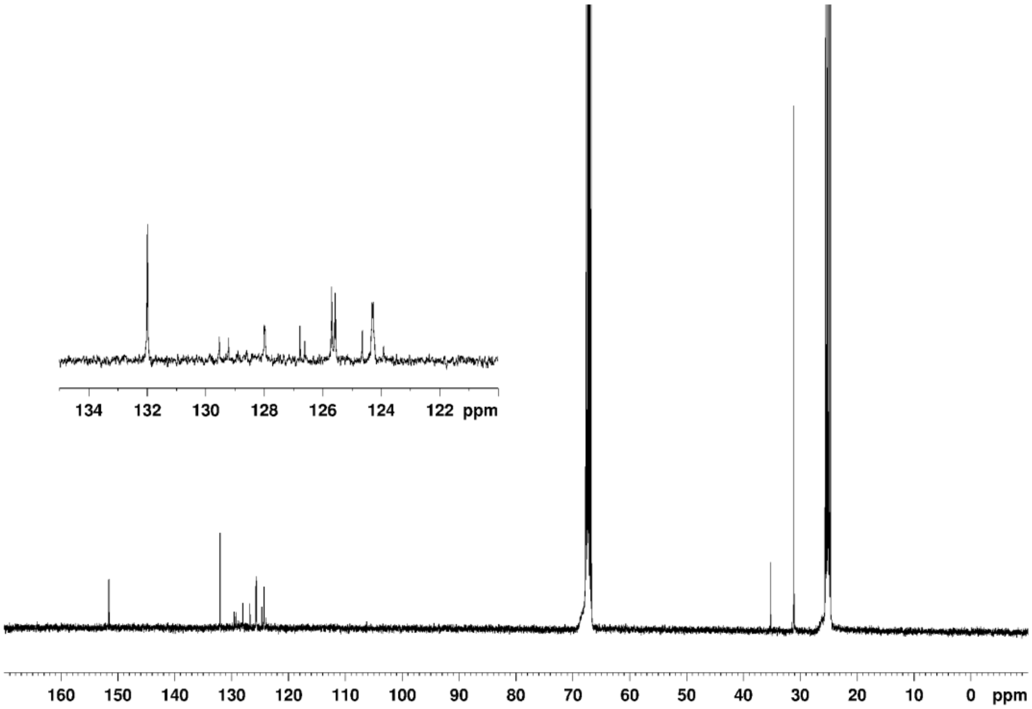

(d) $^{19}F\{^{1}H\}$ NMR (THF-d_8, 470 MHz)

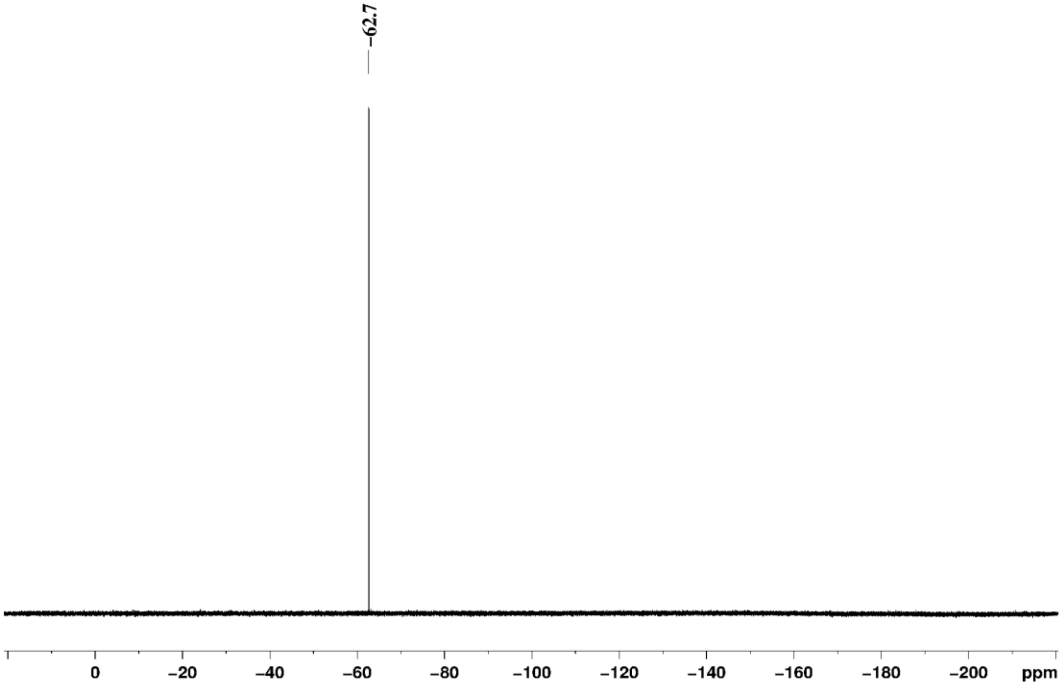

Figure 4.12, continued.

(e) $^{11}B\{^1H\}$ NMR (toluene-*d*$_8$, 128 MHz)

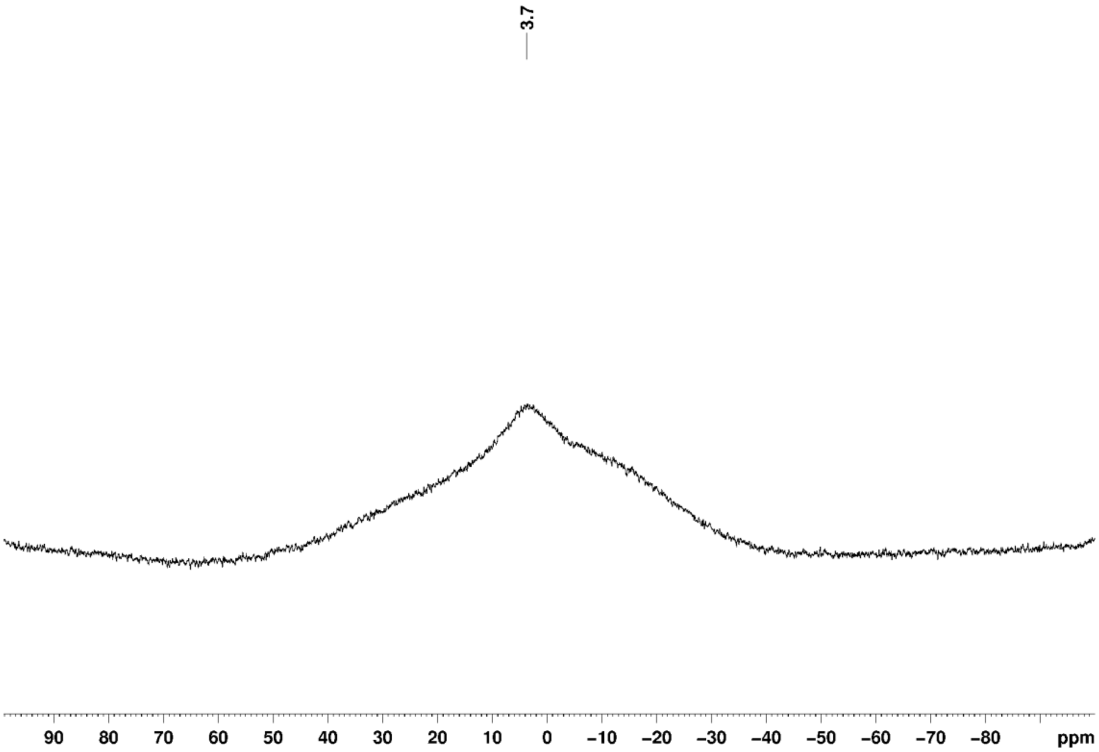

[(3,5-^{t}Bu$_2$-Ph)PO$_3$B(*p*-CHO-Ph)]$_4$ (3d). **3d** was synthesized analogously to **3a** from **1** (75 mg, 0.28 mmol) and 4-formylphenylboronic acid (41 mg, 0.27 mmol) in toluene (110 ml). The volatiles were removed under vacuum to afford a white solid. This material was redissolved in toluene (2 ml), hexane (10 ml) was added and a white precipitate formed. The solid **3d** was collected and washed with hexane. The product was dried under vacuum (46 mg, 44 %). X-ray quality crystals were grown by layering hexane onto a toluene solution of **3d** and stored at −40 °C. $^{31}P\{^1H\}$ NMR (THF-*d*$_8$): δ -6.9. ^1H NMR (THF-*d*$_8$): δ 9.92 (s, 1H, H^{11}), 7.82 (d, $^3J_{HH}$ = 8, 2H, H^9), 7.77-7.74 (m, 5H, H^2, H^4, H^8), 1.23 (s, 18H, H^6). $^{13}C\{^1H\}$ NMR (THF-*d*$_8$): δ 192.0 (s, C^{11}), 152.5 (d, $^3J_{PC}$ = 18, C^3), 150.9 (broad, C^7), 137.3 (s, C^8), 132.0 (s, C^{10}), 129.1 (s, C^9), 128.8 (d, $^4J_{PC}$ = 4, C^4), 125.9 (d, $^1J_{PC}$ = 234, C^1), 125.9 (d, $^2J_{PC}$ = 13, C^2), 35.6 (d, $^4J_{PC}$ = 2, C^5), 31.2 (s, C^6). $^{11}B\{^1H\}$

NMR (toluene-d_8): δ 3.5. HRMS (*m*/*z*): Calcd. for $[C_{84}H_{104}B_4P_4O_{16} + H]^+$ 1537.6725, Found: 1537.6785. ESI-MS (1:1 CH_2Cl_2:acetonitrile, LiCl, positive ion scan): 1543.9 ($[M + Li]^+$ = 1543.6).

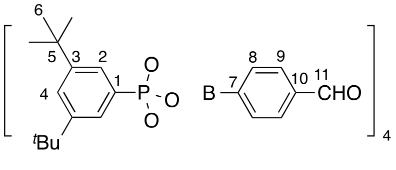

3d

Figure 4.13. NMR spectra of [(3,5-^{t}Bu$_2$-Ph)PO$_3$B(*p*-CHO-Ph)]$_4$ (**3d**)

(a) $^{31}P\{^1H\}$ NMR (THF-d_8, 202 MHz)

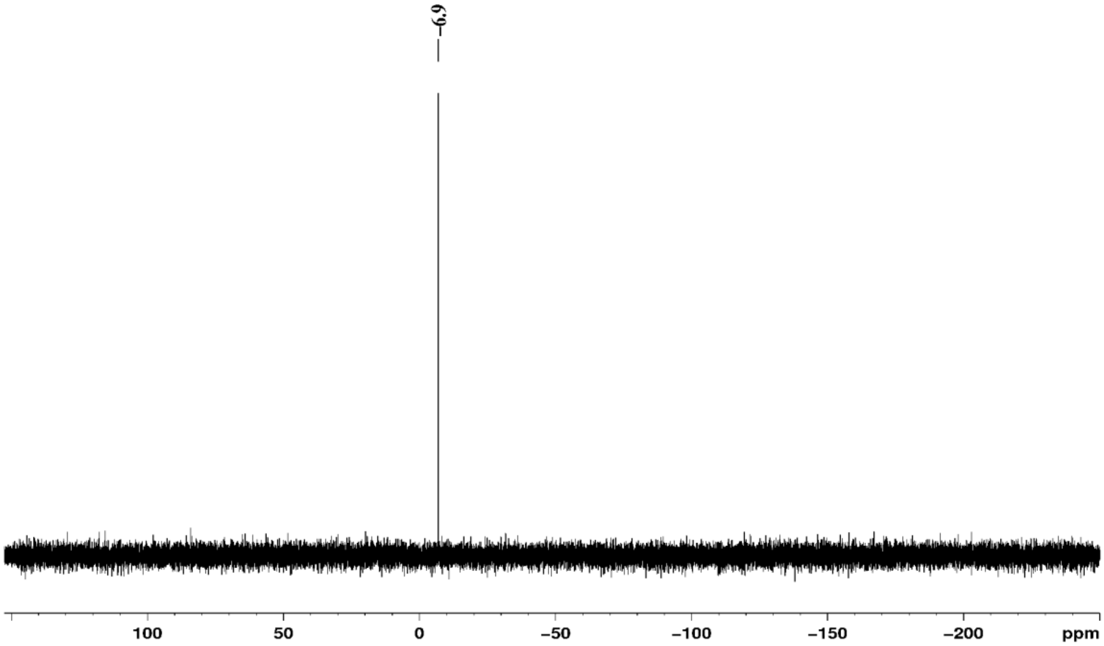

Figure 4.13, continued.

(b) ^{1}H NMR (THF-d_8, 500 MHz)

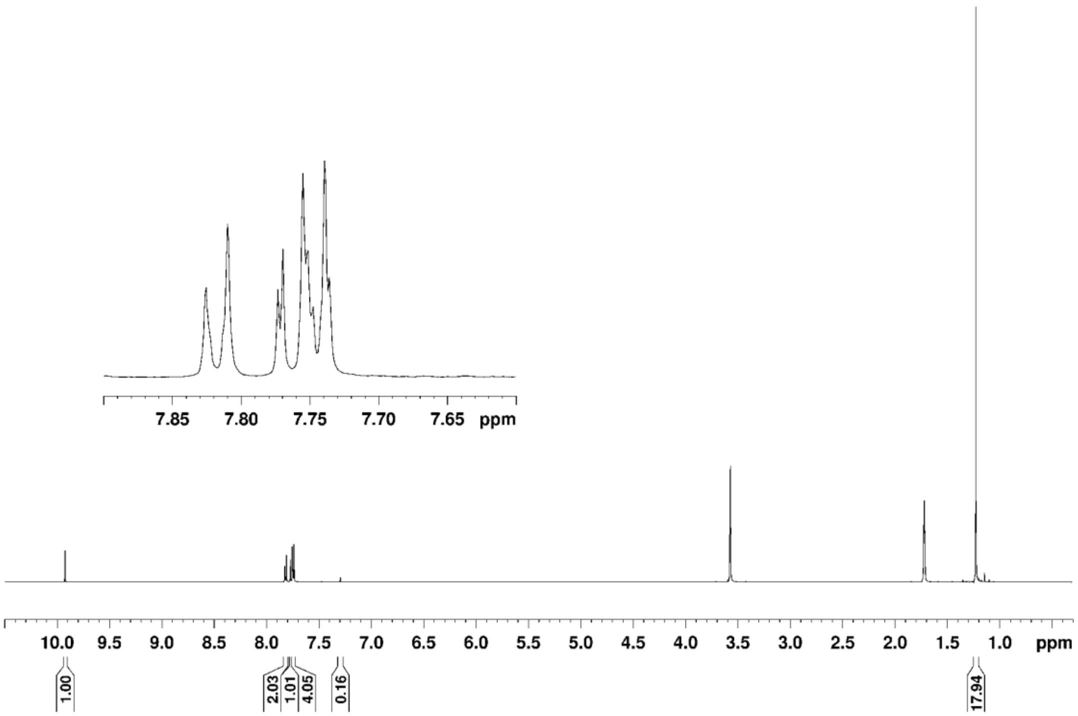

(c) ^{13}C{^{1}H} NMR (THF-d_8, 125 MHz)

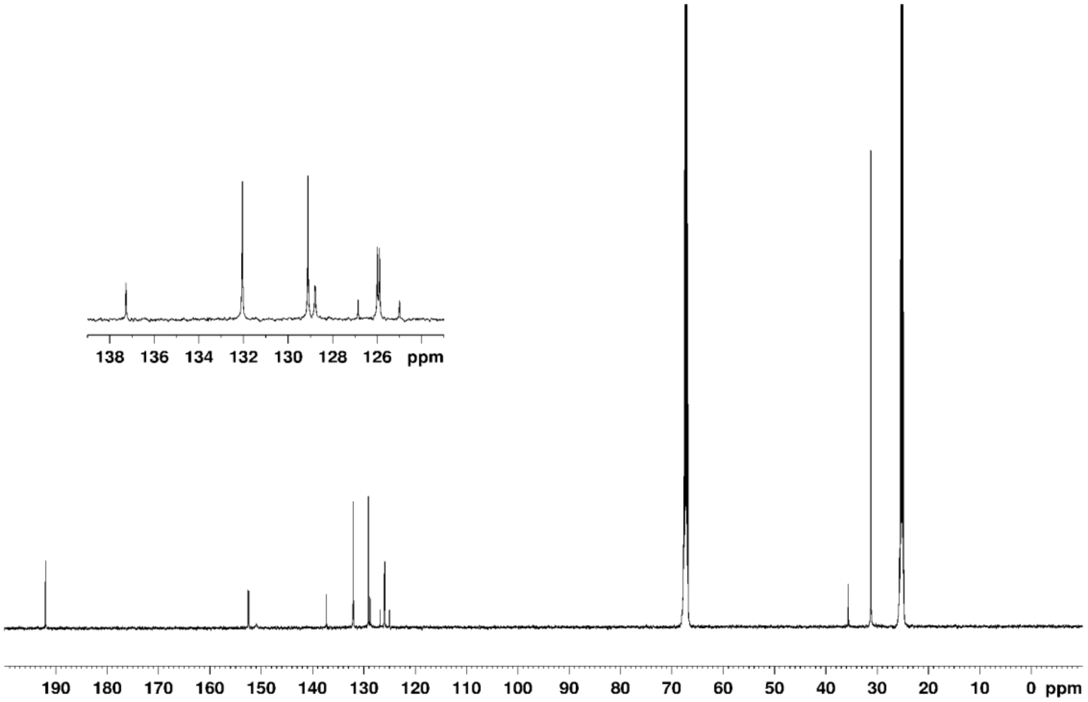

Figure 4.13, continued.

(d) $^{11}B\{^1H\}$ NMR (toluene-d_8, 128 MHz)

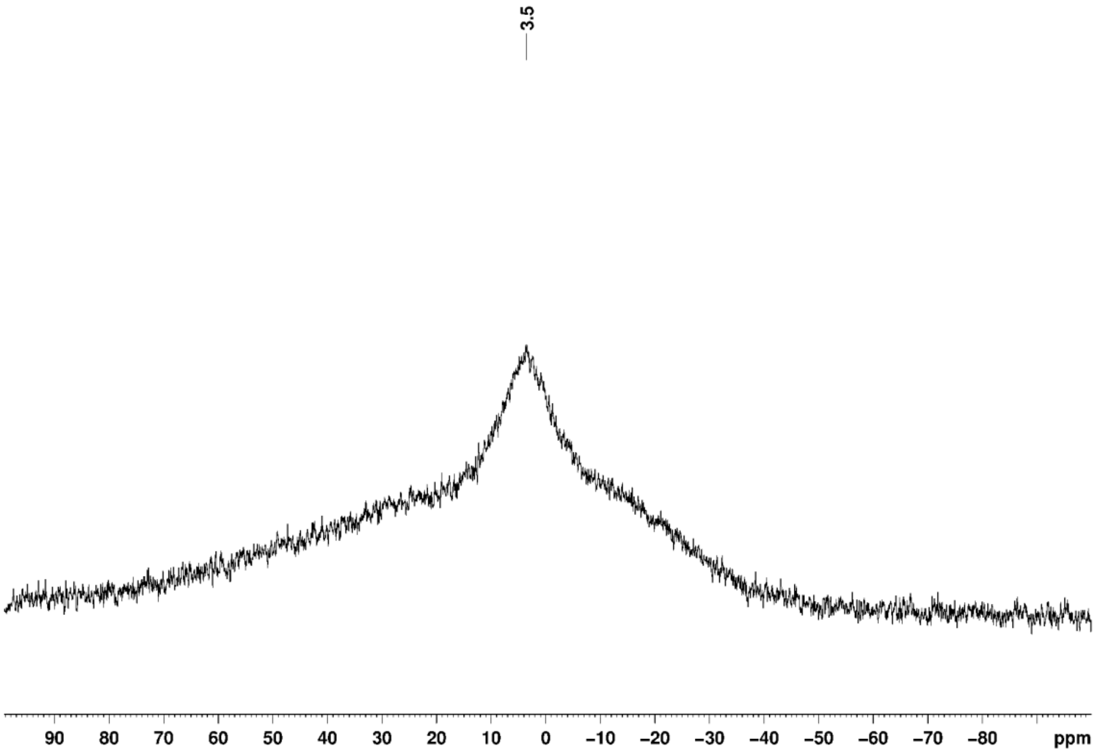

[(3,5-^{t}Bu$_2$-Ph)PO$_3$B(*p*-CHO-Ph)]$_6$ (4d). 4d was synthesized analogously to **3a** from **1** (811 mg, 3.00 mmol), 4-formylphenylboronic acid (450 mg, 3.00 mmol), and toluene (120 ml). The reaction mixture was cooled and left at room temperature for 18 h. The volatiles were removed under vacuum to afford a white solid. This material was redissolved in toluene (25 ml), hexane (20 ml) was added and a white precipitate formed. The precipitate was recrystallized from toluene to afford **4d** as white powder and dried under vacuum (410 mg, 36 %). X-ray quality crystals were grown by slow evaporating a toluene solution of **4d** at −40 °C. $^{31}P\{^1H\}$ NMR (THF-d_8): δ -1.6. ^1H NMR (THF-d_8): δ 9.72 (s, 1H, H^{11}), 7.51 (d, $^3J_{HH}$ = 8, 2H, H^9), 7.44-7.41 (m, 3H, H^2 and H^4), 7.35 (d, $^3J_{HH}$ = 8, 2H, H^8), 1.14 (s, 18H, H^6). $^{13}C\{^1H\}$ NMR (THF-d_8): δ 191.7 (s, C^{11}), 151.5 (d, $^3J_{PC}$ = 17, C^3), 149.8 (broad, C^7), 136.5 (s, C^8), 132.1 (s, C^{10}), 128.7 (s, C^9), 128.0 (d, $^4J_{PC}$ = 3, C^4), 125.9

(d, ${}^1J_{PC}$ = 214, C^1), 125.6 (d, ${}^2J_{PC}$ = 12, C^2), 35.2 (d, ${}^4J_{PC}$ = 2, C^5), 31.2 (s, C^6). ${}^{11}B\{{}^1H\}$ NMR (toluene-d_8): δ 4.1. HRMS (m/z): Calcd. for $[C_{126}H_{156}B_6P_6O_{24} + H]^+$ 2306.0049, Found: 2306.0107.

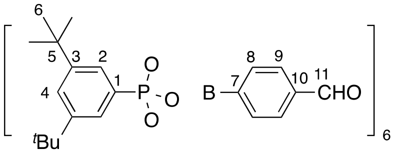

4d

Figure 4.14. NMR spectra of $[(3,5\text{-}{}^tBu_2\text{-}Ph)PO_3B(p\text{-}CHO\text{-}Ph)]_6$ (**4d**)

(a) ${}^{31}P\{{}^1H\}$ NMR (THF-d_8, 202 MHz)

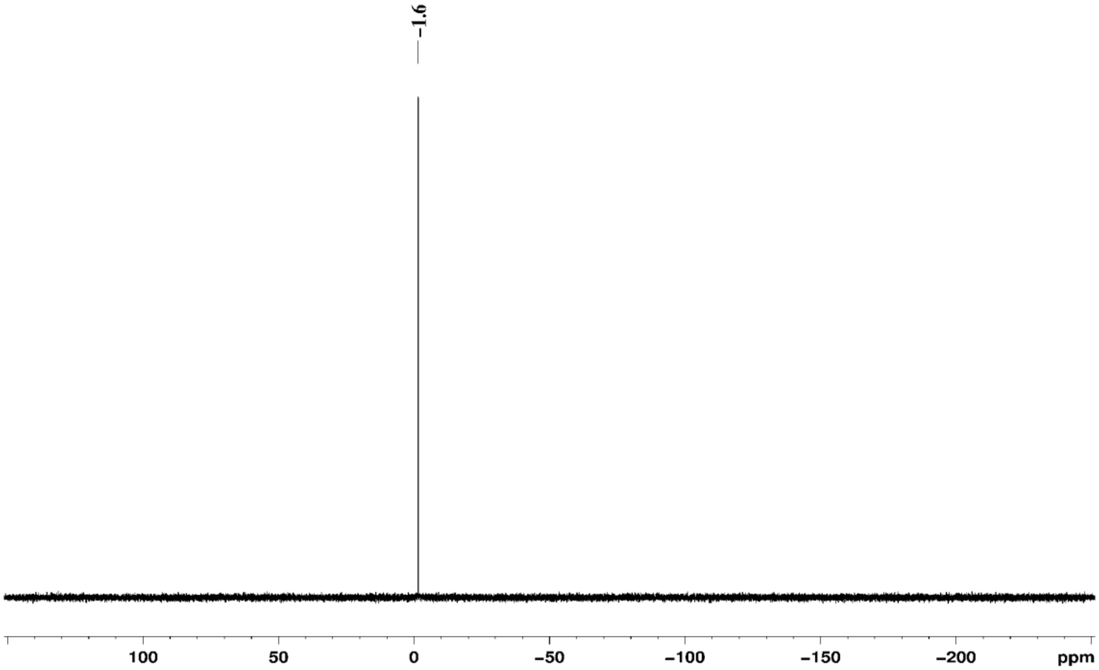

Figure 4.14, continued.

(b) ^{1}H NMR (THF-d_8, 500 MHz)

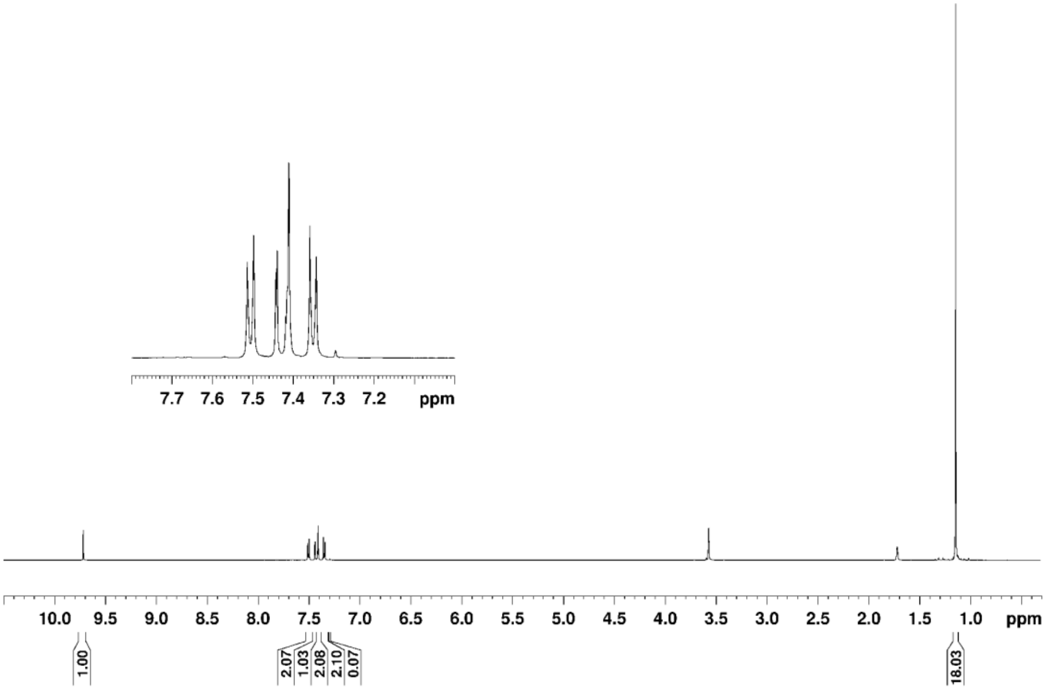

(c) ^{13}C{^{1}H} NMR (THF-d_8, 125 MHz)

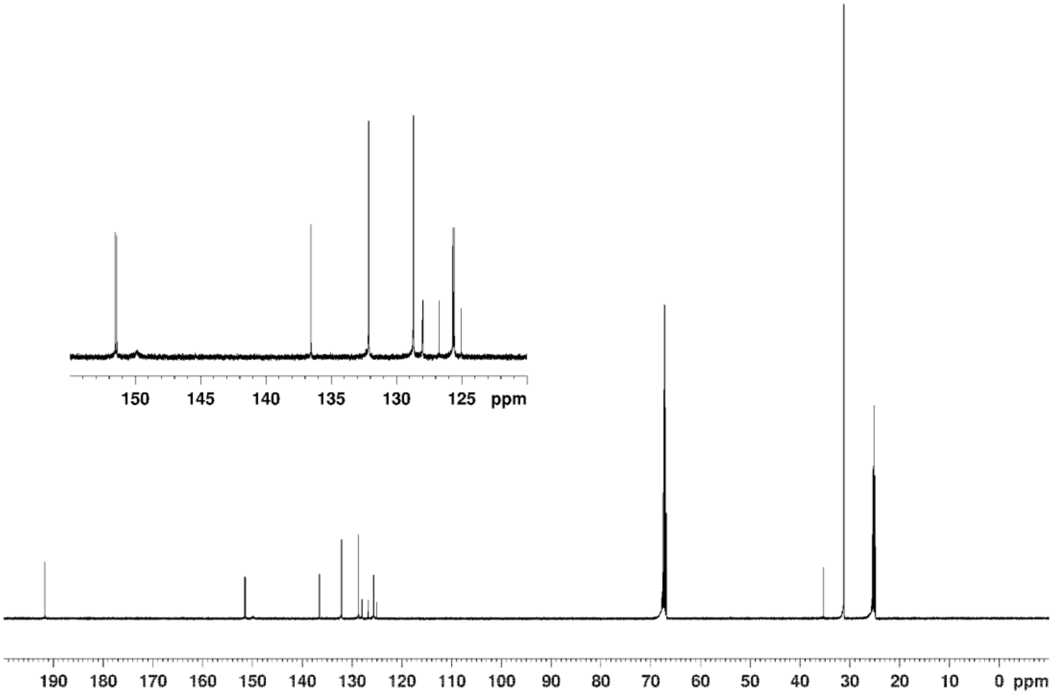

Figure 4.14, continued.

(d) ^{11}B{^{1}H} NMR (toluene-*d*$_8$, 128 MHz)

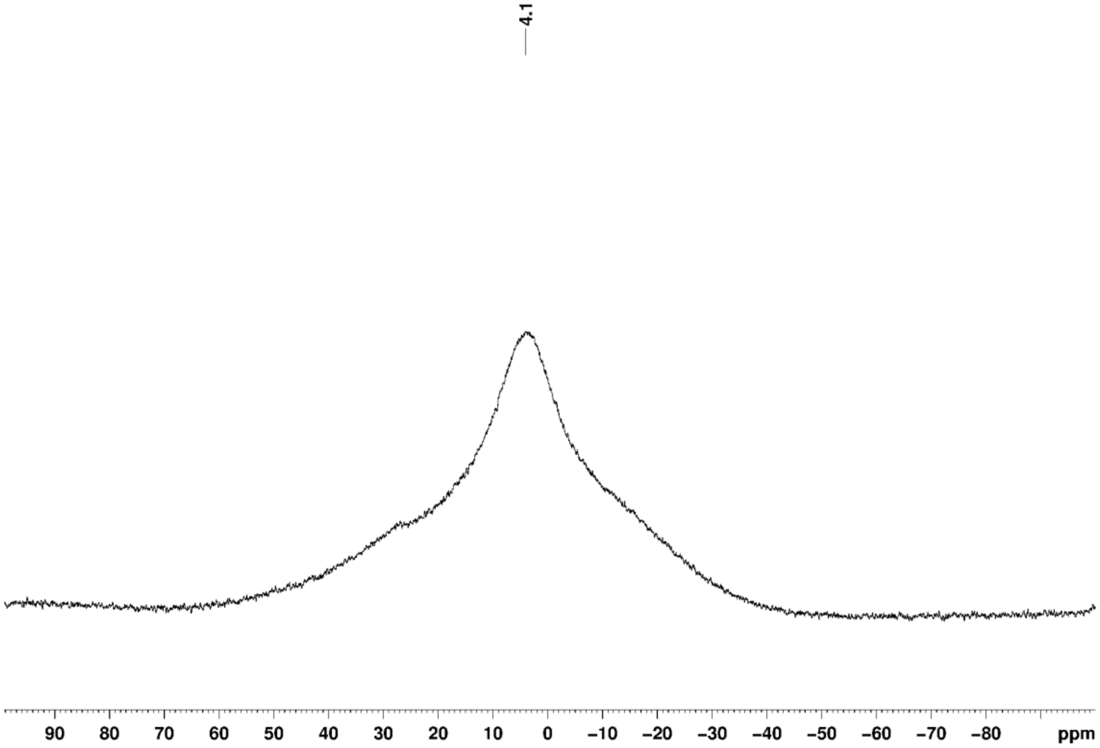

[(2-PPh$_2$-Ph)PO$_3$B(*p*-CF$_3$-Ph)]$_4$ (7c). 7c was synthesized analogously to **3a** from **6** (103 mg, 0.301 mmol) and 4-(trifluoromethyl)phenylboronic acid (57 mg, 0.30 mmol) in toluene (12 ml). The volatiles were removed under vacuum to afford a yellow solid. This material was recrystallized by dissolving it in hot toluene and letting the solution cool when hexane was diffused in to afford **7c** as a white powder, which was dried under vacuum (60 mg, 40 %). ^{31}P{^{1}H} NMR (THF-*d*$_8$): δ -9.9, -15.1. ^{1}H NMR (THF-*d*$_8$): δ 7.81 (dd, $^{3}J_{PH}$ = 16, $^{3}J_{HH}$ = 8; 1H, H^{2}), 7.53 (dt, $^{3}J_{HH}$ = 8, $^{4}J_{PH}$ = 2; 1H, H^{4}), 7.41 (t, $^{3}J_{PH}$ = $^{3}J_{HH}$ = 7, 1H, H^{5}), 7.40 – 7.32 (m, 3H; H^{3} and H^{12}), 7.12 (t, $^{3}J_{HH}$ = 7, 2H, H^{10}), 7.06 (d, $^{3}J_{HH}$ = 8, 2H, H^{13}), 6.92 (t, $^{3}J_{HH}$ = 8, 4H, H^{9}), 6.77 (t, $^{3}J_{PH}$ = $^{3}J_{HH}$ =7, 4H, H^{8}). ^{13}C{^{1}H} NMR (THF-*d*$_8$): δ 147.7 (broad, C^{11}), 143.3 (m, C^{6}), 138.6 (d, $^{2}J_{PC}$ = 19, C^{5}), 138.0 (d, $^{3}J_{PC}$ = 14, C^{3}), 133.9 (m, J_{PC} is obscured due to overlap, C^{2}, C^{4}, C^{8}), 133.6 (dd, $^{1}J_{PC}$ =

236, $^{2}J_{PC}$ = 36; C^{1}), 132.3 (s, C^{12}), 129.8 (d, $^{1}J_{PC}$ = 17, C^{7}), 129.1 (q, $^{2}J_{FC}$ = 31, C^{14}), 128.7 (m, J_{PC} is obscured due to overlap, C^{9}, C^{10}), 125.7 (q, $^{1}J_{FC}$ = 272, C^{15}), 124.3 (q, $^{3}J_{FC}$ = 4, C^{13}). ^{19}F{^{1}H} NMR (THF-d_8): δ -62.5. ^{11}B{^{1}H} NMR (toluene-d_8): δ 3.4. HRMS (*m*/*z*): Calcd. for [$C_{100}H_{72}B_4P_8O_{12}F_{12}$ + H]$^+$ 1985.3184, Found: 1985.3161.

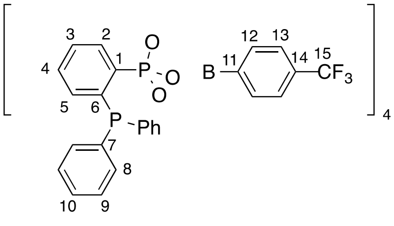

7c

Figure 4.15. NMR spectra of [(2-PPh$_2$-Ph)PO$_3$B(*p*-CF$_3$-Ph)]$_4$ (**7c**)

(a) ^{31}P{^{1}H} NMR (THF-d_8, 202 MHz)

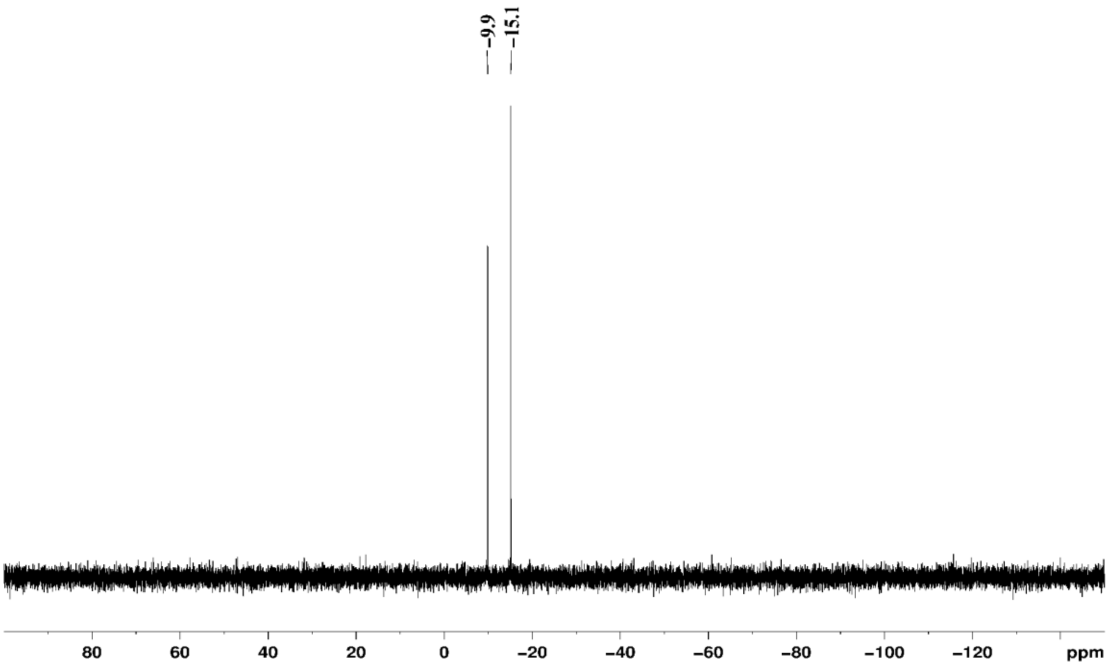

Figure 4.15, continued.

(b) ^{1}H NMR (THF-d_8, 500 MHz)

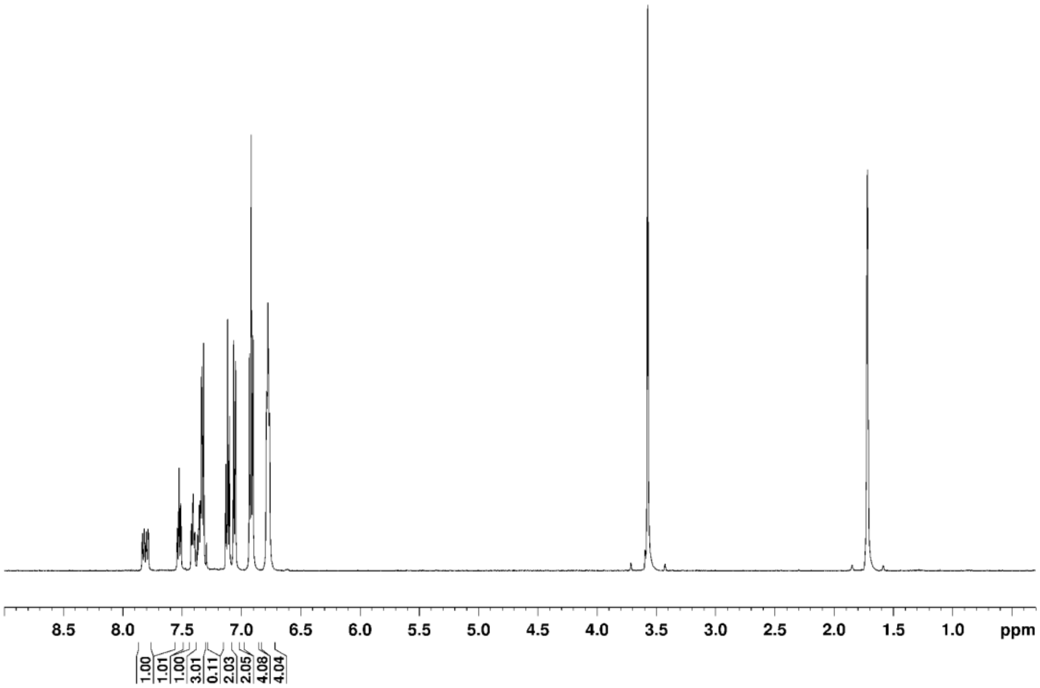

(c) ^{13}C{^{1}H} NMR (THF-d_8, 125 MHz)

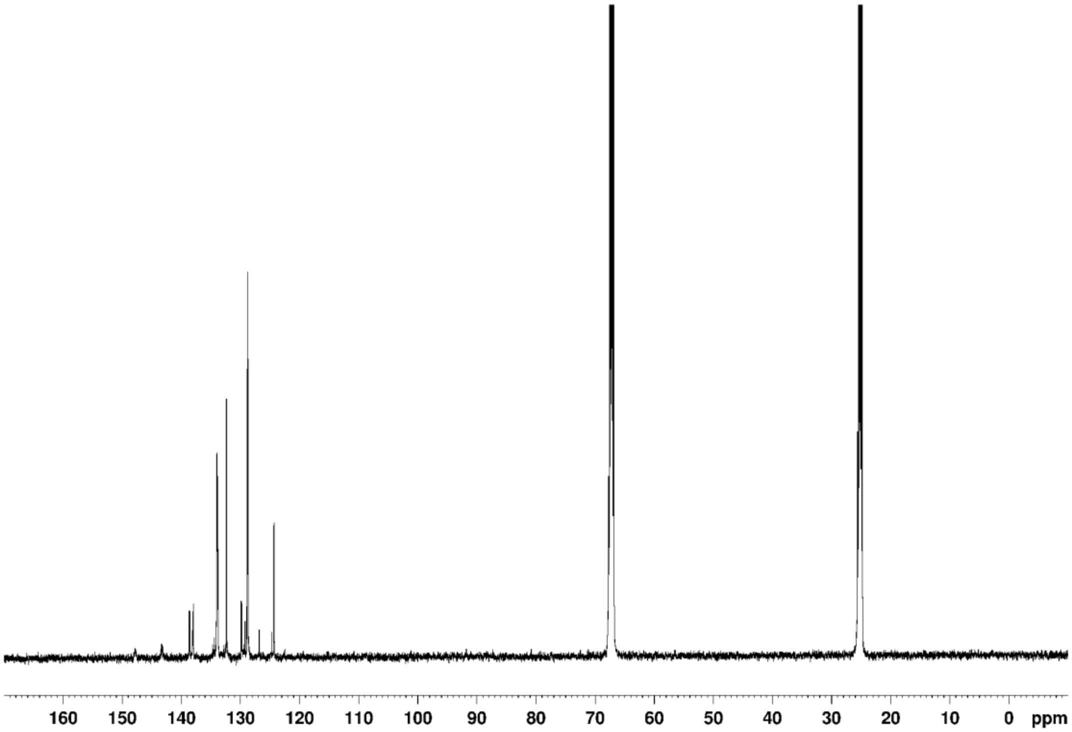

Figure 4.15, continued.

(d) $^{19}F\{^1H\}$ NMR in (THF-d_8, 470 MHz)

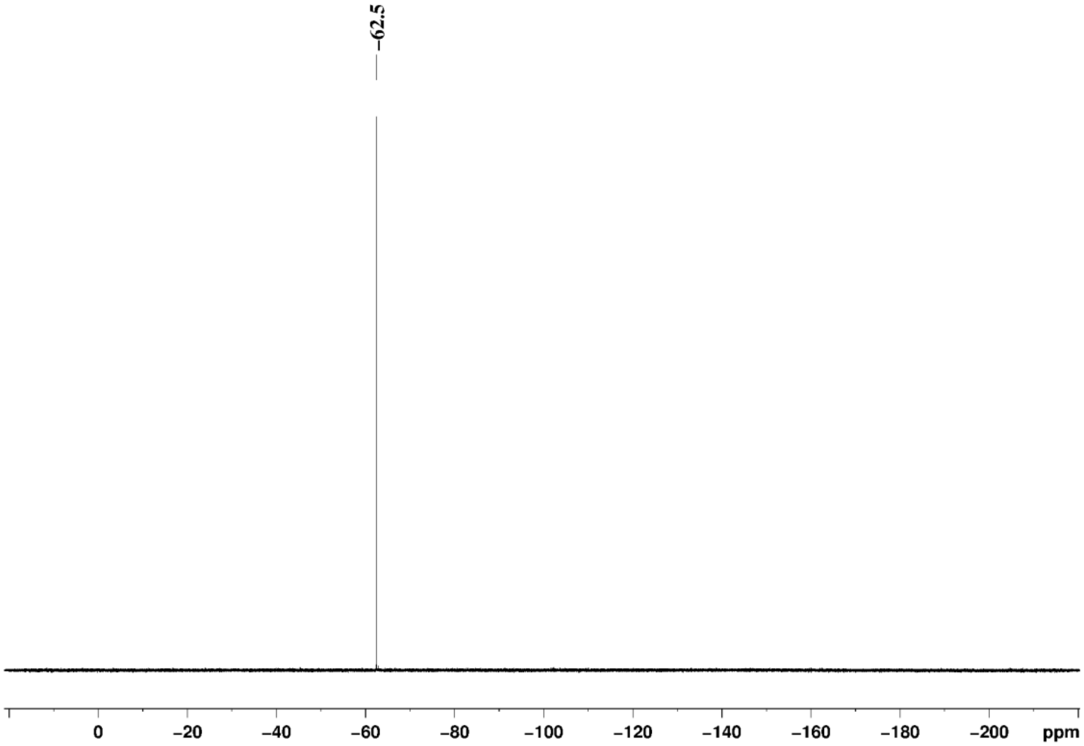

(e) $^{11}B\{^1H\}$ NMR (toluene-d_8, 128 MHz)

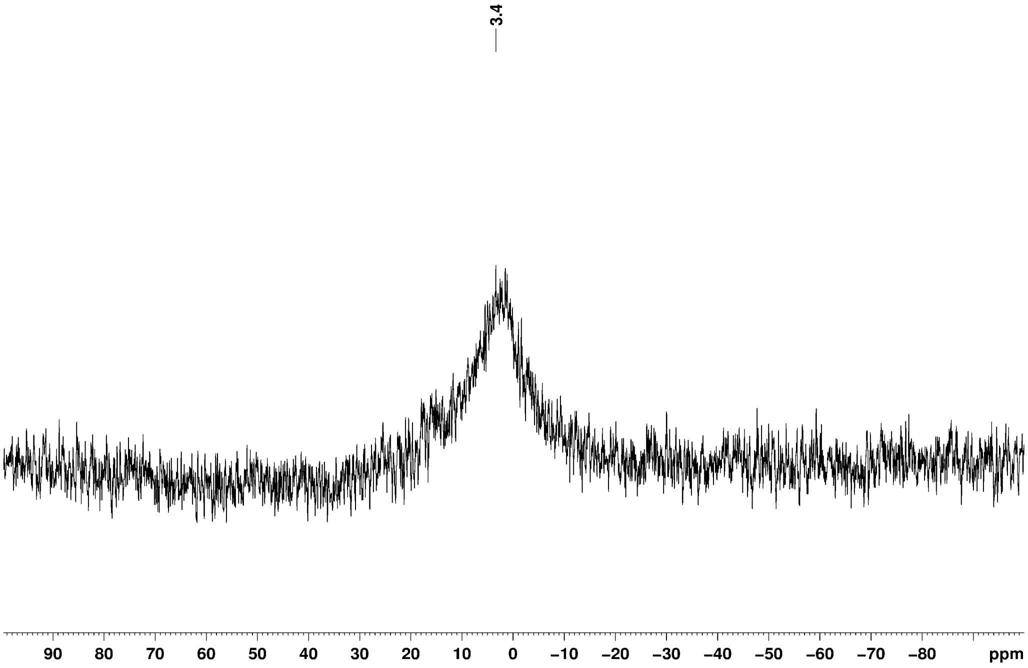

[(2-PPh$_2$-Ph)PO$_3$B(*p*-CHO-Ph)]$_4$ (7d). 7d was synthesized analogously to **3a** from **6** (103 mg, 0.301 mmol) and 4-formylphenylboronic acid (45 mg, 0.30 mmol) in toluene (12 ml). The volatiles were removed under vacuum to afford a white solid. This material was recrystallized from hot toluene to afford **7d** as a white powder, which was dried under vacuum (46 mg, 34 %). ^{31}P{^{1}H} NMR (THF-*d$_8$*): δ -9.7, -14.9. ^{1}H NMR (THF-*d$_8$*): δ 9.85 (s, 1H, H^{15}), 7.80 (dd, $^{3}J_{PH}$ = 17, $^{3}J_{HH}$ = 8; 2H, H^{2}), 7.51 (t, $^{3}J_{HH}$ = 8, 1H, H^{4}), 7.42 (t, $^{3}J_{PH}$ = $^{3}J_{HH}$ = 6, 1H, H^{5}), 7.37 (d, $^{3}J_{HH}$ = 8, 2H, H^{13}), 7.34 – 7.30 (m, 3H, H^{3} and H^{12}), 7.09 (t, $^{3}J_{HH}$ = 7, 2H, H^{10}), 6.88 (t, $^{3}J_{HH}$ = 8, 4H, H^{9}), 6.78 (t, $^{3}J_{PH}$ = $^{3}J_{HH}$ = 6, 4H, H^{8}). ^{13}C{^{1}H} NMR (THF-*d$_8$*): δ 192.3 (s, C^{15}), 143.4 (m, C^{6}), 138.6 (d, $^{2}J_{PC}$ = 19, C^{5}), 138.2 (d, $^{3}J_{PC}$ = 15, C^{3}), 136.6 (s, C^{12}), 134.1 (dd, $^{1}J_{PC}$ = 231, $^{2}J_{PC}$ = 50; C^{1}), 133.9 (m, J_{PC} is obscured due to overlap, C^{2}, C^{4}, C^{8}), 132.5 (s, C^{14}), 129.8 (d, $^{1}J_{PC}$ = 17, C^{7}), 128.7 (m, J_{PC} is obscured due to overlap, C^{9}, C^{10}), 128.7 (s, C^{13}), C^{11} resonance is not observed. ^{11}B{^{1}H} NMR (toluene-*d$_8$*): δ 2.5. HRMS (*m*/*z*): Calcd. for [$C_{100}H_{76}B_4P_8O_{16}$ + H]$^+$ 1825.3485, Found: 1825.3476. ESI-MS (1:1 CH_2Cl_2:acetonitrile, LiCl, positive ion scan): 1831.5 ([M + Li]$^+$ = 1831.3).

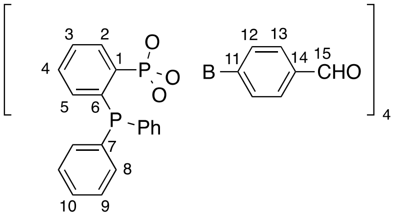

7d

Figure 4.16. NMR spectra of [(2-PPh$_2$-Ph)PO$_3$B(*p*-CHO-Ph)]$_4$ (**7d**)

(a) $^{31}P\{^1H\}$ NMR (THF-*d*$_8$, 202 MHz)

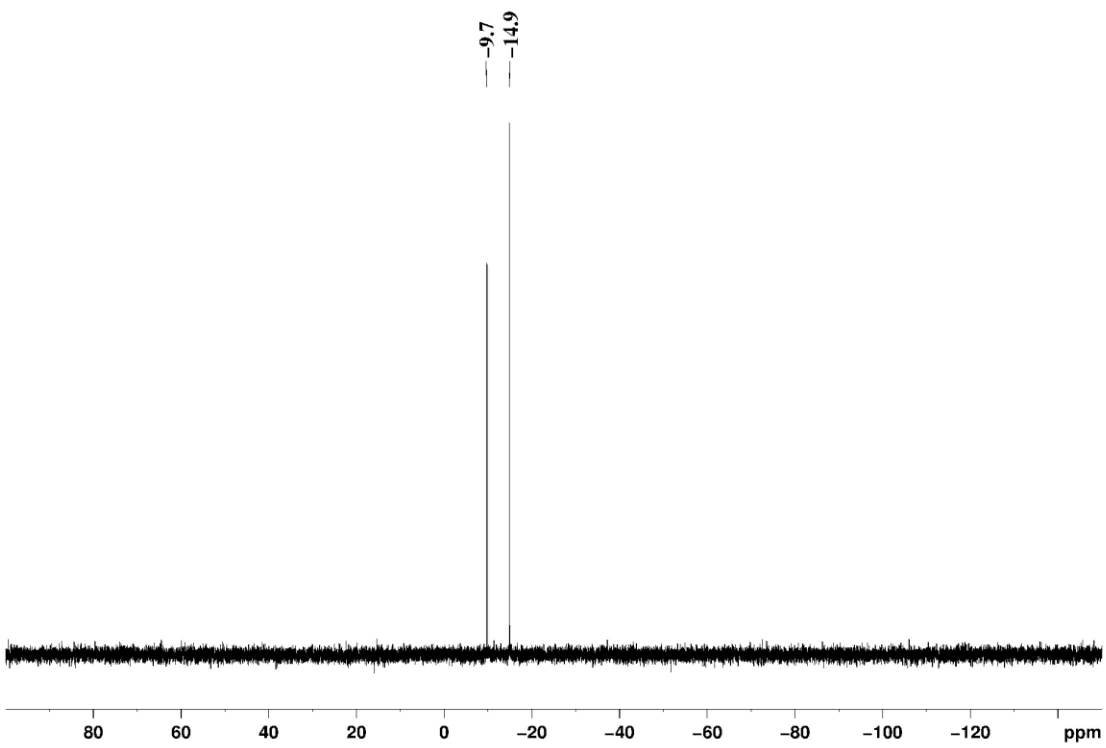

(b) ^1H NMR (THF-*d*$_8$, 500 MHz)

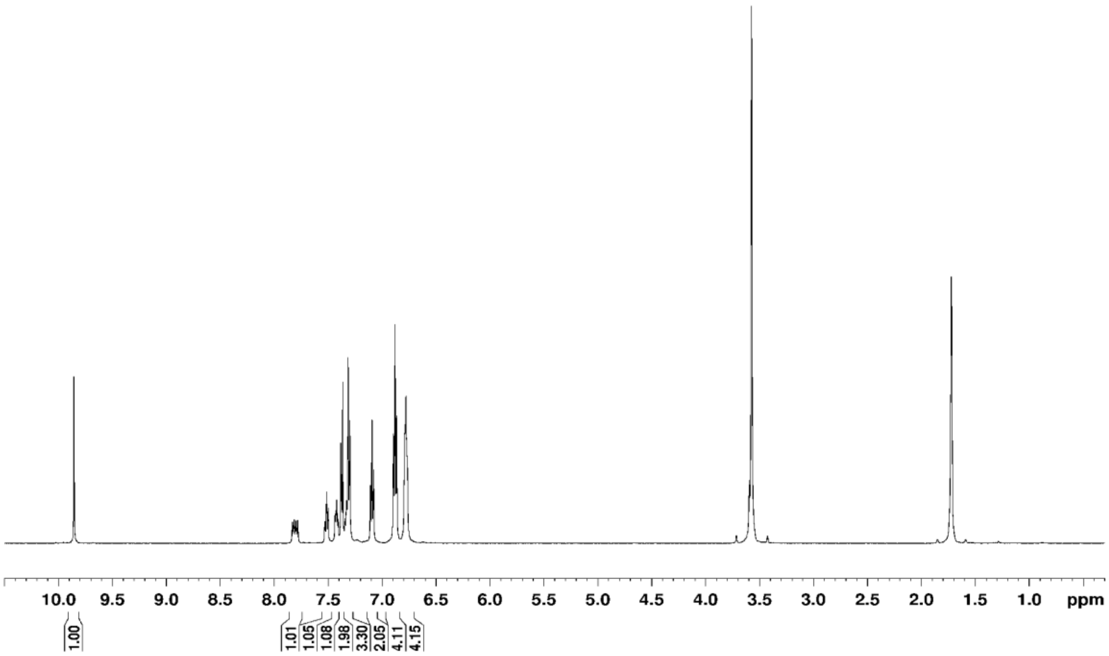

Figure 4.16, continued.

(c) $^{13}C\{^1H\}$ NMR (THF-d_8, 100 MHz)

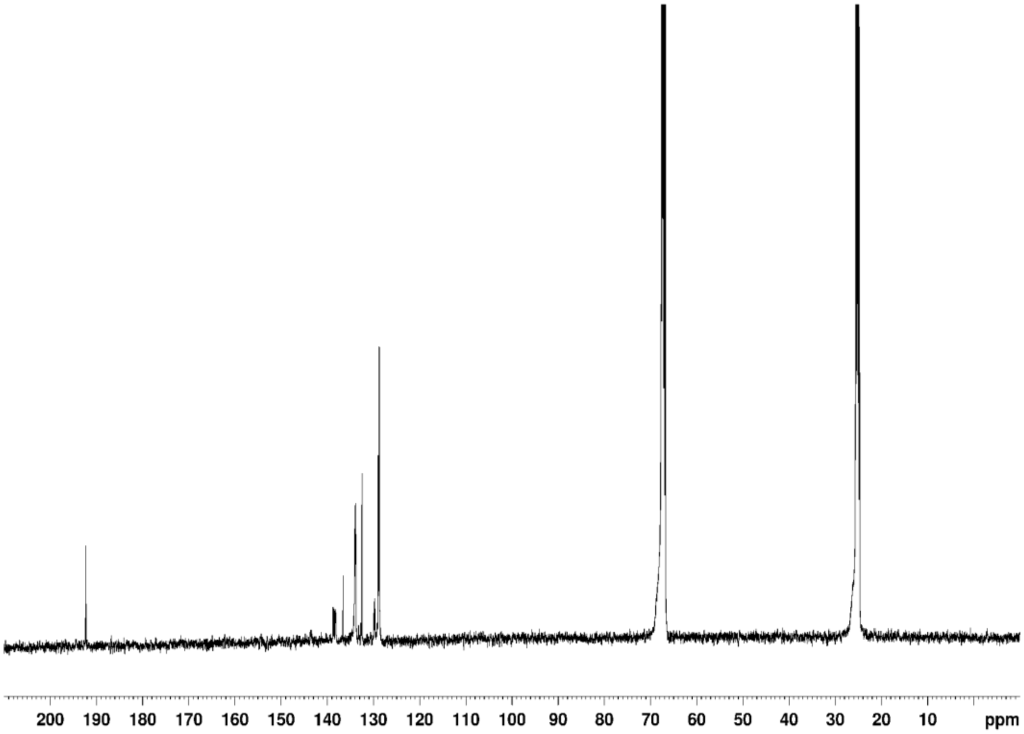

(d) $^{11}B\{^1H\}$ NMR (toluene-d_8, 128 MHz)

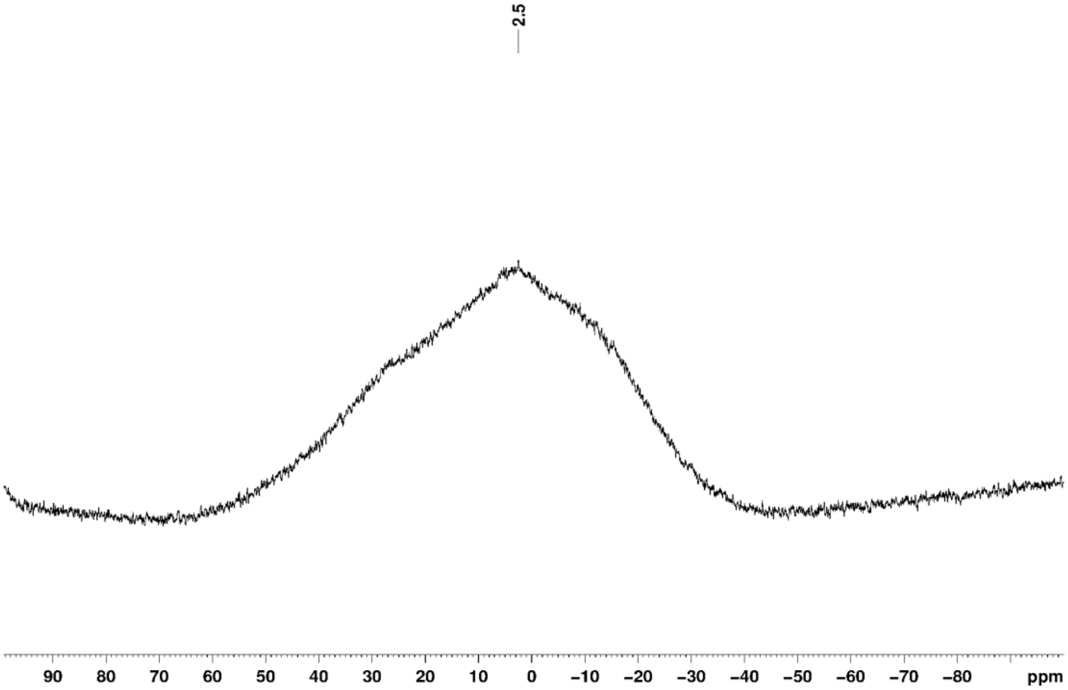

[^{t}BuPO$_3$B(*p*-Br-Ph)]$_4$ (8). **8** was synthesized analogously to **3a** from tert-butylphosphonic acid (0.73 g, 5.3 mmol) and 4-bromo-phenylboronic acid (1.1 g, 5.3 mmol) in toluene (120 ml). The volatiles were removed under vacuum to afford a yellow solid. The crude product was washed with hexanes (60 ml) and recrystallized from toluene/hexanes solution at -40 ˚C to afford **8** as a white solid. The solid was washed with hexane and dried under vacuum (1.2 g, 74 %). ^{31}P{^{1}H} NMR (C_6D_6): δ 9.6. ^{1}H NMR (C_6D_6): δ 7.62 (d, $^3J_{HH}$ = 7, 2H), 7.56 (d, $^3J_{HH}$ = 7, 2H, H), 1.22 (d, $^3J_{PH}$ = 19, 9H).

Figure 4.17. NMR Spectra of **8**

(a) ^{31}P{^{1}H} NMR (C_6D_6, 202 MHz)

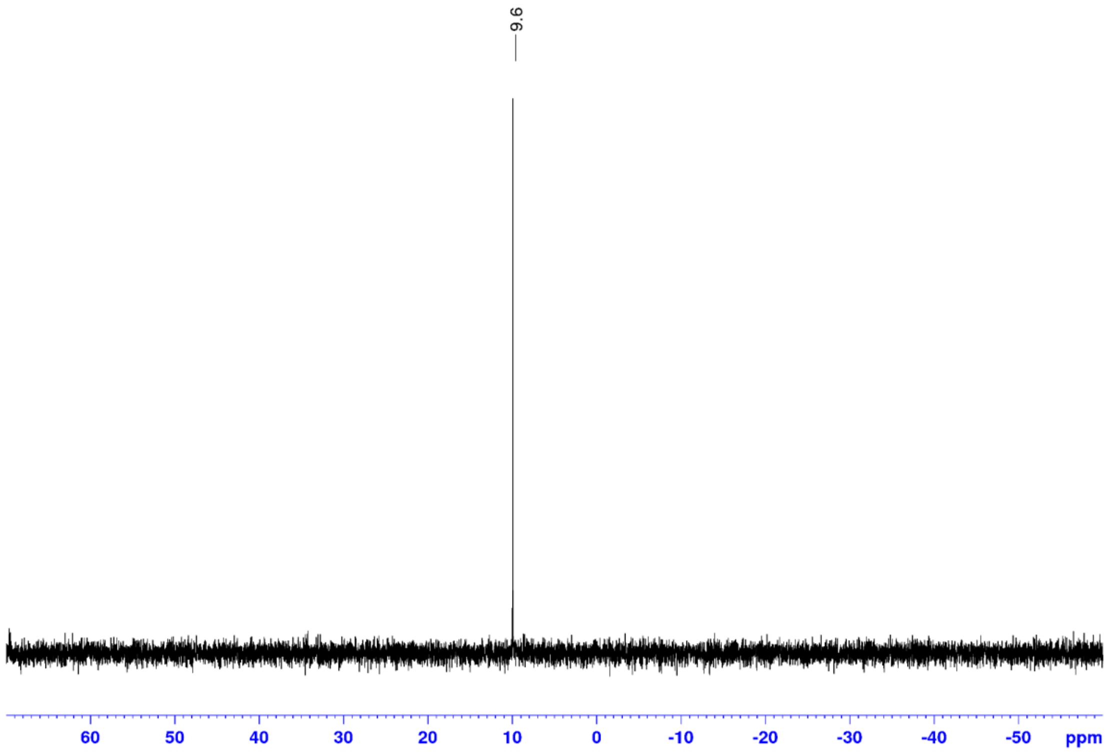

Figure 4.17, continued.

(b) ^{1}H NMR (C_6D_6, 500 MHz)

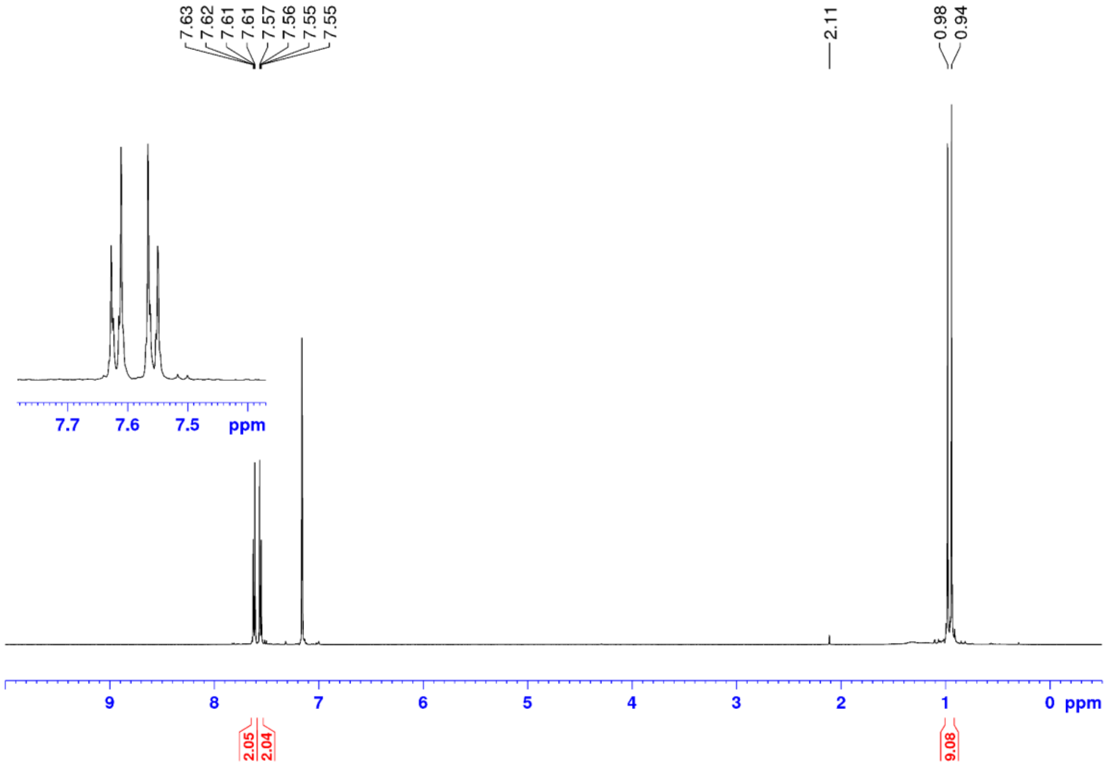

The reaction of (3,5-^{t}Bu$_2$-Ph)P(O)(OH)$_2$ (1) with PhB(OH)$_2$ (2e). A Schlenk flask equipped with Dean-Stark trap was charged with **1** (81 mg, 0.30 mmol), **2e** (37 mg, 0.30 mmol), and toluene (120 ml). The mixture was refluxed for 3 h. A sample of the reaction mixture (1 ml) was transferred to a J-Young NMR tube and the volatiles were removed under vacuum. C_6D_6 was added to obtain the NMR spectra. The rest of the reaction mixture was taken to dryness under vacuum to afford a white solid.

The reaction of 1 with (*p*-tolyl)B(OH)$_2$ (2f). The reaction was conducted analogously to that described above with **1** (54 mg, 0.20 mmol), **2f** (27 mg, 0.20 mmol), and toluene (60 ml). A sample of the reaction mixture (1 ml) was transferred to a J-Young NMR tube and the volatiles were removed under vacuum. C_6D_6 was added to obtain the NMR spectra. The rest of the reaction mixture was taken to dryness under vacuum to afford a white solid.

The reaction of (2-PPh_2-Ph)P(O)$(OH)_2$ (6) with 2f. The reaction was conducted analogously to that described above with **1** (137 mg, 0.40 mmol), **2f** (54 mg, 0.40 mmol), and toluene (120 ml). A sample of the reaction mixture (1 ml) was transferred to a J-Young NMR tube and the volatiles were removed under vacuum. C_6D_6 was added to obtain the NMR spectra. The rest of the reaction mixture was taken to dryness under vacuum to afford a white solid.

The reaction of 1 with (*o*-CF_3-Ph)boroxine (5b). The reaction was conducted analogously to that described above with **1** (57 mg, 0.21 mmol), **5b** (36 mg, 0.070 mmol), and toluene (12 ml). A sample of the reaction mixture (1 ml) was transferred to a J-Young NMR tube and the volatiles were removed under vacuum. C_6D_6 was added to obtain the NMR spectra. The rest of the reaction mixture was taken to dryness under vacuum to afford a white solid.

The reaction of 1 with *p*-tolylboroxine (5f). The reaction was conducted analogously to that described above with **1** (81 mg, 0.30 mmol), **5f** (36 mg, 0.10 mmol), and toluene (90 ml). A sample of the reaction mixture (1 ml) was transferred to a J-Young NMR tube and the volatiles were removed under vacuum. C_6D_6 was added to obtain the NMR spectra. The rest of the reaction mixture was taken to dryness under vacuum to afford a white solid.

The reaction of 6 with (*o*-CF_3-Ph)B$(OH)_2$ (2b). The reaction was conducted analogously to that described above with **6** (103 mg, 0.30 mmol), **2b** (57 mg, 0.30 mmol), and toluene (12 ml). A sample of the reaction mixture (1 ml) was transferred to a J-Young NMR tube and the volatiles were removed under vacuum. C_6D_6 was added to obtain the NMR spectra. The rest of the reaction mixture was taken to dryness under vacuum to afford a white solid.

The self-condensation of 1. A Schlenk flask equipped with a Dean-Stark trap was charged with **1** (23 mg, 0.085 mmol) and toluene (15 ml). The mixture was refluxed overnight. A sample of the reaction mixture (1 ml) was transferred to a J-Young NMR tube and the volatiles were removed under vacuum. C_6D_6 was added to obtain the NMR spectra. The rest of the reaction mixture was taken to dryness under vacuum to afford a white solid.

The reaction of 3a with RLi and Ph_2PCl. A Schlenk flask was charged with 1.0 equiv of **3a** and THF, and cooled to -78 °C. RLi solution (R = ^{n}Bu, 2.5 M in hexanes, 4.0 equiv; R = Me, 1.6 M in diethyl ether, 4.0 equiv; R = ^{t}Bu, 1.7 M in pentane, 8.0 equiv) was added via syringe. The mixture was stirred at -78 °C for 1 h and Ph_2PCl (4.0 equiv) was added. The mixture was stirred at room temperature for 18 h to yield a clear yellow solution. A sample of the reaction mixture (1 ml) was transferred to a J-Young NMR tube and the volatiles were removed under vacuum. THF-d_8 was added and NMR spectra and HRMS data were obtained. These data show low conversion of **3a**. Although the functionalization of **3a** was unsuccessful, these data indicate that borophosphonate cage is stable to the strongly nucleophilic and basic alkyl lithium reagent. Data from the experiment with ^{n}BuLi and 1 h lithiation time are provided below.

Figure 4.18. NMR Spectra of the reaction mixture of **3a** with ^{n}BuLi and Ph$_2$PCl

(a) ^{31}P{^{1}H} NMR (THF-d_8, 202 MHz): δ 34.7 (d, $^{1}J_{PP}$ = 21 Hz) and -23.7 (d, $^{1}J_{PP}$ = 21 Hz) = Ph$_2$(O=)P-PPh$_2$

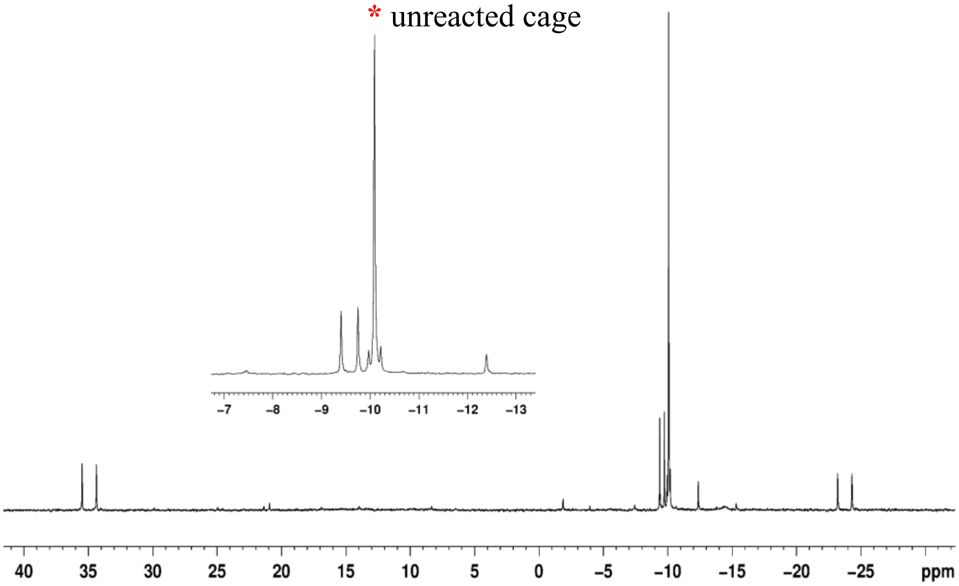

Figure 4.18, continued.

(b) HMRS (APCI-MS, positive, 0 V)

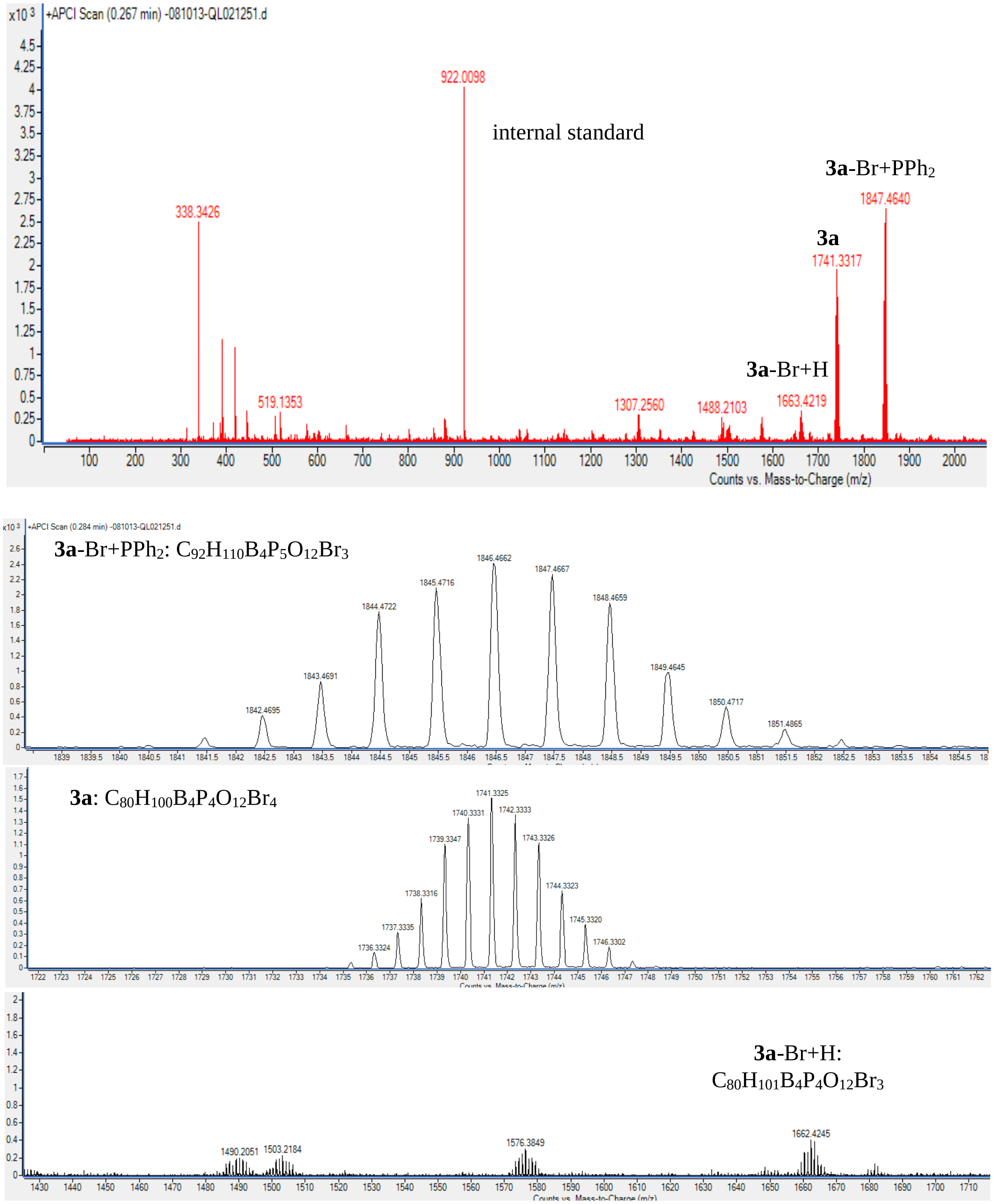

The reaction of 8 with ^{n}BuLi and Ph_2PCl. A Schlenk flask was charged **8** (0.30 g, 0.25 mmol) and THF (8 mL), and cooled to -78 °C. ^{n}BuLi (2.5 M in hexanes, 0.40 mL, 1.0 mmol) was added via syringe over 5 min. The mixture was stirred at -78 °C for 1 h (or 18 h) and Ph_2PCl (0.18 mL, 1.0 mmol) was added. The mixture was stirred at room temperature for 18 h to yield a clear yellow solution. A sample of the reaction mixture (1 ml) was transferred to a J-Young NMR tube. The volatiles were removed under vacuum to afford a yellow solid. C_6D_6 or THF-d_8 was added, and NMR spectra and HRMS data were obtain. These data show that **8** was successfully coverted to the fully Ph_2P-functionalized cage in 68 % yield, with 86 % overall Ph_2P installation based on ${}^{31}P\{{}^{1}H\}$ NMR.

Figure 4.19. NMR Spectra of the reaction mixture of **8** with ^{n}BuLi and Ph_2PCl

(a) ${}^{31}P\{{}^{1}H\}$ NMR (THF, 202 MHz)

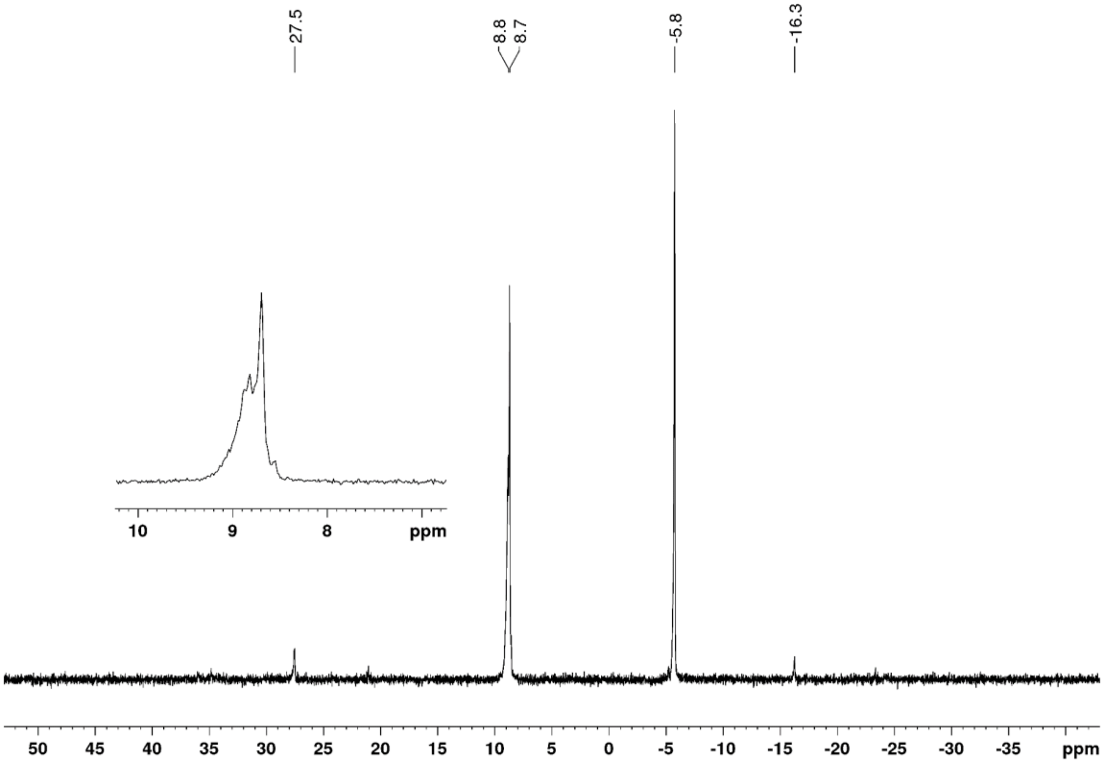

Figure 4.19, continued.

(b) HMRS (APCI-MS, positive, 0 V):

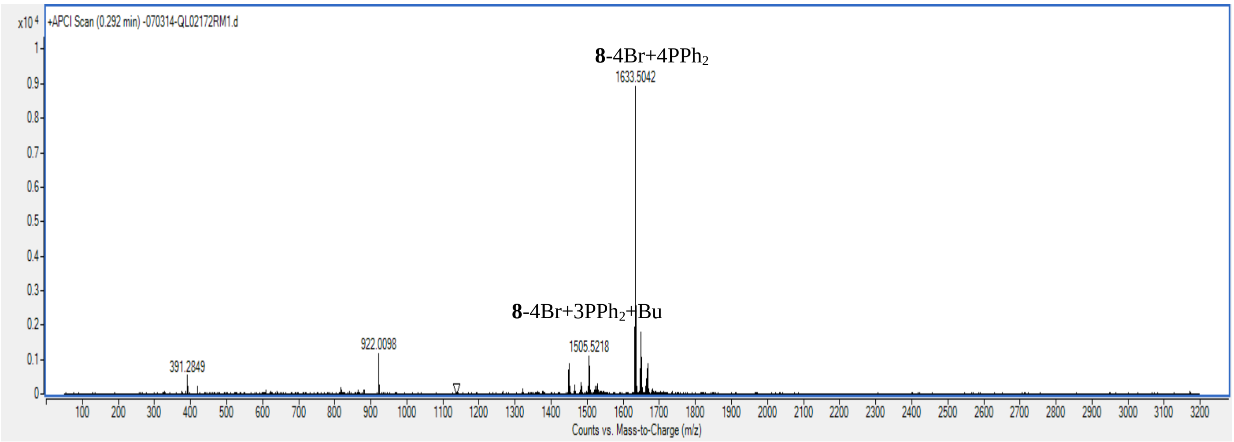

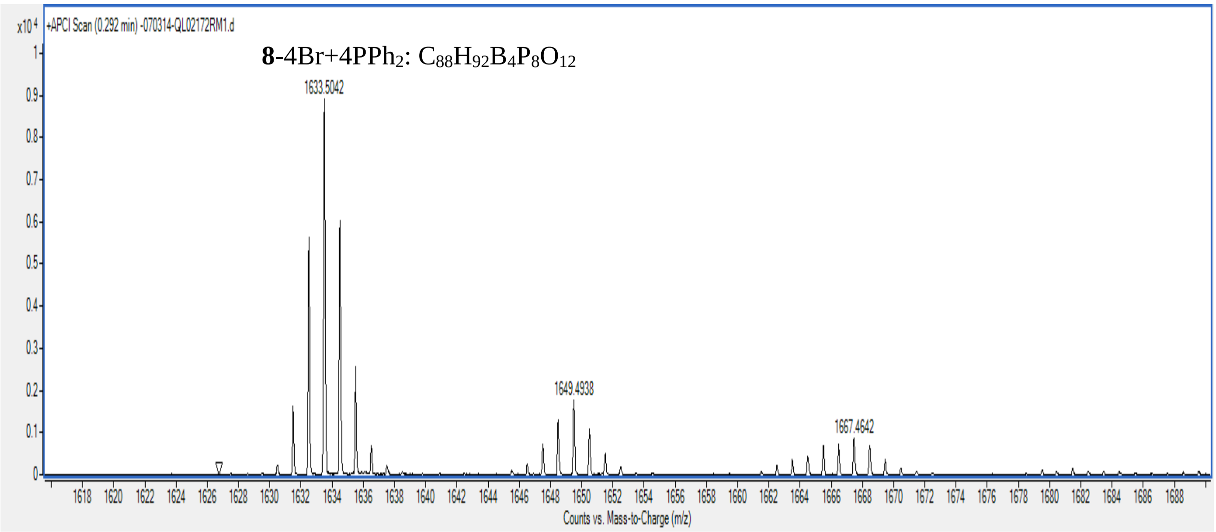

Interconversion of 4c and 3c. Two J-Young NMR tubes were charged with **4c** (2.7 mg and 3.3 mg, respectively) and toluene-*d*$_8$ (0.5 ml) and sealed under nitrogen in glove box. The tubes were brought out of glove box and heated in a 105 °C oil bath. NMR spectra were obtained periodically at room temperature. Equilibrium was reached after 3 weeks. The equilibrium constant $K_{eq} = [\mathbf{3c}]^3/[\mathbf{4c}]^2 = 2.4(1) \times 10^{-3}$ M. The tubes were cooled back to room temperature and

NMR spectra were obtained periodically. Equilibrium was reached after 4 weeks. The equilibrium constant $K_{eq} = [\mathbf{3c}]^3/[\mathbf{4c}]^2 = 1.2(1) \times 10^{-3}$ M.

The interconversion of **4c** and **3c** is shown in Scheme 4.9. In the following calculations, [P] is the total phosphorus concentration.

Scheme 4.9.

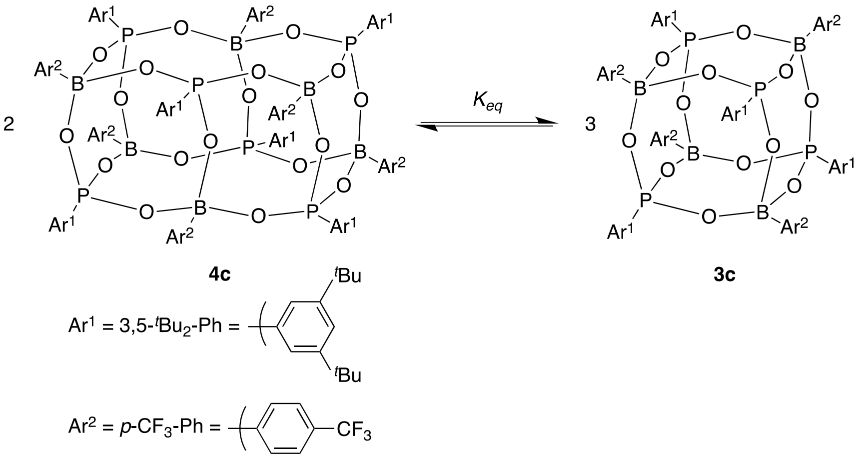

K_{eq} is defined as:

$$K_{eq} = \frac{[\mathbf{3c}]^3}{[\mathbf{4c}]^2}$$

Determination of K_{eq}. A known amount of **4c** and d_8-toluene were added to an NMR tube. The tube was maintained at the desired temperature and NMR spectra were recorded periodically until the concentrations of **4c** and **3c** remained constant, indicating that equilibrium had been reached. The initial concentration of **4c** is:

$$[\mathbf{4c}]_0 = \frac{m/MW}{V}$$

where m is the mass of **4c**, MW is the molecular weight of **4c** ($MW = 2546\ g/mol$) and V is the solution volume.

The initial total concentration of phosphorous $[P]_0$ is:

$$[P]_0 = 6[\mathbf{4c}]_0$$

The equilibrium concentrations of **4c** and **3c** were determined from the integrals of the ^{1}H NMR resonances at δ 7.67 (d, 12H) of **4c** ($I_{\mathbf{4c},^1H}$) and δ 7.95 (d, 8H) of **3c** ($I_{\mathbf{3c},^1H,}$), and the total integral of all of the aromatic resonances $I_{total,^1H}$, and are given by:

$$[\mathbf{4c}]_{eq} = \frac{I_{\mathbf{4c},^1H}/12}{I_{total,^1H}/7} * [P]_0$$

$$[\mathbf{3c}]_{eq} = \frac{I_{\mathbf{3c},^1H}/8}{I_{total,^1H}/7} * [P]_0$$

The factor of 7 reflects the fact that each $Ar^1PO_3BAr^2$ unit contains 7 aromatic hydrogens.

K_{eq} was determined at 105 °C and 23 °C for two independent samples. Data and results are summarized in Table 4.1.

Table 4.1. Determination of K_{eq}.

Sample No.	T (°C)	$[\mathbf{4c}]_0$ (mM)	$[P]_0$ (mM)	$[\mathbf{4c}]_{eq}$ (mM)	$[\mathbf{3c}]_{eq}$ (mM)	K_{eq} (M)
1 (Figure 4.20)	105	2.1	12.7	0.996	1.34	2.4×10^{-3}
1 (Figure 4.21)	23	2.1	12.7	1.08	1.14	1.3×10^{-3}
2 (Figure 4.22)	105	2.6	15.6	1.30	1.58	2.3×10^{-3}
2 (Figure 4.23)	23	2.6	15.6	1.38	1.32	1.2×10^{-3}

The average values for K_{eq} from the two samples are

105 °C:

$$K_{eq} = (2.4 \pm 0.1) \text{ x } 10^{-3} M$$

23 °C:

$$K_{eq} = (1.2 \pm 0.1) \text{ x } 10^{-3}\ M$$

Very similar results were obtained using the integrals of the ^{t}Bu resonances.

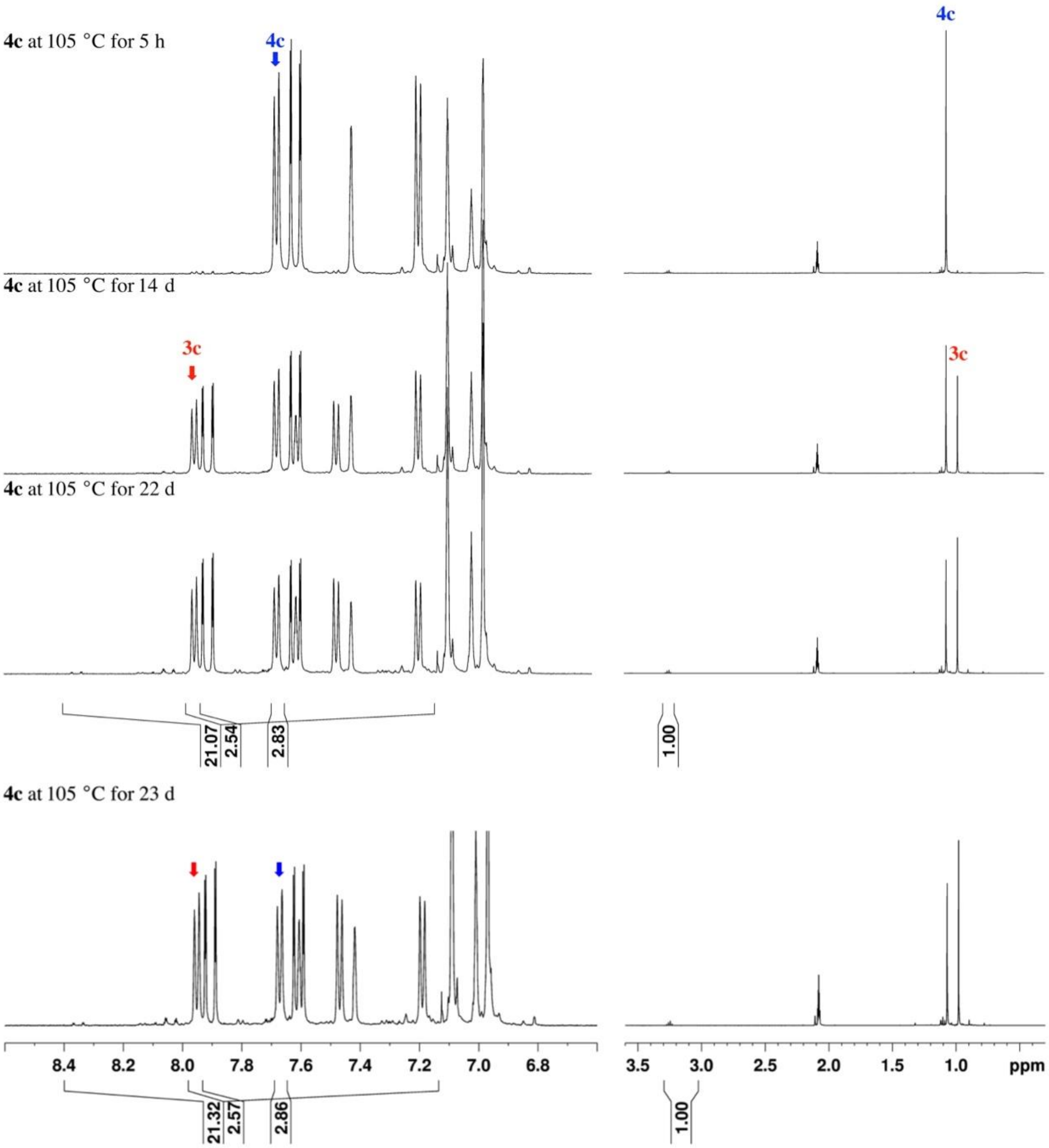

Figure 4.20. ^{1}H NMR for sample 1 at 105 °C (toluene-d_8, 500 MHz). The aromatic region is at the left and the aliphatic region is at the right, and they are at different vertical expansions. **4c** ($I_{\mathbf{4c},{}^{1}H}$): δ 7.67 (d, 12H), **3c** ($I_{\mathbf{3c},{}^{1}H}$): δ 7.95 (d, 8H), and total aromatic resonances ($I_{total,{}^{1}H}$): δ 8.39-7.14.

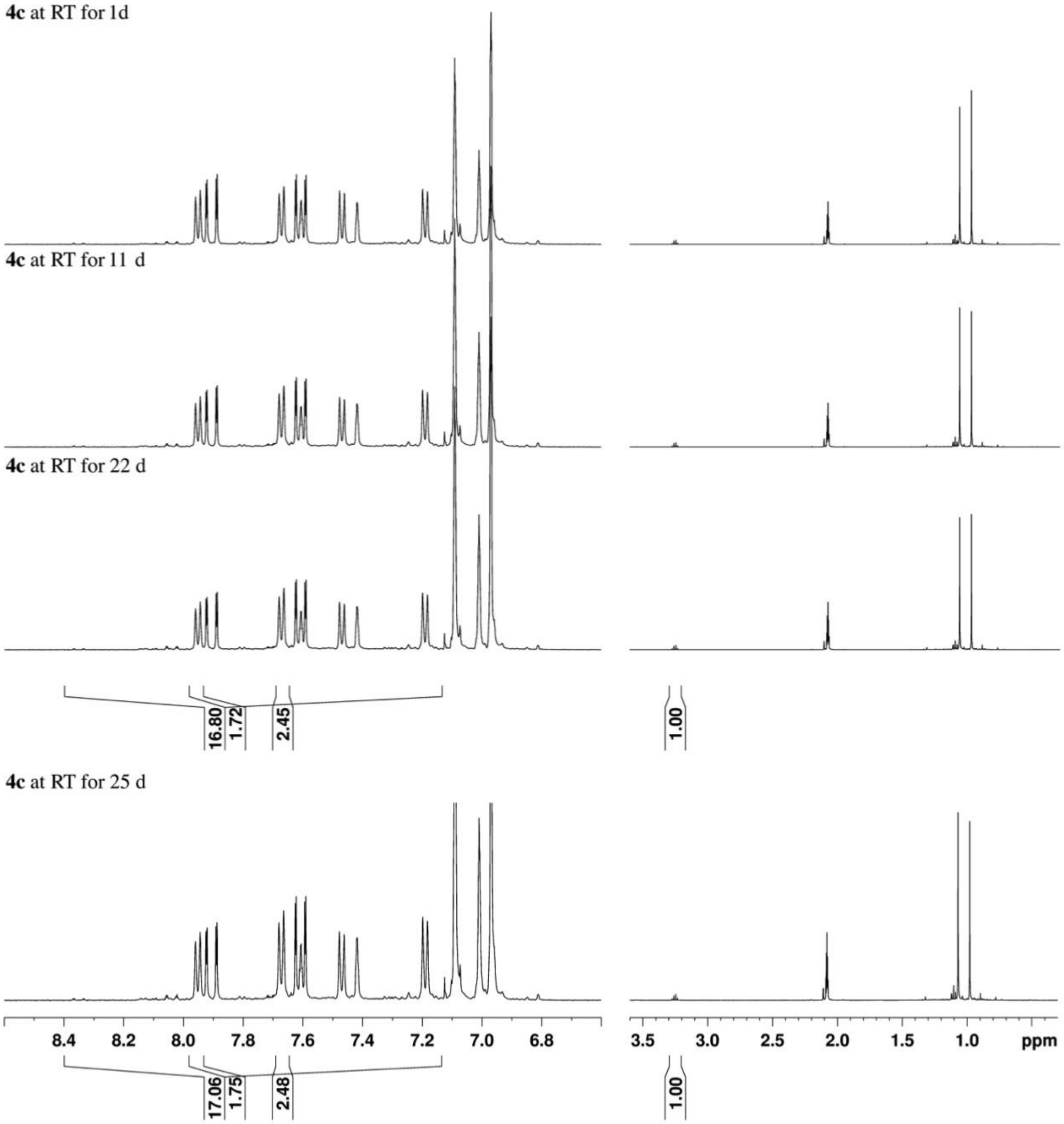

Figure 4.21. ^{1}H NMR for sample 1 at 23 °C (toluene-d_8, 500 MHz). The aromatic region is at the left and the aliphatic region is at the right, and they are at different vertical expansions. **4c** ($I_{\mathbf{4c},^1H}$): δ 7.67 (d, 12H), **3c** ($I_{\mathbf{3c},^1H}$): δ 7.95 (d, 8H), and total aromatic resonances ($I_{total,^1H}$): δ 8.39-7.14.

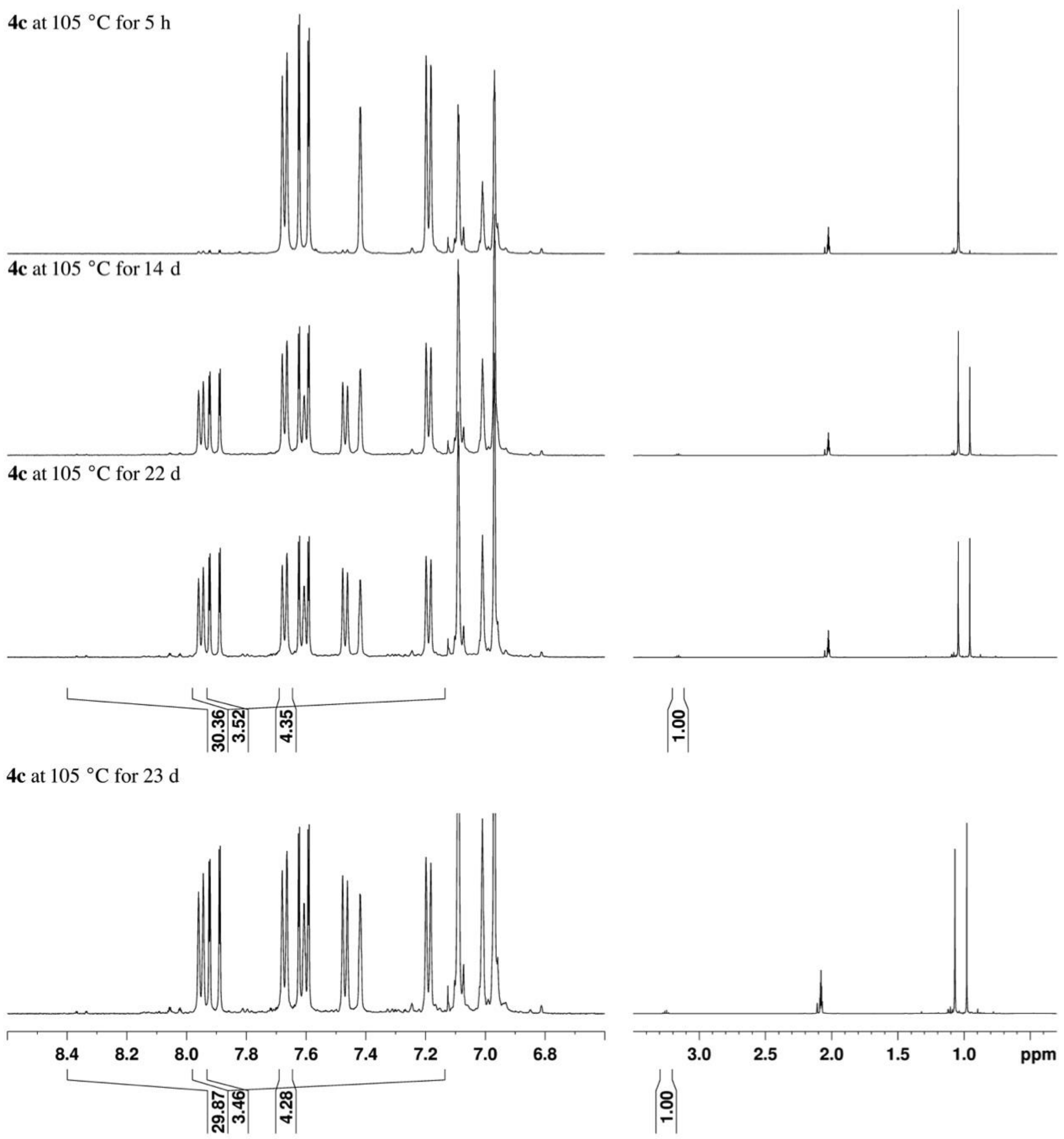

Figure 4.22. ^{1}H NMR for sample 2 at 105 °C (toluene-d_8, 500 MHz). The aromatic region is at the left and the aliphatic region is at the right, and they are at different vertical expansions. **4c** ($I_{\mathbf{4c},{}^1H}$): δ 7.67 (d, 12H), **3c** ($I_{\mathbf{3c},{}^1H}$): δ 7.95 (d, 8H), and total aromatic resonances ($I_{total,{}^1H}$): δ 8.39-7.14.

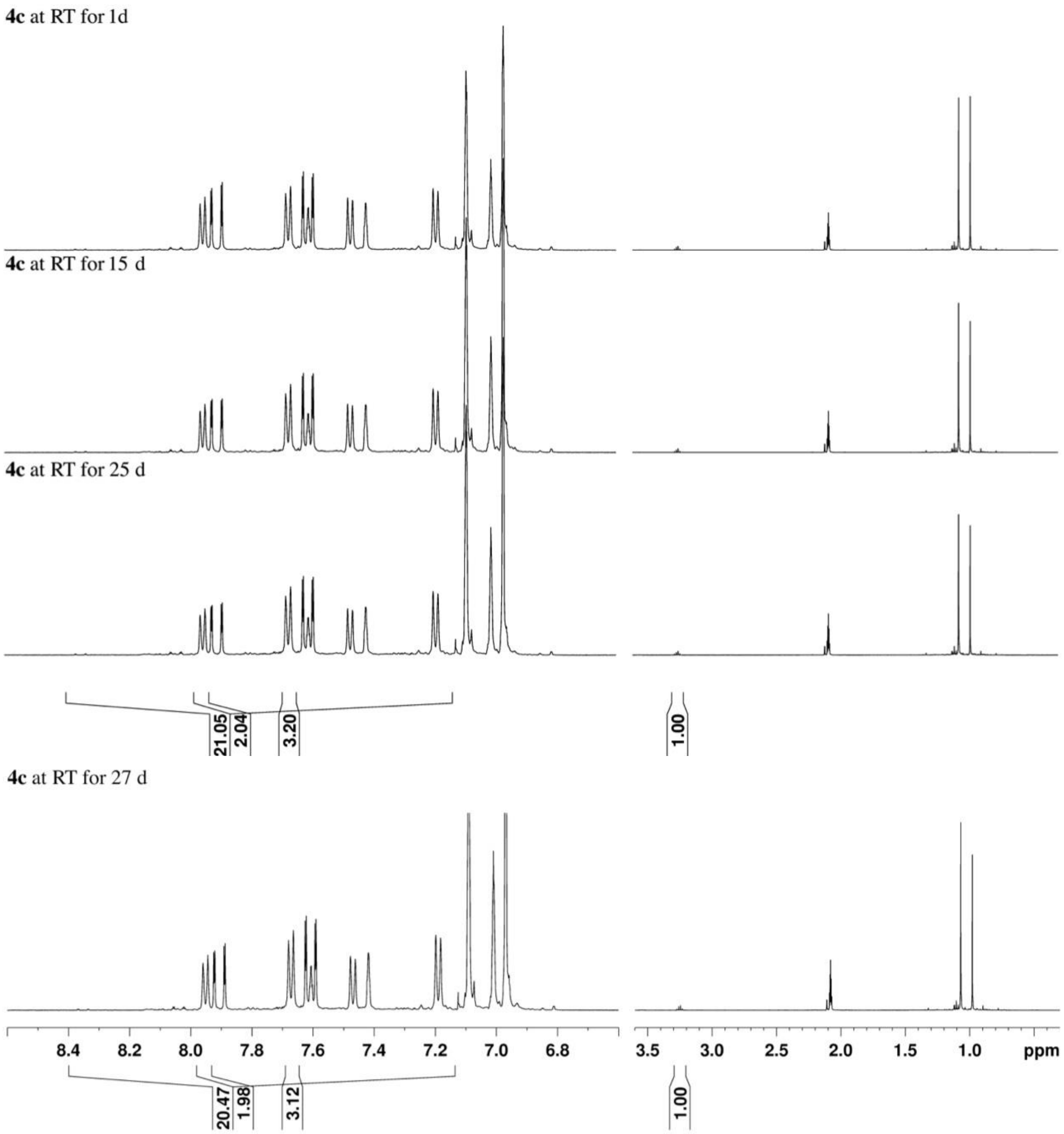

Figure 4.23. ^{1}H NMR for sample 2 at 23 °C (toluene-d_8, 500 MHz). The aromatic region is at the left and the aliphatic region is at the right, and they are at different vertical expansions. **4c** ($I_{\mathbf{4c},{}^1H}$): δ 7.67 (d, 12H), **3c** ($I_{\mathbf{3c},{}^1H}$): δ 7.95 (d, 8H), and total aromatic resonances ($I_{total,{}^1H}$): δ 8.39-7.14.

Assessment of whether the reaction of 1 and 2c generates an equilibrium mixture of 3c and 4c.

Method 1. Objective: Comparsion of reaction quotient Q and K_{eq}. For the low-initial-concentration reaction of **1** and **2c**, an aliquot was taken from the reacion mixture at the end of the reaction period (ca. 3 h, 110 °C). The volatiles were removed rapidly under vacuum, and the residue was analyzed by ^{1}H NMR in C_6D_6. The total concentration of phosphorous $[P]$, is equal to the initial concentration of (3,5-^{t}Bu$_2$-Ph)P(O)(OH)$_2$ (**1**) ($[P] = 2.5\ mM$). $[\boldsymbol{4c}]_t$ and $[\boldsymbol{3c}]_t$ are the concentrations of **4c** and **3c** at time = t. The concentrations of **4c** and **3c** in the reaction mixture can then be determined from the integrals of the ^{1}H NMR resonances at δ 7.72 (d, 12H) of **4c** ($I_{\boldsymbol{4c},{}^1H}$) and δ 8.01 (d, 8H) of **3c** ($I_{\boldsymbol{3c},{}^1H}$), and the total integral of all of the aromatic resonances $I_{total,{}^1H}$ of the NMR sample (Figure 4.24), and are given by:

$$[\boldsymbol{4c}]_t = \frac{I_{\boldsymbol{4c},{}^1H,}/12}{I_{total,{}^1H}/7} * [P]$$

$$[\boldsymbol{3c}]_t = \frac{I_{\boldsymbol{3c},{}^1H}/8}{I_{total,{}^1H}/7} * [P]$$

$$Q = \frac{{[\boldsymbol{3c}]_t}^3}{{[\boldsymbol{4c}]_t}^2}$$

The factor of 7 reflects the fact that each Ar^{1}PO$_3$BAr^2 unit contains 7 aromatic hydrogens.

After the reaction time (ca. 3 h), Q = 73 x 10^{-3} M > K_{eq} =2.4 x 10^{-3} M, i.e. the sample is enriched in **3c** compared to the equilibrium concentration. This is obvious by inspection of the NMR spectrum. Note that the value of Q determined above is a lower limit, since it is possible that some conversion of **3c** to **4c** occurred during the preparation and NMR analysis of the sample.

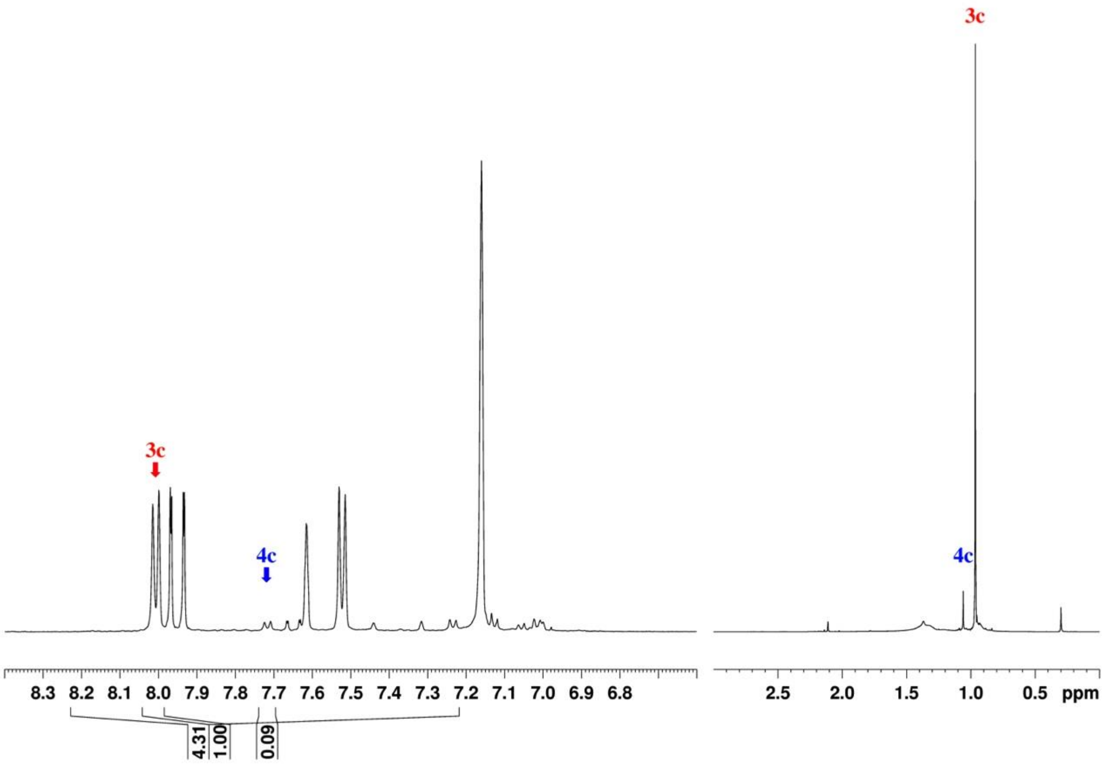

Figure 4.24. ^{1}H NMR of an aliquot from the reaction of **1** and **2c** at low concentration after ca. 3 h at 110 °C, stripped of volatiles and dissolved in C_6D_6 (500 MHz). The aromatic region is at the left and the aliphatic region is at the right, and they are at different vertical expansions. **4c** ($I_{\mathbf{4c},^1H}$): δ 7.72 (d, 12H), **3c** ($I_{\mathbf{3c},^1H}$): δ 8.01 (d, 8H), and total aromatic resonances ($I_{total,^1H}$): δ 8.23-7.22.

For the high-initial-concentration reaction, an aliquot was taken from the reaction mixture and analyzed by ^{31}P{^{1}H} NMR. The total concentration of phosphorous $[P] = 25\,mM$. The concentrations of **4c** and **3c** are determined from the integrals of the ^{31}P{^{1}H} NMR resonances at δ -1 (s, 6P) of **4c** ($I_{\mathbf{4c},^{31}P}$) and δ -7 (s, 4P) of **3c** ($I_{\mathbf{3c},^{31}P}$), and the total integral of the P resonances $I_{total,^{31}P}$ (see Figure 4.1(b)), and are given by:

$$[\mathbf{4c}]_t = \frac{I_{\mathbf{4c},^{31}P}/6}{I_{total,^{31}P}} * [P]$$

$$[\mathbf{3c}]_t = \frac{I_{\mathbf{3c},{}^{31}P}/4}{I_{total,{}^{31}P}} * [P]$$

$$Q = \frac{[\mathbf{3c}]_t{}^3}{[\mathbf{4c}]_t{}^2}$$

In this case, the denominator (1) of the $I_{total,{}^{31}P}$ term reflects the fact that each $Ar^1PO_3BAr^2$ unit contains 1 phosphorous.

After the reaction time (ca. 3 h), $Q = 0.11 \times 10^{-3}$ M < $K_{eq} = 2.4 \times 10^{-3}$ M, i.e. the sample is enriched in **4c** compared to the equilibrium concentration.

Method 2. Objective: Compare observed $\frac{[3c]_t}{[4c]_t}$ *ratio to the equilibrium ratio.* If K_{eq} and the total phosphorus concentration $[P]$ are known, the equilibrium concentration of products can be predicted as follow.

$$K_{eq} = \frac{[\mathbf{3c}]^3}{[\mathbf{4c}]^2}$$

$$[\mathbf{4c}]_{eq} = \sqrt{\frac{[\mathbf{3c}]_{eq}{}^3}{K_{eq}}} \quad (\text{eq.} 1)$$

$[\mathbf{4c}]_{eq}$ and $[\mathbf{3c}]_{eq}$ are related to $[P]$ by

$$4 * [\mathbf{3c}]_{eq} + 6 * [\mathbf{4c}]_{eq} = [P]$$

After substitution,

$$4 * [\mathbf{3c}]_{eq} + 6 * \sqrt{\frac{[\mathbf{3c}]_{eq}{}^3}{K_{eq}}} = [P]$$

After rearrangement,

$$36 * [\mathbf{3c}]_{eq}{}^3 - 16 * K_{eq} * [\mathbf{3c}]_{eq}{}^2 + 8 * K_{eq} * [P] * [\mathbf{3c}]_{eq} - K_{eq} * ([P])^2 = 0 \quad (\text{eq.} 2)$$

This cubic equation was solved by a standard calculator program. $[\mathbf{4c}]_{eq}$ was then determined by equation 1.

In the condensation reactions, **4c**, **3c** and other phosphorous species are observed, and the total phosphorous concentration from **4c** and **3c** at time = t is $[P]_t$. $[P]_t$ can be determined by ^{1}H NMR, and is given by:

$$[P]_t = \frac{\left(I_{\mathbf{4c},^1H} + I_{\mathbf{3c},^1H}\right)/2}{I_{total,^1H}/7} * [P]_0 \quad (\mathrm{eq.}\,3)$$

The factor of 2 in equation 3 reflects the fact that each Ar^{1}PO$_3$BAr^2 unit of **4c** and **3c** contains 2 hydrogens at δ 7.72 (d) of **4c** and δ 8.01 (d) of **3c**. The factor of 7 reflects the fact that each Ar^{1}PO$_3$BAr^2 unit contains 7 aromatic hydrogens. $[P]_t$ also can be determined by ^{31}P{^{1}H} NMR, and is given by:

$$[P]_t = \frac{I_{\mathbf{4c},^{31}P} + I_{\mathbf{3c},^{31}P}}{I_{total,^{31}P}} * [P]_0 \quad (\mathrm{eq.}\,4)$$

This value should be used in equation 1 and 2 to predict the $\frac{[\mathbf{3c}]_{eq}}{[\mathbf{4c}]_{eq}}$ ratio.

At the end (ca. 3 h) of low initial concentration reaction of **1** and **2c** ($[\mathbf{1}]_0 = [\mathbf{2c}]_0 = [P]_0 = 2.5\,mM$, $K_{eq} = 2.4 \text{ x } 10^{-3}\,M$ at 105 °C), $[P]_t$ was determined by ^{1}H NMR (equation 3, Figure 4.24). The results are:

$$[P]_t = 2.2\,mM$$

$$[\mathbf{3c}]_{eq} = 0.35\,mM$$

$$[\mathbf{4c}]_{eq} = 0.13\,mM$$

Therefore, the predicted ratio of the equilibrium concentrations of **4c** and **3c** is

$$\frac{[\mathbf{3c}]_{eq}}{[\mathbf{4c}]_{eq}} = 2.6$$

The observed concentrations of **4c** and **3c** were determined by ^{1}H NMR as described above in the discussion of Method **1**.

$$[\mathbf{3c}]_t = 0.51\,mM$$

$$[\boldsymbol{4c}]_t = 0.030\ mM$$

$$\left(\frac{[\boldsymbol{3c}]_t}{[\boldsymbol{4c}]_t}\right)_{obs} = 17$$

Therefore, the product mixture of the dilute reaction ($[\mathbf{1}]_0$ = $[\mathbf{2c}]_0$ = 2.5 mM) is highly enriched in **3c** relative to the expected equilibrium concentration, consistent with the result of Method **1**.

At the end (ca. 3 h) of high initial concentration reaction of **1** and **2c** ($[\mathbf{1}]_0 = [\boldsymbol{2c}]_0 = [P]_0 = 25\ mM$, $K_{eq} = 2.4 \text{ x } 10^{-3}\ M$ at 105 °C), $[P]_t$ was determined by ^{31}P{^{1}H} NMR (equation 4, see Figure 4.1(b)). The results are:

$$[P]_t = 22\ mM$$

$$[\boldsymbol{3c}]_{eq} = 2.2\ mM$$

$$[\boldsymbol{4c}]_{eq} = 2.2\ mM$$

Therefore, the predicted ratio for equilibrium concentrations of **4c** and **3c** is

$$\frac{[\boldsymbol{3c}]_{eq}}{[\boldsymbol{4c}]_{eq}} = 1.0$$

The observed concentrations of **4c** and **3c** were determined by ^{31}P{^{1}H} NMR as described above in the discussion of Method **1**.

$$[\boldsymbol{3c}]_t = 0.99\ mM$$

$$[\boldsymbol{4c}]_t = 3.0\ mM$$

$$\left(\frac{[\boldsymbol{3c}]_t}{[\boldsymbol{4c}]_t}\right)_{obs} = 0.33$$

Therefore, the product mixture of the high initial concentration reaction ($[\mathbf{1}]_0$ = $[\mathbf{2c}]_0$ = 25 mM) is enriched in **4c** relative to the expected equilibrium concentration, consistent with the result of Method **1**.

$^{11}B\{^1H\}$ NMR Background Subtraction. $^{11}B\{^1H\}$ NMR spectra for borophosphonate cage complexes and background spectra (which contain broad signals from the probe) were acquired in 0.5 ml toluene-*d_8* in a quartz nmr tube. The background-free $^{11}B\{^1H\}$ NMR spectra for the complexes were obtained by subtracting the background spectra from the complex spectra. Figure 4.25 illustrates this procedure for **3a**. All the $^{11}B\{^1H\}$ NMR spectra provided here are the background-free $^{11}B\{^1H\}$ NMR spectra.

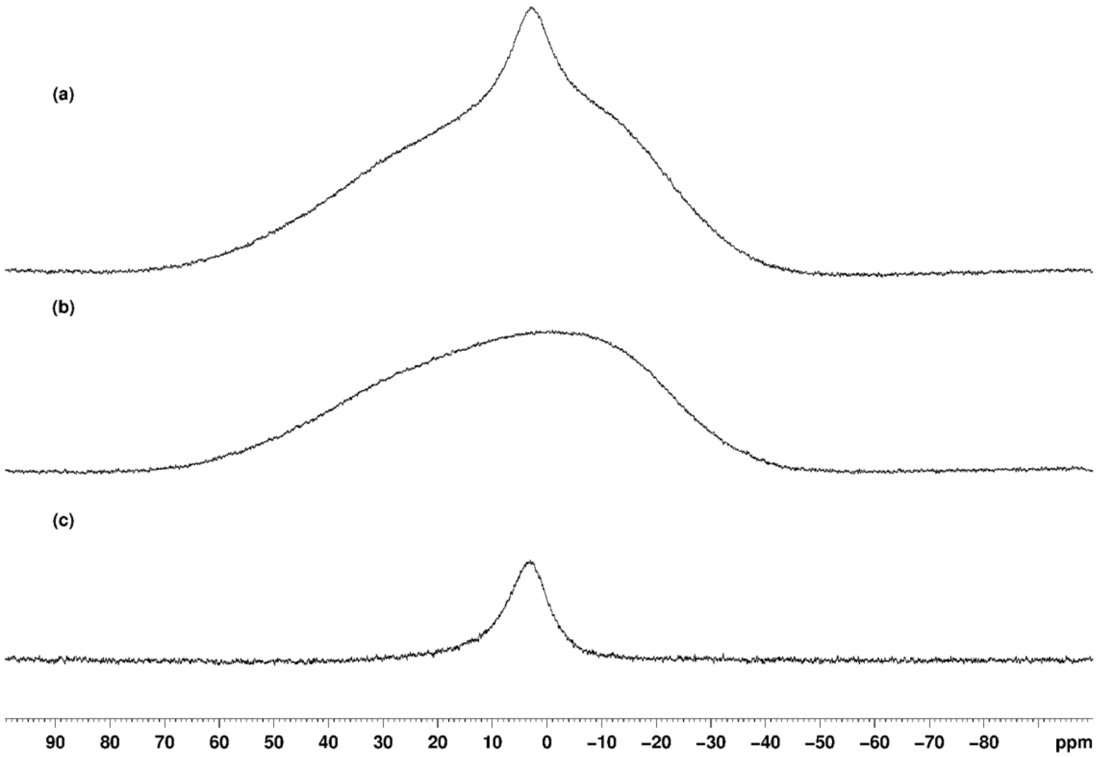

Figure 4.25. $^{11}B\{^1H\}$ NMR spectra for $[(3,5\text{-}^t\text{Bu}_2\text{-Ph})\text{PO}_3\text{B}(o\text{-Br-Ph})]_4$ (**3a**): (a) $^{11}B\{^1H\}$ NMR spectrum for **3a** in toluene-*d_8*; (b) $^{11}B\{^1H\}$ NMR spectrum for toluene-*d_8*; (c) Background-free $^{11}B\{^1H\}$ NMR spectrum for **3a** in toluene-*d_8*, obtained by subtracting spectrum b from spectrum a.

X-ray Data Collection and Structure Refinement. The diffraction data for **3a**, **3d**, and **4d** were measured at 100 K on a Bruker D8 VENTURE with PHOTON 100 CMOS detector system equipped with a Mo-target X-ray tube (λ = 0.71073 Å). Data reduction and integration were performed with the Bruker APEX2 software package. Data were corrected for absorption effects using the empirical methods as implemented in SADABS. The structures were solved and refined by full-matrix least-squares procedures using the Bruker SHELXTL software package.

Specific details for structure refinement for 3a. All atoms were refined with anisotropic thermal parameters except for modelling of minor disorders of a number of ^{t}Bu groups. The ^{t}Bu groups as it is commonly observed were rotationally disordered over two or three positions and were individually modelled. Modelling of two ^{t}Bu moieties was also complicated by the positional disorder. Geometric restrains (DFIX 1.53 and DANG 2.47 with the default standard deviation) were used in the disorder modelling to keep the refinement stable. The main residue atoms are found to be well behaved. Hydrogen atoms were included in idealized positions for structure factor calculations. Crystal contained disordered solvent molecule and this was treated by application of the program SQUEZZE[20] as implemented in Platon[21]. SQUEEZE algorithm located a void, centered at (0, 0.5, 0.5), with a large volume of 1238 Å^3 and the electron count of 246 that can correspond to three molecules of toluene or/and hexanes used for crystallization.

Specific details for structure refinement for 3d. The crystal contained solvent accessible voids with disordered solvent which was treated with the bulk solvent correction of the observed intensities by using the SQEEZE protocol included in PLATON[20,21]. The program accounted for two large voids centered at x, y, z = 0, 0.5, 0 and 0, 0, 0.5 with a volume of 1180 Å^3 and an electron void count of 365 that can correspond to four toluene and/or hexanes molecules.

One of the ^{t}Bu groups found to be disordered over two positions, and this was modeled with 0.55:0.45 relative occupancies. It can be noted that this disordered is also complicated by the spatial shift of both groups (simultaneous rotational and positional disorder). Similarity and “rigid bond” restraints SIMU and DELU were used for modelling the disorder of these moieties. The C22X and C22Y were refined to behave approximately isotropic. The asymmetric unit is presented in Figure 4.26.

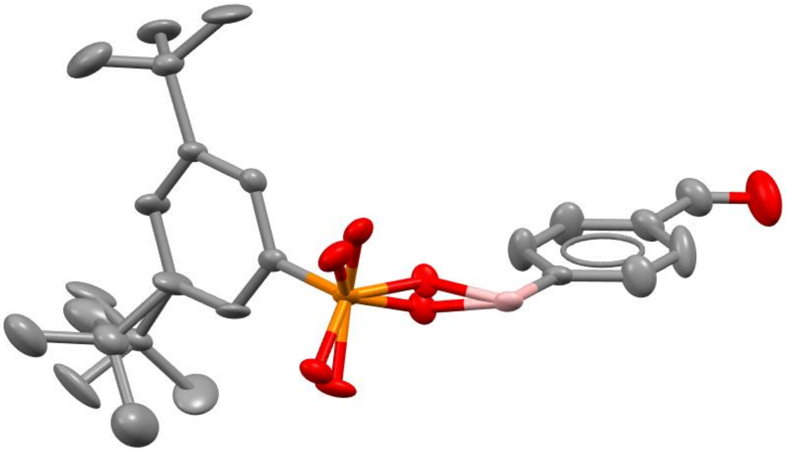

Figure 4.26. Asymmetric unit of **3d** drawn with thermal ellipsoids at the 50% probability level. Both parts of the disordered ^{t}Bu groups and the disordered O-bridges are shown. Hydrogen atoms are omitted for clarity.

The bridging oxygen atoms between P and B atoms are also found to be disordered over two positions, and this fact merits a further detailed discussion. The separation of oxygen over two positions is carried out without the use of any restraints and the relative occupancy of two parts is 1:1. Oxygen atoms that belong to the same group are shown in Figure 4.27 overlaid with yellow (part 1) or blue (part 2) circles.

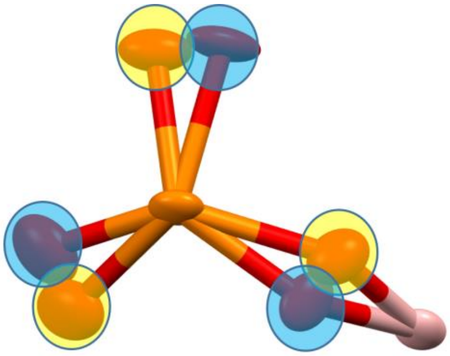

Figure 4.27. A view at the disorder of oxygen bridges. Blue and yellow circles represent oxygen atoms that belong to two different self-assembled cages.

Disorder of oxygen bridges leads to the important consequence: there are two different molecular moieties co-crystallized in the crystal of **3d**. Growing the asymmetric unit reveals how the two cages are overlaid (Figure 4.28).

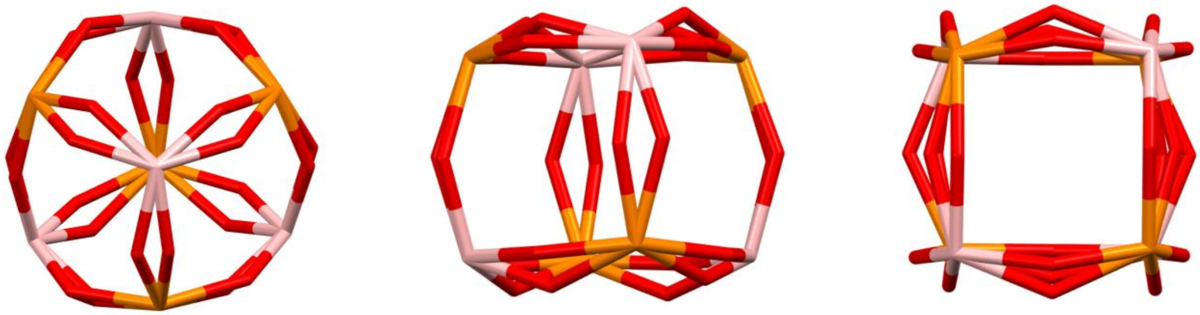

Figure 4.28. Different views of two different overlaid self-assembled cages in **3d**.

Two cages represent two conformational isomers as they have the same atoms connectivity but they differ in the spatial orientation of O-bridges in regard to other bridges. Two neighboring oxygen bridges may lie in the same or perpendicular planes illustrating the conformational flexibility (Figure 4.29).

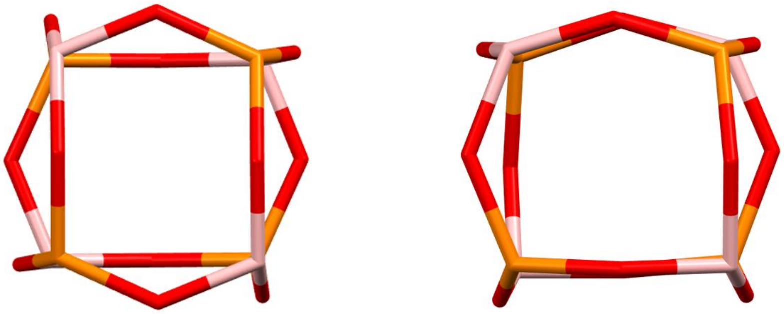

Figure 4.29. Two different co-crystallized cages are represented separately (left and right). Note the difference in the spatial orientation of some oxygen bridges while the overall connectivity and position of all atoms is the same.

Specific details for structure refinement for 4d. All atoms were refined with anisotropic thermal parameters except for modelling of a minor disorder of a formyl group and one of the solvent benzene molecules as discussed below. Hydrogen atoms were included in idealized positions for structure factor calculations.

Formyl group is rotationally disordered and refined with a 1:1 ratio of two parts. C and O atoms are refined with isotropic thermal parameters. The C=O distances were restrained to be 1.20 Å and C_{Ar}-C_{formyl} were restrained to be 1.47 for two disordered parts (DFIX). DANG restraints were also used for 1,3-distances to accommodate the refinement of the formyl group disorder.

There two kinds of solvent molecules present in the structure: two toluene molecules and one benzene molecule per one main residue. Toluene is found to be well defined but benzene is disordered over a center of inversion in such a way that the two parts share two C-atoms. When each C-atom was given 0.5 occupancy and one shared was left with a full occupancy, thermal parameters for all of them except one ½-occuppied refined to be similar. This fact might indicate a possible "contamination" of the position with toluene molecules.

Table 4.2. Crystal data and structure refinement for **3a**.

Identification code	**3a**	
Empirical formula	$C_{80}H_{100}B_4Br_4O_{12}P_4$	
Formula weight	1740.36	
Temperature	100(2) K	
Wavelength	0.71073 Å	
Crystal system	Triclinic	
Space group	P-1	
Unit cell dimensions	a = 13.6221(8) Å	α= 81.418(2)°.
	b = 17.9989(10) Å	β= 80.698(2)°.
	c = 20.9051(11) Å	γ = 86.124(2)°.
Volume	4996.6(5) $Å^3$	
Z	2	
Density (calculated)	1.157 Mg/m^3	
Absorption coefficient	1.723 mm^{-1}	
F(000)	1792	
Crystal size	0.47 x 0.36 x 0.35 mm^3	
Theta range for data collection	1.94 to 28.40°.	
Index ranges	-18<=h<=18, -24<=k<=24, -27<=l<=27	
Reflections collected	104261	
Independent reflections	24855 [R(int) = 0.0550]	
Completeness to theta = 25.00°	100.0 %	
Absorption correction	Semi-empirical from equivalents	
Max. and min. transmission	0.5855 and 0.4988	
Refinement method	Full-matrix least-squares on F^2	
Data / restraints / parameters	24855 / 38 / 978	
Goodness-of-fit on F^2	1.017	
Final R indices [I>2sigma(I)]	R1 = 0.0453, wR2 = 0.0953	
R indices (all data)	R1 = 0.0819, wR2 = 0.1025	
Largest diff. peak and hole	0.752 and -0.505 e.$Å^{-3}$	

Table 4.3. Crystal data and structure refinement for **3d**.

Identification code	**3d**	
Empirical formula	$C_{84}H_{104}B_4O_{16}P_4$	
Formula weight	1536.79	
Temperature	100(2) K	
Wavelength	0.71073 Å	
Crystal system	Tetragonal	
Space group	I -4	
Unit cell dimensions	a = 13.9467(13) Å	α= 90°.
	b = 13.9467(13) Å	β= 90°.
	c = 29.586(3) Å	γ = 90°.
Volume	5754.8(10) $Å^3$	
Z	2	
Density (calculated)	0.887 Mg/m^3	
Absorption coefficient	0.112 mm^{-1}	
F(000)	1632	
Crystal size	0.39 x 0.28 x 0.17 mm^3	
Theta range for data collection	2.07 to 25.10°.	
Index ranges	-16<=h<=16, -16<=k<=16, -35<=l<=35	
Reflections collected	77112	
Independent reflections	5123 [R(int) = 0.1548]	
Completeness to theta = 25.00°	99.9 %	
Max. and min. transmission	0.9812 and 0.9577	
Refinement method	Full-matrix least-squares on F^2	
Data / restraints / parameters	5123 / 62 / 316	
Goodness-of-fit on F^2	1.079	
Final R indices [I>2sigma(I)]	R1 = 0.0622, wR2 = 0.1593	
R indices (all data)	R1 = 0.0652, wR2 = 0.1615	
Absolute structure parameter	0.09(12)	
Largest diff. peak and hole	0.406 and -0.237 e.$Å^{-3}$	

Table 4.4. Crystal data and structure refinement for **4d**.

Identification code	**4d**	
Empirical formula	$C_{146}H_{176}B_6O_{24}P_6$	
Formula weight	2565.56	
Temperature	100(2) K	
Wavelength	0.71073 Å	
Crystal system	Triclinic	
Space group	P-1	
Unit cell dimensions	a = 14.9373(16) Å	α= 70.912(4)°.
	b = 15.3524(15) Å	β= 65.758(3)°.
	c = 18.090(2) Å	γ = 77.708(3)°.
Volume	3559.8(7) Å^3	
Z	1	
Density (calculated)	1.197 Mg/m^3	
Absorption coefficient	0.142 mm^{-1}	
F(000)	1364	
Crystal size	0.18 x 0.17 x 0.13 mm^3	
Theta range for data collection	2.15 to 25.14°.	
Index ranges	-17<=h<=17, -18<=k<=18, -21<=l<=21	
Reflections collected	81635	
Independent reflections	11725 [R(int) = 0.0772]	
Completeness to theta = 25.00°	92.9 %	
Absorption correction	Semi-empirical from equivalents	
Max. and min. transmission	0.982 and 0.975	
Refinement method	Full-matrix least-squares on F^2	
Data / restraints / parameters	11725 / 8 / 830	
Goodness-of-fit on F^2	1.032	
Final R indices [I>2sigma(I)]	R1 = 0.0641, wR2 = 0.1566	
R indices (all data)	R1 = 0.1112, wR2 = 0.1825	
Largest diff. peak and hole	0.947 and -0.755 e.Å^{-3}	

4.5 References and Notes

1. (a) Walawalkar, M. G.; Murugavel, R.; Roesky, H. W.; Schmidt, H.-G. *Inorg. Chem.* **1997**, *36*, 4202. (b) Walawalkar, M. G.; Murugavel, R.; Roesky, H. W.; Schmidt, H.-G. *Organometallics* **1997**, *16*, 516.

2. Cordes, D. B.; Lickiss, P. D.; Rataboul, F. *Chem. Rev.* **2010**, *110*, 2081.

3. (a) Kuehnle, A. *Chem. Abstr.* **2006**, *144*, 276020. (b) Guan, C.; Yang, H.; Li, W.; Zhou, D.; Xu, J.; Chen, Z.-R. *J. Appl. Polym. Sci.* **2014**, *131*, 40847. (c) Kajetanowicz, A.; Czaban, J.; Krishnan, G. R.; Malińska, M.; Woźniak, K.; Siddique, H.; Peeva, L. G.; Livingston, A. G.; Grela, K. *ChemSusChem* **2013**, *6*, 182. (d) Leng, Y.; Liu, J.; Zhang, C.; Jiang, P. *Catalysis Science & Technology* **2014**, *4*, 997. (e) Pescarmona, P. P.; Masters, A. F.; van der Waal, J. C.; Maschmeyer, T. *J. Mol. Catal. A: Chem.* **2004**, *220*, 37. (f) Abbenhuis, H. C. L.; van Herwijnen, H. W. G.; van Santen, R. A. *Chem. Commun.* **1996**, 1941.

4. Tönnemann, J.; Scopelliti, R.; Severin, K. *Eur. J. Inorg. Chem.* **2013**, 5071.

5. (a) Mason, M. R.; Matthews, R. M.; Mashuta, M. S.; Richardson, J. F. *Inorg. Chem.* **1996**, *35*, 5756. (b) Mason, M. *J. Cluster Sci.* **1998**, *9*, 1. (c) Mason, M. R.; Perkins, A. M.; Ponomarova, V. V.; Vij, A. *Organometallics* **2001**, *20*, 4833.

6. (a) Mason, M. R.; Mashuta, M. S.; Richardson, J. F. *Angew. Chem. Int. Ed.* **1997**, *36*, 239. (b) Mason, M. R.; Perkins, A. M.; Matthews, R. M.; Fisher, J. D.; Mashuta, M. S.; Vij, A. *Inorg. Chem.* **1998**, *37*, 3734.

7. Keys, A.; Bott, S.; Barron, A. R. *Chem. Commun.* **1996**, 2339.

8. Landry, C. C.; Cleaver, W. M.; Guzei, I. A.; Rheingold, A. L. *Organometallics* **1998**, *17*, 5209.

9. Yang, Y.; Walawalkar, M. G.; Pinkas, J.; Roesky, H. W.; Schmidt, H.-G. *Angew. Chem. Int. Ed.* **1998**, *37*, 96.

10. (a) Diemert, K.; Englert, U.; Kuchen, W.; Sandt, F. *Angew. Chem. Int. Ed.* **1997**, *36*, 241. (b) Diemert, K.; Kuchen, W.; Mootz, D.; Poll, W.; Sandt, F. *Phosphorus Sulfur Silicon Relat. Elem.* **1996**, *111*, 100.

11. Similar reactions of dialkylphosphonates with cyclohexyldichloroborane gave mixtures of oligomeric condensation products: Mortier, J.; Gridnev, I. D.; Guénot, P. *Organometallics* **2000**, *19*, 4266.

12. Tönnemann, J.; Scopelliti, R.; Zhurov, K. O.; Menin, L.; Dehnen, S.; Severin, K. *Chem. Eur. J.* **2012**, *18*, 9939.

13. Yuji Tokunaga, H. U., Youji Shimomura, and Toshihiro Seo *Heterocycles* **2002**, *57*, 4.

14. Brock, C. P.; Minton, R. P.; Niedenzu, K. *Acta Crystallogr., Sect. C* **1987**, *43*, 1775.

15. (a) Moedritzer, K. *J. Am. Chem. Soc.* **1961**, *83*, 4381. (b) Ohms, G.; Großmann, G.; Schwab, B.; Schiefer, H. *Phosphorus Sulfur Silicon Relat. Elem.* **1992**, *68*, 77. (c) Fuchs, S.; Schmidbauer, H. *Z. Naturforsch., B: Chem. Sci.* **1995**, *50(b)*, 855. (d) Diemert, K.; Kuchen, W.; Poll, W.; Sandt, F. *Eur. J. Inorg. Chem.* **1998**, 361. (e) Kaltbeitzel, A.; Schauff, S.; Steininger, H.; Bingöl, B.; Brunklaus, G.; Meyer, W. H.; Spiess, H. W. *Solid State Ionics* **2007**, *178*, 469. (f) Kudzin, Z. H.; Depczynski, R.; Kudzin, M. H.; Luczak, J.; Drabowicz, J. *Amino Acids* **2007**, *33*, 663.

16. Reisinger, C. M.; Nowack, R. J.; Volkmer, D.; Rieger, B. *Dalton Trans.* **2007**, 272.

17. Anet, F. L., Dynamics of eight-membered rings in the cyclooctane class. In *Dynamic Chemistry*, Springer Berlin Heidelberg: 1974; Vol. 45, pp 169.

18. (a) Dale, J. *Acta Chem. Scand.* **1973**, *27*, 1115. (b) Gotō, H. *Tetrahedron* **1992**, *48*, 7131.

19. (a) Chen, F.-X.; Kina, A.; Hayashi, T. *Org. Lett.* **2005**, *8*, 341. (b) Liao, Y.-X.; Hu, Q.-S. *J. Org. Chem.* **2011**, *76*, 7602.

20. Van der Sluis, P.; Spek, A. L., *Acta Cryst. A.* **1990,** *46* (3), 194-201.

21. Spek, A., *Acta Cryst. D.***2009,** *65* (2), 148-155